STUDIES ON TRANSITION METAL POLYTHIA MACROCYCLIC COMPLEXES

by

Malcolm A. Halcrow

Thesis presented for the Degree of Doctor of Philosophy

University of Edinburgh

1991

To my family, and to Mr. S. Nandi

for getting me into all this.

DECLARATION

Except where specific reference is made to other sources, the work presented in this thesis is the original work of the author. It has not been submitted, in whole or in part, for any other degree. Certain of the results have already been published.

Malcolm A. Halcrow

ACKNOWLEDGEMENTS

I would like to express my appreciation for my supervisor, Dr. M. Schröder, whose advice and encouragement throughout the course of this work have been invaluable. I would also like to thank Drs. A.J. Blake and R.O. Gould for collecting the data for all the x-ray structures, and for help with their solution and refinement. I am also indebted to Drs. L.J. Yellowlees and R.E.P. Winpenny for discussions on electrochemistry and electronic spectroscopy, and on e.p.r. spectroscopy, respectively.

I would like to thank the departmental analytical services, in particular Mr. A.T. Taylor (mass spectrometry), Mrs. E. McDougall (elemental analysis), Dr. D. Reed, Mr. J.A. Miller and Miss H. Grant (n.m.r. spectroscopy). I am also grateful to Dr. S.G.D. Henderson for help with several aspects of n.m.r. spectroscopy and to Dr. J.T. Sharp for explaining the molecular mechanics programs. I am indebted to Dr. D. Coliston (University of Manchester) for e.p.r. simulations, and to Dr. R.D. Peacock (University of Glasgow) for running Raman spectra.

My thanks to Drs. Tim Hyde and Gill Reid and to Anne Taylor for their help and discussions, and to the other members of the group and the inhabitants of lab. 293 for stopping me working too hard.

I would like to acknowledge the S.E.R.C. and I.C.I. Organics Division for a CASE award, Johnson-Matthey for loans of rhodium and iridium salts and the University of Edinburgh for the use of facilities. Finally, my thanks to Mrs. L. Marouf for typing this thesis.

ABSTRACT

Chapter 1

An introduction to macrocyclic coordination chemistry and its relevance to biological systems and catalysis is presented. The general aims of the project are discussed.

Chapter 2

Reaction of $NiCl_2$ with [12]aneS_4, [14]aneS_4, [16]aneS_4 or [9]aneS_3 in CH_3NO_2 yields the dimeric complexes $[Ni_2(S_4)_2(\mu\text{-}Cl)_2]^{2+}$ (S_4 = [12]aneS_4, [14]aneS_4, [16]aneS_4) and $[Ni_2([9]aneS_3)(\mu\text{-}Cl)_3]^{+}$. Single crystal x-ray analyses of $[Ni_2(S_4)_2(\mu\text{-}Cl)_2]^{2+}$ (S_4 = [12]aneS_4, [14]aneS_4, [16]aneS_4) show the Ni centres to adopt octahedral stereochemistries, with the macrocycles bound in *cis*-fashion about the metal ions [Ni-S = 2.37-2.44, Ni-Cl = 2.38-2.44, Ni...Ni = 3.56 Å]. The single crystal structure of $[Ni_2([9]aneS_3)_2(\mu\text{-}Cl)_3]^{+}$ shows the cation to adopt a confacial bi-octahedral geometry [Ni-S = 2.35-2.37, Ni-Cl = 2.41-2.44, Ni...Ni = 2.92 Å]. The electrochemistry of the compounds $[Ni_2(S_4)_21(\mu\text{-}Cl)_2]^{2+}$ is complex, exhibiting several irreversible oxidative and reductive processes which could not be unambiguously assigned.

Treatment of $Ni(BF_4)_2.6H_2O$ with [12]aneS_4 or [16]aneS_4 in CH_3NO_2 in the presence of $(CH_3CO)_2O$ affords the octahedral species $[Ni(S_4)(OH_2)_2]^{2+}$, which readily lose

one H_2O ligand *in vacuo*. The single crystal structure of $[Ni([16]aneS_4)(OH_2)_2](BF_4)_2$ contains a *trans*-octahedral complex cation [Ni-S = 2.43, Ni-O = 2.08 Å]. Comparison of the electronic spectra of $[Ni(S_4)(Solv)_2]^{2+}$ (S_4 = $[12]aneS_4$, $[14]aneS_4$, $[16]aneS_4$; Solv = CH_3CN) with those of octahedral complexes of tetraaza macrocycles shows that these tetrathia crowns exert a weaker ligand field onto the Ni centre than their tetraaza analogues. Cyclic voltammetry of $[Ni(S_4)(Solv)_2]^{2+}$ in CH_3CN/0.1M $^nBu_4NPF_6$ exhibited only irreversible processes.

Chapter 3

The synthesis and characterisation of the series of complexes $[Ni([9]aneS_3)(PP)](PF_6)_2$ (PP = a chelating diphosphine ligand) is described. Single crystal analyses on four of these compounds [PP = $Ph_2PCH_2PPh_2$, $Ph_2PC_2H_4PPh_2$, $CyC_2PC_2H_4PCyc_2$, $CH_3C(CH_2PPh_2)_3$] show the complex cations to adopt *quasi*-square-pyramidal stereochemistries [$Ni\text{-}S_{apical}$ = 2.38-2.65, $Ni\text{-}S_{basal}$ = 2.22-2.24, Ni-P = 2.17-2.22 Å]. N.m.r. and electronic spectral data are consistent with these complexes retaining their five-coordinate structures in solution.

Complexation of $NiX_2.6H_2O$ (X = BF_4^-, PF_6^-) by $[15]aneS_5$ in CH_3NO_2 in the presence of $(CH_3CO)_2O$ yields the square-pyramidal species $[Ni([15]aneS_5)]^{2+}$ [$Ni\text{-}S_{apical}$ = 2.41, $Ni\text{-}S_{basal}$ = 2.15-2.20 Å by x-ray crystallography].

$[Ni([15]aneS_5)]^{2+}$ forms the six-coordinate adducts $[Ni([15]aneS_5)(Solv)]^{2+}$ with pyridine and in CH_3CN solution, which were characterised by U.V./visible spectroscopy: no reaction was observed between $[Ni([15]aneS_5)]^{2+}$ and O_2 or CO in CH_3NO_2. The cyclic voltammogram of $[Ni([15]aneS_5)]^{2+}$ in CH_3CN/0.1M $^nBu_4NPF_6$ exhibited only an irreversible reduction at Ep_C = -1.3V vs. Fc/Fc^+ under Ar, CO or CO_2 atmospheres.

Reaction of $NiCl_2$ with $[15]aneS_5$ in CH_3NO_2 followed by counterion metathesis with NH_4PF_6 affords the mononuclear octahedral complex $[Ni([15]aneS_5)Cl]^+$.

Chapter 4

An electrochemical study of the complexes $[Ni([9]aneS_3)(PP)]^{2+}$ (see Chapter 3) is presented. All complexes in the series exhibit two one-electron reductions by cyclic voltammetry in CH_3CN/0.1M $^nBu_4NPF_6$ at 298K: a chemically reversible couple at $E_{\frac{1}{2}}$ = -0.8 to -1.2V vs. Fc/Fc^+, and a *quasi*-reversible or irreversible wave at Ep_C = -1.3 to -1.9V. Both the first and second reduction products were studied by e.p.r. spectroscopy and *in situ* U.V./visible spectroscopy. On the basis of this data, the species $[Ni([9]aneS_3)(PP)]^+$ were assigned as d^9 metal-centred radical cations, probably with square-pyramidal geometries [$g_{||}$ = 2.14-2.19, $A_{||}(^{31}P)$ = 80-126G, $g_\perp$ = 2.04-2.11, $A_\perp$ = 111-174G]. An e.p.r. study of

enriched $[^{61}Ni([9]aneS_3)(CH_3C(CH_2PPh_2)_3)]^+$ showed this species to have 67% metal radical character. The e.p.r. silent second reduction products $[Ni([9]aneS_3)(PP)]^0$ were tentatively assigned as adopting tetrahedral structures.

In addition to their reductive behaviour, the complexes $[Ni([9]aneS_3)(PP)]^{2+}$ [PP = $Me_2PC_2H_4PMe_2$(dmpe) and $CH_3C(CH_2PPh_2)_3$(tdpme)] each exhibited an irreversible one-electron oxidation, which were assigned as metal- (PP = dmpe) and phosphine ligand-based (PP = tdpme) processes respectively on the basis of e.p.r. data.

Cyclic voltammetry in CH_3CN/0.1M $^nBu_4NPF_6$ under a CO atmosphere showed the complexes $[Ni([9]aneS_3)(PP)]^+$ to form adducts with CO, which regenerated the initial Ni^{II} complex on re-oxidation at 298K. It was shown that different decomposition reactions for the CO adducts occurred at 298K and 243K; it was unclear whether these reactions involved concommitant reduction of the CO ligand. No reaction occurred between $[Ni([9]aneS_3)(PP)]^+$ and CO_2.

A re-investigation of the electrochemistry of $[Ni([9]aneS_3)_2]^{2+}$ is also reported. The cyclic voltammogram of $[Ni([9]aneS_3)_2]^{2+}$ in CH_3CN/0.1M $^nBu_4NPF_6$ at 298K exhibited a chemically reversible one-electron oxidation ($E_{\frac{1}{2}}$ = +1.0V vs. Fc/Vc^+) and a *quasi*-reversible reduction ($E_{\frac{1}{2}}$ = - 1.1V). $[Ni([9]aneS_3)_2]^{3+}$ was characterised by e.p.r. spectroscopy [g_1 = 2.09, g_2 =

2.07, g_3 = 2.03] and *in situ* U.V./visible spectroscopy. E.p.r. spectroscopy of enriched $[^{61}Ni([9]aneS_3)_2]^{3+}$ showed this complex to possess 39 or 54% metal radical character. Electroreduction of bulk samples of $[Ni([9]aneS_3)_2]^{2+}$ yielded a mixture of e.p.r. active products.

Cyclic voltammetry of $[Zn([9]aneS_3)_2]^{2+}$ in CH_3CN/0.1M $^nBu_4NPF_6$ exhibited only irreversible processes which could not be characterised.

Chapter 5

The synthesis and characterisation of $[Rh([9]aneS_3)(L)(L')]^+$ (L = C_2H_4, L' = C_2H_4, P^ipr_3, $Pcyc_3$; L,L' = $\frac{1}{2}C_7H_8$, $\frac{1}{2}C_8H_{12}$, $\frac{1}{2}C_4H_6$; L = CO, L = PPh_3) and $[Rh_2([9]aneS_3)_2(\mu\text{-}CO)_2]^{2+}$ is discussed. $[Rh([9]aneS_3)(C_2H_4)_2]^+$, $[Rh([9]aneS_3)(C_8H_{12})]^+$ and $[Rh([9]aneS_3)(CO)(PPh_3)]^+$ exhibit a range of five-coordinate geometries in the solid state [Rh-S = 2.31-2.47, Rh-C = 2.08-2.22 Å], which are related by rotation of the $[9]aneS_3$ ring about the central Rh-$[9]aneS_3$ axis. The ^1H n.m.r. coalescence temperature for rotation of the ethene ligands in $[Rh([9]aneS_3)(C_2H_4)_2]^+$ is usually low (T_C < 175K; see Chapter 6), implying that the $[Rh([9]aneS_3)]^+$ fragment has high electrophilic character. The single crystal structure of $[Rh([9]aneS_3)(C_4H_6)]^+$ shows the cation to adopt a square-pyramidal geometry analogous to that of $[Fe(CO)_3(C_4H_6)]$ (butadiene C-C = 1.41, 1.39, 1.44 Å].

$[Rh([9]aneS_3)(C_2H_4)_2]^+$ is inert to thermal nucleophilic substitution with CO, PPh_3 or C_8H_{12}. The $[Rh([9]aneS_3)]^+$ fragment exhibits a poor affinity for the electrophilic ligands C_2F_4, tcne and H^+. Reaction of $[Rh([9]aneS_3)(C_2H_4)(L)]^+$ (L = C_2H_4, $Pcyc_3$) with CH_3I, I_2, CH_3COCl, $(CH_3)_3SiCl$, CH_2Cl_2 or $CHCl_3$ yields only the insoluble products $[Rh([9]aneS_3)X_3]$ (X = Cl, I). No reaction was observed between $[Rh([9]aneS_3)(C_2H_4)_2]^+$ and $HSiEt_3$ or C_6H_6 under thermal conditions. The thermal decomposition reaction of $[Rh([9]aneS_3)(C_2H_4)]^+$ is discussed.

Chapter 6

The synthesis and properties of the complexes $[Ir([9]aneS_3)(L)(L')]^+$ (L,L' = C_2H_4, C_8H_{14}, $\frac{1}{2}C_8H_{12}$, $\frac{1}{2}C_4H_6$; L = CO, L' = PPh_3) is described. X-ray structural analyses of $[Ir([9]aneS_3)(L)_2]^+$ (L = C_2H_4, $\frac{1}{2}C_8H_{12}$, $\frac{1}{2}C_4H_6$) showed these complex cations to adopt five-coordinate geometries similar to those of their Rh congeners [Ir-S = 2.32-2.44, Ir-C = 2.12-2.20 Å]. The barrier to rotation of the ethene ligands in $[Ir([9]aneS_3)(C_2H_4)_2]^+$ was measured as 33.3 $kJ.mol^{-1}$ by ^1H n.m.r. spectroscopy (T_C = 177K). The electronic character of $[M([9]aneS_3)(C_2H_4)_2]^+$ and $[M([9]aneS_3)(C_4H_6)]^+$ (M = Rh, Ir) is discussed: ^{13}C n.m.r. spectroscopy showed the complexes $[M([9]aneS_3)(C_4H_6)]^+$ to be M^I η^4-C_4H_6 species, rather than their M^{III}

σ,η^2,σ-C_4H_6 tautomers.

Chapter 7

Single crystal x-ray analyses of two polymorphs of [16]aneS_4 showed this macrocycle to adopt a rectangular [3535] conformation in the solid state, with two S-atoms occupying exodentate positions and two occupying positions neither exo- nor endo-dentate. Molecular mechanics calculations on different conformations of [16]aneS_4 and $C_{16}H_{32}$ imply that the tetrathia macrocycle should be more conformationally flexible than its parent hydrocarbon.

TABLE OF CONTENTS

CHAPTER 2 (Cont'd) Page No.

CHAPTER 2 (Cont'd) Page No.

CHAPTER 4 (Cont'd) Page No.

CHAPTER 5 (Cont'd) Page No.

CHAPTER 6 (Cont'd) Page No.

LIST OF FIGURES

Page No.

Page No.

LIST OF TABLES

CHAPTER 1

INTRODUCTION

1.1 THERMODYNAMICS AND KINETICS OF MACROCYCLIC COMPLEX FORMATION

The increased stability of a macrocyclic complex over an open-chain polychelate analogue was first noted by Cabbiness and Margerum in 1969[1]. This phenomenon was termed the "macrocyclic effect" by analogy with the chelate effect, and was found to be both kinetic and thermodynamic in origin[2-9]. This enhanced stability has led to a wide interest in macrocyclic chemistry[3,4,10-14], since macrocyclic ligands can impose unusual electronic or stereochemical properties onto a metal centre[3,4,13,14] and also act as protecting groups to control metal ion reactivity[10,11,14].

The kinetic macrocyclic effect was quantified in a study of the kinetics of formation and dissociation of $[Cu(1)]^{2+}$ and $[Cu(2)]^{2+}$ [2].

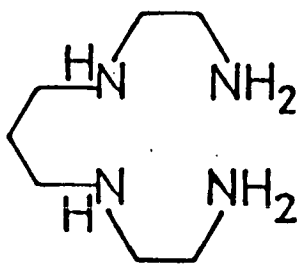

(1)

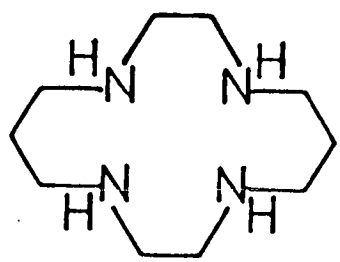

(2)

For the reaction

$$Cu^{2+} + L \underset{k_d}{\overset{k_f}{\rightleftharpoons}} [Cu(L)]^{2+} \qquad (3)$$

the following rate constants k_f, k_d and stability constants K_s were measured:

	$[Cu(1)]^{2+}$	$[Cu(2)]^{2+}$
k_f (M^{-1} s^{-1})	8.9×10^4	5.8×10^{-2}
k_d (s^{-1})	4.1	3.6×10^{-7}
$K_s = k_f/k_d$ (M^{-1})	2.17×10^4	1.61×10^5

The conformational flexibility of the open-chain ligand means that the complexation and decomplexation reactions can occur simply by enfolding, or "unzipping" from, the metal ion (4). In contrast, the formation and dissociation reactions induce strain into the relatively rigid macrocyclic framework (5); this constraining influence of the ring system was labelled "multiple juxtapositional fixedness" by Busch[6].

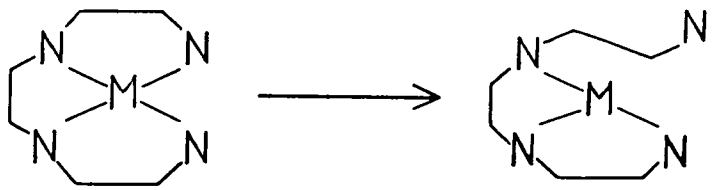

(4)

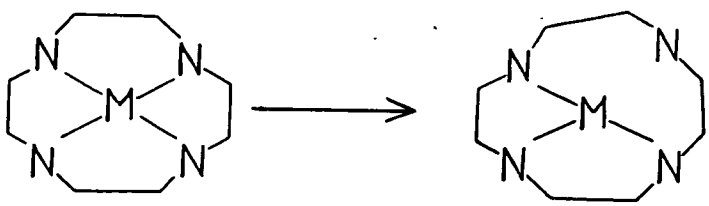

(5)

In practise, the rate of dissociation (k_d) for the macrocyclic system compared to the open-chain ligand is lowered by more than the rate of complexation (k_f), so that the overall stability constant (K_s) is significantly greater for the macrocyclic complex.

The thermodynamic origins of the macrocyclic effect are still the focus of some controversy. Both entropic and enthalpic considerations are involved, and their relative importance varies between systems.

The entropic component of the macrocyclic effect arises from the relative flexibility of a free open-chain ligand compared to a macrocycle. The displacement of an open-chain ligand by a macrocycle:

$$[M(L_{open})]^{n+} + L_{mac} \longrightarrow [M(L_{mac})]^{n+} + L_{open} \quad (6)$$

results in a net gain in configurational entropy, and for this reason it is found that the entropic contribution to such reactions is generally favourable[9,15,16].

The enthalpic term of the macrocyclic effect is mainly derived from the difference in solvation energies of the free open-chain and macrocyclic ligands, and as such is very dependent on the system under study, and the experimental conditions employed[7]. Early studies on nickel and copper complexes of saturated tetra-aza macrocyclic ligands implied that this enthalpic factor was the dominant contributor to the macrocyclic effect[5,8,15].

However, more recent studies on analogous poly-thioether complexes have shown that the enthalpic term is diminished in these systems, and the macrocyclic effect here is entropically driven[9,16]. This is because of the relatively poor hydrogen bonding between the free ligands and solvent molecules for thioethers, in comparison to the more polar poly-aza species.

Consideration of the enthalpic component is further hampered by hole-size effects, and by ligand pre-organisation energies. A serious metal ion/macrocyclic cavity size mis-match will cause a diminution in the enthalpic term, since the M-L bond will be weakened, and the macrocyclic ring strain will be increased. Alternatively, such a mis-match may induce a structural change, e.g. from trans- to cis-octahedral $[M(N_4)(solvent)_2]^{n+}$, and so cause changes in the observed thermodynamic data[18].

Pre-organisation energy becomes important when the conformation of the free macrocycle is different from that required for in-cavity complexation. This is not generally significant for most tetra-aza ligands[17,18], but becomes important when considering the crown thioethers. Most of these adopt exodentate conformations in the unbound state[19,21], and must re-arrange to an endodentate form to allow incorporation of a metal ion within the macrocyclic cavity. Such a process amounts to an additional unfavourable enthalpic contribution to the

macrocyclic effect. One notable exception to this is the small-ring macrocycle 1,4,7-trithiacyclononane ([9]aneS_3, 7), which in the solid state adopts a conformation pre-organised for tri-dentate facial coordination[22]; for this reason [9]aneS_3 generally binds to metal centres more strongly than other crown thioethers[14]. The coordination chemistry of poly-thioether macrocycles is discussed further in Chapters 2 and 3.

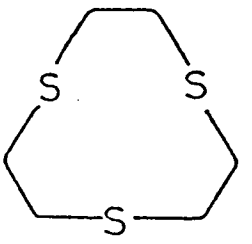

(7)

1.2 METAL IONS IN BIOLOGICAL SYSTEMS

Metal complexes have been found to play an important role in many biological processes[23,24]. The mechanisms of most such reactions are still under investigation, but it is clear that metal ions in enzymic systems can perform a number of functions. They can form the active site of an enzyme, for reversible substrate binding (e.g. O_2 binding by Fe in haemoglobin and myoglobin[25]), or for a catalytic reaction, such as Ni in hydrogenases[26], Fe in cytochrome P_{450}[27] or Zn in carbonic anhydrase[28]. Metal ions are also

known to act as electron-transfer catalysts (Fe-S clusters in ferredoxins[29], Cu in oxidases[30]) and as free-radical initiators (Co in vitamin B_{12}[31]).

Metal ion coordination sites in bio-molecules can be divided broadly into three groups: macrocyclic and non-macrocyclic complexes, and clusters.

i) Macrocyclic metal sites in metalloenzymes are exclusively based around the tetrapyrrole fragment, or its partially reduced derivatives. The most common examples are the haem iron-porphyrin complexes (8), which occur in a variety of enzymes[32]; other examples are the chlorins (9, found in chlorophylls)[33], corrins (10, vitamin B_{12})[31], and the nickel tetrahydroporphinoid complex F_{430} (11)[26]. The function of the metal ions in these compounds varies between systems, but generally involves a metal-based redox process; the macrocycle here acts both as a protecting group, and as a means of "tuning" the metal redox activity. There has been considerable interest in complexes of synthetic porphyrin (12) and phthalocyanin (13) macrocycles, both as models for the above systems[34] and as novel catalysts in their own right.

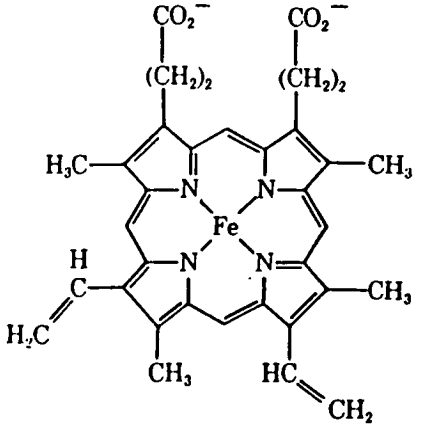

(8)

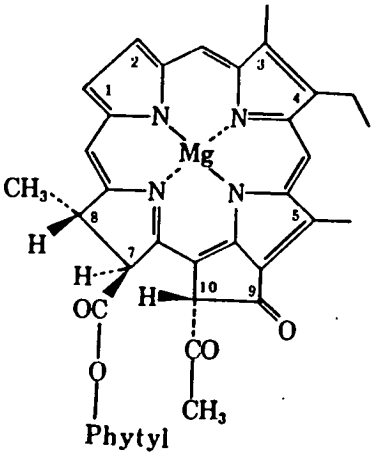

(9)

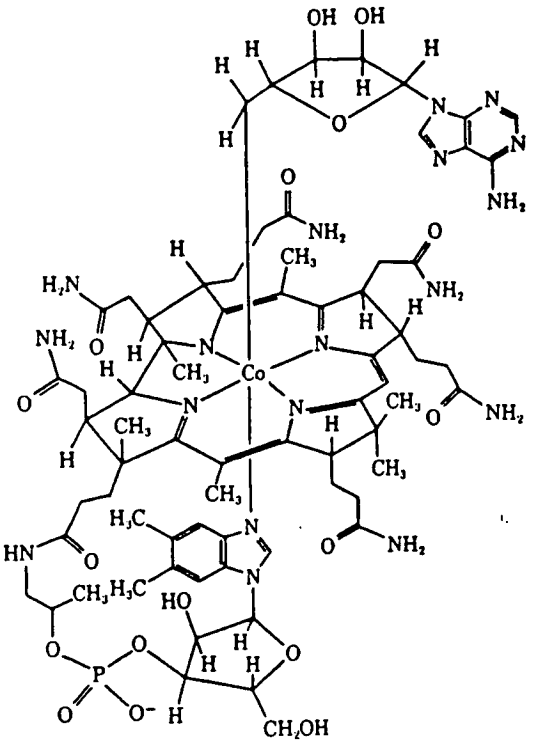

(10)

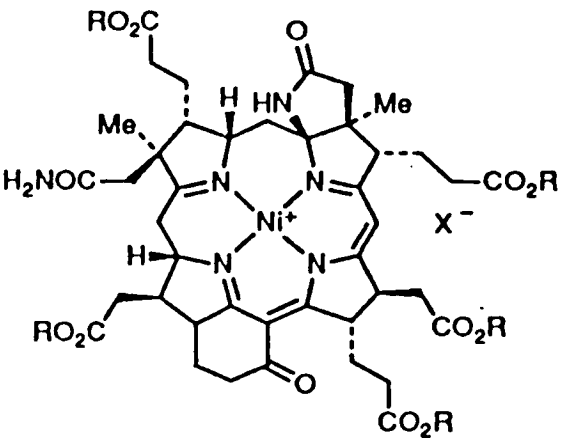

(11)

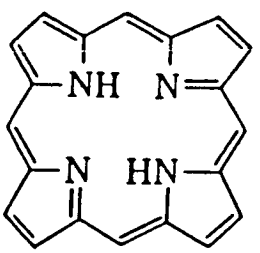

(12)

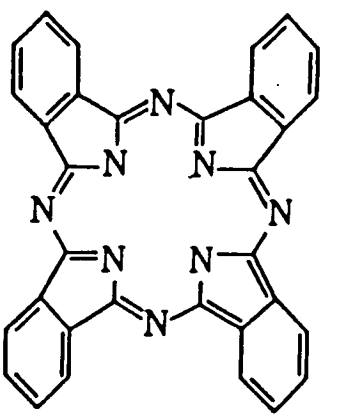

(13)

Another class of biological macrocycles are the siderophores which are secreted by bacteria to sequester iron from their aqueous environment and transfer it through the cell wall[35]. These are chemically varied, but generally consist of a macrocyclic framework, with O-donor side-arms that chelate to the Fe atom (14). All siderophores form extremely stable Fe^{3+} complexes, with stability constants typically $\geq 10^{45}$ [36].

ii) Non-macrocyclic coordination sites in metalloenzymes vary considerably in ligand type, coordination geometry and nuclearity (several homo- and heterometallic dimeric, and some trimeric, metal centres have been identified). Here the metal atom(s) are coordinated directly to amino acid side-chains from the protein; hence a wide range of N-, O- and S-donor ligands are observed, and the (often strained) coordination geometry is maintained by the rigid protein backbone[35]. An example is the "blue" copper site, found in many oxidase enzymes (15)[30]. This has a very distorted, "flattened" tetrahedral N_2S_2 coordination sphere; this strained geometry is adopted to regulate the Cu (II/I) redox couple, and so to facilitate electron transfer. Macrocyclic ligands have received much interest as models for such systems[10,34], since they can be used to impose strained coordination geometries onto metal ions.

iii) Iron-sulphur clusters occur in enzymes that catalyse multiple-electron redox processes. They are

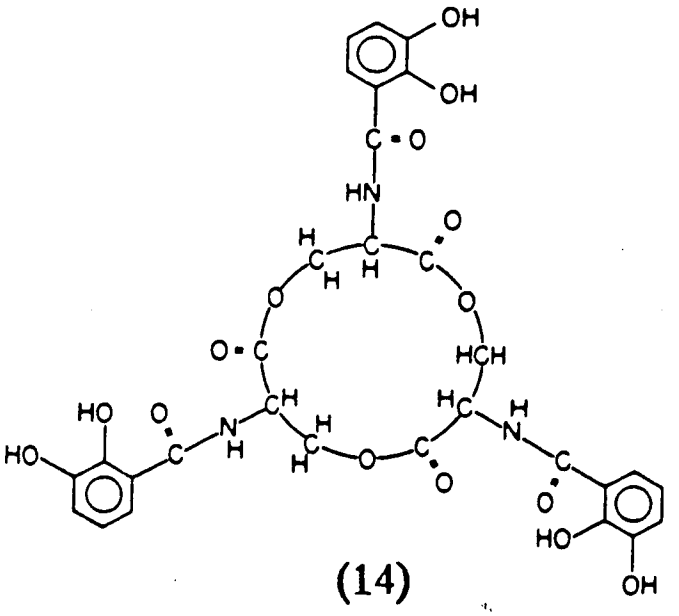
OH
OH
C • O
HN
H
C
H
C • O
O
O
O • C
HCH
HO
O
CH
HC
H
HO
C
N
H
N
H
C
H
O
C
O
O
HO
OH

(14)

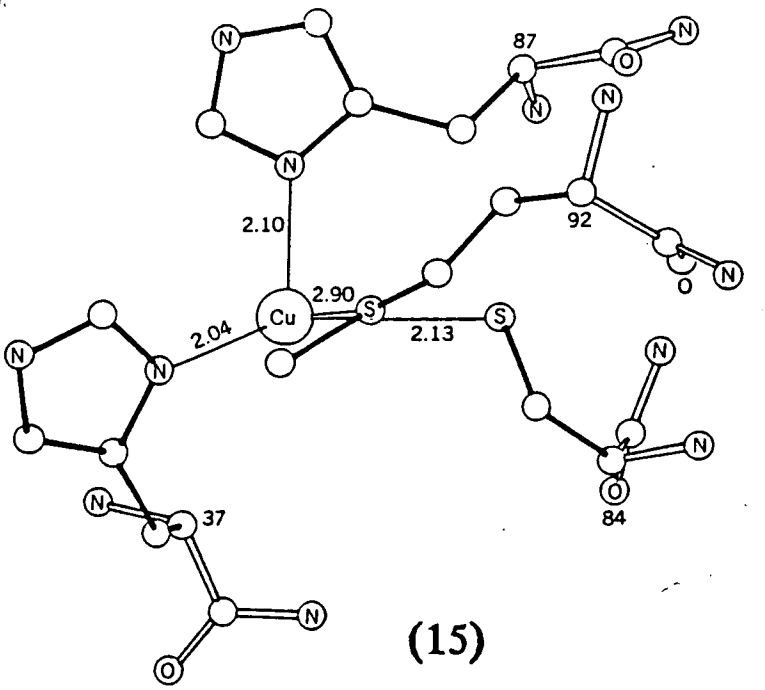
N
87
O
N
N
N
N
2.10
92
O
N
2.90
Cu
S
2.04
2.13
S
N
N
N
N
N
37
O
84

(15)

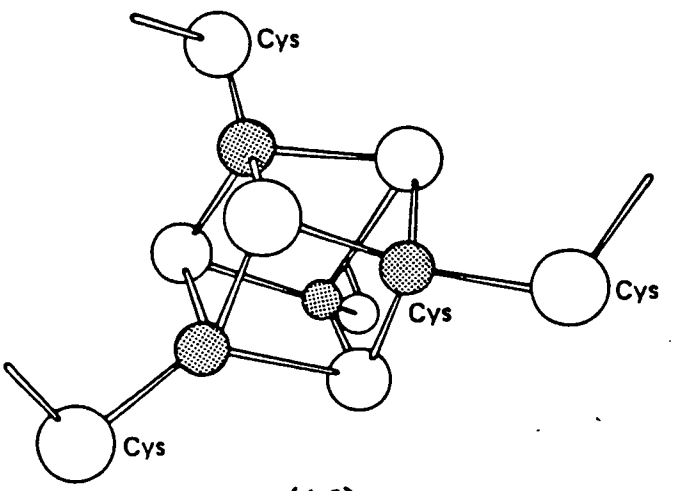
Cys
Cys
Cys
Cys

(16)

often found in conjunction with other metals, such as nickel (in hydrogenases, which catalyse the oxidation of H_2 to $2H^+$) and molybdenum (in nitrogenases, which reduce N_2 to $2NH_3$). They are thought to exist as cubic Fe_3S_4M (M = Fe, Mo, Ni etc.) units, often linked by additional metal-thiolate bridges (16), although only low molecular weight mono-cluster proteins have so far been structurally characterised[29].

1.3 MACROCYCLIC COMPLEXES IN CATALYSIS

The design of an effective homogeneous metal catalyst involves effective control of the stereochemical and electronic properties of the metal centre. Macrocyclic ligands are ideally suited to fulfil these requirements, and there has been considerable interest in the catalytic properties of synthetic macrocyclic complexes. Given the known roles of such complexes in metalloenzymes (*vide supra*), most attention has been paid to the ability of metalloporphyrins and analogous species to bind and activate small molecule substrates such as CO_2[37-40], CO[41], O_2[42-44], H_2[41,45], N_2[46-48], NO_3^-[49] and C_2H_4[50].

Two processes that have received particular attention are the electrocatalytic reductions of CO_2 and O_2. Several Co and Ni complexes of tetra-aza macrocycles have been shown to reduce CO_2 to CO in aqueous solution[37-39]. $[Ni(cyclam)]^{2+}$ has been shown to be a particularly efficient catalyst for this process, whilst avoiding the

competing reduction of H_2O to H_2[38]. The cyclam amine H atoms have been implicated in the mechanism of this process (Figure 1.1). In contrast, Ag^{II} and Pd^{II} porphyrin complexes reduce CO_2 to $C_2O_4^{2-}$ under similar conditions[40].

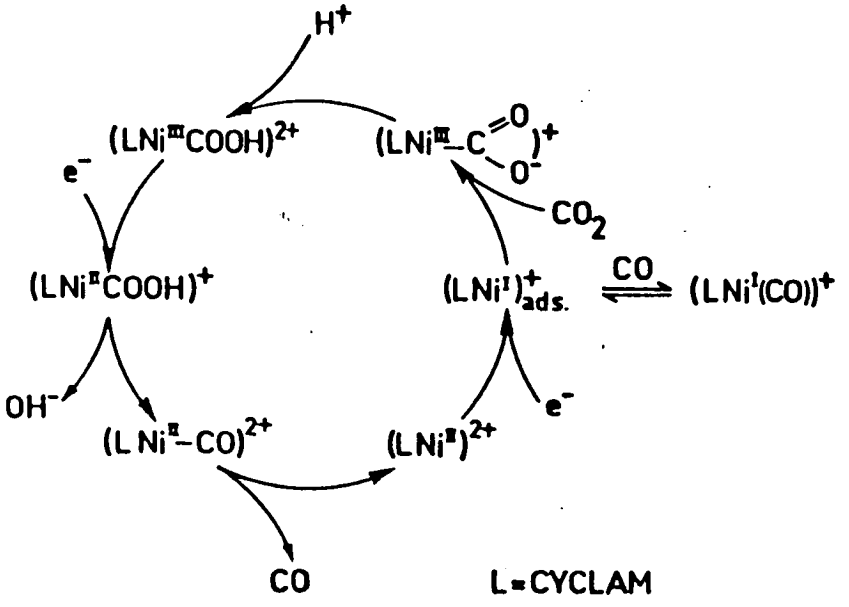

Figure 1.1: Proposed mechanism for the electroreduction of CO_2 to CO by $[Ni(cyclam)]^{2+}$ (from Reference 38).

The reduction of O_2 to H_2O has potential applications in fuel cells[51]. Two metal porphyrin systems have been shown to be effective catalysts for this process; a di-cobalt co-facial porphyrin dimer[42] and the complex [Ir(OEP)H] adsorbed onto graphite electrodes[43]. Both these reductions are thought to proceed via a dimeric superoxide-bridged intermediate (17).

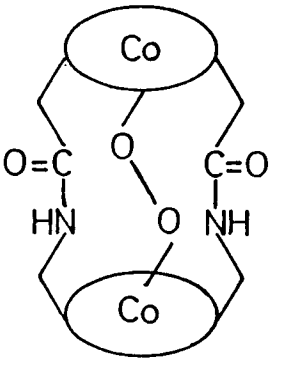

(17)

The organometallic chemistry of square-planar macrocyclic complexes is also of interest[11,52], since the absence of cis-coordination sites in these species means that several common processes, such as α- or β-elimination or insertion reactions, must follow novel mechanisms. An example of this is the photochemical production of methanol and formaldehyde from CO and H_2 using a $[Rh(OEP)]_2$ catalyst[41]. This proceeds by insertion of CO into an Rh-H bond via a free-radical mechanism[41,53]:

$$[Rh(OEP)]_2 + H_2 \rightleftharpoons 2[HRh(OEP)]$$

$$[Rh(OEP)]_2 \overset{h\nu}{\rightleftharpoons} 2[\cdot Rh(OEP)]$$

$$[\cdot Rh(OEP)] + CO \rightleftharpoons [\cdot(OC)Rh(OEP)]$$

$$[\cdot(OC)Rh(OEP)]+[HRh(OEP)] \rightleftharpoons [(OHC)Rh(OEP)]+[\cdot Rh(OEP)]$$

$$+ \text{ termination steps}$$

Several metal-carbon σ-bonded derivatives have been produced by oxidative additions to low-valent macrocyclic precursors[52,54]; in many cases these can undergo further

transformations to species such as carbenes under redox conditions.

1.4 AIMS OF WORK

In contrast to monodentate and chelate thioether ligands[55], macrocyclic poly-thioethers have been shown to bind effectively to a range of metal centres[14,56,57]. Unlike the saturated polyamine macrocycles, crown thioethers can act as both π-donor and π-acceptor ligands via filled sulphur 3p- and vacant sulphur 3d- and/or S-C σ^* orbitals: both types of bonding have been observed experimentally[58,59]. In addition, the conformational flexibility of the crown thioethers allows them to accommodate a range of metal coordination geometries[14], whereas polyamine macrocycles are generally restricted to in-cavity binding of metal ions. As a result, the chemistry of the poly-thioether macrocycles is distinct from that of other classes of macrocycle.

Like their N-donor analogues, the crown thioethers have been shown to stabilise a range of unusual transition metal oxidation states. The ligand [9]aneS$_3$ is particularly efficient in this regard, because of its enhanced binding abilities (Chapter 3). The high and medium oxidation state complex chemistry of these ligands has been well studied; for example the hexathia donor set in [M([9]aneS$_3$)$_2$]$^{n+}$ complexes has been found to stabilise mononuclear Rh^{II}[60,61], Pd^{III}[62], Pt^{III}[63], Ag^{II}[66b] and

Au^{II}[64] metal centres. However, with the exception of the copper triad[65-67], the chemistry of the crown thioethers with metal centres in the Ø or +1 oxidation states has not been well investigated. It was therefore decided to initiate a study of some novel low oxidation state complexes containing poly-thioether macrocycles, with emphasis both on the characterisation of these compounds, and on their potential for substrate activation and catalysis.

The first area of investigation was concerned with the study of nickel crown thioether complexes. Several such nickel (II) compounds are known[68-72]; however, the electrochemistry of these species has not been well characterised[73,74]. Recent results have shown that the electrochemical reduction of square-planar Pd^{II} and Pt^{II} tetrathia complexes results in the formation of dimeric M^{I}-M^{I} species[75], in contrast to the mononuclear, Pd^{I} centres formed by their substituted tetra-aza analogues[76]. We argued that dimerization reactions were less likely to occur for the analogous nickel systems, because of the less diffuse nature of the Ni 3d frontier orbitals. So, a re-examination of the Ni^{II} chemistry with the tetrathia ligands [12]aneS_4, [14]aneS_4 and [16]aneS_4 was undertaken (Chapter 2). Secondly, it has been observed that $[Ni([9]aneS_3)_2]^{2+}$ cannot be reduced to a stable Ni^{I} species[74]. We proposed that the cause of this was probably stereochemical in nature, since no stable

octahedral Ni^{I} species are known[77,78]. Hence a novel series of five-coordinate Ni^{II} complexes of formula $[Ni([9]aneS_3)(PP)]^{2+}$ was synthesised, where PP is a chelating diphosphine ligand, with the aim of stabilising the Ni (II/I) redox couple (Chapters 3 and 4). There was also interest in the structures of these compounds, since their Pd^{II} and Pt^{II} analogues $[M([9]aneS_3)(PP)]^{2+}$ have been shown to adopt unusual quasi-five-coordinate geometries[73,79,80]. Any Ni^{I} complexes that might be obtained would be of considerable interest as an electro-reduction catalyst for small molecule substrates.

Another topic of investigation was suggested by the observation that, in addition to its role as a "traditional" macrocycle, the facially binding six-electron-donor $[9]aneS_3$ ligand could act as a protecting group similar to the cyclopentadienyl moiety (18).

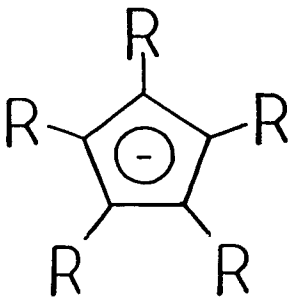

Cp^- : R=H

$(Cp^*)^-$: $R=CH_3$

(18)

There has been considerable interest recently in the organometallic chemistry of $[C_5R_5]^-$ and related ligands such as hydridotris(pyrazolyl)borate, $[C(CH_2P(O)Ph_2)_3]^-$ (triso) and $[MeC(CH_2PPh_2)_3]$ (tdpme). The $Rh^{I/III}$ and $Ir^{I/III}$ chemistry of these ligands is particularly rich, especially with respect to C-H and Si-H bond activation reactions[81-86]. With this in mind, the synthesis and characterisation of a series of half-sandwich Rh^I and Ir^I complexes of [9]aneS_3 was undertaken, with the aim of examining their activity towards oxidative addition reactions (Chapters 5 and 6). We argued that these compounds might exhibit unusual reactivity arising from the properties imposed on the metal ion by the neutral trithia macrocycle; other cp^- analogues are usually tripodal N-, O- or P-donor ligands with a uninegative charge.

One feature of the chemistry of crown thioethers is their conformational flexibility (*vide supra*). This is particularly evident in the coordination chemistry of the tetrathia ligands [12]aneS_4 and [14]aneS_4[14] which are known to bind metal ions in both endo- and exo-dentate manner (Chapter 2). This variety arises from the conformational preferences of the free ligands, which adopt exodentate conformations in the solid state[19,20]. Such diversity is not evident in the complexes formed by [16]aneS_4, as no exodentate complex of this ligand has been structurally characterised to date. A conformational

study of [16]aneS_4 was therefore initiated, involving X-ray crystallography and molecular mechanics calculations, to try to explain these differences (Chapter 7).

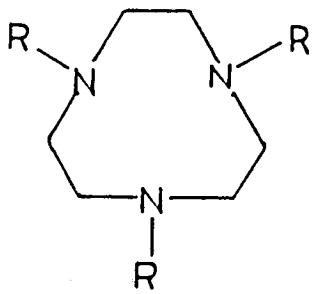

R=H: [9]aneN$_3$

R=CH$_3$: Me$_3$[9]aneN$_3$

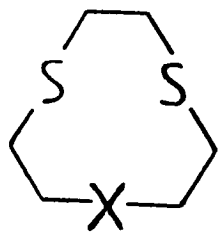

X=NH: [9]aneNS$_2$

X=S: [9]aneS$_3$

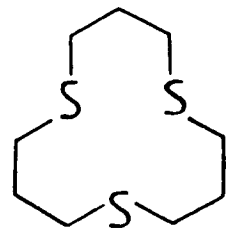

[12]aneS$_3$

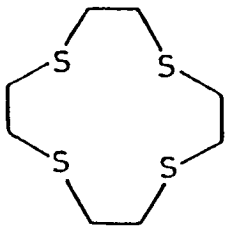

[12]aneS$_4$

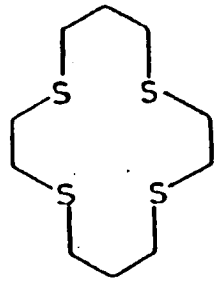

[14]aneS$_4$

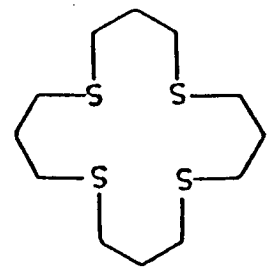

[16]aneS$_4$

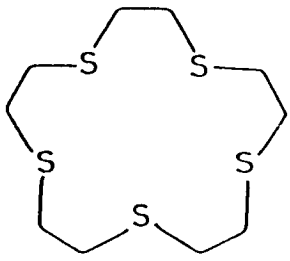

[15]aneS$_5$

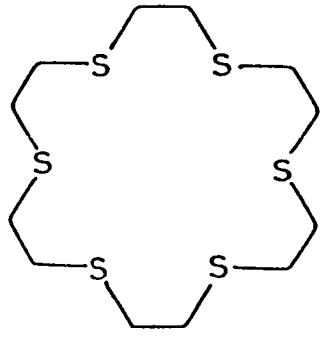

[18]aneS$_6$

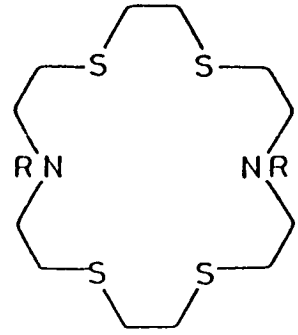

R=H: [18]aneN$_2$S$_4$

R=CH$_3$: Me$_2$[18]aneN$_2$S$_4$

Figure 1.2: Macrocyclic ligands referred to in this work

CHAPTER 2

OCTAHEDRAL NICKEL (II) COMPLEXES OF CROWN THIOETHERS

2.1 INTRODUCTION

The ability of saturated and unsaturated tetra-aza macrocycles to stabilise mononuclear Ni^{I} metal centres is well known[87-90]. Several of these four-coordinate Ni^{I} complexes have been shown to bind external substrates such as CO[90-92] and CO_2[37-39]; $[Ni(cyclam)]^+$ is an efficient catalyst for the electroreduction of CO_2 to CO[38] (Section 1.3). The cathodic nature of the Ni(II)/Ni(I) couple in such systems (typically between -1.2 and -1.8V vs. F_C/F_C^+) implies that the stability of the reduced species is predominantly kinetic in origin. This is supported by the observation that the stability of $[Ni(N_4)]^+$ complexes is enhanced by sterically bulky macrocycles[88,89], which inhibit attack at the metal centre. We proposed that the replacement of a hard aza donor by a softer polythia macrocycle might further stabilise the Ni(II/I) redox couple, leading to Ni^{I} complexes that could exhibit novel reactivity.

The Edinburgh group has recently studied the electrochemical reduction of Pd^{II} complexes of some saturated tetrathia macrocycles[75]. It was found that whilst the tetrathia ionophores did promote more accessible Pd(II)/(I) reduction potentials than their tetra-aza analogues, these reductions were rapidly followed by the formation of intensely coloured diamagnetic products, for which dimeric structures were proposed:

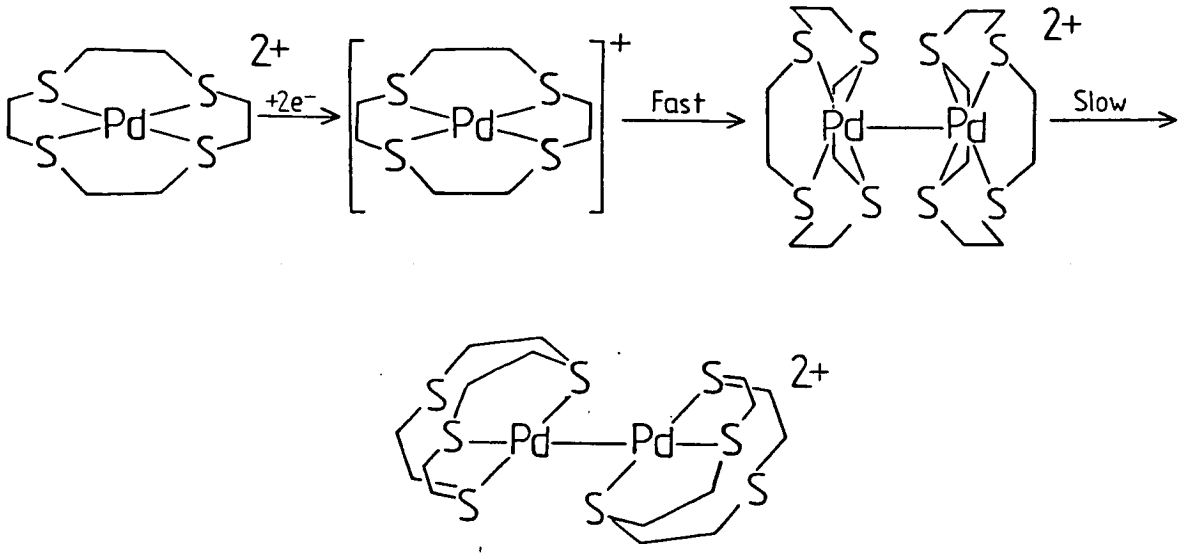

This type of dimerisation is well known for Pd^{I} complexes, as well as many other second and third row transition metal systems. However, the only known example of a first row metal-metal bonded complex containing a non-porphinoid macrocycle is the reduction product of $[Ni(cyclops)]^{+}$ (19)[93]:

$$2[Ni^{II}(cyclops)]^{+} \xrightarrow{+2e^{-}} 2[Ni^{I}(cyclops)] \longrightarrow [Ni^{I}(cyclops)]_2$$

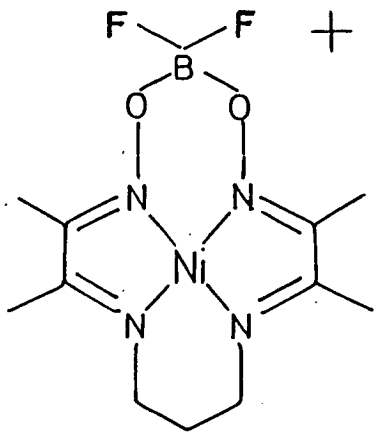

(19)

We argued that any $[Ni(S_4)]^+$ complexes were less likely to dimerise than their Pd^I analogues. Therefore, we decided to investigate the chemistry of nickel with the tetrathia macrocycles [12]aneS_4, [14]aneS_4 and [16]aneS_4.

A survey of the chemistry of these ligands is now described[14].

LIGAND SYNTHESIS

The synthesis of [12]aneS_4 and [14]aneS_4 was first reported by Rosen and Busch in 1969[68,69], following the methodology originally developed by Tucker and Reid[94]:

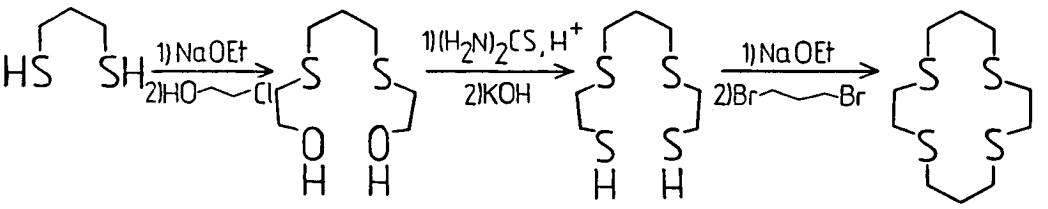

This, and a later modified preparation by Ochrymowycz[95], depended on high dilution conditions to achieve the final cyclisation, resulting in yields of below 35%. This was much improved in 1981, with the discovery that Cs_2CO_3 could be used to promote ring closure[96], so increasing yields to 75%. It is not known whether Cs^+ acts as as a template in this reaction. The Cs^+ method is now the method of choice for the synthesis of crown thioethers[97], although the open chain polythia

intermediates are highly toxic. [12]aneS$_4$, [14]aneS$_4$ and [16]aneS$_4$ are now available from a commercial supplier.

COORDINATION CHEMISTRY OF TETRATHIA MACROCYCLES

i) [12]aneS$_4$ and [14]aneS$_4$

The X-ray structures of both of these molecules have been determined[19,20]; they show that these macrocycles adopt all-exodentate conformations in the solid state, with the sulphur atoms lying at the corners of a square ([12]aneS$_4$) or rectangular ([14]aneS$_4$) ring (Figure 2.1, Chapter 7). This implies a substantial barrier for in-cavity binding of a metal ion, since the ligands must completely invert their conformations such that every *gauche* torsion in the free ligand becomes *anti*, and vice versa. This is reflected in the complex chemistry of these ligands, which have been shown to coordinate to metal centres in both endodentate and exodentate fashion[14]. The chemistry of [14]aneS$_4$ has been investigated in greater detail than that of [12]aneS$_4$, but both exhibit similar features.

The first exodentate S$_4$ complex to be structurally characterised was [NbCl$_5$]$_2$([14]aneS$_4$)[98] (Figure 2.2a), which was found to consist of approximately square-pyramidal NbCl$_5$ fragments, with one macrocyclic S atom occupying the sixth coordination site (Nb....S = 2.71(1) Å). Similar structures have been observed for the Al complexes [Al(CH$_3$)$_3$]$_4$([14]aneS$_4$)[99] and [Al(CH$_3$)$_3$]-

Figure 2.1: Views of the single crystal structures of [12]aneS$_4$ and [14]aneS$_4$.

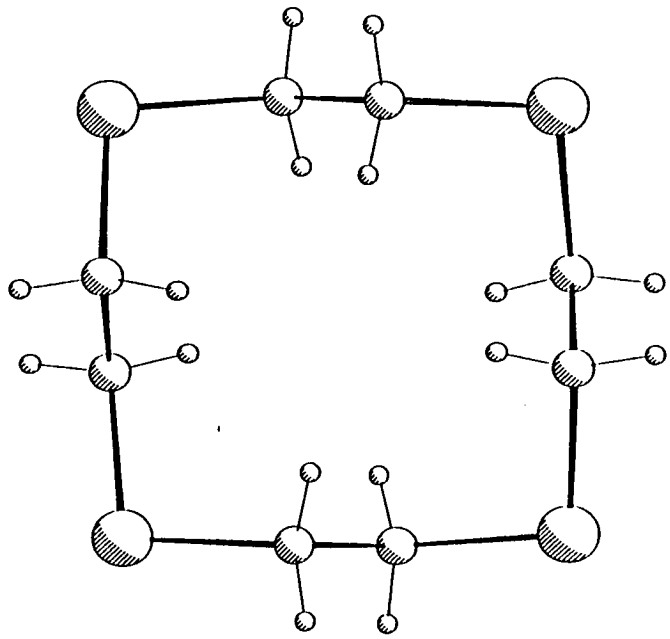

a) [12]aneS$_4$

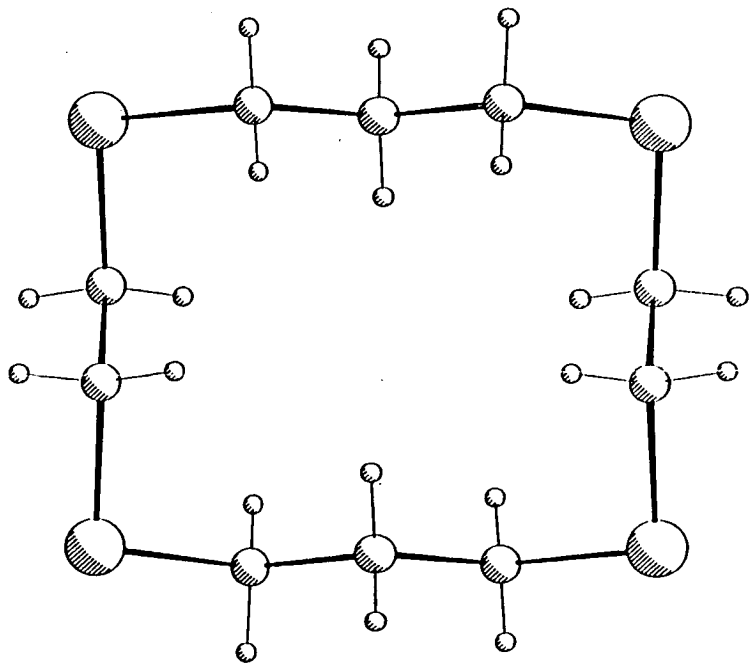

b) [14]aneS$_4$

([12]aneS$_4$)[100], and proposed for some high valent Mo adducts[101]. The crystal structure of [HgCl$_2$]$_2$([14]aneS$_4$) has also been reported, and shows [14]aneS$_4$ acting as an exodentate chelate ligand to two tetrahedral Hg^{II} centres[102] (Figure 2.2b). This latter mode of coordination is also observed in [(C$_5$Me$_5$)RhCl]$_2$ ([14]aneS$_4$)[103]. It should be noted that the conformation of the macrocycle in these complexes is often different from that observed for the free ligand.

Endocyclic complexes of [12]aneS$_4$ and [14]aneS$_4$ are also well known. The most common geometries for these species are square-planar (e.g. [M(S$_4$)]$^{2+}$; M = Ni, S$_4$ = [14]aneS$_4$; M = Pd, Pt, S$_4$ = [12]-, [14]aneS$_4$; Figure 2.2c)[75,103,104] and *cis*- or *trans*-octahedral (such as *cis*-[M(S$_4$)Cl$_2$]$^+$; M = Rh, Ir, S$_4$ = [12]-, [14]aneS$_4$ and *trans*-[Cu([14]aneS$_4$)(OClO$_3$)$_2$])[75,105,106]. The formation of *cis*- against *trans*-octahedral complexes is favoured by the use of metal ions larger than the macrocyclic cavity; [14]aneS$_4$ generally forms *trans*-octahedral complexes with first row transition metal ions and *cis*-complexes with second and third row metals, whilst all structurally characterised octahedral [12]aneS$_4$ complexes have shown *cis* configurations. The structure of [Cu([12]aneS$_4$)(OH$_2$)](ClO$_4$)$_2$ exhibits a square-pyramidal geometry, with the macrocycle forming the basal plane of the complex[107].

Figure 2.2: Views of the single crystal structures of some complexes of [14]aneS$_4$.

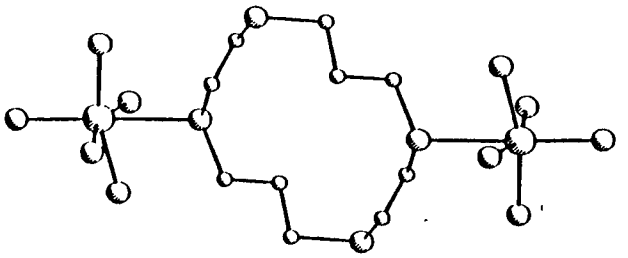

a) [NbCl$_5$]$_2$([14]aneS$_4$)

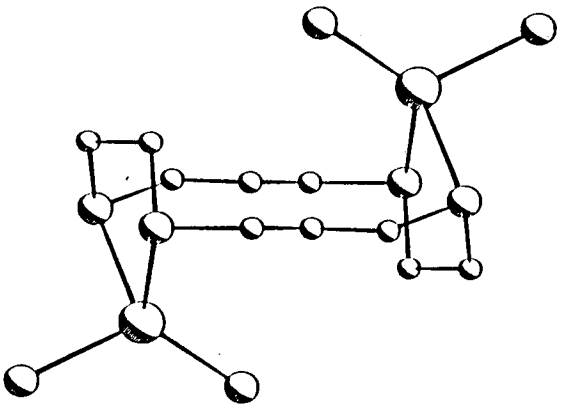

b) [HgCl$_2$]$_2$([14]aneS$_4$)

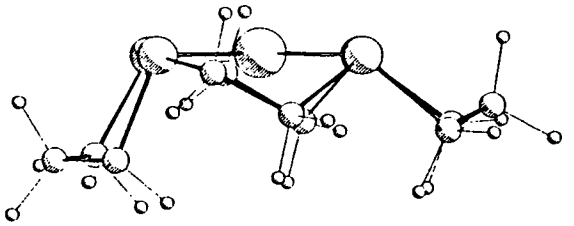

c) [Pd([14]aneS$_4$)](PF$_6$)$_2$

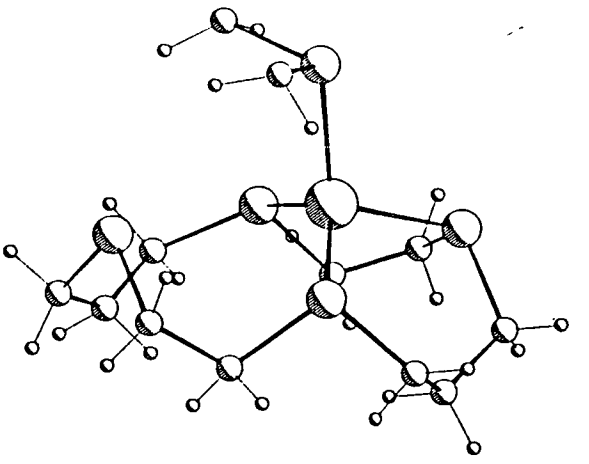

d) [Cu([14]aneS$_4$)]ClO$_4$

A square-planar or tetragonal tetradentate macrocyclic complex can adopt one of five conformational isomers, depending on the orientation of the macrocycle chelate rings (Figure 2.3).

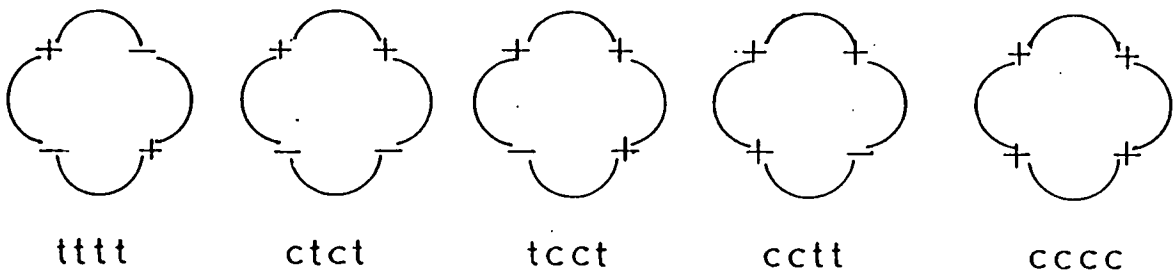

Figure 2.3: Conformational isomers for an in-plane $[M(S_4)]^{n+}$ complex (+ and - refer to the orientation of the S non-bonding lone-pairs above and below the square plane).

In practice, tetrathia macrocyclic complexes generally adopt the cccc or ctct forms, with equilibria between the two isomers being observed in solution[75,108].

Finally, some tridentate complexes of these ligands have also been reported, such as $[Re([12]aneS_4)(CO)_3]PF_6$[109] and $[Cu([14]aneS_4)]ClO_4$[110] (Figure 2.2d). The

latter species has a polymeric structure, with each tetrahedral Cu^{I} ion bound to three S atoms from one macrocycle, and to one from an adjacent ligand.

ii) [16]aneS_4

In contrast to the smaller tetrathia ligands, no exo-dentate complexes of [16]aneS_4 have been structurally characterised, and this macrocycle binds to metal ions almost exclusively in an endo-dentate in-plane manner. Relatively few such complexes have been structurally characterised; examples that have been reported include *trans*-[Cu([16]aneS_4)($OClO_3$)$_2$][107], [Mo([16]aneS_4)(O)(SH)]$^+$ (20)[111], *trans*-[Rh([16]aneS_4)Cl_2]$^+$[112] and [Pd([16]-aneS_4)]$^{2+}$ [75].

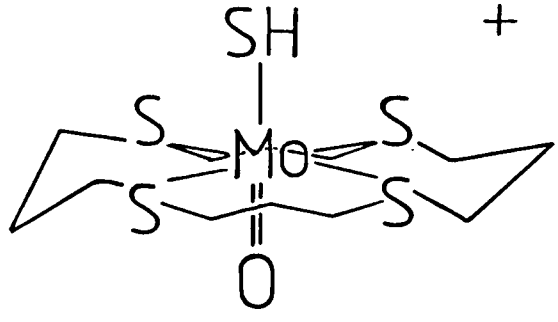

(20)

Yoshida et al have prepared a series of octahedral $Mo^{O/II}$ complexes of the related ligand $Me_8[16]aneS_4$[113]. The reduction of *trans*-$[Mo(Me_8[16]aneS_4)Br_2]$ with Na/Hg under N_2 yields *trans*-$[Mo(Me_8[16]aneS_4)(N_2)_2]$[48], which contains exceptionally nucleophilic N_2 ligands.

$[Ru([16]aneS_4)(PPh_3)Cl](PF_6)$ and $[Ru([16]aneS_4)(NCMe)_2](PF_6)_2$ have been shown to adopt a *cis*-octahedral structure[80].

2.2 RESULTS AND DISCUSSION

2.2.1 $[Ni_2(S_4)_2(\mu\text{-}Cl)_2](BF_4)_2$ (S_4 = [12]aneS$_4$, [16]aneS$_4$)

The reaction of anhydrous $NiCl_2$ with one equivalent of [12]aneS$_4$ or [16]aneS$_4$ in CH_3NO_2 at room temperature affords a pale green solid. Addition of excess $NaBF_4$, followed by gentle heating of the mixture, yielded a green solution from which a green solid product could be isolated by the addition of diethyl ether. Recrystallisation of the crude compounds from CH_3NO_2/Et_2O gave pale green crystals which rapidly lost solvent on exposure to air.

The I.R. spectra of these products confirmed the presence of the S_4 macrocycles and BF_4^- counter-ion, and their elemental analyses were consistent with the formulation $[Ni(S_4)Cl](BF_4)$. However, their f.a.b. mass spectra showed molecular ions consistent with dimeric

structures:

Molecular Ion	S_4 = [12]aneS_4	S_4 = [16]aneS_4
$[^{58}Ni_2(S_4)_2{}^{35}Cl_2(^{11}BF_4)]^+$	M^+ = 753 (calculated 753)	-(865)
$[^{58}Ni_2(S_4)_2{}^{35}Cl_2]^+$	666(666)	M^+ = 778(778)
$[^{58}Ni(S_4){}^{35}Cl]^+$	333(333)	389(389)

Hence, these compounds were assigned chloro-bridged dimeric species $[Ni_2(S_4)_2(\mu\text{-}Cl)_2](BF_4)_2$ (21). This was supported by U.V./visible spectroscopy, which showed weak (ε = 20-40 $dm^3\ M^{-1}\ cm^{-1}$) d-d transitions at ca. 950 and 600 nm, which is consistent with an octahedral geometry about each Ni^{II} centre[114].

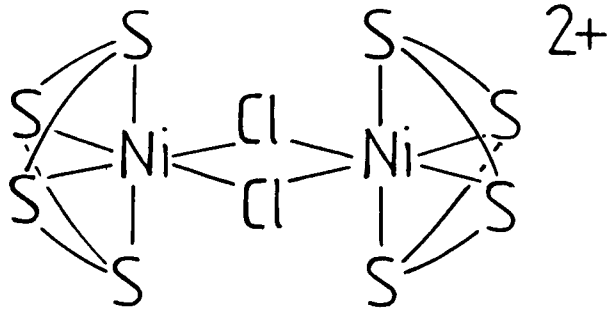

(21)

This type of binuclear structure is well known both for Ni^{II}[114] and other octahedral metal centres[13,59,115]. For Ni^{II}, examples containing octahedral[116] and trigonal bipyramidal[117] Ni^{II} centres have been structurally

characterised with one, two or three bridging ligands (22-24). Halide or pseudo-halide (e.g. NCO^-, NCS^-, N_3^-) bridges are most commonly observed. For doubly bridged dimers, Ni...Ni distances of 3.50-3.80 Å are typical, and magnetic measurements indicate a weak exchange interaction between the Ni centres which can be ferromagnetic or antiferromagnetic in nature[114].

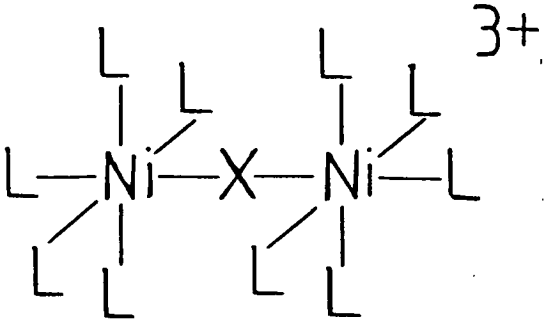

(22)

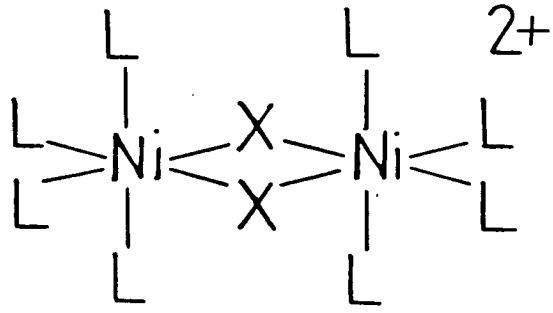

(23)

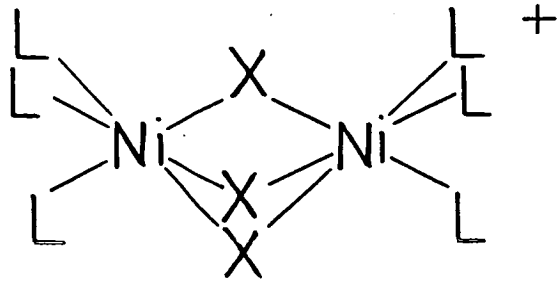

(24)

The only previously known macrocyclic Ni^{II}-Ni^{II} bridged dimers are $[Ni_2(TMC)_2(N_3)_2(\mu\text{-}N_3)]^+$ and

$[Ni_2(HMC)_2(\mu\text{-}C_2O_4)]^{2+}$ [118] (TMC = N,N',N'',N'''-tetramethylcyclam, HMC = 5,7,7,12,14,14-hexamethylcyclam), and the triply bridged complex $[Ni_2(Me_3[9]aneN_3)_2(\mu\text{-}CH_3CO_2)_2(\mu\text{-}OH)]ClO_4$ [119]; no such species incorporating thioether donors has been reported.

In order to confirm the dimeric nature of these complexes, and to investigate the effect of macrocyclic hole size on the metal-ligand and metal-metal interaction, single crystal X-ray analyses for both compounds were undertaken.

2.2.2 Single Crystal Structure of $[Ni_2([12]aneS_4)_2(\mu\text{-}Cl)_2](BF_4)_2.2CH_3NO_2$

Details of the structure solution and refinement are given in the Experimental Section. Relevant bond lengths, angles and torsions are presented in Table 2.1, and an ORTEP plot revealing the geometry of the complex is given in Figure 2.4.

The structure shows the cation to possess crystallographically imposed 2/m symmetry, with the Ni_2Cl_2 bridge and the equatorial S donors S(1) and S(7) lying on a crystallographic mirror plane, and an inversion centre at the midpoint of the Ni..Ni vector. The complex adopts the expected chloro-bridged dimeric structure, with each Ni atom bound to a *cis*-octahedral S_4Cl_2 donor set. The angles about the metal are significantly distorted from an ideal octahedral geometry [<S(1)-Ni-Cl = 178.82(10)°,

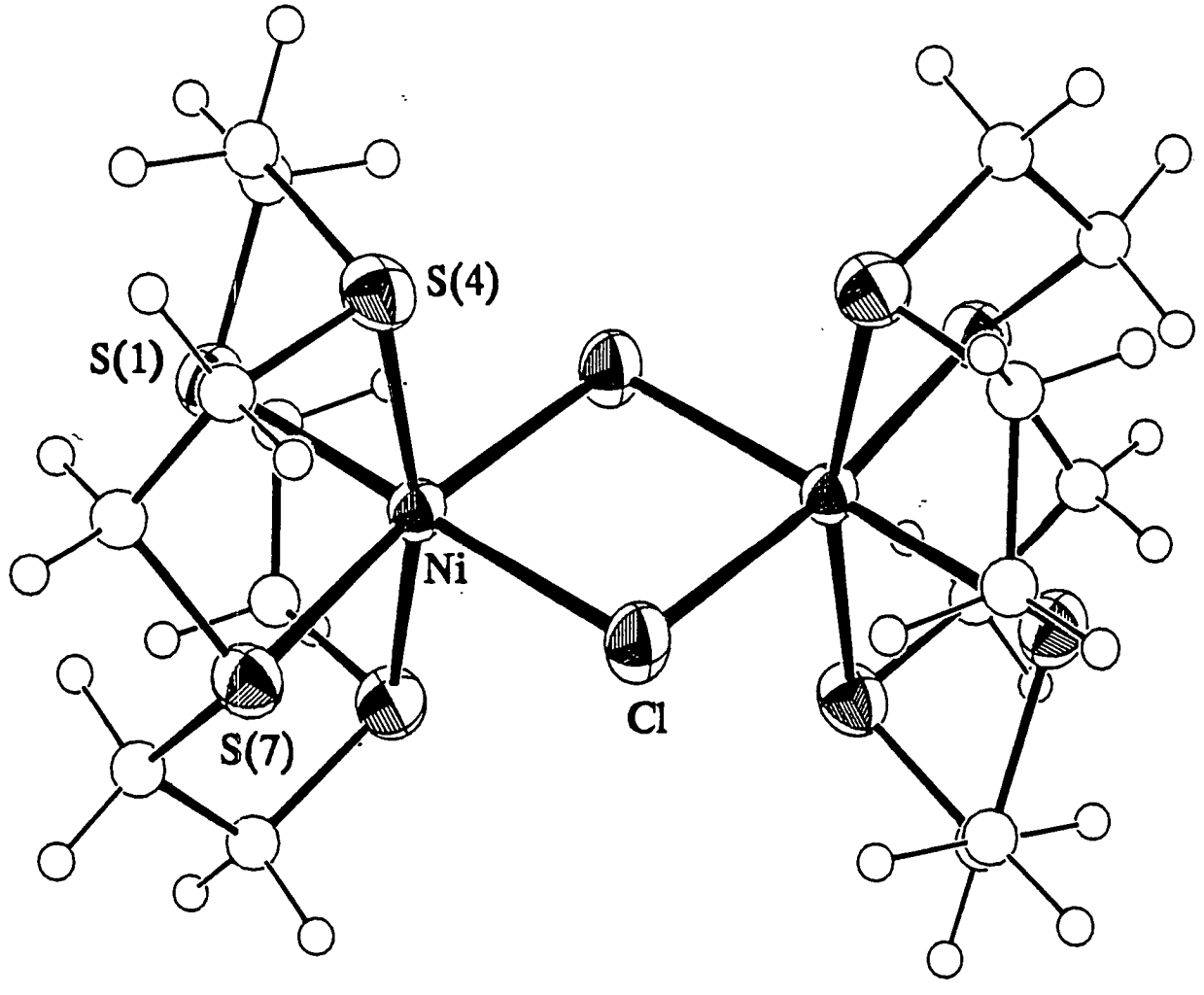

Figure 2.4: View of the Single Crystal Structure of $[Ni_2([12]aneS_4)_2(\mu\text{-}Cl)_2]^{2+}$

Single Crystal Structure of $[Ni_2([12]aneS_4)_2(\mu\text{-}Cl)_2](BF_4)_2.2CH_3NO_2$

Table 2.1. Bond Lengths(A), angles(degrees) and torsion angles(degrees) with standard deviations

Ni	- Ni'	3.5559(17)	S(1)	- C(2)	1.806(9)
Ni	- S(1)	2.412(3)	C(2)	- C(3)	1.548(12)
Ni	- S(4)	2.4144(25)	C(3)	- S(4)	1.823(9)
Ni	- S(7)	2.373(3)	S(4)	- C(5)	1.841(9)
Ni	- Cl	2.411(3)	C(5)	- C(6)	1.512(13)
Ni	- Cl'	2.382(3)	C(6)	- S(7)	1.810(9)

S(1)	- Ni - S(4)	83.73(9)	Ni	- S(1) - C(2)	97.0(3)
S(1)	- Ni - S(7)	94.42(10)	Ni	- S(4) - C(3)	103.2(3)
S(1)	- Ni - Cl	178.82(10)	Ni	- S(4) - C(5)	99.9(3)
S(1)	- Ni - Cl'	94.61(9)	Ni	- S(7) - C(6)	98.9(3)
S(4)	- Ni -S(4')	166.14(9)	C(2)	- S(1) -C(2')	107.0(4)
S(4)	- Ni - S(7)	87.54(9)	S(1)	- C(2) - C(3)	106.0(6)
S(4)	- Ni - Cl	96.32(9)	C(2)	- C(3) - S(4)	112.5(6)
S(4)	- Ni - Cl'	93.44(9)	C(3)	- S(4) - C(5)	101.2(4)
S(7)	- Ni - Cl	86.76(9)	S(4)	- C(5) - C(6)	114.5(6)
S(7)	- Ni - Cl'	170.97(10)	C(5)	- C(6) - S(7)	108.0(6)
Cl	- Ni - Cl'	84.21(9)	C(6)	- S(7) -C(6')	106.6(4)
Ni	- Cl - Ni'	95.79(9)			

C(2')	- S(1) - C(2) - C(3)	163.2(6)	C(3)	- S(4) - C(5) - C(6)	-75.2(7)
S(1)	- C(2) - C(3) - S(4)	-59.0(7)	S(4)	- C(5) - C(6) - S(7)	-60.7(7)
C(2)	- C(3) - S(4) - C(5)	125.0(6)	C(5)	- C(6) - S(7) -C(6')	157.9(6)

<S(7)-Ni-Cl' = 170.97(10)°, <S(4)-Ni-S(4') = 166.14(9)°, because of the small cavity size of the [12]aneS$_4$ macrocycle. The cation exhibits a tetragonal shortening along the S(7)-Ni-Cl' axis [Ni-S(1) = 2.412(3), Ni-S(4) = 2.414(3), Ni-S(7) = 2.373(3), Ni-Cl = 2.411(3), Ni-Cl' = 2.382(3) Å]. This contrasts with the analogous complex $[Ni_2(en)_4Cl_2]Cl_2$ (en = 1,2-diaminoethane), which exhibits a tetragonal elongation along the same axis[116b], and reflects the presence of a π-acceptor S donor *trans* to a π-donor Cl^- ligand as opposed to a purely σ-donating amine ligand. The Ni-S bond lengths are longer than those observed in other Ni^{II} crown thioether complexes[70,71,120], a result of the macrocyclic cavity to metal ion size mismatch; however, they are significantly shorter than the Ni-S distances reported for trans-$[Ni(dtco)_2Cl_2]$ (25)[121] [Ni-S = 2.478(3), 2.497(3) Å].

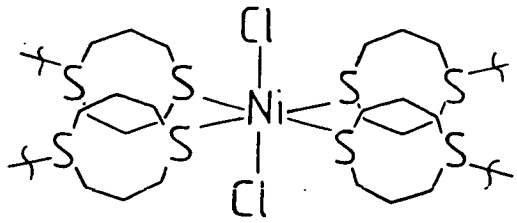

(25)

The Ni...Ni distance of 3.5559(17) Å is typical for a dichloro-bridged Ni^{II}-Ni^{II} dimer[114].

2.2.3 Single Crystal Structure of $[Ni_2([16]aneS_4)_2(\mu\text{-}Cl)_2](BF_4)_2.2CH_3NO_2$

Details of the structure solution are given in the Experimental Section. Selected bond lengths, angles and torsions are listed in Tables 2.2, 2.3 and 2.4 respectively. An ORTEP plot showing the structure of the complex cation is shown in Figure 2.5.

The structure shows the complex to be isostructural with the $[12]aneS_4$ dimer. Interestingly, there is no internal crystallographic symmetry within the molecule, and bond lengths and angles are seemingly randomly distributed throughout the complex [Ni-S = 2.4098(22)-2.4421(22) Å, Ni-Cl = 2.3860(21)-2.4205(20) Å]. Examination of space-filling models shows that for the ligand conformation observed, the imposition of an inversion centre between the Ni atoms would cause unfavourable steric interaction between methylene groups on the two macrocycles (Figure 2.6). The Ni-S bond lengths are similar to those of the $[12]aneS_4$ complex. However, the internal angles about Ni are now close to ideal for an octahedral geometry [*trans*-<S-Ni-Cl = 174.40(8)-176.22(7)°, <S(1)-Ni-S(9) = 178.50(9)°, <S(21)-Ni-S(29) = 179.20(8)°]. The Ni...Ni distance is identical to that of the $[12]aneS_4$ dimer [3.5534(12) Å], despite the increased steric crowding associated with the larger macrocycle.

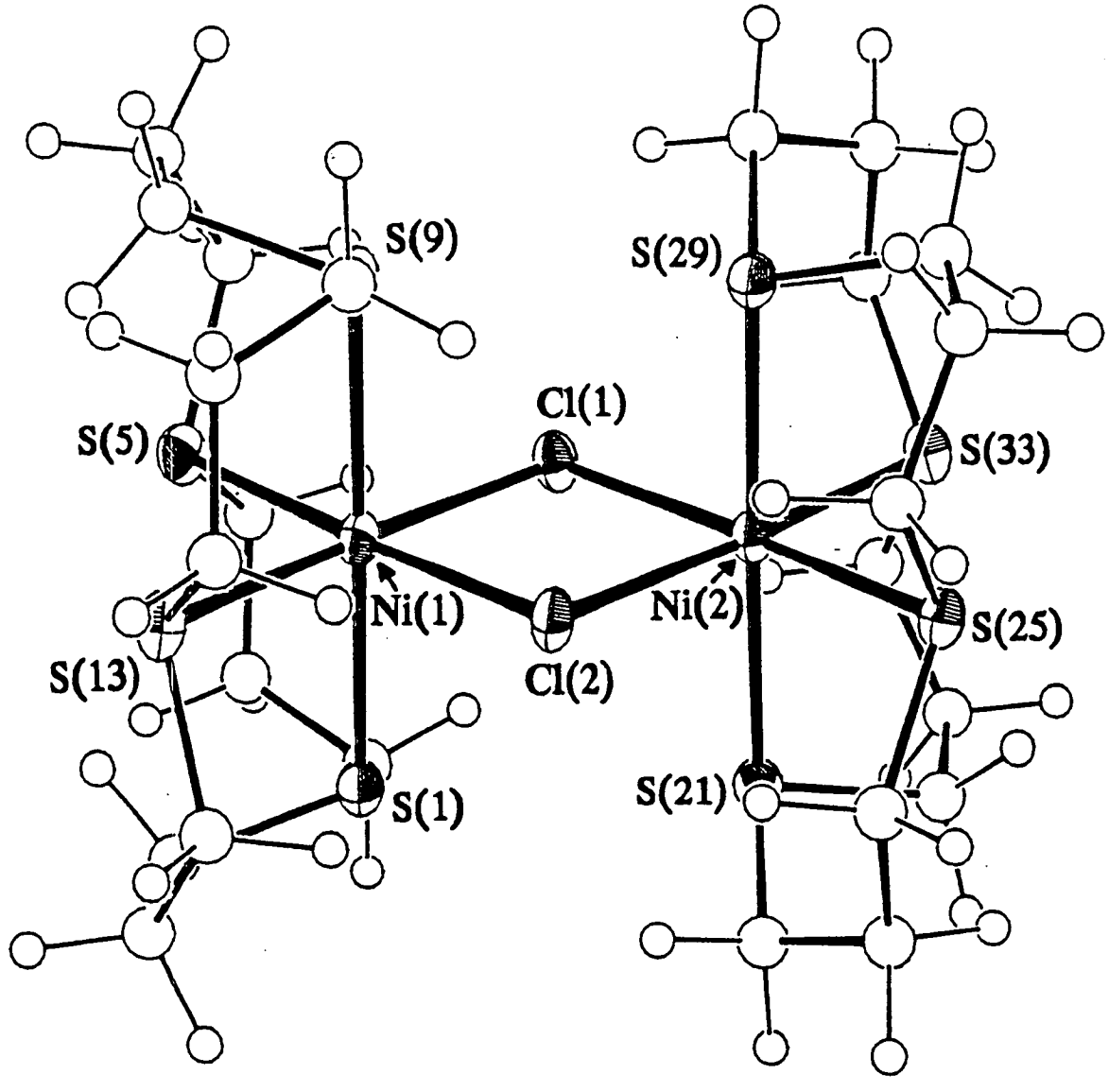

Figure 2.5: View of the Single Crystal Structure of $[Ni_2([16]aneS_4)_2(\mu\text{-}Cl)_2]^{2+}$

Single Crystal Structure of $[Ni_2([16]aneS_4)_2(\mu\text{-}Cl)_2](BF_4)_2.2CH_3NO_2$

Table 2.2. Bond Lengths(A) with standard deviations

Ni(1) -Ni(2)	3.5534(12)	C(10) -C(11)	1.529(12)
Ni(1) - S(1)	2.4309(23)	C(11) -C(12)	1.518(12)
Ni(1) - S(5)	2.4166(23)	C(12) -S(13)	1.815(8)
Ni(1) - S(9)	2.4259(24)	S(13) -C(14)	1.831(9)
Ni(1) -S(13)	2.4388(25)	C(14) -C(15)	1.523(12)
Ni(1) -Cl(1)	2.4182(23)	C(15) -C(16)	1.518(12)
Ni(1) -Cl(2)	2.4118(22)	S(21) -C(22)	1.821(9)
Ni(2) -S(21)	2.4421(22)	S(21) -C(36)	1.813(9)
Ni(2) -S(25)	2.4321(21)	C(22) -C(23)	1.533(13)
Ni(2) -S(29)	2.4098(22)	C(23) -C(24)	1.521(13)
Ni(2) -S(33)	2.4258(22)	C(24) -S(25)	1.840(9)
Ni(2) -Cl(1)	2.3860(21)	S(25) -C(26)	1.828(9)
Ni(2) -Cl(2)	2.4205(20)	C(26) -C(27)	1.505(12)
S(1) - C(2)	1.835(8)	C(27) -C(28)	1.557(12)
S(1) -C(16)	1.831(9)	C(28) -S(29)	1.822(9)
C(2) - C(3)	1.510(11)	S(29) -C(30)	1.815(8)
C(3) - C(4)	1.540(12)	C(30) -C(31)	1.524(12)
C(4) - S(5)	1.837(8)	C(31) -C(32)	1.527(12)
S(5) - C(6)	1.819(8)	C(32) -S(33)	1.822(9)
C(6) - C(7)	1.535(12)	S(33) -C(34)	1.813(9)
C(7) - C(8)	1.519(12)	C(34) -C(35)	1.536(13)
C(8) - S(9)	1.814(8)	C(35) -C(36)	1.505(13)
S(9) -C(10)	1.824(8)		

Table 2.3. Angles(degrees) with standard deviations

Cl(1) -Ni(1) -Cl(2)	84.71(7)	C(4) - S(5) - C(6)	95.2(4)
Cl(1) -Ni(1) - S(1)	89.55(8)	S(5) - C(6) - C(7)	113.0(6)
Cl(1) -Ni(1) - S(5)	89.90(8)	C(6) - C(7) - C(8)	116.1(7)
Cl(1) -Ni(1) - S(9)	91.77(8)	C(7) - C(8) - S(9)	117.4(6)
Cl(1) -Ni(1) -S(13)	175.59(9)	Ni(1) - S(9) - C(8)	110.3(3)
Cl(2) -Ni(1) - S(1)	90.11(8)	Ni(1) - S(9) -C(10)	103.9(3)
Cl(2) -Ni(1) - S(5)	174.40(8)	C(8) - S(9) -C(10)	100.5(4)
Cl(2) -Ni(1) - S(9)	90.72(8)	S(9) -C(10) -C(11)	111.0(6)
Cl(2) -Ni(1) -S(13)	90.88(8)	C(10) -C(11) -C(12)	114.2(7)
S(1) -Ni(1) - S(5)	88.32(8)	C(11) -C(12) -S(13)	111.6(6)
S(1) -Ni(1) - S(9)	178.50(9)	Ni(1) -S(13) -C(12)	102.9(3)
S(1) -Ni(1) -S(13)	90.55(8)	Ni(1) -S(13) -C(14)	107.8(3)
S(5) -Ni(1) - S(9)	90.96(8)	C(12) -S(13) -C(14)	97.2(4)
S(5) -Ni(1) -S(13)	94.51(8)	S(13) -C(14) -C(15)	112.9(6)
S(9) -Ni(1) -S(13)	88.19(8)	C(14) -C(15) -C(16)	116.5(7)
Cl(1) -Ni(2) -Cl(2)	85.21(7)	S(1) -C(16) -C(15)	117.2(6)
Cl(1) -Ni(2) -S(21)	90.81(7)	Ni(2) -S(21) -C(22)	104.8(3)
Cl(1) -Ni(2) -S(25)	176.22(7)	Ni(2) -S(21) -C(36)	109.9(3)
Cl(1) -Ni(2) -S(29)	90.00(7)	C(22) -S(21) -C(36)	100.5(4)
Cl(1) -Ni(2) -S(33)	90.88(7)	S(21) -C(22) -C(23)	110.7(6)
Cl(2) -Ni(2) -S(21)	89.59(7)	C(22) -C(23) -C(24)	115.2(7)
Cl(2) -Ni(2) -S(25)	91.04(7)	C(23) -C(24) -S(25)	112.5(6)
Cl(2) -Ni(2) -S(29)	90.48(7)	Ni(2) -S(25) -C(24)	102.7(3)
Cl(2) -Ni(2) -S(33)	176.09(7)	Ni(2) -S(25) -C(26)	107.5(3)
S(21) -Ni(2) -S(25)	88.70(7)	C(24) -S(25) -C(26)	96.4(4)
S(21) -Ni(2) -S(29)	179.20(8)	S(25) -C(26) -C(27)	114.3(6)
S(21) -Ni(2) -S(33)	90.24(7)	C(26) -C(27) -C(28)	114.9(7)
S(25) -Ni(2) -S(29)	90.50(7)	C(27) -C(28) -S(29)	116.5(6)
S(25) -Ni(2) -S(33)	92.87(7)	Ni(2) -S(29) -C(28)	110.1(3)
S(29) -Ni(2) -S(33)	89.74(7)	Ni(2) -S(29) -C(30)	104.5(3)
Ni(1) -Cl(1) -Ni(2)	95.40(8)	C(28) -S(29) -C(30)	101.0(4)
Ni(1) -Cl(2) -Ni(2)	94.67(7)	S(29) -C(30) -C(31)	110.8(6)
Ni(1) - S(1) - C(2)	105.3(3)	C(30) -C(31) -C(32)	115.7(7)
Ni(1) - S(1) -C(16)	110.8(3)	C(31) -C(32) -S(33)	112.6(6)
C(2) - S(1) -C(16)	100.1(4)	Ni(2) -S(33) -C(32)	102.4(3)
S(1) - C(2) - C(3)	110.2(5)	Ni(2) -S(33) -C(34)	107.2(3)
C(2) - C(3) - C(4)	115.8(7)	C(32) -S(33) -C(34)	96.8(4)
C(3) - C(4) - S(5)	111.9(6)	S(33) -C(34) -C(35)	115.1(6)
Ni(1) - S(5) - C(4)	103.9(3)	C(34) -C(35) -C(36)	116.5(8)
Ni(1) - S(5) - C(6)	106.5(3)	S(21) -C(36) -C(35)	117.7(6)

Table 2.4. Torsion angles(degrees) with standard deviations

C(16)	- S(1)	- C(2)	- C(3)	163.3(6)	C(36)	-S(21)	-C(22)	-C(23)	164.6(6)
C(2)	- S(1)	-C(16)	-C(15)	55.3(7)	C(22)	-S(21)	-C(36)	-C(35)	52.4(7)
S(1)	- C(2)	- C(3)	- C(4)	47.3(8)	S(21)	-C(22)	-C(23)	-C(24)	45.4(9)
C(2)	- C(3)	- C(4)	- S(5)	40.7(9)	C(22)	-C(23)	-C(24)	-S(25)	44.2(9)
C(3)	- C(4)	- S(5)	- C(6)	169.8(6)	C(23)	-C(24)	-S(25)	-C(26)	167.4(6)
C(4)	- S(5)	- C(6)	- C(7)	176.0(6)	C(24)	-S(25)	-C(26)	-C(27)	173.5(6)
S(5)	- C(6)	- C(7)	- C(8)	-78.8(8)	S(25)	-C(26)	-C(27)	-C(28)	-77.3(8)
C(6)	- C(7)	- C(8)	- S(9)	70.1(9)	C(26)	-C(27)	-C(28)	-S(29)	72.0(9)
C(7)	- C(8)	- S(9)	-C(10)	54.1(7)	C(27)	-C(28)	-S(29)	-C(30)	51.1(7)
C(8)	- S(9)	-C(10)	-C(11)	163.1(6)	C(28)	-S(29)	-C(30)	-C(31)	164.7(6)
S(9)	-C(10)	-C(11)	-C(12)	45.6(8)	S(29)	-C(30)	-C(31)	-C(32)	46.3(9)
C(10)	-C(11)	-C(12)	-S(13)	45.1(8)	C(30)	-C(31)	-C(32)	-S(33)	43.2(9)
C(11)	-C(12)	-S(13)	-C(14)	165.7(6)	C(31)	-C(32)	-S(33)	-C(34)	169.1(6)
C(12)	-S(13)	-C(14)	-C(15)	174.2(6)	C(32)	-S(33)	-C(34)	-C(35)	172.6(7)
S(13)	-C(14)	-C(15)	-C(16)	-78.5(8)	S(33)	-C(34)	-C(35)	-C(36)	-75.5(9)
C(14)	-C(15)	-C(16)	- S(1)	71.2(9)	C(34)	-C(35)	-C(36)	-S(21)	69.6(9)

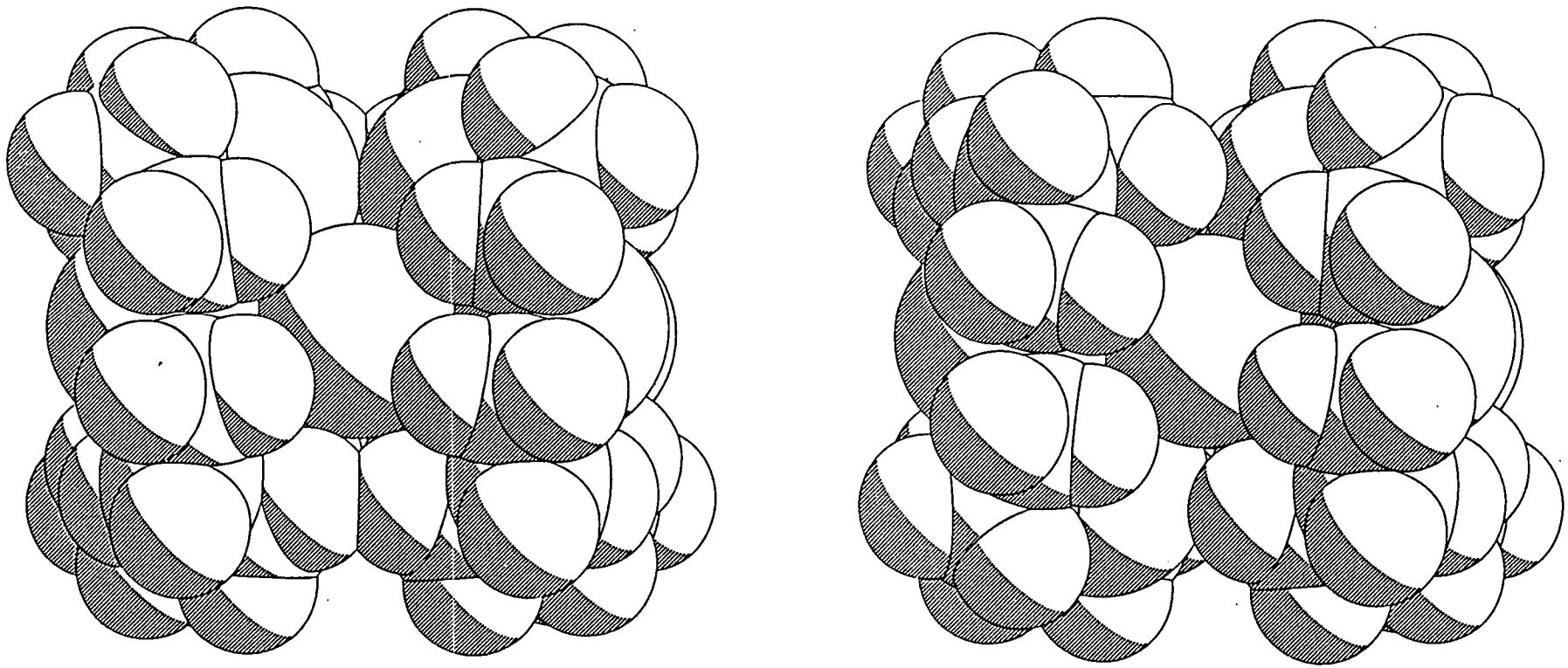

a) Centrosymmetric

b) Non-centrosymmetric

Figure 2.6: Space-filling Diagrams of $[Ni_2([16]aneS_4)_2(\mu\text{-}Cl)_2]^{2+}$

2.2.4 $[Ni_2([14]aneS_4)_2(\mu\text{-}Cl)_2](BF_4)_2$

The reaction of anhydrous $NiCl_2$ and $[14]aneS_4$ in the manner described in Section 2.2.1 yielded a microcrystalline blue solid product. The I.R. spectrum and elemental analysis of this product were consistent with the formulation $[Ni([14]aneS_4)Cl]BF_4$.

The f.a.b. mass spectrum of the complex shows peaks at M^+ = 809, 722 and 361, corresponding to $[^{58}Ni_2([14]aneS_4)_2{}^{35}Cl_2(^{11}BF_4)]^+$, $[^{58}Ni_2([14]aneS_4)_2{}^{35}Cl_2]^+$ and $[^{58}Ni([14]aneS_4){}^{35}Cl]^+$. Therefore, this product was assigned the same dimeric structure as the analogous $[12]aneS_4$ and $[16]aneS_4$ species despite its different colour.

Heating this complex to 60°C in CH_3NO_2 causes rapid decomposition to the red square-planar compound $[Ni([14]aneS_4)]^{2+}$ [68].

A single crystal X-ray analysis of the complex was performed, to confirm the structural assignment.

2.2.5 Single Crystal Structure of $[Ni_2([14]aneS_4)_2(\mu\text{-}Cl)_2](BF_4)_2.6CH_3NO_2$

Details of the structure solution and refinement are described in Section 2.4.4. Selected bond lengths, angles and torsions are presented in Tables 2.5, 2.6 and 2.7. ORTEP plots showing the molecular geometry of the cation, and the disposition of solvent molecules within the structure, are given in Figures 2.7 and 2.8.

The dimeric cation lies across a crystallographic inversion centre, at the centre of the Ni_2Cl_2 bridge. The Ni-S bond lengths are rather shorter than for the [12]aneS_4 and [16]aneS_4 dimers [Ni-S(1) = 2.3694(22), Ni-S(4) = 2.3765(21), Ni-S(8) = 2.3756(21), Ni-S(11) = 2.3798(21) Å], and are close to those observed for the octahedral hexathia complexes $[Ni([9]aneS_3)_2]^{2+}$ [Ni-S = 2.377(1), 2.380(1), 2.400(1) Å][70] and $[Ni([18]aneS_6)]^{2+}$ [Ni-S = 2.377(1), 2.389(1), 2.397(1) Å][71]. This reflects the improved macrocyclic cavity to metal ion size fit between Ni^{II} and [14]aneS_4 : for $[Ni([14]aneS_4)]^{2+}$, the macrocyclic hole size R_A = 1.21 Å, cf the ionic radius of low spin Ni^{II} of 1.20 Å[18]. The tetragonal contraction observed for $[Ni_2([12]aneS_4)(\mu\text{-}Cl)_2]^{2+}$ is not present in this complex. The Ni-Cl and Ni...Ni distances are similar to those of the other Ni/S_4 dimers [Ni-Cl = 2.4416(20), Ni-Cl′ = 2.4252(20), Ni...Ni = 3.5692(12) Å], and the bond angles around the Ni^{II} centres are close to 90 and 180°. There are no close interactions between any of the solvent molecules and the complex cation (c.f. the inclusion complex $[Ru([9]aneS_3)_2(DMSO)_2](BPh_4)_2$[122]).

2.2.6 Electrochemical Study of $[Ni_2(S_4)_2(\mu\text{-}Cl)_2]^{2+}$

Cyclic voltammetry of these compounds in CH_3CN/0.1 M $^nBu_4NPF_6$ at 298K yielded complex results, which are summarised in Table 2.8.

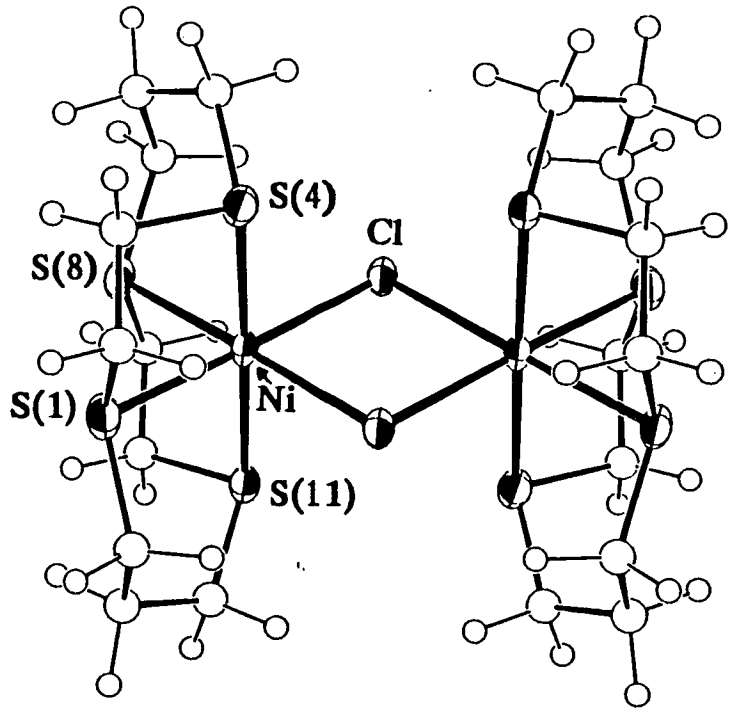

Figure 2.7: View of the Single Crystal Structure of $[Ni_2([14]aneS_4)_2(\mu\text{-}Cl)_2]^{2+}$.

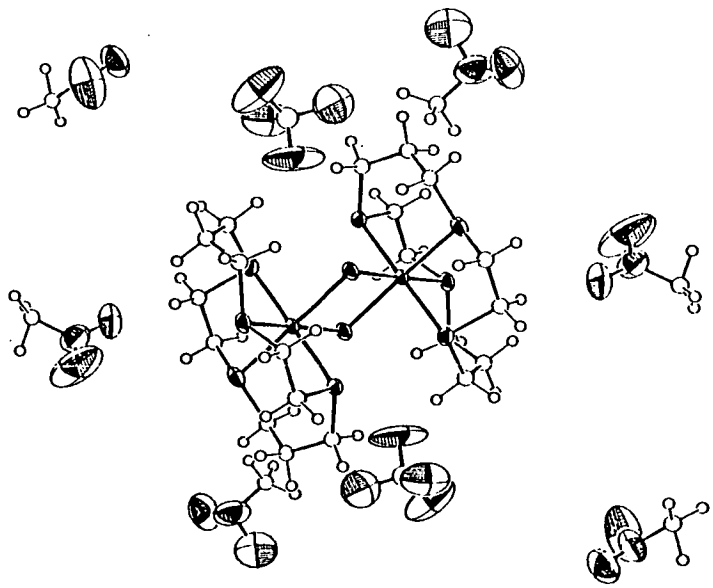

Figure 2.8: Alternative View of the Single Crystal Structure of $[Ni_2([14]aneS_4)_2(\mu\text{-}Cl)_2](BF_4)_2 \cdot 6CH_3NO_2$.

Single Crystal Structure of $[Ni_2([14]aneS_4)_2(\mu\text{-}Cl)_2](BF_4)_2.6CH_3NO_2$.

Table 2.5. Bond Lengths(A) with standard deviations

Ni	- Ni'	3.5692(12)	S(4)	- C(5)	1.826(8)
Ni	- S(1)	2.3694(22)	C(5)	- C(6)	1.503(12)
Ni	- S(4)	2.3765(21)	C(6)	- C(7)	1.512(12)
Ni	- S(8)	2.3756(21)	C(7)	- S(8)	1.804(8)
Ni	-S(11)	2.3798(21)	S(8)	- C(9)	1.848(8)
Ni	- Cl	2.4416(20)	C(9)	-C(10)	1.514(11)
Ni	- Cl'	2.4252(20)	C(10)	-S(11)	1.829(8)
S(1)	- C(2)	1.834(9)	S(11)	-C(12)	1.810(9)
S(1)	-C(14)	1.815(9)	C(12)	-C(13)	1.507(13)
C(2)	- C(3)	1.547(12)	C(13)	-C(14)	1.518(12)
C(3)	- S(4)	1.822(8)			

Table 2.6. Angles(degrees) with standard deviations

Cl	- Ni	- S(1)	178.09(8)		Ni	- S(4)	- C(5)	112.3(3)
Cl	- Ni	- S(4)	90.93(7)		Ni	- S(8)	- C(7)	106.9(3)
Cl	- Ni	- S(8)	94.13(7)		Ni	- S(8)	- C(9)	99.1(3)
Cl	- Ni	-S(11)	89.95(7)		Ni	-S(11)	-C(10)	101.0(3)
S(1)	- Ni	- S(4)	87.28(7)		Ni	-S(11)	-C(12)	112.3(3)
S(1)	- Ni	- S(8)	85.28(7)		C(2)	- S(1)	-C(14)	106.1(4)
S(1)	- Ni	-S(11)	91.83(7)		S(1)	- C(2)	- C(3)	105.9(6)
S(1)	- Ni	- Cl'	94.99(7)		C(2)	- C(3)	- S(4)	107.9(6)
S(4)	- Ni	- S(8)	91.45(7)		C(3)	- S(4)	- C(5)	104.5(4)
S(4)	- Ni	-S(11)	178.70(8)		S(4)	- C(5)	- C(6)	120.8(6)
S(4)	- Ni	- Cl'	90.47(7)		C(5)	- C(6)	- C(7)	116.8(7)
S(8)	- Ni	-S(11)	87.53(7)		C(6)	- C(7)	- S(8)	108.3(6)
S(8)	- Ni	- Cl'	178.07(7)		C(7)	- S(8)	- C(9)	106.0(4)
S(11)	- Ni	- Cl'	90.55(7)		S(8)	- C(9)	-C(10)	106.6(5)
Cl	- Ni	- Cl'	85.65(7)		C(9)	-C(10)	-S(11)	109.2(5)
Ni	- Cl	- Ni'	94.35(7)		C(10)	-S(11)	-C(12)	104.9(4)
Ni	- S(1)	- C(2)	99.3(3)		S(11)	-C(12)	-C(13)	120.5(6)
Ni	- S(1)	-C(14)	108.2(3)		C(12)	-C(13)	-C(14)	117.9(8)
Ni	- S(4)	- C(3)	101.4(3)		S(1)	-C(14)	-C(13)	107.6(6)

Table 2.7. Torsion angles(degrees) with standard deviations

C(14) - S(1) - C(2) - C(3)	167.3(5)	C(6) - C(7) - S(8) - C(9)	178.9(5)
C(2) - S(1) -C(14) -C(13)	-179.2(6)	C(7) - S(8) - C(9) -C(10)	164.7(5)
S(1) - C(2) - C(3) - S(4)	-68.9(6)	S(8) - C(9) -C(10) -S(11)	-68.0(6)
C(2) - C(3) - S(4) - C(5)	161.6(6)	C(9) -C(10) -S(11) -C(12)	161.0(5)
C(3) - S(4) - C(5) - C(6)	-67.6(7)	C(10) -S(11) -C(12) -C(13)	-66.7(8)
S(4) - C(5) - C(6) - C(7)	-63.1(9)	S(11) -C(12) -C(13) -C(14)	-64.9(10)
C(5) - C(6) - C(7) - S(8)	81.5(8)	C(12) -C(13) -C(14) - S(1)	80.5(8)

$[Ni_2([12]aneS_4)_2(\mu\text{-}Cl)_2]^{2+}$ exhibits one irreversible oxidation at Ep_a = +1.06V vs. Fc/Fc^+ (scan rate 400 mV/s) together with a weak return wave at Ep_c = +0.14V due to an unstable daughter product, which decreases in intensity relative to the parent oxidation at slow scan rates. An irreversible reduction is also observed at Ep_c = -1.39V, with an approximately equal intensity return wave at Ep_a = -0.31V. On addition of a ten-fold excess of $^nBu_4NCl$, the solution becomes more intensely coloured, and the cyclic voltammogram changes to show an irreversible oxidation at Ep_a = +0.82V (scan rate 400 mV/s) and a irreversible reduction at Ep_c = -1.98V with a return wave at Ep_a = -0.60V.

The electrochemical properties of $[Ni_2([14]aneS_4)_2(\mu\text{-}Cl)_2]^{2+}$ and $[Ni_2([16]aneS_4)_2(\mu\text{-}Cl)_2]^{2+}$ were different from those of the $[12]aneS_4$ dimer. Both these complexes exhibited two irreversible oxidations, at Ep_a ca. +0.75V and +1.25V vs. Fc/Fc^+ (scan rate 400 mV/s).

On addition of a ten-fold excess of $^nBu_4NCl$, the first of these oxidations became quasi-reversible ($E_{\frac{1}{2}} \simeq 0.60V$, ΔEp = 350 mV), whilst the second process became reduced in intensity (Figure 2.9). No reduction waves were observed for these compounds.

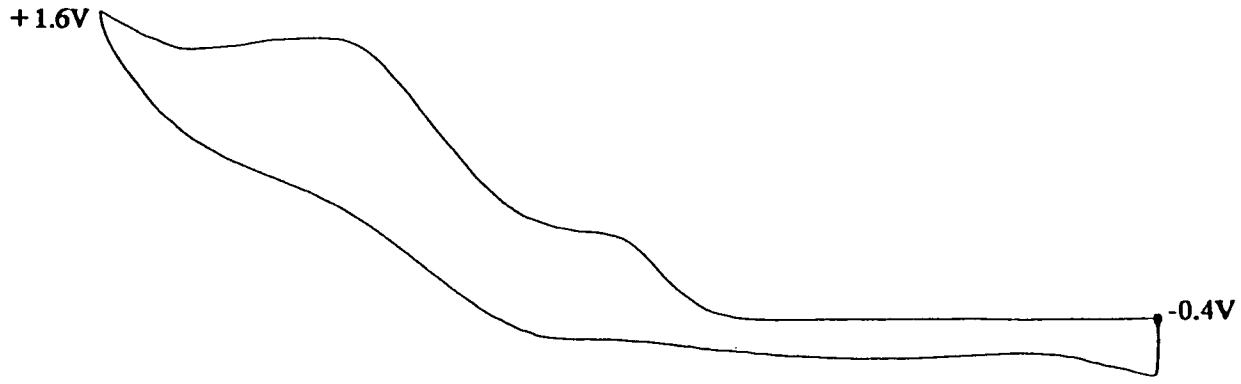

a) $CH_3CN/^nBu_4NPF_6$

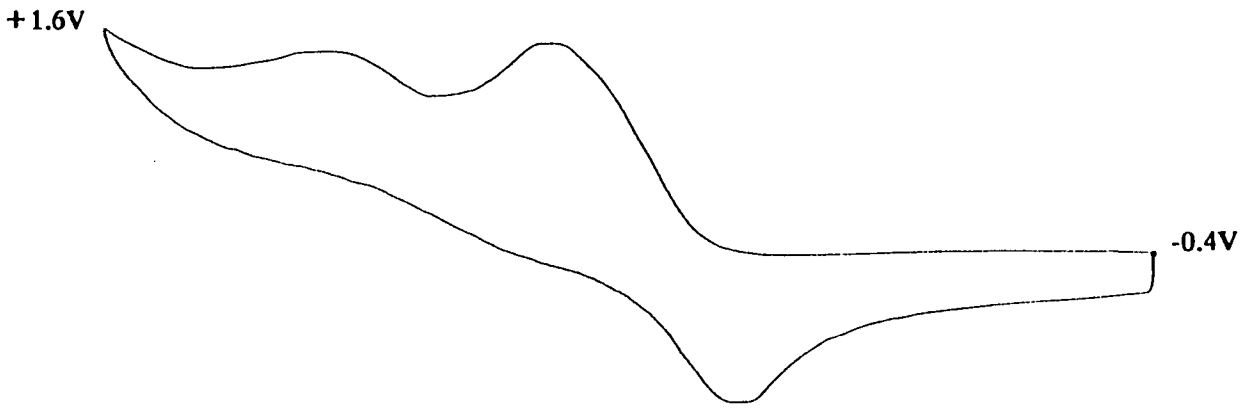

b) $CH_3CN/^nBu_4PF_6$ + excess $^nBu_4NCl$.

Figure 2.9: Cyclic Voltammograms of $[Ni_2([14]aneS_4)_2(\mu\text{-}Cl)_2](BF_4)_2$ (298K, scan rate 400 mV/s).

Attempts to electrogenerate bulk samples of the redox products described above resulted in diamagnetic solutions and/or Ni metal plating onto the Pt working electrode, demonstrating the instability of the oxidised and reduced species.

On the basis of purely cyclic voltammetric data, no firm interpretation of the above experiments can be given. In particular, it is not known if the oxidation processes are metal based, or whether they correspond to the oxidation of free Cl^- [$E(Cl^{-/0}) \simeq +1.0V$] released by dissociation of the dimeric species in solution. The reduction observed for $[Ni_2([12]aneS_4)_2(\mu\text{-}Cl)_2]^{2+}$ may correspond to the formation of an Ni^I-Ni^I dimer, with loss of Cl^- (26). Ni-Ni bond formation should be less favoured for the other dimers, since close approach of the two metal ions would be hindered by steric interactions between the macrocyclic ligands of the type shown in Figure 2.6.

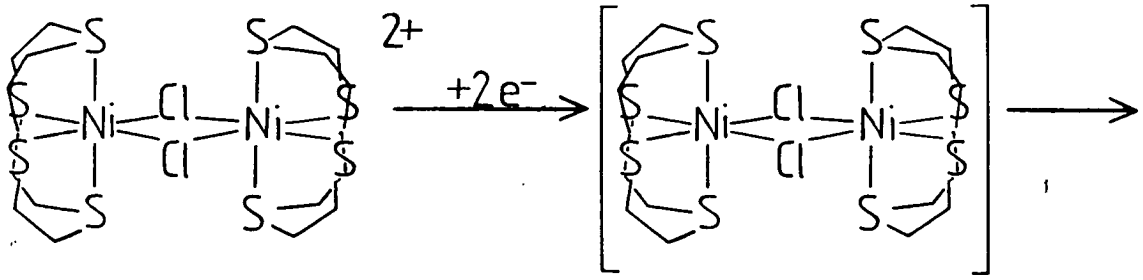

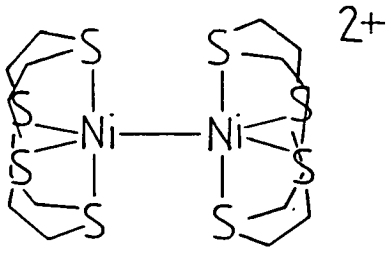

(26)

S_4	First Oxidation E(V)	First Oxidation ΔEp(mV)	First Oxidation E(return wave,V)	Second Oxidation E(V)	Reduction E(V)	Reduction E(return wave,V)
[12]aneS_4	+1.06(i)	-	+0.14(w)	-	-1.39(i)	-0.31(i)
+excess $^nBu_4NCl$	+0.82(i)	-	-	-	-1.98(i)	-0.60(i)
[14]aneS_4	+0.78(i)	-	-	+1.25(i)	-	-
+excess $^nBu_4NCl$	+0.59(q)	350	-	+1.25(w)	-	-
[16]aneS_4	+0.72(i)	-	-	+1.21(i)	-	-
+excess $^nBu_4NCl$	+0.61(q)	330	-	+1.21(w)	-	-

q = quasi-reversible, i = irreversible, w = weak

All measurements performed in CH_3CN/0.1M $^nBu_4NPF_6$ at 298K, scan rate 400 mV/s.

All potentials quoted vs. Fc/Fc^+.

Table 2.8: Electrochemical Data for $[Ni_2(S_4)_2(\mu\text{-}Cl)_2]^{2+}$.

2.2.7 $[Ni_2([9]aneS_3)_2(\mu\text{-}Cl)_3]BF_4$

Treatment of $NiCl_2$ with one molar equivalent of [9]aneS_3 in CH_3NO_2 yielded a mustard yellow precipitate (Section 3.2.1). The addition of one equivalent of $NaBF_4$ gave two products in roughly equal amounts, which could be separated by fractional crystallisation from $MeCN/Et_2O$. The first product, a pink crystalline solid, was identified as $[Ni([9]aneS_3)_2]^{2+}$ by comparison with a genuine sample (Section 4.3).

The second product was a pale green solid. The f.a.b. mass spectrum of this compound exhibited peaks at M^+ = 581, 546 and 238, which had the correct isotopic distributions for the assignments $[^{58}Ni_2([9]aneS_3)_2{}^{35}Cl_3]^+$, $[^{58}Ni_2([9]aneS_3)_2{}^{35}Cl_2]^+$ and $[^{58}Ni([9]aneS_3)]^+$. The complex was therefore assigned as the octahedral dimeric species $[Ni_2([9]aneS_3)_2(\mu\text{-}Cl)_3]BF_4$ (27). The I.R. spectrum and elemental analysis of the complex supported this assignment.

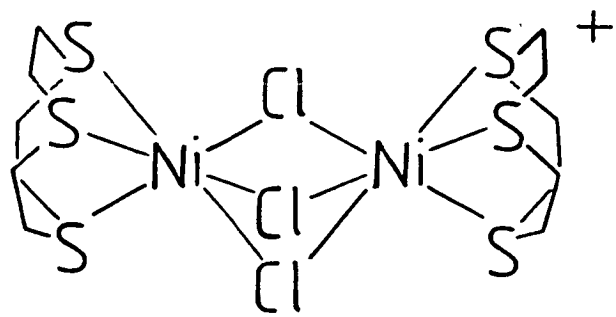

(27)

An X-ray structure determination was carried out, to verify the dimeric nature of the complex.

2.2.8 Single Crystal Structure of $[Ni_2([9]aneS_3)_2(\mu\text{-}Cl)_3]BF_4.CH_3CN$

Details of structure solution and refinement are given in Section 2.4.7. Selected bond lengths, angles and torsions are presented in Tables 2.9, 2.10 and 2.11, and an ORTEP plot of the complex cation is given in Figure 2.10.

The analysis confirms the face-sharing bi-octahedral structure proposed for the complex. The Ni-S bond lengths of 2.345(3)-2.370(3) Å are shorter than those in $[Ni([9]aneS_3)_2]^{2+}$ [70], illustrating the improved π-donation capability of a Cl^- ligand *trans* to a π-accepting thioether. The bond angles about the Ni centres are close to 90 and 180°. The Ni...Ni distance [2.9211(20) Å] is similar to that in $[Ni_2(acac)_2(\mu\text{-}O{:}O,O'\text{-}acac)_2(\mu\text{-}OAsPh_3)]$, which has an Ni_2O_3 bridge [Ni...Ni = 2.90 Å][123].

2.2.9 $[Ni(S_4)(OH_2)_2](BF_4)_2$ (S_4 = [12]aneS$_4$, [16]aneS$_4$)

In order to examine the Ni^{II} chemistry of the S_4 macrocycles in the absence of a coordinating anion, [12]aneS$_4$ and [16]aneS$_4$ were reacted with $Ni(BF_4)_2.6H_2O$ in nitromethane, with a trace of acetic anhydride to remove water from the reaction mixture. Both reactions afforded blue solutions from which pale blue solids could

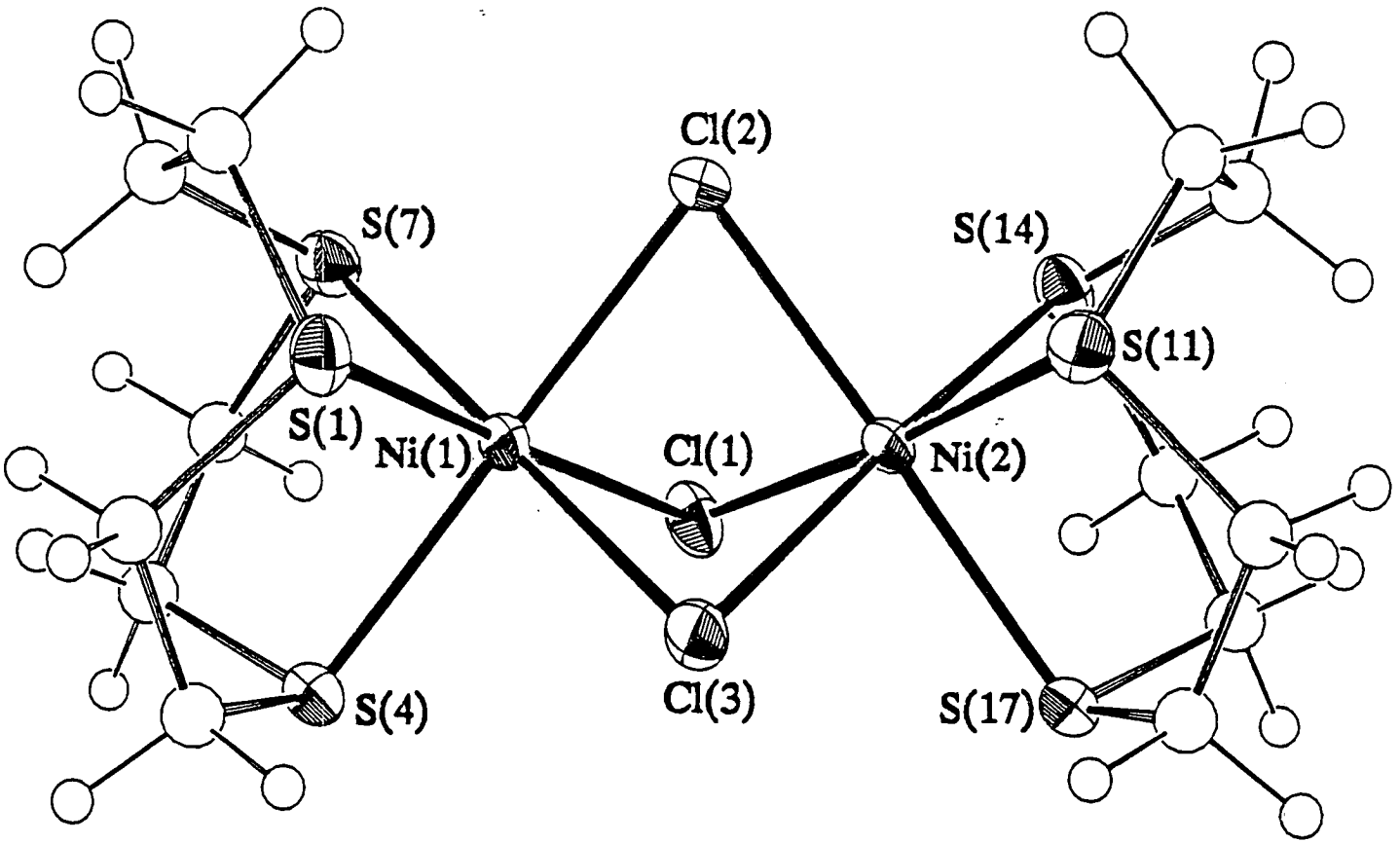

Figure 2.10: View of the Single Crystal Structure of $[Ni_2([9]aneS_3)_2(\mu\text{-}Cl)_3]^+$

Single Crystal Structure of $[Ni_2([9]aneS_3)_2(\mu\text{-}Cl)_3]BF_4 . CH_3CN$

Table 2.9. Bond Lengths(A) with standard deviations

Ni(1) -Ni(2)	2.9211(20)	C(3) - S(4)	1.821(13)
Ni(1) -Cl(1)	2.416(3)	S(4) - C(5)	1.834(12)
Ni(1) -Cl(2)	2.419(3)	C(5) - C(6)	1.524(17)
Ni(1) -Cl(3)	2.415(3)	C(6) - S(7)	1.810(12)
Ni(1) - S(1)	2.345(3)	S(7) - C(8)	1.822(13)
Ni(1) - S(4)	2.370(3)	C(8) - C(9)	1.529(17)
Ni(1) - S(7)	2.361(3)	S(11) -C(12)	1.788(12)
Ni(2) -Cl(1)	2.440(3)	S(11) -C(19)	1.828(12)
Ni(2) -Cl(2)	2.411(3)	C(12) -C(13)	1.524(17)
Ni(2) -Cl(3)	2.396(3)	C(13) -S(14)	1.815(12)
Ni(2) -S(11)	2.351(3)	S(14) -C(15)	1.815(12)
Ni(2) -S(14)	2.354(3)	C(15) -C(16)	1.495(17)
Ni(2) -S(17)	2.357(3)	C(16) -S(17)	1.795(13)
S(1) - C(2)	1.826(12)	S(17) -C(18)	1.793(13)
S(1) - C(9)	1.836(12)	C(18) -C(19)	1.502(17)
C(2) - C(3)	1.501(17)		

Table 2.10. Angles(degrees) with standard deviations

Cl(1) -Ni(1) -Cl(2)	86.58(11)	Ni(1) -Cl(3) -Ni(2)	74.76(10)
Cl(1) -Ni(1) -Cl(3)	86.86(11)	Ni(1) - S(1) - C(2)	102.7(4)
Cl(1) -Ni(1) - S(1)	175.61(12)	Ni(1) - S(1) - C(9)	99.2(4)
Cl(1) -Ni(1) - S(4)	93.04(11)	C(2) - S(1) - C(9)	103.1(6)
Cl(1) -Ni(1) - S(7)	93.20(11)	S(1) - C(2) - C(3)	112.4(8)
Cl(2) -Ni(1) -Cl(3)	88.19(11)	C(2) - C(3) - S(4)	116.2(9)
Cl(2) -Ni(1) - S(1)	90.05(11)	Ni(1) - S(4) - C(3)	98.2(4)
Cl(2) -Ni(1) - S(4)	179.60(12)	Ni(1) - S(4) - C(5)	103.7(4)
Cl(2) -Ni(1) - S(7)	90.66(11)	C(3) - S(4) - C(5)	102.0(5)
Cl(3) -Ni(1) - S(1)	90.23(11)	S(4) - C(5) - C(6)	112.5(8)
Cl(3) -Ni(1) - S(4)	91.90(11)	C(5) - C(6) - S(7)	116.1(8)
Cl(3) -Ni(1) - S(7)	178.84(12)	Ni(1) - S(7) - C(6)	100.6(4)
S(1) -Ni(1) - S(4)	90.34(12)	Ni(1) - S(7) - C(8)	103.3(4)
S(1) -Ni(1) - S(7)	89.65(12)	C(6) - S(7) - C(8)	102.3(6)
S(4) -Ni(1) - S(7)	89.25(11)	S(7) - C(8) - C(9)	111.4(8)
Cl(1) -Ni(2) -Cl(2)	86.21(11)	S(1) - C(9) - C(8)	113.9(8)
Cl(1) -Ni(2) -Cl(3)	86.73(11)	Ni(2) -S(11) -C(12)	100.1(4)
Cl(1) -Ni(2) -S(11)	175.09(12)	Ni(2) -S(11) -C(19)	102.8(4)
Cl(1) -Ni(2) -S(14)	90.09(11)	C(12) -S(11) -C(19)	102.4(6)
Cl(1) -Ni(2) -S(17)	95.05(11)	S(11) -C(12) -C(13)	117.5(9)
Cl(2) -Ni(2) -Cl(3)	88.83(11)	C(12) -C(13) -S(14)	113.7(8)
Cl(2) -Ni(2) -S(11)	88.88(11)	Ni(2) -S(14) -C(13)	103.3(4)
Cl(2) -Ni(2) -S(14)	93.48(11)	Ni(2) -S(14) -C(15)	99.3(4)
Cl(2) -Ni(2) -S(17)	177.17(12)	C(13) -S(14) -C(15)	102.5(6)
Cl(3) -Ni(2) -S(11)	93.36(11)	S(14) -C(15) -C(16)	115.5(9)
Cl(3) -Ni(2) -S(14)	175.94(12)	C(15) -C(16) -S(17)	112.2(9)
Cl(3) -Ni(2) -S(17)	88.71(11)	Ni(2) -S(17) -C(16)	103.4(4)
S(11) -Ni(2) -S(14)	90.02(11)	Ni(2) -S(17) -C(18)	98.5(4)
S(11) -Ni(2) -S(17)	89.86(12)	C(16) -S(17) -C(18)	102.2(6)
S(14) -Ni(2) -S(17)	89.05(12)	S(17) -C(18) -C(19)	116.8(9)
Ni(1) -Cl(1) -Ni(2)	73.96(10)	S(11) -C(19) -C(18)	112.0(8)
Ni(1) -Cl(2) -Ni(2)	74.42(10)		

Table 2.11. Torsion angles(degrees) with standard deviations

C(9)	S(1)	C(2)	C(3)	133.1(9)	C(19)	-S(11)	-C(12)	-C(13)	66.0(10)
C(2)	S(1)	C(9)	C(8)	-58.7(10)	C(12)	-S(11)	-C(19)	-C(18)	-131.1(9)
S(1)	C(2)	C(3)	S(4)	-52.7(11)	S(11)	-C(12)	-C(13)	-S(14)	45.8(12)
C(2)	C(3)	S(4)	C(5)	-62.2(10)	C(12)	-C(13)	-S(14)	-C(15)	-127.5(9)
C(3)	S(4)	C(5)	C(6)	129.5(9)	C(13)	-S(14)	-C(15)	-C(16)	62.6(10)
S(4)	C(5)	C(6)	S(7)	-49.0(11)	S(14)	-C(15)	-C(16)	-S(17)	53.2(11)
C(5)	C(6)	S(7)	C(8)	-64.2(10)	C(15)	-C(16)	-S(17)	-C(18)	-133.8(9)
C(6)	S(7)	C(8)	C(9)	135.0(9)	C(16)	-S(17)	-C(18)	-C(19)	60.4(10)
S(7)	C(8)	C(9)	S(1)	-54.3(10)	S(17)	-C(18)	-C(19)	-S(11)	51.9(11)

isolated; both compounds gradually turned a deep purple colour on drying *in vacuo*.

Elemental analyses on the dried complexes suggested the formulation $[Ni(S_4)(OH_2)](BF_4)_2$. This was supported by f.a.b. mass spectral data:

Assignment	[12]aneS$_4$	[16]aneS$_4$
$[^{58}Ni(S_4)(OH_2)(^{11}BF_4)]^+$	M^+=404 (calculated 403)	459(459)
$[^{58}Ni(S_4)(OH_3)]^+$	317(317)	373(373)
$[^{58}Ni(S_4)]^+$	298(298)	354(354)

However, an X-ray analysis on blue crystals of the [16]aneS$_4$ complex revealed this to be the octahedral species *trans*-$[Ni([16]aneS_4)(OH_2)_2](BF_4)_2$ (*vide infra*). The initial product of the [12]aneS$_4$ reaction is therefore also assigned as the octahedral *bis*-aquo complex $[Ni([12]aneS_4)(OH_2)_2](BF_4)_2$ probably with a *cis*-configuration. Both complexes undergo facile loss of one water ligand under vacuum, to give a five-coordinate species, or possibly an aquo- or hydroxo-bridged dimer of the type described above. Given the intense purple colour of the dried compounds, the former structure seems more likely, however.

The complexation of [14]aneS$_4$ by $Ni(BF_4)_2.6H_2O$ in CH_3NO_2 at 298K yielded the known square-planar compound $[Ni([14]aneS_4)](BF_4)_2$ (Figure 2.11)[68,120]. In our hands, the blue octahedral dimeric complex $[Ni_2([12]aneS_4)_3]^{4+}$

(28) reported previously by Rosen and Busch could not be prepared[69].

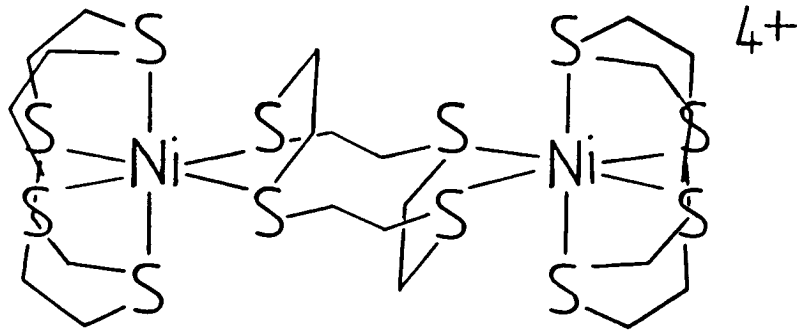

(28)

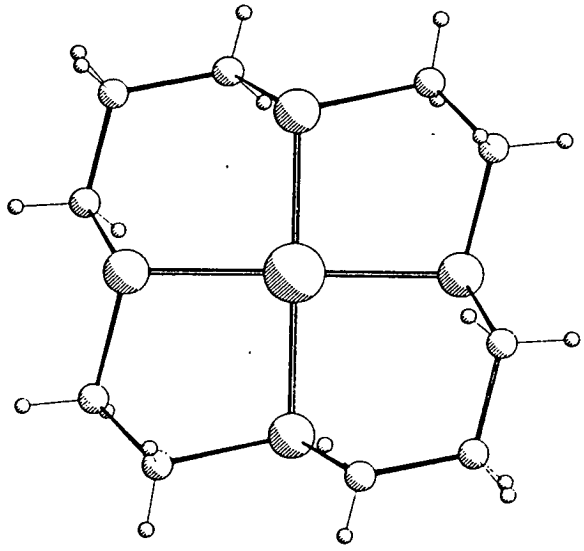

Figure 2.11: View of the Single Crystal Structure of $[Ni([14]aneS_4)]^{2+}$

2.2.10 Single Crystal Structure of $[Ni([16]aneS_4)(OH_2)_2](BF_4)_2$

An X-ray analysis of this complex was undertaken to unambiguously identify its molecular structure. Details

of the structure solution are described in Section 2.4.12. Important bond lengths, angles and torsions are given in Table 2.12, and the complex molecular geometry is displayed in Figure 2.12.

The Ni^{II} ion lies on a crystallographic inversion centre, and adopts a *trans*-octahedral geometry with two axially coordinated aquo ligands. The Ni-S bond lengths are similar to those of the *cis*-octahedral dimer $[Ni_2([16]aneS_4)_2(\mu\text{-}Cl)_2]^{2+}$ described above [Ni-S(1) = 2.4290(10), Ni-S(5) = 2.4231(10) Å]; the Ni-OH_2 distance of 2.083(3) Å is at the high end of the range commonly observed (e.g. Ni-O = 2.02-2.10 Å in $[Ni(OH_2)_6]^{2+}$ [128], and probably corresponds to a slight tetragonal elongation. All internal angles about the Ni centre are close to 90°; the Ni atom lies precisely in the plane of the macrocycle, as a consequence of the crystallographic symmetry. The water H atom positions were allowed to refine, with fixed O-H and H-O-H distances. They imply that the water ligand adopts a planar geometry, which may reflect disorder in the orientation of the non-bonding O lone pair. There is a hydrogen bond from the water molecule to one F atom of the BF_4^- counter-ion [H(12)...F(1) = 1.736(29) Å, <O...H(12)...F(1) = 173.94(27), <H(12)...F(1)...B = 116.3(9)°].

2.2.11 Electronic Spectra of $[Ni(S_4)]^{2+}$ Complexes

The electronic spectra of octahedral or near-

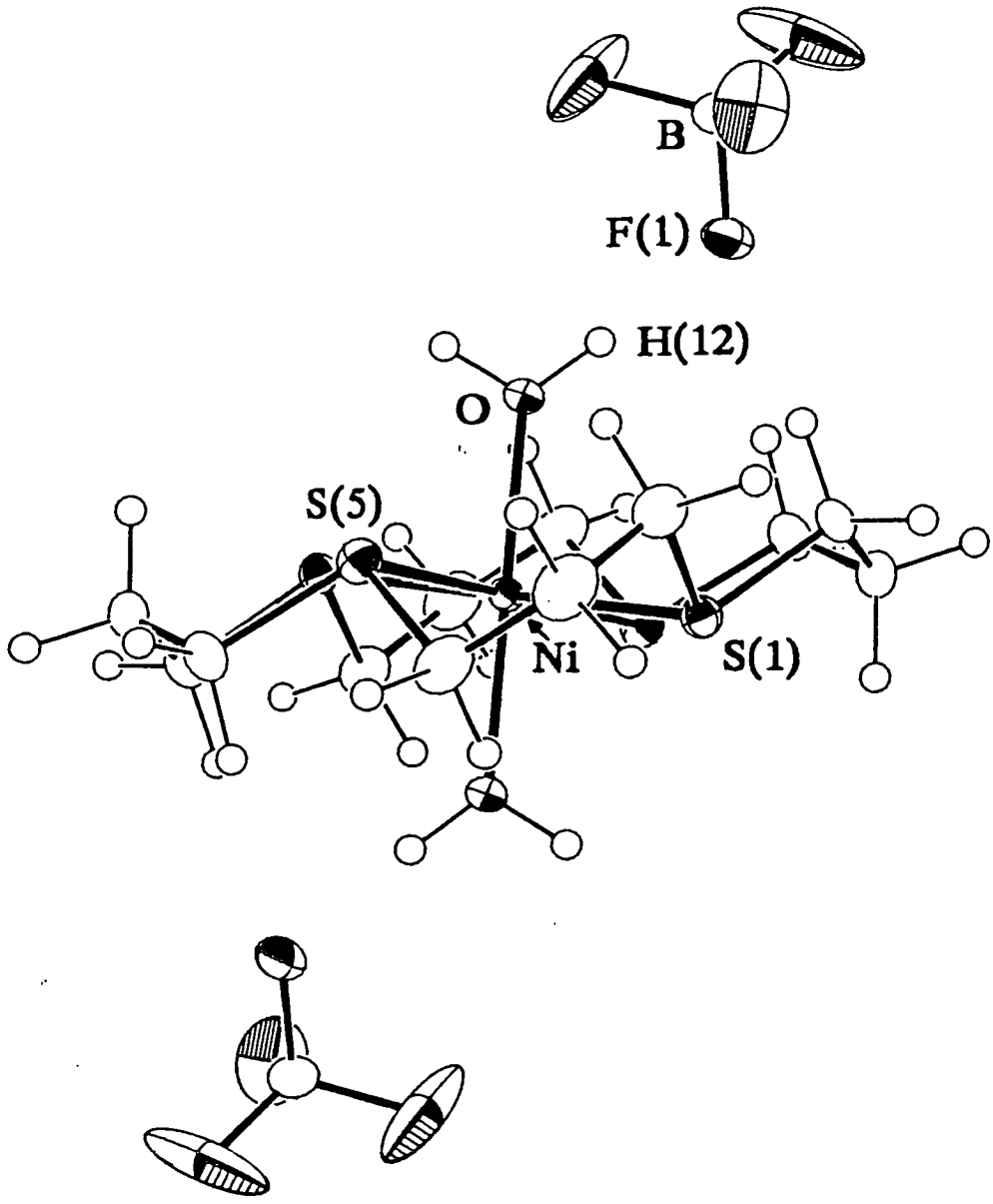

Figure 2.12: View of the Single Crystal Structure of $[Ni([16]aneS_4)(OH_2)_2](BF_4)_2$

Single Crystal Structure of $[Ni([16]aneS_4)(OH_2)_2](BF_4)_2$

Table 2.12. Bond Lengths(A), angles(degrees) and torsion angles(degrees) with standard deviations

Ni	- S(1)	2.4290(10)	C(3)	- C(4)	1.524(6)
Ni	- S(5)	2.4231(10)	C(4)	- S(5)	1.828(5)
Ni	- O	2.083(3)	S(5)	- C(6)	1.817(4)
S(1)	- C(2)	1.820(5)	C(6)	- C(7)	1.526(6)
S(1')	- C(8)	1.821(4)	C(7)	- C(8)	1.514(6)
C(2)	- C(3)	1.532(6)			

S(1)	- Ni - S(5)	89.85(3)	C(3)	- C(4) - S(5)	111.3(3)
S(1)	- Ni - O	92.85(8)	Ni	- S(5) - C(4)	101.59(15)
S(5)	- Ni - O	87.04(8)	Ni	- S(5) - C(6)	110.32(14)
Ni	- S(1) - C(2)	102.80(14)	C(4)	- S(5) - C(6)	98.85(20)
Ni	-S(1') - C(8)	108.53(14)	S(5)	- C(6) - C(7)	112.8(3)
C(8)	-S(1') -C(2')	99.59(19)	C(6)	- C(7) - C(8)	115.0(3)
S(1)	- C(2) - C(3)	110.5(3)	S(1')	- C(8) - C(7)	112.1(3)
C(2)	- C(3) - C(4)	115.1(4)			

C(2')	-S(1') - C(8) - C(7)	173.0(3)	C(3)	- C(4) - S(5) - C(6)	-163.4(3)
C(8)	-S(1') -C(2') -C(3')	166.2(3)	C(4)	- S(5) - C(6) - C(7)	-167.4(3)
S(1)	- C(2) - C(3) - C(4)	-46.2(5)	S(5)	- C(6) - C(7) - C(8)	78.9(4)
C(2)	- C(3) - C(4) - S(5)	-45.4(5)	C(6)	- C(7) - C(8) -S(1')	-81.9(4)

octahedral Ni^{II} complexes generally exhibit three d-d bands, corresponding to the transitions $^3A_{2g} \rightarrow {}^3T_{2g}$ (in O_h symmetry, lowest energy band), $^3A_{2g} \rightarrow {}^3T_{1g}$ and $^3A_{2g} \rightarrow {}^3T_{1g}(P)$ (highest energy, often obscured by charge-transfer bands)[114]. The energy of the first of these transitions corresponds to the ligand field splitting energy 10Dq[125], which allows a comparison of ligand field strengths for a series of related complexes.

The U.V./visible spectra of $[Ni(S_4)(OH_2)_2](BF_4)_2$ (S_4 = [12]aneS_4, [16]aneS_4) in CH_3NO_2 exhibit two d-d bands, at *ca.* 950 and 580 nm (ε_{max} = 30-100 $dm^3mol^{-1}cm^{-1}$). This is consistent with these complexes maintaining an octahedral structure in solution. The extinction coefficients of these bands for $[Ni([12]aneS_4)(OH_2)_2]^{2+}$ are roughly twice those for the [16]aneS_4 complex; this supports the assignment of a *cis*-octahedral structure for the former compound. The red square-planar complex $[Ni([14]aneS_4)]^{2+}$ forms a pale blue solution in CH_3CN, which gives d-d bands at λ_{max} = 925 nm (ε_{max} = 7.8 $dm^3\,mol^{-1}\,cm^{-1}$) and 562 nm (10.3). This implies the formation of an octahedral species in this solvent, via the coordination of two axial solvent molecules to give $[Ni([14]aneS_4)(NCCH_3)_2]^{2+}$. Attempts to isolate this adduct were unsuccessful, however, giving a pale blue solid that rapidly turned red on exposure to air. It is likely that the aquo ligands in $[Ni(S_4)(OH_2)_2]^{2+}$ will also be displayed in CH_3CN solutions of these complexes, forming $[Ni(S_4)(NCCH_3)_2]^{2+}$.

Table 2.13: Electronic Spectral Data for Octahedral Ni^{II} Complexes of Thia- and Aza-Macrocycles

	$\lambda_{max}(^3A_{2g} \rightarrow {}^3T_{2g})$ (nm)	10Dq (cm^{-1})	Ref.
$[Ni([12]aneS_4)(NCCH_3)_2]^{2+}$	943	10,600	This Work
$[Ni([14]aneS_4)(NCCH_3)_2]^{2+}$	925	10,810	This Work
$[Ni([16]aneS_4)(NCCH_3)_2]^{2+}$	972	10,290	This Work
$[Ni([14]aneS_4)X_2]$*	939	10,700	68
$[Ni([14]aneN_4)X_2]$*	-†	14,800	126
$[Ni([16]aneN_4)X_2]$*	-†	11,100	126
$[Ni([9]aneS_3)_2]^{2+}$	785	12,740	70
$[Ni([12]aneS_3)_2]^{2+}$	890	11,240	71
$[Ni([9]aneNS_2)_2]^{2+}$	840	11,930	124
$[Ni([9]aneN_3)_2]^{2+}$	816	12,500	127
$[Ni([15]aneS_5)(NCCH_3)]^{2+}$	902	11,090	This Work (Section 3.2)
$[Ni([18]aneS_6)]^{2+}$	815	12,290	71
$[Ni([18]aneN_2S_4)]^{2+}$	824	12,135	75
$[Ni([18]aneN_6)]^{2+}$	893	11,200	129

* X = Cl^-, Br^-. † Tetragonal Complex

Electronic spectral data for several octahedral and tetragonal Ni^{II} complexes of polythia- and polyaza-macrocycles is listed in Table 2.13. The ligand field exerted on Ni^{II} by the S_4 macrocycles is lower than for other crown thioethers, possibly reflecting the decreased macrocyclic compression exerted by an in-plane bound tetrathia ligand. The highest ligand field is exerted by [14]aneS_4 as a result of the good metal ion to cavity size match.

However, in contrast to [9]aneS_3 or [18]aneS_6, the tetrathia macrocycles are weaker field ligands than their poly-aza analogues. This is a result of the increased pre-organisational energy required for endo complexation by the tetrathia crowns compared to the tetraaza macrocycles.

2.2.12 Electrochemical Study of $[Ni(S_4)(Solvent)_2]^{2+}$; ($S_4$ = [12]aneS_4, [14]aneS_4, [16]aneS_4)

No reversible electrochemical couples were observed in the cyclic voltammograms of $[Ni([12]aneS_4)(OH_2)_2]^{2+}$, $[Ni([14]aneS_4)]^{2+}$ and $[Ni([16]aneS_4)(OH_2)_2]^{2+}$ in $CH_3CN/{}^nBu_4NPF_6$ at 298K. All three complexes exhibited an irreversible reduction, with an associated desorption spike at *ca.* oV vs. Fc/Fc^+, corresponding to the desorption of Ni metal onto the Pt electrodes. In addition, $[Ni([14]aneS_4)]^{2+}$ exhibited an irreversible oxidation at +1.02V (scan rate 400 mV/s), with no

observable daughter products. All these processes remained irreversible at high scan rates, and were not studied further. The redox data for these complexes ~~is~~ are summarised in Table 2.14.

	Oxidation Ep_a(V)	Reduction Ep_c(V)
S_4 = [12]aneS_4	-	-1.60
[14]aneS_4	+1.02	-1.18
[16]aneS_4	-	-1.51

Table 2.14: Electrochemical Data for $[Ni(S_4)(NCCH_3)_2]^{2+}$ (All measurements in CH_3CN/0.1M $^nBu_4NPF_6$, scan rate 400 mV/s).

2.3 CONCLUSIONS

The chemistry of Ni^{II} with the crown tetrathioethers [12]aneS_4, [14]aneS_4 and [16]aneS_4 has been investigated. In the absence of a coordinating anion, the ligands [12]aneS_4 and [16]aneS_4 form octahedral complexes $[Ni(S_4)(Solv)_2]^{2+}$ (Solv = H_2O, CH_3CN). The known square-planar compound $[Ni([14]aneS_4)]^{2+}$ also coordinates solvent ligands in CH_3CN. Analysis of the electronic spectra of $[Ni(S_4)(NCCH_3)_2]^{2+}$ shows that these tetrathia macrocycles exert a relatively weak ligand field onto a Ni^{II} ion, explaining their tendency to form octahedral

rather than square-planar Ni^{II} complexes.

Reaction of the S_4 macrocycles with $NiCl_2$ yields the dimeric species $[Ni_2(S_4)_2(\mu\text{-}Cl)_2]^{2+}$. These have been structurally characterised; the Ni...Ni distance in these compounds is insensitive to the macrocyclic cavity size, even though the Ni-S bond lengths do vary between the complexes. Complexation of $NiCl_2$ by [9]aneS_3 affords the triply bridged dimer $[Ni_2([9]aneS_3)_2(\mu\text{-}Cl)_3]^{+}$, together with $[Ni([9]aneS_3)_2]^{2+}$. If the bridging ligands in these species can be replaced by carboxylate or thiolate moieties, such dimers may have use as models for Ni sites in biological systems such as hydrogenases. However, the low stability of all the Ni/S_4 complexes towards hydrolysis may limit their effectiveness in this regard (all the compounds are highly sensitive towards H_2O and other O-donor solvents).

The in-plane Ni^{II} complexes $[Ni([14]aneS_4)]^{2+}$, and $[Ni([16]aneS_4)(OH_2)_2]^{2+}$, and the *cis*-octahedral dimers $[Ni_2(S_4)_2(\mu\text{-}Cl)_2]^{2+}$ (S_4 = [14]aneS_4, [16]andeS_4), have now been structurally characterised. This type of *cis-trans* isomerism about the same metal ion has not been previously observed for these ligands; it further demonstrates the poor ability of the tetrathia crowns to impose a tetragonal geometry onto a metal ion, in contrast to their tetraaza analogues.

No stable Ni^{III} or Ni^{I} species could be generated from any of the above Ni/S_4 complexes. This is unsurprising,

given the low stability of the Ni^{II} precursors. The investigation of Ni^{I} thioether complexes will require ligands more effective at encapsulating metal ions that these S_4 macrocycles (Chapter 4).

2.4 EXPERIMENTAL

2.4.1 Synthesis of $[Ni_2([12]aneS_4)_2Cl_2](BF_4)_2$

Reaction of anhydrous $NiCl_2$ (0.021 g, $1.6x10^{-4}$ mol) with $[12]aneS_4$ (0.036 g, $1.6x10^{-4}$ mol) in nitromethane (4 cm^3) at 298K for 30 mins afforded a pale green precipitate. Addition of an excess of $NaBF_4$ caused this precipitate to dissolve, giving a green solution. The solution was filtered, and reduced to half its volume. Addition of diethyl ether yielded a green solid product, which was recrystallised from nitromethane/diethyl ether and dried *in vacuo* (yield: 46 mg, 68%). Mol. wt. 842.76. Elemental analysis: found C = 22.5, H = 3.83%; calculated for $[C_{16}H_{32}S_8Cl_2Ni_2](BF_4)_2$: C = 22.8, H = 3.80%. F.a.b. mass spectrum: found M^+ = 753, 666, 333, 298; calculated for

$[^{58}Ni_2{}^{35}Cl_2([12]aneS_4)_2(^{11}BF_4)]^+$	M^+ = 753
$[^{58}Ni_2{}^{35}Cl_2([12]aneS_4)_2]^+$	M^+ = 666
$[^{58}Ni{}^{35}Cl([12]aneS_4)]^+$	M^+ = 333
$[^{58}Ni([12]aneS_4)]^+$	M^+ = 298

UV/vis spectrum (MeCN): λ_{max} = 980 nm (ε = 25.6 $dm^3 mol^{-1} cm^{-1}$), 608 (30.7), 384 (93.2), 288 (407), 244 (4,125). I.R. spectrum (KBr disc): 2960 m, 2920 m, 2840 w, 1425 s, 1410 s, 1300 m, 1255 s, 1205 s, 1180 w, 1060 vs, 1030 w, 990 w, 950 m, 915 m, 895 w, 850 m, 840 w, 820m, 800 m, 770 w, 675 w, 655 w, 525 s, 425 w cm^{-1}.

2.4.2 Single Crystal Structure of $[Ni_2([12]aneS_4)_2Cl_2](BF_4)_2.2CH_3NO_2$

Pale green plates suitable for X-ray diffraction were obtained by vapour diffusion of diethyl ether into a solution of the complex in $MeNO_2$.

Crystal Data:

$[C_{16}H_{32}S_8Cl_2Ni_2](BF_4)_2(CH_3NO_2)_2$, Mr = 964.82, a = 11.0651(20), b = 13.4977(24); c = 12.7222(21) Å, β = 104.824(21)°, V = 1836.86 Å^3 (by least squares refinement on diffraction angles for 44 reflections measured at $\pm\omega$ [$20<2\theta<25°$, λ = 0.71073 Å]), Z = 2, D_C = 1.616 g cm^{-3}. Crystal dimensions 0.27 x 0.39 x 0.06 mm, μ(Mo-K_α) = 1.683 mm^{-1}, $F(000)$ = 984.

Data Collection and Processing:

Stöe STADI-4 four-circle diffractometer, $\omega/2\theta$ scan mode, with ω scan width (1.20 + 0.347 tan θ)°. Graphite-monochromated Mo-K_α radiation; 1266 reflections measured ($2\theta_{max}$ = 45°, h - 11→11, k0→14, l0→13), giving 809 with $F>6\sigma(F)$. No absorption correction. Crystal decay of 18% was observed, and corrected for, during data collection.

Structure Analysis and Refinement:

The Ni position was located using a Patterson synthesis, and input to DIRDIF which located the Cl and S atoms. Iterative rounds of least-squares refinement and

difference Fourier synthesis located all other non-H atoms. At isotropic convergence, an empirical absorption correction was made using DIFABS (maximum correction 1.185, minimum 0.691). Anisotropic thermal parameters were refined for all non-H atoms, and H atoms were included in fixed, calculated positions. The weighting scheme $w^{-1} = \sigma^2(F) + 0.001158F^2$ gave satisfactory agreement analyses. At final convergence $R = 0.0439$, $R_w = 0.0557$ and $S = 1.131$ for 119 independent parameters, and the final difference Fourier synthesis showed maximum and minimum residuals +0.61 and -0.44 eÅ^{-3} respectively.

2.4.3 Synthesis of $[Ni_2([14]aneS_4)_2Cl_2](BF_4)_2$

Method as for 2.4.1 above, using $[14]aneS_4$ (0.040 g, 1.6×10^{-4} mol). The product was isolated as a pale blue microcrystalline solid (yield: 45 mg, 67%). Mol. wt. 898.87. Elemental analysis: found C = 26.7, H = 4.39%; calculated for $[C_{20}H_{40}S_8Cl_2Ni_2](BF_4)_2$: C = 26.7, H = 4.45%. F.a.b. mass spectrum: found M^+ = 809, 722, 361, 326; calculated for

$[^{58}Ni_2{}^{35}Cl_2([14]aneS_4)_2(^{11}BF_4)]^+$ $M^+ = 809$

$[^{58}Ni_2{}^{35}Cl_2([14[aneS_4)_2]^+$ $M^+ = 722$

$[^{58}Ni{}^{35}Cl([14]aneS_4)]^+$ $M^+ = 361$

$[^{58}Ni([14]aneS_4)]^+$ $M^+ = 326$

UV/vis spectrum (MeCN): λ_{max} = 915 nm (ε_{max} = 35.9 dm^{3}mol^{-1} cm^{-1}), 598 (25.7), 380 (sh), 284 (922), 244 (4,670). I.R. spectrum (KBr disc): 2950 m, 2910 m, 2840 w, 1400 s, 1305

m, 1290 m, 1255 w, 1245 m, 1195 w, 1155 w, 1060 vs, 1030 w, 980 w, 920 m, 865 s, 845 m, 810 w, 800 w, 770 w, 690 w, 525 s, 460 w cm^{-1}.

2.4.4 Single Crystal Structure of $[Ni_2([14]aneS_4)_2Cl_2)](BF_4)_2.6CH_3NO_2$

Vapour diffusion of diethyl ether into a nitromethane solution of the complex yielded blue columns of crystallographic quality. A suitable single crystal was selected, and kept under solid CO_2 whilst being mounted on a glass fibre, and then cooled to 173K with an Oxford Cryosystems low temperature device.

Crystal Data:

$[C_{20}H_{40}S_8Cl_2Ni_2](BF_4)_2(CH_3NO_2)_6$, Mr = 1,265.05, Triclinic, space group $P\bar{1}$, a = 10.6341(18), b = 11.6841(22), c = 12.2457(25) Å, α = 88.547(7), β = 67.288(12), γ = 68.647(6)°, V = 1,295.37 $Å^3$ (by least squares refinement on diffraction angles for 32 reflections measured at $\pm\omega$ [$30<2\theta<32°$, λ = 0.71073 Å]), Z = 1, D_C = 1.621 g cm^{-3}. Crystal dimensions 0.77 x 0.23 x 0.17 mm, μ(Mo-K_α) = 1.226 mm^{-1}, $F(000)$ = 652.

Data Collection and Processing:

Stöe STADI-4 diffractometer, $\omega/2\theta$ scan mode using the learnt profile method. Graphite monochromated Mo-K_α radiation; 3300 reflections measured ($2\theta_{max}$ = 45°,

h-10→10, k-12→12, l0→13) giving 2790 with $F>6\sigma(F)$. No crystal decay, no absorption correction.

Structure Solution and Refinement:

The structure was solved using automatic direct methods in the space group $P1$, and developed by least squares refinement and difference Fourier synthesis. After an initial refinement, the observed high number of matrix correlations implied that this model was of too low a symmetry. Hence, after remerging the data and shifting the atomic coordinates so that the crystallographic inversion centre lay between the Ni atoms, a further refinement was carried out in the space group $P\bar{1}$. During refinement, the BF_4^- counterion was found to be disordered; this was modelled using partial F atoms, such that the total number of F atoms equalled four. One nitromethane solvent molecule was also disordered, and was similarly modelled using partial O atoms. Anisotropic thermal parameters were refined for Ni, S, Cl, F, N and O atoms with site occupancy factor >½, and H atoms were included in fixed, calculated positions. The weighting scheme $w^{-1} = \sigma^2(F) + 0.000031\ F^2$ gave satisfactory agreement analyses. At convergence $R = 0.0630$, $R_w = 0.0742$, $S = 1.146$ for 245 parameters, and in the final ΔF synthesis the maximum and minimum residual peaks were +1.15 and -0.73 eÅ^{-3} respectively.

2.4.5 Synthesis of $[Ni_2([16]aneS_4)_2Cl_2](BF_4)_2$

The method described for 2.4.1 was followed, using $[16]aneS_4$ (0.044 g, $1.6x10^{-4}$ mol). The product was a green solid (yield: 52 mg, 73%). Mol. wt. 954.98. Elemental analysis: found C = 29.8, H = 5.08%; calculated for $[C_{24}H_{48}S_8Cl_2Ni_2](BF_4)_2$: C = 30.2, H = 5.03%. F.a.b. mass spectrum: found M^+ = 778, 389, 354; calculated for

$[^{58}Ni_2{}^{35}Cl_2([16]aneS_4)_2]^+$ $M^+ = 778$

$[^{58}Ni^{35}Cl([16]aneS_4)]^+$ $M^+ = 389$

$[^{58}Ni([16]aneS_4)]^+$ $M^+ = 354$

UV/vis spectrum (MeCN): λ_{max} = 970 nm (ε_{max} = 19.1 $dm^3 mol^{-1} cm^{-1}$), 566 (32.5), 370 (sh), 312 (8,520), 256 (7,180). I.R. spectrum (KBr disc): 2900 s, 2840 m, 1440 s, 1425 s, 1290 s, 1250 m, 1190 w, 1145 w, 1060 vs, 990 w, 945 w, 930 w, 880 s, 840 m, 770 s, 720 w, 695 w, 650 w, 525 s, 460 w cm^{-1}.

2.4.6 Single Crystal Structure of $[Ni_2([16]aneS_4)_2Cl_2](BF_4)_2.2CH_3NO_2$

Vapour diffusion of diethyl ether into a solution of the complex in nitromethane gave green plates suitable for x-ray diffraction. A single crystal was selected and placed in a 0.5 mm capillary tube to prevent solvent loss. The tube was then cooled to 173K with an Oxford Cryosystems low temperature device.

Crystal Data:

$[C_{24}H_{48}S_8Cl_2Ni_2](BF_4)_2(CH_3NO_2)_2$, Mr = 1,077.04, Monoclinic, space group Cc, a = 16.0240(49), b = 13.6862(17), c = 19.7329(24) Å, β = 92.042(19)°, V = 4324.82 Å^3 (by least squares refinement on diffraction angles for 28 reflections measured at $\pm\omega$ [$30<2\theta<32°$, λ = 0.71073 Å]), Z = 4, D_C = 1.654 g cm^{-3}. Crystal dimensions 0.60 x 0.35 x 0.25 mm, μ(Mo-K$_\alpha$) = 1.439 mm^{-1}, $F(000)$ = 2224.

Data Collection and Processing:

Stöe STADI-4 diffractometer, $\omega/2\theta$ scan mode using the learnt profile method. Graphite monochromated Mo-K$_\alpha$ radiation; 3925 reflections measured ($2\theta_{max}$ = 45°, h-17→17, k0→14, l0→21), 2834 unique (R_{int} = 0.0290), giving 2800 with $F>6\sigma(F)$. No significant crystal decay, no absorption correction.

Structure Analysis and Refinement:

The Ni positions were deduced from a Patterson synthesis, and iterative cycles of least squares refinement and difference Fourier syntheses located the other non-hydrogen atoms. During refinement one BF_4^- counterion was found to be disordered; this was modelled using partially occupied F atoms, such that the total number of F atoms equalled four. H atoms were included in fixed, calculated positions. Anisotropic thermal

parameters were refined for all Ni, S, N, O, B and F atoms. The weighting scheme $w^{-1} = \sigma^2(F) + 0.000041 F^2$ gave satisfactory agreement analyses. At final convergence $R = 0.0373$, $R_w = 0.0498$, $S = 1.158$ for 370 independent parameters, and the final difference Fourier synthesis showed no feature above 0.41 or below -0.39 eÅ^{-3}.

2.4.7 Synthesis of $[Ni_2([9]aneS_3)_2Cl_3]BF_4$

Method as in 2.4.1, substituting [9]aneS$_3$ (0.030 g, 1.6x10^{-4} mol) as the macrocyclic ligand. Fractional recrystallisation from MeCN/ether was necessary to remove a substantial amount of $[Ni([9]aneS_3)_2](BF_4)_2$ by-product[70]. The complex was a green crystalline solid (yield = 25 mg, 45%). Mol. wt. 671.22. Elemental analysis: found C = 21.5, H = 3.80%; calculated for $[C_{12}H_{24}S_6Cl_3Ni_2](BF_4)$ C = 21.5, H = 3.60%. F.a.b. mass spectrum: found M^+ = 581, 546, 238; calculated for

$[^{58}Ni_2{}^{35}Cl_3([9]aneS_3)_2]^+$ $M^+ = 581$

$[^{58}Ni_2{}^{35}Cl_2([9]aneS_3)_2]^+$ $M^+ = 546$

$[^{58}Ni([9]aneS_3)]^+$ $M^+ = 238$

UV/vis spectrum (MeCN): λ_{max} = 1026 nm (ε_{max} = 79.9 dm^3 mol^{-1}cm^{-1}), 653 (37.3), 352 (sh), 286 (9,150), 256 (6,770), 210 (sh). I.R. spectrum (KBr disc): 2950 m, 2920 m, 2840 w, 1445 m, 1410 s, 1380 w, 1300 m, 1280 m, 1255 w, 1060 vs, 930 m, 900 m, 825 m, 765 w, 720 w, 700 w, 670 w, 620 w, 550 w, 525 m, 470 w, 430 m cm^{-1}.

2.4.8 Single Crystal Structure of $[Ni_2([9]aneS_3)_2Cl_3](BF_4).CH_3CN$

Single crystals of X-ray quality were obtained by vapour diffusion of diethyl ether into an acetonitrile solution of the compound. A single crystal was selected, sealed in a "3-in-1" oil film to prevent solvent loss, mounted on a glass fibre and cooled to 150K with an Oxford Cryosystems low temperature device.

Crystal Data:

$[C_{12}H_{24}S_6Cl_3Ni_2](BF_4).CH_3CN$, Mr = 712.28, Monoclinic, space group $P2_1/c$, a = 12.379(5), b = 13.790(6), c = 16.031(6) Å, β = 99.73(4)°, V = 2697 Å^3 (by least squares refinement on diffraction angles for 23 reflections measured at $\pm\omega$ [$20<2\theta<22°$, λ = 0.71073 Å]), Z = 4, D_C = 1.754 g cm^{-3}. Crystal dimensions 0.70 x 0.21 x 0.08 mm, μ(Mo-K_α) = 2.184 mm^{-1}, $F(000)$ = 1448.

Data Collection and Processing:

Stöe STADI-4 diffractometer, $\omega/2\theta$ scan mode with ω scan width (1.32 + 0.347 tan θ)°. Graphite-monochromated Mo-K_α radiation; 4448 reflections measured ($2\theta_{max}$ = 45°, h-13→13, k0→14, l0→17), 3084 unique (R_{int} = 0.0496), giving 2173 with $F>4\sigma(F)$. No significant crystal decay, no absorption correction.

Structure Analysis and Refinement:

A Patterson synthesis located the Ni atom positions, and the structure was developed by successive cycles of least squares refinement and difference Fourier syntheses. During refinement the BF_4^- counterion was found to be disordered; this was modelled with partially occupied F atoms, such that the total number of F atoms equalled four. Anisotropic thermal parameters were refined for all Ni, S, Cl, C, N, B and ordered F atoms, and H atoms were included in fixed, calculated positions. The weighting scheme $w^{-1} = \sigma^2(F) + 0.000664\ F^2$ gave satisfactory agreement analyses. At final convergence $R = 0.0562$, $R_w = 0.0640$ and $S = 1.059$ for 282 parameters, and the final difference Fourier synthesis showed no feature above +0.84 or below -1.11 eÅ^{-3}.

2.4.9 Synthesis of $[Ni([12]aneS_4)(OH_2)_2](BF_4)_2$

Reaction of $Ni(BF_4)_2.6H_2O$ (0.053 g, 1.5×10^{-4} mol) and $[12]aneS_4$ (0.036 g, 1.5×10^{-4} mol) in nitromethane (4 cm^3) and acetic anhydride (1 drop) yielded a deep blue solution. This solution was filtered, and the blue solid product crystallised with diethyl ether (yield 0.042 g, 56%). Mol. wt. 508.70. Elemental analysis: found C = 20.2, H = 3.75%; calculated for $[C_8H_{16}S_4Ni(OH_2)](BF_4)_2$ C = 19.6, H = 3.70%. F.a.b. mass spectrum: found M^+ = 404, 385, 317, 298; calculated for

$[^{58}Ni([12]aneS_4)(OH_3)(^{11}BF_4)]^+$ $M^+ = 404$

$[^{58}Ni([12]aneS_4)(^{11}BF_4)]^+$ $M^+ = 385$

$[^{58}Ni([12]aneS_4)(OH_3)]^+$ $M^+ = 317$

$[^{58}Ni([12]aneS_4)]^+$ $M^+ = 298$

UV/vis spectrum (CH_3NO_2): λ_{max} = 1035 nm (ε_{max} = 74.0 $dm^3 mol^{-1} cm^{-1}$), 951 (97), 577 (33.3). UV/vis spectrum (CH_3CN): λ_{max} = 1020 nm (sh), 943 (ε_{max} = 13.8 $dm^3 mol^{-1} cm^{-1}$), 578 (8.1), 306 (485). I.R. spectrum (KBr disc) 2980 w, 2960 w, 2920 w, 1430 s, 1410 s, 1380 w, 1305 m, 1285 w, 1255 m, 1205 w, 1190 w, 1060 vs, 950 w, 930 w, 910 m, 890 m, 855 s, 840 m, 820 w, 770 m, 740 w, 705 w, 690 m, 675 m, 655 w, 615 m, 525 s, 430 m, 415 w, 330 w cm^{-1}.

2.4.10 Synthesis of $[Ni([14]aneS_4)](PF_6)_2$[68]

$NiCl_2.6H_2O$ (0.032 g, $1.4x10^{-4}$ mol) was stirred with $TlPF_6$ (0.094 g, $2.8x10^{-4}$ mol) in nitromethane (4 cm^3) in the presence of acetic anhydride (1 drop) for 30 mins. The resulting pale green solution was filtered, and $[14]aneS_4$ (0.040 g, $1.4x10^{-4}$ mol) added to the filtrate. After a further 30 mins stirring the red solution was reduced to ½ its original volume, and the red crystalline product crystallized with diethyl ether (yield 0.065 g, 78%). Mol. wt. 617.02. Elemental analysis: found C = 19.7, H = 3.33%; calculated for $[C_{10}H_{20}S_4Ni](PF_6)_2$ C = 19.5, H = 3.27%. F.a.b. mass spectrum: found M^+ = 471, 326; calculated for:

$[^{58}Ni([14]aneS_4)(PF_6)]^+$ $M^+ = 471$

$[^{58}Ni([14]aneS_4)]^+$ $M^+ = 326$

^{1}H nmr spectrum (200.13 MHz, CD_3NO_2, 298 K) δ = 3.80 - 1.95 ppm (M, CH_2). ^{13}C D.E.P.T. nmr spectrum[108] (50.32 MHz, CD_3NO_2, 298 K). δ = 36.21 ppm (s), 35.19 (s), 24.37 (s) (major isomer), 37.95 (s), 33.07 (s), 23.76 (s) (minor isomer) (CH_2). UV/vis spectrum (CH_3NO_2): λ_{max} = 490 nm (ε_{max} = 310 $dm^3 mol^{-1} cm^{-1}$), 423 (127). UV/vis spectrum (CH_3CN): λ_{max} = 925 nm (ε_{max} = 7.8 $dm^3 mol^{-1} cm^{-1}$), 562 (10.3), 304 (495). I.R. spectrum (KBr disc) 3000 s, 2940 m, 2840 w, 1425 s, 1380 w, 1365 w, 1300 w, 1285 s, 1250 w, 1235 w, 1200 w, 1155 w, 1120 m, 1050 w, 1010 w, 935 w, 840 vs, 740 m, 680 w, 645 w, 550 s, 470 m, 435 m, 385 w cm^{-1}.

2.4.11 Synthesis of $[Ni([16]aneS_4)(OH_2)_2](BF_4)_2$

$Ni(BF_4)_2.6H_2O$ (0.053 g, $1.5x10^{-4}$ mol) and $[16]aneS_4$ (0.044 g, $1.5x10^{-4}$ mol) were stirred in nitromethane (4 cm^3) in the presence of a trace of acetic anhydride, yielding a blue solution. This was filtered, and the pale blue solid product crystallised with diethyl ether (yield 0.027 g, 32%). Mol. wt. 564.82. Elemental analysis: found C = 26.7, H = 4.73%; calculated for $[C_{12}H_{24}S_4Ni(OH_2)](BF_4)_2$ C = 26.4, H = 4.79%. F.a.b. mass spectrum: found M^+ = 459, 373, 354; calculated for:

$[^{58}Ni([16]aneS_4)(OH_2)(^{11}BF_4)]^+$ M^+ = 459

$[^{58}Ni([16]aneS_4)(OH_3)]^+$ M^+ = 373

$[^{58}Ni([16]aneS_4)]^+$ M^+ = 354

UV/vis spectrum (CH_3NO_2): λ_{max} = 1005 nm (sh), 928 (ε_{max} = 35.3 $dm^3 mol^{-1} cm^{-1}$), 580 (29.2). UV/vis spectrum (CH_3CN:

λ_{max} = 972 nm (ε_{max} = 7.6 $dm^3 mol^{-1} cm^{-1}$), 580 (11.5), 324 (440). I.R. spectrum (KBr disc): 2940 w, 2900 m, 2840 w, 1440 s, 1420 s, 1300 m, 1290 s, 1250 m, 1060 vs, 990 w, 950 w, 925 m, 875 m, 860 s, 845 m, 795 w, 770 s, 755 w, 745 w, 720 w, 695 w, 645 w, 525 s, 455 m cm^{-1}.

2.4.12 Single Crystal Structure of $[Ni([16]aneS_4)(OH_2)_2](BF_4)_2$

Blue tablets suitable for X-ray diffraction were grown by vapour diffusion of diethyl ether into a nitromethane solution of the complex. A suitable crystal was coated in "3-in-1" oil, mounted on a glass fibre, and placed in the cold stream of an Oxford Cryosystems low temperature device at 150 K.

Crystal Data:

$[C_{12}H_{28}S_4O_2Ni](BF_4)_2$, Mr = 564.82. Triclinic, space group $P\bar{1}$, a = 7.927(4), b = 8.657(5), c = 9.351(5) Å, α = 67.106(20), β = 79.764(23), γ = 66.898 (24)°, V = 543.5 $Å^3$ (by least-squares refinement on diffraction angles for 38 reflections measured at $\pm\omega[31<2\theta<32°$, λ = 0.71073 Å]), Z = 1, D_C = 1.725 g cm^{-3}. Crystal dimensions 0.95 x 0.82 x 0.51 mm, μ(Mo-K_α) = 1.338 mm^{-1}, $F(000)$ = 290.

Data Collection and Processing:

Stöe STADI-4 diffractometer, $\omega/2\theta$ scan mode with ω scan width (0.99 + 0.347 tan θ)°. Graphite monochromated

Mo-K_α radiation; 1427 reflections measured ($2\theta_{max}$ = 45°, h = -8→8, k = -8→9, l = 0→10), 1424 unique, giving 1393 with $F>4\sigma(F)$. An initial absorption correction was applied using ψ-scan data (maximum transition factor 0.5387, minimum 0.2398). No significant crystal decay.

Structure Analysis and Refinement:

Consideration of the observed unit cell volume, together with the assumed unit cell contents, implied that the Ni atom must lie on the crystallographic inversion centre. This assumption was confirmed when the structure was developed, using iterative cycles of least-squares refinement and difference Fourier synthesis. Anisotropic thermal parameters were refined for all non-H atoms; an isotropic thermal parameter was also refined for the H atoms. Macrocyclic H atoms were included in fixed, calculated positions; the water H atom positions were refined, using the constrained distances O-H = 0.96 Å, H-O-H = 1.568 Å. The weighting scheme $w^{-1} = \sigma^2(F) + 0.000010F^2$ gave satisfactory agreement analysis. At final convergence R = 0.0381, R_w = 0.0488, S = 1.366 for 140 independent parameters, and in the final difference Fourier synthesis the maximum and minimum residuals were +0.86 and -0.75 eÅ^{-3} respectively.

CHAPTER 3

FIVE-COORDINATE NICKEL (II) COMPLEXES OF [9]aneS$_3$ AND [15]aneS$_5$

3.1 INTRODUCTION

One of the first complexes of the small ring macrocycle [9]aneS_3 to be characterised was the homoleptic hexathia species $[Ni([9]aneS_3)_2]^{2+}$ [70]. This was shown to adopt an octahedral geometry, with a small tetragonal elongation (Figure 3.1). The electrochemistry of this complex was first reported by Wieghardt *et al.*[130], and was found to show a chemically reversible oxidation (at +0.97V vs Fc/Fc^+) and a quasi-reversible reduction (at -1.11V).

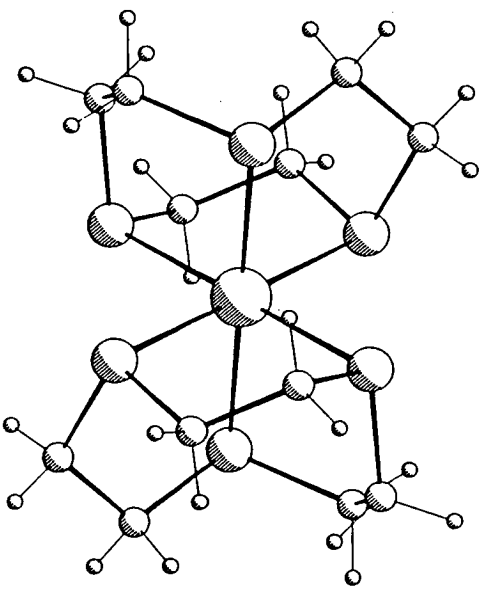

Figure 3.1: View of the Single Crystal Structure of $[Ni([9]aneS_3)_2]^{2+}$

A more recent study showed that the reduction product of $[Ni([9]aneS_3)_2]^{2+}$ was highly unstable, preventing its full characterisation[74], this was surprising, given the known ability of multidentate S- and P-donor ligands to stabilise Ni^I (Section 4.1). We argued that the

instability of $[Ni([9]aneS_3)_2]^+$ was likely to be stereochemical in origin, as the vast majority of known Ni^I complexes adopt four- or five-coordinate geometries. Therefore, the synthesis and characterisation of a series of five-coordinate complexes of type $[Ni([9]aneS_3)(PP)]^{2+}$ was undertaken, (PP = chelating diphosphine ligand), in the hope of using these as precursors to stable Ni^I complexes. The homoleptic pentathia complex $[Ni([15]aneS_5)]^{2+}$ was also investigated for the same reason.

The synthesis and structural characterisation of these compounds is reported here; their electrochemistry is described in Chapter 4. An introductory account of the chemistry of $[9]aneS_3$ is now presented[114].

LIGAND SYNTHESIS

The original synthesis of $[9]aneS_3$ utilised the same high-dilution cyclisation methodology as the early syntheses of the S_4 macrocycles[70,131] (Section 2.1). Yields from these preparations were correspondingly low (< 5%), and the in-depth study of the coordination chemistry of this ligand only became feasible with the publication by Sellman and Zapf of a high yield synthesis based on a $[Mo(CO)_3]$ template[132].

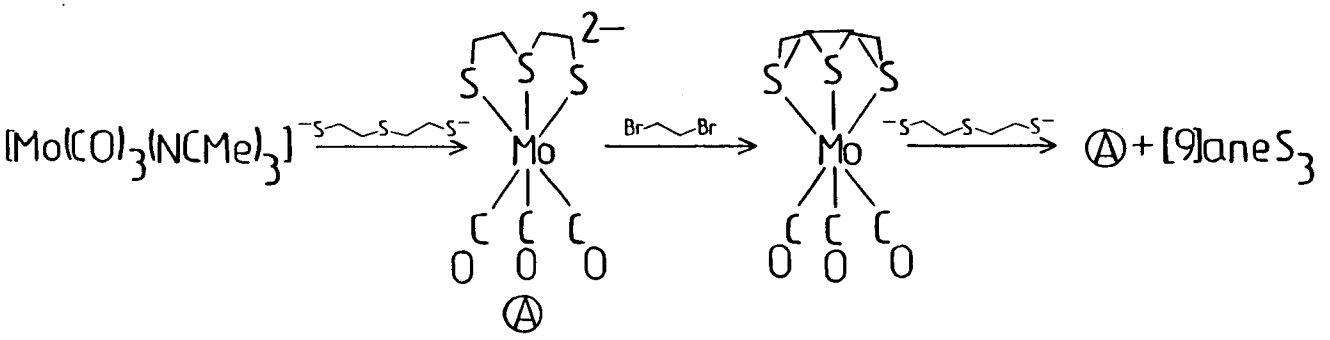

More recently, a synthesis using a Cs_2CO_3-promoted cyclisation has also been reported[133].

COORDINATION CHEMISTRY

The single crystal structure of [9]aneS_3 shows the macrocycle to adopt an endo conformation, with internal C_3 symmetry (Figure 3.2)[22]. An electron diffraction study concluded that the C_3 conformation was also present in the gas phase, possibly in equilibrium with other forms[134]. Hence, in contrast to the other crown thioethers, [9]aneS_3 is pre-organised for facial, tridentate binding to a metal

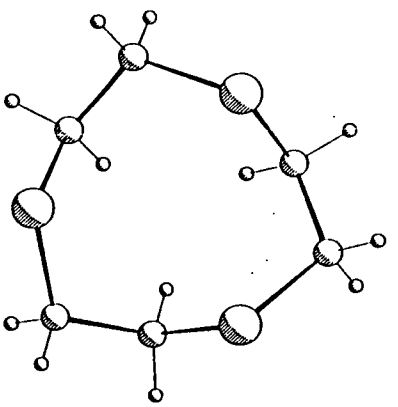

Figure 3.2: View of the Single Crystal Structure of [9]aneS_3

ion, and its complex chemistry is dominated by this mode of coordination[14]. This ligand pre-organisation together with the conformational rigidity of the nine-membered macrocyclic ring, means that [9]aneS$_3$ forms more stable complexes than other poly-thioether macrocycles, with shorter metal-sulphur bond lengths[14].

The homoleptic hexathia complexes [M([9]aneS$_3$)$_2$]$^{n+}$ have been particularly well studied. In these compounds, [9]aneS$_3$ has shown a remarkable ability to adapt to the conformational requirements of a particular metal ion. At the same time, however, the inherent preference of the *bis*-[9]aneS$_3$ ligand set for octahedral coordination tends to stabilise any metal centre favouring an octahedral geometry, leading to some novel redox behaviour. The metal ions in such octahedral complexes are fully encapsulated by the macrocyclic ligands, and so are protected from attack by external agents.

A good example of both these properties is the series of complexes [Au([9]aneS$_3$)$_2$]$^{+/2+/3+}$ [64,67a]. [Au([9]aneS$_3$)$_2$]$^+$ can be prepared by the reaction of [9]aneS$_3$ with [Au(tht)$_2$]$^+$ (tht = tetrahydrothiophene) or [AuCl$_4$]$^-$ under reducing conditions. The single crystal structure of [Au([9]aneS$_3$)$_2$]$^+$ shows a "tetrahedrally distorted linear" geometry about the Au centre, with one mono-dentate and one asymmetric facially bound [9]aneS$_3$ ligand [Au-S = 2.302(6), 2.350(7), 2.733(8), 2.825(8) Å, Figure 3.3c]. Chemical oxidation of this complex in HClO$_4$

a) $[Au([9]aneS_3)_2]^{3+}$

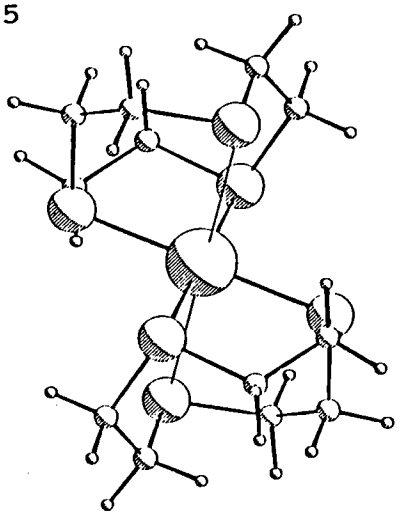

b) $[Au([9]aneS_3)_2]^{2+}$

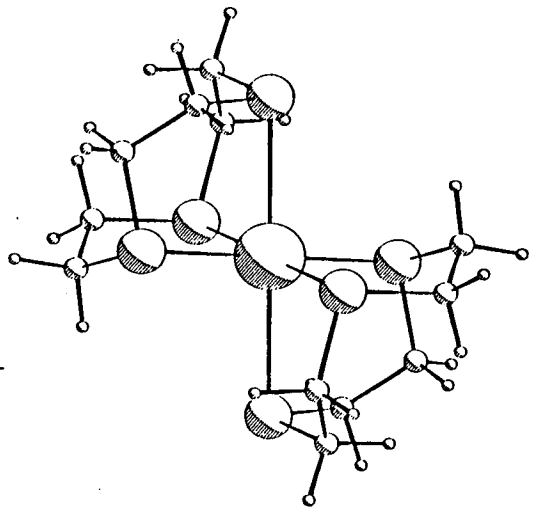

c) $[Au([9]aneS_3)_2]^{+}$

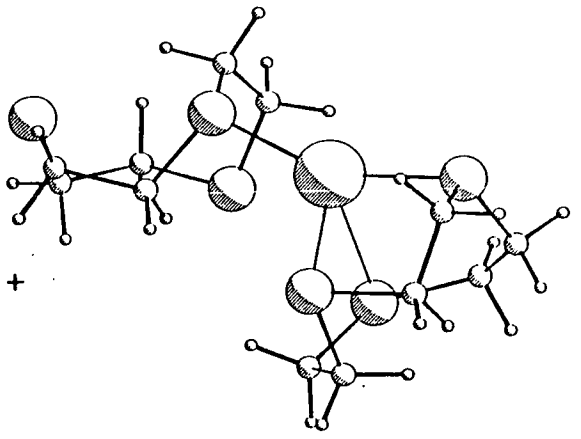

Figure 3.3: Views of the Single Crystal Structures of $[Au([9]aneS_3)_2]^{n+}$

yields the tetragonal $[Au([9]aneS_3)_2]^{3+}$ [Au-S = 2.348(4), 2.354(4), 2.926(4) Å, Figure 3.3a]. Oxidation of the Au^{I} complex in HBF_4 affords the green paramagnetic species $[Au([9]aneS_3)_2]^{2+}$, which also adopts a tetragonally elongated octahedral stereochemistry [Au-S = 2.452(5), 2.462(5), 2.839(5) Å, Figure 3.3b]. The stabilisation of mononuclear Au^{II} is highly unusual; here it is achieved by a combination of the stereochemical preference of $[9]aneS_3$ for tridentate coordination, together with the preference of the thioether donors for a softer metal centre. Similar considerations have led to the stabilisation of octahedral d^7 Rh^{II}, Pd^{III} and Pt^{III} metal centres by this ligand[60-63].

Several half- and mixed-sandwich complexes of $[9]aneS_3$ have also been prepared and structurally characterised. A series of octahedral Ru^{II} and Os^{II} complexes $[M([9]aneS_3)(L^1)(L^2)(L^3)]^{n+}$ (L^1-L^3 = Hal^-, H^-, CO, CS, PR_3, NCMe), has been described[59,80]. A structural and spectro-electrochemical investigation has shown that $[9]aneS_3$ can act as both a Π-donor and Π-acceptor ligand in these compounds[59]. $[Ru([9]aneS_3)(PPh_3)Cl_2]$ has been shown to oxidise diethyl ether or THF to furan (29)[80].

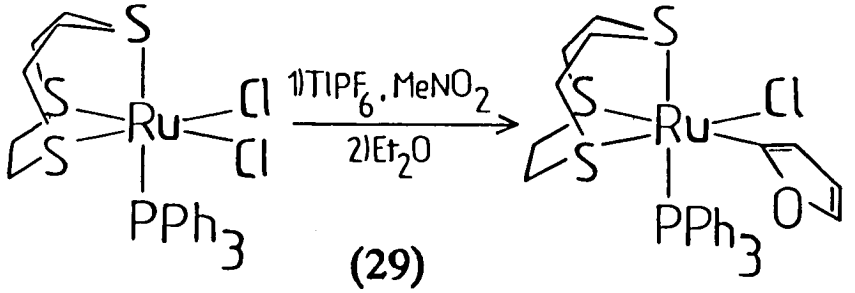

(29)

The mixed sandwich complexes $[M([9]aneS_3)(L)]^{n+}$ (M = Ru, Os, Rh, Ir; L = $(C_5Me_5)^-$, C_6Me_6, p-cymene) have been characterised[135]. $[Fe([9]aneS_3(C_5H_5)]^+$ exhibits a one-electron oxidation at +0.44V vs. Fc/Fc^+ in $CH_3CN/^nBu_4NPF_6$, midway between those of $[Fe([9]aneS_3)_2]^{2+}$ and $[Fe(C_5H_5)_2]$[136].

In contrast to $[9]aneS_3$, $[12]aneS_3$ adopts a square exodentate conformation in the solid state. As a result, the coordination chemistry of this ligand resembles that of the tetrathia macrocycles (Chapter 2), with exo- and endocyclic complexes being known[21,61,66b,137]. The single crystal structures of the 10-membered macrocyclic complexes $[Fe([10]aneS_3)]^{2+}$ and $[Ni(keto\text{-}[10]aneS_3)_2]^{2+}$ (30) have recently been reported[138]; both exhibit octahedral stereochemistries.

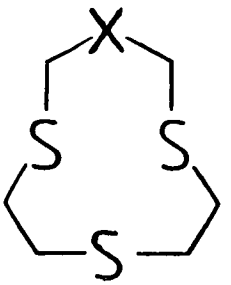

X=CH$_2$: [10]aneS$_3$
X=CO: keto-[10]aneS$_3$

(30)

3.2 RESULTS AND DISCUSSION

3.2.1 $[Ni([9]aneS_3)(PP)](PF_6)_2$ (PP = dppm, dppe, dppv, dcpe, dmpe, dppp, tdpme).

The reaction of the known starting materials $[Ni(PP)Cl_2]$ (Figure 3.4)[139-139] with $[9]aneS_3$ in the presence of a halide abstracting agent such as NH_4PF_6 or $TlPF_6$ yielded intense green or red solutions, from which solid products could be isolated in high yields by the addition of diethyl ether.

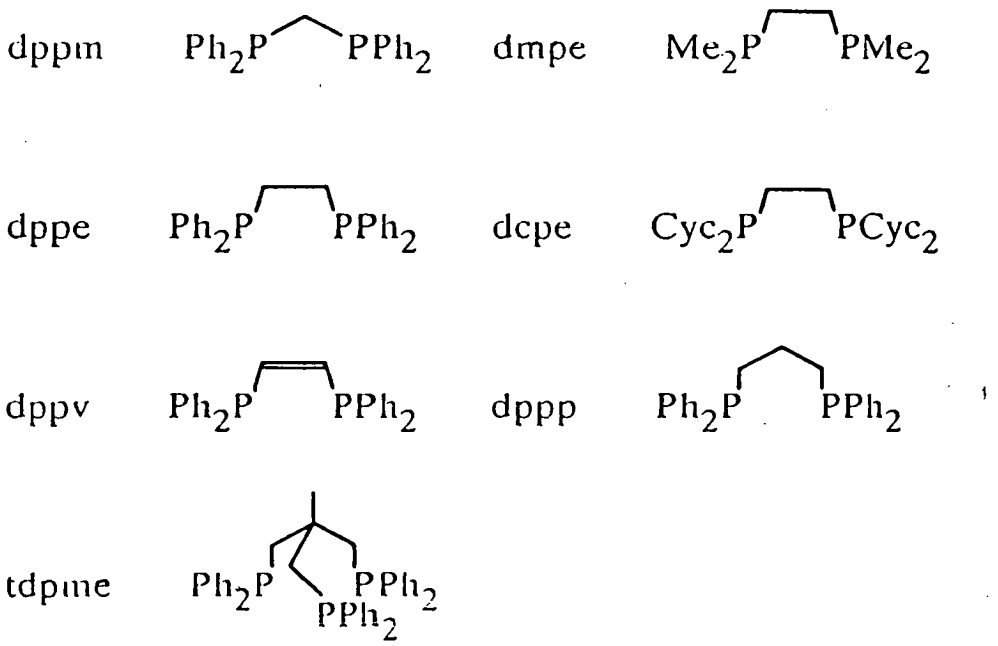

Figure 3.4: Phosphine Ligands Used in This Work.

Fractional recrystallisation of these compounds by vapour diffusion of diethyl ether into CH_3CN solutions of the products enabled the removal of a relatively insoluble pink impurity, which was identified as $[Ni([9]aneS_3)_2]^{2+}$.

This contamination was particularly severe for compounds containing strained or sterically crowded phosphine ligands (PP = dppm, dcpe, dppp).

All seven of these products exhibited similar physical and spectral characteristics. Their elemental analyses, and I.R. and f.a.b. mass spectra (Table 3.1) were all consistent with the proposed formulation. The complexes were all diamagnetic in solution, and gave well resolved n.m.r. spectra (Figure 3.5). In particular, their ^{13}C n.m.r. spectra exhibited a single resonance in the region expected for [9]aneS_3, implying that the macrocyclic C atoms are equivalent in solution. No decoalescence of this [9]aneS_3 ^{13}C resonance was observed down to 218K for $[Ni([9]aneS_3)(dppe)]^{2+}$; a similar study of $[Ni([9]aneS_3)(dcpe)]^{2+}$ was not possible due to the lower solubility of this complex. The U.V/visible spectra of these compounds in CH_3CN contained two intense d-d bands, at λ_{max} = 500-600 nm (ε_{max} = 40-150 $dm^3\,mol^{-1}\,cm^{-1}$) and 415-450 nm (600-1800). These are consistent with a five-coordinate geometry, and are assigned to the transitions $^1A_1 \rightarrow {}^1B_1$ and $^1A_1 \rightarrow {}^1E$ for square-pyramidal symmetry (*vide infra*)[114]. The third transition expected for this geometry, $^1A_1 \rightarrow {}^1A_2$, was not observed, however, and was possibly obscured beneath an intense charge-transfer band at *ca.* 320 nm. These data are consistent with the desired five-coordinate species, $[Ni([9]aneS_3)(PP)]^{2+}$ (31).

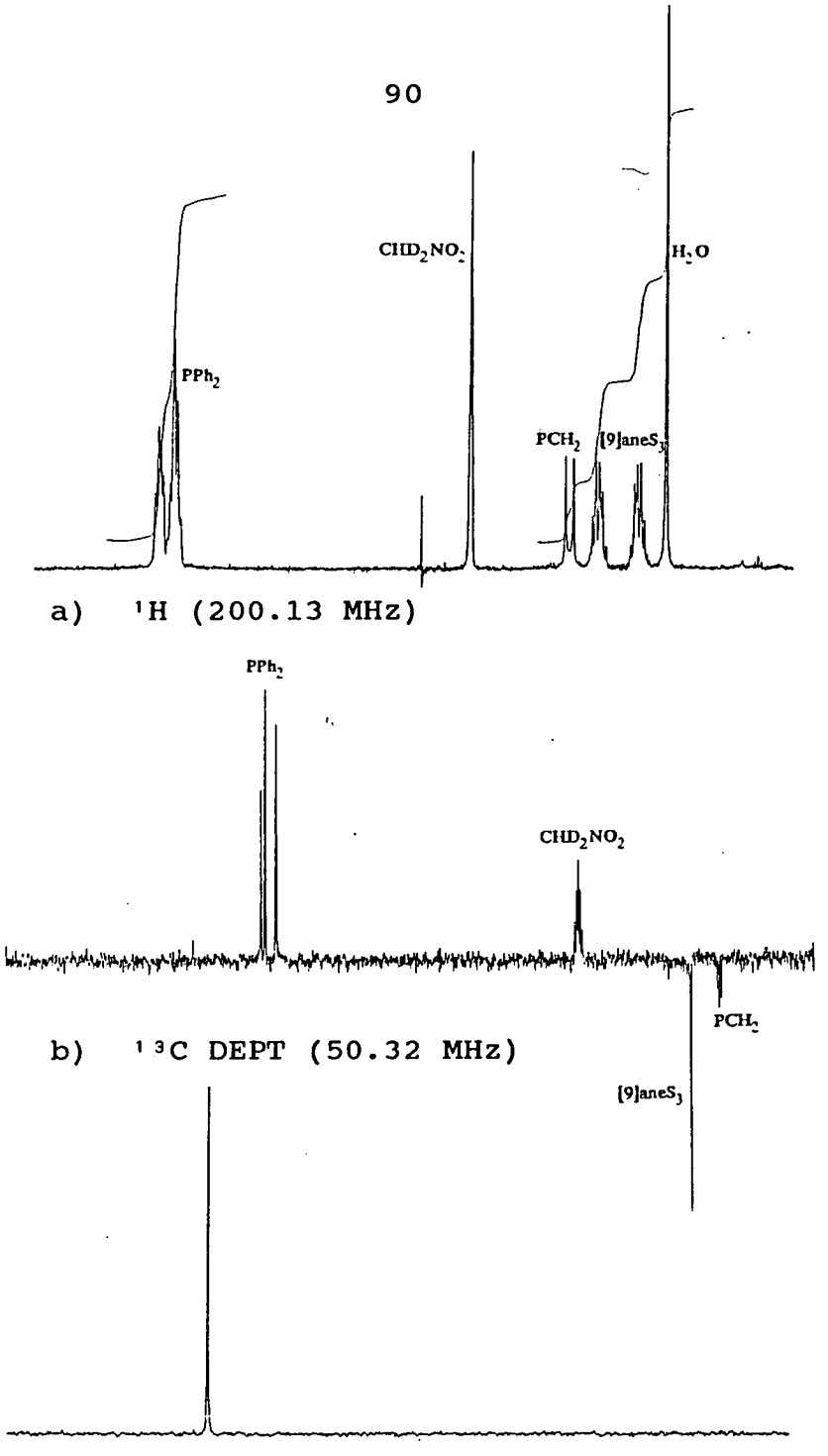

Figure 3.5: N.m.r. Spectra of [Ni([9]aneS$_3$)(dppe)]$(BF_4)_2$(CD_3CN, 298K)

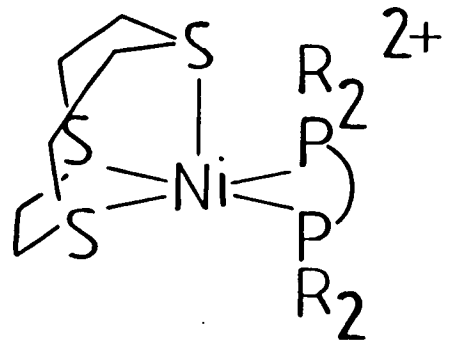

(31)

Molecular ions observed for:

PP	$[^{58}Ni([9]aneS_3)(PP)(PF_6)]^+$	$[^{58}Ni([9]aneS_3)(PP)]^+$
dppm	M^+ = 766 (calculated 767)	622(622)
dppe	781(781)	635(636)
dppv	779(779)	634(634)
dcpe	805(805)	660(660)
dmpe	533(533)	388(388)
dppp	794(795)	650(650)
tdpme	1007(1007)	861(862)

Table 3.1: F.a.b. Mass Spectral Data for $[Ni([9]aneS_3)(PP)](PF_6)_2$

Attempts to synthesise analogous complexes with monodentate phosphines (from $[Ni(PPh_3)_2Cl_2]$[142] and $[Ni(PEt_3)_2Cl_2]$[143], from a sample prepared by E.J.M. Hamilton) and a diarsine chelate (from $[Ni(diars)Cl_2]$[144]) gave $[Ni([9]aneS_3)_2]^{2+}$ as the only isolable product. The reaction of $[Ni(NN)_2Cl_2]$ (NN = 2,2'-bipy, 1,10-phen)[145] with $[9]aneS_3$ under similar conditions afforded a mixture of the pink $[Ni([9]aneS_3)_2]^{2+}$ and maroon $[Ni(NN)_3]^{2+}$ [146]. The reaction of $NiCl_2$ with $[9]aneS_3$ yielded a yellow precipitate, of composition $[Ni([9]aneS_3)Cl_2]$ from its elemental analysis. Surprisingly, the addition of bipy or dppe to this gave only $[Ni([9]\ aneS_3)_2]^{2+}$. This contrasts with the behaviour of $[M([9]aneS_3)Cl_2]$ (M = Pd, Pt), which react with PR_3 or bipy/phen to give $[M([9]aneS_3)(LL)]^{2+}$ in high yields[80].

The single crystal structures of four $[Ni([9]aneS_3)(PP)]^{2+}$ complexes were obtained, for comparison with their Pd and Pt analogues and as an aid to the discussion of their redox behaviour (Chapter 4). Important structural parameters derived from these analyses are listed in Tables 3.15 and 3.16.

3.2.2 Single Crystal Structures of $[Ni([9]aneS_3)(dppm)](PF_6)_2$ and $[Ni([9]aneS_3)(dppe)](PF_6)_2$

The solution and refinement of these structures is described in Sections 3.4.9 and 3.4.11. Relevant bond lengths, angles and torsions are listed in Tables 3.2-3.7,

and ORTEP plots of the two molecules are given in Figures 3.6 and 3.7.

The structure of $[Ni([9]aneS_3)(dppm)](PF_6)_2$ shows the cation to adopt a distorted square-pyramidal geometry. The Ni atom lies 0.262 Å above the basal least-squares S_2P_2 plane (Table 3.16), with a lengthened apical Ni-S bond as expected for a d^8 square-pyramidal species[147] [Ni-S(1) = 2.4007(21), Ni-S(4) = 2.2179(25), Ni-S(7) = 2.2336(24) Å]. The slight asymmetry in the equatorial Ni-S bond lengths may reflect steric interactions between the macrocyclic ring and the dppm phenyl groups (Figure 3.12a). The internal S-Ni-S angles are all *ca.* 90°, because of the rigidity of the $[9]aneS_3$ ring, and the apical Ni-S bond is bent back by 8° from the vertical. The angles within the basal plane are typical for a square pyramidal complex [*trans*-<S-Ni-P = 164.26(9), 162.52(8)°].

The crystal structure of $[Ni([9]aneS_3)(dppe)](BF_4)_2$ was found to contain two independent molecules per asymmetric unit; only minimal structural differences were observed between the two crystallographic cations. The coordination geometry about the Ni centres in this structure is similar to that of the dppm complex [$Ni\text{-}S(1)_{av}$ = 2.390(3), $Ni\text{-}S(4)_{av}$ = 2.246(3), $Ni\text{-}S(7)_{av}$ = 2.226(3), $Ni\text{-}P(1)_{av}$ = 2.190(3), $Ni\text{-}P(2)_{av}$ = 2.190(3) Å]. However, the basal S_2P_2 plane is now slightly distorted [$<S(4)\text{-}Ni\text{-}P(1)_{av}$ = 161.56(13), $<S(7)\text{-}Ni\text{-}P(2)_{av}$ = 169.14(13)°]. It is not known whether this is a result of

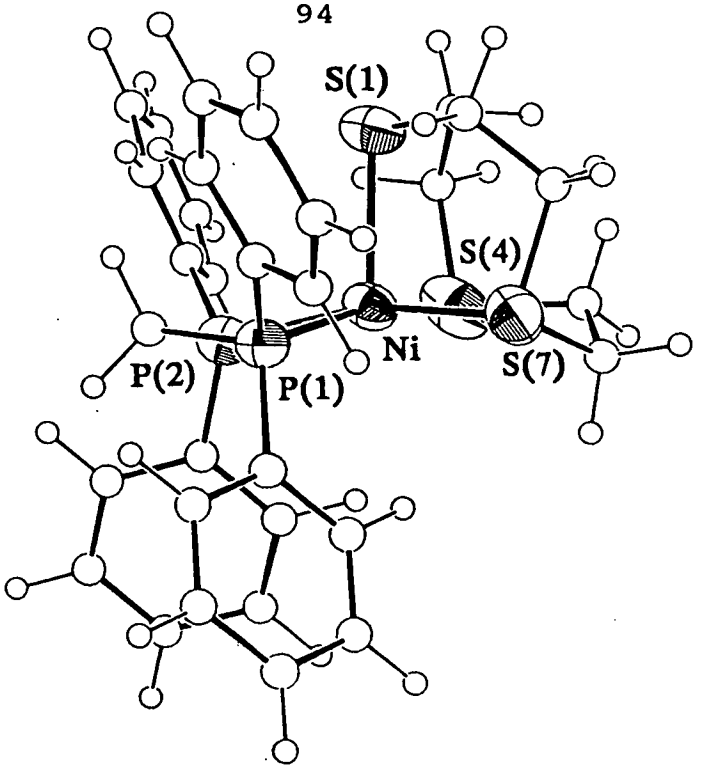

Figure 3.6: View of the Single Crystal Structure of $[Ni([9]aneS_3)(dppm)]^{2+}$

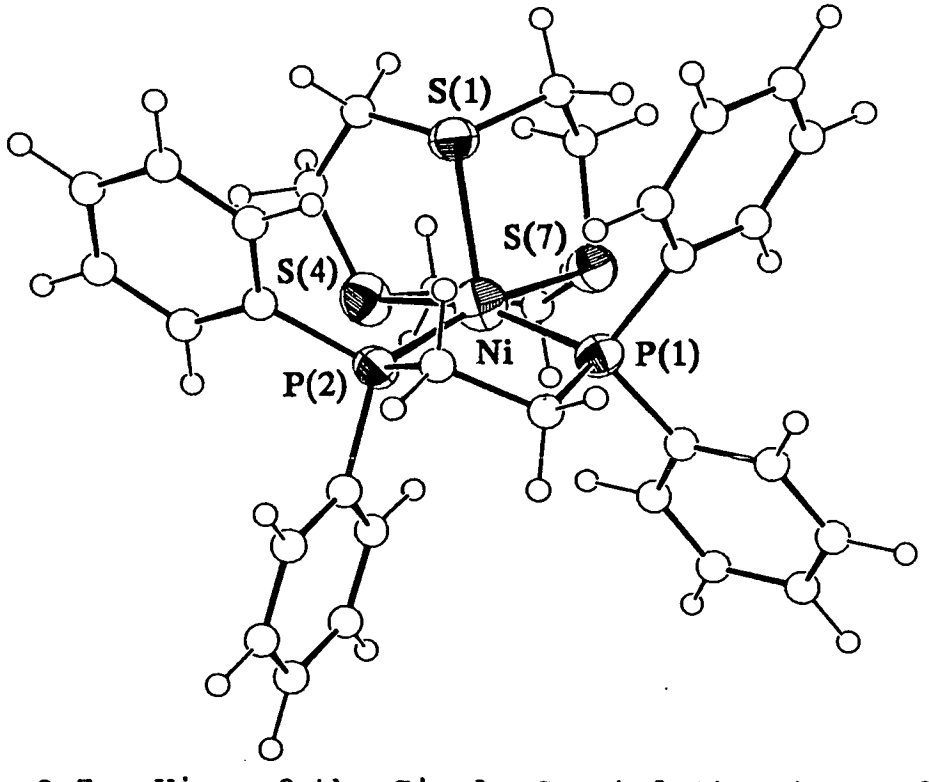

Figure 3.7: View of the Single Crystal Structure of $[Ni([9]aneS_3)(dppe)]^{2+}$ (molecule 1)

Single Crystal Structure of $[Ni([9]aneS_3)(dppm)](PF_6)_2$

Table 3.2. Bond Lengths(A) with standard deviations

Ni	- S(1)	2.4007(21)	P(1)	-C(26)	1.785(5)
Ni	- S(4)	2.2179(25)	P(1)	-C(36)	1.802(5)
Ni	- S(7)	2.2336(24)	P(2)	-C(10)	1.823(7)
Ni	- P(1)	2.1747(19)	P(2)	-C(46)	1.781(5)
Ni	- P(2)	2.1820(20)	P(2)	-C(56)	1.789(7)
P(1)	-C(10)	1.811(7)			

Table 3.3. Angles(degrees) with standard deviations

S(1)	- Ni	- S(4)	91.38(8)		Ni	- S(7)	-C(6')	103.2(6)
S(1)	- Ni	- S(7)	91.28(8)		Ni	- S(7)	-C(8')	100.0(6)
S(1)	- Ni	- P(1)	102.17(7)		C(6')	- S(7)	-C(8')	103.8(8)
S(1)	- Ni	- P(2)	104.08(7)		Ni	- P(1)	-C(26)	116.18(17)
S(4)	- Ni	- S(7)	91.77(9)		Ni	- P(1)	-C(36)	118.60(17)
S(4)	- Ni	- P(1)	164.26(9)		Ni	- P(1)	-C(10)	95.36(23)
S(4)	- Ni	- P(2)	96.09(8)		C(26)	- P(1)	-C(36)	106.93(22)
S(7)	- Ni	- P(1)	95.83(8)		C(26)	- P(1)	-C(10)	108.9(3)
S(7)	- Ni	- P(2)	162.52(8)		C(36)	- P(1)	-C(10)	110.0(3)
P(1)	- Ni	- P(2)	73.05(7)		P(1)	-C(26)	-C(21)	120.6(4)
Ni	- S(1)	- C(2)	99.1(4)		P(1)	-C(26)	-C(25)	119.3(4)
Ni	- S(1)	- C(9)	97.5(4)		P(1)	-C(36)	-C(31)	118.8(3)
C(2)	- S(1)	- C(9)	100.6(5)		P(1)	-C(36)	-C(35)	121.0(3)
Ni	- S(4)	- C(3)	100.7(4)		P(1)	-C(10)	- P(2)	91.0(3)
Ni	- S(4)	- C(5)	103.8(4)		Ni	- P(2)	-C(10)	94.77(23)
C(3)	- S(4)	- C(5)	100.8(6)		Ni	- P(2)	-C(46)	120.62(19)
Ni	- S(7)	- C(6)	100.5(4)		Ni	- P(2)	-C(56)	115.11(22)
Ni	- S(7)	- C(8)	103.0(3)		C(10)	- P(2)	-C(46)	107.6(3)
C(6)	- S(7)	- C(8)	99.9(5)		C(10)	- P(2)	-C(56)	112.0(3)
Ni	- S(1)	-C(2')	97.7(5)		C(46)	- P(2)	-C(56)	106.1(3)
Ni	- S(1)	-C(9')	98.7(5)		P(2)	-C(46)	-C(41)	121.0(4)
C(2')	- S(1)	-C(9')	99.8(7)		P(2)	-C(46)	-C(45)	119.0(4)
Ni	- S(4)	-C(3')	102.4(5)		P(2)	-C(56)	-C(51)	118.3(5)
Ni	- S(4)	-C(5')	100.3(6)		P(2)	-C(56)	-C(55)	121.2(5)
C(3')	- S(4)	-C(5')	97.9(8)					

Table 3.4. Torsion angles(degrees) with standard deviations

C(9)	S(1)	C(2)	C(3)	134.6(8)	C(26)	P(1)	C(36)	C(35)	-148.6(4)
C(2)	S(1)	C(9)	C(8)	-58.7(9)	C(10)	P(1)	C(36)	C(31)	153.9(4)
S(1)	C(2)	C(3)	S(4)	-56.6(10)	C(10)	P(1)	C(36)	C(35)	-30.5(5)
C(2)	C(3)	S(4)	C(5)	-60.8(9)	C(26)	P(1)	C(10)	P(2)	-100.5(3)
C(3)	S(4)	C(5)	C(6)	136.9(9)	C(36)	P(1)	C(10)	P(2)	142.59(25)
S(4)	C(5)	C(6)	S(7)	-51.7(11)	C(22)	C(21)	C(26)	P(1)	177.1(4)
C(5)	C(6)	S(7)	C(8)	-62.1(9)	C(24)	C(25)	C(26)	P(1)	-177.2(4)
C(6)	S(7)	C(8)	C(9)	137.6(8)	C(32)	C(31)	C(36)	P(1)	175.7(4)
S(7)	C(8)	C(9)	S(1)	-54.3(9)	C(34)	C(35)	C(36)	P(1)	-175.6(4)
C(9')	S(1)	C(2')	C(3')	58.6(12)	P(1)	C(10)	P(2)	C(46)	104.8(3)
C(2')	S(1)	C(9')	C(8')	-134.3(13)	P(1)	C(10)	P(2)	C(56)	-139.0(3)
S(1)	C(2')	C(3')	S(4)	57.9(14)	C(10)	P(2)	C(46)	C(41)	-121.9(5)
C(2')	C(3')	S(4)	C(5')	-142.8(12)	C(10)	P(2)	C(46)	C(45)	58.5(5)
C(3')	S(4)	C(5')	C(6')	57.6(14)	C(56)	P(2)	C(46)	C(41)	118.0(5)
S(4)	C(5')	C(6')	S(7)	54.4(15)	C(56)	P(2)	C(46)	C(45)	-61.6(5)
C(5')	C(6')	S(7)	C(8')	-137.7(13)	C(10)	P(2)	C(56)	C(51)	-159.0(5)
C(6')	S(7)	C(8')	C(9')	58.7(14)	C(10)	P(2)	C(56)	C(55)	29.2(6)
S(7)	C(8')	C(9')	S(1)	58.0(15)	C(46)	P(2)	C(56)	C(51)	-41.9(6)
C(36)	P(1)	C(26)	C(21)	-127.5(4)	C(46)	P(2)	C(56)	C(55)	146.3(5)
C(36)	P(1)	C(26)	C(25)	49.6(4)	C(42)	C(41)	C(46)	P(2)	-179.6(4)
C(10)	P(1)	C(26)	C(21)	113.6(4)	C(44)	C(45)	C(46)	P(2)	179.6(4)
C(10)	P(1)	C(26)	C(25)	-69.2(5)	C(52)	C(51)	C(56)	P(2)	-171.9(5)
C(26)	P(1)	C(36)	C(31)	35.8(4)	C(54)	C(55)	C(56)	P(2)	171.6(5)

Single Crystal Structure of $[Ni([9]aneS_3)(dppe)](BF_4)_2$

Table 3.5. Bond Lengths(A) with standard deviations

Ni - S(1)	2.381(3)	Ni(') -S(1')	2.399(3)
Ni - S(4)	2.248(3)	Ni(') -S(4')	2.243(3)
Ni - S(7)	2.225(3)	Ni(') -S(7')	2.226(3)
Ni - P(1)	2.195(3)	Ni(') -P(1')	2.184(3)
Ni - P(2)	2.193(3)	Ni(') -P(2')	2.187(3)
S(1) - C(2)	1.787(14)	S(1') -C(2')	1.815(12)
S(1) - C(9)	1.785(12)	S(1') -C(9')	1.796(11)
C(2) - C(3)	1.490(20)	C(2') -C(3')	1.518(16)
C(3) - S(4)	1.813(15)	C(3') -S(4')	1.811(12)
S(4) - C(5)	1.854(16)	S(4') -C(5')	1.838(12)
C(5) - C(6)	1.452(21)	C(5') -C(6')	1.467(17)
C(6) - S(7)	1.776(14)	C(6') -S(7')	1.844(12)
S(7) - C(8)	1.845(12)	S(7') -C(8')	1.851(12)
C(8) - C(9)	1.515(16)	C(8') -C(9')	1.517(16)
P(1) -C(26)	1.815(7)	P(1') -C(26')	1.796(7)
P(1) -C(36)	1.791(8)	P(1') -C(36')	1.799(7)
P(1) -C(10)	1.828(12)	P(1') -C(10')	1.836(10)
C(10) -C(11)	1.555(16)	C(10')-C(11')	1.499(14)
C(11) - P(2)	1.816(11)	C(11')-P(2')	1.822(10)
P(2) -C(46)	1.803(7)	P(2') -C(46')	1.799(7)
P(2) -C(56)	1.802(8)	P(2') -C(56')	1.815(7)

Table 3.6. Angles(degrees) with standard deviations

S(1) - Ni - S(4)	90.85(11)	S(1') -Ni(') -S(4')	90.84(11)
S(1) - Ni - S(7)	91.16(11)	S(1') -Ni(') -S(7')	90.47(11)
S(1) - Ni - P(1)	106.89(11)	S(1') -Ni(') -P(1')	108.31(11)
S(1) - Ni - P(2)	98.86(11)	S(1') -Ni(') -P(2')	100.49(11)
S(4) - Ni - S(7)	90.05(12)	S(4') -Ni(') -S(7')	90.98(12)
S(4) - Ni - P(1)	162.27(13)	S(4') -Ni(') -P(1')	160.85(13)
S(4) - Ni - P(2)	92.11(12)	S(4') -Ni(') -P(2')	92.11(11)
S(7) - Ni - P(1)	89.62(12)	S(7') -Ni(') -P(1')	88.81(12)
S(7) - Ni - P(2)	169.71(13)	S(7') -Ni(') -P(2')	168.57(13)
P(1) - Ni - P(2)	85.26(12)	P(1') -Ni(') -P(2')	84.68(11)
Ni - S(1) - C(2)	102.4(4)	Ni(') -S(1') -C(2')	101.0(4)
Ni - S(1) - C(9)	100.1(4)	Ni(') -S(1') -C(9')	99.6(4)
C(2) - S(1) - C(9)	100.8(6)	C(2') -S(1') -C(9')	102.0(5)
S(1) - C(2) - C(3)	121.0(10)	S(1') -C(2') -C(3')	115.2(8)
C(2) - C(3) - S(4)	118.5(10)	C(2') -C(3') -S(4')	115.5(8)
Ni - S(4) - C(3)	105.6(5)	Ni(') -S(4') -C(3')	103.1(4)
Ni - S(4) - C(5)	103.9(5)	Ni(') -S(4') -C(5')	104.8(4)
C(3) - S(4) - C(5)	103.8(7)	C(3') -S(4') -C(5')	101.5(5)
S(4) - C(5) - C(6)	114.7(11)	S(4') -C(5') -C(6')	110.9(8)
C(5) - C(6) - S(7)	116.7(10)	C(5') -C(6') -S(7')	114.2(9)
Ni - S(7) - C(6)	102.7(5)	Ni(') -S(7') -C(6')	100.7(4)
Ni - S(7) - C(8)	103.0(4)	Ni(') -S(7') -C(8')	105.1(4)
C(6) - S(7) - C(8)	101.8(6)	C(6') -S(7') -C(8')	103.0(5)
S(7) - C(8) - C(9)	113.0(8)	S(7') -C(8') -C(9')	112.8(8)
S(1) - C(9) - C(8)	113.9(8)	S(1') -C(9') -C(8')	115.1(8)
Ni - P(1) -C(26)	110.6(3)	Ni(') -P(1') -C(26')	116.53(24)
Ni - P(1) -C(36)	117.8(3)	Ni(') -P(1') -C(36')	110.3(3)
Ni - P(1) -C(10)	110.4(4)	Ni(') -P(1') -C(10')	110.5(3)
C(26) - P(1) -C(36)	106.1(4)	C(26')-P(1') -C(36')	106.5(3)
C(26) - P(1) -C(10)	106.8(4)	C(26')-P(1') -C(10')	105.4(4)
C(36) - P(1) -C(10)	104.5(5)	C(36')-P(1') -C(10')	107.1(4)
P(1) -C(26) -C(21)	119.1(5)	P(1') -C(26')-C(21')	121.2(5)
P(1) -C(26) -C(25)	120.5(5)	P(1') -C(26')-C(25')	118.7(5)
P(1) -C(36) -C(31)	119.1(6)	P(1') -C(36')-C(31')	120.0(5)
P(1) -C(36) -C(35)	120.8(6)	P(1') -C(36')-C(35')	119.6(5)
P(1) -C(10) -C(11)	108.2(8)	P(1') -C(10')-C(11')	110.3(7)
C(10) -C(11) - P(2)	105.9(7)	C(10')-C(11')-P(2')	107.0(7)
Ni - P(2) -C(11)	106.8(4)	Ni(') -P(2') -C(11')	107.3(3)
Ni - P(2) -C(46)	114.8(3)	Ni(') -P(2') -C(46')	115.9(3)
Ni - P(2) -C(56)	114.9(3)	Ni(') -P(2') -C(56')	115.82(25)
C(11) - P(2) -C(46)	107.2(4)	C(11')-P(2') -C(46')	105.8(4)
C(11) - P(2) -C(56)	105.9(5)	C(11')-P(2') -C(56')	105.6(4)
C(46) - P(2) -C(56)	106.7(4)	C(46')-P(2') -C(56')	105.5(3)
P(2) -C(46) -C(41)	120.7(5)	P(2') -C(46')-C(41')	118.8(5)
P(2) -C(46) -C(45)	119.3(5)	P(2') -C(46')-C(45')	121.1(5)
P(2) -C(56) -C(51)	118.7(6)	P(2') -C(56')-C(51')	119.2(5)
P(2) -C(56) -C(55)	120.8(6)	P(2') -C(56')-C(55')	120.7(5)

Table 3.7. Torsion angles(degrees) with standard deviations

C(9)	S(1)	C(2)	C(3)	109.8(11)	C(9')	S(1')	C(2')	C(3')	128.6(9)
C(2)	S(1)	C(9)	C(8)	-67.3(9)	C(2')	S(1')	C(9')	C(8')	-64.0(9)
S(1)	C(2)	C(3)	S(4)	-14.5(16)	S(1')	C(2')	C(3')	S(4')	-44.3(11)
C(2)	C(3)	S(4)	C(5)	-95.1(12)	C(2')	C(3')	S(4')	C(5')	-71.2(9)
C(3)	S(4)	C(5)	C(6)	120.3(11)	C(3')	S(4')	C(5')	C(6')	133.7(9)
S(4)	C(5)	C(6)	S(7)	-32.9(15)	S(4')	C(5')	C(6')	S(7')	-47.5(11)
C(5)	C(6)	S(7)	C(8)	-67.8(12)	C(5')	C(6')	S(7')	C(8')	-64.6(10)
C(6)	S(7)	C(8)	C(9)	141.7(9)	C(6')	S(7')	C(8')	C(9')	133.8(8)
S(7)	C(8)	C(9)	S(1)	-51.1(10)	S(7')	C(8')	C(9')	S(1')	-47.8(10)
C(36)	P(1)	C(26)	C(21)	-141.1(6)	C(36')	P(1')	C(26')	C(21')	-132.4(5)
C(36)	P(1)	C(26)	C(25)	46.4(7)	C(36')	P(1')	C(26')	C(25')	50.5(6)
C(10)	P(1)	C(26)	C(21)	-30.0(7)	C(10')	P(1')	C(26')	C(21')	114.1(6)
C(10)	P(1)	C(26)	C(25)	157.5(6)	C(10')	P(1')	C(26')	C(25')	-63.1(6)
C(26)	P(1)	C(36)	C(31)	41.5(7)	C(26')	P(1')	C(36')	C(31')	38.1(7)
C(26)	P(1)	C(36)	C(35)	-143.1(7)	C(26')	P(1')	C(36')	C(35')	-148.2(6)
C(10)	P(1)	C(36)	C(31)	-71.2(8)	C(10')	P(1')	C(36')	C(31')	150.5(6)
C(10)	P(1)	C(36)	C(35)	104.2(8)	C(10')	P(1')	C(36')	C(35')	-35.8(7)
C(26)	P(1)	C(10)	C(11)	94.6(8)	C(26')	P(1')	C(10')	C(11')	-146.2(6)
C(36)	P(1)	C(10)	C(11)	-153.2(7)	C(36')	P(1')	C(10')	C(11')	100.7(7)
C(22)	C(21)	C(26)	P(1)	-172.5(5)	C(22')	C(21')	C(26')	P(1')	-177.1(5)
C(24)	C(25)	C(26)	P(1)	172.4(5)	C(24')	C(25')	C(26')	P(1')	177.2(5)
C(32)	C(31)	C(36)	P(1)	175.4(6)	C(32')	C(31')	C(36')	P(1')	173.8(5)
C(34)	C(35)	C(36)	P(1)	-175.3(6)	C(34')	C(35')	C(36')	P(1')	-173.8(5)
P(1)	C(10)	C(11)	P(2)	47.2(8)	P(1')	C(10')	C(11')	P(2')	41.9(8)
C(10)	C(11)	P(2)	C(46)	72.6(8)	C(10')	C(11')	P(2')	C(46')	75.6(7)
C(10)	C(11)	P(2)	C(56)	-173.8(7)	C(10')	C(11')	P(2')	C(56')	-172.8(6)
C(11)	P(2)	C(46)	C(41)	-129.1(6)	C(11')	P(2')	C(46')	C(41')	47.9(7)
C(11)	P(2)	C(46)	C(45)	52.3(7)	C(11')	P(2')	C(46')	C(45')	-133.3(6)
C(56)	P(2)	C(46)	C(41)	117.8(6)	C(56')	P(2')	C(46')	C(41')	-63.7(6)
C(56)	P(2)	C(46)	C(45)	-60.7(6)	C(56')	P(2')	C(46')	C(45')	115.1(6)
C(11)	P(2)	C(56)	C(51)	-155.0(7)	C(11')	P(2')	C(56')	C(51')	46.1(7)
C(11)	P(2)	C(56)	C(55)	33.2(8)	C(11')	P(2')	C(56')	C(55')	-137.8(6)
C(46)	P(2)	C(56)	C(51)	-41.1(7)	C(46')	P(2')	C(56')	C(51')	157.9(5)
C(46)	P(2)	C(56)	C(55)	147.1(6)	C(46')	P(2')	C(56')	C(55')	-26.1(6)
C(42)	C(41)	C(46)	P(2)	-178.5(5)	C(42')	C(41')	C(46')	P(2')	178.8(5)
C(44)	C(45)	C(46)	P(2)	178.6(5)	C(44')	C(45')	C(46')	P(2')	-178.8(5)
C(52)	C(51)	C(56)	P(2)	-171.9(6)	C(52')	C(51')	C(56')	P(2')	176.1(5)
C(54)	C(55)	C(56)	P(2)	171.7(6)	C(54')	C(55')	C(56')	P(2')	-176.0(5)

steric repulsions within the molecule (Figure 3.12b), or if it corresponds to an electronic distortion of the type proposed for the square-planar complexes $[Ni(PP)_2]^{2+}$ (PP = dppm, dppe, dppp etc.)[148]. The Ni atom lies 0.27 Å above the least-squares basal plane (Table 3.16).

X-ray structural analyses of $[Pd([9]aneS_3)(dppm)]^{2+}$ and $[Pt([9]aneS_3)(dppm)]^{2+}$ have been reported previously by the Edinburgh group[80]. These complexes adopt square pyramidal geometries, with unusually short apical M-S distances [$Pd\text{-}S_{apical}$ = 2.698(3), $Pt\text{-}S_{apical}$ = 2.673(3) Å, Figure 3.8a]. However, whilst $[Pd([9]aneS_3)(PPh_3)_2]^{2+}$ also exhibits this geometry [Pd-S = 2.877(3), 2.4068(25), 2.3753(23) Å], $[Pt([9]aneS_3)(PPh_3)_2]^{2+}$ is trigonal bipyramidal in the solid state [Pt-S = 2.5835(20), 2.5359(18), 2.3511(18) Å, Figure 3.8b][80].

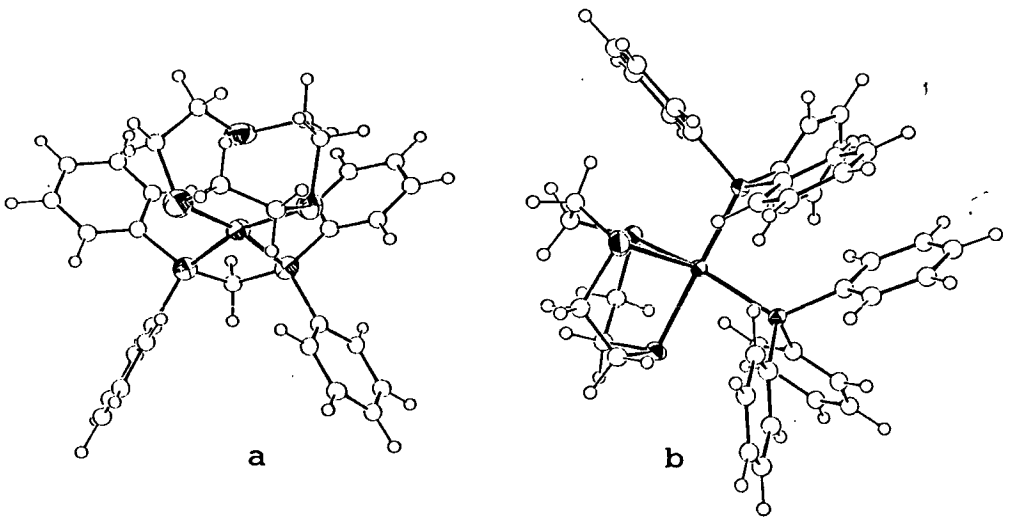

Figure 3.8: Views of the Single Crystal Structures of
a) $[Pd([9]aneS_3)(dppm)]^{2+}$ and
b) $[Pt([9]aneS_3)(PPh_3)_2]^{2+}$

3.2.3 Single Crystal Structure of [Ni([9]aneS$_3$)(dcpe)](PF$_6$)$_2$.1.25CH$_3$CN

The structure's solution and refinement are described in Section 3.4.14. Selected bond lengths, angles and torsions are given in Tables 3.8, 3.9 and 3.10, and an ORTEP plot of the complex cation is displayed in Figure 3.9.

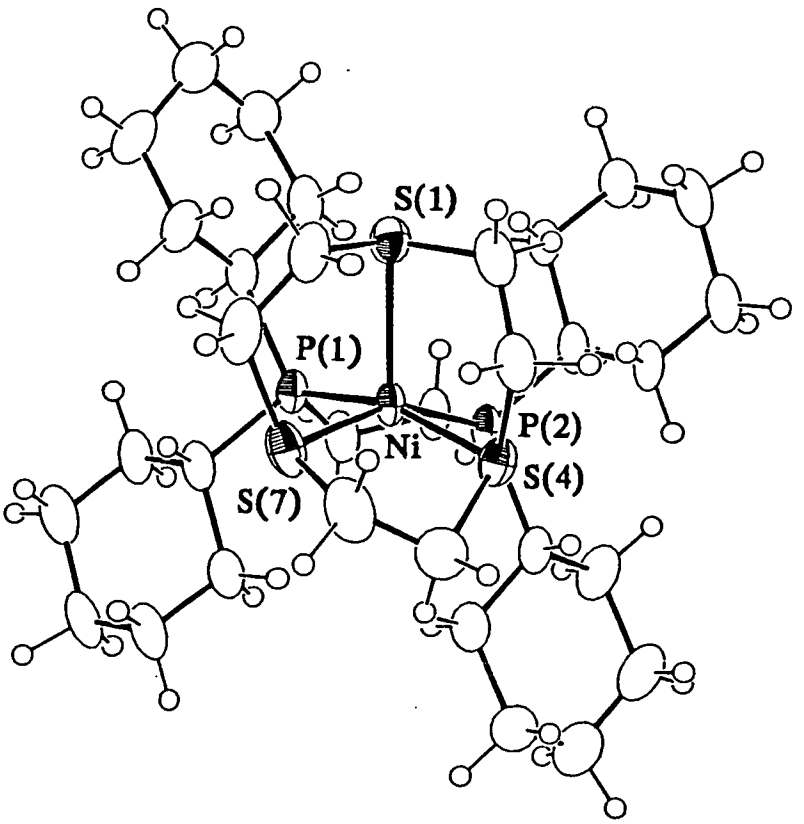

Figure 3.9: View of the Single Crystal Structure of [Ni([9]aneS$_3$)(dcpe)]$^{2+}$

Single Crystal Structure of [Ni([9]aneS$_3$(dcpe)](PF$_6$)$_2$.1.25CH$_3$CN

Table 3.8. Bond Lengths(A) with standard deviations

Ni	- S(1)	2.6521(20)	C(6)	- S(7)	1.868(8)
Ni	- S(4)	2.2260(19)	S(7)	- C(8)	1.962(8)
Ni	- S(7)	2.2402(20)	C(8)	- C(9)	1.501(11)
Ni	- P(1)	2.1654(19)	P(1)	-C(26)	2.038(7)
Ni	- P(2)	2.2173(19)	P(1)	-C(36)	1.808(7)
S(1)	- C(2)	1.766(8)	P(1)	-C(11)	1.857(7)
S(1)	- C(9)	1.804(8)	C(11)	-C(12)	1.447(9)
C(2)	- C(3)	1.657(10)	C(12)	- P(2)	1.803(7)
C(3)	- S(4)	1.882(7)	P(2)	-C(46)	1.815(7)
S(4)	- C(5)	1.872(8)	P(2)	-C(56)	2.030(7)
C(5)	- C(6)	1.524(11)			

Table 3.9. Angles(degrees) with standard deviations

S(1) - Ni - S(4)	95.65(7)	S(1) - C(9) - C(8)	112.1(5)
S(1) - Ni - S(7)	89.06(7)	Ni - P(1) -C(26)	119.61(20)
S(1) - Ni - P(1)	102.66(7)	Ni - P(1) -C(36)	108.98(22)
S(1) - Ni - P(2)	116.98(7)	Ni - P(1) -C(11)	108.72(22)
S(4) - Ni - S(7)	84.95(7)	C(26) - P(1) -C(36)	109.4(3)
S(4) - Ni - P(1)	161.69(8)	C(26) - P(1) -C(11)	106.9(3)
S(4) - Ni - P(2)	87.46(7)	C(36) - P(1) -C(11)	101.7(3)
S(7) - Ni - P(1)	95.53(7)	P(1) -C(26) -C(21)	121.0(5)
S(7) - Ni - P(2)	153.50(8)	P(1) -C(26) -C(25)	116.1(5)
P(1) - Ni - P(2)	84.02(7)	P(1) -C(36) -C(31)	108.9(5)
Ni - S(1) - C(2)	93.4(3)	P(1) -C(36) -C(35)	116.1(4)
Ni - S(1) - C(9)	101.9(3)	P(1) -C(11) -C(12)	111.0(5)
C(2) - S(1) - C(9)	96.5(4)	C(11) -C(12) - P(2)	107.3(5)
S(1) - C(2) - C(3)	117.5(5)	Ni - P(2) -C(12)	112.61(23)
C(2) - C(3) - S(4)	118.9(5)	Ni - P(2) -C(46)	116.56(22)
Ni - S(4) - C(3)	99.97(23)	Ni - P(2) -C(56)	110.21(20)
Ni - S(4) - C(5)	108.32(24)	C(12) - P(2) -C(46)	97.7(3)
C(3) - S(4) - C(5)	104.3(3)	C(12) - P(2) -C(56)	107.3(3)
S(4) - C(5) - C(6)	105.3(5)	C(46) - P(2) -C(56)	111.6(3)
C(5) - C(6) - S(7)	110.4(5)	P(2) -C(46) -C(41)	117.7(4)
Ni - S(7) - C(6)	109.5(3)	P(2) -C(46) -C(45)	108.2(5)
Ni - S(7) - C(8)	101.35(24)	P(2) -C(56) -C(51)	118.8(5)
C(6) - S(7) - C(8)	106.7(3)	P(2) -C(56) -C(55)	115.3(5)
S(7) - C(8) - C(9)	121.2(5)		

Table 3.10. Torsion angles(degrees) with standard deviations

C(9)	S(1)	C(2)	C(3)	68.2(6)	C(22)	C(21)	C(26)	P(1)	172.4(5)
C(2)	S(1)	C(9)	C(8)	-119.3(6)	C(24)	C(25)	C(26)	P(1)	-172.1(5)
S(1)	C(2)	C(3)	S(4)	48.1(7)	C(32)	C(31)	C(36)	P(1)	-175.7(5)
C(2)	C(3)	S(4)	C(5)	-139.9(5)	C(34)	C(35)	C(36)	P(1)	171.8(5)
C(3)	S(4)	C(5)	C(6)	57.9(5)	P(1)	C(11)	C(12)	P(2)	42.7(5)
S(4)	C(5)	C(6)	S(7)	46.4(6)	C(11)	C(12)	P(2)	C(46)	-152.8(5)
C(5)	C(6)	S(7)	C(8)	-136.8(5)	C(11)	C(12)	P(2)	C(56)	91.6(5)
C(6)	S(7)	C(8)	C(9)	74.7(7)	C(12)	P(2)	C(46)	C(41)	68.7(5)
S(7)	C(8)	C(9)	S(1)	44.9(8)	C(12)	P(2)	C(46)	C(45)	-161.3(5)
C(36)	P(1)	C(26)	C(21)	-170.8(5)	C(56)	P(2)	C(46)	C(41)	-179.2(4)
C(36)	P(1)	C(26)	C(25)	60.4(6)	C(56)	P(2)	C(46)	C(45)	-49.2(5)
C(11)	P(1)	C(26)	C(21)	-61.4(6)	C(12)	P(2)	C(56)	C(51)	-71.5(6)
C(11)	P(1)	C(26)	C(25)	169.9(5)	C(12)	P(2)	C(56)	C(55)	56.0(5)
C(26)	P(1)	C(36)	C(31)	48.0(5)	C(46)	P(2)	C(56)	C(51)	-177.4(5)
C(26)	P(1)	C(36)	C(35)	173.1(4)	C(46)	P(2)	C(56)	C(55)	-49.9(6)
C(11)	P(1)	C(36)	C(31)	-64.8(5)	C(42)	C(41)	C(46)	P(2)	-173.4(5)
C(11)	P(1)	C(36)	C(35)	60.2(5)	C(44)	C(45)	C(46)	P(2)	174.0(5)
C(26)	P(1)	C(11)	C(12)	90.1(5)	C(52)	C(51)	C(56)	P(2)	-173.0(5)
C(36)	P(1)	C(11)	C(12)	-155.2(5)	C(54)	C(55)	C(56)	P(2)	174.9(4)

$[Ni([9]aneS_3(dcpe)]^{2+}$ adopts a highly distorted square-pyramidal geometry, with an extremely long apical Ni-S bond [Ni-S(1) = 2.6521(20), Ni-S(4) = 2.2260(19), Ni-S(7) = 2.2402(20), Ni-P(1) = 2.1654(19), Ni-P(2) = 2.2173(19) Å]. As in $[Ni([9]aneS_3)(dppe)]^{2+}$ the basal S_2P_2 donors show significant deviations from planarity [<S(4)-Ni-P(1) = 161.69(8), <S(7)-Ni-P(2) = 153.50(8)°]. The Ni ion lies 0.422 Å above the least-squares basal plane (Table 3.16). Examination of space-filling diagrams of this complex show it to be extremely crowded, with severe steric interactions between the dcpe cyclohexyl substituents and the $[9]aneS_3$ ring (Figure 3.12c). Therefore, the structure of the cation appears to be dominated by steric considerations, and no clear inferences about the electronic properties of the dcpe ligand can be drawn.

3.2.4 Single Crystal Structure of $[Ni([9]aneS_3)(tdpme)](PF_6)_2$

Details of the structure solution and refinement are described in Section 3.4.18. Relevant bond lengths, angles and torsions are listed in tables 3.11-3.13, and the molecular geometry of the complex cation is displayed in Figure 3.10.

$[Ni([9]aneS_3)(tdpme)]^{2+}$ exhibits a square-pyramidal stereochemistry [Ni-S(1) = 2.458(5), Ni-S(4) = 2.266(5), Ni-S(7) = 2.242(5), Ni-P(1) = 2.224(4), Ni-P(2) =

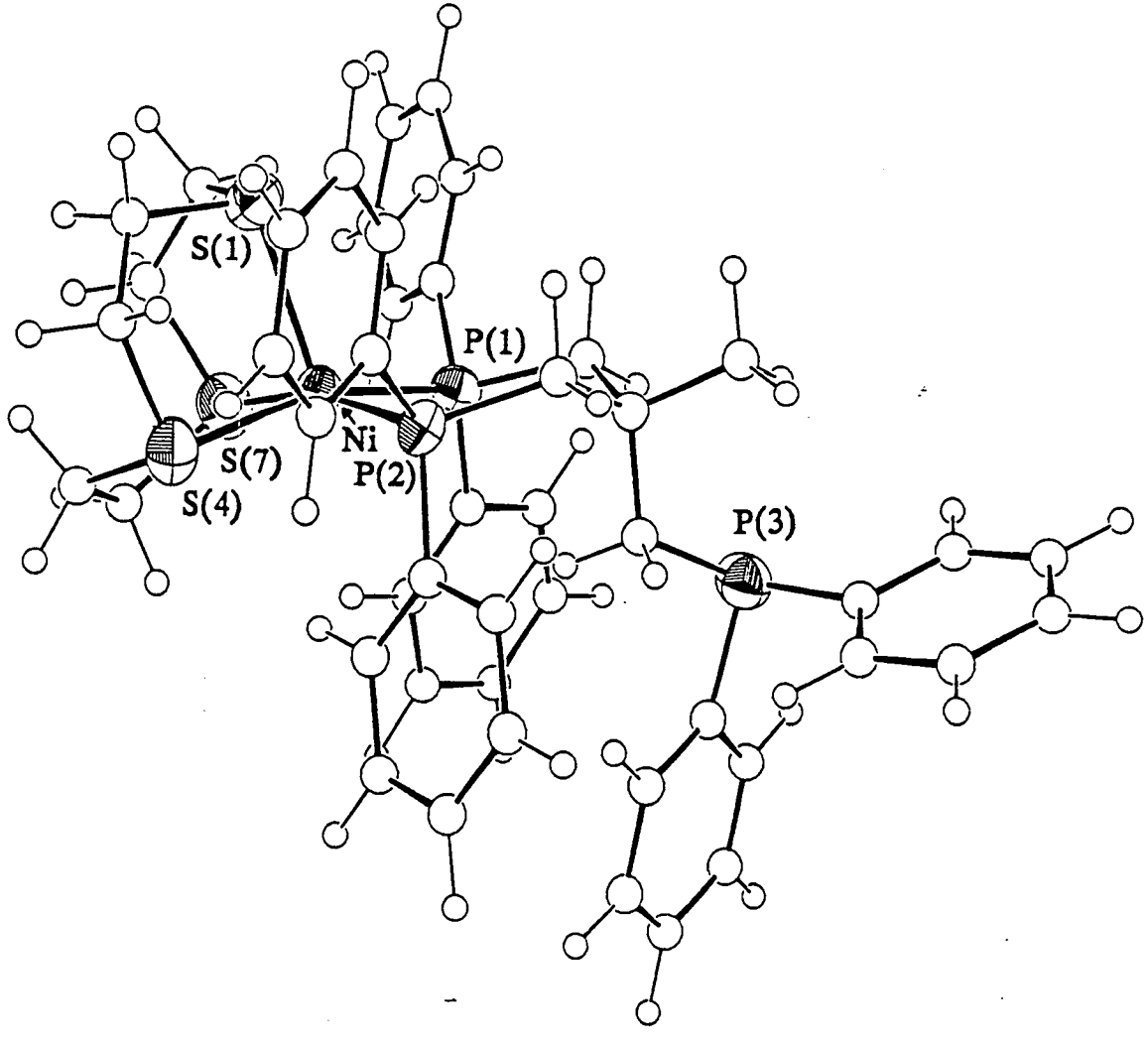

Figure 3.10: View of the Single Crystal Structure of $[Ni([9]aneS_3)(tdpme)]^{2+}$

Single Crystal Structure of [Ni([9]aneS$_3$)(tdpme)](PF$_6$)$_2$

Table 3.11. Bond Lengths(A) with standard deviations

Ni	- S(1)	2.458(5)	P(1)	-C(26)	1.802(11)
Ni	- S(4)	2.266(5)	P(1)	-C(36)	1.824(10)
Ni	- S(7)	2.242(5)	P(1)	-C(13)	1.813(16)
Ni	- P(1)	2.224(4)	P(2)	-C(46)	1.808(11)
Ni	- P(2)	2.214(4)	P(2)	-C(56)	1.817(10)
S(1)	- C(2)	1.827(21)	P(2)	-C(14)	1.792(14)
S(1)	- C(9)	1.778(18)	P(3)	-C(66)	1.817(12)
C(2)	- C(3)	1.46(3)	P(3)	-C(76)	1.868(12)
C(3)	- S(4)	1.849(19)	P(3)	-C(15)	1.860(16)
S(4)	- C(5)	1.787(19)	C(11)	-C(12)	1.536(22)
C(5)	- C(6)	1.49(3)	C(12)	-C(13)	1.573(21)
C(6)	- S(7)	1.819(20)	C(12)	-C(14)	1.533(20)
S(7)	- C(8)	1.850(21)	C(12)	-C(15)	1.533(21)
C(8)	- C(9)	1.52(3)			

Table 3.12. Angles(degrees) with standard deviations

S(1)	- Ni -	S(4)	88.99(16)
S(1)	- Ni -	S(7)	89.40(16)
S(1)	- Ni -	P(1)	107.69(16)
S(1)	- Ni -	P(2)	105.90(16)
S(4)	- Ni -	S(7)	89.27(16)
S(4)	- Ni -	P(1)	162.71(17)
S(4)	- Ni -	P(2)	88.56(16)
S(7)	- Ni -	P(1)	86.48(16)
S(7)	- Ni -	P(2)	164.50(16)
P(1)	- Ni -	P(2)	91.07(15)
Ni	- S(1) -	C(2)	101.6(7)
Ni	- S(1) -	C(9)	98.9(6)
C(2)	- S(1) -	C(9)	100.7(9)
S(1)	- C(2) -	C(3)	117.6(14)
C(2)	- C(3) -	S(4)	116.6(14)
Ni	- S(4) -	C(3)	104.4(6)
Ni	- S(4) -	C(5)	105.1(6)
C(3)	- S(4) -	C(5)	105.1(8)
S(4)	- C(5) -	C(6)	115.0(13)
C(5)	- C(6) -	S(7)	112.4(13)
Ni	- S(7) -	C(6)	102.4(6)
Ni	- S(7) -	C(8)	105.7(7)
C(6)	- S(7) -	C(8)	100.6(9)
S(7)	- C(8) -	C(9)	111.4(13)
S(1)	- C(9) -	C(8)	116.8(13)
Ni	- P(1) -	C(26)	113.0(4)
Ni	- P(1) -	C(36)	108.1(4)
Ni	- P(1) -	C(13)	122.4(5)
C(26)	- P(1) -	C(36)	105.4(5)
C(26)	- P(1) -	C(13)	105.2(6)
C(36)	- P(1) -	C(13)	101.0(6)
P(1)	-C(26) -	C(21)	119.1(8)
P(1)	-C(26) -	C(25)	120.8(8)
P(1)	-C(36) -	C(31)	120.9(7)
P(1)	-C(36) -	C(35)	118.9(7)
Ni	- P(2) -	C(46)	110.9(4)
Ni	- P(2) -	C(56)	113.7(3)
Ni	- P(2) -	C(14)	118.7(5)
C(46)	- P(2) -	C(56)	105.3(5)
C(46)	- P(2) -	C(14)	99.7(6)
C(56)	- P(2) -	C(14)	106.9(6)
P(2)	-C(46) -	C(41)	121.1(8)
P(2)	-C(46) -	C(45)	118.9(8)
P(2)	-C(56) -	C(51)	121.7(7)
P(2)	-C(56) -	C(55)	118.3(7)
C(66)	- P(3) -	C(76)	100.6(5)
C(66)	- P(3) -	C(15)	101.4(6)
C(76)	- P(3) -	C(15)	101.6(6)
P(3)	-C(66) -	C(61)	115.4(8)
P(3)	-C(66) -	C(65)	124.5(8)
P(3)	-C(76) -	C(71)	115.5(8)
P(3)	-C(76) -	C(75)	124.5(8)
C(11)	-C(12) -	C(13)	106.2(12)
C(11)	-C(12) -	C(14)	107.8(12)
C(11)	-C(12) -	C(15)	110.0(12)
C(13)	-C(12) -	C(14)	109.3(12)
C(13)	-C(12) -	C(15)	109.7(12)
C(14)	-C(12) -	C(15)	113.5(12)
P(1)	-C(13) -	C(12)	119.4(11)
P(2)	-C(14) -	C(12)	119.9(10)
P(3)	-C(15) -	C(12)	115.7(10)

Table 3.13. Torsion angles(degrees) with standard deviations

C(9)	S(1)	C(2)	C(3)	122.5(15)	C(14)	P(2)	-C(56) -C(55)	45.1(9)
C(2)	S(1)	C(9)	C(8)	-64.9(15)	C(46)	P(2)	-C(14) -C(12)	-177.9(11)
S(1)	C(2)	C(3)	S(4)	-38.1(20)	C(56)	P(2)	-C(14) -C(12)	72.7(12)
C(2)	C(3)	S(4)	C(5)	-76.1(16)	C(42)	-C(41)	-C(46) - P(2)	-179.9(8)
C(3)	S(4)	C(5)	C(6)	129.4(14)	C(44)	-C(45)	-C(46) - P(2)	179.9(8)
S(4)	C(5)	C(6)	S(7)	-41.7(18)	C(52)	-C(51)	-C(56) - P(2)	177.4(7)
C(5)	C(6)	S(7)	C(8)	-66.9(15)	C(54)	-C(55)	-C(56) - P(2)	-177.5(7)
C(6)	S(7)	C(8)	C(9)	138.2(14)	C(76)	- P(3)	-C(66) -C(61)	-96.5(9)
S(7)	C(8)	C(9)	S(1)	-49.8(17)	C(76)	- P(3)	-C(66) -C(65)	82.2(10)
C(36)	- P(1)	-C(26)	-C(21)	54.4(9)	C(15)	- P(3)	-C(66) -C(61)	159.2(9)
C(36)	- P(1)	-C(26)	-C(25)	-128.5(9)	C(15)	- P(3)	-C(66) -C(65)	-22.1(11)
C(13)	- P(1)	-C(26)	-C(21)	-51.9(10)	C(66)	- P(3)	-C(76) -C(71)	123.7(9)
C(13)	- P(1)	-C(26)	-C(25)	125.2(9)	C(66)	- P(3)	-C(76) -C(75)	-58.6(11)
C(26)	- P(1)	-C(36)	-C(31)	26.0(9)	C(15)	- P(3)	-C(76) -C(71)	-132.2(9)
C(26)	- P(1)	-C(36)	-C(35)	-159.7(8)	C(15)	- P(3)	-C(76) -C(75)	45.5(11)
C(13)	- P(1)	-C(36)	-C(31)	135.3(9)	C(66)	- P(3)	-C(15) -C(12)	-166.4(10)
C(13)	- P(1)	-C(36)	-C(35)	-50.4(10)	C(76)	- P(3)	-C(15) -C(12)	90.2(11)
C(26)	- P(1)	-C(13)	-C(12)	-88.4(12)	C(62)	-C(61)	-C(66) - P(3)	178.8(8)
C(36)	- P(1)	-C(13)	-C(12)	162.2(11)	C(64)	-C(65)	-C(66) - P(3)	-178.6(9)
C(22)	-C(21)	-C(26)	- P(1)	177.1(8)	C(72)	-C(71)	-C(76) - P(3)	177.8(9)
C(24)	-C(25)	-C(26)	- P(1)	-177.1(8)	C(74)	-C(75)	-C(76) - P(3)	-177.6(9)
C(32)	-C(31)	-C(36)	- P(1)	174.2(7)	C(11)	-C(12)	-C(13) - P(1)	-174.2(11)
C(34)	-C(35)	-C(36)	- P(1)	-174.3(7)	C(14)	-C(12)	-C(13) - P(1)	-58.1(15)
C(56)	- P(2)	-C(46)	-C(41)	-17.1(10)	C(15)	-C(12)	-C(13) - P(1)	67.0(15)
C(56)	- P(2)	-C(46)	-C(45)	163.0(8)	C(11)	-C(12)	-C(14) - P(2)	-177.6(10)
C(14)	- P(2)	-C(46)	-C(41)	-127.8(10)	C(13)	-C(12)	-C(14) - P(2)	67.4(14)
C(14)	- P(2)	-C(46)	-C(45)	52.4(10)	C(15)	-C(12)	-C(14) - P(2)	-55.4(16)
C(46)	- P(2)	-C(56)	-C(51)	122.2(8)	C(11)	-C(12)	-C(15) - P(3)	-45.8(15)
C(46)	- P(2)	-C(56)	-C(55)	-60.4(8)	C(13)	-C(12)	-C(15) - P(3)	70.7(14)
C(14)	- P(2)	-C(56)	-C(51)	-132.4(8)	C(14)	-C(12)	-C(15) - P(3)	-166.7(10)

2.214(4) Å], with one dangling non-interacting P donor. The bond lengths about the Ni centre are longer than for the dppm and dppe complexes, a result of steric repulsions between the [9]aneS$_3$ ring and phosphine phenyl moieties (Figure 3.12d). The basal S_2P_2 plane is not significantly twisted, however [*trans*-<S(4)-Ni-P(1) = 162.71(17), <S(7)-Ni-P(2) = 164.50(16)°]; the Ni atom lies 0.318 Å above this plane (Table 3.16).

The analogous Pd^{II} species [Pd([9]aneS$_3$)(oxy-tdpme)]$^{2+}$, in which the unbound P-donor has been oxidised to a phosphine oxide (P=O), exhibits a similar geometry [Pd-S = 2.722(4), 2.376(4), 2.398(4); Pd-P = 2.280(4), 2.290(4) Å][80]. This latter complex adopts a conformation with the non-bonding $CH_2P(O)Ph_2$ moiety occupying an equatorial position on the six-membered P-Ni-P chelate ring (Figure 3.11). This contrasts with [Ni([9]aneS$_3$)(tdpme)]$^{2+}$, where the dangling CH_2PPh_2 group adopts an axial orientation (Figure 3.10). Such differences will have minimal effect on the environment of the metal centres, however.

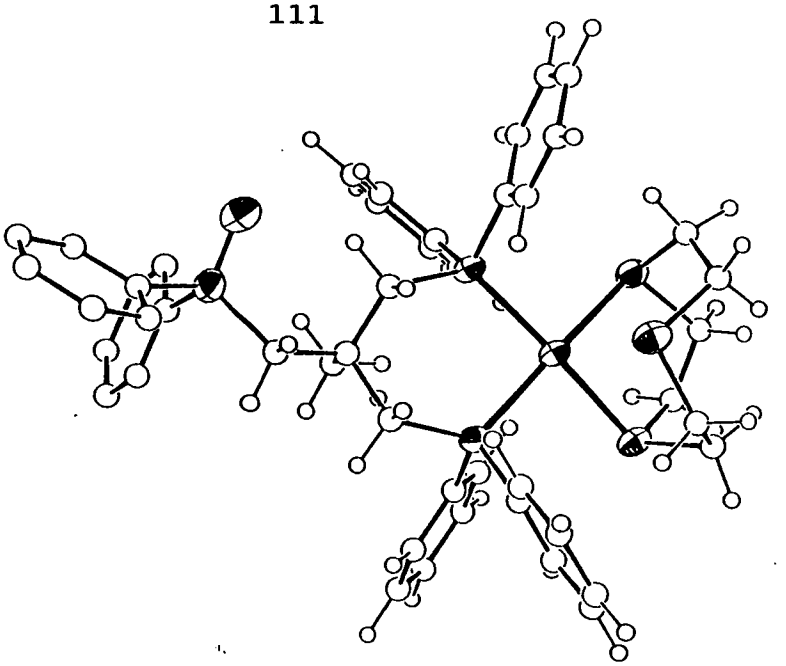

Figure 3.11: View of the Single Crystal Structure of $[Pd([9]aneS_3)(oxy\text{-}tdpme)]^{2+}$

3.2.5 $[Ni([15]aneS_5)](BF_4)_2$

The complexation of $Ni(BF_4)_2.6H_2O$ with $[15]aneS_5$ in CH_3NO_2 in the presence of a trace of acetic anhydride (to remove water from the reaction mixture) afforded a deep purple solution, from which a purple solid could be isolated by the addition of diethyl ether. The f.a.b. mass spectrum of this product showed molecular ions at M^+ = 444 and 358, which were assigned to $[^{58}Ni([15]aneS_5\text{-}H)(^{11}BF_4)]^+$ and $[^{58}Ni([15]aneS_5)]^+$ respectively. The product was therefore formulated as $[Ni([15]aneS_5)](BF_4)_2$, an assignment that was supported by elemental analytical and I.R. spectral data.

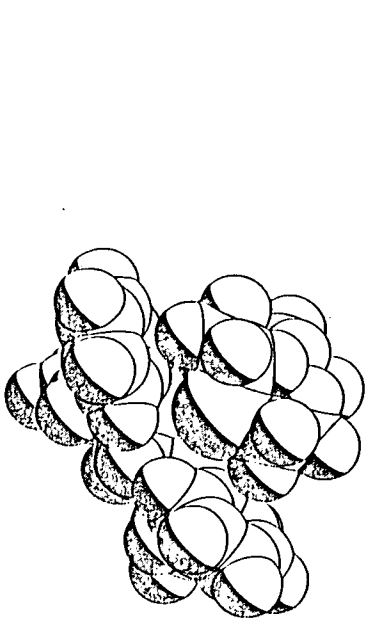

a) PP = dppm

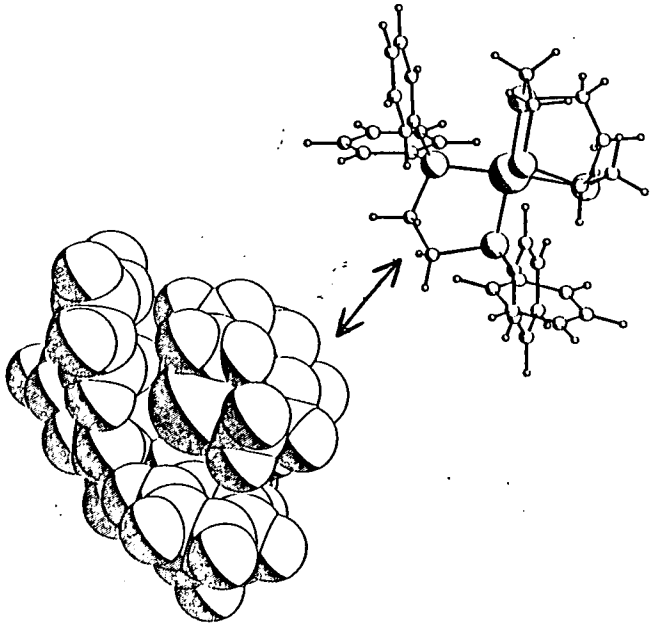

b) PP = dppe

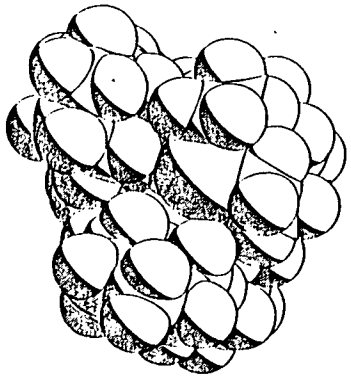

c) PP = dcpe

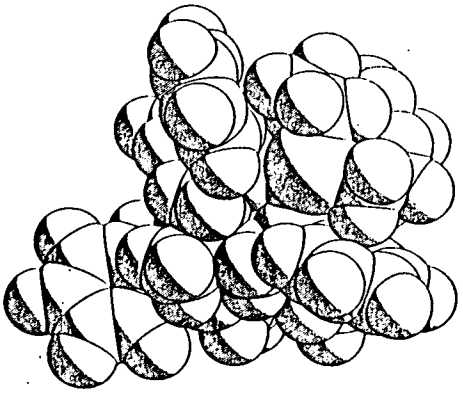

d) PP = tdpme

Figure 3.12: Space-Filling Diagrams of $[Ni([9]aneS_3)(PP)]^{2+}$

In contrast to the complexes $[Ni([9]aneS_3)(PP)]^{2+}$, $[Ni([15]aneS_5)]^{2+}$ is paramagnetic in solution and did not give an observable ^1H n.m.r. spectrum in CD_3NO_2 at 298K: this demonstrates the lower Π-acidity of thioether S- compared to tertiary phosphine P-donors. The U.V./visible spectrum of the complex in CH_3NO_2 shows 4 d-d bands, at λ_{max} = 1060 nm (sh), 823 (ε_{max} = 81 $dm^3mol^{-1}cm^{-1}$), 538 (118), 475 (sh); this is consistent with the cation adopting a five-coordinate geometry in this solvent, although the assignment of these bands is uncertain[114]. Interestingly, solutions of the compound in CH_3CN are pale blue, and exhibit absorptions at λ_{max} = 902 nm (ε_{max} = 11.4 $dm^3mol^{-1}cm^{-1}$), and 572 nm (9.7) in addition to charge transfer bands. This implies the coordination of a solvent molecule, to give perhaps the octahedral species $[Ni([15]aneS_5)(NCMe)]^{2+}$ (32). The addition of pyridine to CH_3NO_2 solutions of $[Ni([15]aneS_5)]^{2+}$ also produced a blue colour. Attempts to isolate these six-coordinate adducts yielded pale blue microcrystalline solids, which rapidly turned purple on exposure to air. Attempts to bind O_2 to $[Ni([15]aneS_5)]^{2+}$ were unsuccessful (Ni^{II} complexes of some penta-aza macrocycles form $[Ni^{III}(N_5)(O_2^-)]^{2+}$ adducts[152]). The compounds $[Ni([9]aneS_3)(PP)]^{2+}$ do not exhibit this behaviour.

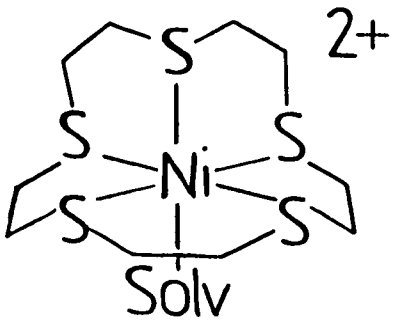

(32)

The cyclic voltammogram of $[Ni([15]aneS_5)(NCMe)](BF_4)_2$ in $CH_3CN/^nBu_4NPF_6$ showed a single irreversible reduction at Ep_C = -1.26V vs. Fc/Fc^+ (scan rate 400 mV/s), with an associated desorption spike at $Ep_a \triangleq$ OV due to the deposition of Ni metal onto the Pt working electrode. No oxidation was observed. No change in this electrochemical response was observed in the presence of CO or CO_2.

3.2.6 $[Ni([15]aneS_5)Cl](PF_6)$

The reaction of $NiCl_2$ with $[15]aneS_5$ in CH_3NO_2 yielded a blue precipitate, which dissolved on addition of one molar equivalent of NH_4PF_6. Filtration, reduction of the solution and addition of diethyl ether gave a blue microcrystalline product. The I.R. spectrum and elemental analysis of this compound were consistent with the formulation $[Ni([15]aneS_5)Cl](PF_6)$. Its f.a.b. mass spectrum showed peaks at M^+ = 392 and 358, which correspond to $[^{58}Ni([15]aneS_5)^{35}Cl]^+$ and

$[^{58}Ni([15]aneS_5)]^+$; no higher mass fragments were observed (cf $[Ni_2(S_4)_2(\mu\text{-}Cl)_2]^{2+}$, Chapter 2). Therefore, a monomeric octahedral stereochemistry was assigned for this compound (32, Solv = Cl^-). This demonstrates that $[Ni([15]aneS_5)]^{2+}$ can indeed accommodate a sixth ligand, as postulated earlier.

3.2.7 Single Crystal Structure of $[Ni([15]aneS_5)](PF_6)_2$

In order to compare the molecular structure of $[Ni([15]aneS_5)]^{2+}$ with those of the $[Ni([9]aneS_3)(PP)]^{2+}$ complexes, an X-ray analysis of the PF_6^- salt of the complex was undertaken. The structure solution and refinement are described in Section 3.4.21. Selected bond lengths, angles and torsions are given in Table 3.14, and the geometry of the complex cation is displayed in Figures 3.13 and 3.14.

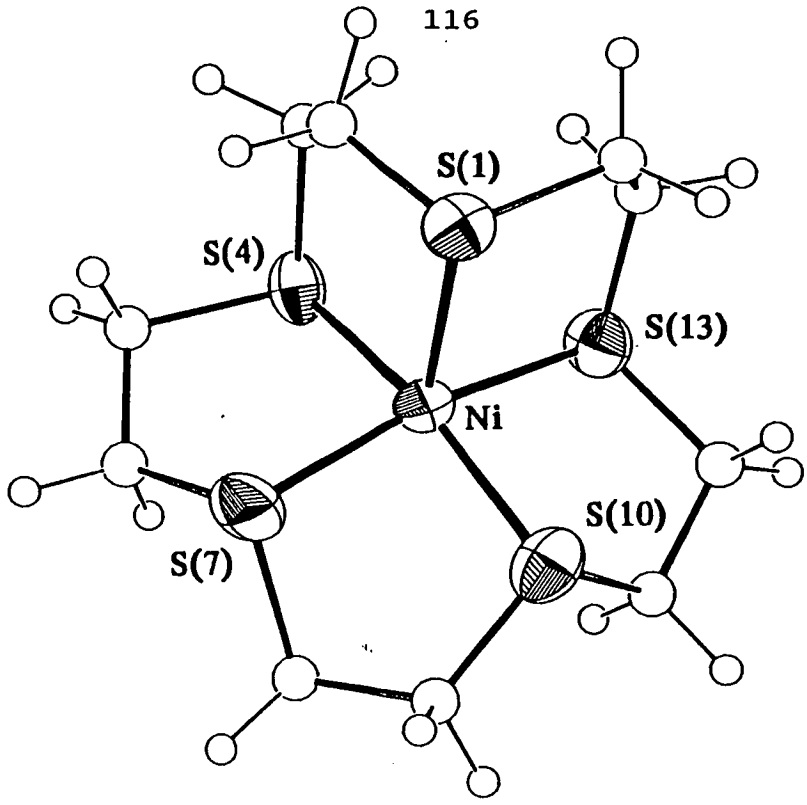

Figure 3.13: View of the Single Crystal Structure of $[Ni([15]aneS_5)]^{2+}$

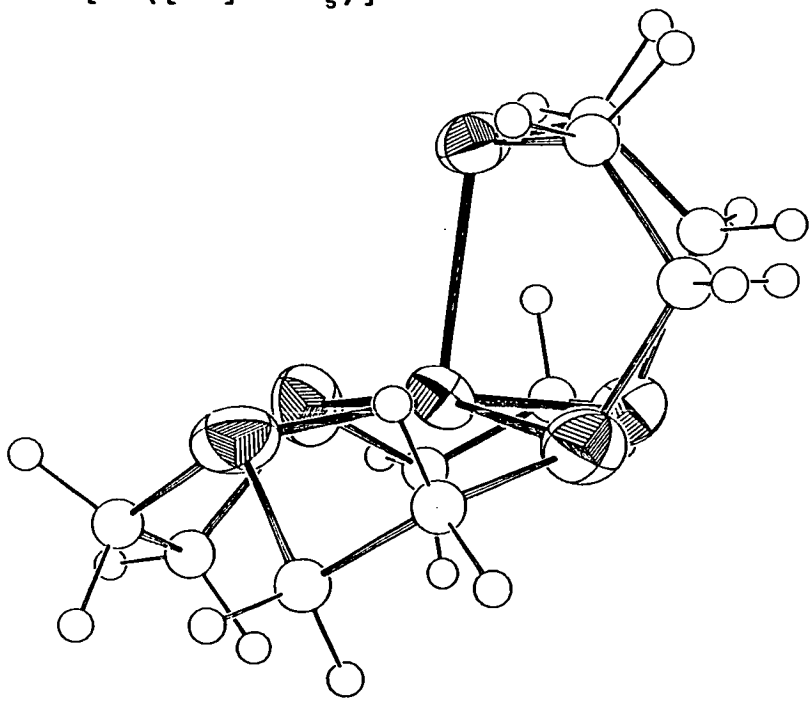

Figure 3.14: Alternative View of the Single Crystal Structure of $[Ni([15]aneS_5)]^{2+}$

Single Crystal Structure of $[Ni([15]aneS_5)](PF_6)_2$

Table 3.14. Bond Lengths(A), angles(degrees) and torsion angles(degrees) with standard deviations

Ni	- S(1)	2.413(5)	C(5)	- C(6)	1.498(18)
Ni	- S(4)	2.177(6)	C(6)	- S(7)	1.801(14)
Ni	- S(7)	2.146(7)	S(7)	- C(8)	1.842(15)
Ni	-S(10)	2.169(6)	C(8)	- C(9)	1.511(19)
Ni	-S(13)	2.198(6)	C(9)	-S(10)	1.730(15)
S(1)	- C(2)	1.697(14)	S(10)	-C(11)	1.781(14)
S(1)	-C(15)	1.856(13)	C(11)	-C(12)	1.490(19)
C(2)	- C(3)	1.440(19)	C(12)	-S(13)	1.835(15)
C(3)	- S(4)	1.883(15)	S(13)	-C(14)	1.723(13)
S(4)	- C(5)	1.792(14)	C(14)	-C(15)	1.556(17)

S(1)	- Ni -	S(4) 92.02(21)	S(4)	- C(5) - C(6)	106.6(9)
S(1)	- Ni -	S(7) 103.00(22)	C(5)	- C(6) - S(7)	109.2(9)
S(1)	- Ni	-S(10) 101.51(20)	Ni	- S(7) - C(6)	102.8(5)
S(1)	- Ni	-S(13) 91.18(20)	Ni	- S(7) - C(8)	99.7(5)
S(4)	- Ni -	S(7) 89.46(25)	C(6)	- S(7) - C(8)	102.8(7)
S(4)	- Ni	-S(10) 166.45(23)	S(7)	- C(8) - C(9)	105.2(9)
S(4)	- Ni	-S(13) 90.42(23)	C(8)	- C(9) -S(10)	116.4(10)
S(7)	- Ni	-S(10) 86.82(24)	Ni	-S(10) - C(9)	104.9(5)
S(7)	- Ni	-S(13) 165.82(25)	Ni	-S(10) -C(11)	99.0(5)
S(10)	- Ni	-S(13) 90.03(23)	C(9)	-S(10) -C(11)	104.9(7)
Ni	- S(1) -	C(2) 98.7(5)	S(10)	-C(11) -C(12)	101.9(9)
Ni	- S(1)	-C(15) 98.8(4)	C(11)	-C(12) -S(13)	109.6(9)
C(2)	- S(1)	-C(15) 105.5(6)	Ni	-S(13) -C(12)	100.0(5)
S(1)	- C(2) -	C(3) 118.6(10)	Ni	-S(13) -C(14)	106.6(5)
C(2)	- C(3) -	S(4) 115.7(10)	C(12)	-S(13) -C(14)	114.5(7)
Ni	- S(4) -	C(3) 101.4(5)	S(13)	-C(14) -C(15)	115.2(9)
Ni	- S(4) -	C(5) 106.0(5)	S(1)	-C(15) -C(14)	115.4(8)
C(3)	- S(4) -	C(5) 97.4(6)			

C(15)	- S(1) - C(2) -	C(3) 66.8(12)	S(7)	- C(8) - C(9)	-S(10) -37.2(12)
C(2)	- S(1)	-C(15) -C(14) -76.3(10)	C(8)	- C(9)	-S(10) -C(11) -99.9(11)
S(1)	- C(2) - C(3) -	S(4) 44.8(14)	C(9)		-S(10) -C(11) -C(12) 169.4(9)
C(2)	- C(3) - S(4) -	C(5) 81.2(11)	S(10)		-C(11) -C(12) -S(13) -64.4(10)
C(3)	- S(4) - C(5) -	C(6) -140.6(9)	C(11)		-C(12) -S(13) -C(14) 148.8(9)
S(4)	- C(5) - C(6) -	S(7) 55.0(10)	C(12)		-S(13) -C(14) -C(15) -74.5(11)
C(5)	- C(6) - S(7) -	C(8) -151.5(9)	S(13)		-C(14) -C(15) - S(1) -42.1(12)
C(6)	- S(7) - C(8) -	C(9) 158.6(9)			

The geometry of $[Ni([15]aneS_5)]^{2+}$ is similar to that observed for the complexes $[Ni([9]aneS_3)(PP)]^{2+}$. The cation exhibits a square pyramidal stereochemistry [$Ni-S_{apical}$ = 2.413(5), $Ni-S_{basal}$ = 2.146(7)-2.198(6) Å], with internal angles close to ideal for this stereochemistry [<S(4)-Ni-S(10) = 166.45(23), <S(7)-Ni-S(13) = 165.82(25)°]. The apical S atom is bent back slightly from the vertical, in common with related $[9]aneS_3$ complexes[14]. The Ni atom lies 0.260 Å above the basal S_4 plane (Table 3.16).

The structure of this complex is similar to those of $[Cu([15]aneS_5)]^{2+}$ [149] and $[Pt([15]aneS_5)]^{2+}$ [$Pt-S_{apical}$ = 2.894(9), $Pt-S_{basal}$ = 2.283(7)-2.309(7) Å, Figure 3.15b][150]. The $[15]aneS_5$ macrocycle can accommodate other stereochemistries, however. $[Pd([15]aneS_5)]^{2+}$ has a distorted trigonal bipyramidal structure [Pd-S = 2.278(8), 2.294(12), 2.336(11), 2.532(11), 2.540(11) Å, Figure 3.15a][148], whilst $[Cu([15]aneS_5)]^{+}$ is tetrahedral with one

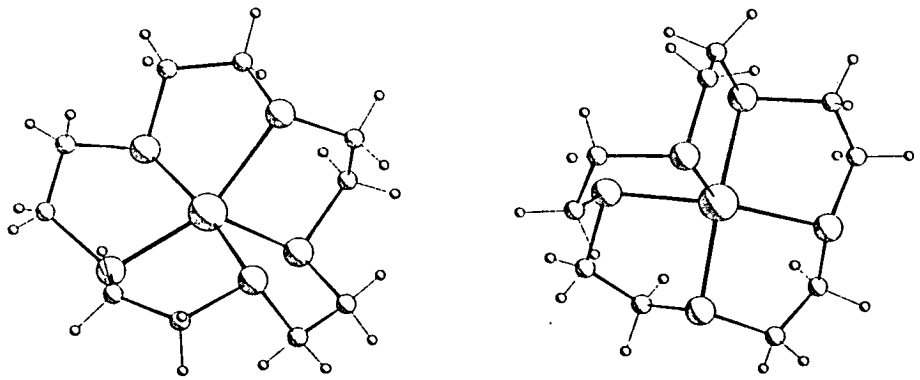

Figure 3.15: Views of the Single crystal Structure of
a) $[Pd([15]aneS_5)]^{2+}$ and
b) $[Pt([15]aneS_5)]^{2+}$

non-interacting S donor[149]. The bidentate, exocyclic complex [Re([15]aneS$_5$)(CO)$_3$Br] has also been structurally characterised in Edinburgh[109]. The solid state structure of [Ag([15]aneS$_5$)]$^+$ has been found to vary depending upon the counterion used[151].

3.3 CONCLUSIONS

A series of half-sandwich Ni^{II} complexes containing [9]aneS$_3$ and a diphosphine chelate ligand has been synthesised and characterised. Single crystal X-ray analyses on four of the compounds have shown them to adopt distorted square-pyramidal geometries in the solid state. U.V./visible spectroscopy implies that the complexes remain five-coordinate in solution, and their n.m.r. spectra show them to be fluxional, with all [9]aneS$_3$ CH$_2$ groups being equivalent at room temperature. This equilibration probably occurs via rotation of the [9]aneS$_3$ ring about the central Ni-[9]aneS$_3$ axis. Only limited low temperature n.m.r. studies on these compounds were possible, due to their low solubility in suitable solvents; however, evidence for such a process in the five-coordinate d^8 species [Rh([9]aneS$_3$)(L)$_2$]$^+$ (L = alkene) is described in Chapter 5. It is likely that steric considerations play an important role in influencing the molecular structures observed for these compounds. Unfortunately, the failure of attempts to synthesise analogous complexes containing monodentate

phosphines, or N donor chelate ligands, prevented further study of this effect.

The complexation of Ni^{II} by [15]aneS_5 has also been investigated. $[Ni([15]aneS_5)]^{2+}$ is square-pyramidal in the solid state, and five-coordinate in CH_3NO_2. However, in the presence of donor solvents (CH_3CN, pyridine) or Cl^-, six-coordinate adducts $[Ni([15]aneS_5)(L)]^{n+}$ are formed. $[Ni([15]aneS_5)]^{2+}$ resembles the Ni^{II} tetrathia complexes in this regard (Chapter 2), rather than the $[Ni[9]aneS_3)(PP)]^{2+}$ compounds.

No reversible electrochemical processes were observed for $[Ni([15]aneS_5)(NCCH_3)]^{2+}$ in $CH_3CN/^nBu_4NPF_6$, either in the absence or presence of CO, CO_2 or O_2. Hence, this complex is not a useful model for Ni sites in metalloproteins (Section 4.1), even though the Ni coordination spheres in such systems are known to contain S donor ligands[26]. The electrochemistry of the $[Ni([9]aneS_3)(PP)]^{2+}$ complexes is described in Chapter 4.

	dppe					
	PP = dppm	Molecule 1	Molecule 2	dcpe	tdpme	$[Ni([15]aneS_5)]^{2+}$
Ni-S(1) (Å)	2.4007(21)	2.381(3)	2.399(3)	2.6521(20)	2.458(5)	2.413(5)
Ni-S(4) (Å)	2.2179(25)	2.248(3)	2.243(3)	2.2260(19)	2.266(5)	2.177(6)
Ni-S(7) (Å)	2.2336(24)	2.225(3)	2.226(3)	2.2402(20)	2.242(5)	2.146(7)
Ni-P(1)/S(10)* (Å)	2.1747(19)	2.195(3)	2.184(3)	2.1654(19)	2.224(4)	2.169(6)
Ni-P(2)/S(13)* (Å)	2.1820(20)	2.193(3)	2.187(3)	2.2173(19)	2.214(4)	2.198(6)
S(4)-Ni-P(1)/S(10)* (o)	164.26(9)	162.27(13)	160.85(13)	161.69(8)	162.71(17)	166.45(23)
S(7)-Ni-P(2)/S(13)* (o)	162.52(8)	169.71(13)	168.57(13)	153.50(8)	164.50(16)	165.82(25)
P(1)-Ni-P(2) (o)	73.05(7)	85.26(12)	84.68(11)	84.02(7)	91.07(15)	-

* $[Ni([15]aneS_5)]^{2+}$

Table 3.15: Selected Structural Parameters for $[Ni([9]aneS_3)(PP)]^{2+}$ and $[Ni([15]aneS_5)]^{2+}$

	PP = dppm	dppe Molecule 1	dppe Molecule 2	dcpe	tdpme	$[Ni([15]aneS_5)]^{2+}$
Distance (Å) above plane† of						
S(4)	0.0170	-0.0747	-0.0790	0.0852	-0.0172	0.0065
S(7)	-0.0170	0.0768	0.0819	-0.0801	0.0176	-0.0068
P(1)/S(10)*	0.0210	-0.0817	-0.0886	0.0825	-0.0176	0.0067
P(2)/S(13)*	-0.0210	0.0796	0.0857	-0.0876	0.0172	-0.0064
Ni	0.2618	0.2634	0.2830	0.4219	0.3178	0.2600
σ(Plane) (Å)	0.0191	0.0783	0.0839	0.0839	0.0174	0.0066

* $[Ni([15]aneS_5)]^{2+}$. σ(Plane) = Average deviation of the basal donors from the least-squares plane.

†Plane of best fit through the four based donor atoms of the square-pyramidal complex cation.

Table 3.16: Least-Squares Basal Planes for $[Ni([9]aneS_3)(PP)]^{2+}$ and $[Ni([15]aneS_5)]^{2+}$

3.4 EXPERIMENTAL

3.4.1 The Synthesis of $[Ni(dppm)Cl_2]$[139]

A solution of $NiCl_2.6H_2O$ (0.62 g, $2.6x10^{-3}$ mol) in 60 cm^3 2:1 2-propanol/methanol was mixed with dppm (1.00 g, $2.6x10^{-3}$ mol) in 100 cm^3 warm 2-propanol. The mixture was refluxed for 2 hrs, giving a red precipitate. The mixture was cooled and filtered, and the solid product washed with cold 2-propanol (yield: 0.92 g, 69%). Mol. wt. 514.01. Elemental analysis: found C = 57.9, H = 4.28%; calculated for $[C_{25}H_{22}P_2Cl_2Ni]$ C = 58.4, H = 4.31%. F.a.b. mass spectrum: found M^+ = 477, 442, 383; calculated for:

$[^{58}Ni(dppm)^{35}Cl]^+$ $M^+ = 477$

$[^{58}Ni(dppm)]^+$ $M^+ = 442$

$[dppm-H]^+$ $M^+ = 383$

I.R. spectrum (KBr disc): 3060 w, 3040 w, 2950 w, 2910 w, 1585 w, 1570 w, 1480 m, 1460 w, 1435s, 1400 w, 1380 w, 1355 w, 1335 m, 1310 m, 1280 w, 1260 w, 1235 w, 1185 m, 1160 m, 1100 s, 1080 w, 1055 w, 1025 m, 1000 m, 975 w, 920 w, 845 w, 785 w, 745s, 735 m, 720 s, 690 s, 655 m, 620 w, 545 m, 525 w, 505 s, 480 m, 445 m, 360 w, 315 s cm^{-1}.

3.4.2 The Synthesis of $[Ni(dppe)Cl_2]$[140]

Method as for 3.4.1, using $NiCl_2.6H_2O$ (0.60 g, $2.5x10^{-3}$ mol) and dppe (1.00 g, $2.5x10^{-3}$ mol). The product was a fine orange solid (yield 1.05 g, 80%). Mol. wt. 528.04. Elemental analysis: found C = 58.7, H = 4.50%; calculated for $[(C_{26}H_{24}P_2Cl_2Ni]$ C = 59.1, H =

4.55%. F.a.b. mass spectrum: M^+ = 561, 491; calculated for

$[^{58}Ni^{35}Cl_3(dppe)]^+$ $M^+ = 561$

$[^{58}Ni^{35}Cl(dppe)]^+$ $M^+ = 491$

^{31}P n.m.r. spectrum (36.23 MHz, $CDCl_3$, 298 K) δ = 57.35 ppm. I.R. spectrum (KBr disc): 3050 w, 2970 w, 2840 w, 1585 w, 1570 w, 1480 m, 1435 s, 1415 w, 1400 m, 1335 w, 1310 w, 1265 w, 1230 w, 1190 m, 1160 w, 1120 w, 1100 s, 1065 w, 1025 m, 995 m, 920 w, 875 m, 850 w, 815 s, 750 s, 715 s, 700 s, 690 s, 655 m, 615 w, 530 s, 480 s, 450 w, 430 w, 390 w, 340 m, 325 s cm^{-1}.

3.4.3 The Synthesis of $[Ni(dppv)Cl_2]$[141]

Anhydrous $NiCl_2$ (0.41 g, $3.2x10^{-3}$ mol) and dppv (0.50 g, $1.3x10^{-3}$ mol) were refluxed in 50 cm^3 absolute ethanol for 1 hr. The resulting orange precipitate was filtered hot, and washed with cold ethanol. Yield = 0.61 g, 92%. Mol. wt. 526.03. Elemental analysis: found C = 59.3, H = 4.17%; calculated for $[C_{26}H_{22}P_2Cl_2Ni]$ C = 59.3, H = 4.18%. F.a.b. mass spectrum: found M^+ = 559, 524, 489, 454; calculated for:

$[^{58}Ni^{35}Cl_3(dppv)]^+$ $M^+ = 559$

$[^{58}Ni^{35}Cl_2(dppv)]^+$ $M^+ = 524$

$[^{58}Ni^{35}Cl(dppv)]^+$ $M^+ = 489$

$[^{58}Ni(dppv)]^+$ $M^+ = 454$

^{31}P n.m.r. spectrum (36.23 MHz, $CDCl_3$, 298 K) δ = 64.62 ppm. I.R. spectrum (KBr disc): 3060 w, 2980 m, 1580 w,

1570 w, 1480 m, 1430 s, 1335 w, 1310 w, 1275 w, 1185 w, 1160 w, 1100 s, 1070 w, 1025 w, 1000 m, 970 w, 850 w, 780 s, 740 s, 705 s, 690 s, 620 w, 560 s, 535 m, 510 w, 480 m, 460 m, 340 m, 315 m cm^{-1}.

3.4.4 The Synthesis of [Ni(dcpe)Cl_2]

Method as for 3.4.1, using $NiCl_2.6H_2O$ (0.282 g, $1.2x10^{-3}$ mol) and dcpe (0.50 g, $1.2x10^{-3}$ mol) and reducing solvent volumes accordingly. The product was isolated as an orange micro-crystalline solid (yield 0.58 g, 87%). Mol. wt. 552.23. Elemental analysis: found C = 56.5, H = 8.81%; calculated for [$C_{26}H_{48}P_2Cl_2Ni$] C = 56.6, H = 8.76%. F.a.b. mass spectrum: found M^+ = 585, 550, 515, 480; calculated for

$[^{58}Ni^{35}Cl_3(dcpe)]^+$	$M^+ = 585$
$[^{58}Ni^{35}Cl_2(dcpe)]^+$	$M^+ = 550$
$[^{58}Ni^{35}Cl(dcpe)]^+$	$M^+ = 515$
$[^{58}Ni(dcpe)]^+$	$M^+ = 480$

^{31}P n.m.r. spectrum (36.23 MHz, $CDCl_3$, 298 K) δ = 82.65 ppm. I.R. spectrum (KBr disc): 2920 vs, 2840 s, 2640 w, 1440 s, 1400 s, 1340 m, 1320 m, 1300 m, 1290 m, 1265 m, 1200 m, 1170 m, 1145 w, 1115 m, 1080 w, 1045 w, 1005 s, 915 m, 885 s, 860 s, 845 s, 815 s, 790 s, 750 s, 735 m, 670 s, 650 m, 535 s, 510 m, 485 m, 460 m, 440 m, 400 m, 370 m, 340 m, 315 s cm^{-1}.

3.4.5 The Synthesis of $[Ni(dmpe)Cl_2]$[140a]

The method of 3.4.1 was followed, using $NiCl_2.6H_2O$ (0.39 g, $1.7x10^{-3}$ mol) and dmpe (0.25 g, $1.7x10^{-3}$ mol), reducing solvent volumes accordingly. The product was a microcrystalline orange solid (yield 0.37 g, 79%). Mol. wt. 279.76. Elemental analysis: found C = 25.0, H = 5.65%; calculated for $[C_6H_{16}P_2Cl_2Ni]$ C = 25.6, H = 5.72%. F.a.b. mass spectrum: found M^+ = 278, 243; calculated for

$[^{58}Ni^{35}Cl_2(dmpe)]^+$ $M^+ = 278$

$[^{58}Ni^{35}Cl(dmpe)]^+$ $M^+ = 243$

^{31}P n.m.r. spectrum (36.23 MHz, $CDCl_3$, 298 K) δ = 50.62 ppm. I.R. spectrum (KBr disc): 2970 w, 2940 w, 2900 w, 1420 s, 1405 m, 1295 m, 1280 s, 1245 m, 1135 w, 1085 m, 985 m, 950 s, 910 s, 865 m, 840 m, 800 w, 760 s, 735 m, 720 s, 665 m, 650 w, 460 m, 320 m, 300 m cm^{-1}.

3.4.6 The Synthesis of $[Ni(dppp)Cl_2)$[140b]

Method as for 3.4.1, using $NiCl_2.6H_2O$ (0.58 g, $2.4x10^{-3}$ mol) and dppp (1.00 g, $2.4x10^{-3}$ mol), giving a red solid product (yield 1.00 g, 75%). Mol. wt. 542.07. Elemental analysis: found C = 59.8, H = 4.88%; calculated for $[C_{27}H_{26}P_2Cl_2Ni]$ C = 59.8, H = 4.84%. F.a.b. mass spectrum: found M^+ = 575, 505, 470; calculated for

$[^{58}Ni^{35}Cl_3(dppp)]^+$ $M^+ = 575$

$[^{58}Ni^{35}Cl(dppp)]^+$ $M^+ = 505$

$[^{58}Ni(dppp)]^+$ $M^+ = 470$

I.R. spectrum (KBr disc): 3040 w, 2960 w, 2910 w, 1580 w,

1570 w, 1480 m, 1450 w, 1430 s, 1405 s, 1330 w, 1310 w, 1240 w, 1185 w, 1145 m, 1095 s, 1065 w, 1025 w, 995 m, 940 m, 915 w, 845 w, 815 m, 740 s, 715 w, 700 s, 660 m, 540 m, 510 s, 475 w, 455 m, 360 w, 345 w, 320 s cm^{-1}.

3.4.7 The Synthesis of $[Ni(tdpme)Cl_2]$

The method described in 3.4.1 was followed, using $NiCl_2.6H_2O$ (0.38 g, $1.6x10^{-3}$ mol) and tdpme (1.00 g, $1.6x10^{-3}$ mol), reducing solvent volumes as required. The product was an orange solid (yield 0.99 g, 82%). Mol. wt. 754.30. Elemental analysis: found C = 63.3, H = 5.21%; calculated for $[C_{41}H_{39}P_3Cl_2Ni]$ C = 65.3, H = 5.17%. F.a.b. mass spectrum: found M^+ = 717, 682; calculated for

$[^{58}Ni^{35}Cl(tdpme)]^+$ $M^+ = 717$

$[^{58}Ni(tdpme)]^+$ $M^+ = 682$

^{31}P n.m.r. spectrum (36.23 MHz, $CDCl_3$, 298 K) δ = 29.21 (1P), 25.98 ppm (2P). I.R. spectrum (KBr disc): 3045 m, 2980 w, 2960 w, 1585 m, 1570 w, 1545 m, 1480 s, 1450 w, 1435 s, 1400 w, 1380 w, 1335 w, 1310 m, 1280 w, 1260 w, 1185 m, 1160 m, 1115 m, 1100 s, 1070 w, 1055 w, 1025 m, 1000 m, 970 w, 935 w, 840 m, 815 w, 800 m, 745 s, 725 m, 710 m, 700 s, 655 w, 580 m, 560 m, 550 w, 530 m, 515 s, 485 w, 450 m, 345 w, 330 m cm^{-1}.

3.4.8 The Synthesis of $[Ni([9]aneS_3(dppm)](PF_6)_2$

$[9]aneS_3$ (0.030 g, $1.6x10^{-4}$ mol) and $TlPF_6$ (0.112 g, $3.2x10^{-4}$ mol) were added to a solution of $[Ni(dppm)Cl_2]$

(0.172 g, 3.2×10^{-4} mol) in nitromethane (6 cm^3). The mixture was stirred for 30 mins, yielding an intense red solution and a fine white precipitate. The precipitate was filtered, and the product crystallised from the filtrate with diethyl ether. Fractional recrystallisation from $MeCN/Et_2O$ was necessary to remove a substantial amount of $[Ni([9]aneS_3)_2](PF_6)_2$[70] impurity. The product was a dark green crystalline solid (yield: 30 mg, 20%).

Alternatively, $[Ni(dppm)Cl_2]$ (0.172 g, 3.2×10^{-4} mol) and $[9]aneS_3$ (0.030 g, 1.6×10^{-4} mol) were stirred at room temperature in methanol (10 cm^3) for 1 hr. NH_4PF_6 (0.052 g, 3.2×10^{-4} mol) was then added to the resulting red solution, and the mixture stirred for a further 30 mins, giving a green precipitate. The product was collected, and recrystallised as above (yield: 35 mg, 23%). Mol. wt. 913.25. Elemental analysis: found C = 41.0, H = 3.79%; calculated for $[C_{31}H_{34}S_3P_2Ni](PF_6)_2$; C = 40.8, H = 3.75%. F.a.b. mass spectrum (3-NOBA matrix): found M^+ = 766, 622, 442, 423; calculated for:

$[^{58}Ni([9]aneS_3\text{-}H)(dppm)(PF_6)]^+$ $M^+ = 766$

$[^{58}Ni([9]aneS_3)(dppm)]^+$ $M^+ = 622$

$[^{58}Ni(dppm)]^+$ $M^+ = 442$

$[^{58}Ni([9]aneS_3)(PPh_2)]^+$ $M^+ = 423$

^1H n.m.r. spectrum (200.13 MHz, CD_3CN, 298 K): δ = 7.81-7.22 ppm (m, 20H, PPh_2), 4.55 (t, $^2J_{P-H}$ = 4.8 Hz, 2H, PCH_2P), 2.95-2.40 (m, 12H, $[9]aneS_3$). ^{13}C D.E.P.T. n.m.r. spectrum (50.32 MHz, CD_3CN, 298 K): δ = 133.08 ppm (s,

p-PPh_2), 132.24 (s, m-PPh_2), 129.50 (s, o-PPh_2), 35.38 (s, [9]aneS_3), 31.45 (t, $^1J_{P-C}$ = 25 Hz, PCH_2P). ^{31}P n.m.r. spectrum (36.23 MHz, CD_3CN, 298 K) δ = -27.85 ppm. U.V./vis spectrum (MeCN): λ_{max} = 563 nm (ε_{max} = 124 dm^3 mol^{-1} cm^{-1}), 418 (1,920), 317 (14,520), 268 (20,180). I.R. spectrum (KBr disc): 3060 w, 3000 w, 2970 m, 2910 w, 1585 w, 1570 w, 1480 m, 1440 s, 1410 m, 1375 w, 1360 m, 1335 w, 1310 m, 1285 w, 1260 w, 1185 m, 1165 w, 1100 s, 1070 w, 1025 w, 1000 m, 940 w, 840 vs, 750 m, 720 m, 705 w, 690 s, 660 w, 615 w, 565 s, 540 s, 500 s, 480 m, 455 w, 420 w, 385 w cm^{-1}.

3.4.9 Single Crystal Structure of [Ni([9]aneS_3)(dppm)]$(PF_6)_2$

Vapour diffusion of diethyl ether into an acetonitrile solution of the complex yielded dark green tablets of crystallographic quality.

Crystal Data:

$[C_{31}H_{34}S_3P_2Ni](PF_6)_2$, Mr = 913.25. Triclinic, space group $P\bar{1}$, a = 10.9748(25), b = 13.9702(20), c = 15.7688(24) Å, α = 80.071(7), β = 70.817(8), γ = 76.441(8)°, V = 2207.8 $Å^3$ (by least-squares refinement on diffraction angles for 30 reflections measured at $\pm\omega[31<2\theta<32°$, λ = 0.71073 Å]), Z = 2, D_C = 1.374 g cm^{-3}. Crystal dimensions 0.47 x 0.39 x 0.19 mm, μ(Mo-k_α) = 0.789 mm^{-1}, $F(000)$ = 928.

Data Collection and Processing:

Stöe STADI-4 four-circle diffractometer, $\omega/2\theta$ scan mode using the learnt profile method. Graphite-monochromated Mo-k_α radiation: 5762 reflections ($2\theta_{max}$ = 45°, h = -10→11, k = -14→15, l = 0→16), 5392 unique giving 4405 with $F>6\sigma(F)$. No significant crystal decay, no absorption correction.

Structure Analysis and Refinement:

A Patterson synthesis located the Ni atom, and the structure was then developed using least-squares refinement and difference Fourier synthesis. During refinement, the [9]aneS_3 carbon atoms were found to be disordered over two orientations; this was successfully modelled using the constrained distances S-C = 1.83 Å, C-C = 1.52 Å, S-C-C = 2.74 Å. One PF_6^- counterion was also disordered, and was modelled over two distinct orientations, with a 70:30 occupancy ratio. The phosphine phenyl groups were refined as rigid groups. Anisotropic thermal parameters were refined for all non-H atoms with site occupancy factory > ½, and H atoms were included in fixed, calculated positions. The weighting scheme $w^{-1} = \sigma^2(F) + 0.000405\ F^2$ gave satisfactory agreement analyses. At final convergence R = 0.0689, R_W = 0.0970, S = 1.191 for 434 independent parameters, and the final difference Fourier synthesis showed no peak above or below +0.86 or

-0.48 eÅ^{-3}.

3.4.10 The Synthesis of [Ni([9]aneS$_3$)(dppe)](PF$_6$)$_2$

Method as for 3.4.8, with [Ni(dppe)Cl$_2$] (0.088 g, 1.6x10^{-4} mol) and [9]aneS$_3$ (0.030 g, 1.6x10^{-4} mol). The product was a dark green crystalline solid (yield 0.133 g, 86%). Mol. wt. 927.28. Elemental analysis: found C = 41.4, H = 3.96%; calculated for [C$_{32}$H$_{36}$S$_3$P$_2$Ni](PF$_6$)$_2$ C = 41.5, H = 3.91%. F.a.b. mass spectrum: found M^+ = 781, 635, 455; calculated for

[^{58}Ni([9]aneS$_3$)(dppe)(PF$_6$)]$^+$ M^+ = 781

[^{58}Ni([9]aneS$_3$-H)(dppe)]$^+$ M^+ = 635

[^{58}Ni(dppe-H)]$^+$ M^+ = 455

^{1}H n.m.r. spectrum (360.13 MHz, CD_3NO_2, 298 K) δ = 7.88-7.63 ppm (m, 20H, PPh_2), 3.22 (d, $^2J_{P-H}$ = 19 Hz, PCH_2), 2.96-2.38 (m, 12H, [9]aneS$_3$). ^{13}C n.m.r. D.E.P.T. spectrum (50.32 MHz, CD_3NO_2, 298 K) δ = 132.52 ppm, (s, p-PPh_2), 131.61 (d, $^3J_{P-C}$ = 4.4 Hz, m-PPh_2), 129.08 (d, $^2J_{P-C}$ = 5.2 Hz, o-PPh_2), 35.16 (s, [9]aneS$_3$), 28.71(dd, $^1J_{P-C}$ = 24 Hz, $^2J_{P-C}$ = 24 Hz, PCH_2). ^{31}P n.m.r. spectrum (36.23 MHz, CD_3NO_2, 298 K) δ = 67.58 ppm. U.V./vis spectrum (CH_3CN): λ_{max} = 560 nm (ε_{max} = 110.1 dm^3 mol^{-1} cm^{-1}), 427 (1,765), 316 (16,970), 256 (23,585). I.R. spectrum (KBr disc) 3040 w, 2980 m, 2940 m, 1580 m, 1570 w, 1480 m, 1435 s, 1410 m, 1380 w, 1340 w, 1305 m, 1290 m, 1235 w, 1180 m, 1160 w, 1100 w, 1060 w, 995 m, 945 w, 905 m, 875 m, 840 vs, 810 m, 755 s, 725 m, 715 m,

705 s, 690 s, 660 m, 615 w, 560 s, 510 w, 485 s, 460 m, 450 w, 430 m, 385 m, 365 w cm^{-1}.

3.4.11 Single Crystal Structure of [Ni([9]aneS$_3$(dppe)](BF$_4$)$_2$

A sample of [Ni([9]aneS$_3$)(dppe)](BF$_4$)$_2$ was prepared as for the PF_6^- salt, using $AgBF_4$ to perform the counterion metathesis. Elemental analysis: found C = 46.9, H = 4.48%; calculated for $[C_{32}H_{36}S_3P_2Ni](BF_4)_2$ C = 47.4, H = 4.47%. Vapour diffusion of diethyl ether into a solution of the complex in nitromethane gave olive green plates.

Crystal Data

$[C_{32}H_{36}S_3P_2Ni](BF_4)_2$, M_r = 811.00. Monoclinic, space group $P2_1/n$, a = 12.8730(10), b = 39.8212(3), c = 14.1368(9) Å, β = 91.666(6)°, V = 7243.8 Å^3 (by least-squares refinement on diffraction angles for 56 reflections measured at $\pm\omega[32,2\theta<34°$, λ = 1.54184 Å]), Z = 8, D_C = 1.487 g cm^{-3}. Crystal dimensions 0.46 x 0.31 x 0.09 mm, μ(Cu-k$_\alpha$) = 3.789 mm^{-1}, $F(000)$ = 3328.

Data Collection and Processing:

Stöe STADI-4 four-circle diffractometer, $\omega/2\theta$ scan mode using the learnt profile method. Graphite-monochromated Cu-k$_\alpha$ radiation : 7127 reflections measured ($2\theta_{max}$ = 95°, h = -12→12, k = 0→38, l = 0→13), 5946 unique (R_{int} 0.0143) giving 4449 with $F>6\sigma(F)$. An initial

absorption correction was applied using ψ-scans (maximum and minimum transmission factors 0.4576, 0.1603 respectively). No crystal decay.

Structure Analysis and Refinement:

The Ni atom positions were deduced from a Patterson synthesis, and repeated cycles of least-squares refinement and difference Fourier synthesis located all other non-H atoms. During refinement three of the four BF_4^- counterions were found to be disordered. These were modelled using partially occupied F atoms, such that the total number of F atoms associated with each boron atom equalled four. A partially occupied water solvent molecule was also included. The phenyl rings were refined as rigid groups, and H atoms were included in fixed, calculated positions. Anisotropic thermal parameters were refined for Ni, S, P, F and non-aryl C atoms. The weighting scheme $w^{-1} = \sigma^2(F) + 0.000373F^2$ gave satisfactory agreement analyses. At convergence, $R = 0.0720$, $R_w = 0.0929$, $S = 1.196$ for 580 independent parameters, and in the final difference Fourier synthesis no peak was observed above +0.54 or below -0.49 eÅ^3.

3.4.12 The Synthesis of $[Ni([9]aneS_3)(dppv)](PF_6)_2$

The method described in section 3.4.8 was followed, using $[Ni(dppv)Cl_2]$ (0.088 g, 1.6×10^{-4} mol) and $[9]aneS_3$ (0.030 g, 1.6×10^{-4} mol). The product was isolated as a

dark green solid (yield 0.128 g, 82%). Mol. wt. 925.27. Elemental analysis: found C = 41.1, H = 3.74%; calculated for $[C_{32}H_{34}S_3P_2Ni](PF_6)_2$ C = 41.5, H = 3.70%. F.a.b. mass spectrum: found M^+ = 779, 634, 454; calculated for

$[^{58}Ni([9]aneS_3)(dppv)(PF_6)]^+$ $M^+ = 779$

$[^{58}Ni([9]aneS_3)(dppv)]^+$ $M^+ = 634$

$[^{58}Ni(dppv)]^+$ $M^+ = 454$

^1H n.m.r. spectrum (200.13 MHz, CD_3CN, 298 K) δ = 7.86-7.40 ppm (m, 20H, PPh_2), 2.90-2.28 (m, 12H, [9]aneS_3), 2.08 (s, 2H, PC*H*). ^{13}C {^1H} n.m.r. spectrum (50.32 MHz, CD_3CN, 298 K) δ = 146.35 ppm (dd, $^1J_{P-C}$ = 37.5, $^2J_{P-C}$ = 37.5 Hz, P*C*H), 133.40 (s, p-PPh_2), 132.40 (s, m-PPh_2), 129.81 (s, o-PPh_2), 126.18 (dd, $^1J_{P-C}$ = 26.4, J_{P-C} = 26.4 Hz, b-PPH_2), 36.12 (s, [9]aneS_3). ^{31}P n.m.r. spectrum (36.23 MHz, CD_3CN, 298 K) δ = 75.52 ppm. U.V./vis spectrum (CH_3CN): λ_{max} = 580 nm (ε_{max} = 64.7 dm^3 $mol^{-1}cm^{-1}$), 423 (1,795), 320 (14,630), 250 (28,650). I.R. spectrum (KBr disc) 3050 w, 3020 m, 2960 w, 1580 w, 1570 w, 1480 m, 1440 s, 1410 m, 1375 w, 1340 w, 1310 m, 1270 w, 1250 w, 1190 m, 1165 w, 1100 s, 1070 w, 1025 w, 1000 m, 985 w, 940 w, 835 vs, 760 s, 735 s, 700 s, 620 w, 560 s, 525 m, 480 m, 455 m, 410 m, 370 w cm^{-1}.

3.4.13 The Synthesis of $[Ni([9]aneS_3)(dcpe)](PF_6)_2$

Method as in 3.4.8, using $[Ni(dcpe)Cl_2]$ (0.092, $1.6x10^{-4}$ mol) and [9]aneS_3 (0.030 g, $1.6x10^{-4}$ mol). The product was a red microcrystalline solid (yield 0.139 g,

88%). Mol. wt. 951.47. Elemental analysis: found C = 41.1, H = 6.43, N = 1.52%; calculated for $[C_{32}H_{60}S_3P_2Ni](PF_6)_2$. CH_3CN C = 41.1, H = 6.40, N = 1.42%. F.a.b. mass spectrum: found M^+ = 805, 660, 480; calculated for

$[^{58}Ni([9]aneS_3)(dcpe)(PF_6)]^+$ $M^+ = 805$

$[^{58}Ni([9]aneS_3)(dcpe)]^+$ $M^+ = 660$

$[^{58}Ni(dcpe)]^+$ $M^+ = 480$

^1H n.m.r. spectrum (200.13 MHz, CD_3CN, 298 K) δ = 3.42-2.95 ppm (m, 12H, [9]aneS$_3$), 2.19 (d, $^2J_{P-H}$ = 14.6 Hz, 4H, PCH_2), 2.12-1.07 (m, 44H, PCyc$_2$). ^{13}C D.E.P.T. n.m.r. spectrum (50.32 MHz, CD_3CN, 298 K), δ = 36.98 ppm (dd, $^1J_{P-C}$ = 9.8 Hz, b-Pcyc$_3$), 36.25 (s, [9]aneS$_3$), 28.51 (s, α-Pcyc$_2$), 27.41 (s, α-PCyc$_2$), 25.91 (s, β-Cyc$_2$), 25.60 (s, β-PCyc$_2$), 24.70 (s, γ-PCyc$_2$), 21.88 (dd, $^1J_{P-C}$ = 20.1 Hz, PCH_2). ^{31}P n.m.r. spectrum (36.23 MHz, CD_3CN, 298 K) δ = 89.65 ppm. U.V./vis spectrum (MeCN): λ_{max} = 570 nm (ε_{max} = 200 $dm^3 mol^{-1} cm^{-1}$), 448 (775), 325 (6,730), 293 (12,670), 245 (13,190). I.R. spectrum (KBr disc): 2990 m, 2920 s, 2840 s, 2800 w, 1440 s, 1405 s, 1370 w, 1345 m, 1330 m, 1320 m, 1300 w, 1290 m, 1270 s, 1245 w, 1205 s, 1175 s, 1150 w, 1115 s, 1090 w, 1070 m, 1040 m, 1005 s, 940 m, 910 w, 835 vs, 750 w, 735 m, 670 m, 650 m, 620 w, 550 s, 530 s, 515 m, 480 m, 455 m, 440 w, 390 m, 360 m cm^{-1}.

3.14.4 Single Crystal Structure of [Ni([9]aneS$_3$)(dcpe)](PF$_6$)$_2$.1.25 CH$_3$CN

Red platelets of X-ray quality were grown by vapour diffusion of diethyl ether into a solution of the complex in acetonitrile. A suitable crystal was sealed in a Lindeman tube to prevent solvent loss.

Crystal Data:

$[C_{32}H_{60}S_3P_2Ni](PF_6)_2 \cdot {}^5/_4CH_3CN$, M_r = 1002.79. Triclinic, space group $P\bar{1}$, a = 12.432(8), b = 13.382(4), c = 15.070(6) Å, α = 86.83(2), β = 70.47(3), γ = 77.82(2)°, V = 2304.5 Å^3 (by least squares refinement on diffraction angles for 36 reflections measured at ± w [30<2σ<32°, λ = 0.71073 Å]), Z = 2, D_c = 1.445 g cm^{-3}, crystal dimensions 0.58 x 0.51 x 0.12 mm, μ(Mo-K$_\alpha$) = 1.526 mm^{-1}, F(000) = 2094.

Data Collection and Processing:

Stoë STADI-4 four-circle diffractometer, $\omega/2\theta$ scan mode with ω scan width (0.99 + 0.347 tan θ)°. Graphite monochromated Mo-K$_\alpha$ radiation : 6021 reflections measured ($2\theta_{max}$ = 45°, h-12→13, k-14→14, l0→16), 5271 unique, giving 3667 with $F>4\sigma(F)$. No crystal decay, no absorption correction.

Structure Analysis and Refinement:

A Patterson synthesis revealed the Ni atom position, and the structure was developed by repeated cycles of

least squares refinement and difference Fourier synthesis. During refinement, a partially occupied CH_3CN molecule was found to be disordered, about a crystallographic inversion centre at the centre of the C≡N bond. Anisotropic thermal parameters were refined for all wholly occupied non-H atoms, and the H atoms were included in fixed, calculated positions. The weighting scheme $w^{-1} = \sigma^2(F) + 0.001001\,F^2$ gave satisfactory agreement analyses. At convergence R = 0.0491, R_W = 0.0627, S = 1.053 for 508 independent parameters. The maximum and minimum residuals in the final difference Fourier synthesis were +0.51 and -0.29 eÅ^{-3} respectively.

3.4.15 The Synthesis of $[Ni([9]aneS_3)(dmpe)](PF_6)_2$

Method as for 3.4.8, with $[Ni(dmpe)Cl_2]$ (0.047 g, 1.6x10^{-4} mol) and $[9]aneS_3$ (0.030 g, 1.6x10^{-4} mol). The product was isolated as a dark red crystalline solid (yield 0.080 g, 71%). Mol. wt. 679.00. Elemental analysis: found C = 21.0, H = 4.18%; calculated for $[C_{12}H_{28}S_3P_2Ni](PF_6)_2$: C = 21.2, H = 4.16%. F.a.b. mass spectrum: found M^+ = 533, 388; calculated for

$[^{58}Ni([9]aneS_3)(dmpe)(PF_6)]^+$ $M^+ = 533$

$[^{58}Ni([9]aneS_3)(dmpe)]^+$ $M^+ = 388$

^1H n.m.r. spectrum (200.13 MHz, CD_3CN, 298 K) δ = 3.22-2.91 ppm (m, 12H, $[9]aneS_3$), 2.17 (br, 4H, PCH_2), 1.66 (m, 12H, PCH_3). ^{13}C D.E.P.T. n.m.r. spectrum (50.32 MHz, CD_3CN, 298 K) δ = 35.69 ppm (s, $[9]aneS_3$), 26.89 (dd,

$^{1}J_{P-C}$ = 25.9, $^{2}J_{P-C}$ = 25.9 Hz, PCH_2), 13.58 (dd, $^{1}J_{P-C}$ = 14.7, $^{3}J_{P-C}$ = 14.7 Hz, PCH_3), 13.49 (dd, $^{1}J_{P-C}$ = 14.4, $^{3}J_{P-C}$ = 14.4 Hz, PCH_3). ^{31}P n.m.r. spectrum (36.23 MHz, CD_3CN, 298 K) δ = 58.02 ppm. U.V./vis spectrum (CH_3CN) λ_{max} = 540 nm (ε_{max} = 166 dm^{-3} mol^{-1} cm^{-1}), 415 (662), 284 (13,150), 249 (17,380). I.R. spectrum (KBr disc) 3000 m, 2945 w,, 2920 w, 1450 s, 1420 s, 1295 s, 1275 w, 1240 m, 1180 w, 1140 w, 1085 m, 1010 w, 995 w, 950 s, 920 m, 905 s, 860 vs, 745 m, 720 m, 690 w, 665 m, 650 w, 620 w, 560 s, 485 w, 470 w, 460 m, 440 w, 380 m, 360 m cm^{-1}.

3.4.16 The Synthesis of $[Ni([9]aneS_3)(dppp)](PF_6)_2$

The method of 3.4.8 was followed, using $[Ni(dppp)Cl_2]$ (0.090 g, $1.6x10^{-4}$ mol) and $[9]aneS_3$ (0.030 g, $1.6x10^{-4}$ mol). The product was a green microcrystalline solid (yield 0.125 g, 80%). Mol. wt. 941.31. Elemental analysis: found C = 43.4, H = 4.33, N = 2.07%; calculated for $[C_{33}H_{38}S_3P_2Ni](PF_6)_2$. $3/2CH_3CN$ C = 43.1, H = 4.27, N = 2.09%. F.a.b. mass spectrum: found M^+ = 794, 650, 470; calculated for:

$[^{58}Ni([9]aneS_3\text{-}H)(dppp)(PF_6)]^+$ M^+ = 794

$[^{58}Ni([9]aneS_3)(dppp)]^+$ M^+ = 650

$[^{58}Ni(dppp)]^+$ M^+ = 470

^{1}H n.m.r. spectrum (200.13 MHz, CD_3CN, 298 K) δ = 7.69-7.50 ppm (m, 20H, PPh_2), 2.81 (dt, $^{2}J_{P-H}$ = 9.7, J_{H-H} = 5.8 Hz, 4H, PCH_2CH_2), 2.75-2.32 (m, 12H, $[9]aneS_3$), 2.19 (br, 2H, PCH_2CH_2). ^{13}C D.E.P.T. n.m.r. spectrum

(50.32 MHz, CD_3CN, 298 K) δ = 132.51 ppm (s, p-PPh_2), 132.29 (s, m-PPh_2), 129.17 (s, o-PPh_2), 36.39 (s, [9]aneS_3), 23.27 (dd, $^1J_{P-C}$ = 18.5, $^3J_{P-C}$ = 18.5 Hz, PCH_2CH_2), 16.39 (s, PCH_2CH_2). ^{31}P n.m.r. spectrum (36.23 MHz, CD_3CN, 298 K) δ = 2.29 ppm. U.V./vis spectrum (CH_3CN): λ_{max} = 600 nm (ε_{max} = 133 dm^3 mol^{-1} cm^{-1}), 452 (1,365), 335 (15,860), 260 (11,990). I.R. spectrum (KBr disc): 3070 w, 3050 m, 2990 m, 2950 w, 2920 m, 2850 w, 1580 m, 1570 w, 1480 m, 1445 w, 1435 s, 1415 m, 1395 w, 1370 w, 1340 w, 1320 m, 1300 m, 1270 w, 1250 w, 1190 w, 1150 m, 1130 w, 1090 s, 1070 w, 1050 w, 1025 w, 995 s, 975 s, 930 w, 915 w, 910 m, 860 vs, 780 m, 755 s, 745 s, 700 s, 665 m, 615 w, 555 s, 530 w, 510 s, 490 s, 480 w, 425 m, 375 m cm^{-1}.

3.4.17 The Synthesis of [Ni([9]aneS_3)(tdpme)]$(PF_6)_2$

Method as for 3.4.8, using [Ni(tdpme)Cl_2] (0.128 g, $1.6x10^{-4}$ mol) and [9]aneS_3 (0.030 g, $1.6x10^{-4}$ mol). The product was an olive-green microcrystalline solid (yield 0.152 g, 78%). Mol. wt. 1153.54. Elemental analysis: found C = 48.4, H = 4.46%; calculated for $[C_{47}H_{51}S_3P_3Ni](PF_6)_2$ C = 48.9, H = 4.42%. F.a.b. mass spectrum: found M^+ = 1007, 861, 682; calculated for

$[^{58}Ni([9]ane S_3)(tdpme)(PF_6)]^+$ M^+ = 1007

$[^{58}Ni([9]ane S_3\text{-}H)(tdpme)]^+$ M^+ = 861

$[^{58}Ni(tdpme)]^+$ M^+ = 682

^1H n.m.r. spectrum (200.13 MHz, CD_3CN, 298 K) δ =

7.87-7.06 ppm (m, 30H, PPh_2), 2.74-2.07 (m, 18H, [9]aneS_3 + PCH_2C), 0.42 (s, 3H, CCH_3). $^{13}C\{^1H\}$ n.m.r. spectrum (50.32 MHz, CD_3CN, 298 K) δ = 133.25-128.07 ppm (m, PPh_2), 36.53 (s, [9]aneS_3), 35.70 (dd, $^1J_{P-C}$ = 15.4, $^3J_{P-C}$ = 15.4 Hz, bound PCH_2C), 35.20 (dd, $^1J_{P-C}$ = 17.8, $^3J_{P-C}$ = 17.8 Hz, free PCH_2C). ^{31}P n.m.r. spectrum (36.23 MHz, CD_3CN, 298 K) δ = 9.02 ppm (2P, bound PPh_2), 7.54 (1P, free PPh_2). U.V./vis spectrum (MeCN): λ_{max} = 593 nm (ε_{max} = 46.1 $dm^3\ mol^{-1}\ cm^{-1}$), 445 (1,280), 333 (11,300), 250 (19,900). I.R. spectrum (KBr disc) 3060 m, 3000 m, 2960 w, 2940 w, 2910 m, 1585 w, 1570 w, 1480 s, 1460 w, 1445 w, 1435 s, 1410 m, 1385 w, 1320 w, 1300 m, 1270 w, 1245 w, 1200 m, 1190 w, 1170 w, 1160 m, 1115 s, 1090 s, 1065 w, 1040 w, 1000 m, 960 w, 940 w, 835 vs, 745 s, 715 w, 700 s, 615 w, 560 s, 535 m, 510 s, 500 s, 485 w, 455 w, 440 m, 410 w cm^{-1}.

3.4.18 Single Crystal Structure of [Ni([9]aneS_3)(tdpme)]$(PF_6)_2$

Brown needles suitable for X-ray diffraction were obtained by vapour diffusion of diethyl ether into an acetonitrile solution of the complex.

Crystal Data:

$[C_{47}H_{51}S_3P_3Ni](PF_6)_2$, M_r = 1153.54. Monoclinic, space group Cc, a = 10.759(16), b = 37.399(5), c = 13.1038(29) Å, β = 103.746(11)°, V = 5139 $Å^3$ (by least-squares

refinement on diffraction angles for 39 reflections at $\pm\omega[20<2\theta<22°$, λ = 0.71073 Å]), Z = 4, D_C = 1.491 g cm^{-3}. Crystal dimensions 0.65 x 0.062 x 0.046 mm, μ(Mo-k$_\alpha$) = 0.72 mm^{-1}, $F(000)$ = 2368.

Data Collection and Processing:

Stöe STADI-4 four-circle diffractometer, $\omega/2\theta$ scan mode using the learnt profile method. Graphite-monochromated Mo-k$_\alpha$ radiation; 3962 data collected ($2\theta_{max}$ = 45°, h-11→11, k0→40, l0→14), 3034 unique (R_{int} = 0.0251), giving 2204 with $F>6\sigma(F)$. No significant crystal decay, no absorption correction.

Structure Analysis and Refinement:

The Ni atom was located using a Patterson synthesis, and the structure was then developed by successive least-squares cycles and difference Fourier synthesis. During refinement both PF_6^- ions were found to be disordered, one over two distinct orientations and one by rotation about a F-P-F axis; both were satisfactorily modelled. The phenyl rings were refined as rigid groups. Anisotropic thermal parameters were refined for Ni, S, P, non-aryl C and wholly-occupied F-atoms, and H atoms were included in fixed, calculated positions. The weighting scheme w^{-1} = $\sigma^2(F)$ + 0.000378 F^2 gave satisfactory agreement analyses. At convergence R = 0.0567, R_w = 0.0663, S = 1.164 for 352

independent parameters, and the final difference Fourier synthesis showed no feature between 0.60 and -0.27 eÅ^{-3}.

3.4.19 The Synthesis of [Ni([9]aneS$_3$)Cl$_2$]

The reaction of $NiCl_2.6H_2O$ (0.040 g, 1.6x10^{-4} mol) with [9]aneS$_3$ (0.030 g, 1.6x10^{-4} mol) in CH_3OH at 298K for 1 hr afforded a mustard yellow precipitate, which was filtered, washed with CH_3OH and dried *in vacuo* (yield 0.047 g, 91%). Mol. wt. 309.96. Elemental analysis : found C = 23.8, H = 4.86%; calculated for $[C_6H_{12}S_3Cl_2Ni].CH_3OH.\frac{1}{2}H_2O$ C = 23.9, H = 4.88%. I.R. spectrum (KBr disc) : 2960 w, 2915 w, 1440 s, 1400 s, 1280 m, 1250 w, 1180 w, 1140 m, 1125 m, 1010 w, 990 w, 930 s, 895 s, 820 s, 690 w, 670 w, 620 w, 440 m cm^{-1}.

3.4.20 The Synthesis of [Ni([15]aneS$_5$)](BF$_4$)$_2$

$Ni(BF_4)_2.6H_2O$ (0.045 g, 1.33x10^{-4} mol) was dissolved in 4 cm^3 nitromethane with 2 drops of acetic anhydride. Addition of [15]aneS$_5$ (0.040 g, 1.33x10^{-4} mol) immediately gave a deep purple solution, which was filtered and reduced to half its volume. Addition of an excess of diethyl ether yielded a purple solid product (yield 52 mg, 73%). Mol. wt. 532.80. Elemental analysis: found C = 22.4, H = 3.78%; calculated for $[C_{10}H_{20}S_5Ni](BF_4)_2$: C = 22.5, H = 3.78%. F.a.b. mass spectrum: found M^+ = 444, 358; calculated for:

$[^{58}Ni([15]aneS_5-H)(^{11}BF_4)]^+$ $M^+ = 444$

$[^{58}Ni([15]aneS_5)]^+$ $M^+ = 358$

U.V./visible spectrum ($MeNO_2$): λ_{max} = 1060 nm (sh), 823 (ε_{max} = 81 mol^{-1} M^{-1} cm^{-1}), 538 (118), 475 (sh, 89). U.V./visible spectrum (MeCN): λ_{max} = 902 nm (ε_{max} = 11.4 dm^3 mol^{-1} cm^{-1}), 572 (9.7), 312 (325), 283 (270), 254 (1,600). I.R. spectrum (KBr disc): 2990 m, 2940 m, 2840 w, 1430 s, 1285 m, 1260 w, 1060 vs, 945 w, 930 w, 900 w, 860 m, 825 w, 810 w, 680 w, 620 w, 525 s, 410 w cm^{-1}.

3.4.21 The Synthesis of $[Ni([15]aneS_5)](PF_6)_2$

A solution of $Ni(PF_6)_2$ was generated by stirring $NiCl_2.6H_2O$ (0.032 g, $1.33x10^{-4}$ mol) with an excess of $TlPF_6$ in 4 cm^3 nitromethane with a trace of acetic anhydride for 30 mins. This solution was filtered, then reacted as above. The product was a purple microcrystalline solid (yield 70 mg, 80%). Mol. wt. 649.08. Elemental analysis: found C = 18.6, H = 3.18%; calculated for $[C_{10}H_{20}S_5Ni](PF_6)_2$: C = 18.5, H = 3.11%.

3.4.22 Single Crystal Structure of $[Ni([15]aneS_5)](PF_6)_2$

Vapour diffusion of diethyl ether into a nitromethane solution of the complex yielded purple needles of crystallographic quality.

Crystal Data:

$[C_{10}H_{20}S_5Ni](PF_6)_2$, M_r = 649.08. Monoclinic, space group $P2_1$, a = 5.9862(30), b = 10.1460(67), c =

17.4024(90) Å, β = 96.038(40)°, V = 1048 Å^3 (by least-squares refinement on diffraction angles for 10 reflections measured at $\pm\omega$[26<2θ<28°, λ = 0.71073 Å]). Z = 2, D_C = 2.057 g cm^{-3}. Crystal dimensions 0.50 x 0.10 x 0.10 mm, μ(Mo-k$_\alpha$) = 1.659 mm^{-1}, F(000) = 652.

Data Collection and Processing:

Stöe STADI-4 four-circle diffractometer, $\omega/2\theta$ scan mode with ω scan-width (0.66 + 0.347 tan θ)°. Graphite-monochromated Mo-k$_\alpha$ radiation, 1485 reflections measured ($2\theta_{max}$ = 45°, h = -6→6, k = Ø→10, l = Ø→18), 1324 unique, giving 1233 with $F>2\sigma(F)$. No absorption correction. Slight crystal decay (2%) was noted during collection, and corrected for during data reduction.

Structure Analysis and Refinement:

The Ni atom was located using a Patterson synthesis, and repeated cycles of least-squares refinement followed by different Fourier synthesis identified the remaining H atoms. During refinement, one PF_6^- counterion was found to be disordered over two distinct orientations by rotation about a F-P-F axis; this was successfully modelled. Anisotropic thermal parameters were refined for Ni, S, P and ordered F atoms, and H atoms were included at fixed, calculated positions. The weighting scheme $w^{-1} = \sigma^2(F) + 0.000382F^2$ gave satisfactory agreement analyses. At final convergence R, R_W = 0.0599 and 0.0720

respectively, S = 1.623 for 216 parameters, and the final difference Fourier synthesis exhibited no feature above 0.87 or below -0.56 eÅ^{-3}.

3.4.23 The Synthesis of [Ni([15]aneS$_5$)Cl](PF$_6$)

The reaction of anhydrous $NiCl_2$ (0.022 g, 1.6x10^{-4} mol) with $TlPF_6$ (0.058 g, 1.6x10^{-4} mol) in nitromethane (4 cm^3) yielded a pale green solution and a white precipitate. The solution was filtered, and [15]aneS$_5$ (0.050 g, 1.6x10^{-4} mol) added to the filtrate. The resulting pale blue solution was stirred for 30 mins, filtered, and the blue microcrystalline product crystallised with diethyl ether (yield 0.065 g, 72%). Mol. wt. 539.63. Elemental analysis: found C = 22.4, H = 3.68%; calculated for [$C_{10}H_{20}S_5ClNi$](PF$_6$) C = 22.3, H = 3.74%. F.a.b. mass spectrum: found M^+ = 392,358; calculated for:

[^{58}Ni^{35}Cl([15]aneS$_5$-H)]$^+$ M^+ = 392

[^{58}Ni([15]aneS$_5$)]$^+$ M^+ = 358

U.V./vis spectrum (CH_3CN): λ_{max} = 920 nm (ε_{max} = 58.7 dm^3 mol^{-1} cm^{-1}), 582 (43.8), 334 (86.8), 312 (3,100), 227 (7,450). I.R. spectrum (KBr disc): 3000 w, 2940 m, 2860 w, 1460 s, 1410 m, 1390 w, 1310 w, 1290 m, 1260 s, 1250 w, 1220 w, 1200 w, 1180 w, 1160 w, 1145 w, 1120 m, 1060 w, 1025 w, 990 w, 970 w, 945 s, 930 w, 915 w, 880 w, 840 vs, 780 w, 740 m, 700 w, 685 m, 650 w, 630 w, 610 w, 560 s, 530 m, 485 w, 460 w, 425 m cm^{-1}.

CHAPTER 4

ELECTROCHEMICAL STUDIES ON NICKEL COMPLEXES OF [9]aneS$_3$

4.1 INTRODUCTION

The redox chemistry of Ni complexes has attracted intense interest. Whilst the most common oxidation state for Ni is +2, complexes of Ni in the 0, +1, +3 and +4 states are also known[77,78]. These latter species are usually highly reactive, and the catalytic properties of Ni^0 compounds in particular have been well studied. Ni complexes have been shown to be particularly effective at catalysing coupling and oligomerisation reactions of alkenes, alkynes and organic halides, and carbonylation reactions[153]. An example of such a reaction is the coupling of ethene to form 1-butene, catalysed by Ni^{II} complexes in the presence of a Lewis acid (Figure 4.1). In addition the reactivity of Ni^I complexes towards small molecule substrates such as CO, CO_2, O_2 and alkyl halides has been investigated[38,90-92,154]: $[Ni(cyclam)]^+$ has been proven to be an efficient catalyst for the electro-reduction of CO_2 to CO (Section 1.3)[38].

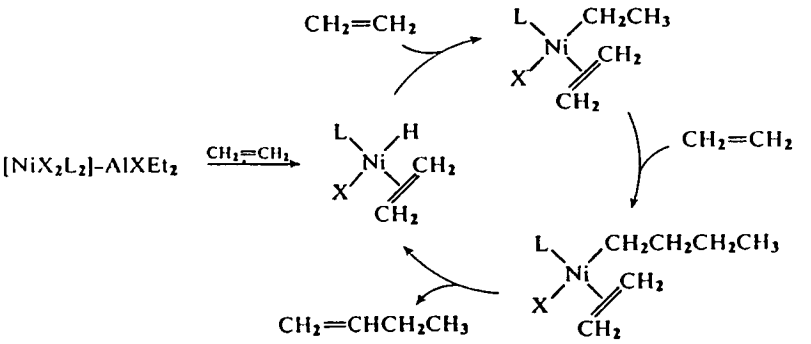

Figure 4.1: Proposed Mechanism for the Ni-catalysed conversion of ethene to 1-butene (from Reference 153).

This chapter describes the electrochemistry of the complexes $[Ni([9]aneS_3)(PP)]^{2+}$ (PP = diphosphine chelate), the syntheses of which are described in Chapter 3. A re-investigation of the electrochemistry of $[Ni([9]aneS_3)_2]^{2+}$ is also discussed.

The cyclic voltammogram of $[Ni([9]aneS_3)_2]^{2+}$ was first reported by Wieghardt *et al.*, who described a chemically reversible one-electron oxidation at $E_{\frac{1}{2}}$ = +0.97V vs. Fc/Fc^+[130]. This was originally assigned as a ligand-based oxidation, as the oxidation of free $[9]aneS_3$ occurs at a similar potential (Ep_a = +0.99V)[130]. However, a preliminary investigation of the redox behaviour of $[Ni([9]aneS_3)_2]^{2+}$ by the Edinburgh group suggested the formulation of $[Ni([9]aneS_3)_2]^{3+}$ as a metal-centred Ni^{III} radical[74], whilst a similar investigation of $[Fe([9]aneS_3)_2]^{2+}$ [$E_{\frac{1}{2}}$(Fe(II)/Fe(III)) = +0.98V][130] showed this complex to form a metal-based Fe^{III} oxidation product $[Fe([9]aneS_3)_2]^{3+}$ [156]. In separate studies, the oxidation product of $[9]aneS_3$ under anaerobic conditions was shown to be the bicyclic sulphonium cation (33)[155], whilst the chemical oxidation of $[Fe([9]aneS_3)_2]^{2+}$ with H_2O_2 yielded the mono-sulphoxo species $[Fe([9]aneS_3)(oxy\text{-}[9]aneS_3)]^{2+}$ (34)[159]. Given this ambiguous evidence about the ease of oxidation of the $[9]aneS_3$ ligand, a full characterisation of $[Ni([9]aneS_3)_2]^{3+}$ was undertaken.

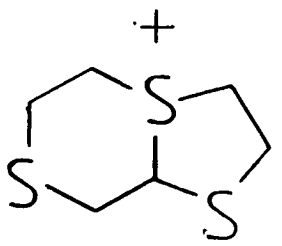

(33)

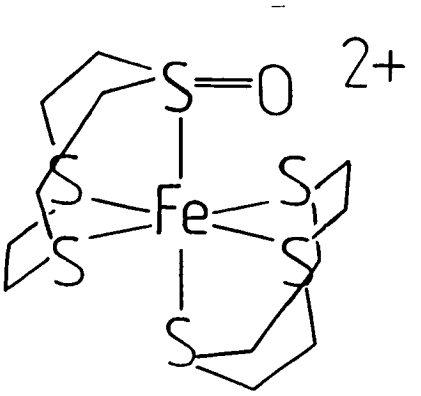

(34)

THE BIOCHEMISTRY OF NICKEL

Further impetus for the study of Ni redox chemistry was provided by the discovery of paramagnetic Ni centres in several biological systems[26]. Four types of enzyme are now known to contain Ni; in three of these, the Ni is thought to take part in redox reactions.

(i) Ureases catalyse the hydrolysis of urea to NH_3 and CO_2. The Ni in Jack Bean urease is diamagnetic, and is thought to exist as Ni^{II} in an octahedral environment. The function of the Ni centre(s) in this enzyme is thought to be analogous to that of Zn^{2+} in carbonic anhydrase, to activate the urea substrate electrostatically to nucleophilic attack[158].

(ii) Methyl-Coenzyme M reductase requires an

Ni-containing prosthetic group for activity, Factor F_{430}. This is a square-planar Ni complex of a tetrahydro-porphinoid macrocycle (11), which forms an octahedral Ni centre in the intact protein. The active ("reduced") form of this enzyme is e.p.r. active ($g_{||}$ = 2.23, $g_{\perp}$ = 2.17)[159], which is thought to imply the existence of an Ni^{I} centre. The role of the Ni in this enzyme is unclear.

(iii) Carbon monoxide oxidoreductase is a bacterial enzyme that catalyses the interconversion of CO with CO_2. This is thought to contain a mixed-metal [$NiFe_3$-4S] cluster with a formally Ni^{III} centre, on the bases of e.p.r. evidence[160]. Labelling experiments have shown that this cluster interacts directly with the CO/CO_2 substrate molecules[161].

(iv) Several hydrogenase enzymes, which oxidise H_2 to $2H^+$, are known to contain Ni centres, in addition to at least one [4Fe-4S] cluster. Inactive ("oxidised") samples of these enzymes are e.p.r. active, giving spectra that have been attributed to the presence of a low spin Ni^{III} ion, in a distorted octahedral or square-pyramidal environment (e.g. for *D. Gigas* hydrogenase g_1 = 2.32, g_2 = 2.21, g_3 = 2.01)[162]. Further e.p.r. experiments have shown that the Ni centre is

coordinated by at least one S donor (via ^{33}S enrichment), and that the H_2 substrate interacts directly with the Ni complex, possibly causing its reduction to Ni^{I}. The mechanism of the enzymic reaction is not known; one proposed mechanism is shown in Figure 4.2[163]. Alternatively, a $Ni^{III}.(H_2)$ complex may be involved[164]. Crabtree *et al.* have recently published the first example of a Ni^{II} complex that interacts directly with H_2[165].

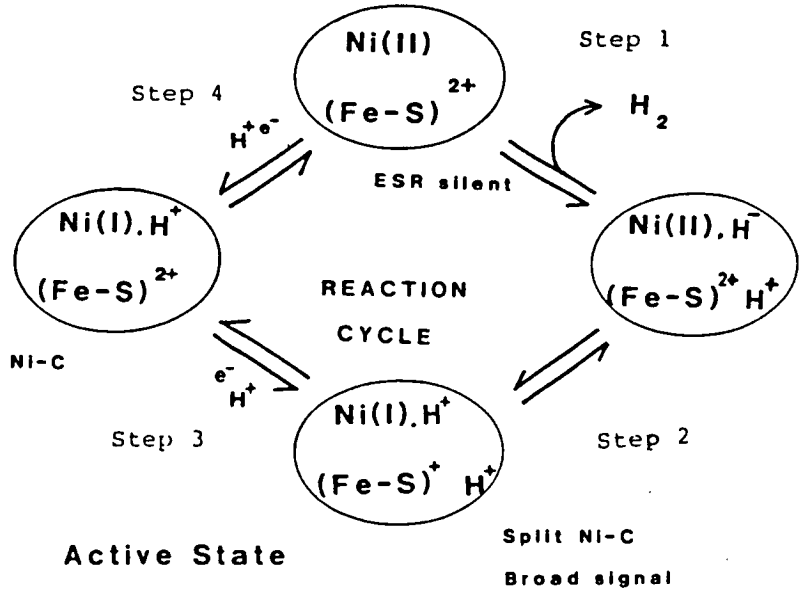

Figure 4.2: Proposed mechanism for the oxidation of H_2 to $2H^+$ by hydrogenases.

THE CHEMISTRY OF NICKEL (I)

In comparison with the relatively large number of Ni^0 and Ni^{III} complexes known, relatively few Ni^{I} compounds have been well characterised. Those that have been

reported can be broadly divided into macrocyclic and non-macrocyclic systems.

The reductive chemistry of several Ni^{II} complexes of tetraaza macrocycles has been investigated[88-92]. It has been found that the electroreduction of $[Ni(N_4)]^{2+}$, where N_4 is a saturated or partially unsaturated tetraaza ligand, yields a square planar, metal-based Ni^{I} radical, typically with $g_{\perp}$ = 2.18-2.33, $g_{||}$ = 2.05-2.07[88,89]. As expected, the Ni(II)/(I) couple in these systems becomes less cathodic for complexes with larger ring macrocycles. However, reduced Ni complexes of ligands containing conjugated π-systems (e.g. α-diimines, porphyrins) have been formulated as Ni^{II}-stabilised ligand-radical anions, with g = 1.99-2.01[90-92]. Some reduced Ni porphyrins of intermediate character have been reported[90]; the complex (35) exhibits two e.p.r. signals at room temperature (g = 2.113, 2.048); this has been interpreted as evidence for an equilibrium between $[Ni^{I}(L)]^{+}$ and $[Ni^{II}(L^{\cdot -})]^{+}$ valence isomers[91]. The Ni catenand complex $[Ni(cat\text{-}30)]^{2+}$ (36) has been shown to form an exceptionally stable Ni^{I} reduction product, due to the imposed tetrahedral coodination at the Ni centre[166].

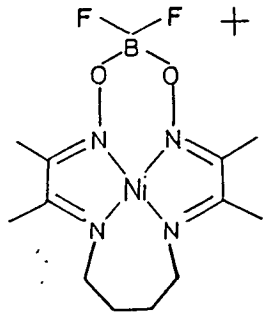

(35)

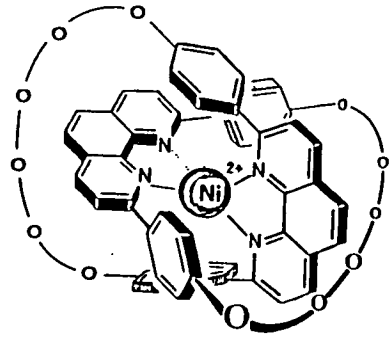

(36)

Both $[Ni^{I}(N_4)]^{+}$ and $[Ni^{II}(N_4^{\cdot -})]^{+}$ species have been shown to bind substrates such as CO to form five-coordinate metal-centered radicals[90-92]. The single crystal structures of two square-planar Ni^{I} macrocyclic complexes have recently been published; [Ni(SDPDTP)] (SDPDTP = diphenyldi-p-tolyl-21-thiaporphyrin, Figure 4.3a)[167] and $[Ni(Me_6[14]4,11\text{-dieneN}_4)]^{+}$ ($Me_6[14]4,11$-dieneN$_4$ = 5,7,7,12,14,14-hexamethyl-1,4,8,11-tetrazacyclotetradeca-4,11-diene, Figure 4.3b)[168].

All of the known non-macrocyclic Ni^{I} complexes contain S- or P-donor ligands. The first such species to be reported were the complexes $[Ni(PPh_3)_3X]$ (X = halide)[169], which were later shown to have a tetrahedral stereochemistry (Figure 4.3c)[170]. Several similar complexes containing tripodal P- or As-donor ligands have been synthesised[171]; all those structurally characterised exhibit tetrahedral or trigonal bipyramidal geometries, depending on the donacity of the tripodal ligand (Figure 4.3d,e)[172]. The reductive electrochemistry of several Ni^{II} dithiolate complexes has been examined[173-175]. On the basis of e.p.r. evidence and S.C.F. calculations, $[Ni(SS)_2]^{3-}$ are best formulated as Ni^{I} complexes for SS = dithiocarbamate and 1,2-dithiolene ligands, and as Ni^{II}-stabilised ligand-radical anions for SS = dithio-β-diketonate. One three-coordinate Ni^{I} complex has been characterised (Figure 4.3f)[176].

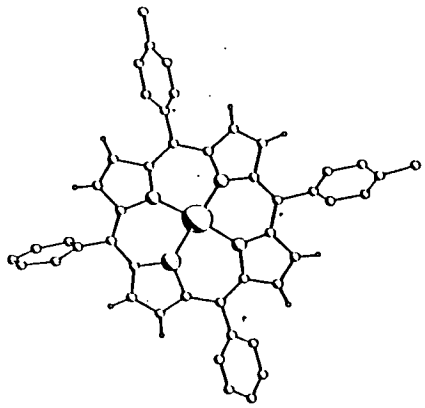

a) [Ni(SDPDTP)]

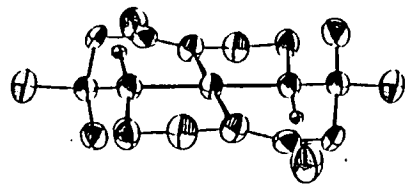

b) [Ni(N_4-diene)]$^+$

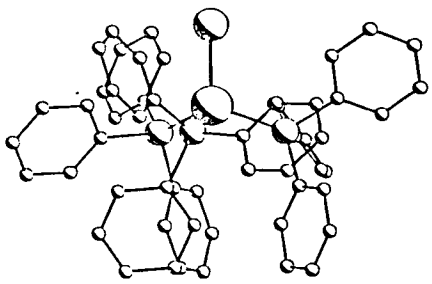

c) [Ni(PPh_3)$_3$Br]

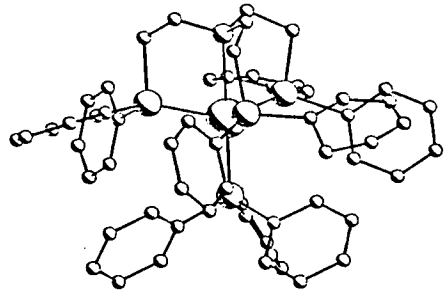

d) [Ni(N{$C_2H_4AsPh_2$}$_3$)(PPh_3)]$^+$

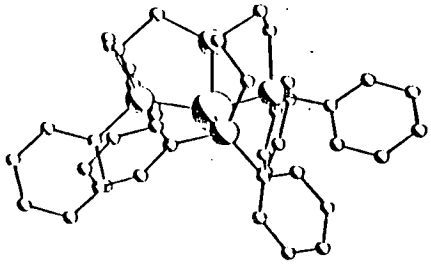

e) [Ni(P{$C_2H_4PPh_2$}$_3$)]$^+$

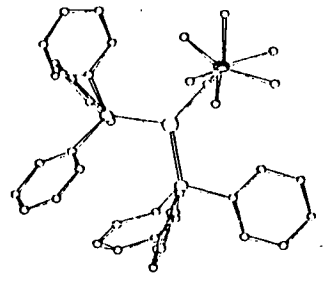

f) [Ni(PPh_3)$_2$(N{$SiMe_3$}$_2$)]

SDPDTP = diphenyldi-p-tolyl-21-thiaporphyrin

N_4-diene = 5,7,7,12,14,14-hexamethyl-1,4,8,11-tetraazacyclotetradeca-4,11-diene

Figure 4.3: Views of the Single Crystal Structures of Some Ni^I Complexes.

4.2 RESULTS AND DISCUSSION

4.2.1 Electrochemical Study of $[Ni([9]aneS_3)(PP)](PF_6)_2$ (PP = dppm, dppe, dppv, dcpe, dmpe, dppp, tdpme)

The complexes $[Ni([9]aneS_3)(PP)](PF_6)_2$ (PP = diphosphine chelate, Figure 3.4) were prepared as described in Chapter 3.

The cyclic voltammograms of the complexes $[Ni([9]aneS_3)(PP)](PF_6)_2$ in $CH_3CN/^nBu_4NPF_6$ at 298K each exhibited two reduction waves (Table 4.1, Figures 4.4-4.6). A chemically reversible couple was observed between $^1E_{\frac{1}{2}}$ = -0.77 to -1.16V vs. Fc/Fc^+ (ΔEp = 61-92 mV, scan rate 400 mV/s) together with a quasi-reversible or irreversible reduction ranging between -1.31 and -1.93V. Coulometric determinations were consistent with both couples corresponding to one-electron processes (Table 4.1). This is consistent with the assignment of these processes as $[Ni([9]aneS_3)(PP)]^{2+/+}$ and $[Ni([9]aneS_3)(PP)]^{+/0}$ couples respectively. Only a small variation in reduction potential was observed with differing P-Ni-P chelate ring size. This contrasts with the complexes $[Ni(PP)_2]^{2+}$, for which the Ni(II)/(I) couples were observed to become significantly less cathodic with increasing P-Ni-P chelate ring size, this was related to a tetrahedral distortion about the Ni^{II} centre caused by steric repulsions between the phosphine ligands[148]. The reduction potentials for $[Ni([9]aneS_3)(dcpe)]^{2+}$ and $[Ni([9]aneS_3)(dmpe)]^{2+}$ are more cathodic than those of the

other complexes examined. This is unsurprising, given the greater Lewis basicity of the dcpe and dmpe ligands compared to the diphenylphosphino chelates.

Controlled potential electrolysis of $[Ni([9]aneS_3)(PP)](PF_6)_2$ at potentials corresponding to the first reduction process afforded paramagnetic solutions, which exhibited e.p.r. spectra of axial or rhombic symmetry at 77K with observed hyperfine coupling to two ^{31}P nuclei (Table 4.2). Electrogenerated solutions of the second reduction products were e.p.r. silent. No transient e.p.r. active intermediates were observed during the electrogeneration of any of the reduction products. The $[Ni([9]aneS_3)(PP)]^{2+}$ species for PP = dppe, dppv, dcpe, dppp and tdpme could also be chemically generated using $NaBH_4$ in CH_3OH: e.p.r. spectra at 77K and 298K of the resultant solutions were identical to those shown by the electrogenerated solutions in CH_3CN (Figure 4.9), suggesting that no coordination of solvent molecules occurs on reduction.

The reductions were followed by u.v./visible spectroscopy using an O.T.E. system (Optically Transparent Electrode, see Appendix). Except for PP = dppm, the $[Ni([9]aneS_3)(PP)]^{2+/+}$ conversions proceeded isosbestically in $CH_3CN/^nBu_4NPF_6$ at 253K (Table 4.3), and re-oxidation of all the reduced solutions (including PP = dppm) at 0V gave quantitative regeneration of the Ni^{II} precursors. The $[Ni([9]aneS_3)(PP)]^{+/0}$ reductions did not

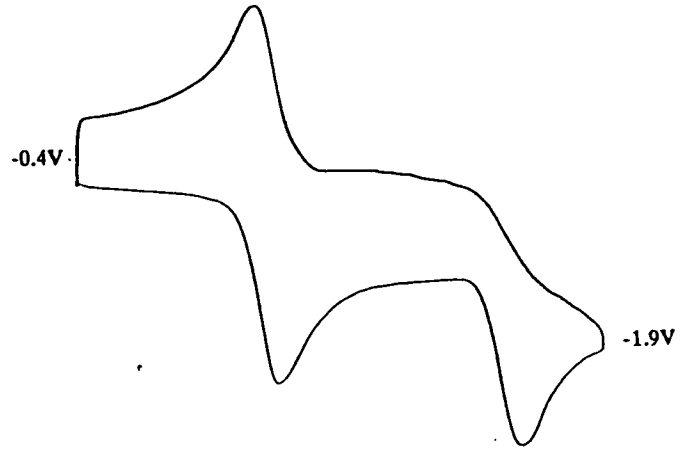

Figure 4.4: Cyclic Voltammogram of [Ni([9]aneS$_3$)(dppe)] $(PF_6)_2$ ($CH_3CN/^nBu_4NPF_6$, 298K, 400 mV/s).

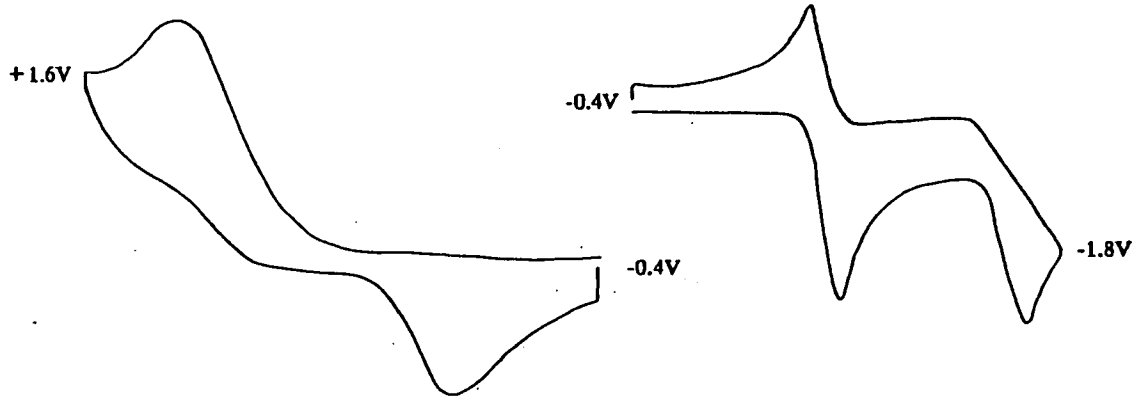

Figure 4.5: Cyclic Voltammogram of [Ni([9]aneS$_3$)(dmpe)] $(PF_6)_2$ ($CH_3CN/^nBu_4NPF_6$, 298K, 400 mV/s).

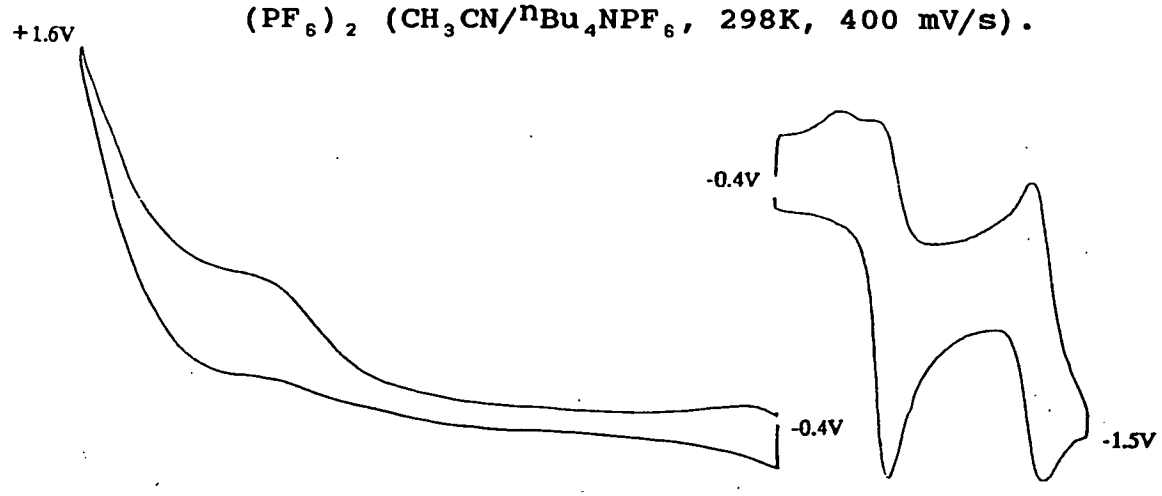

Figure 4.6: Cyclic Voltammogram of [Ni([9]aneS$_3$)(tdpme)] $(PF_6)_2$ ($CH_3CN/^nBu_4NPF_6$, 298K, 400 mV/s).

proceed isosbestically at 253K (Table 4.3), and re-oxidation at a potential intermediate between the two reductive couples did <u>not</u> quantitatively regenerate the $[Ni([9]aneS_3)(PP)]^+$ species. However, in some cases, re-oxidation of the $[Ni([9]aneS_3)(PP)]^0$ (PP = dppe, dppv, dppp, tdpme) solutions at 0.0V did result in quantitative regeneration of the Ni^{II} complexes.

In addition to the reductions described above, $[Ni([9]aneS_3)(dmpe)](PF_6)_2$ and $[Ni([9]aneS_3)(tdpme)](PF_6)_2$ also exhibited irreversible, one-electron oxidations at +1.22 and +1.04V vs. Fc/Fc^+ respectively (scan rate 400 mV/s, Figures 4.5, 4.6, Table 4.1).

The characterisation of all the redox products described above is discussed further in Sections 4.2.2-4.2.5.

4.2.2 Characterisation of the Reduction Products of $[Ni([9]aneS_3)(dppe)](PF_6)_2$ and $[Ni([9]aneS_3)(dppv)](PF_6)_2$

Controlled potential electrolysis of bulk samples of $[Ni([9]aneS_3)(PP)](PF_6)_2$ (PP = dppe, dppv) in $CH_3CN/0.1M$ $^nBu_4NPF_6$ at 298K at a potential between the first and second reduction potentials for these species afforded dark red e.p.r. active solutions. The e.p.r. spectra of these reduced species in mobile solution at 298K, exhibited a triplet resonance arising from hyperfine coupling to the ^{31}P nuclei of the diphosphine ligands;

PP	Oxidation E(V)[a]	n	First Reduction E(V)[a]	n	ΔEp(mV)	Second Reduction E(V)[a]	Total n	ΔEp(mV)
dppm	-	-	-0.77(r)	0.90	91	-1.50(i)	1.99	-
dppe	-	-	-0.88(r)	1.03	64	-1.65(i)	1.91	-
dppv	-	-	-0.82(r)	0.93	61	-1.59(i)	2.08	-
dcpe	-	-	-0.96(r)	0.98	84	-1.84(i)	-	-
dmpe	+1.22(i)[b]	0.95	-1.16(r)	0.96	72	-1.93(i)	-	-
dppp	-	-	-0.79(r)	1.00	92	-1.63(i)	1.91	-
tdpme	+1.04(i)	0.91	-0.77(q)	1.08	c	-1.31(q)	1.94	71

a. Electrochemical redox potential, measured at 298K, in CH_3CN/0.1M $^nBu_4NPF_6$, scan rate 400 mV/s, under an Ar atmosphere. Potentials quoted vs. Fc/Fc^+.
n = coulometric determination, r = chemically reversible, q = quasi-reversible, i = irreversible.

b. Exhibits a return wave at Ep_a = +0.21V.

c. Exhibits two return waves.

Table 4.1: Electrochemical Data for [Ni([9]aneS_3)(PP)](PF_6)$_2$

PP	Mobile Solution[a]		Frozen Glass[b]					
	g_{iso}	$A_{iso}(G)^c$	g_1	$A_1(G)^c$	g_2	$A_2(G)^c$	g_3	$A_3(G)^c$
dppm	2.110	127*	2.193	98	2.098	149	2.041	167
dppe	2.086	118	2.136	98	2.051	111	2.051	152
dppv	2.086	118	2.141	98	2.053	122	2.053	147
dcpe	2.104	107	2.167	80	2.107	127	2.037	133
dmpe	2.090	127*	2.149	94	2.090	149	2.042	174
dppp	2.098	120	2.158	120		2.060	132	
tdpme[d]	2.095	126	2.154	126		2.060	137	

All assignments of frozen glass spectra are provisional in the absence of simulations.

a. Solution spectra measured at 298K in CH_3OH except * in $CH_3CN/0.1M\ ^nBu_4NPF_6$.

b. Frozen glass spectra measured at 77K in $CH_3CN/0.1M\ ^nBu_4NPF_6$.

c. Hyperfine coupling to ^{31}P.

d. Hyperfine constants to ^{61}Ni (I = 3/2) A_{iso} = 21G, A_1 = 53G, A_2, A_3 = 8G.

Table 4.2: E.p.r. Data for $[Ni([9]aneS_3)(PP)]^+$

PP	Ni^{II} spectrum $\lambda_{max}(\varepsilon_{max})$[nm,$dm^3mol^{-1}cm^{-1}$]	Ni(II)/(I) λ_{iso}[nm]	Ni^{I} spectrum $\lambda_{max}(\varepsilon_{max})$[nm,$dm^3mol^{-1}cm^{-1}$]	Ni^{o} Spectrum $\lambda_{max}(\varepsilon_{max})$[nm,$dm^3mol^{-1}cm^{-1}$]
dppm	418(2,130),320(14,880), 266(13,715)	-	460(sh),408(2,420), 319(9,800),265(13,150)	466(sh),395(sh),320(sh), 265(10,610)
dppe	422(1,650),316(17,390), 266(13,070)	343,284,278, 260	512(1,580),398(2,060), 327(7,300),262(11,840)	460(sh),319(sh), 262(9,470)
dppv	420(2,320),318(18,340) 260(19,190)	445,412,350, 293,273	514(1,740),395(2,220), 325(9,200),266(sh)	482(sh),380(sh),320(sh), 265(16,850)
dcpe	435(835),325(7,015), 292(12,990),243(14,580)	398,344,272, 256,217	320(4,220),287(8,580), 249(12,590)	-
dmpe	413(650),283(13,350), 244(12,740)	394,316	350(1,760),308(sh), 267(sh),244(10,650)	-
dppp	452(1,250),329(11,270), 260(10,480)	365,293	477(1,250),398(1,545), 319(7,830),263(10,880)	462(sh),398(sh),323(sh), 262(10,050)
tdpme	443(1,860),328(14,640), 260(18,710)	478,420,364, 293,272	488(1,250),380(sh), 322(8,270),260(17,090)	386(7,725),328(8,600), 260(14,290)

All spectra recorded in O.T.E. cell in CH_3CN/0.1M $^nBu_4NPF_6$ at 253K.

Table 4.3: U.V./Visible data for $[Ni([9]aneS_3)(PP)]^{2+/+/0}$

which indicates that both P-donors remain coordinated to the Ni centre on reduction. In frozen solution at 77K, the reduced complexes gave complex e.p.r. spectra, which were tentatively interpreted using axial symmetry in g, and rhombic symmetry for hyperfine coupling; equal coupling to both ^{31}P nuclei was also assumed (Figures 4.8, 4.12, Table 4.2). These assignments are consistent with the averaged A_{iso} values measured from the isotropic solution spectra (Table 4.2); however, they must remain speculative in the absence of complete simulation data. The complexity of the frozen glass e.p.r. spectra, together with the observed g_{iso} = 2.086, A_{iso} = 118G for both complexes, are consistent with the formulation of $[Ni([9]aneS_3)(PP)]^+$ (PP = dppe,dppv) as genuine metal-based Ni^I species. Both mobile and frozen solution spectra also show the presence of residual peaks due to paramagnetic impurities. These trace signals are reproducible between different samples of the Ni^{II} precursors, and it is unclear whether or not they correspond to decomposition products, or conformational isomers, of the species $[Ni([9]aneS_3)(PP)]^+$.

Both $[Ni([9]aneS_3)(dppe)]^+$ and $[Ni([9]aneS_3)(dppv)]^+$ could also be generated chemically using $NaBH_4$ in CH_3OH at 298K under N_2; the resultant deep red solutions exhibited identical e.p.r. spectra to the electrogenerated samples described previously (Figure 4.9). These chemically generated Ni^I solutions were stable for several hours at

298K under N_2 but spontaneously re-oxidised to the corresponding Ni^{II} complex on exposure to air. Filtration and reduction in volume of the Ni^{I} solutions followed by addition of diethyl ether afforded a low yield (<10%) of wine-red solid, which could be recrystallised from CH_2Cl_2/^{n}hexane. These products gave I.R. spectra that indicated the presence of [9]aneS_3 and diphosphine ligands, and PF_6^- counterion. Further characterisation of the reduced products in the solid state was prevented by their sensitivity to air.

Bowmaker, Boyd *et al.* have studied the electrochemistry of a series of complexes $[Ni(SS)(PP)]^{n+}$ (SS = dithiocarbamate, 1,2-dithiolene or 1,3-dithio-β-diketonate, PP = *bis*-diphenylphosphino chelate)[174,175]. They found that reduction of these Ni^{II} compounds ($E_{\frac{1}{2}}$ = -0.70 to -1.20V *vs.* Fc/Fc^+) gave the square-planar Ni^{I} radicals $[Ni(SS)(PP)]^{(n-1)+}$, which exhibited axial or rhombic e.p.r. spectra in frozen solution. Whilst a detailed comparison of the e.p.r. spectra of the species $[Ni([9]aneS_3)(PP)]^+$ and $[Ni(SS)(PP)]^{(n-1)+}$ cannot currently be made, it is clear that the isotropic hyperfine coupling constants to the ^{31}P nuclei of the diphosphine ligand are greater for the [9]aneS_3 complexes (e.g. for $[Ni([9]aneS_3)(dppe)]^+$ A_{iso} = 118G; c.f. for $[Ni(Et_2NCS_2)(dppe)]$ A_{iso} = 83G, $[Ni(mnt)(dppe)]^-$ A_{iso} = 107G (mnt = maleonitrile-dithiolate)[174,175a]). This is consistent with the reduced π-acceptor capability of

[9]aneS$_3$ compared to a conjugated dithiolate ligand, resulting in more unpaired spin density residing on the phosphine centres.

In situ experiments using an O.T.E. system (see Appendix) to monitor the reductions of [Ni([9]aneS$_3$)-(PP)]$^{2+}$ to [Ni([9]aneS$_3$)(PP)]$^{+}$ (PP = dppe, dppv) by U.V./visible spectroscopy showed that both processes occurred isosbestically and reversibly in CH_3CN/0.1M $^nBu_4NPF_6$ at 253K (Figures 4.10 and 4.13, Table 4.3), proving that no intermediate species or decomposition reactions were involved in the formation of the reduced complexes. During the reductions, loss of intensity of the Ni^{II} d-d band at $\lambda_{max} \simeq 420$ nm was observed, with concommitant growth of two new bands at $\lambda_{max} \simeq 512$ nm ($\varepsilon_{max} \simeq 1{,}650$ dm^3 mol^{-1} cm^{-1}) and 396 (2,200), which can be assigned either as d-d transitions, or as πS$\rightarrow$Ni charge-transfer bands. The former assignment is more likely, since the energies of these bands vary significantly between the other [Ni([9]aneS$_3$)(PP)]$^{+}$ complexes (Sections 4.2.3, 4.2.4), and because πS$\rightarrow$metal charge-transfer bands have not been previously observed in first-row transition metal complexes of [9]aneS$_3$[59]. The two charge transfer bands in the electronic spectra of the Ni^{II} complexes also lost intensity during the reduction, with the lower energy band becoming shifted to higher wavelength whilst the higher energy band did not move to higher or lower energy ($\lambda_{max} \simeq 316$ nm ($\varepsilon_{max} = 17{,}390$ dm^3 mol^{-1} cm^{-1}), 266

(13,070) for $[Ni([9]aneS_3)(dppe)]^{2+}$; λ_{max} = 327 nm (ε_{max} = 7,300 $dm^3.mol^{-1}.cm^{-1}$), 262 (11,840) for $[Ni([9]aneS_3)(dppe)]^{+}$). This is consistent with the tentative assignment of these bands as Ni→πP and intra-[9]aneS$_3$ charge transfer bands respectively[59].

Unfortunately, the U.V./visible spectra observed for the complexes $[Ni([9]aneS_3)(PP)]^{+}$ (PP = dppe, dppv) cannot be used to unambiguously assign the stereochemistry adopted by these species, since all possible four- or five-coordinate geometries have low point symmetries and hence would exhibit up to four d-d transitions (Figure 4.7). However, the fact that the frozen glass e.p.r. spectra of all of the series of complexes $[Ni([9]aneS_3)(PP)]^{+}$ can be interpreted using equal hyperfine coupling to both ^{31}P nuclei of the diphosphine ligand (Sections 4.2.3-4.2.5), and the observed high degree of interaction between the Ni-based $d_{x^2-y^2}$ S.O.M.O. and the phosphine P-donors (Section 4.2.3), imply that these species exhibit square-planar or square-pyramidal structures with an S_2P_2 basal plane. The latter assignment is more likely, because the narrow peak separation observed in the $[Ni([9]aneS_3)(PP)]^{2+/+}$ couples from cyclic voltammetry ($\Delta E_p \simeq 65$ mV in CH_3CN/0.1M $^nBu_4NPF_6$ at 298K at scan rate 400 mV/s for PP = dppe, dppv, Table 4.1) suggests that major stereochemical changes such as de-coordination of the apical S-donor are unlikely to be occurring during the reductions. The high extinction

coefficients of the *d-d* bands in the electronic spectra of the reduced complexes are also consistent with the lower symmetry structure (Figure 4.7). Therefore, the species $[Ni([9]aneS_3)(PP)]^+$ were assigned to have square-pyramidal geometries similar to those of the Ni^{II} complexes $[Ni([9]aneS_3)(PP)]^{2+}$ (Chapter 3), although this assignment must remain provisional in the absence of an x-ray structural analysis.

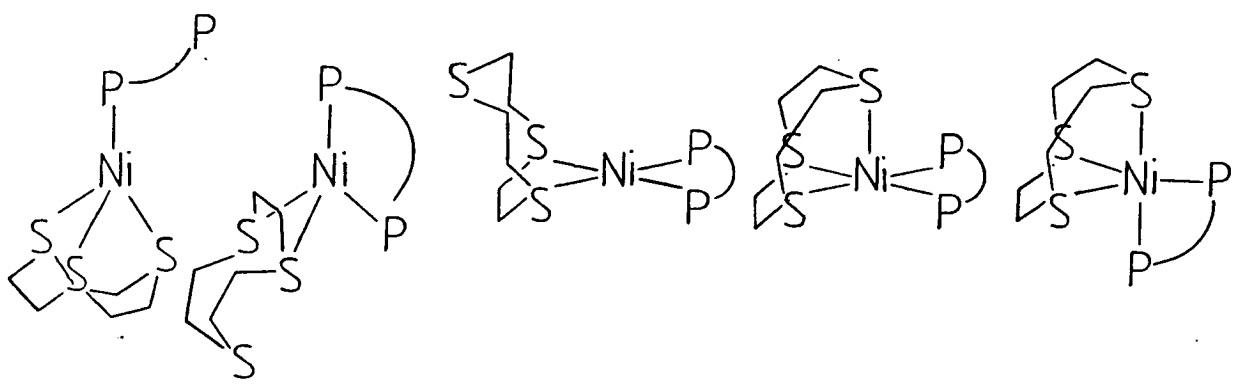

Figure 4. 7: Possible Stereochemistries of the complexes $[Ni([9]aneS_3)(PP)]^+$

The second reduction couples observed in the cyclic voltammograms of $[Ni([9]aneS_3)(PP)](PF_6)_2$ (PP = dppe, dppv) in CH_3CN/0.1M $^nBu_4NPF_6$ at 298K did not exhibit a significant return wave at scan rates 100-1000 mV/s (Figure 4.4), resulting in these reductions being classified as formally irreversible processes. However, the fact that the original Ni^{II} complexes can be regenerated quantitatively from electro-generated

solutions of these second reduction products (from O.T.E. experiments, *vide infra*), together with the appearance of return waves for the Ni(II)/(I) couples after the "irreversible" $[Ni([9]aneS_3)(PP)]^{+/0}$ reductions had been scanned by cyclic voltammetry (Figures 4.4-4.6), implies that these second reductions are in fact chemically reversible processes, and that the return $[Ni([9]aneS_3)(PP)]^{0/+}$ oxidations occur at a significantly slower rate than the initial $[Ni([9]aneS_3)(PP)]^{+/0}$ reductions. Experiments using an O.T.E. system to follow the second reductions by U.V./visible spectroscopy showed that these processes did not occur isosbestically in $CH_3CN/0.1M$ $^nBu_4NPF_6$ at 253K (Table 4.3, Figure 4.11). Attempted re-oxidation of the fully reduced solutions at -0.90V *vs.* Ag/Ag^+ did not quantitatively regenerate the $[Ni([9]aneS_3)(PP)]^+$ species; however, re-oxidation at 0V *vs.* Ag/Ag^+ did result in quantitative production of the initial $[Ni([9]aneS_3)(PP)]^{2+}$ complexes. These results are consistent with the $[Ni([9]aneS_3)(PP)]^{+/0}$ (PP = dppe, dppv) reductions being accompanied by a gross stereochemical change about the Ni centre, to form a stable reduced Ni^0 species.

Reduction of $[Ni([9]aneS_3)(PP)]^+$ to $[Ni([9]aneS_3)(PP)]^0$ (PP = dppe, dppv) resulted in collapse of the two d-d bands exhibited by the Ni^I species, resulting in spectra containing only broad charge-transfer absorbtions (Figure 4.10). The intra-$[9]aneS_3$

at $\lambda_{max} \simeq 260$ nm lost intensity during the reduction, but did not shift to higher or lower wavelength (λ_{max} = 262 nm (ε_{max} = 11,840 $dm^3.mol^{-1}.cm^{-1}$) for $[Ni([9]aneS_3)(dppe)]^+$; λ_{max} = 262 nm (ε_{max} = 9,470 $dm^3.mol^{-1}.cm^{-1}$) for $[Ni([9]aneS_3)(dppe)]^0$}, implying that the mode of coordination of the $[9]aneS_3$ ligand does not change during the reduction process. The broad, relatively featureless spectra given by the fully reduced complexes are typical for complexes of d^{10} metal ions (Table 4.3). Controlled potential electrolysis of bulk solutions of $[Ni([9]aneS_3)(PP)](PF_6)_2$ in CH_3CN/0.1M $^nBu_4NPF_6$ at 243K yielded yellow, e.p.r. silent solutions, which are also consistent with the formation of d^{10} Ni^0 species.

These data imply that further reduction of the five-coordinate d^9 complexes $[Ni([9]aneS_3)(PP)]^+$ (PP = dppe, dppv) leads to the formation of d^{10} $[Ni([9]aneS_3)(PP)]^0$ species, which would be expected to adopt a tetrahedral stereochemistry with a dangling P-donor (37, cf $[Cu([9]aneS_3)(AsPh_3)]^+$ [190]). Re-oxidation of the species $[Ni([9]aneS_3)(PP)]^0$ would be followed by rearrangement of a d^9 complexes $[Ni([9]aneS_3)(PP)]^+$ from a tetrahedral to five-coordinate geometry, which would be expected to be slower than the corresponding rearrangement of a five-coordinate d^{10} Ni^0 species to a tetrahedral stereochemistry (37). Further spectroscopic, structural and kinetic data would be necessary to confirm this assignment.

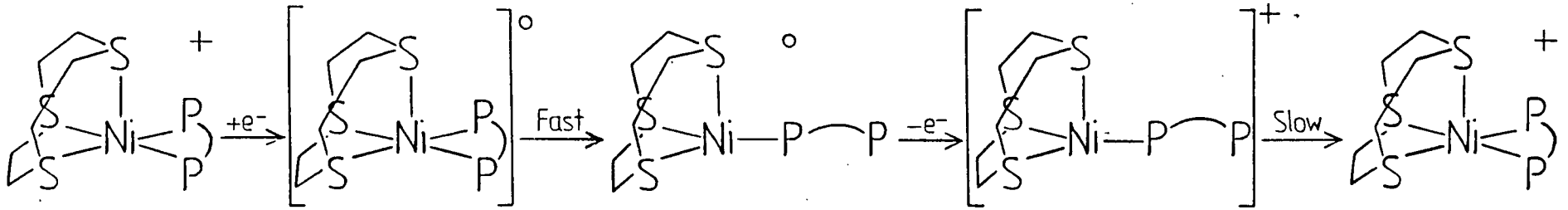

(37)

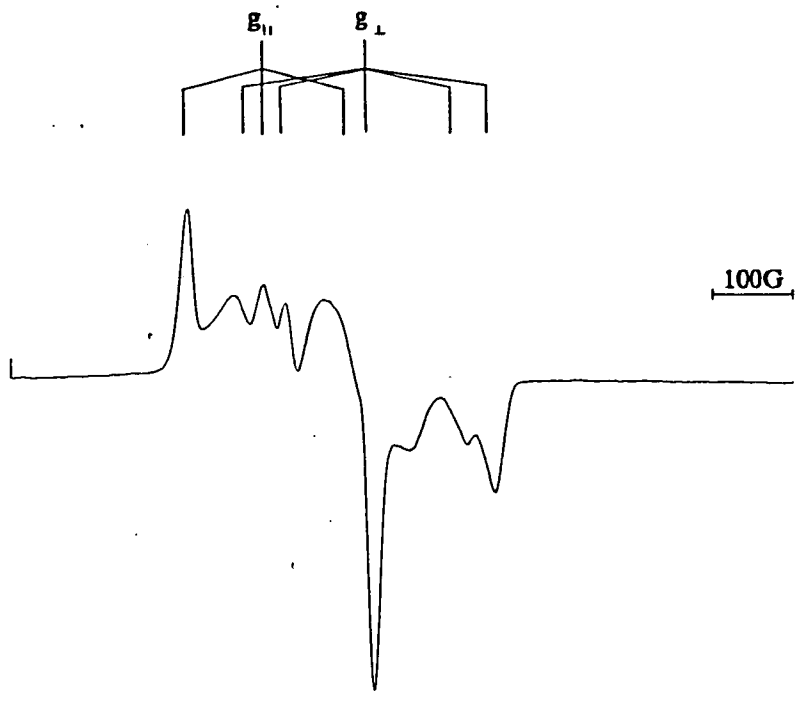

Figure 4.8: E.p.r. spectrum of $[Ni([9]aneS_3)(dppe)]^+$ (CH_3CN/0.1M $^nBu_4NPF_6$, 77K).

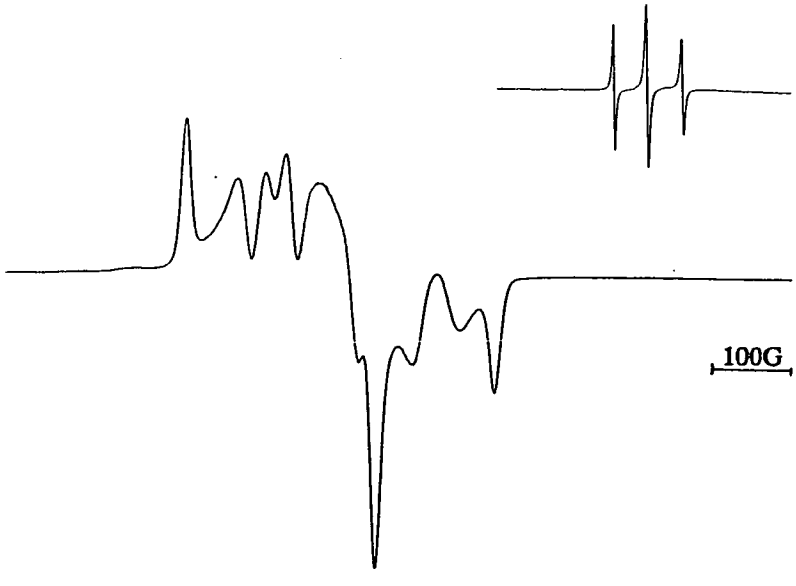

Figure 4.9: E.p.r. spectrum of $[Ni([9]aneS_3)(dppe)]^+$ (CH_3OH, 77K). Inset isotropic spectrum (CH_3OH, 298K).

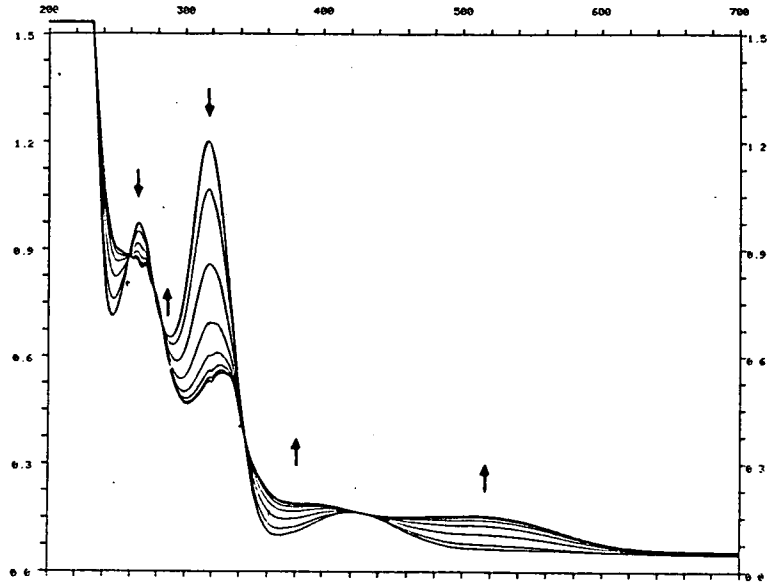

Figure 4.10: Electronic spectrum showing the reduction of $[Ni([9]aneS_3)(dppe)]^{2+}$ to $[Ni([9]aneS_3)(dppe)]^{+}$ (CH_3CN/0.1M $^nBu_4NPF_6$, 243K).

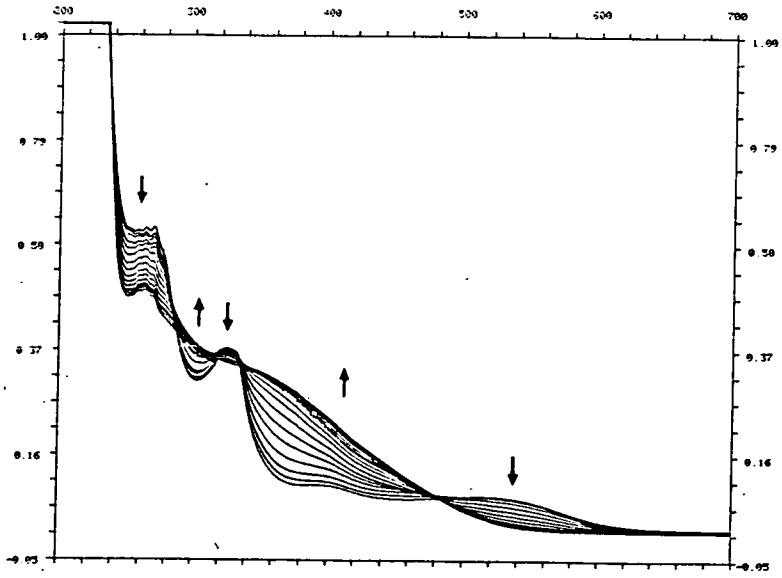

Figure 4.11: Electronic spectrum showing the reduction of $[Ni([9]aneS_3)(dppe)]^{+}$ to $[Ni([9]aneS_3)(dppe)]^{0}$ (CH_3CN/0.1M $^nBu_4NPF_6$, 243K).

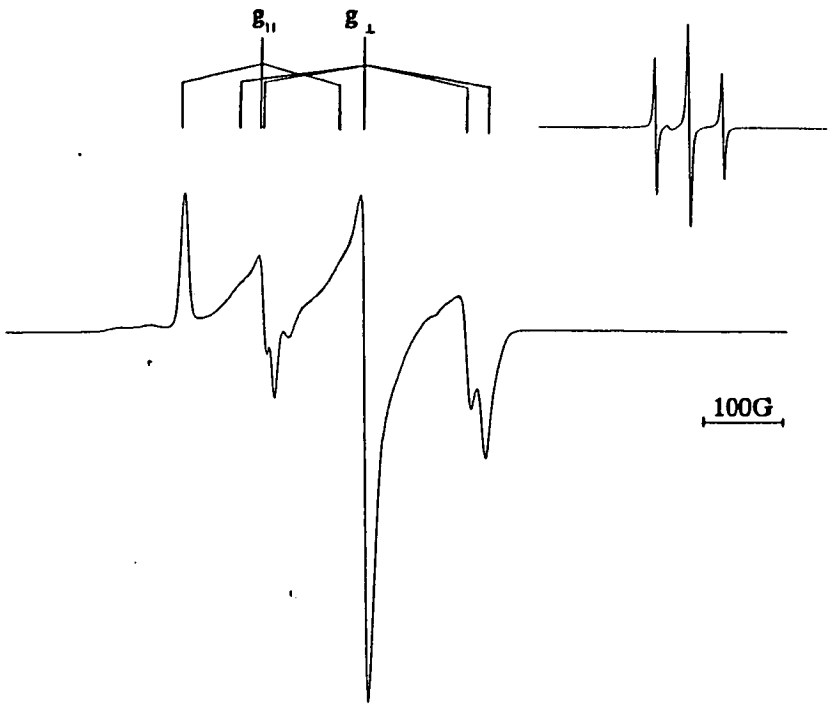

Figure 4.12: E.p.r. spectrum of $[Ni([9]aneS_3)(dppv)]^+$ (CH_3OH, 77K). Inset isotropic spectrum (CH_3OH, 298K).

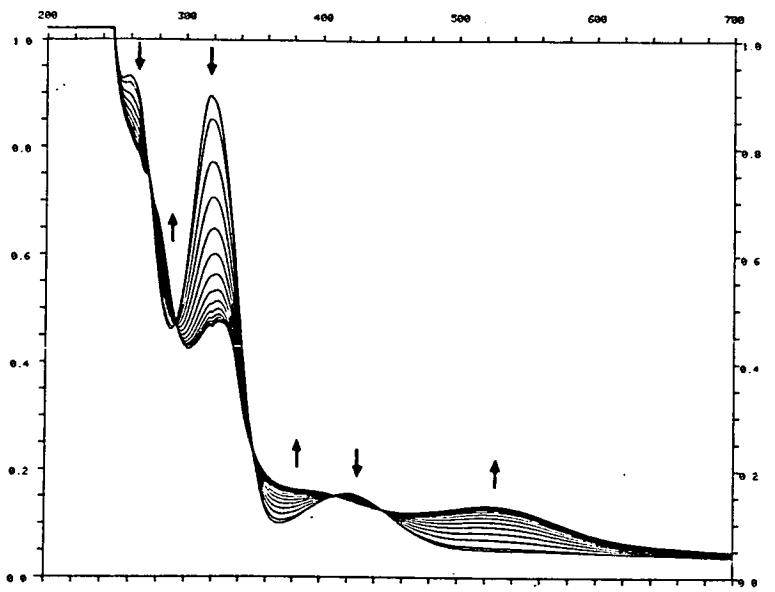

Figure 4.13: Electronic spectrum showing the reduction of $[Ni([9]aneS_3)(dppv)]^{2+}$ to $[Ni([9]aneS_3)(dppv)]^+$ (CH_3CN/0.1M $^nBu_4NPF_6$, 253K).

4.2.3 Characterisation of the Redox Products of $[Ni([9]aneS_3)(dppp)](PF_6)_2$ and $[Ni([9]aneS_3)(tdpme)](PF_6)_2$

The cyclic voltammogram of $[Ni([9]aneS_3)(tdpme)](PF_6)_2$ in $CH_3CN/0.1M\ ^nBu_4NPF_6$ at 298K exhibited slightly different features from those of the other $[Ni([9]aneS_3)(PP)](PF_6)_2$ complexes (Figure 4.5). The first reduction at $E_{\frac{1}{2}} = -0.77V$ *vs.* Fc/Fc^+ (scan rate 400 mV/s) for this complex showed two return waves, at $Ep_a = -0.59$ and $-0.69V$, which could reflect partial decomposition of the reduced species. However, the fact that no significant impurities were observed in the e.p.r. spectra of $[Ni([9]aneS_3)(tdpme)]^+$, and the reversibility and isosbesticity of the reductive process (*vide infra*), suggest that this double return wave may reflect partial adsorption of the reduced species onto the Pt electrode through the non-bonding P-donor of the tdpme ligand. A similar split return wave is observed in the cyclic voltammogram of $[Ni([9]aneS_3)(tdpme)](PF_6)_2$ under a CO atmosphere (Section 4.2.6). The $[Ni([9]aneS_3)(tdpme)]^{+/0}$ couple occurs at a less cathodic potential than those of the other complexes in the series, and is quasi-reversible, rather than irreversible, over the cyclic voltammogram timescale (Table 4.1): this is discussed below.

Controlled potential electrolysis of solutions of $[Ni([9]aneS_3)(dppp)](PF_6)_2$ and $[Ni([9]aneS_3)(tdpme)](PF_6)_2$

in CH_3CN/0.1M $^nBu_4NPF_6$ at 298K at -0.95V *vs.* Ag/AgCl yielded orange solutions. The frozen solution e.p.r. spectra of these species were less complex than those of the Ni^I dppe and dppv complexes (Section 4.2.2), and were successfully simulated by assuming axial symmetry for both g and hyperfine splitting (Figures 4.14 and 4.16, Table 4.2). In mobile solution, these samples gave triplet e.p.r. signals, which yielded g_{iso} and A_{iso} values in good agreement with those derived from the frozen glass spectra (Table 4.2). The observed pattern of g values ($g_{||}<g_{\perp}$) is consistent with metal-centered d^9 Ni^I radicals, with a $d_{x^2-y^2}$ ground state. The increased symmetry of the frozen glass spectra of $[Ni([9]aneS_3)(PP)]^+$ (PP = dppp, tdpme) is not inconsistent with their adopting the same geometry as the other $[Ni([9]aneS_3)(PP)]^+$ species. The perpendicular component of the ^{31}P hyperfine coupling for a complex containing a *cis*-NiS_2P_2 basal plane can be described by the equations:

$$A_X^2 = A_{X'}^2\sin^2(\alpha/2) + A_{Y'}^2\cos^2(\alpha/2) \qquad (38)$$

$$A_X^2 = A_{X'}^2\cos^2(\alpha/2) + A_{Y'}^2\sin^2(\alpha/2) \qquad (39)$$

where A_X and A_Y are the observed hyperfine constants, $A_{X'}$ and $A_{Y'}$ are the hyperfine constants along the principle axes for the ^{31}P nuclei, and α is the P-Ni-P angle (40)[124].

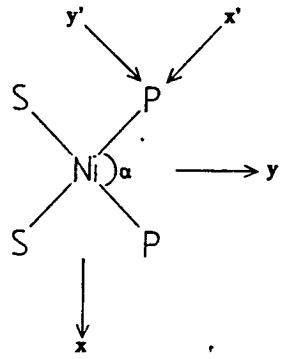

(40)

Z,Z' are perpendicular to the plane of the paper.

The P-Ni-P angle α can be estimated as 82° for $[Ni([9]aneS_3)(dppe)]^+$ and $[Ni([9]aneS_3)(dppv)]^+$ from the single crystal structure of $[Ni([9]aneS_3)(dppe)](BF_4)_2$ (Section 3.2.2), leading to rhombic hyperfine coupling to the diphosphine P-donors. For the species $[Ni([9]aneS_3)(PP)]^+$ (PP = dppp, tdpme), $\alpha \simeq 90°$ from the single crystal structure of $[Ni([9]aneS_3)(tdpme)](PF_6)_2$, so that equations 38 and 39 collapse to:

$$A_X^2 = A_Y^2 = \tfrac{1}{2}(A_{X1}^2 + A_{Y1}^2) \qquad (41)$$

giving rise to axial hyperfine coupling. Hence, given the similarity of the g and A values observed for the Ni^I dppp and tdpme complexes to those shown by $[Ni([9]aneS_3)(PP)]^+$ (PP = dppe, dppv), it is likely that these four complexes have similar electronic structures, and therefore that they adopt similar geometries.

Solutions of the complexes $[Ni([9]aneS_3)(dppp)]^+$ and $[Ni([9]aneS_3)(tdpme)]^+$ were also prepared chemically using $NaBH_4$ in CH_3OH at 298K under N_2. These orange solutions gave identical e.p.r. spectra to the electrogenerated

solutions described above, and did not decompose significantly on standing at 298K under N_2 for 3 hrs. Small amounts of orange solid could be isolated by the same procedure described for the Ni^I dppe and dppv species. As for these latter compounds, the air sensitivity of the orange products prevented full characterisation, although I.R. spectroscopy confirmed the presence of [9]aneS_3, diphosphine and PF_6^- counterion.

In order to quantify the electronic character of the $[Ni([9]aneS_3)(PP)]^+$ species, the e.p.r. spectroscopy of a 62%-enriched sample of $[^{61}Ni([9]aneS_3)(tdpme)]^+$ (^{61}Ni: I = 3/2) was examined. In mobile CH_3CN/0.1M $^nBu_4NPF_6$ solution at 298K, this enriched species showed a triplet of four-lines e.p.r. signal, with g_{iso} = 2.095, $A_{iso}(^{31}P)$ = 126G, $A_{iso}(^{61}Ni)$ = 21G (Figure 4.17, Table 4.2). In frozen solution in CH_3CN/0.1M $^nBu_4NPF_6$ or CH_3OH, the parallel component of the ^{61}Ni hyperfine is clearly resolvable at 53G (Figure 4.16). In CH_3OH, additional features in the perpendicular region of the spectrum can be observed, which may correspond to the outermost components of an $A_\perp(^{61}Ni)$ coupling of 8±1G: this value is in good agreement with that expected from the $A_{iso}(^{61}Ni)$ and $A_{||}(^{61}Ni)$ values quoted above. These hyperfine coupling constants to ^{61}Ni are similar to those reported for other Ni^I species (e.g. for $[Ni(mnt)_2]^{3-}$ $A_{||}$ = 55G, $A_\perp$ = 6G[173b]).

For an $S = \frac{1}{2}$ complex with a $d_{x^2-y^2}$ ground state, consideration of metal-ligand σ-bonding only leads to the

following equations for hyperfine coupling to the metal nucleus:

$$A_{\parallel} = -K + P_O[-4/7\alpha^2 + (g_{\parallel}-g_e) + 3/7(g_{\perp}-g_e) \quad (42)$$

$$A_{\perp} = -K + P_O[2/7\alpha^2 + 11/14(g_{\perp}-g_e)] \quad (43)$$

where K is the Fermi contact term for isotropic hyperfine coupling to the metal nucleus, P_O is the coupling constant for dipole-dipole coupling to the free metal ion, and α^2 is a covalency factor that gives the reduction in the observed dipole-dipole coupling from the free ion value P_O[173b,177]. Purely ionic metal-ligand bonding gives $\alpha^2=1$ (i.e. 100% metal character for the unpaired electron), whilst metal-ligand covalency leads to $\alpha^2<1$. Solving equations 42 and 43 using $A_{\parallel}$ = -43G, $A_{\perp}$ = -8G and P_O for ^{61}Ni (102G)[178], we obtain α^2 = 0.67 for [Ni([9]aneS$_3$)(tdpme)]$^+$, i.e. the unpaired electron in this complex has 67% metal character. This is a lower value than those previously reported for other Ni^I complexes (Table 4.4), showing that [Ni([9]aneS$_3$)(tdpme)]$^+$ has a greater degree of σ-covalency than these other species. However, these results show that the complexes [Ni([9]aneS$_3$)(PP)]$^+$ are best regarded as genuine Ni^I radical species.

Complex	Covalency Factor	Reference
$[Ni([9]aneS_3)(tdpme)]^+$	0.67	This work
$[Ni(tmc)]^+$	0.74	179
$[Ni(mnt)_2]^{3-}$	0.70 or 0.85	173b
$[Ni(Bu_2NCS_2)_2]^-$	0.80	174
$[Ni(tpo)_2]^-$	0.87	180

tmc = N,N',N'',N'''-tetramethylcyclam

mnt = maleonitriledithiolate

tpo = 2-thiopyridine-N-oxide

Table 4.4: Covalency factors for some Ni^I Complexes

The reductions of $[Ni([9]aneS_3)(PP)]^{2+}$ to $[Ni([9]aneS_3)(PP)]^+$ (PP = dppp, tdpme) were monitored by U.V./visible spectroscopy using an O.T.E. system. These reductions were shown to proceed both isosbestically and reversibly in CH_3CN/0.1M $^nBu_4NPF_6$ at 253K (Figures 4.15, 4.18, Table 4.3). As for $[Ni([9]aneS_3)(dppe)]^+$ and $[Ni([9]aneS_3)(dppv)]^+$, the reduced dppp and tdpme complexes exhibited two *d-d* bands at $\lambda_{max} \simeq 480$ nm ($\varepsilon_{max} \simeq 1,250$ $dm^3.mol^{-1}.cm^{-1}$) and 390 (1,500), supporting further the conclusion that these four Ni^I complexes adopt the same five-coordinate geometry (Section 4.2.2). The first of these bands occurs at *ca.* 30 nm lower wavelength for $[Ni([9]aneS_3)(PP)]^+$ (PP = dppp, tdpme) than for PP =

dppe and dppv, showing that the energies of these d-d transitions are very sensitive to the diphosphine ligand used. This observation, and the high intensity of the d-d bands, are consistent with the relatively high metal-ligand covalency data derived from the e.p.r. spectra of $[Ni([9]aneS_3)(tdpme)]^+$, since the S.O.M.O of the complex will have a significant degree of P- as well as Ni $d_{x^2-y^2}$-character. The two charge transfer bands in the electronic spectra of $[Ni([9]aneS_3)(PP)]^{2+}$ (PP = dppp, tdpme) behaved in a similar way to the analogous bands exhibited by the Ni dppe and dppv complexes during reduction to $[Ni([9]aneS_3)(PP)]^+$, and were therefore given the same assignments (Section 4.2.2).

The reduction potential and slow reversibility of the $[Ni([9]aneS_3)(dppp)]^{+/0}$ couple, and the electronic spectrum of the final reduced product, are similar to those exhibited by the reductions $[Ni([9]aneS_3)(PP)]^{+/0}$ (PP = dppe, dppv, Tables 4.1 and 4.3). The species $[Ni([9]aneS_3)(dppp)]^0$ is therefore probably isostructural with those of the Ni^0 dppe and dppv complexes (Section 4.2.2). In contrast, the $[Ni([9]aneS_3)(tdpme)]^{+/0}$ couple is quasi-reversible by cyclic voltammetry, exhibiting a well-defined return wave (Figure 4.5), and occurs at a significantly less cathodic potential (Table 4.1). The formation of the e.p.r. inactive second reduction product of $[Ni([9]aneS_3)(tdpme)](PF_6)_2$ was shown to be fully reversible but non-isosbestic at 253K in CH_3CN/0.1M

$^{n}Bu_4NPF_6$ by U.V./visible spectroscopy using an O.T.E. system (Figure 4.19), and the electronic spectrum of the reduced species showed an extra charge transfer band compared to those of the Ni^0 dppe, dppv and dppp complexes [λ_{max} = 386 nm (ε_{max} = 7,725 $dm^3.mol^{-1}.cm^{-1}$), 328 (8,600) and 260 (14,290), Table 4.3]. These data might suggest that the dangling P-donor of the tdpme ligand becomes coordinated to the Ni centre after reduction to Ni^0, possibly to give a tetrahedral species containing a monodentate [9]aneS_3 ligand:

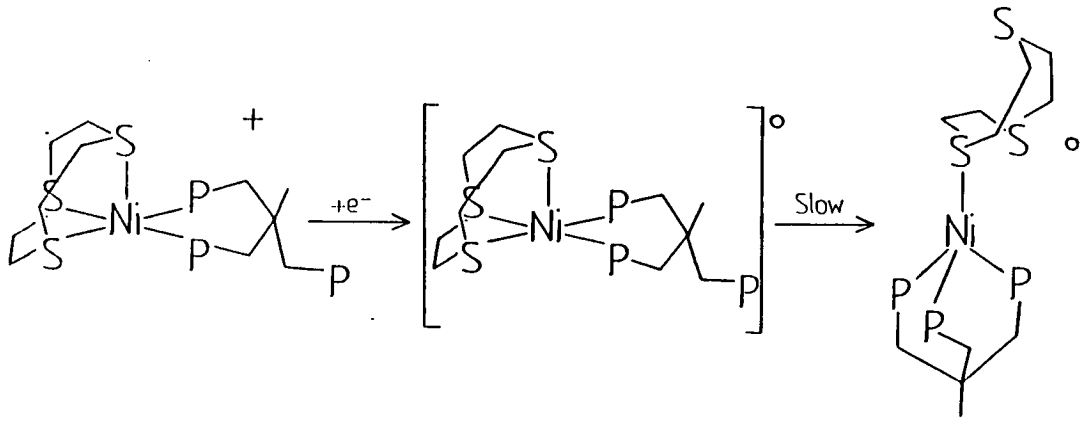

This monodentate coordination for [9]aneS_3 has been observed previously for d^{10} metal complexes[65c,67a]. However, this structural assignment must remain speculative in the absence of corroborating data.

In addition to the reductive chemistry described

above, $[Ni([9]aneS_3)(tdpme)](PF_6)_2$ exhibits an irreversible one-electron oxidation at Ep_a = +1.04V *vs.* Fc/Fc^+ in CH_3CN/0.1M $^nBu_4NPF_6$ at 298K (scan rate 400 mV/s), with no observable return wave (Figure 4.5, Table 4.1). Electrogeneration of bulk samples of this oxidation product by controlled potential electrolysis in CH_3CN/0.1M $^nBu_4NPF_6$ proceeded very slowly, and gave an e.p.r. silent solution identical in colour to the original Ni^{II} complex. No current flow was observed on attempting re-reduction of the oxidised species at 0V *vs.* Ag/AgCl. This oxidative process was assigned to an oxidation of the dangling P-donor of the complex to a phosphonium radical centre, which then rapidly reacts further to give an unknown final product: aerial oxidation of dangling P centres in tdpme complexes is known to occur[80].

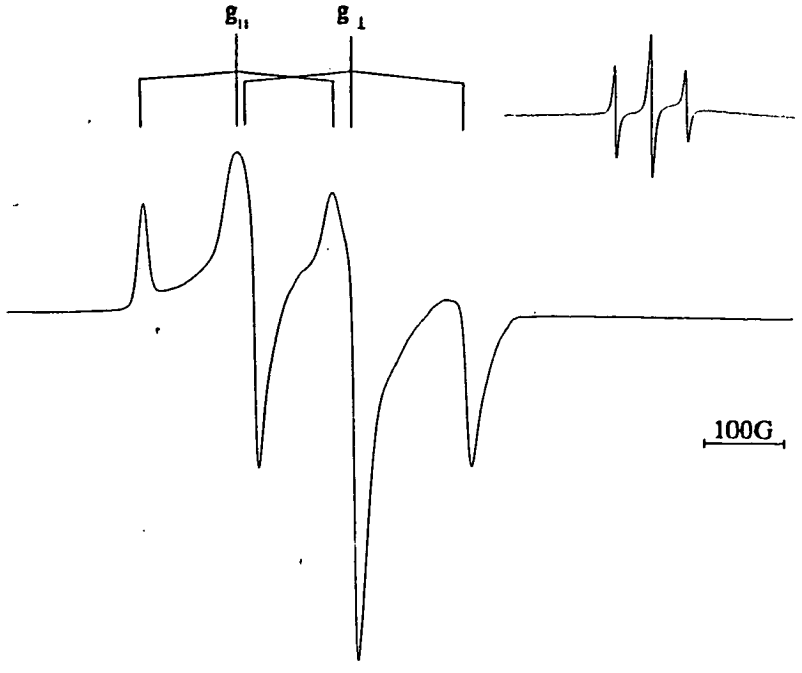

Figure 4.14: E.p.r. spectrum of $[Ni([9]aneS_3)(dppp)]^+$ (CH_3CN/0.1M $^nBu_4NPF_6$, 77K). Inset isotropic spectrum (CH_3OH, 298K).

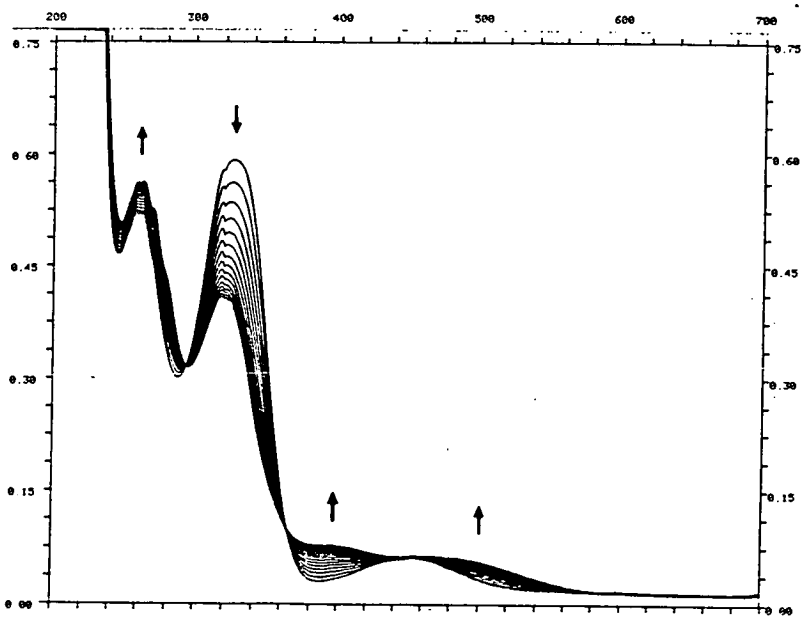

Figure 4.15: Electronic spectrum showing the conversion of $[Ni([9]aneS_3)(dppp)]^{2+}$ to $[Ni([9]aneS_3)(dppp)]^+$ (CH_3CN/0.1M $^nBu_4NPF_6$, 253K).

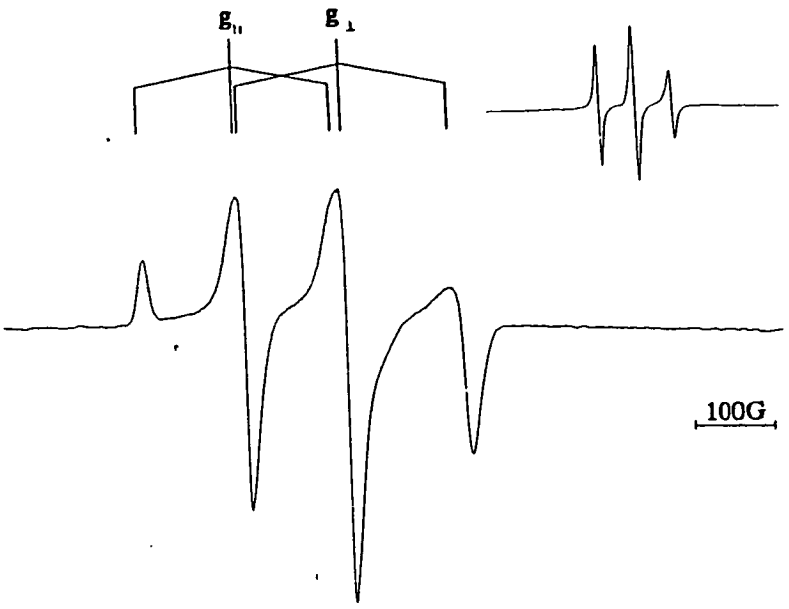

Figure 4.16: E.p.r. spectrum of $[Ni([9]aneS_3)(tdpme)]^+$ (CH_3CN/0.1M $^nBu_4NPF_6$, 77K). Inset isotropic spectrum (CH_3OH, 298K).

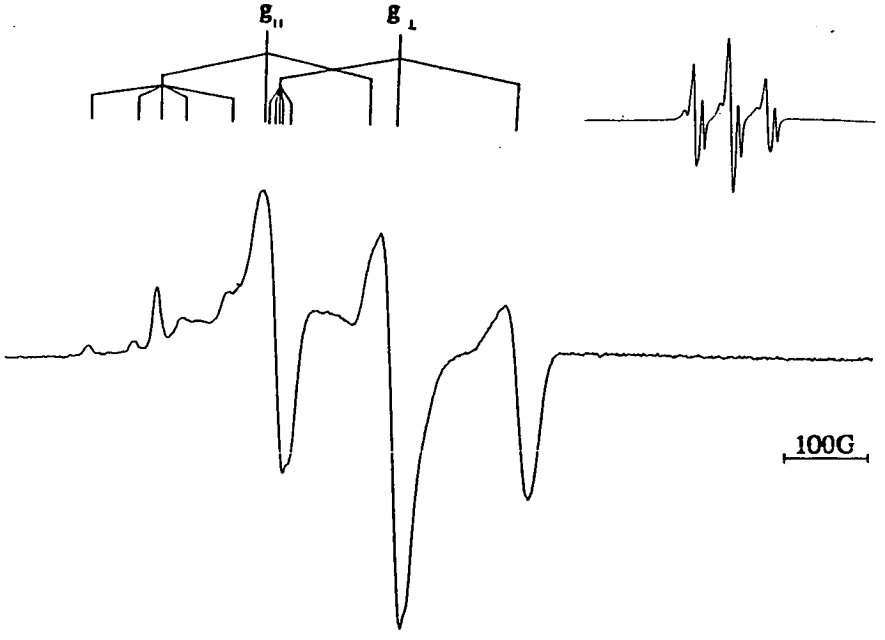

Figure 4.17: E.p.r. spectrum of 62%-enriched $[^{61}Ni([9]aneS_3)(tdpme)]^+$ (CH_3OH, 77K). Inset isotropic spectrum (CH_3CN/0.1M $^nBu_4NPF_6$), 298K).

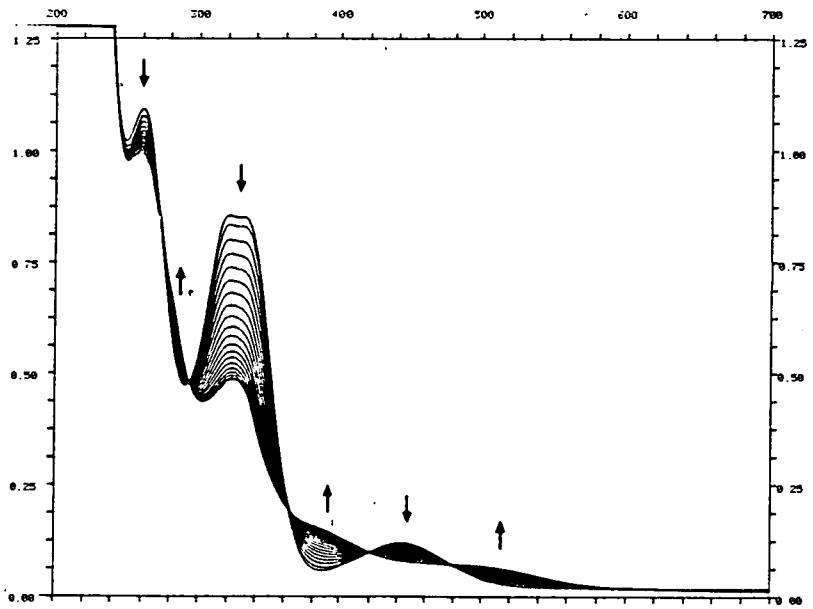

Figure 4.18: Electronic spectrum showing the reduction of $[Ni([9]aneS_3)(tdpme)]^{2+}$ to $[Ni([9]aneS_3)(tdpme)]^{+}$ (CH_3CN/0.1M $^nBu_4NPF_6$, 253K).

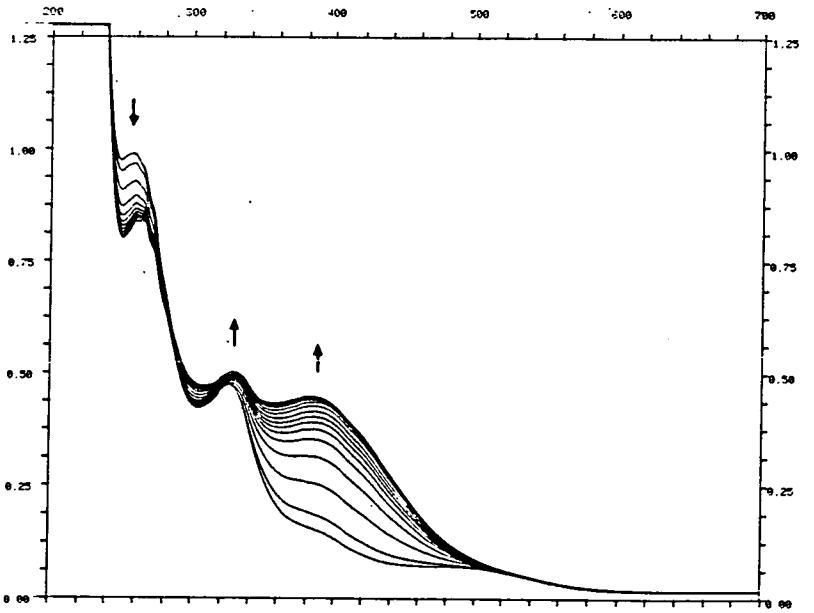

Figure 4.19: Electronic spectrum showing the reduction of $[Ni([9]aneS_3)(tdpme)]^{+}$ to $[Ni([9]aneS_3)(tdpme)]^{0}$ (CH_3CN/0.1M $^nBu_4NPF_6$, 253K).

4.2.4 Characterisation of the Redox Products of $[Ni([9]aneS_3)(dcpe)](PF_6)_2$ and $[Ni([9]aneS_3)(dmpe)](PF_6)_2$

The first reduction products of $[Ni([9]aneS_3)(dcpe)]^{2+}$ and $[Ni([9]aneS_3)(dmpe)]^{2+}$ were much less thermally stable than those of the diphenylphosphine chelate complexes described above, reflecting the more cathodic reduction potentials of the dcpe and dmpe species. Generation of the species $[Ni([9]aneS_3)(PP)]$ (PP = dcpe, dmpe) by controlled potential electrolysis in $CH_3CN/0.1M\ ^nBu_4NPF_6$ at 298K resulted in pale, cloudy, e.p.r. inactive solutions, and deposition of Ni metal onto the Pt working electrode. At 243K, however, electrogeneration of bulk $CH_3CN/0.1M\ ^nBu_4NPF_6$ solutions of the relevant Ni^{II} precursor afforded yellow and green solutions of $[Ni([9]aneS_3)(dcpe)]^+$ and $[Ni([9]aneS_3)(dmpe)]^+$ respectively. Weak solutions of $[Ni([9]aneS_3)(dcpe)]^+$ could be generated chemically using $NaBH_4$ in CH_3OH under N_2; these solutions showed the same e.p.r. spectrum as electrogenerated samples of this species, but decomposed after standing at room temperature for 10 minutes. $[Ni([9]aneS_3)(dmpe)]^+$ could not be chemically generated by this method.

The e.p.r. spectra of $[Ni([9]aneS_3)(PP)]^+$ (PP = dcpe, dmpe) in frozen solution are complex (Figures 4.20, 4.22), and were tentatively interpreted by assuming rhombic symmetry and equal hyperfine coupling to both ^{31}P nuclei

(Table 4.2). In mobile solution, both species gave triplet e.p.r. resonances (Table 4.2, Figures 4.20 and 4.22). In common with the other complexes in the series, the e.p.r. spectra of $[Ni([9]aneS_3)(dcpe)]^+$ and $[Ni([9]aneS_3)(dmpe)]^+$ also show additional weak signals which were reproducible between different samples of each compound. It is unclear whether these correspond to decomposition products of the initial Ni^I complexes, or to conformational isomers of the $[Ni([9]aneS_3)(PP)]^+$ species.

In situ experiments using an O.T.E. system to monitor the conversions of $[Ni([9]aneS_3)(PP)]^{2+}$ to $[Ni([9]aneS_3)(PP)]^+$ (PP = dcpe, dmpe) showed that both processes occurred isosbestically and reversibly at 253K (for dcpe) and 243K (for dmpe - this reduction was not completely reversible at 253K) (Table 4.3, Figures 4.21 and 4.23). The U.V./visible spectrum of $[Ni([9]aneS_3)(dmpe)]^+$ showed two bands of similar intensity to the *d-d* bands observed for the *bis*-diphenylphosphine chelate Ni^I complexes, as well as two charge-transfer bands [λ_{max} = 350 nm (ε_{max} = 1,760 $dm^3.mol^{-1}.cm^{-1}$), 308 (sh), 267 (sh), 244 (10,650)]. Despite their occurring at 100-150 nm lower wavelength than the analogous bands in $[Ni([9]aneS_3)(PP)]^+$ (PP = dppe, dppv, dppp, tdpme), it is likely that these two lower energy bands for $[Ni([9]aneS_3)(dmpe)]^+$ are analogous to the *d-d* bands exhibited by the Ni^I dppe, dppv, dppp and tdpme species, since it has been noted that the energies of these *d-d* transitions are very sensitive to the

phosphine ligand used (Section 4.2.3). This being the case, the geometry adopted by $[Ni([9]aneS_3)(dmpe)]^+$ is probably five-coordinate, as for the Ni^I dppe, dppv, dppp and tdpme complexes discussed previously (Sections 4.2.2 and 4.2.3). Unfortunately, no *d-d* type bands are observed in the electronic spectrum of $[Ni([9]aneS_3)(dcpe)]^+$, athough they could be obscured by a third charge-transfer band observed for this species [λ_{max} = 320 nm (ε_{max} = 4,220 $dm^3\ mol^{-1}\ cm^{-1}$), 287 (8,580), 249 (12,590)]. Hence, no firm inferences about the structure of this complex can be drawn, although the similarity of its e.p.r. spectrum to that exhibited by $[Ni([9]aneS_3)(dmpe)]^+$ implies that the two complexes have similar electronic structures.

The second reduction products of $[Ni([9]aneS_3)(PP)]^{2+}$ (PP = dcpe, dmpe) were highly unstable. Generation of the second reduction products for these complexes by controlled potential electrolysis in CH_3CN/0.1M $^nBu_4NPF_6$ at 243K gave colourless e.p.r. silent solutions, together with deposition of Ni metal onto the Pt basket working electrode. No current flow was observed on attempting re-oxidation of these reduced solutions at 0V *vs.* Ag/AgCl at 243K. Coulometric measurements on the first and second reductions for these compounds consistently gave $n<2$ electrons. Hence, no information about the structures of any Ni^0 dcpe or dmpe species could be obtained, and no further experiments on these species were attempted.

In addition to the reductive chemistry described

above, $[Ni([9]aneS_3)(dmpe)](PF_6)_2$ also exhibits an irreversible oxidation at Ep_a = +1.22V *vs.* Fc/Fc^+ (scan rate 400 mV/s) in CH_3CN/0.1M $^nBu_4NPF_6$, together with a return wave of roughly equal intensity to the parent oxidation at Ep_c = +0.21V (Figure 4.5). A coulometric determination of this process at 298K gave n=0.95, consistent with an overall one-electron oxidation, and re-reduction of the oxidised solution at OV *vs.* Ag/AgCl regenerated $[Ni([9]aneS_3)(dmpe)]^{2+}$ (identified from its cyclic voltammogram). Controlled potential electrolysis of bulk solutions of $[Ni([9]aneS_3)(dmpe)](PF_6)_2$ in CH_3CN/ 0.1M $^nBu_4NPF_6$ at 1.85V *vs.* Ag/AgCl at 298K afforded green solution, that surprisingly showed an axial e.p.r. spectrum at 77K, with hyperfine coupling to 2 equivalent ^{15}N nuclei ($g_\perp$ = 2.120, $A_\perp$ = 17G, $g_{||}$ = 2.023, $A_{||}$ = 19G, g_{iso} = 2.098, A_{iso} = 18G, Figure 4.24). This implies the coordination of two axial CH_3CN ligands to the oxidised Ni^{III} centre, presumably *via* the decoordination of one macrocyclic S-donor. Chemical oxidation of $[Ni([9]aneS_3)(dmpe)]^{2+}$ with 98% H_2SO_4 or 70% $HClO_4$ gave red solutions, which exhibited one major axial e.p.r. signal at 77K ($g_{||}$ = 2.153, $g_\perp$ = 2.018, g_{iso} = 2.117, Figure 4.25) together with weaker peaks due to paramagnetic impurities. These results suggest the formation of a metal-based d^7 $[Ni([9]aneS_3)(dmpe)]^{3+}$ radical, which probably corresponds to the major species in the e.p.r. spectra of the chemically oxidised samples; this species appears to bind

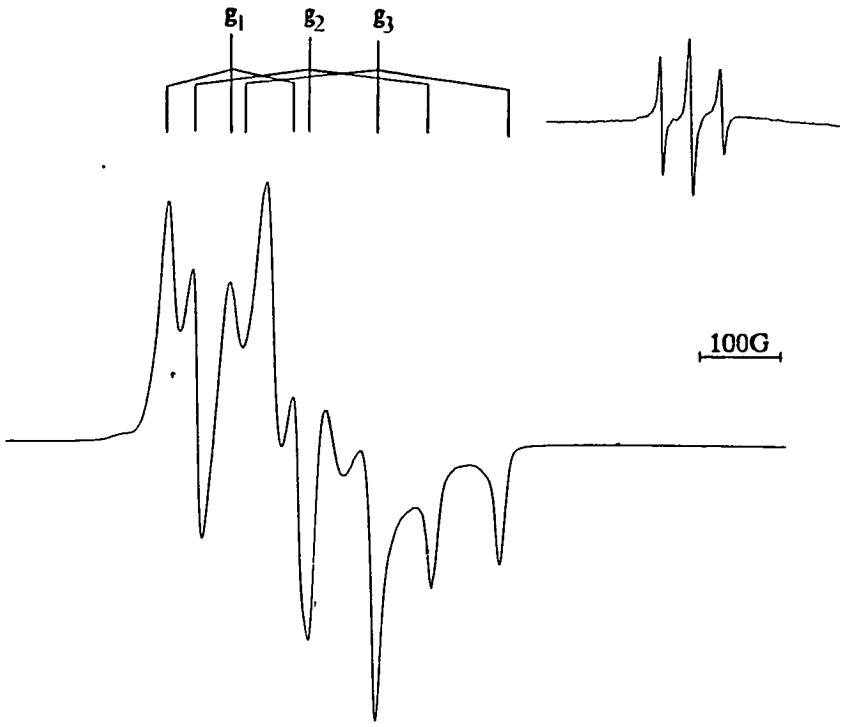

Figure 4.20: E.p.r. spectrum of [Ni([9]aneS$_3$)(dcpe)]$^+$ (CH_3CN/0.1M $^nBu_4NPF_6$, 77K). Inset isotropic spectrum (CH_3OH, 298K).

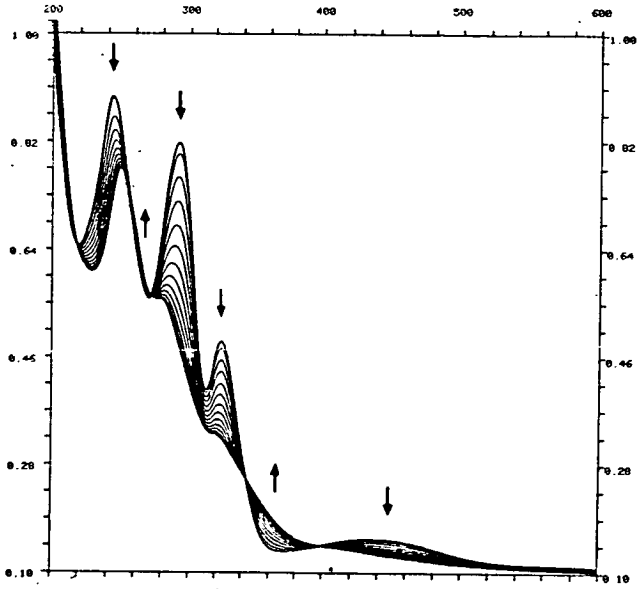

Figure 4.21: Electronic spectrum showing the conversion of [Ni([9]aneS$_3$)(dcpe)]$^{2+}$ to [Ni([9]aneS$_3$)(dcpe)]$^+$ (CH_3CN/0.1M $^nBu_4NPF_6$, 253K).

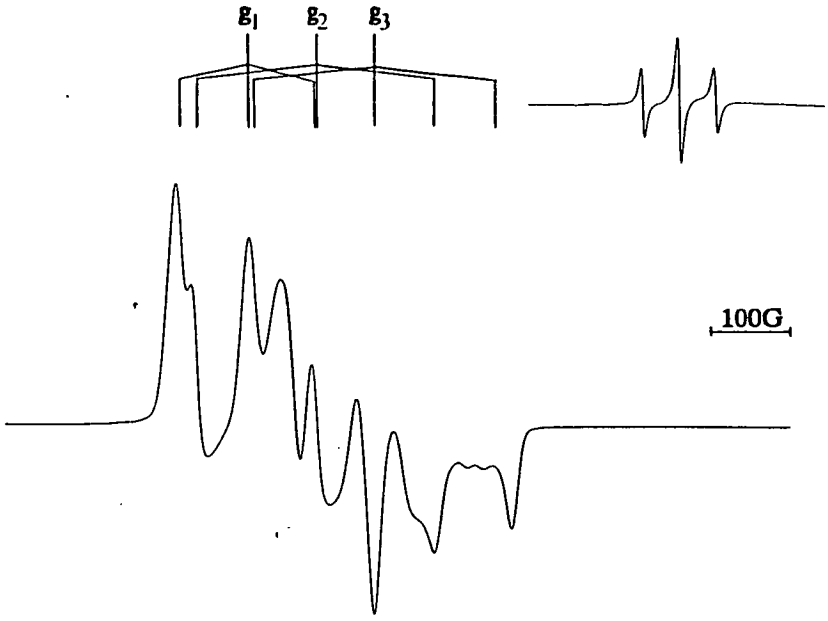

Figure 4.22: E.p.r. spectrum of $[Ni([9]aneS_3)(dmpe)]^+$ (CH_3CN/0.1M $^nBu_4NPF_6$, 77K). Inset isotropic spectrum (CH_3OH, 298K).

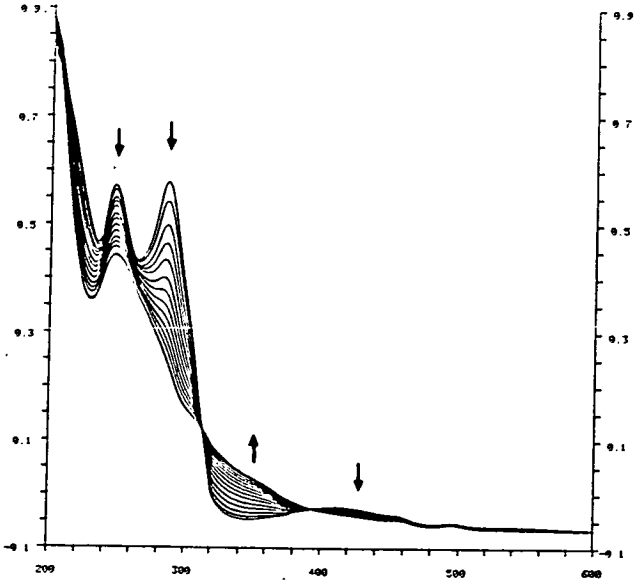

Figure 4.23: Electronic spectrum showing the conversion of $[Ni([9]aneS_3(dmpe)]^{2+}$ to $[Ni([9]aneS_3)(dmpe)]^+$ (CH_3CN/0.1M $^nBu_4NPF_6$, 243K).

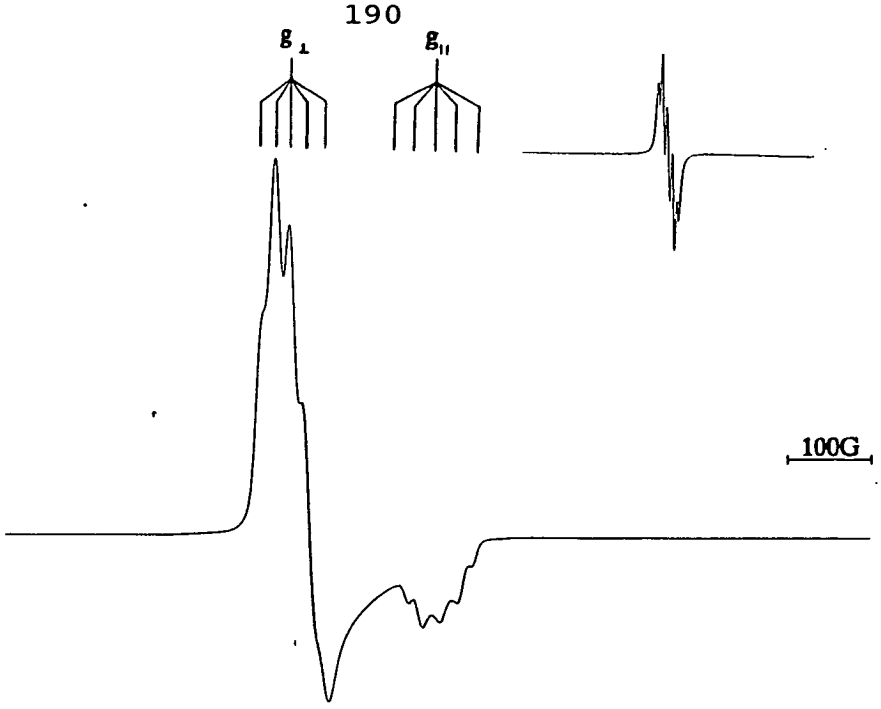

Figure 4.24: E.p.r. spectrum of the electrogenerated oxidation product of $[Ni([9]aneS_3)(dmpe)]^{2+}$ (CH_3CN/0.1M $^nBu_4NPF_6$, 77K). Inset isotropic spectrum (CH_3CN/0.1M $^nBu_4NPF_6$, 298K).

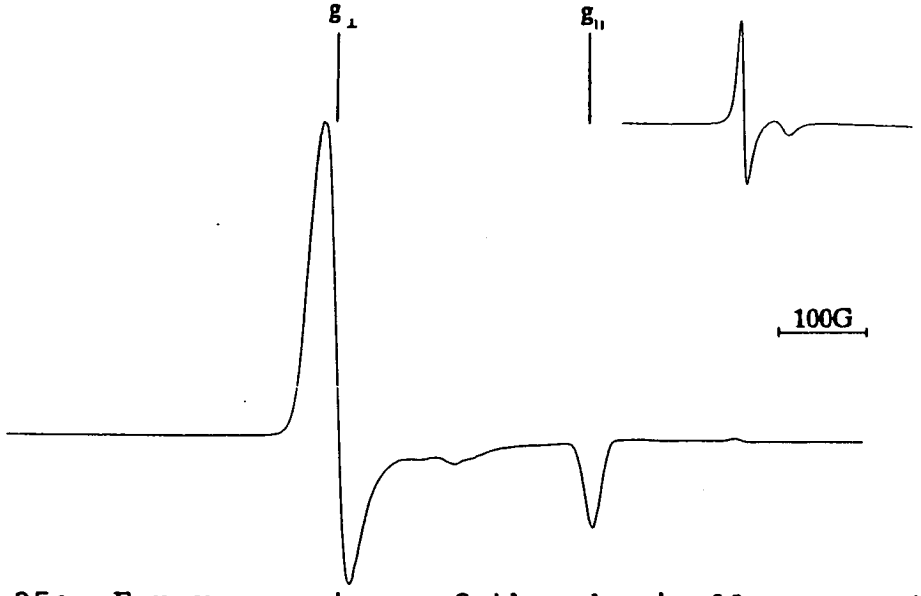

Figure 4.25: E.p.r. spectrum of the chemically generated oxidation product of $[Ni([9]aneS_3)(dmpe)]^{2+}$ (98% H_2SO_4, 77K). Inset isotropic spectrum (98% H_2SO_4, 298K).

axial ligands in coordinating media to give octahedral Ni^{III} species. Further experiments would be necessary to confirm these conclusions, and to fully characterise the oxidation products, however.

4.2.5 Characterisation of the Reduction Products of $[Ni([9]aneS_3)(dppm)](PF_6)_2$

In contrast to the other Ni *bis*-diphenylphosphine chelate systems described previously, the reduction products of $[Ni([9]aneS_3)(dppm)]^{2+}$ are thermally unstable. Attempts to electrogenerate bulk samples of $[Ni([9]aneS_3)(dppm)]^{+}$ in CH_3CN/0.1M $^nBu_4NPF_6$ at 298K were unsuccessful, giving pale yellow e.p.r. inactive solutions and deposition of Ni metal onto the Pt electrodes. At 243K, controlled potential electrolysis of CH_3CN/0.1M $^nBu_4NPF_6$ solutions of $[Ni([9]aneS_3)(dppm)](PF_6)_2$ at -0.9V *vs.* Ag/AgCl afforded orange solutions, which gave complex e.p.r. spectra at 77K (Figure 4.26). The mobile solution e.p.r. spectra of these solutions at 298K showed that they contained one major e.p.r. active component which exhibited a triplet signal similar to those of the other $[Ni([9]aneS_3)(PP)]^{+}$ species, as well as at least one paramagnetic impurity (Figure 4, Table 4.2). The frozen solution e.p.r. spectrum of $[Ni([9]aneS_3)(dppm)]^{+}$ was therefore tentatively assigned assuming rhombic symmetry and equal hyperfine coupling to both ^{31}P nuclei of the dppm ligand (Table 4.2).

Spectro-electrochemical experiments to follow the reduction of $[Ni([9]aneS_3)(dppm)]^{2+}$ to $[Ni([9]aneS_3)(dppm)]^{+}$ by U.V./visible spectroscopy using an O.T.E. system showed that this process does not occur isosbestically in $CH_3CN/0.1M\ ^nBu_4NPF_6$ at 253K, in contrast to the other $[Ni([9]aneS_3)(PP)]^{2+/+}$ reductions (Figure 4.27). Re-oxidation of the reduction solution at OV *vs.* Ag/Ag^+ quantitatively regenerated $[Ni([9]aneS_3)(dppm)]^{2+}$, however, and the electronic spectrum of the reduced species shows similar features to those of the Ni^I dppe, dppv, dppp and tdpme complexes (Table 4.3). Hence, it is possible that the non-isosbesticity of the $[Ni([9]aneS_3)(dppm)]^{2+/+}$ reduction is caused by conformational isomerism of the reduced species, possibly giving a dimeric five-coordinate complex with bridging dppm ligands, or a mononuclear species in equilibrium between five- and four-coordinate geometries:

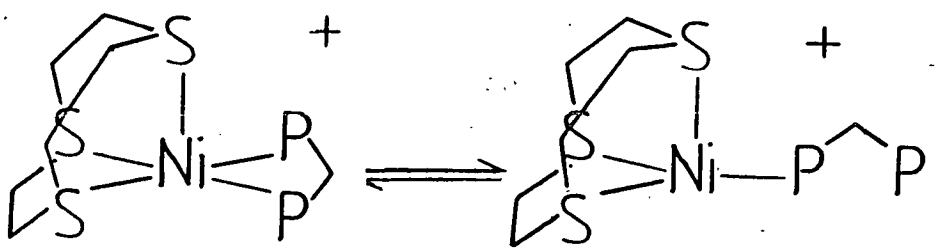

The instability of $[Ni([9]aneS_3)(dppm)]^{2+}$ towards decomposition to $[Ni([9]aneS_3)_2]^{2+}$ has been noted previously (Section 3.2.1), confirming the strain associated with the four-membered P-Ni-P chelate ring.

Controlled potential electrolysis of the second reduction product of $[Ni([9]aneS_3)(dppm)]^{2+}$ in CH_3CN/0.1M $^nBu_4NPF_6$ at 243K yielded a yellow e.p.r. silent solution, and deposition of Ni metal onto the Pt basket working electrode. *In situ* spectro-electrochemical experiments showed that this process was neither isosbestic nor quantitatively reversible in CH_3CN/0.1M $^nBu_4NPF_6$ at 253K, confirming the instability of this second reduction product. No conclusions about the nature of $[Ni([9]aneS_3)(dppm)]^0$ can be drawn from these data, and no further experiments were attempted.

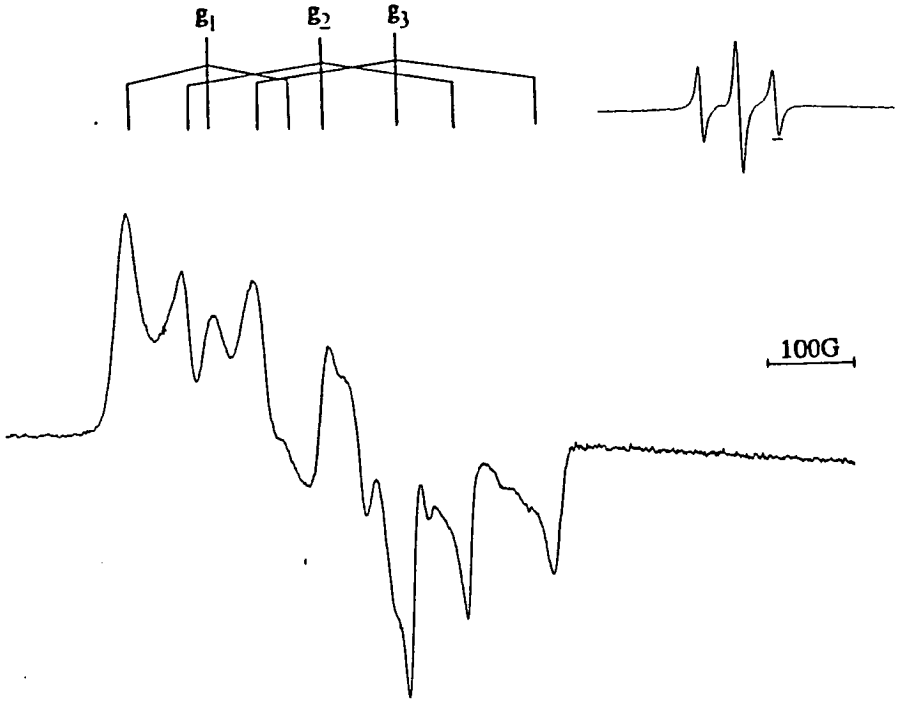

Figure 4.26: E.p.r. spectrum of $[Ni([9]aneS_3)(dppm)]^+$ (CH_3CN/0.1M $^nBu_4NPF_6$, 77K). Inset isotropic spectrum (CH_3CN/0.1M $^nBu_4NPF_6$, 298K).

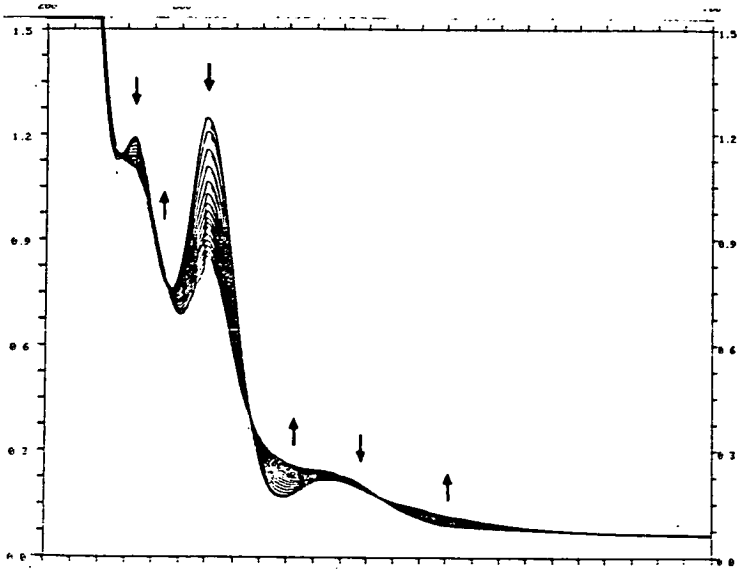

Figure 4.27: Electronic spectrum showing the conversion of $[Ni([9]aneS_3)(dppm)]^{2+}$ to $[Ni([9]aneS_3)(dppm)]^+$ (CH_3CN/0.1M $^nBu_4NPF_6$, 253K).

4.2.6 Electrochemical Study of $[Ni([9]aneS_3)(PP)](PF_6)_2$ under CO and CO_2 Atmospheres

The ability of many Ni^I complexes to bind and activate small molecule substrates has been discussed previously (Sections 1.3 and 4.1). With this in mind, a preliminary study of the electrochemistry of the $[Ni([9]aneS_3)(PP)]^{2+}$ complexes in the presence of the reagent gases CO and CO_2 was undertaken.

Under a CO atmosphere, the cyclic voltammograms of $[Ni([9]aneS_3)(PP)]^{2+}$ in $CH_3CN/0.1M\ ^nBU_4NPF_6$ at 298K exhibit a quasi-reversible or irreversible reduction at similar potentials to the $[Ni([9]aneS_3)(PP)]^{2+/+}$ couples observed under Ar (Tables 4.1 and 4.5, Figure 4.28a). In all cases, a return wave due to a daughter product is observed at $Ep_a \approx 0V$ *vs.* Fc/Fc^+, with 1/3-2/3 the intensity of the reduction wave at scan rate 400 mV/s. This return oxidation becomes more intense relative to the initial reduction at increased scan rates, which suggests that the initial reaction of $[Ni([9]aneS_3)(PP)]^+$ with CO is fast, to form an unstable adduct which then rapidly decomposes. In some cases, a weak second irreversible reduction is also observed, at similar potential to those of the $[Ni([9]aneS_3)(PP)]^{+/0}$ reductions found under an Ar atmosphere (Tables 4.1, 4.5). No significant decay in intensity of these processes was observed on repeat cycling of the cyclic voltammograms, implying that both decomposition and re-oxidation of the CO adducts

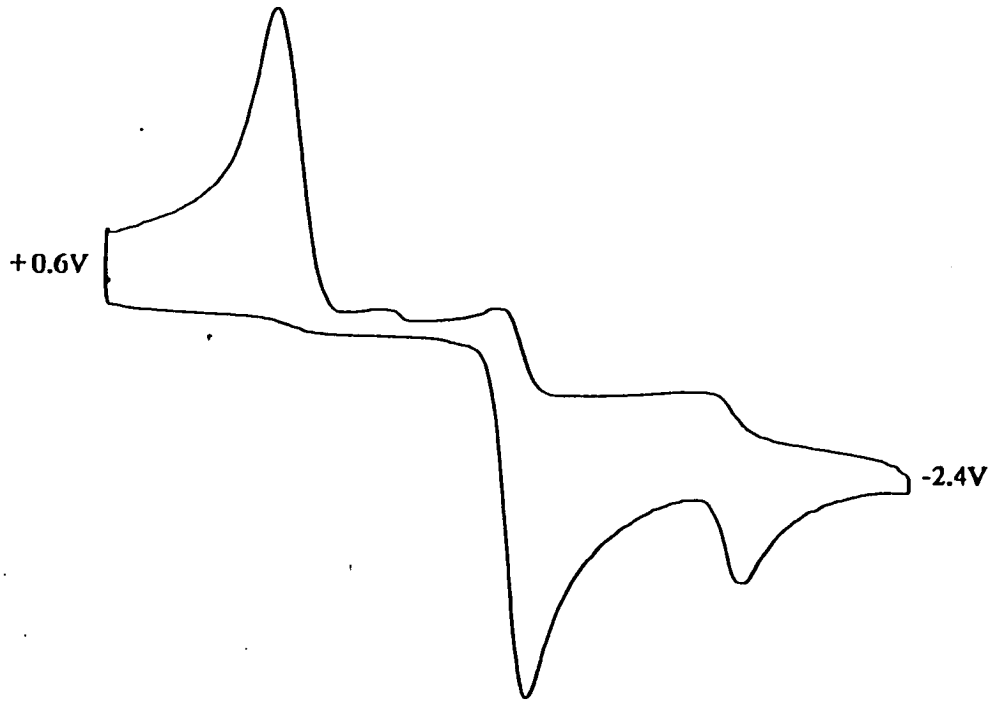

a) CO atmosphere

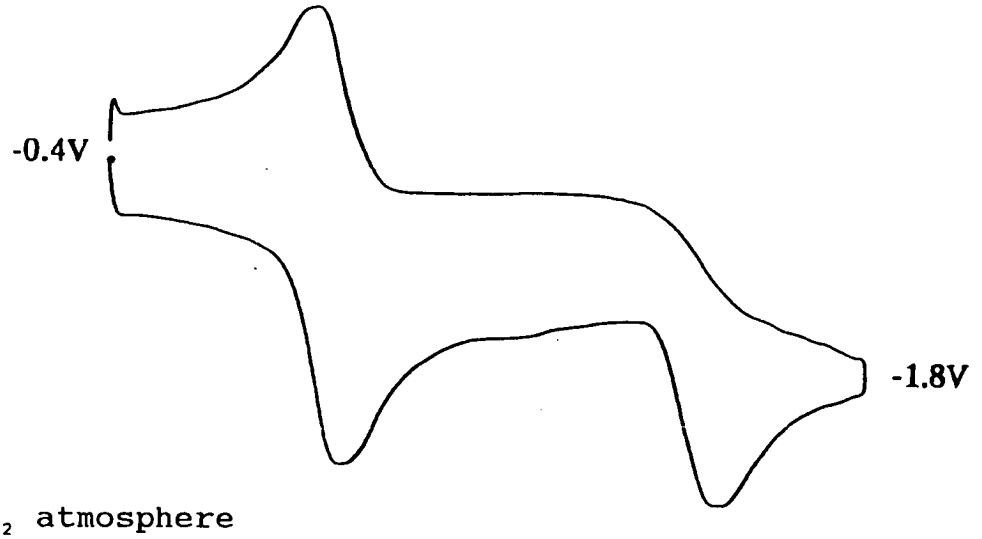

b) CO_2 atmosphere

Figure 4.28: Cyclic Voltammograms of [Ni([9]aneS_3)(dppe)] $(PF_6)_2$ under a) CO and b) CO_2 Atmospheres ($CH_3CN/^nBu_4NPF_6$, 298K, scan rate 400 mV/s).

PP	E(First reduction,V)[a]	E(Second reduction,V)[a]	E(Return oxidation,V)[a]
dppm	-0.77(i)	-	-0.03(i,w)
dppe	-0.88(q)	-1.76(i,w)	0.00(i)
dppv	-0.80(q)	-1.65(i,w)	+0.02(i)
dcpe	-0.98(i)	-	-0.11(i)
dmpe	-1.14(i)	-	-0.19(i)
dppp	-0.78(i)	-1.76(i,w)	-0.07(i)
tdpme	-0.80(i)	-	-0.32(i), +0.05(i)

a. Electrochemical redox potential measured at 298K, in CH_3CN/0.1M $^nBu_4NPF_6$, scan rate 400 mV/s, under a CO atmosphere. Potentials quoted *vs.* Fc/Fc^+
q = quasi-reversible, i = irreversible, w = weak.

Table 4.5: Electrochemical Data for $[Ni([9]aneS_3)(PP)](PF_6)_2$ under a CO Atmosphere.

regenerates the initial $[Ni([9]aneS_3)(PP)]^{2+}$ complexes.

Controlled potential electrolysis of bulk solutions of the complexes $[Ni([9]aneS_3)(PP)]^{2+}$ under CO gave continuous current flow, with no obvious colour change in the solution. On cooling to 243K, current decay was observed and the electrogenerated solutions became almost colourless. Most of these reduced solutions were e.p.r. silent; however, for reduced samples of $[Ni([9]aneS_3)(dppp)]^{2+}$ and $[Ni([9]aneS_3)(tdpme)]^{2+}$ a weak axial e.p.r. signal was sometimes observed with $g_{||} = 2.093$, $g_{\perp} = 2.015$, exhibiting no obvious hyperfine coupling to ^{31}P (Figure 4.29). This may indicate the presence of a CO-based radical species, although other Ni^{I}-CO adducts have exhibited e.p.r. spectra characteristic of metal-based radicals[91,92]. Warming these samples to 298K does not result in re-generation of $[Ni([9]aneS_3)(PP)]^{2+}$, showing that these colourless products are not intermediates in the re-oxidation reaction observed at room temperature.

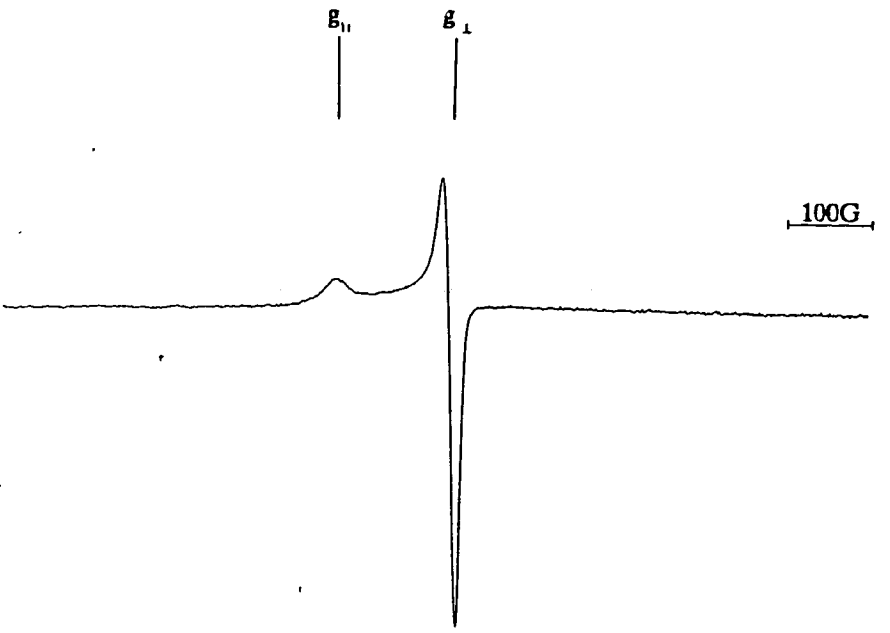

Figure 4.29: E.p.r. spectrum of a solution of $[Ni([9]aneS_3)(tdpme)](PF_6)_2$ electrogenerated at -0.90V *vs.* Ag/AgCl under a CO atmosphere ($CH_3CN/^nBu_4NPF_6$, 77K).

These results show that the complexes $[Ni([9]aneS_3)(PP)]^+$ react rapidly with CO, presumably to form an initial adduct $[Ni([9]aneS_3)(PP)(CO)]^+$ which is observed by cyclic voltammetry. At 298K, this adduct rapidly re-oxidises to form $[Ni([9]aneS_3)(PP)]^{2+}$: it is not known whether this oxidation is coupled to reduction of the bound CO ligand. At 243K this decomposition pathway is blocked, and an alternative e.p.r. silent product is formed; an e.p.r. active species is also observed in some samples generated at this temperature. The electro-reduction of alkyl halides by Ni^I tetra-aza macrocyclic complexes is known to follow a free radical

mechanism, via an initial one-electron transfer[154]:

$$[Ni(N_4)]^+ + R\text{-}X \longrightarrow [Ni(N_4)]^{2+} + R^\circ + X^-$$

It is possible that the radical species detected in the low temperature $[Ni([9]aneS_3)(PP)]^{2+/+}$ reductions under CO may be evidence for a similar process. Further experiments to follow these reactions *in situ* using e.p.r. and U.V./visible spectroscopy would be necessary to fully characterise the processes and products involved in these reactions.

In contrast to the above results, cyclic voltammograms of the complexes $[Ni([9]aneS_3)(PP)]^{2+}$ in $CH_3CN/0.1M$ $^nBu_4NPF_6$ at 298K under a CO_2 atmosphere were identical to those run under Ar (Figures 4.4 and 4.28b), showing that the species $[Ni([9]aneS_3)(PP)]^+$ do not react with CO_2 under these conditions.

4.2.7 Electrochemical Study of $[Ni([9]aneS_3)_2]^{2+}$

The cyclic voltammogram of $[Ni([9]aneS_3)_2](PF_6)_2$ in $CH_3CN/^nBu_4NPF_6$ at 298K exhibited the processes previously reported for this compound[128,74]: a chemically reversible oxidation at $E_{\frac{1}{2}}$ = +0.97V *vs.* Fc/Fc^+ (ΔEp = 83 mV, scan rate 400 mV/s) and a quasi-reversible reduction at -1.14V (ΔEp = 98 mV).

A coulometric determination of the above oxidation at 253K gave n = 0.94 electrons. Controlled potential electrolysis of $[Ni([9]aneS_3)_2]^{2+}$ at +1.60V *vs.* Ag/AgCl at 253K yielded an intense red solution, which exhibited a rhombic e.p.r. spectrum with g_1 = 2.093, g_2 = 2.075, g_3 = 2.027 (measured as a CH_3CN glass at 77K, Figure 4.30). A similar spectrum was obtained by chemical oxidation in 70% $HClO_4$, giving g_1 = 2.094, g_2 unresolved, g_3 = 2.025 (at 77K), g_{iso} = 2.065 (at 298K, Figure 4.30). This data is consistent with the formation of an octahedral d^7 Ni^{III} cation (Table 4.6), with the $g_\perp > g_{||}$ pattern implying a d_{z^2} electronic ground state.

The e.p.r. spectrum of 62% enriched $[^{61}Ni([9]aneS_3)_2]^{3+}$ showed an additional e.p.r. coupling to ^{61}Ni (I = 3/2), with g_1 = 2.093, A_1 = 28G, g_2 and A_2 unresolved, g_3 = 2.027, A_3 = 7G (in CH_3CN at 77K, Figures 4.31 and 4.32), g_{iso} = 2.065, A_{iso} unresolved (in 70% $HClO_4$, 298K, Figure 4.31). For an $S = \frac{1}{2}$ radical with a d_{z^2} ground state, a similar analysis to that described for $[^{61}Ni([9]aneS_3)(tdpme)]^+$ (Section 4.2.3) leads to the

equations:

$$A_1 = -K + P_0[-2/7\alpha^2 + 15/14(g_1 - g_e)] \quad (44)$$

$$A_3 = -K + P_0[4/7\alpha^2 - 1/7(g_1 - g_e)] \quad (45)$$

where K, P_0, α^2 and g_e have the meanings discussed in Section 4.2.3[174,177]. The solution of these equations using the values for g_1, A_1 and A_3 quoted above for $[Ni([9]aneS_3)_2]^{3+}$ gives

$$\alpha^2 = 0.39 \text{ for } A_1 = +28G, A_3 = +7G$$

or $$\alpha^2 = 0.56 \text{ for } A_1 = +28G, A_3 = -7G$$

Both of these solutions must be considered, because the relative signs of A_1 and A_3 cannot be derived from the isotropic e.p.r. spectrum of the enriched cation. Very little ^{61}Ni e.p.r. data has been reported for Ni^{III} complexes. ^{61}Ni hyperfine constants have been reported for several oxidised Ni 1,2-dithiolene radicals[177,185]; e.g. for $[Ni(mnt)_2]^-$ (46), $g_1 = 2.156$, $A_1 = 14.1G$, $g_2 = 2.042$, $A_2 = -5.1G$, $g_3 = 1.996$, $A_3 = 4.1G$ giving $\alpha^2 = 0.21$[177]. This has led to these species being formulated as Ni^{II}-stabilised ligand-based radicals. No ^{61}Ni couplings could be resolved for an enriched sample of $[^{61}Ni([9]aneN_3)_2]^{3+}$ [186]. However, an e.p.r. analysis of $[^{61}Ni(phmp)_2Cl_2]^+$ [47, $g_1 = 2.116$, $A_1(^{61}Ni) = -12.3G$, $g_2 = 2.112$, $A_2 = -13.3G$, $g_3 = 2.009$, $A_3 = +26.6G$] implied that

Table 4.6: E.p.r. data for some Octahedral Ni^{III} Complexes

	g_1	g_2	g_3	Reference
$[Ni([9]aneS_3)_2]^{3+}$	2.093	2.075	2.027	This work
$[Ni([9]aneNS_2)_2]^{3+}$	2.121		2.019[a]	124
$[Ni([9]aneN_3)_2]^{3+}$	2.127		2.030	181
$[Ni([18]aneN_2S_4)]^{3+}$	2.108	2.071	2.027	75
$[Ni(bipy)_3]^{3+}$	2.137		2.027	182
$[Ni(Me_2y)]^{2+}$	2.134		2.030	183
$[Ni(phmp)_2Cl_2]^{+}$	2.116	2.112	2.009[b]	184

a $A_{1,1}(^{14}N) = 20G$

b $A_3(^{31}P) = -46.5G$. $A_1(^{35}Cl^-) = -18.5G$, $A_2 = -17.8G$, $A_3 = -16.3G$

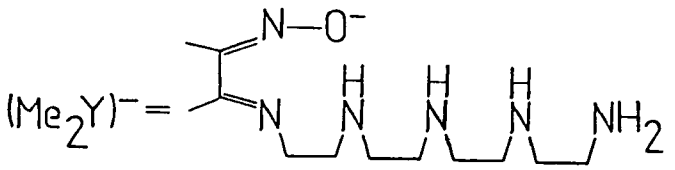

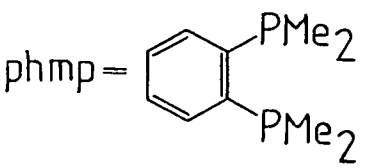

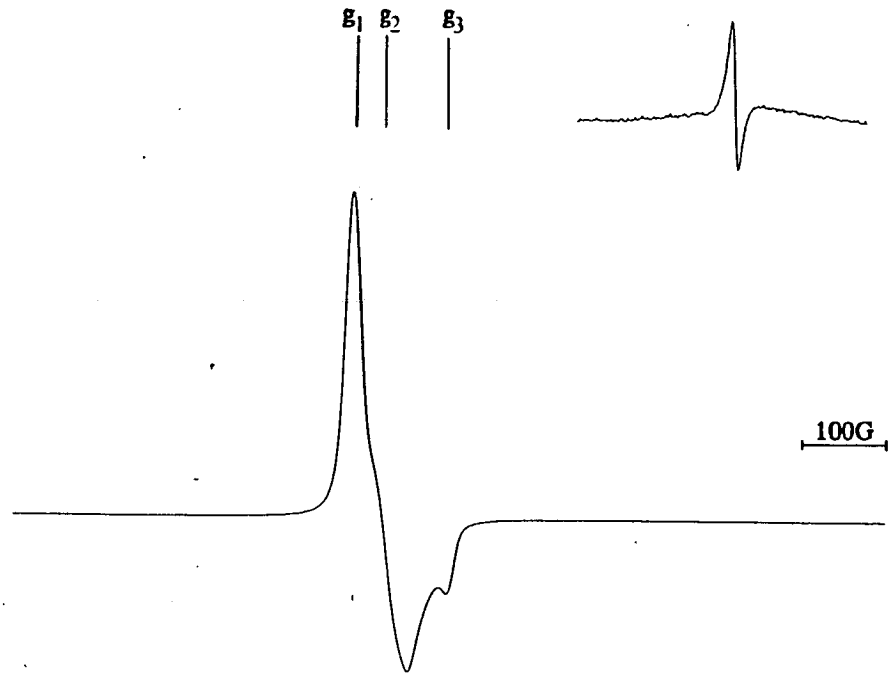

Figure 4.30: E.p.r. spectrum of $[Ni([9]aneS_3)_2]^{3+}$ $CH_3CN/^nBu_4NPF_6$, 77K). Inset isotropic spectrum (70% $HClO_4$, 298K).

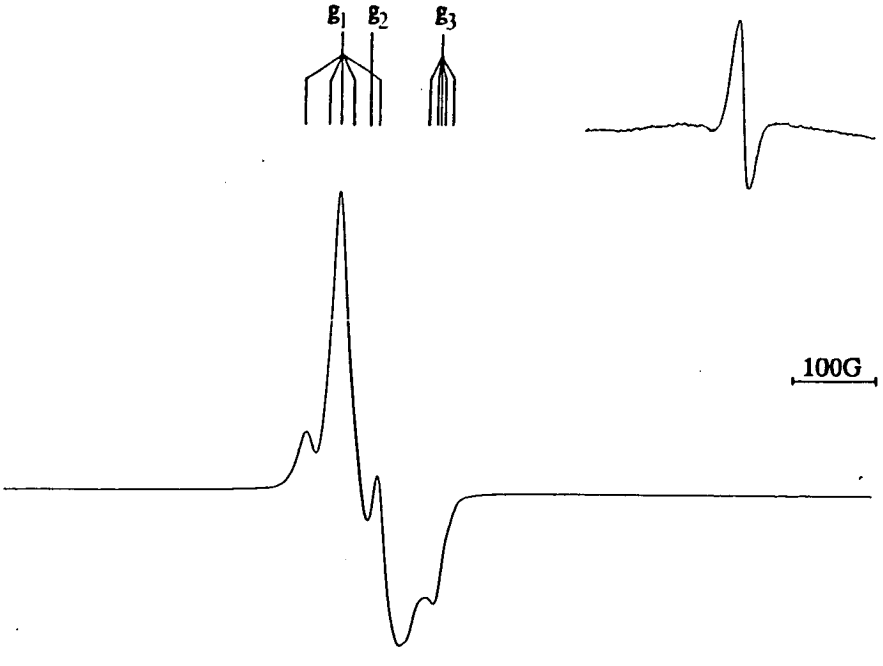

Figure 4.31: E.p.r. spectrum of 62% enriched $[^{61}Ni([9]aneS_3)_2]^{3+}$ $CH_3CN/^nBu_4NPF_6$, 77K). Inset isotropic spectrum (70% $HClO_4$, 298K).

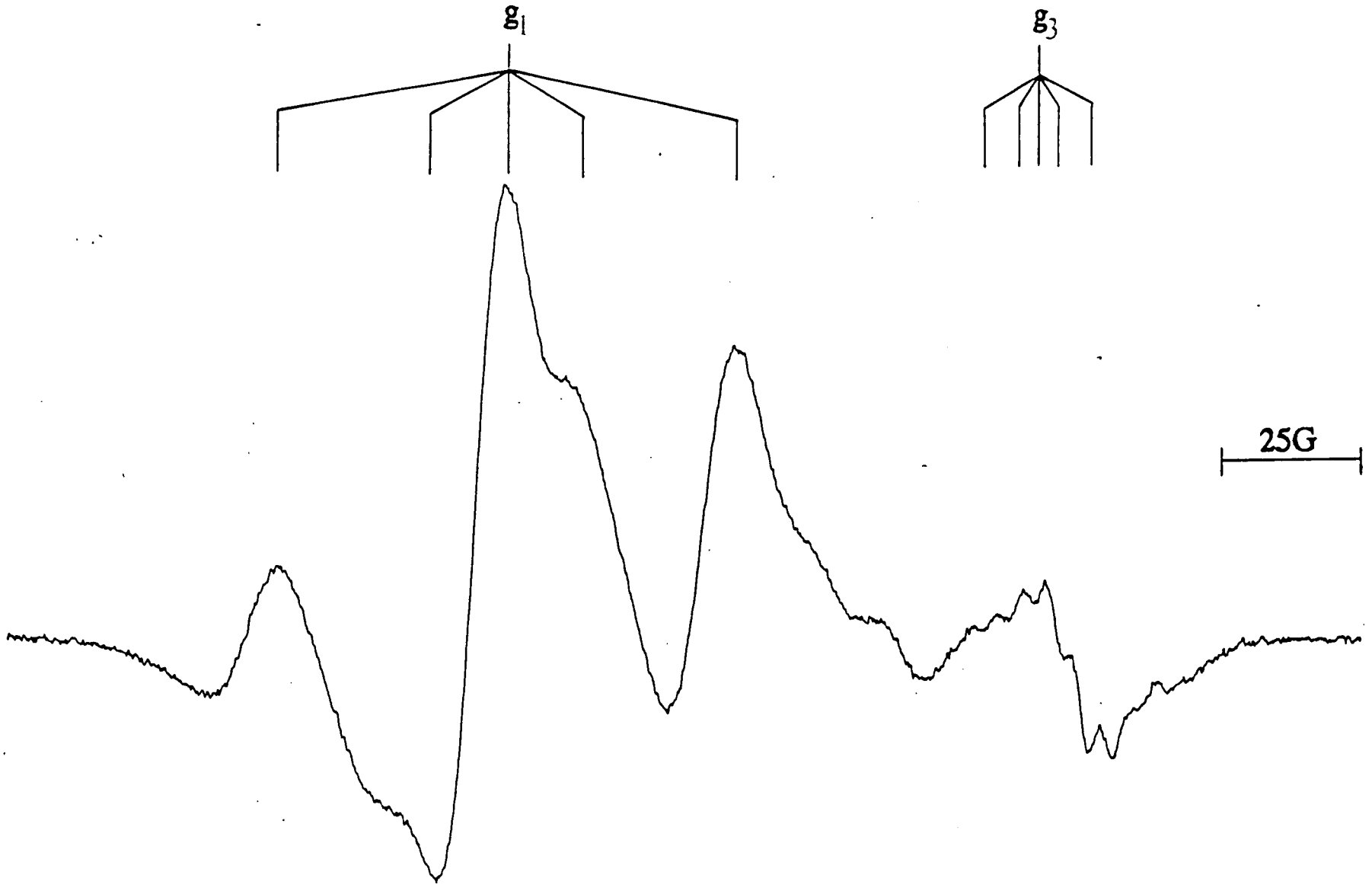

Figure 4.32. E.p.r. spectrum of 62% enriched $[^{61}Ni([9]aneS_3)_2]^{3+}$, second derivative ($CH_3CN$/0.1M $^nBu_4NPF_6$, 77K).

42% of the unpaired spin density resided on the Ni centre for this complex[187], a figure similar to those derived above for $[Ni([9]aneS_3)_2]^{3+}$.

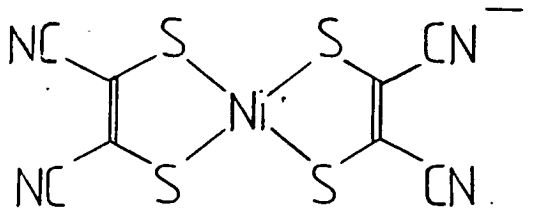

(46)

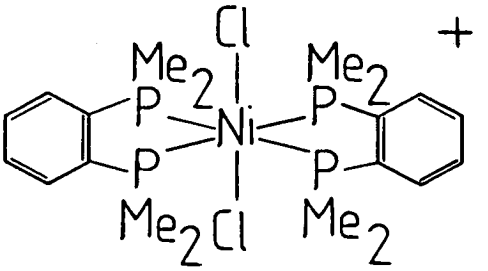

(47)

The oxidation of $[Ni([9]aneS_3)_2]^{3+}$ was followed by U.V./visible spectroscopy at 253K, using an *in situ* O.T.E. system (Appendix). The oxidation occurs isosbestically (Figure 4.33), with λ_{iso} = 320, 290 nm. During electrogeneration, the Ni^{II} charge-transfer band at λ_{max} = 316 nm (ε_{max} = 16,680 $dm^3.mol^{-1}.cm^{-1}$) lost intensity, with concommitant growth of new charge-transfer bands at λ_{max} = 492 nm (sh), 428 (sh), 387 (ε_{max} = 13,870 $dm^3.mol^{-1}.cm^{-1}$), 326 (6,03S), 271 (sh) and 235 (9,900). No more specific assignment of these transitions can be made. Re-reduction of the sample at 0V at 253K gave quantitative regeneration of $[Ni([9]aneS_3)_2]^{2+}$.

The single crystal structure of $[Ni([9]aneS_3)_2]^{3+}$ has been determined in Edinburgh[188]. This confirms the expected octahedral geometry for the complex cation (Figure 4.34). Unfortunately, the Ni^{III} ion lies on a site of $\bar{3}$ crystallographic symmetry, so that all Ni-S bond

lengths are averaged to a single value [Ni-S = 2.3129(25) Å]. This distance is shorter than those observed for $[Ni([9]aneS_3)_2]^{2+}$ [Ni–S = 2.377(1), 2.380 (1), 2.400 (1) Å[70]] as expected for the oxidation of a d^8 ion to a d^7 species via the loss of an electron from a (formally Ni-S, anti-bonding) Ni e_g 3d-orbital. The absence of a Jahn-Teller distortion in the structure is attributed to crystallographic disorder; the observed three-fold symmetry is not consistent with the rhombic symmetry of the e.p.r. spectrum of this complex. The $[Ni([9]aneS_3)_2]^{3+}$ cation was only stable in the presence of $HClO_4/ClO_4^-$ or H_2SO_4, so crystals of this complex with alternative anions could not be grown.

The reduction of $[Ni([9]aneS_3)_2]^{2+}$ at -1.00V *vs.* Ag/AgCl at 253K afforded a pale green solution, together with some deposition of Ni metal onto the Pt basket working electrode. These solutions yielded complex e.p.r. spectra (Figure 4.35), which appeared to contain peaks from more than one paramagnetic species. Coulometric determination of this process consistently gave n>1 electron (typically n ≈ 1.4), also implying decomposition of the initial reduction product. Monitoring the reduction by U.V./visible spectroscopy showed that this process does not occur isosbestically (Figure 4.36). These results are consistent with the initial formation of a highly reactive $[Ni([9]aneS_3)_2]^{+}$ species, which rapidly decomposes, possibly by disproportionation to

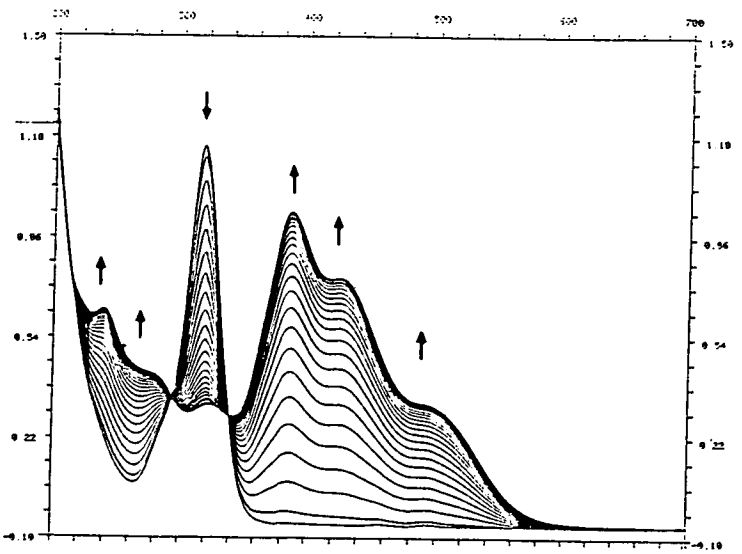

Figure 4.33: Electronic Spectrum showing the Oxidation of $[Ni([9]aneS_3)_2]^{2+}$ to $[Ni([9]aneS_3)_2]^{3+}$ ($CH_3CN/^nBu_4NPF_6$, 253K).

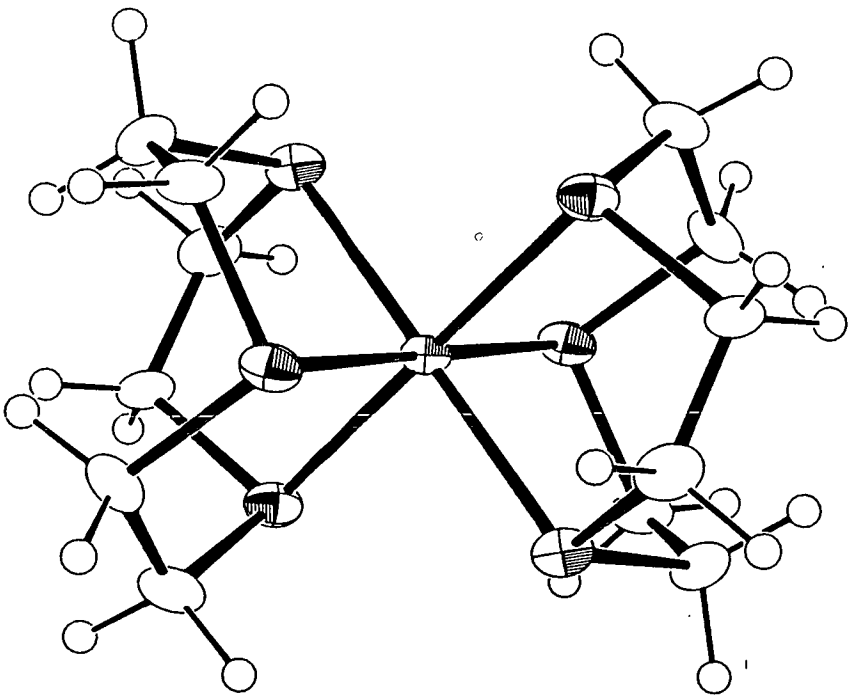

Figure 4.34: View of the Single Crystal Structure of $[Ni([9]aneS_3)_2]^{3+}$

$[Ni([9]aneS_3)_2]^{2+}$ and Ni metal, or by loss of one or more $[9]aneS_3$ ligands. Further experiments to characterise the final paramagnetic products of the reduction were not attempted. However, the related complex $[Ni([9]aneNS_2)_2]^{2+}$ has been shown to form tetrahedral Ni^I species on reduction, via loss of one macrocyclic ligand[124].

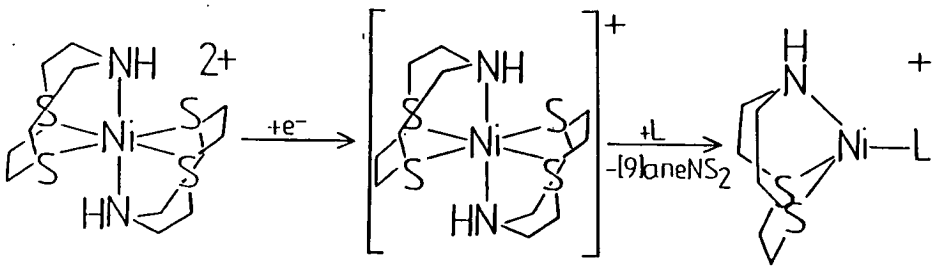

A similar electrochemical study of $[Ni([18]aneS_6)]^{2+}$ was not possible, due to the low solubility of this complex.

4.2.8 Electrochemical Study of $[Zn([9]aneS_3)_2]^{2+}$

In order to investigate whether a genuine metal-stabilised ligand radical species could be generated from a $[M([9]aneS_3)_2]^{n+}$ complex, the electrochemistry of $[Zn([9]aneS_3)_2]^{2+}$ was examined. The single crystal

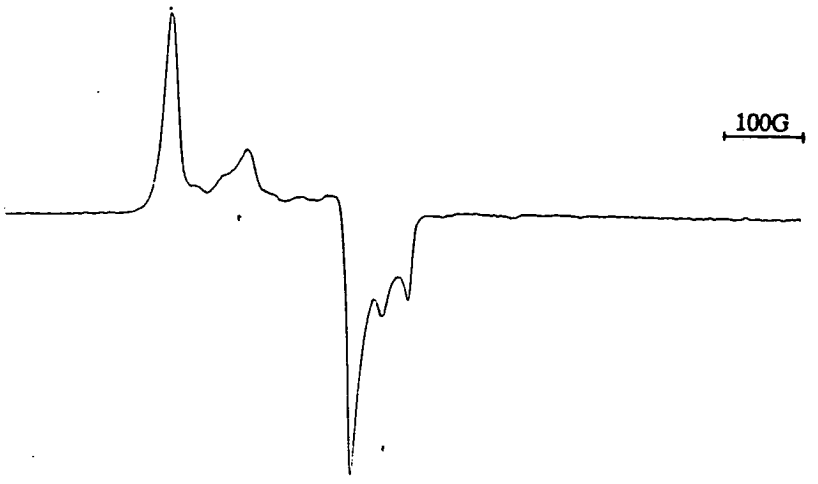

Figure 4.35: E.p.r. spectrum of the reduction products of $[Ni([9]aneS_3)_2]^{2+}$ (CH_3CN, 77K).

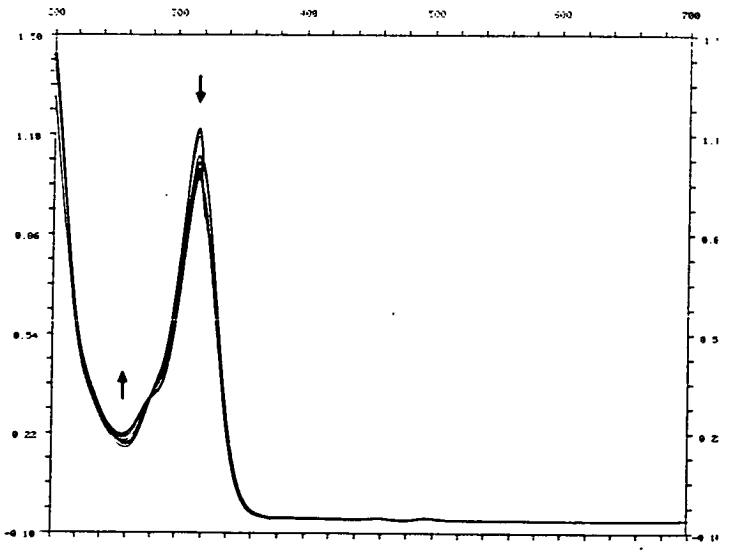

Figure 4.36: Electronic spectrum showing the reduction of $[Ni([9]aneS_3)_2]^{2+}$ (CH_3CN/ $^nBu_4NPF_6$, 253K).

structure of $[Zn([9]aneS_3)_2](ClO_4)_2$ has been previously reported, and shows the cation to adopt an octahedral stereochemistry[189].

The PF_6^- salt of $[Zn([9]aneS_3)_2]^{2+}$ was prepared by the reaction of $Zn(NO_3)_2.6H_2O$ with two molar equivalents of [9]aneS$_3$ in CH_3CN at 298K, followed by counterion metathesis with NH_4PF_6. The crude product was recrystallised from CH_3NO_2, to give an off-white crystalline solid, which was identified as the desired product from its I.R. and f.a.b. mass spectra and elemental analysis. The cyclic voltammogram of this complex in $CH_3CN/^nBu_4NPF_6$ at 298K showed a broad irreversible oxidation at Ep_a = +1.30V *vs.* Fc/Fc^+ (scan rate 400 mV/s), with no observable return waves. An irreversible reduction was also observed at Ep_c = -1.77V, with an associated desorption spike at Ep_a = -0.60V due to deposition of Zn metal onto the working electrode. These processes remained irreversible at high scan rates, and at 273K. Hence, no stable redox products could be generated from this compound, and it was not investigated further.

4.3 CONCLUSIONS

The electrochemistry of the complexes $[Ni([9]aneS_3)(PP)](PF_6)_2$ (PP = dppm, dppe, dppv, dcpe, dmpe, dppp and tdpme, Figure 3.4) has been studied. Each of these complexes exhibited one chemically reversible, and one quasi- or irreversible, one-electron reduction by

cyclic voltammetry at CH_3CN/0.1M $^nBu_4NPF_6$ at 298K. The first reduction products of these complexes exhibit complex frozen glass e.p.r. spectra showing substantial hyperfine coupling to the ^{31}P donors of the phosphine chelate ligands. Analysis of the e.p.r. spectra of an enriched sample of $[^{61}Ni([9]aneS_3)(tdpme)]^+$ has shown that this species is a genuine d^9 metal-based Ni^I radical. The other complexes in the series should also be metal-based radicals, since they exhibit similar g-values and ^{31}P hyperfine coupling constants to the Ni^I tdpme complex. On the basis of cyclic voltammetric, e.p.r. and electronic spectral data the species $[Ni([9]aneS_3)(PP)]^+$ were assigned square-pyramidal geometries similar to those exhibited by the Ni^{II} precursor complexes (Chapter 3), although $[Ni([9]aneS_3)(dppm)]^+$ may exist in equilibrium with one or more other conformational isomers. The second reduction products $[Ni([9]aneS_3)(PP)]^0$ (PP = dppe, dppv, dppp, tdpme) were e.p.r. silent, and were formulated as d^{10} Ni^0 species with tetrahedral stereochemistries. The Ni^0 dppm, dcpe and dmpe species could not be studied due to their thermal instability. Additional structural data would be necessary to confirm these assignments: single crystals obtained from CH_2Cl_2 solutions of $[Ni([9]aneS_3)$-$(dppe)]^+$ and $[Ni([9]aneS_3)(tdpme)]^+$ decomposed on the diffractometer (unit cell for $[Ni([9]aneS_3)(dppe)](PF_6)$ a = 10.370, b = 23.459, c = 16.382 Å α = 90, β = 107.40, γ = 90°).

The complexes $[Ni([9]aneS_3)(PP)]^+$ have been shown to react with CO, forming an initial adduct which rapidly decomposes at 298K to reform the complexes $[Ni([9]aneS_3)(PP)]^{2+}$. At 243K, a different decomposition reaction occurred, giving diamagnetic products; an e.p.r. active species was also sometimes detected in these samples. Further experiments should be carried out to further characterise these reactions, and to study the reactivity of these Ni^I complexes towards other substrates such as NO_2, SO_2, H_2 and alkyl halides.

The electrochemistry of $[Ni([9]aneS_3)_2](PF_6)_2$ has also been examined. Electrochemical or chemical oxidation of this complex affords an octahedral complex, $[Ni([9]aneS_3)_2]^{3+}$ which was formulated as a metal-based d^7 Ni^{III} radical complex on the basis of e.p.r. spectra of an enriched sample of $[^{61}Ni([9]aneS_3)_2]^{3+}$, despite the earlier assignment of this complex as an Ni^{II}-stabilised ligand radical species[130]. Electrochemical reduction of $[Ni([9]aneS_3)_2]^{2+}$ afforded a mixture of e.p.r. active products which could not be characterised. In addition, the cyclic voltammogram of $[Zn([9]aneS_3)_2](PF_6)_2$ was shown to exhibit no reversible processes at 298K, proving that the formation of a ligand-based radical species $[M^{II}([9]aneS_3^{\cdot+})([9]aneS_3)]^{3+}$ is not a favourable process.

4.4 EXPERIMENTAL

The compounds $[Ni([9]aneS_3)(PP)](PF_6)_2$ (PP = dppm,

dppe, dppv, dcpe, dmpe, dppp, tdpme) were prepared as described in Chapter 3.

4.4.1 $^{61}Ni(NO_3)_2.6H_2O$

^{61}Ni foil (0.050 g, 8.2 x 10^{-4} mol) was dissolved in 70% w/w nitric acid (20 cm^3). After 24 hrs the resulting green solution was reduced to the minimum possible volume (< 1 cm^3), and the product was allowed to crystallise out. The green crystals were filtered, washed with ethyl acetate, and dried in *in vacuo*. Yield 210 mg (87%).

4.4.2 $[^{61}Ni([9]aneS_3)(tdpme)](PF_6)_2$

The reaction of $^{61}Ni(NO_3)_2.6H_2O$ (0.027 g, 9.4 x 10^{-5} mol) with tdpme (0.058 g, 9.4 x 10^{-5} mol) in refluxing methanol (15 cm^3) yielded an olive green solution. $[9]aneS_3$ (0.017 g, 9.4 x 10^{-5} mol) was added, and the mixture refluxed for a further 30 mins. Addition of NH_4PF_6 (0.031 g, 1.9 x 10^{-4} mol) quickly gave a dark green precipitate, which was filtered, recrystallised from acetonitrile/diethyl ether, and dried *in vacuo*. Yield 0.060 g, 55%. Elemental analysis: found C = 48.9, H = 4.52%; calculated for $[C_{47}H_{51}S_3P_3{}^{61}Ni](PF_6)_2$ C = 48.8, H = 4.45%.

4.4.3 $[Ni([9]aneS_3)_2](PF_6)_2$

$NiCl_2.6H_2O$ (0.059 g, 2.5 x 10^{-4} mol) and $[9]aneS_3$

(0.090 g, 5.0 x 10^{-4} mol) were refluxed in methanol (15 cm^3) for 1 hr. NH_4PF_6 (0.082 g, 5.0 x 10^{-4} mol) was then added, and the mixture refluxed for a further 1 hr. The pink precipitate product was filtered and recrystallised from acetonitrile/diethyl ether. Yield 0.145 g, 82%. Mol. wt. 709.20. Elemental analysis: found C = 20.4, H = 3.40%; calculated for $[C_{12}H_{24}S_6Ni](PF_6)_2$ C = 20.3, H = 3.41%. F.a.b. mass spectrum: found M^+ = 562, 418; calculated for

$[^{58}Ni([9]aneS_3)([9]aneS_3\text{-}H)(PF_6)]^+$ $M^+ = 562$

$[^{58}Ni([9]aneS_3)_2]^+$ $M^+ = 418$

U.V./vis spectrum (MeCN): λ_{max} = 785 nm (ε_{max} = 37.0 dm^3 mol^{-1} cm^{-1}), 529 (36.0), 319 (17,270). I.R. spectrum (KBr disk): 3000 m, 2940 m, 1445 s, 1415 s, 1300 m, 1285 s, 1255 m, 1180 m, 1140 m, 1010 w, 985 w, 930 m, 900 w, 840 vs, 740 m, 690 w, 670 m, 635 w, 620 m, 555 s, 480 m, 435 m cm^{-1}.

4.4.4 $[^{61}Ni([9]aneS_3)_2](PF_6)_2$

Method as in 4.5.3, using $^{61}Ni(NO_3)_2.6H_2O$ (0.041 g, 1.4 x 10^{-4} mol) and $[9]aneS_3$ (0.050 g, 2.8 x 10^{-4} mol). Yield 0.070 g, 70%. Elemental analysis: found C = 20.6, H = 3.53%; calculated for $[C_{12}H_{24}S_6{}^{61}Ni](PF_6)_2$ C = 20.3, H = 3.40%.

4.4.5 $[Zn([9]aneS_3)_2](PF_6)_2$[189]

$Zn(NO_3)_2.6H_2O$ (0.050 g, 1.6 x 10^{-4} mol) and $[9]aneS_3$

(0.060 g, 3.2 x 10^{-4} mol) were stirred in acetonitrile (10 cm^3) at room temperature for 1 hr, whereupon a white precipitate formed. NH_4PF_6 (0.052 g, 3.2 x 10^{-4} mol) was added, and the mixture stirred for a further 1 hr. The resulting colourless solution was filtered, reduced to $^1/_3$ its original volume, and the product crystallised with diethyl ether. The product was a white microcrystalline solid (Yield 0.093 g, 78%). Mol. wt. 715.86. Elemental analysis: found C = 20.0, H = 3.49, N = 1.10%; calculated for $[C_{12}H_{24}S_6Zn](PF_6)_2 . 0.6\ CH_3NO_2$ C = 20.1, H = 3.46, N = 1.11%. F.a.b. mass spectrum: found M^+ = 569, 423, 243; calculated for:

$[^{64}Zn([9]aneS_3)_2(PF_6)]^+$	$M^+ = 569$
$[^{64}Zn([9]aneS_3)([9]aneS_3\text{-}H)]^+$	$M^+ = 423$
$[^{64}Zn([9]aneS_3\text{-}H)]^+$	$M^+ = 243$

^1H nmr spectrum (80.13 MHz, CD_3CN, 298K) δ = 3.09 ppm (s). I.R. spectrum (KBr disk): 2960 w, 2920 m, 2900 w, 2800 w, 1450 m, 1410 s, 1380 w, 1300 m, 1285 s, 1255 w, 1220 w, 1190 w, 1155 m, 1135 w, 1100 w, 940 w, 855 s, 775 w, 700 w, 670 m, 655 m, 615 m, 560 s, 475 w, 430 m cm^{-1}.

CHAPTER 5

HALF SANDWICH RHODIUM (I) COMPLEXES OF [9]aneS$_3$

5.1 INTRODUCTION

The design of a metal complex to act as an efficient homogeneous catalyst, or as a reagent for organometallic transformations, requires the selective incorporation of protected (blocked) and labile coordination sites at the metal centre. This is generally achieved using bi- or polydentate ligands as protecting groups to give either coordinatively unsaturated complexes, or coordinatively saturated complexes from which transient unsaturated species can be generated by thermal or photochemical activation. Macrocyclic complexes have often been utilised in this regard (Section 1.3).

Over the last twenty-five years there has been intense interest in the coordination chemistry of the cyclopentadienyl [$C_5H_5^-$, cp^-] or pentamethylcyclopentadienyl [C_5Me_5, $(cp^*)^-$, 8] anions[81-83,191-194]. These ligands have been shown to form η^5 π-complexes with most metals of the transition series, in both high and low oxidation states, as well as with several main group elements[195]. Cyclopentadienyl complexes of both early and late transition metals have been shown to catalyse a variety of organometallic reactions, with the cp^- moiety acting as a protecting group to shield one face of the metal ion from attack (*vide infra*). More recently, the reactivity of complexes containing tri-dentate, facially binding ligands analogous to cp^- has also been studied: such ligands include hydrido-*tris*-pyrazolylborate ($HBPz_3$,

48), $[C(CH_2P(O)Ph_2)_3]^-$ (triso, 49), $CH_3C(CH_2PPh_2)_3$ (tdpme, Figure 3.4) and $P_3O_9^{3-}$ (50)[84-86,196-198]. The Rh and Ir chemistry of these ligands has been particularly well studied, with each protecting group imposing a different reactivity onto the metal centres. For example, the complexes $[(HBPz^*_3)Rh(L)_2]$ (L = CO, C_2H_4) have been shown to undergo oxidative addition reactions across aryl, vinyl and alkyl C-H bonds under mild thermal conditions[84], whilst $[Ir(triso)(L)_2]$ (L = CO, C_2H_4) catalyses the stereo-selective hydrosilylation of alkynes[85].

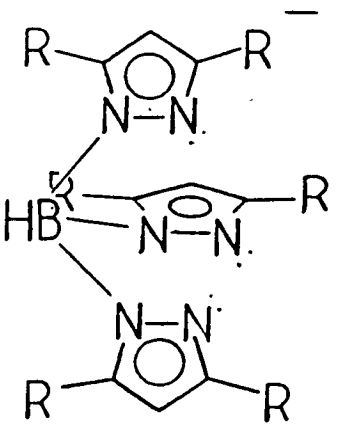

R=H: $(HBPz_3)^-$

R=CH_3: $(HBPz^*_3)^-$

(48)

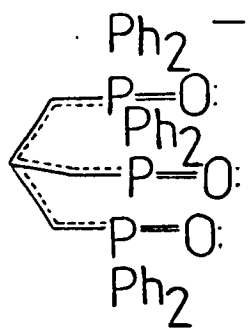

(49)

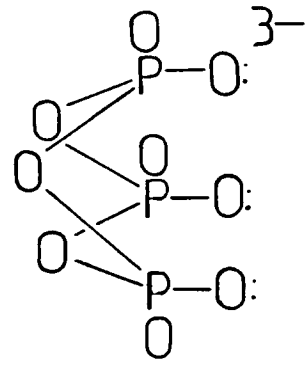

(50)

We argued that [9]aneS$_3$ could also act as a protecting group analogous to the cyclopentadienyl ligand, and that the complexes $[M([9]aneS_3)(L)_2]^+$ (M = Rh, Ir; L = alkene,

CO, PR_3) might exhibit novel reactivity. The synthesis and characterisation of these compounds was therefore undertaken. This chapter describes the characterisation of the Rh^I complexes $[Rh([9]aneS_3)(L)_2]^+$ (L = C_2H_4, $\frac{1}{2}C_7H_8$, $\frac{1}{2}C_8H_{12}$, $\frac{1}{2}C_4H_6$, CO, PR_3), and a preliminary study of the reactivity of these species. The synthesis and characterisation of the Ir congeners of these compounds, and a detailed discussion of the metal-alkene bonding in the complexes $[M([9]aneS_3)(C_2H_4)_2]^+$ and $[M([9]aneS_3)(C_4H_6)]^+$ (M = Rh, Ir) are described in Chapter 6. Some of the results described in this chapter have been published[317].

Relatively few Rh complexes containing thioether ligands have been reported. Several octahedral complexes *fac*- or *mer*-$[Rh(SR_2)_3X_3]$ and $[Rh_2(SR_2)_4Cl_4(\mu\text{-}Cl)_2]$ (R = alkyl, aryl) have been synthesised[199]: $[Rh(SR_2)_3Cl_3]$ (R = Et, Bz) was shown to catalyse the hydrogenation of alkenes under mild thermal conditions[200]. The reaction of $[Rh_2(CO)_4Cl_2]$ with 2,5-dithiahexane (dth) afforded a polymeric species $[Rh(dth)(CO)Cl]_n$[199]; a similar reaction with SEt_2 gave the monomeric complex $[Rh(SEt_2)_2(CO)Cl]$[201]. The synthesis of $[Rh([14]aneS_4)]^+$ was reported by Busch *et al.*[202]. This complex was found to be a strong nucleophile, forming adducts with O_2, SO_2, tcne and H^+, and undergoing oxidative addition reactions with CH_3I, CH_3COCl and CH_2Cl_2, although none of the Rh^{III} products from these reactions was fully characterised[202,203]. The

single crystal structure of this compound shows the complex cation to adopt a square-planar geometry, with weak inter-molecular contacts between adjacent cations to form a dimeric structure [Rh...Rh = 3.313(1) Å, Figure 5.1][203].

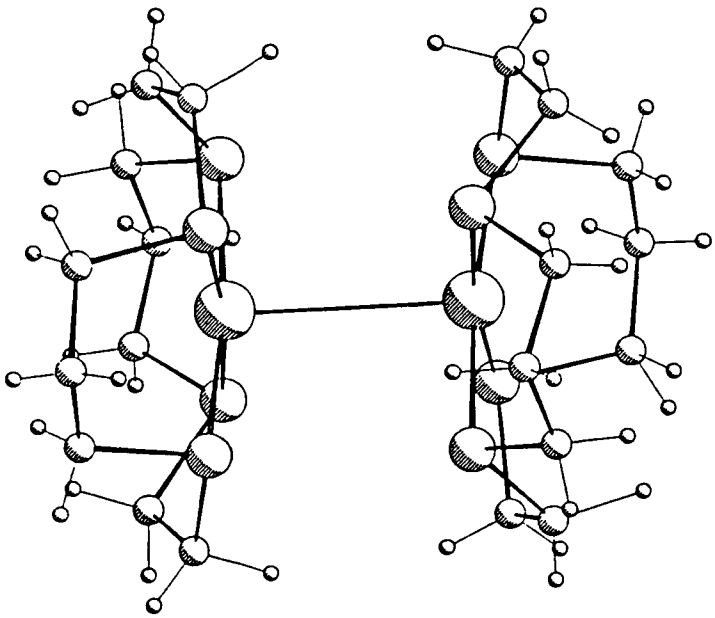

Figure 5.1: View of the Single Crystal Structure of $[Rh([14]aneS_4)]^+$.

The Edinburgh group, and Cooper *et al.*, have independently studied the complexes $[Rh([9]aneS_3)_2]^{n+}$ (n = 1, 2, 3)[60,61]. Reaction of $RhCl_3.3H_2O$ with two molar equivalents of $[9]aneS_3$ in refluxing water: methanol gave the colourless complex $[Rh([9]aneS_3)_2]^{3+}$, which adopts an octahedral stereochemistry in the solid state (Figure 5.2a). $[Rh([9]aneS_3)_2](PF_6)_3$ exhibits two chemically

reversible one-electron reductions by cyclic voltammetry in $CH_3CN/0.1M\ ^nBu_4NPF_6$ at 298K, at $E_{\frac{1}{2}}$ = -0.71 and -1.08V *vs.* Fc/Fc^+. The first reduction product was e.p.r. active, and was assigned as a mononuclear octahedral d^7 Rh^{II} species similar to the isoelectronic complex $[Pd([9]aneS_3)_2]^{3+}$ [62]. The second reduction product of $[Rh([9]aneS_3)]^{3+}$ was e.p.r. silent, and was formulated as the d^8 complex $[Rh([9]aneS_3)_2]^+$, which was assumed to adopt a tetragonal geometry by analogy with $[Pd([9]aneS_3)_2]^{2+}$ and $[Au([9]aneS_3)]^{3+}$[204,67a]. However, neither $[Rh([9]aneS_3)_2]^{2+}$ nor $[Rh([9]aneS_3)_2]^+$ has been structurally characterised. For $[M([9]aneS_3)_2]^{3+}$ (M = Co, Rh, Ir), it was found that deprotonation of the parent complex at pH>4 in H_2O led to a ring-opening reaction of one coordinated macrocycle (51, Figure 5.2b)[205]. This reaction is thought to be general for crown thioether complexes of high valent metal ions. Some octahedral Rh^{III} complexes of larger ring polythia macrocycles have also been characterised in Edinburgh, such as $[Rh(S_4)Cl_2]^+$ (S_4 = [14]aneS$_4$, [16]aneS$_4$)[112], $[Rh([18]aneN_2S_4)]^{3+}$ [206] and $[Rh_2(C_5Me_5)_2Cl_2([14]aneS_4)]^{2+}$ [56b]. The binuclear species $[Rh_2(cod)_2([20]aneS_6)]^{2+}$ was found to adopt a five-coordinate geometry, with each Rh centre bound to three S-donors[207].

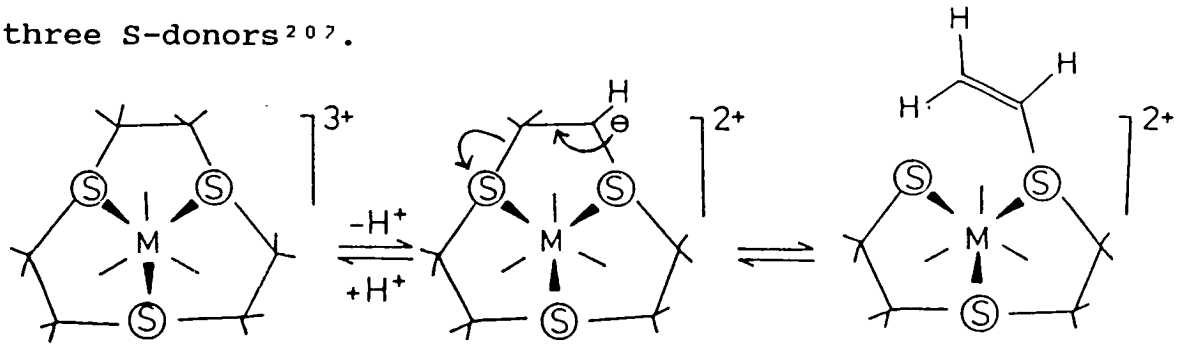

(51)

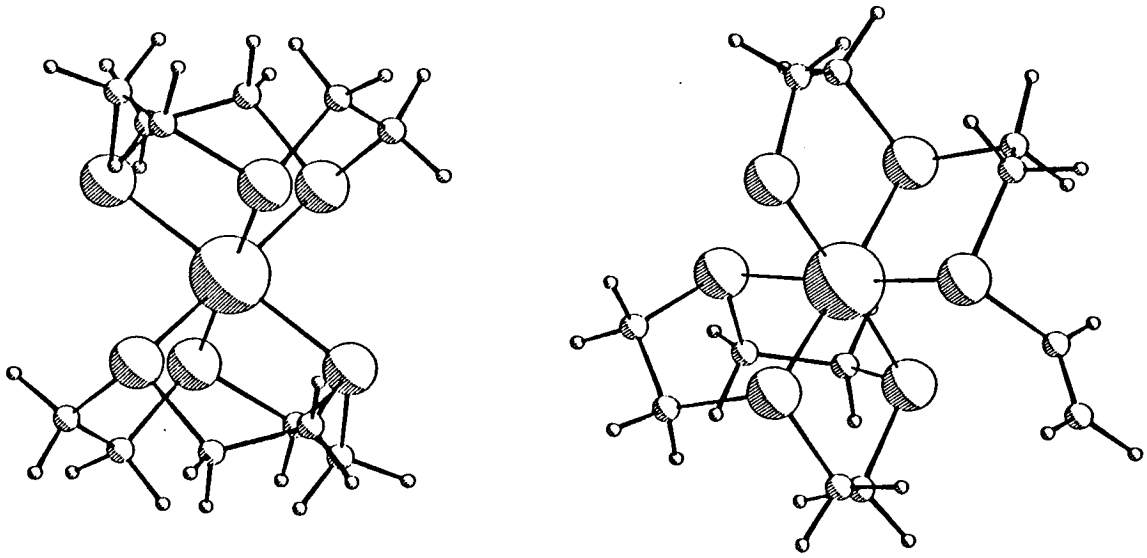

Figure 5.2: Views of the Single Crystal Structures of a) $[Rh([9]aneS_3)_2]^{3+}$ and b) $[Rh([9]aneS_3)\{H_2C{=}CHS(CH_2)_2S(CH_2)_2S\}]^{2+}$.

CHEMISTRY OF RHODIUM AND IRIDIUM HALF-SANDWICH CYCLOPENTADIENYL COMPLEXES

The syntheses of the Rh^I complexes $[Rh(cp)(L)_2]$ (L = C_2H_4, CO) were first reported in the early 1960s[208]. Early studies on $[Rh(cp)(C_2H_4)_2]$ centred on its dynamic n.m.r. behaviour; it was shown that equilibration of the "inner" and "outer" H-environments of the ethene ligands (52) occurred by rotation of the ethene molecules about a central Rh-ethene axis, and that ethene exchange and thermal ligand substitution reactions occurred slowly at 298K[209]. This contrasted with the analogous complex

$[Rh(acac)(C_2H_4)_2]$ (acac = 2,4-pentanedionate), which underwent rapid ligand exchange and substitution at room temperature. These differences were explained by postulating that ligand substitution at the 16-electron species $[Rh(acac)(C_2H_4)_2]$ occurred via an associative mechanism which was not possible for the coordinatively saturated 18-electron $[Rh(cp)(C_2H_4)_2]$ complex[209]. More recently, some associative substitution reactions at $[Rh(cp)(C_2H_4)_2]$ have been shown to occur under forcing conditions, possibly via slippage of the cp^- ligand from an η^5 to an η^3-mode of coordination (53) to generate a transient 16-electron Rh centre[210,211]. This type of slippage is also known to occur in indenyl complexes[211,212]. Many analogous compounds of type $[(cp^*)M(L)_2]$ or $[(C_5R_4X)M(L)_2]$ (M = Rh, Ir; R = H, Me, Ph; X = H, hal, NO_2 etc.; L = alkene, CO, PR_3) have been characterised, and exhibit similar properties to the parent complexes[210,213, .

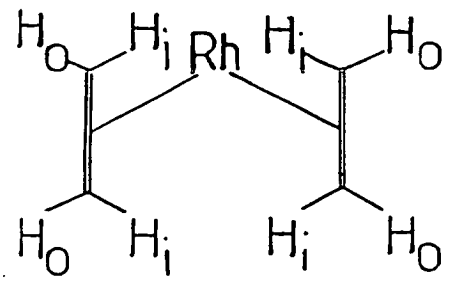

(52)

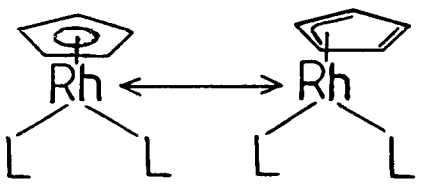

(53)

The complexes $[(C_5R_5)M(L)_2]$ (M = Rh, Ir; R = H, Me; L = C_2H_4, CO, PR_3) are highly nucleophilic, and form adducts with electrophiles such as SO_2 and tcne (tcne = tetracyanoethene)[214]. They also undergo oxidative addition reactions with a variety of substrates under thermal or photochemical conditions:

$$[(C_5R_5)M(L)(L')] + X\text{-}Y \xrightarrow{\Delta \text{ or } h\nu} \begin{matrix} [(C_5R_5)M(L)(L')(X)]^+Y^- \\ \text{or} \\ [(C_5R_5)M(L)(X)(Y)] \\ \text{or} \\ \text{insertion products for} \\ L = CO \end{matrix} \quad (54)$$

where X-Y = I_2, R-X (R = CH_3, C_3H_5, $C_6H_5CH_2$, X = Br, I), CH_3COCl, R_3Si-H, R-H (R = alkyl)[213a,215-217]. There is some controversy as to whether these reactions proceed via initial ligand dissociation to create a coordinately unsaturated $[(C_5R_5)M(L)]$ fragment, or by η^5-η^3 slippage of the cp^- ring to give a 16-electron $[(\eta^3\text{-}C_5R_5)M(L)_2]$ intermediate[217-219].

A reaction that has received particular interest is the photochemical activation of hydrocarbons by the complexes $[(cp^*)M(PMe_3)H_2]$ (M = Rh, Ir)[220,221]. This occurs by initial loss of H_2 from the Rh^{III} or Ir^{III} precursors to form a highly reactive 16-electron fragment $[(cp^*)M(PMe_3)]$, which then oxidatively adds across alkyl, alkenyl or aryl C-H bonds:

$$[(cp^*)M(PMe_3)H_2] \xrightarrow[-H_2]{h\nu} [(cp^*)M(PMe_3)] \xrightarrow{R-H} [(cp^*)M(PMe_3)(R)(H)] \quad (55)$$

This reaction has been used to examine the relative rates of intra- *vs.* inter-molecular C-H bond activation, the relative reactivities of alkyl, alkenyl and aryl C-H bonds towards oxidative addition, and the possibility of pre-coordination of the hydrocarbon substrate molecules to the unsaturated fragment $[(cp^*)M(PMe_3)]$[222,223].

Another system that has been well studied is the dimeric Rh^{III} and Ir^{III} compounds $[M_2(cp^*)_2X_2(\mu\text{-}X)_2]$ (M = Rh, Ir; X = Cl, Br, I)[81]. These complexes display an extensive nucleophilic substitution chemistry, particularly with anionic ligands, to form a range of mono-, bi- and polynuclear products[81,224]. The binuclear compounds $[M_2(cp^*)_2X_2(\mu\text{-}Y)_2]$ (M = Rh, Ir; X = Cl, Br, I; Y = Cl, Br, I, H) were found to be efficient catalysts for the hydrogenation of alkenes and arenes under basic conditions[225], via heterolytic activation of H_2 by an electrophilic metal centre (56). This contrasts with Rh^I and Ir^I-based hydrogenation catalysts such as $[Rh(PPh_3)_3Cl]$, which activate H_2 via an oxidative addition (i.e. homolytic) pathway using a nucleophilic metal centre (57)[226].

$$[M(L)_n]^{m+} + H_2 + \ddot{B} \longrightarrow [M(L)_n]^{(m-1)+} + BH^+ \quad (56)$$

$$[M(L)_n]^{m+} + H_2 \longrightarrow [M(L)_n(H)_2]^{m+} \quad (57)$$

5.2 RESULTS AND DISCUSSION

5.2.1 $[Rh([9]aneS_3)(C_2H_4)_2](BF_4)$

Treatment of $[Rh_2(C_2H_4)_4Cl_2]$ with two molar equivalents of [9]aneS$_3$ and $NaBF_4$ in acetone (6 cm^3) under N_2 at 298K for 15 mins gave a bright yellow solution, which was filtered and reduced to 1 cm^3 volume. Addition of an excess of diethyl ether afforded a yellow solid product, which was recrystallised from CH_2Cl_2/hexane at 253K. The product was oxygen sensitive in solution, but was stable for 1 hr in acetone or THF solution and for 2 days in the solid state at 298K in the absence of air. The compound reacted rapidly with chlorinated solvents at 298K (Section 5.2.12).

The f.a.b. mass spectrum of the complex showed peaks at M^+ = 339, 311 and 283, which were assigned to the fragments $[^{103}Rh([9]aneS_3)(C_2H_4)_2]^+$, $[^{103}Rh([9]aneS_3)(C_2H_4)]^+$ and $[^{103}Rh([9]aneS_3)]^+$ respectively. On the basis of this data, together with I.R. spectroscopy and elemental analysis, the compound was formulated as $[Rh([9]aneS_3)(C_2H_4)_2](BF_4)$. The U.V./visible spectrum of this complex in CH_3CN at 298K exhibited bands at λ_{max} = 380 nm (ε_{max} = 590 dm^3.mol^{-1}.cm^{-1}), 298 (2,360) and 234 (9,295). The first two bands were tentatively assigned to S(π)$\rightarrow$Rh charge-transfer transitions by analogy with the electronic spectra of the complexes $[Ru([9]aneS_3)(L_1)(L_2)(L_3)]^{n+}$ studied by R.M. Christie[59]. The assignment of the high energy band is uncertain.

The ^{13}C d.e.p.t. n.m.r. spectrum of $[Rh([9]aneS_3)(C_2H_4)_2](BF_4)$ in d^6-acetone at 233K exhibited a doublet resonance at δ = 51.4 ppm ($^1J_{Rh-C}$ = 9.6 Hz), assigned to the ethene C atoms, and a singlet at 33.78 ppm from the macrocyclic SCH_2 groups. This shows that the six methylene groups of the [9]aneS$_3$ ligands are equivalent in solution, which implies that rotation of the [9]aneS$_3$ ring about the central Rh-[9]aneS$_3$ axis is a facile process (Section 5.2.2), in contrast to the behaviour exhibited by $[Rh([9]aneS_3)(C_4H_6)]^+$ (Section 5.2.5). The ^1H n.m.r. spectrum of $[Rh([9]aneS_3)(C_2H_4)_2](BF_4)$ under identical conditions to the ^{13}C spectrum shows a multiplet at δ = 3.22-3.02 ppm (12H) arising from the [9]aneS$_3$ ligand, and a doublet at 2.76 ppm ($^2J_{Rh-H}$ = 1.6 Hz, 4H) from the protons of the ethene ligands (Figure 5.3). No change in this spectrum was observed down to 188K (the limit of the solvent, Figure 5.3), showing that equilibration of the "inner" and "outer" H environments of the C_2H_4 ligands (52) is a highly facile process. This equilibration could occur via one of two possible mechanisms; by inter-molecular exchange of ethene ligands, or by rotation of the ethene molecules about the central Rh-C_2H_4 axis[209]. Given the inertness of $[Rh([9]aneS_3)(C_2H_4)_2]^+$ towards thermal nucleophilic substitution (*vide infra*) the latter mechanism is the more likely, although labelling experiments using C_2D_4 would be required to confirm this.

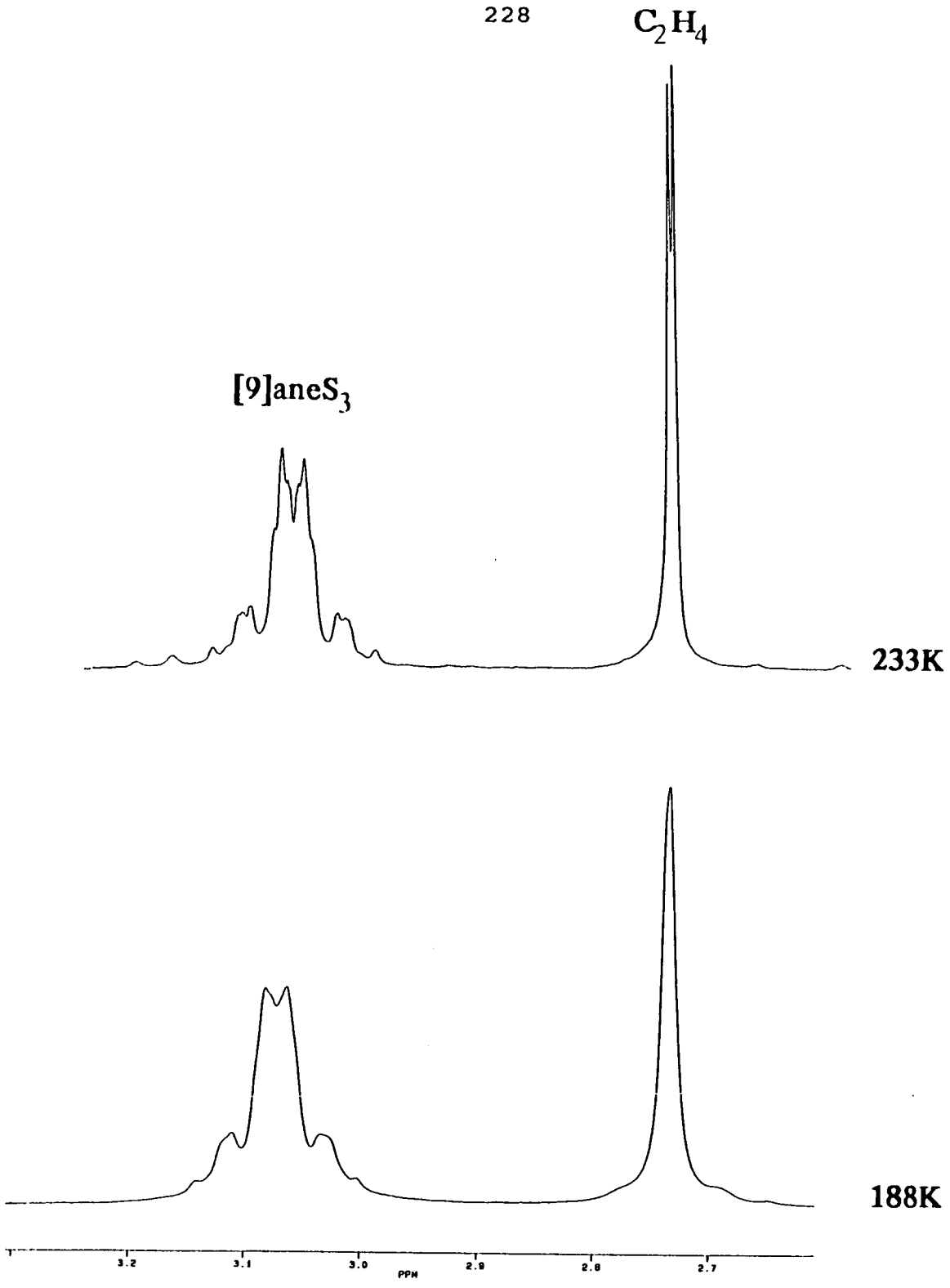

Figure 5.3: Low Temperature ^1H n.m.r. Spectra of $[Rh([9]aneS_3)(C_2H_4)_2](BF_4)$ (360.13 MHz, d^6-acetone).

This being the case, an n.m.r. decoalescence temperature of below 180K represents an unusually low barrier to ethene rotation for a d^8 complex, suggesting that Rh→ethene back-bonding is very weak for $[Rh([9]aneS_3)(C_2H_4)_2]^+$: this is discussed further in Section 6.2.2. Attempts to quantify the Rh-ethene bonding in $[Rh([9]aneS_3)(C_2H_4)_2]^+$ by measuring the ethene C=C stretching frequency by Raman spectroscopy were unsuccessful, due to the intense colour and low thermal stability of the complex (Section 5.2.7).

Attempted reactions of $[Rh([9]aneS_3)(C_2H_4)_2]^+$ with CO, PPh_3 or 1,5-cyclooctadiene in acetone or THF at 298K gave only the Rh^I *bis*-ethene starting material, with no incorporation of the attacking nucleophiles (by I.R. spectroscopy and f.a.b. mass spectrometry). This inertness to nucleophilic substitution implies that $[Rh([9]aneS_3)(C_2H_4)_2]^+$ adopts a five-coordinate 18-electron structure in solution, and that formation of a coordinatively unsaturated Rh centre via decoordination of an ethene ligand or S-donor is not a favourable process[209]:

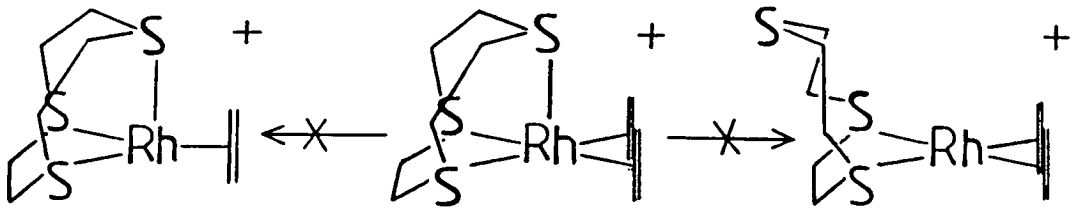

This contrasts with the analogous complexes $[M(HBPz_3)(C_2H_4)_2]$ (48, M = Rh, Ir) and $[Ir(triso)(C_2H_4)_2]$ (49), which undergo rapid nucleophilic substitution at 298K and are therefore thought to adopt four-coordinate geometries, although none of these compounds have been structurally characterised[84,85,269]. Attempted nucleophilic substitution at $[Rh([9]aneS_3)(C_2H_4)_2]^+$ by CO or PPh_3 in acetone at 313K resulted in thermal decomposition of the complex (Section 5.2.12), with no peaks due to CO or PPh_3 being observed in the I.R. and f.a.b. mass spectra of the dark red solid products.

The attempted preparation of $[Rh([9]aneS_3)(C_8H_{14})_2](PF_6)$ by the reaction of $[Rh_2(C_8H_{14})_4Cl_2]$ with two molar equivalents of $[9]aneS_3$ and NH_4PF_6 in THF under N_2 at 298K was unsuccessful, yielding only a red oily product that could not be characterised. Carrying out the reaction at 233K afforded a low yield of yellow solid product, which decomposed at *ca.* 2 hrs under vacuum at 298K. I.R. spectroscopy showed this compound to contain $[9]aneS_3$ and C_8H_{14} ligands and PF_6^- counterion; no further characterisation of the product was possible. Treatment of $[Rh_2(C_2H_4)_4Cl_2]$ with two molar equivalents of $[9]aneS_3$ in acetone yielded a yellow precipitate, which was identified by I.R. spectroscopy and f.a.b. mass spectrometry as the chloride salt $[Rh([9]aneS_3)(C_2H_4)_2]Cl$, rather than the expected product $[Rh([9]aneS_3)(C_2H_4)Cl]$[227].

In order to determine the mode of coordination of the [9]aneS_3 ligand in [Rh([9]aneS_3)$(C_2H_4)_2$]$^+$, and to examine further the Rh-ethene bonding in this complex, a single crystal structure determination was undertaken.

5.2.2 Single Crystal Structure of [Rh([9]aneS_3)-$(C_2H_4)_2$](BF_4)

The solution and refinement of this structure are described in Section 5.4.7. Selected bond lengths, angles and torsions are listed in Tables 5.1-5.3, and the geometry of the complex is displayed in Figures 5.4 and 5.5

The structure contains two crystallographically independent molecules per asymmetric unit, which exhibit different stereochemistries. Molecule 1 of the structure exhibited one short and two long Rh-S bonds, and the internal S-Rh-X angles (X = midpoint of ethene C=C bonds) showed this cation to possess a trigonal bipyramidal geometry [Rh(1)-S(1) = 2.322(9), Rh(1)-S(4) = 2.437(9), Rh(1)-S(7) = 2.432(9) Å, <S(1)-Rh(1)-X(1) = 178.2(12), <S(4)-Rh(1)-X(2) = 140.3(13), <S(7)-Rh(1)-X(2) = 132.8(13)^0, Table 6.8]. Molecule 2 contained two short and one long Rh-S bonds, and the internal S-Rh-X angles are consistent with a square-pyramidal geometry [Rh(2)-S(21) = 2.337(9), Rh(2)-S(24) = 2.327(10), Rh(2)-S(27) = 2.469(10) Å, <S(21)-Rh(2)-X(31) = 161.7(11), <S(24)-Rh(2)-X(32) = 160.1(10), <S(27)-Rh(2)-X(31) =

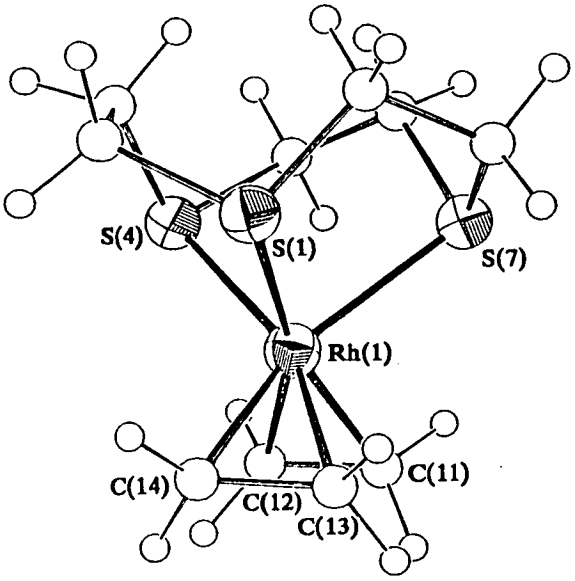

a) Molecule 1.

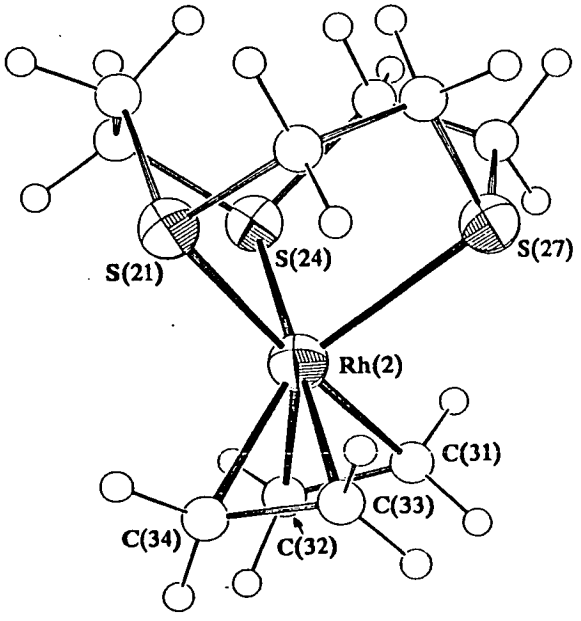

b) Molecule 2

Figure 5.4: Views of the Single Crystal Structure of $[Rh([9]aneS_3)(C_2H_4)_2]^+$.

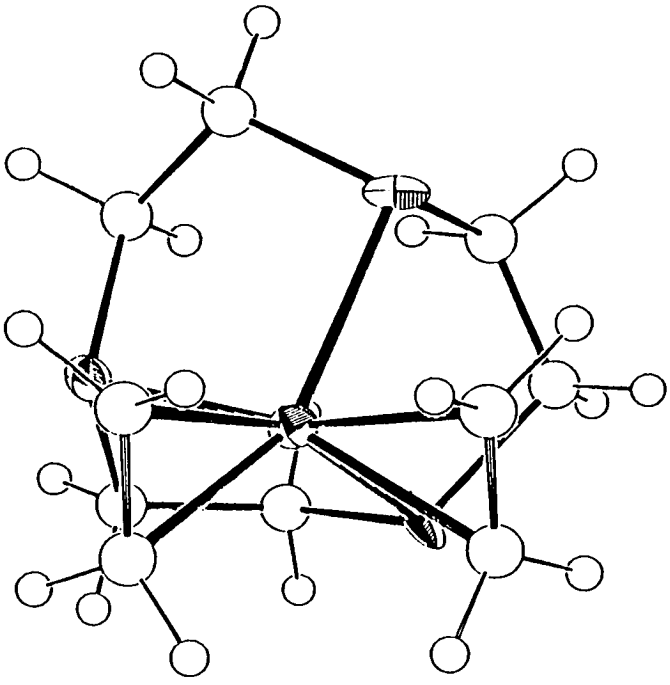

a) Molecule 1

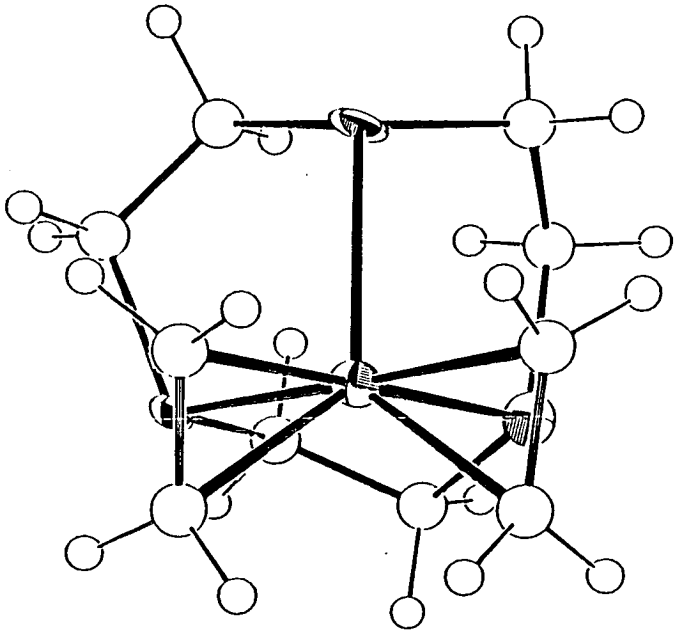

b) Molecule 2

Figure 5.5: Alternative Views of the Single Crystal Structure of $[Rh([9]aneS_3)(C_2H_4)_2]^+$.

Single Crystal Structure of $[Rh([9]aneS_3)(C_2H_4)_2](BF_4)$

Table 5.1. Bond Lengths(A) with standard deviations

Rh(1) - S(1)	2.322(9)	Rh(2) -S(21)	2.337(9)
Rh(1) - S(4)	2.437(9)	Rh(2) -S(24)	2.327(10)
Rh(1) - S(7)	2.432(9)	Rh(2) -S(27)	2.469(10)
Rh(1) -C(11)	2.21(4)	Rh(2) -C(31)	2.11(3)
Rh(1) -C(12)	2.21(5)	Rh(2) -C(32)	2.18(4)
Rh(1) -C(13)	2.12(5)	Rh(2) -C(33)	2.15(4)
Rh(1) -C(14)	2.05(4)	Rh(2) -C(34)	2.22(3)
S(1) - C(2)	1.83(4)	S(21) -C(22)	1.84(4)
S(1) - C(9)	1.80(4)	S(21) -C(29)	1.81(3)
C(2) - C(3)	1.58(5)	C(22) -C(23)	1.52(5)
C(3) - S(4)	1.81(4)	C(23) -S(24)	1.82(3)
S(4) - C(5)	1.83(3)	S(24) -C(25)	1.87(3)
C(5) - C(6)	1.51(5)	C(25) -C(26)	1.47(5)
C(6) - S(7)	1.81(3)	C(26) -S(27)	1.79(4)
S(7) - C(8)	1.75(3)	S(27) -C(28)	1.82(4)
C(8) - C(9)	1.61(5)	C(28) -C(29)	1.50(5)
C(11) -C(12)	1.33(6)	C(31) -C(32)	1.43(5)
C(13) -C(14)	1.43(6)	C(33) -C(34)	1.41(5)

Table 5.2. Angles(degrees) with standard deviations

S(1) -Rh(1) - S(4)	87.3(3)	S(21) -Rh(2) -S(24)	86.4(3)
S(1) -Rh(1) - S(7)	86.3(3)	S(21) -Rh(2) -S(27)	86.3(3)
S(1) -Rh(1) -C(11)	163.9(10)	S(21) -Rh(2) -C(31)	176.0(10)
S(1) -Rh(1) -C(12)	161.0(14)	S(21) -Rh(2) -C(32)	142.8(10)
S(1) -Rh(1) -C(13)	87.7(13)	S(21) -Rh(2) -C(33)	94.1(10)
S(1) -Rh(1) -C(14)	84.6(11)	S(21) -Rh(2) -C(34)	83.5(9)
S(4) -Rh(1) - S(7)	85.6(3)	S(24) -Rh(2) -S(27)	86.1(3)
S(4) -Rh(1) -C(11)	104.6(9)	S(24) -Rh(2) -C(31)	90.3(10)
S(4) -Rh(1) -C(12)	80.3(14)	S(24) -Rh(2) -C(32)	86.1(10)
S(4) -Rh(1) -C(13)	159.9(13)	S(24) -Rh(2) -C(33)	178.9(10)
S(4) -Rh(1) -C(14)	119.9(11)	S(24) -Rh(2) -C(34)	141.7(9)
S(7) -Rh(1) -C(11)	83.9(9)	S(27) -Rh(2) -C(31)	91.2(10)
S(7) -Rh(1) -C(12)	106.8(14)	S(27) -Rh(2) -C(32)	129.3(10)
S(7) -Rh(1) -C(13)	113.5(13)	S(27) -Rh(2) -C(33)	94.9(10)
S(7) -Rh(1) -C(14)	152.4(11)	S(27) -Rh(2) -C(34)	129.8(9)
C(11) -Rh(1) -C(12)	35.0(16)	C(31) -Rh(2) -C(32)	38.9(14)
C(11) -Rh(1) -C(13)	84.5(15)	C(31) -Rh(2) -C(33)	89.3(13)
C(11) -Rh(1) -C(14)	98.3(14)	C(31) -Rh(2) -C(34)	100.5(13)
C(12) -Rh(1) -C(13)	99.0(18)	C(32) -Rh(2) -C(33)	92.9(14)
C(12) -Rh(1) -C(14)	89.2(17)	C(32) -Rh(2) -C(34)	80.2(13)
C(13) -Rh(1) -C(14)	40.2(16)	C(33) -Rh(2) -C(34)	37.5(13)
Rh(1) - S(1) - C(2)	102.6(12)	Rh(2) -S(21) -C(22)	106.4(13)
Rh(1) - S(1) - C(9)	108.4(12)	Rh(2) -S(21) -C(29)	102.3(11)
C(2) - S(1) - C(9)	102.4(16)	C(22) -S(21) -C(29)	101.4(16)
S(1) - C(2) - C(3)	112.1(24)	S(21) -C(22) -C(23)	111.6(25)
C(2) - C(3) - S(4)	113.2(24)	C(22) -C(23) -S(24)	111.6(23)
Rh(1) - S(4) - C(3)	104.2(12)	Rh(2) -S(24) -C(23)	104.5(11)
Rh(1) - S(4) - C(5)	101.1(11)	Rh(2) -S(24) -C(25)	105.7(10)
C(3) - S(4) - C(5)	104.8(16)	C(23) -S(24) -C(25)	99.9(14)
S(4) - C(5) - C(6)	114.7(23)	S(24) -C(25) -C(26)	113.4(23)
C(5) - C(6) - S(7)	112.5(23)	C(25) -C(26) -S(27)	114.5(26)
Rh(1) - S(7) - C(6)	105.4(11)	Rh(2) -S(27) -C(26)	101.4(13)
Rh(1) - S(7) - C(8)	100.8(11)	Rh(2) -S(27) -C(28)	103.9(12)
C(6) - S(7) - C(8)	102.2(15)	C(26) -S(27) -C(28)	102.3(17)
S(7) - C(8) - C(9)	114.7(23)	S(27) -C(28) -C(29)	112.2(24)
S(1) - C(9) - C(8)	108.8(23)	S(21) -C(29) -C(28)	116.5(24)
Rh(1) -C(11) -C(12)	72.5(27)	Rh(2) -C(31) -C(32)	73.2(21)
Rh(1) -C(12) -C(11)	72.5(27)	Rh(2) -C(32) -C(31)	67.9(20)
Rh(1) -C(13) -C(14)	67.2(23)	Rh(2) -C(33) -C(34)	73.9(20)
Rh(1) -C(14) -C(13)	72.7(24)	Rh(2) -C(34) -C(33)	68.6(19)

Table 5.3. Torsion angles(degrees) with standard deviations

C(9) - S(1) - C(2) - C(3)	65.2(27)	C(29) -S(21) -C(22) -C(23)	134.8(25)
C(2) - S(1) - C(9) - C(8)	-136.1(23)	C(22) -S(21) -C(29) -C(28)	-64.1(28)
S(1) - C(2) - C(3) - S(4)	48.9(31)	S(21) -C(22) -C(23) -S(24)	-48.3(30)
C(2) - C(3) - S(4) - C(5)	-130.2(25)	C(22) -C(23) -S(24) -C(25)	-64.7(26)
C(3) - S(4) - C(5) - C(6)	62.8(27)	C(23) -S(24) -C(25) -C(26)	137.3(25)
S(4) - C(5) - C(6) - S(7)	52.4(29)	S(24) -C(25) -C(26) -S(27)	-50.1(32)
C(5) - C(6) - S(7) - C(8)	-135.1(24)	C(25) -C(26) -S(27) -C(28)	-63.9(29)
C(6) - S(7) - C(8) - C(9)	62.6(26)	C(26) -S(27) -C(28) -C(29)	130.0(26)
S(7) - C(8) - C(9) - S(1)	51.5(29)	S(27) -C(28) -C(29) -S(21)	-48.7(32)

110.6(11), <S(27)-Rh(2)-X(32) = 112.8(10)°, Table 6.8]. Interconversion of the two geometries involves the rotation of the [9]aneS$_3$ ring by 22° about the central Rh-[9]aneS$_3$ axis; the existence of both forms in this crystal structure confirms that rotation of the [9]aneS$_3$ ligand is a low energy process, as postulated from n.m.r. data (Section 5.2.1). This type of structural isomerism has been observed previously for Rh^{I} complexes of tripodal phosphines: [Rh{RC(CH$_2$PPh$_2$)$_3$}(nbd)]$^+$ (nbd = 2,5-norbornadiene) exhibits a square-pyramidal stereochemistry in the solid state for R = CH$_3$, but adopts a trigonal bipyramidal geometry for R = H[228]. Neither molecule in the structure of [Rh([9]aneS$_3$)(C$_2$H$_4$)$_2$](PF$_4$) exhibits any unusually long Rh-S distances, unlike the [4+1]-coordinate Pd^{II} complexes [Pd([9]aneS$_3$)(L)$_2$]$^+$ (L = PPh$_3$, $^1/_3$tdpme, $^1/_2$bipy, $^1/_2$phen, Cl$^-$, Br$^-$)[80].

Unfortunately, the poor quality of the sample crystal means that no meaningful conclusions can be drawn from the Rh-C and C=C bond lengths exhibited by the structure.

5.2.3 [Rh([9]aneS$_3$)(C$_7$H$_8$)](PF$_6$) and [Rh([9]aneS$_3$)-(C$_8$H$_{12}$)](PF$_6$)

Reaction of [Rh$_2$(L)$_2$Cl$_2$] [L = 2,5-norbornadiene (nbd) and 1,5-cyclooctadiene (cod)] with two molar equivalents of [9]aneS$_3$ and NH$_4$PF$_6$ in CH$_2$Cl$_2$ (L = nbd) or acetone (L = cod) at 298K under N$_2$ afforded yellow solutions. These solutions were filtered, reduced to 1/6 their original

volumes, and the bright yellow microcrystalline products crystallised by addition of diethyl ether.

I.R. spectroscopy showed that these compounds contained both [9]aneS$_3$ and dialkene ligands, and PF_6^- counterion. The f.a.b. mass spectra of these complexes exhibited peaks at M^+ = 375 (L = nbd) and 391 (L = cod) from the molecular ions $[^{103}Rh([9]aneS_3)(L)]^+$, and at M^+ = 282 (L = nbd, cod) for $[^{103}Rh([9]aneS_3\text{-}H)]^+$. The products were therefore formulated as $[Rh([9]aneS_3)(L)](PF_6)$ (L = nbd, cod); these assignments were supported by micro-analytical data.

The ^1H n.m.r. spectrum of $[Rh([9]aneS_3)(nbd)](PF_6)$ in d^6-acetone at 298K exhibited peaks at δ = 3.58 ppm (4H) from the vinyl H atoms of the nbd ligand, 3.49 (2H) from the nbd alkyl CH groups, 2.87-2.66 (12H) from the [9]aneS$_3$ macrocyclic SCH_2 protons and 1.17 (2H) from the nbd bridging CH_2 moiety. The ^{13}C d.e.p.t. n.m.r. spectrum of this complex showed peaks at δ = 59.32 ppm due to the nbd bridging CH_2 group, 46.10 from the nbd alkyl CH C atoms, 41.45 from the coordinated nbd vinyl C atoms, and 33.71 from the [9]aneS$_3$ ligand. The ^1H n.m.r. spectrum of $[Rh([9]aneS_3)(cod)](PF_6)$ in CD_3NO_2 at 298K showed resonances at δ = 4.10 ppm (4H) for the vinyl protons of the cod ligand, 3.01-2.79 (12H) for the [9]aneS$_3$ ligand, 2.52 (4H) and 2.20 (4H) for the cod alkyl CH_2 H atoms. The ^{13}C d.e.p.t .n.m.r. spectrum of $[Rh([9]aneS_3)(cod)](PF_6)$ exhibited peaks at δ = 78.33 ppm arising from the

cod vinyl CH groups, 33.84 from the [9]aneS$_3$ ligand, and 30.80 from the cod alkyl C atoms (Figure 5.6). On the basis of these spectra, both complexes were assigned as Rh^I complexes containing η^2,η^2-coordinated dialkene ligands.

In order to confirm this structural assignment, and to ascertain the mode of coordination of the [9]aneS$_3$ ligand, a single crystal analysis of [Rh([9]aneS$_3$)(cod)]$^+$ was undertaken.

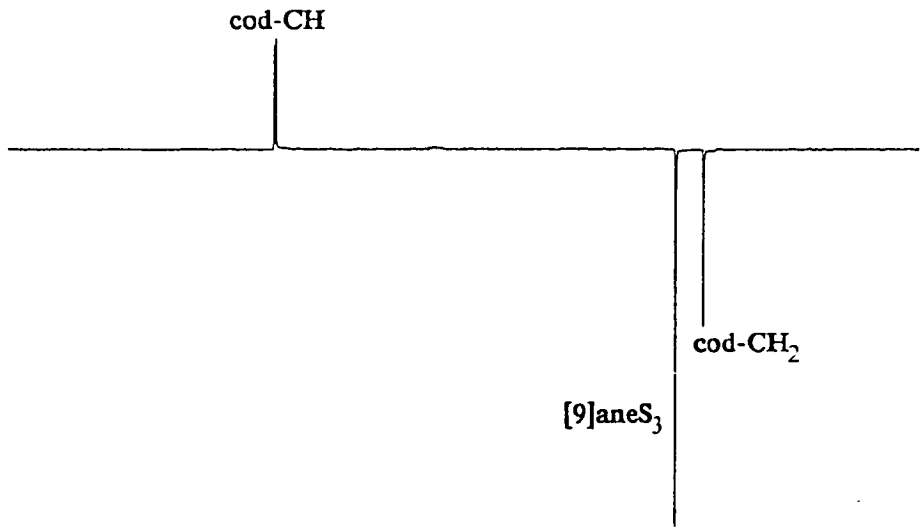

Figure 5.6: ^{13}C d.e.p.t n.m.r. Spectrum of [Rh([9]aneS$_3$)(C_8H_{12})](PF$_6$) (50.32 MHz, CD_3NO_2, 298K).

5.2.4 Single Crystal Structure of [Rh([9]aneS$_3$)-(C$_8$H$_{12}$)](BF$_4$)

Details of the structure solution and refinement are given in Section 5.4.9. Selected bond lengths, angles and torsions are shown in Tables 5.4-5.6, and an ORTEP plot displaying the geometry of the complex is given in Figures 5.7 and 5.8.

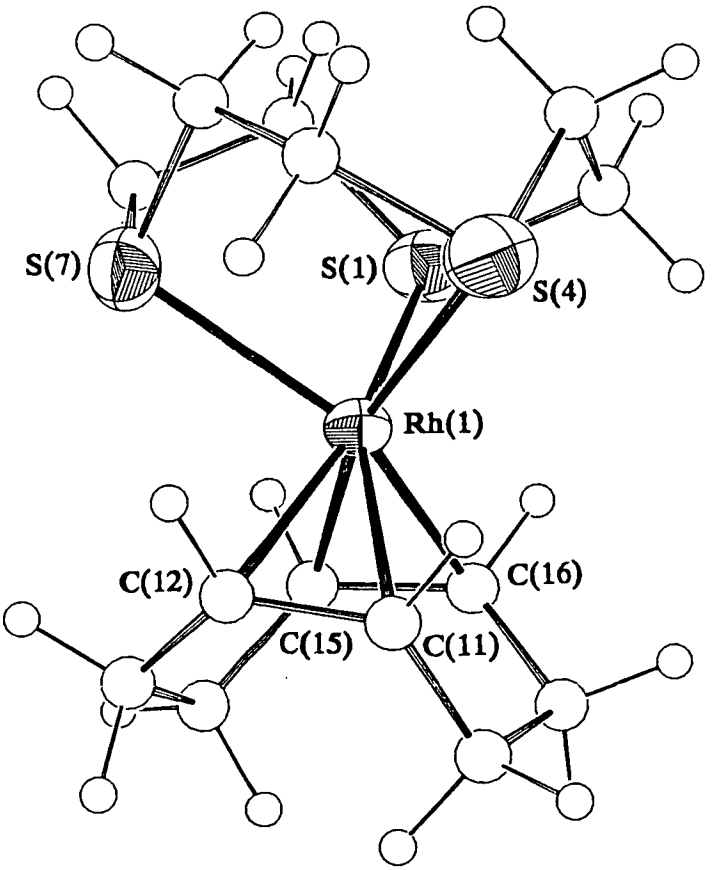

Figure 5.7: View of the Single Crystal Structure of [Rh([9]aneS$_3$)(C$_8$H$_{12}$)]$^+$ (molecule 1).

a) Molecule 1

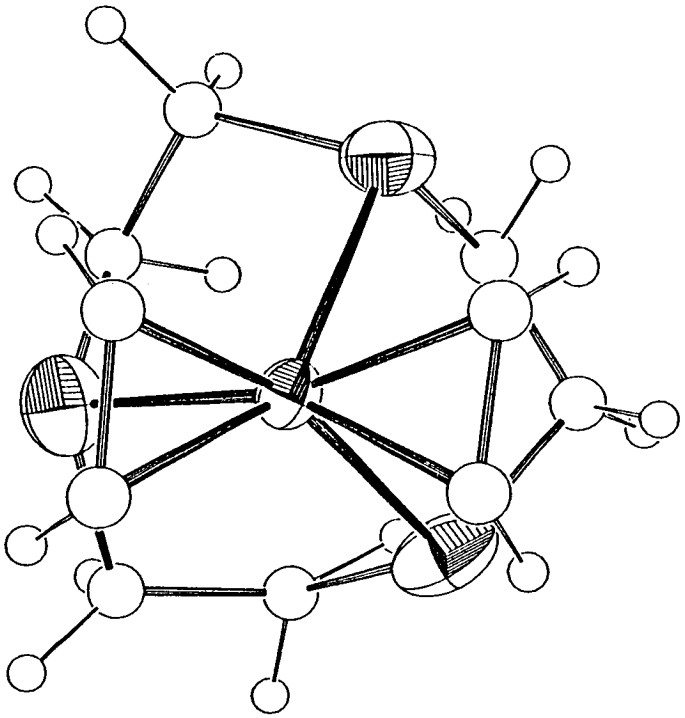

b) Molecule 2

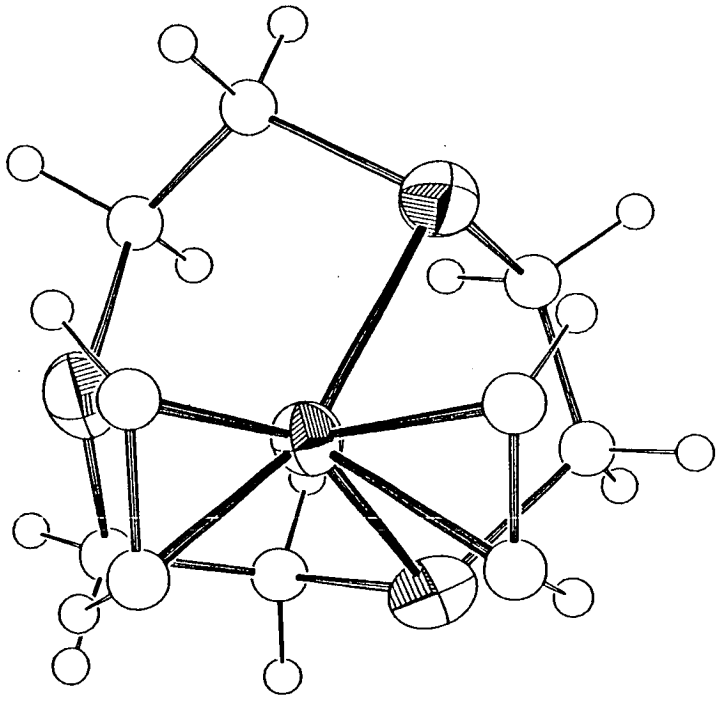

Figure 5.8: Alternative View of the Single Crystal Structure of $[Rh([9]aneS_3)(C_8H_{12})]^+$ (alkyl groups of the C_8H_{12} ligand omitted for clarity).

Single Crystal Structure of [Rh([9]aneS$_3$)(C$_8$H$_{12}$)](BF$_4$)

Table 5.4. Bond Lengths(A) with standard deviations

Rh(1) - S(1)	2.3213(25)	Rh(2) -C(35)	2.116(9)
Rh(1) - S(4)	2.3966(25)	Rh(2) -C(36)	2.083(8)
Rh(1) - S(7)	2.4457(24)	S(21) -C(22)	1.802(9)
Rh(1) -C(11)	2.222(8)	S(21) -C(29)	1.842(8)
Rh(1) -C(12)	2.201(9)	C(22) -C(23)	1.542(12)
Rh(1) -C(15)	2.081(9)	C(23) -S(24)	1.833(9)
Rh(1) -C(16)	2.121(9)	S(24) -C(25)	1.852(9)
C(11) -C(12)	1.397(12)	C(25) -C(26)	1.498(12)
C(11) -C(18)	1.491(12)	C(26) -S(27)	1.830(9)
C(12) -C(13)	1.485(13)	S(27) -C(28)	1.825(9)
C(13) -C(14)	1.517(14)	C(28) -C(29)	1.509(12)
C(14) -C(15)	1.500(13)	C(31) -C(32)	1.314(14)
C(15) -C(16)	1.424(12)	C(31) -C(38)	1.484(15)
C(16) -C(17)	1.511(13)	C(32) -C(33)	1.415(16)
C(17) -C(18)	1.500(13)	C(33) -C(34)	1.418(17)
Rh(2) -S(21)	2.3059(24)	C(34) -C(35)	1.544(14)
Rh(2) -S(24)	2.4443(24)	C(35) -C(36)	1.403(12)
Rh(2) -S(27)	2.4358(23)	C(36) -C(37)	1.483(13)
Rh(2) -C(31)	2.184(9)	C(37) -C(38)	1.440(15)
Rh(2) -C(32)	2.224(10)		

Table 5.5. Angles(degrees) with standard deviations

S(1)	-Rh(1)	- S(4)	87.07(9)	S(21)	-Rh(2)	-C(32)	161.4(3)
S(1)	-Rh(1)	- S(7)	86.25(8)	S(21)	-Rh(2)	-C(35)	88.6(3)
S(1)	-Rh(1)	-C(11)	156.21(23)	S(21)	-Rh(2)	-C(36)	89.48(24)
S(1)	-Rh(1)	-C(12)	165.05(23)	S(24)	-Rh(2)	-S(27)	86.20(8)
S(1)	-Rh(1)	-C(15)	91.36(25)	S(24)	-Rh(2)	-C(31)	84.7(3)
S(1)	-Rh(1)	-C(16)	85.61(25)	S(24)	-Rh(2)	-C(32)	110.0(3)
S(4)	-Rh(1)	- S(7)	86.39(8)	S(24)	-Rh(2)	-C(35)	154.9(3)
S(4)	-Rh(1)	-C(11)	88.37(23)	S(24)	-Rh(2)	-C(36)	116.24(24)
S(4)	-Rh(1)	-C(12)	103.82(23)	S(27)	-Rh(2)	-C(31)	108.1(3)
S(4)	-Rh(1)	-C(15)	164.15(25)	S(27)	-Rh(2)	-C(32)	86.2(3)
S(4)	-Rh(1)	-C(16)	124.55(25)	S(27)	-Rh(2)	-C(35)	118.2(3)
S(7)	-Rh(1)	-C(11)	116.74(23)	S(27)	-Rh(2)	-C(36)	157.07(24)
S(7)	-Rh(1)	-C(12)	84.28(23)	C(31)	-Rh(2)	-C(32)	34.7(4)
S(7)	-Rh(1)	-C(15)	109.26(25)	C(31)	-Rh(2)	-C(35)	92.4(4)
S(7)	-Rh(1)	-C(16)	147.43(25)	C(31)	-Rh(2)	-C(36)	80.2(3)
C(11)	-Rh(1)	-C(12)	36.8(3)	C(32)	-Rh(2)	-C(35)	79.4(4)
C(11)	-Rh(1)	-C(15)	86.7(3)	C(32)	-Rh(2)	-C(36)	90.0(4)
C(11)	-Rh(1)	-C(16)	77.8(3)	C(35)	-Rh(2)	-C(36)	39.0(3)
C(12)	-Rh(1)	-C(15)	80.9(3)	Rh(2)	-S(21)	-C(22)	102.6(3)
C(12)	-Rh(1)	-C(16)	96.2(3)	Rh(2)	-S(21)	-C(29)	107.3(3)
C(15)	-Rh(1)	-C(16)	39.6(3)	C(22)	-S(21)	-C(29)	102.4(4)
Rh(1)	- S(1)	- C(2)	99.8(3)	S(21)	-C(22)	-C(23)	115.3(6)
Rh(1)	- S(1)	- C(9)	105.8(3)	C(22)	-C(23)	-S(24)	109.3(6)
C(2)	- S(1)	- C(9)	104.8(5)	Rh(2)	-S(24)	-C(23)	104.7(3)
Rh(1)	- S(4)	- C(3)	103.8(3)	Rh(2)	-S(24)	-C(25)	100.5(3)
Rh(1)	- S(4)	- C(5)	101.4(3)	C(23)	-S(24)	-C(25)	101.7(4)
C(3)	- S(4)	- C(5)	105.7(4)	S(24)	-C(25)	-C(26)	115.7(6)
Rh(1)	- S(7)	- C(6)	102.9(3)	C(25)	-C(26)	-S(27)	112.6(6)
Rh(1)	- S(7)	- C(8)	100.7(3)	Rh(2)	-S(27)	-C(26)	105.4(3)
C(6)	- S(7)	- C(8)	97.9(4)	Rh(2)	-S(27)	-C(28)	99.6(3)
Rh(1)	-C(11)	-C(12)	70.8(5)	C(26)	-S(27)	-C(28)	102.2(4)
Rh(1)	-C(11)	-C(18)	114.7(6)	S(27)	-C(28)	-C(29)	114.6(6)
C(12)	-C(11)	-C(18)	125.9(8)	S(21)	-C(29)	-C(28)	111.0(6)
Rh(1)	-C(12)	-C(11)	72.4(5)	Rh(2)	-C(31)	-C(32)	74.3(6)
Rh(1)	-C(12)	-C(13)	107.8(6)	Rh(2)	-C(31)	-C(38)	109.9(7)
C(11)	-C(12)	-C(13)	124.0(8)	C(32)	-C(31)	-C(38)	121.2(9)
C(12)	-C(13)	-C(14)	113.3(8)	Rh(2)	-C(32)	-C(31)	71.0(6)
C(13)	-C(14)	-C(15)	113.1(8)	Rh(2)	-C(32)	-C(33)	112.3(8)
Rh(1)	-C(15)	-C(14)	114.6(6)	C(31)	-C(32)	-C(33)	129.9(10)
Rh(1)	-C(15)	-C(16)	71.7(5)	C(32)	-C(33)	-C(34)	116.5(11)
C(14)	-C(15)	-C(16)	124.9(8)	C(33)	-C(34)	-C(35)	117.7(9)
Rh(1)	-C(16)	-C(15)	68.7(5)	Rh(2)	-C(35)	-C(34)	110.9(6)
Rh(1)	-C(16)	-C(17)	113.5(6)	Rh(2)	-C(35)	-C(36)	69.2(5)
C(15)	-C(16)	-C(17)	125.1(8)	C(34)	-C(35)	-C(36)	120.4(8)
C(16)	-C(17)	-C(18)	112.7(8)	Rh(2)	-C(36)	-C(35)	71.7(5)
C(11)	-C(18)	-C(17)	111.2(7)	Rh(2)	-C(36)	-C(37)	115.2(6)
S(21)	-Rh(2)	-S(24)	86.74(8)	C(35)	-C(36)	-C(37)	124.1(8)
S(21)	-Rh(2)	-S(27)	87.06(8)	C(36)	-C(37)	-C(38)	114.3(8)
S(21)	-Rh(2)	-C(31)	162.0(3)	C(31)	-C(38)	-C(37)	118.1(9)

Table 5.6. Torsion angles(degrees) with standard deviations

C(9)	- S(1)	- C(2)	- C(3)	56.9(8)	C(29)	-S(21)	-C(22)	-C(23)	62.8(7)
C(2)	- S(1)	- C(9)	- C(8)	-139.9(7)	C(22)	-S(21)	-C(29)	-C(28)	-135.1(6)
S(1)	- C(2)	- C(3)	- S(4)	53.1(8)	S(21)	-C(22)	-C(23)	-S(24)	51.5(8)
C(2)	- C(3)	- S(4)	- C(5)	-131.2(7)	C(22)	-C(23)	-S(24)	-C(25)	-131.6(6)
C(3)	- S(4)	- C(5)	- C(6)	61.1(7)	C(23)	-S(24)	-C(25)	-C(26)	63.3(7)
S(4)	- C(5)	- C(6)	- S(7)	57.0(8)	S(24)	-C(25)	-C(26)	-S(27)	51.0(8)
C(5)	- C(6)	- S(7)	- C(8)	-138.0(7)	C(25)	-C(26)	-S(27)	-C(28)	-132.5(6)
C(6)	- S(7)	- C(8)	- C(9)	58.6(7)	C(26)	-S(27)	-C(28)	-C(29)	62.4(7)
S(7)	- C(8)	- C(9)	- S(1)	55.8(8)	S(27)	-C(28)	-C(29)	-S(21)	50.7(7)
C(18)	-C(11)	-C(12)	-C(13)	-7.2(14)	C(38)	-C(31)	-C(32)	-C(33)	-0.4(18)
C(12)	-C(11)	-C(18)	-C(17)	97.8(10)	C(32)	-C(31)	-C(38)	-C(37)	71.0(14)
C(11)	-C(12)	-C(13)	-C(14)	-45.1(12)	C(31)	-C(32)	-C(33)	-C(34)	-67.1(17)
C(12)	-C(13)	-C(14)	-C(15)	-29.2(11)	C(32)	-C(33)	-C(34)	-C(35)	-5.8(16)
C(13)	-C(14)	-C(15)	-C(16)	91.5(11)	C(33)	-C(34)	-C(35)	-C(36)	69.3(13)
C(14)	-C(15)	-C(16)	-C(17)	-3.2(14)	C(34)	-C(35)	-C(36)	-C(37)	5.8(14)
C(15)	-C(16)	-C(17)	-C(18)	-44.2(12)	C(35)	-C(36)	-C(37)	-C(38)	-73.7(12)
C(16)	-C(17)	-C(18)	-C(11)	-31.7(10)	C(36)	-C(37)	-C(38)	-C(31)	1.8(13)

The structure contains two crystallographically independent molecules per asymmetric unit. Both cations adopt distorted trigonal bipyramidal geometries similar to that of molecule 1 of the structure of [Rh([9]aneS$_3$)-(C$_2$H$_4$)$_2$](BF$_4$) (Section 5.2.2), with a shortened axial Rh-S bond [for molecule 1 Rh(1)-S(1) = 2.3213(25), Rh(1)-S(4) = 2.3966(25), Rh(1)-S(7) = 2.4457(24) Å; for molecule 2 Rh(2)-S(21) = 2.3059(24), Rh(2)-S(24) = 2.4443(24), Rh(2)-S(27) = 2.4358(23) Å]. However, whilst molecule 2 in the crystal structure has a symmetrical geometry with equal Rh-S distances and S-Rh-X angles (X = midpoint of cod C=C double bond) for both equatorial S-donors, molecule 1 has a significantly more distorted structure [for molecule 1 <S(1)-Rh(1)-X(1) = 172.40(24), <S(4)-Rh(1)-X(2) = 144.16(26), <S(7)-Rh(1)-X(2) = 128.74(26)^0; for molecule 2 <S(21)-Rh(2)-X(31) = 174.07(28), <S(24)-Rh(2)-X(32) = 135.80(26), <S(27)-Rh(2)-X(32) = 137.48(26)^0]. Interconversion of the geometries exhibited by the two cations in the structure involves rotation of the [9]aneS$_3$ ring by 6° about the central Rh-[9]aneS$_3$ axis (Figure 5.8, c.f. [Rh([9]aneS$_3$)-(C$_2$H$_4$)$_2$](BF$_4$), Section 5.2.2), again implying that such rotation is a facile process in solution. For both cations, the Rh-C bond lengths to the axial C=C donor are longer than those to the equatorial alkene donor [Rh-C$_{ax}$(average) = 2.208(9), Rh-C$_{eq}$(average) = 2.100(9) Å], demonstrating a *trans*-effect for an alkene C=C donor

trans to a thioether S-donor. The C=C distances for the axial alkene donors are correspondingly shorter than for the equatorial C=C groups, although this is less marked in the less symmetrical cation of molecule 1 [for molecule 1 C(11)-C(12) = 1.397(12), C(15)-C(16) = 1.424(12) Å; for molecule 2 C(31)-C(32) = 1.314(14), C(35)-C(36) = 1.403(12) Å]. It is unclear whether this *trans*-effect is caused by a greater capacity for σ-donation or for π-back bonding for a thioether S-donor compared to a coordinated alkene.

The geometry of the cation in molecule 2 of this crystal structure is similar to that exhibited by $[Ir([9]aneS_3)(C_2H_4)_2]^+$ (Section 6.2.3), and by the dimeric complex $[Rh_2(cod)_2([20]aneS_6)]^{2+}$ [207].

5.2.5 $[Rh([9]aneS_3)(C_4H_6)](PF_6)$

A bright yellow solution of $[Rh(C_4H_6)_2Cl]$ was generated by bubbling butadiene through a CH_2Cl_2 solution of $[Rh_2(C_2H_4)_4Cl_2]$ at 298K for 10 mins[229]. Addition of one molar equivalent of $[9]aneS_3$ and NH_4PF_6 afforded a pale yellow solution on stirring for 10 mins at 298K under N_2, which was filtered and reduced to *ca.* 1 cm^3 volume. Addition of excess ^{n}hexane yielded a microcrystalline yellow air-stable product, which was analysed without further purification.

F.a.b. mass spectrometry showed peaks at M^+ = 337 and 282, which were assigned to the molecular ions

$[^{103}Rh([9]aneS_3)(C_4H_6)]^+$ and $[^{103}Rh([9]aneS_3\text{-}H)]^+$ respectively. Hence, the complex was formulated as $[Rh([9]aneS_3)(C_4H_6)](PF_6)$: I.R. spectral and elemental analytical data were also consistent with this assignment.

The ^1H n.m.r. spectrum of $[Rh([9]aneS_3)(C_4H_6)](PF_6)$ in d^6-acetone at 298K showed multiplet resonances at δ = 5.60, 2.32 and 1.08 ppm (each 2H) corresponding to the butadiene H atoms, and a broad asymmetric peak at δ = 3.22-2.85 ppm (12H) from the $[9]aneS_3$ ligand (Figure 5.9). The ^{13}C d.e.p.t. n.m.r. spectrum at 298K exhibited resonances at δ = 89.98 ppm (d, $^1J_{Rh-C}$ = 5.0 Hz) from the C_4H_6 CH C atoms, 35.37 (d, $^1J_{Rh-C}$ = 12.1 Hz) from the C_4H_6 CH_2 C atoms, and two broad peaks in the region expected for the $[9]aneS_3$ macrocyclic C atoms at δ = 36.25 and 34.69 ppm with an integral ratio of approximately 1:2 (Figure 5.11a). A variable temperature ^1H n.m.r. study in d^6-acetone showed that between 204K and 273K the $[9]aneS_3$ resonance was resolved into two second order multiplets centred at δ = 3.15 ppm (4H) and δ = 2.91 ppm (8H), whilst above the coalescence temperature of approximately 306K the resonance was resolved into a broad singlet at δ = 3.01 ppm (Figure 5.10). A ^{13}C d.e.p.t n.m.r. spectrum in d^6-acetone at 319K showed one broad singlet for the $[9]aneS_3$ ligand at δ = 35.9 ppm. The ^1H and ^{13}C resonances due to the butadiene ligand were unaffected by changes in temperature between 204 and 327K.

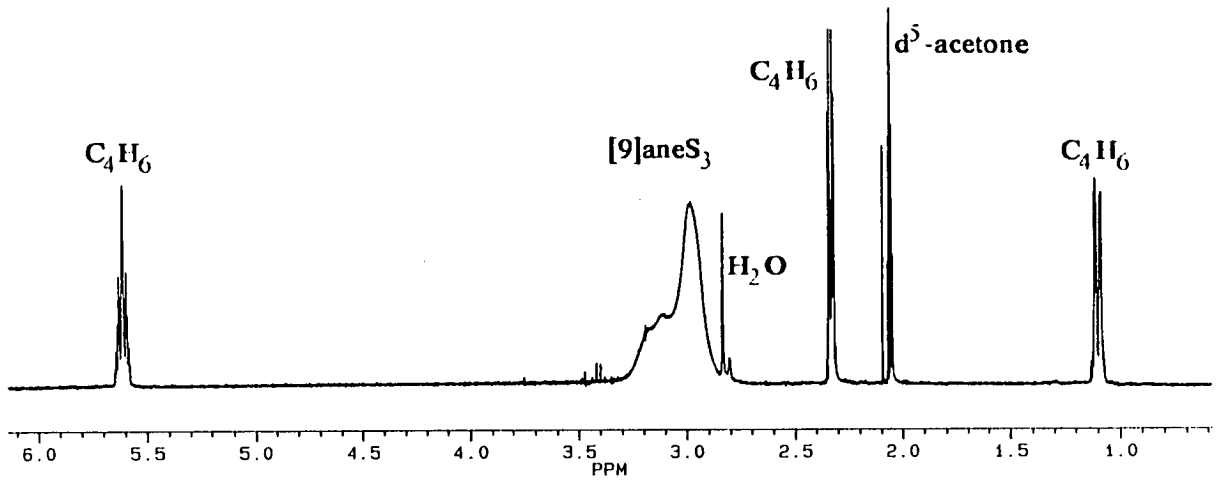

Figure 5.9: ^{1}H n.m.r. Spectrum of [Rh([9]aneS$_3$)(C$_4$H$_6$)] (PF_6) (360.13 MHz, d^6-acetone, 298K).

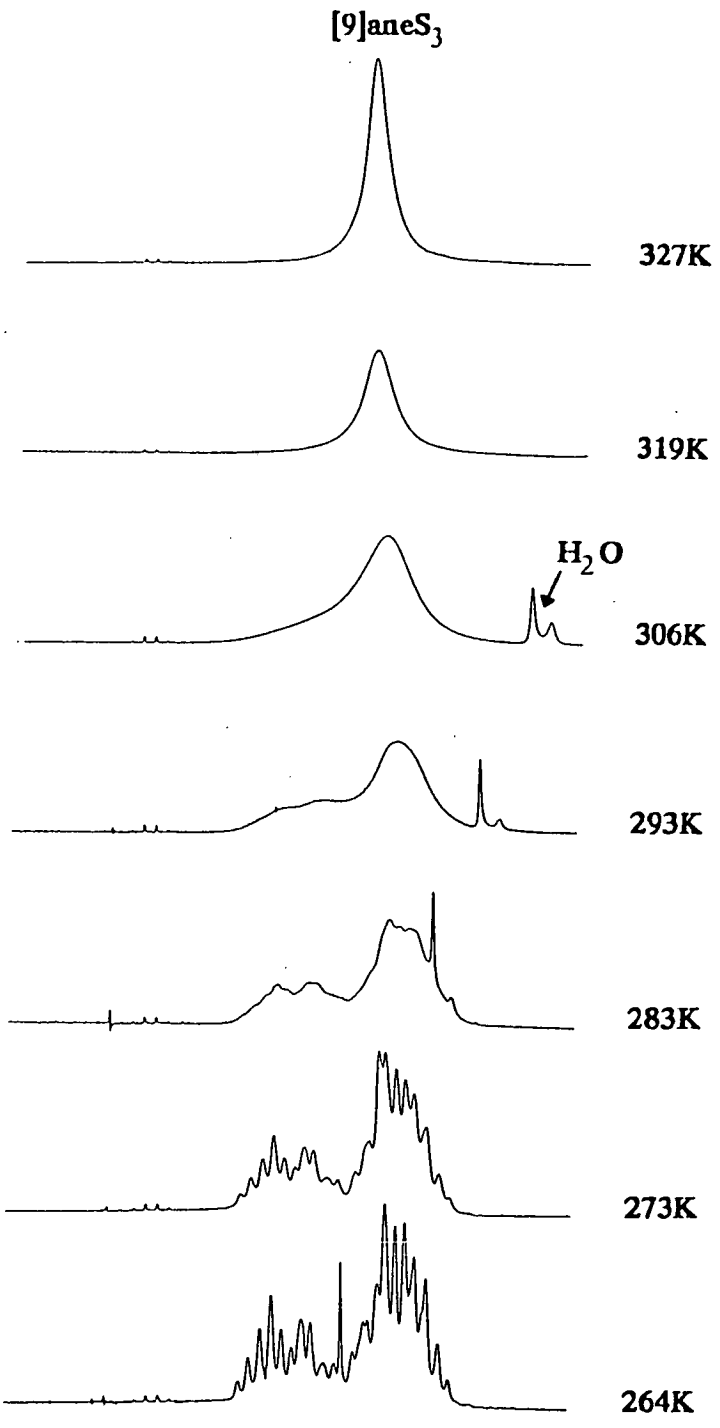

Figure 5.10: Variable Temperature ^1H n.m.r. spectra of $[Rh([9]aneS_3)(C_4H_6)](PF_6)$ (360.13 MHz, d^6-acetone).

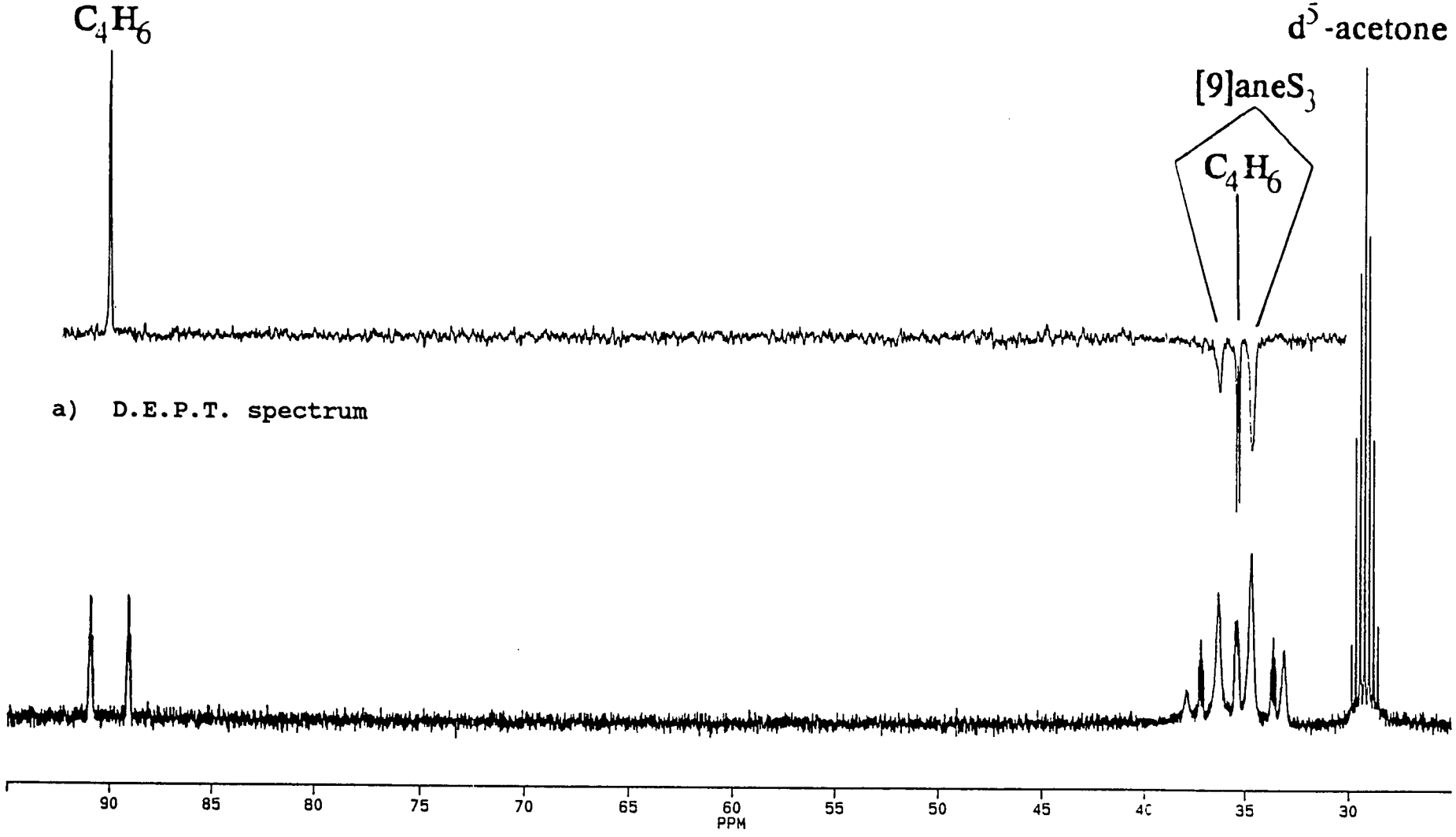

Figure 5.11: ^{13}C n.m.r. Spectra of $[Rh([9]aneS_3)(C_4H_6)](PF_6)$ (90.56 MHz, d^6-acetone, 298K).

This n.m.r. behaviour contrasts with that of $[Rh([9]aneS_3)(C_2H_4)_2]^+$, where no decoalescence of the resonances due to the $[9]aneS_3$ macrocycle is observed above 188K (Section 5.2.1), and with $[Ir([9]aneS_3)(C_4H_6)]^+$ which exhibits a static n.m.r. structure at 298K with three ^{13}C resonances from the $[9]aneS_3$ ligand (Section 6.2.7). The nature of the fluxional process operating below 306K for $[Rh([9]aneS_3)(C_4H_6)]^+$ is unclear: if it is assumed that the complex maintains a five-coordinate structure in solution (Section 5.2.6), there is no mechanism involving rotation of the $[9]aneS_3$ ring relative to the C_4H_6 ligand that would equilibrate two out of the three possible CH_2-environments for the $[9]aneS_3$ macrocycle (a, b and c, 58). A square-pyramidal/square-planar equilibrium via decoordination of the apical macrocyclic S-donor would also not cause this equilibration, whilst a pseudo-rotation mechanism cannot be involved because of the rigidity of the $[9]aneS_3$ ring. It is possible that at the lower temperatures the complex may adopt a static n.m.r. structure similar to that exhibited by its Ir analogue at 298K (Section 6.2.7), with two of the three macrocyclic CH_2-environments being coincidently n.m.r.-equivalent or near-equivalent. The n.m.r behaviour of analogous Rh complexes containing substituted 1,3-dienes and/or substituted trithia macrocycles would have to be examined to confirm this, however.

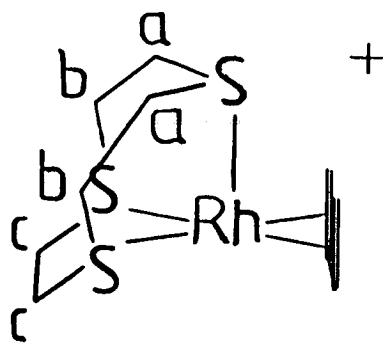

(58)

In order to determine the stereochemistry adopted by the complex, and to quantify the Rh-butadiene bonding, an x-ray structural analysis of $[Rh([9]aneS_3)(C_4H_6)](PF_6)$ was performed. As an aid to characterisation of the electronic character of the complex cation, a ^1H-coupled ^{13}C n.m.r. spectrum of the compound was also measured (Figure 5.10b): the ^{13}C-^1H coupling constants thus obtained are discussed in Section 6.2.8.

5.2.6 Single Crystal Structure of $[Rh([9]aneS_3)(C_4H_6)](PF_6).\frac{1}{4}(C_2H_5OC_2H_5)$

The structure solution and refinement are described in Section 5.4.12. Relevant bond lengths, angles and torsions are listed in Table 5.7, and the geometry of the complex cation is displayed in Figure 5.12.

Single Crystal Structure of [Rh([9]aneS$_3$)(C$_4$H$_6$)](PF$_6$).

½(C$_2$H$_5$OC$_2$H$_5$)

Table 5.7. Bond Lengths(A), angles(degrees) and torsion angles(degrees) with standard deviations

Rh	- S(1)	2.3417(15)	C(3)	- S(4)	1.840(6)
Rh	- S(4)	2.3374(14)	S(4)	- C(5)	1.816(6)
Rh	- S(7)	2.3580(12)	C(5)	- C(6)	1.527(7)
Rh	-C(11)	2.136(5)	C(6)	- S(7)	1.818(5)
Rh	-C(12)	2.126(5)	S(7)	- C(8)	1.824(5)
Rh	-C(13)	2.119(5)	C(8)	- C(9)	1.507(8)
Rh	-C(14)	2.113(5)	C(11)	-C(12)	1.409(7)
S(1)	- C(2)	1.814(6)	C(12)	-C(13)	1.386(7)
S(1)	- C(9)	1.830(6)	C(13)	-C(14)	1.443(7)
C(2)	- C(3)	1.489(8)			

S(1)	- Rh -	S(4) 88.62(5)	Rh	- S(1) -	C(9) 101.47(20)
S(1)	- Rh -	S(7) 87.90(5)	C(2)	- S(1) -	C(9) 101.7(3)
S(1)	- Rh -C(11)	168.72(14)	S(1)	- C(2) -	C(3) 112.5(4)
S(1)	- Rh -C(12)	130.38(13)	C(2)	- C(3) -	S(4) 114.3(4)
S(1)	- Rh -C(13)	100.72(14)	Rh	- S(4) -	C(3) 100.70(20)
S(1)	- Rh -C(14)	94.54(14)	Rh	- S(4) -	C(5) 105.46(18)
S(4)	- Rh -	S(7) 88.70(4)	C(3)	- S(4) -	C(5) 101.2(3)
S(4)	- Rh -C(11)	95.58(14)	S(4)	- C(5) -	C(6) 112.9(4)
S(4)	- Rh -C(12)	99.01(13)	C(5)	- C(6) -	S(7) 115.5(4)
S(4)	- Rh -C(13)	127.30(14)	Rh	- S(7) -	C(6) 101.20(16)
S(4)	- Rh -C(14)	167.17(14)	Rh	- S(7) -	C(8) 105.30(18)
S(7)	- Rh -C(11)	102.62(14)	C(6)	- S(7) -	C(8) 102.04(24)
S(7)	- Rh -C(12)	140.77(13)	S(7)	- C(8) -	C(9) 112.0(4)
S(7)	- Rh -C(13)	142.74(14)	S(1)	- C(9) -	C(8) 114.6(4)
S(7)	- Rh -C(14)	103.82(13)	Rh	-C(11)	-C(12) 70.3(3)
C(11)	- Rh -C(12)	38.61(19)	Rh	-C(12)	-C(11) 71.1(3)
C(11)	- Rh -C(13)	68.44(19)	Rh	-C(12)	-C(13) 70.7(3)
C(11)	- Rh -C(14)	79.14(19)	C(11)	-C(12)	-C(13) 117.8(4)
C(12)	- Rh -C(13)	38.11(19)	Rh	-C(13)	-C(12) 71.2(3)
C(12)	- Rh -C(14)	69.54(18)	Rh	-C(13)	-C(14) 69.8(3)
C(13)	- Rh -C(14)	39.88(19)	C(12)	-C(13)	-C(14) 117.4(4)
Rh	- S(1) - C(2)	104.55(20)	Rh	-C(14)	-C(13) 70.3(3)

C(9)	- S(1) - C(2) - C(3)	135.0(4)	S(4)	- C(5) - C(6) - S(7)	-45.8(5)
C(2)	- S(1) - C(9) - C(8)	-63.9(5)	C(5)	- C(6) - S(7) - C(8)	-67.8(4)
S(1)	- C(2) - C(3) - S(4)	-50.4(5)	C(6)	- S(7) - C(8) - C(9)	132.5(4)
C(2)	- C(3) - S(4) - C(5)	-65.1(5)	S(7)	- C(8) - C(9) - S(1)	-48.7(5)
C(3)	- S(4) - C(5) - C(6)	129.9(4)	C(11)	-C(12) -C(13) -C(14)	1.0(7)

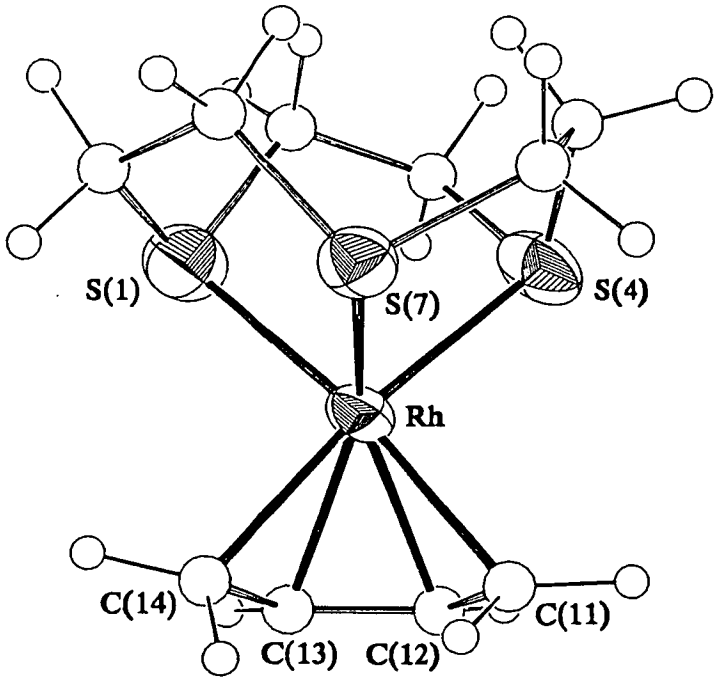

Figure 5.12: View of the Single Crystal Structure of $[Rh([9]aneS_3)(C_4H_6)]^+$.

The complex cation adopts a *quasi*-square-pyramidal stereochemistry with all three Rh-S and four Rh-C bond lengths being equal [Rh-S(1) = 2.3417(15), Rh-S(4) = 2.3374(14), Rh-S(7) = 2.3580(12), Rh-C(11) = 2.136(5), Rh-C(12) = 2.126(5), Rh-C(13) = 2.119(5), Rh-C(14) = 2.113(5) Å; <S(1)-Rh-X(1) = 149.68(14), <S(4)-Rh-X(2) = 147.21(15), <S(7)-Rh-X(1) = 121.70(14), <S(7)-Rh-X(2) = 123.42(15)° where X(1), X(2) are the midpoints of the C(11)=C(12) and C(13)=C(14) double bonds respectively, Table 6.8]. This geometry is analogous to that adopted by other d^8 metal complexes $[M(L)_3(C_4H_6)]^{n+}$ (M = Fe^0, Ru^0, Co^I etc., L = CO, PR_3, Section 6.2.7). The C-C bond

lengths within the butadiene ligand are more distorted from those of free butadiene than is generally observed for butadiene complexes of d^8 metal ions [C(11)-C(12) = 1.409(7), C(12)-C(13) = 1.386(7), C(13)-C(14) = 1.443(7) Å; c.f. for $[Rh(C_4H_6)_2Cl]$ C=C = 1.38(2), C-C = 1.45(2) Å[230]]. This variation in C-C bond lengths could arise from unusually strong σ-donation or π-back donation components to the Rh-butadiene bonding; alternatively it could be indicative of significant tautomerism between formal $[Rh^{I}([9]aneS_3)(\eta^4\text{-}C_4H_6)]^+$ and $[Rh^{III}([9]aneS_3)(\sigma,\eta^2,\sigma\text{-}C_4H_6)]^+$ structures. The nature of the Rh-butadiene bonding in $[Rh([9]aneS_3)(C_4H_6)]^+$ is discussed further in Section 6.2.8.

5.2.7 $[Rh([9]aneS_3)(C_2H_4)(PR_3)](PF_6)$ (R = Phenyl, i-Propyl, c-Hexyl)

Treatment of a solution of $[Rh_2(C_2H_4)_4Cl_2]$ in CH_2Cl_2 with two molar equivalents of PPh_3 under N_2 at 298K for 15 mins afforded a red solution. Addition of two molar equivalents of $[9]aneS_3$ and NH_4PF_6 and stirring for a further 10 mins yielded a deep red solution, which was filtered and reduced to 1 cm^3 volume. Addition of excess ^{n}hexane gave an orange solid product, which was recrystallised from CH_2Cl_2/hexane. I.R. spectroscopy showed that the product contained $[9]aneS_3$ and PPh_3 ligands and PF_6^- counterion, and microanalytical data was consistent with the formulation $[Rh([9]aneS_3)(C_2H_4)$-

$(PPh_3)](PF_6)$ (found C = 43.5, H = 4.32%; calculated for $[C_{26}H_{31}S_3PRh](PF_6)$ C = 43.5, H = 4.37%). However, the f.a.b. mass spectrum of the product exhibited peaks at M^+ = 807, 573 and 339, which were assigned to the fragments $[^{103}Rh([9]aneS_3)(PPh_3)_2]^+$, $[^{103}Rh([9]aneS_3)(C_2H_4)(PPh_3)]^+$ and $[^{103}Rh([9]aneS_3)(C_2H_4)_2]^+$ respectively. Hence, the product was assigned as a mixture of the complexes $[Rh([9]aneS_3)(C_2H_4)_2](PF_6)$, $[Rh([9]aneS_3)(C_2H_4)(PPh_3)](PF_6)$ and $[Rh([9]aneS_3)(PPh_3)_2](PF_6)$: this was supported by ^{31}P n.m.r. spectroscopy, which showed the presence of two phosphorus-containing species at δ = 46.17 ppm (d, $^1J_{Rh-P}$ = 134 Hz) and 43.15 (d, $^1J_{Rh-P}$ = 169 Hz) in CD_3CN at 298K.

In order to prevent the formation of the complexes $[Rh([9]aneS_3)(PR_3)_2]^+$, this reaction was repeated using phosphine ligands with Tolman angles greater than that of PPh_3 (θ = 145°[231]). Following the method described for $[Rh([9]aneS_3)(C_2H_4)(PPh_3)](PF_6)$ using $Pcyc_3$ (θ = 170°[231]) in place of PPh_3 yielded a pale yellow solid product. This compound decomposed after 3 days at 298K *in vacuo*, but could be stored at 253K in air for a week. The f.a.b. mass spectrum of the complex showed peaks at M^+ = 591 and 562, arising from the molecular ions $[^{103}Rh([9]aneS_3)(C_2H_4)(Pcyc_3)]^+$ and $[^{103}Rh([9]aneS_3\text{-}H)(Pcyc_3)]^+$; no peaks attributable to the fragments $[^{103}Rh([9]aneS_3)(Pcyc_3)_2]^+$ (M^+ = 843) or $[^{103}Rh([9]aneS_3)(C_2H_4)_2]^+$ (M^+ = 339) were observed. This result, together with I.R. spectroscopic

and microanalytical data, led to the formulation of the product as the desired species $[Rh([9]aneS_3)(C_2H_4)(Pcyc_3)](PF_6)$.

The ^{13}C d.e.p.t. n.m.r. spectrum of $[Rh([9]aneS_3)(C_2H_4)(Pcyc_3)](PF_6)$ in d^6-acetone at 298K exhibited resonances at δ = 34.43 ppm from the $[9]aneS_3$ macrocycle, 29.15 (d, $^1J_{Rh-C} \simeq 12Hz$) from the ethene ligand, and at 35.02, 28.85, 26.66 and 25.28 ppm due to the $Pcyc_3$ alkyl C atoms. The ^1H n.m.r. spectrum of this complex under identical conditions showed multiplet resonances at δ = 3.08-2.95 (12H) and 2.04-1.28 ppm (33H) from the $[9]aneS_3$ and $Pcyc_3$ ligands respectively, and two multiplets at δ = 2.52 (2H) and 2.18 ppm (2H) due to a non-rotating C_2H_4 ligand (Figure 5.13). This contrasts with $[Rh([9]aneS_3)(C_2H_4)_2]^+$, where the ethene ligands gave one doublet resonance which did not decoalesce above 188K. The non-fluxionality of the ethene ligand in $[Rh([9]aneS_3)(C_2H_4)(Pcyc_3)]^+$ is likely to reflect the steric demands of the neighbouring $[9]aneS_3$ (θ = 220° [232]) and $Pcyc_3$ (θ = 170° [231]) ligands, rather than any difference in electronic character between this complex and $[Rh([9]aneS_3)(C_2H_4)_2]^+$, although an x-ray structural analysis would be needed to confirm this. A high temperature ^1H n.m.r. study of $[Rh([9]aneS_3)(C_2H_4)(Pcyc_3)]^+$ was not possible, because of the low thermal stability of this complex.

$[Rh([9]aneS_3)(C_2H_4)(Pcyc_3)](PF_6)$ gave only a weak

Raman spectrum due to fluorescence and the thermal instability of the complex. However, a band was observed at 1550 cm^{-1} which was provisionally assigned to the C=C stretching vibration of the coordinated C_2H_4 ligand. This compares with $\nu_{C=C}$ = 1493 cm^{-1} for $[(C_5H_5)Rh(C_2H_4)_2]$[209], and is consistent with the reduced $Rh \rightarrow C_2H_4$ back-donation observed for $[Rh([9]aneS_3)(C_2H_4)_2]^+$.

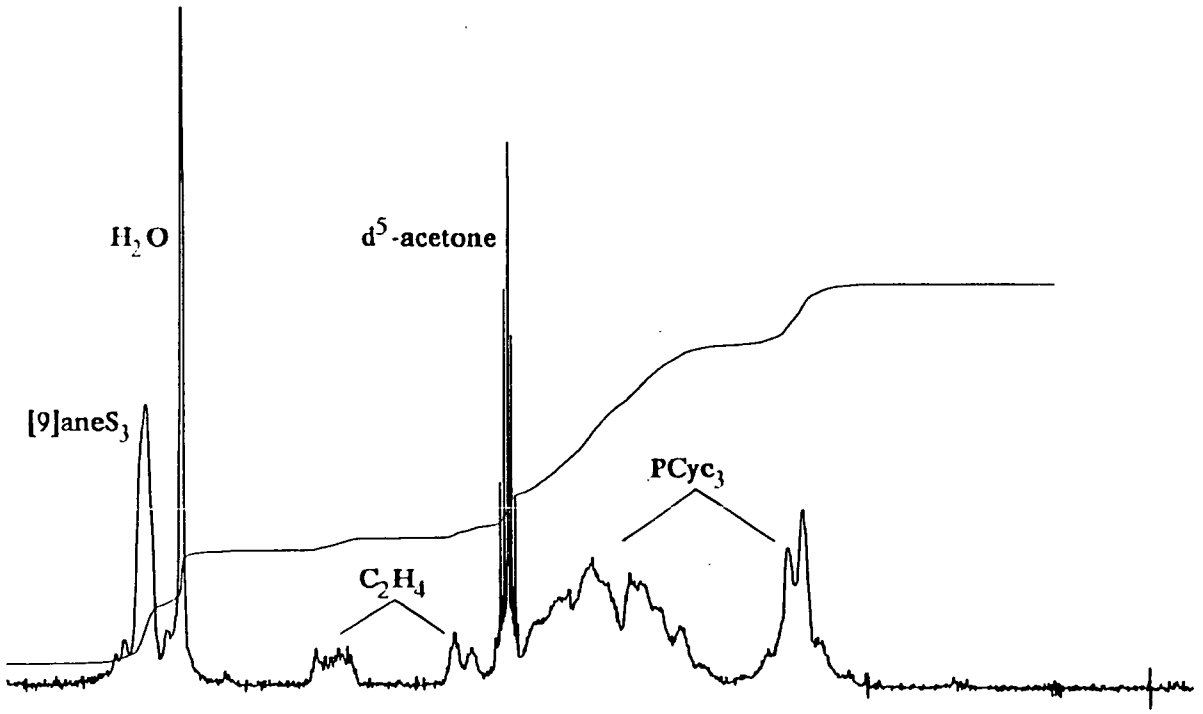

Figure 5.13: ^1H n.m.r. Spectrum of $[Rh([9]aneS_3)(C_2H_4)(Pcyc_3)](PF_6)$ (200.13 MHz, d^6-acetone, 298K).

Carrying out the above synthesis using $P(^{i}pr)_3$ (θ = 160° [231]) led to the isolation of a pale yellow solid product, which decomposed to an orange species after *ca.* 2 days at 298K *in vacuo* in the solid state. F.a.b. mass spectrometry of the yellow complex gave peaks at M^+ = 471 and 443, which were assigned to the fragments $[^{103}Rh([9]aneS_3)(C_2H_4)(P^{i}pr_3)]^+$ and $[^{103}Rh([9]aneS_3)(P^{i}pr_3)]^+$; again, no peaks arising from $[^{103}Rh([9]aneS_3)(P^{i}pr_3)_2]^+$ (M^+ = 603) or from $[^{103}Rh([9]aneS_3(C_2H_4)_2]^+$ (M^+ = 339) were observed. Hence this compound was assigned as $[Rh([9]aneS_3)(C_2H_4)(P^{i}pr_3)](PF_6)$, a formulation supported by microanalysis. An n.m.r. study of this complex was not possible, because of its low stability in solution.

Attempts to prepare $[Rh([9]aneS_3)(C_2H_4)(PMe_3)](PF_6)$ using an analogous method to that described earlier in acetone, THF or CH_2Cl_2 at 298K or 243K afforded only red oil products which could not be characterised.

5.2.8 $[Rh_2([9]aneS_3)_2(\mu\text{-}CO)_2](PF_6)_2$

Reaction of $[Rh_2(CO)_4Cl_2]$ with two molar equivalents of $[9]aneS_3$ and NH_4PF_6 in acetone under N_2 at 298K initially afforded a yellow solution, which became dark green after stirring for 15 mins at 298K. Both products could be isolated as microcrystalline solids after stirring the mixture for 5 mins or 30 mins for the yellow and green compounds respectively, by filtration and reduction of the solutions and addition of diethyl ether.

All samples of the yellow complex were contaminated with the green species, however (by I.R. spectroscopy), and solid state samples of the yellow product became green on standing at 298K for 2 days.

In addition to peaks from the [9]aneS$_3$ ligand and PF_6^- counterion, the initial yellow product exhibited two intense I.R. absorbances in the region expected for a terminally bound CO ligand ($\nu_{C\equiv O}$ = 2080 and 2012 cm^{-1} in CH_3NO_2 solution; c.f. for $[Rh_2(CO)_4Cl_2]$ $\nu_{C\equiv O}$ = 2095, 2030 cm^{-1} in CH_3NO_2 solution), and its f.a.b. mass spectrum exhibited peaks at M^+ = 339, 311 and 283, due to the molecular ions $[^{103}Rh([9]aneS_3)(CO)_2]^+$, $[^{103}Rh([9]aneS_3)(CO)]^+$ and $[^{103}Rh([9]aneS_3)]^+$ respectively. On the basis of the above data this compound was tentatively assigned as the mononuclear complex $[Rh([9]aneS_3)(CO)_2](PF_6)$, although its complete characterisation was not possible because of its instability with respect to the green species.

The I.R. spectrum of the green product showed peaks due to [9]aneS$_3$ and PF_6^-, and a single peak in the bridging CO region of the spectrum ($\nu_{C\equiv O}$ = 1855 cm^{-1} in CH_3NO_2 solution). Its f.a.b. mass spectrum exhibited peaks at M^+ = 622, 593, 339 and 283, which correspond to the fragments $[^{103}Rh_2([9]aneS_3)_2(CO)_2]^+$, $[^{103}Rh_2([9]aneS_3)_2(CO)]^+$, $[^{103}Rh([9]aneS_3)(CO)_2]^+$ and $[^{103}Rh([9]aneS_3)]^+$ respectively. The ^{1}H n.m.r. spectrum of the complex in CD_3NO_2 at 298K exhibited a narrow

multiplet at δ = 3.22 ppm from the [9]aneS$_3$ ligand, whilst the $^{13}C\{^1H\}$ n.m.r. spectrum gave a singlet resonance at δ = 32.71 ppm corresponding to the macrocyclic SCH_2 groups, and a triplet at δ = 202.51 ppm ($^1J_{Rh-C}$ = 26.9 Hz) arising from a μ_2-CO ligand environment (Figure 5.14). From these data, the product was formulated as the dimeric complex $[Rh_2([9]aneS_3)_2(\mu\text{-}CO)_2](PF_6)_2$ (59).

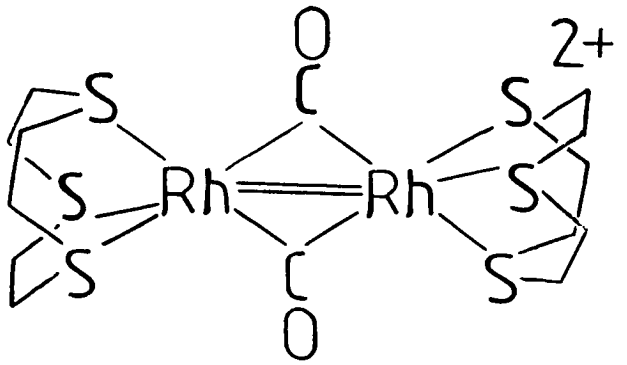

(59)

The electronic spectrum of this compound in CH_3CN exhibited a narrow band at λ_{max} = 895 nm (ε_{max} = 75.1 $dm^3.mol^{-1}.cm^{-1}$) in addition to charge-transfer bands. This low-energy band at 895 nm was tentatively assigned as a $\pi \rightarrow \pi^*$ transition within the Rh-Rh bond although this transition is not observed in the U.V./visible spectra of $[(cp^*)_2M_2(\mu\text{-}CO)_2]$ (M = Rh, Ir)[234]. The cyclic voltammogram of this complex is CH_3CN/0.1M $^nBu_4NPF_6$ at 298K exhibited an irreversible oxidation at Ep_a = + 1.30V

vs. Fc/Fc^+ (scan rate 400 mV/s) and a broad irreversible reduction at Ep_C = -1.67V. Repeated scans caused the appearance of additional waves due to daughter products at $E_{\frac{1}{2}}$ = -0.31V (ΔE_p = 250 mV at scan rate 400 mV/s) and Ep_a = +0.1V. Further characterisation of these processes was not attempted. The complexes $[(cp^*)_2M_2(\mu\text{-}CO)_2]$ (M = Rh, Ir) have been characterised[233,234], and exhibit spectral properties similar to those of $[Rh_2([9]aneS_3)_2(\mu\text{-}CO)_2]^{2+}$.

The reaction of $[Rh_2(C_2H_4)_2(CO)_2Cl_2]$[235] with $[9]aneS_3$ and NH_4PF_6 under identical conditions to those described above also afforded $[Rh_2([9]aneS_3)_2(\mu\text{-}CO)_2](PF_6)_2$ in similar yield to that obtained from $[Rh_2(CO)_4Cl_2]$.

Refluxing an acetone solution of the green $[Rh_2([9]aneS_3)_2(\mu\text{-}CO)_2](PF_6)_2$ under N_2 for 30 mins yielded an intense blue solution, from which a blue solid product could be isolated. The I.R. spectrum of this species exhibited five peaks in the region 2100-1700 cm^{-1} ($\nu_{C\equiv O}$ = 2060 m, 1865 s, 1812 m, 1789 w, 1717 m cm^{-1} in CH_3NO_2 solution) and a weak absorbance at 2340 cm^{-1} which could be assigned to a Rh-H stretching vibration, as well as peaks from coordinated $[9]aneS_3$ and from PF_6^- counterion. The f.a.b. mass spectrum of the blue product showed no significant peaks apart from those assignable to the 3-NOBA matrix. Unfortunately, due to time constraints, this compound could not be characterised further.

Reaction of $[Rh_2(CO)_4Cl_2]$ with two molar equivalents of $[9]aneS_3$ in the absence of NH_4PF_6 in CH_3OH, acetone or

CH_3CN under N_2 at 298K rapidly led to a blue insoluble product which exhibited five C≡O stretching vibrations ($\nu_{C\equiv O}$ = 2055 s, 1995 s, 1835 s, 1778 s, 1750 m cm^{-1} as a KBr disc) in addition to I.R. absorptions due to coordinated [9]aneS_3. The insolubility of this compound prevented further characterisation.

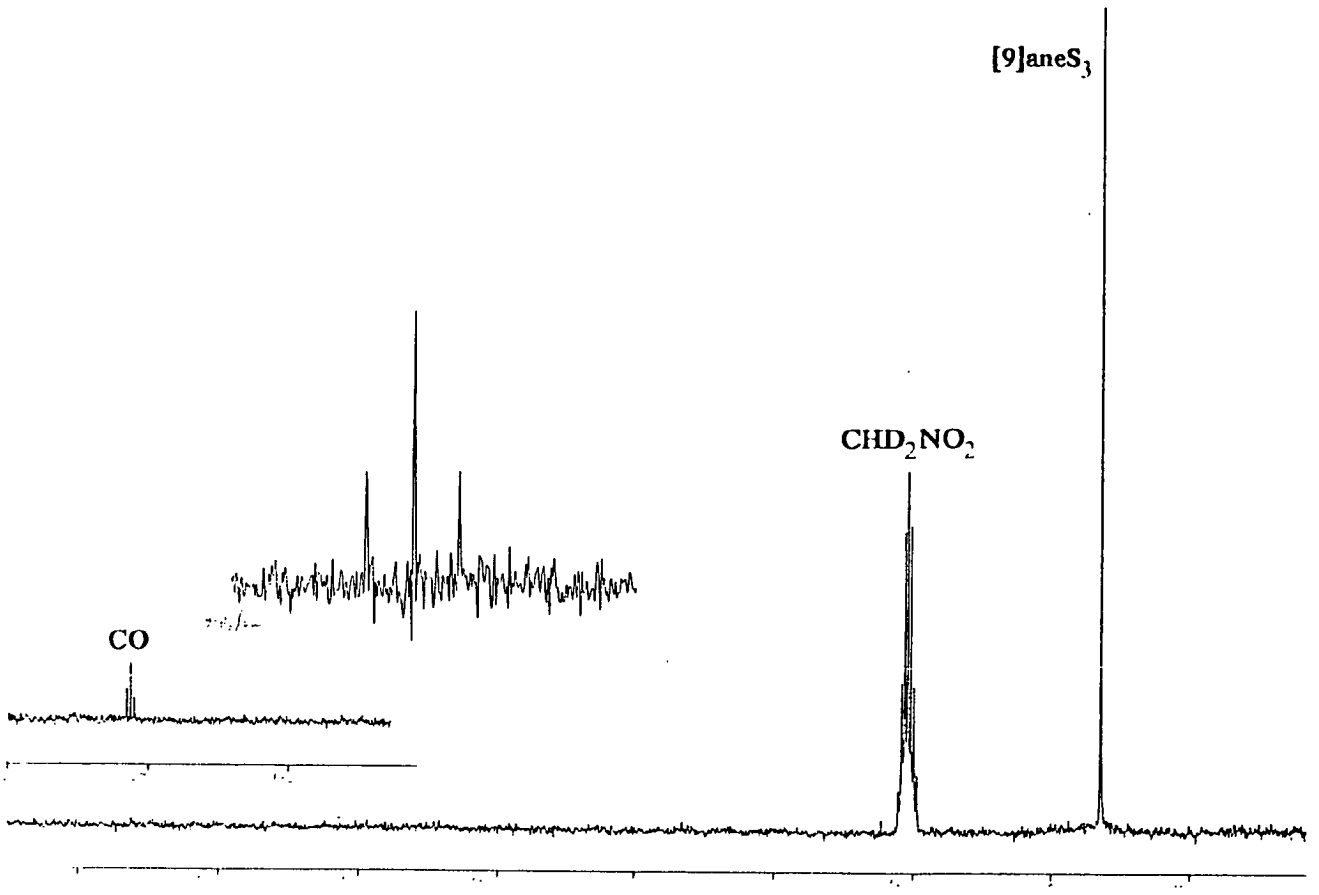

Figure 5.14: ^{13}C n.m.r. Spectrum of $[Rh_2([9]aneS_3)_2(\mu\text{-}CO)_2](PF_6)_2$ (50.32 MHz, CD_3NO_2, 298K).

5.2.9 [Rh([9]aneS$_3$)(CO)(PPh$_3$)](PF$_6$)

Treatment of [Rh(CO)Cl(PPh$_3$)$_2$] with one molar equivalent of [9]aneS$_3$ and of NH$_4$PF$_6$ in CH$_2$Cl$_2$ under N$_2$ at 298K for 15 mins afforded a bright yellow solution. Filtration of this solution, reduction to *ca.* 1 cm^3 volume, and addition of an excess of ^{n}hexane yielded a yellow microcrystalline product, which was analysed without further purification.

I.R. spectroscopy of this compound confirmed the presence of [9]aneS$_3$, PPh$_3$ and CO ligands [$\nu_{C\equiv O}$ = 1,960 cm^{-1} in CH$_3$NO$_2$ solution, and 1,955 cm^{-1} as a KBr disc] and PF$_6^-$ counterion. The f.a.b. mass spectrum of the product showed peaks at M$^+$ = 573, 545 and 468, which were assigned to the fragments [^{103}Rh([9]aneS$_3$)(CO)(PPh$_3$)]$^+$, [^{103}Rh([9]aneS$_3$)(PPh$_3$)]$^+$ and [^{103}Rh([9]aneS$_3$)(PPh$_2$)]$^+$ respectively; no higher mass peaks were observed, ruling out a bi- or polynuclear structure for this species. The ^{1}H n.m.r. spectrum of the complex in d^6-acetone at 298K exhibited multiplets at δ = 7.80-7.45 (15H) and 2.57-2.40 ppm (12H), assigned to the PPh$_3$ and [9]aneS$_3$ ligands respectively. The ^{13}C {^{1}H} n.m.r. spectrum under identical conditions showed peaks at δ = 133.51, 131.75, 131.06 and 128.43 ppm for the o-, b-, m- and p-phenyl C-atoms of the PPh$_3$ ligand, and at 33.44 ppm from the SCH$_2$ groups of the [9]aneS$_3$ macrocycle: no peaks were observed in the region of the spectrum expected for a coordinated CO ligand, due to the low solubility of

the compound. On the basis of the above data, the complex was formulated as the desired product $[Rh([9]aneS_3)(CO)(PPh_3)](PF_6)$; this was confirmed by microanalysis.

A single crystal structural analysis of this compound was performed, in order to ascertain the stereochemistry adopted by the complex cation.

5.2.10 Single Crystal Structure of $[Rh([9]aneS_3)(CO)(PPh_3)](PF_6)$

The solution and refinement of the structure are described in Section 5.4.16. Relevant bond lengths, angles and torsions are listed in Table 5.8, and the geometry of the complex is displayed in Figure 5.15.

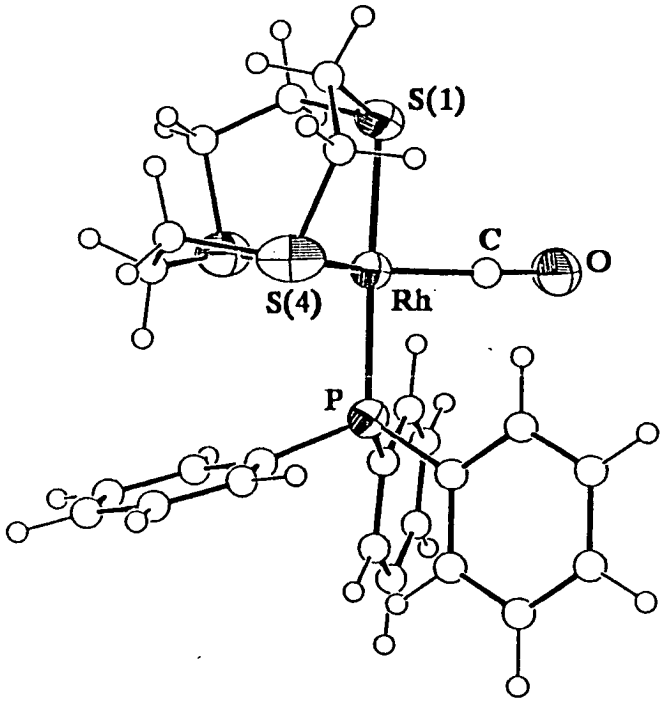

Figure 5.15: View of the Single Crystal Structure of $[Rh([9]aneS_3)(CO)(PPh_3)]^+$.

Single Crystal Structure of [Rh([9]aneS$_3$)(CO)(PPh$_3$)]-(PF$_6$)

Table 5.8. Bond Lengths(A), angles(degrees) and torsion angles(degrees) with standard deviations

Rh	- S(1)	2.335(3)	C	- O	1.129(11)
Rh	- S(4)	2.4504(23)	P	-C(26)	1.828(5)
Rh	- P	2.2972(24)	P	-C(34)	1.822(5)
Rh	- C	1.828(9)			

S(1)	- Rh -	S(4) 86.51(8)	Rh	- S(4) -C(13)	101.8(3)
S(1)	- Rh -	P 178.03(9)	Rh	- S(4) - C(5)	104.2(3)
S(1)	- Rh -	C 88.8(3)	Rh	- S(4) -C(15)	103.8(3)
S(4)	- Rh -S(4')	83.50(8)	C(3)	- S(4) - C(5)	99.3(4)
S(4)	- Rh -	P 94.96(8)	C(13)	- S(4) -C(15)	94.3(4)
S(4)	- Rh -	C 137.9(3)	Rh	- P -C(26)	115.26(18)
P	- Rh -	C 89.2(3)	Rh	- P -C(34)	112.18(18)
Rh	- C -	O 178.0(8)	C(26)	- P -C(26')	105.83(23)
Rh	- S(1) -	C(2) 104.88(25)	C(26)	- P -C(34)	103.54(23)
Rh	- S(1) -C(12)	100.8(3)	P	-C(26) -C(21)	120.4(3)
C(2)	- S(1) -C(12')	103.6(3)	P	-C(26) -C(25)	119.4(3)
C(12)	- S(1) -C(2')	103.6(3)	P	-C(34) -C(31)	120.1(3)
Rh	- S(4) -	C(3) 96.47(24)	P	-C(34) -C(31')	119.0(3)

C(12')	- S(1) - C(2) -	C(3) 138.8(5)	C(26')	- P -C(26) -C(21)	-57.6(4)
C(2')	- S(1) -C(12) -C(13)	53.9(6)	C(26')	- P -C(26) -C(25)	118.2(4)
S(1)	- C(2) - C(3) -	S(4) -63.1(5)	C(34)	- P -C(26) -C(21)	50.9(4)
S(1)	-C(12) -C(13) -	S(4) 63.0(6)	C(34)	- P -C(26) -C(25)	-133.3(4)
C(2)	- C(3) - S(4) -	C(5) -48.7(5)	C(26)	- P -C(34) -C(31)	39.1(4)
C(12)	-C(13) - S(4) -C(15)	-142.4(5)	C(26)	- P -C(34) -C(31')	-148.7(4)
C(3)	- S(4) - C(5) -C(15')	144.0(5)	C(22)	-C(21) -C(26) - P	175.8(4)
C(13)	- S(4) -C(15) -C(5')	56.9(6)	C(24)	-C(25) -C(26) - P	-175.8(4)
S(4)	- C(5) -C(15')	-S(4') -61.8(6)	C(32)	-C(31) -C(34) - P	171.3(3)
S(4)	-C(15) -C(5')	-S(4') 61.8(6)	C(32')	-C(31') -C(34) - P	-171.4(3)

The complex adopts a trigonal bipyramidal stereochemistry, with axial PPh_3 and equatorial CO ligands. The cation lies on a crystallographic mirror plane, which passes through the Rh centre, the axial S- and P-donors, and the CO ligand. The $S-CH_2-CH_2-S$ linkages of the [9]aneS_3 macrocycle were disordered over two distinct orientations about this mirror plane; the high thermal parameters of the C atoms of the phenyl ring perpendicular to the mirror plane implied that these may also be disordered, although this latter disorder was not modelled. The Rh-S distances are similar to those exhibited by the other Rh^I [9]aneS_3 complexes [Rh-S(1) = 2.335(3), Rh-S(4) = 2.4504(23) Å]. The *trans* angle S(1)-Rh-P is close to 180°, but the angles within the equatorial plane are distorted by the rigidity of the [9]aneS_3 ring [<S(1)-Rh-P = 178.03(9), <S(4)-Rh-C = 137.9(3), <S(4)-Rh-S(4′) = 83.50(8)°]. This geometry is similar to that exhibited by the analogous d^8 complex $[Pt([9]aneS_3)(PPh_3)_2]^{2+}$ [80].

5.2.11 Reactions of $[Rh([9]aneS_3)(L)_2]^+$ (L = C_2H_4, $\frac{1}{2}C_8H_{12}$) with Electrophiles

Reaction of $[Rh([9]aneS_3)(C_2H_4)_2]^+$ or $[Rh([9]aneS_3)(C_8H_{12})]^+$ with one molar equivalent of tetracyanoethene (tcne) in acetone, CH_3CN or CH_2Cl_2 under N_2 at 298K or under reflux led to the formation of intense orange or green solutions, from which solid products could be

isolated by reduction of the solutions to approximately 1 cm^3 volume and the addition of excess diethyl ether. Solutions of the orange products became green on addition of excess tcne.

Both orange and green products obtained from $[Rh([9]aneS_3)(C_8H_{12})](PF_6)$ exhibited similar spectral properties. Their I.R. spectra exhibited peaks arising from $[9]aneS_3$, cod and tcne ligands and PF_6^- counterion, with one C≡N stretching vibration at 2200 cm^{-1} (c.f. for free tcne $\nu_{C\equiv N}$ = 2258 and 2220 cm^{-1}), and f.a.b. mass spectrometry showed peaks at M^+ = 391 and 283, assigned to the molecular ions $[^{103}Rh([9]aneS_3)(C_8H_{12})]^+$ and $[^{103}Rh([9]aneS_3)]^+$; no mass peaks consistent with coordination of the tcne ligand were observed. Elemental analytical data was consistent with the formation of adducts $[Rh([9]aneS_3)(C_8H_{12})].(tcne)_n(PF_6)$ (n = 0-1). Cyclic voltammograms of the products in CH_3CN/0.1M $^nBu_4NPF_6$ at 298K showed a broad irreversible oxidation at $Ep_a \simeq +0.45V$ *vs.* Fc/Fc^+ (scan rate 400 mV/s), and two chemically reversible reduction processes at $E_{\frac{1}{2}}$ = - 0.16V and -1.19V [c.f. for $[Rh([9]aneS_3)(C_8H_{12})]^+$ Ep_a = + 0.29V (Section 5.2.13), for free tcne $E_{\frac{1}{2}}$ = -0.17V and -1.17V under identical conditions]. On the basis of these results, the orange and green products were formulated as charge transfer complexes $[Rh([9]aneS_3)(C_8H_{12})(tcne)](PF_6)$, rather than as the formally oxidised species $[Rh([9]aneS_3)(C_8H_{12})]^{2+}[tcne]^-(PF_6)$. Both types of

metal/tcne compound are well known: for example, reaction of ferrocene with tcne affords a charge transfer complex $[(cp)_2Fe(tcne)]$, whilst $[(C_5Me_5)_2Fe]$ undergoes formal electron transfer with tcne to form a salt $[(C_5Me_5)_2Fe]^+[tcne]^-$ [236,237]. The analogous products derived from $[Rh([9]aneS_3)(C_2H_4)_2](PF_6)$ were much less stable than $[Rh([9]aneS_3)(C_8H_{12})(tcne)]^+$, and hence were not well characterised. I.R. spectroscopy showed that the ethene complexes also contained [9]aneS$_3$, tcne and PF_6^- with $\nu_{C\equiv N}$ = 2200 cm^{-1}, however, and these species were therefore also assigned as charge-transfer complexes $[Rh([9]aneS_3)(C_2H_4)_2(tcne)](PF_6)$.

In contrast to the above results, reaction of $[Rh([9]aneS_3)(C_8H_{12})](BF_4)$ with tcne in refluxing CH_3CN under N_2 for 1 hr afforded a yellow solution, from which a pale yellow solid could be isolated by reduction of the solution to 1 cm^3 followed by addition of diethyl ether. The I.R. spectrum of this compound exhibited peaks due to coordinated [9]aneS$_3$ and tcne ($\nu_{C\equiv N}$ = 2320 m, 2295 m, 2245 w, 2220 s, 2150 cm^{-1}) and BF_4^- counterion. F.a.b. mass spectrometry gave peaks at M^+ = 452, 411, 323 and 283, which were consistent with the fragments $[^{103}Rh([9]aneS_3)(tcne)(CH_3CN)]^+$, $[^{103}Rh([9]aneS_3)(tcne)]^+$, $[^{103}Rh([9]aneS_3\text{-}H)(CH_3CN)]^+$ and $[^{103}Rh([9]aneS_3)]^+$ respectively. The product was therefore formulated as $[Rh([9]aneS_3)(tcne)(CH_3CN)](BF_4)$, an assignment supported by microanalysis. The ^{1}H n.m.r. spectrum of this complex

in CD_3CN at 298K showed two identical multiplets at δ = 3.64 and 1.79 ppm, consistent with a non-fluxional [9]aneS_3 ligand bound to a d^6 Rh^{III} centre. The $^{13}C\{^1H\}$ n.m.r. spectrum gave three resonances in the region expected for coordinated [9]aneS_3 at δ = 37.27, 34.06 and 33.53 ppm, also implying a static structure for the complex: no resonances from the tcne ligand could be observed because of the low solubility of the compound. Cyclic voltammetry of $[Rh([9]aneS_3)(tcne)(CH_3CN)]^+$ in CH_3CN/0.1M $^nBu_4NPF_6$ at 298K showed two overlapping irreversible one-electron reduction waves at Ep_C = -1.36V *vs.* Fc/Fc^+ (scan rate 400 mV/s; n = 1.93 electrons for the two reductions by coulometry), and a third irreversible reduction at Ep_C = 2.14V: no oxidative processes or reversible waves due to free tcne were observed. Hence, the compound was tentatively assigned as the Rh^{III} complex $[Rh([9]aneS_3)(\eta^2\text{-tcne})(CH_3CN)](BF_4)$ (60), where formal oxidative addition across the tcne C=C bond has occurred. Improved ^{13}C n.m.r. data or an x-ray structural analysis would be needed to confirm this assignment. Reaction of $[Rh([9]aneS_3)(C_2H_4)_2]^+$ with tcne under identical conditions led to insoluble decomposition products, which could not be characterised.

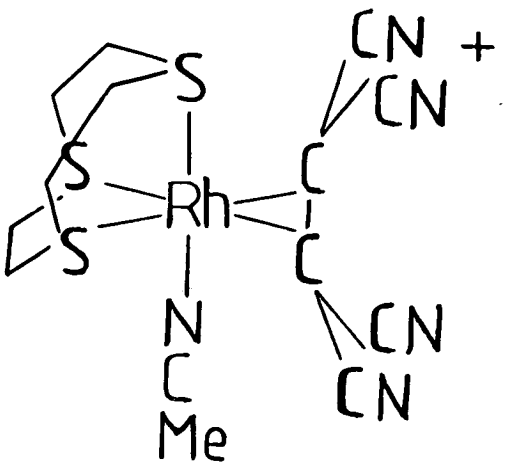

(60)

Treatment of a solution of $[Rh_2(C_2H_4)_2(C_2F_4)_2Cl_2]$ (generated by bubbling C_2F_4 through a THF solution of $[Rh_2(C_2H_4)_4Cl_2]$ at 298K for 30 mins[238]) with one molar equivalent of [9]aneS_3 and NH_4PF_6 at 298K under N_2 gave a pale yellow solution, from which a pale tan solid could sometimes be isolated after filtration and reduction of the solution by addition of diethyl ether. I.R. spectroscopy confirmed the presence of [9]aneS_3, C_2F_4 and NH_4PF_6 in this product, and f.a.b. mass spectrometry showed peaks at M^+ = 411, 383 and 282, attributable to the molecular ions $[^{103}Rh([9]aneS_3)(C_2H_4)(C_2F_4)]^+$, $[^{103}Rh([9]aneS_3)(C_2F_4)]^+$ and $[^{103}Rh([9]aneS_3\text{-}H)]^+$, leading to the tentative assignment of the product as $[Rh([9]aneS_3)(C_2H_4)(C_2F_4)](PF_6)$. Unfortunately the compound was thermally unstable, decomposing to a red oil after 24 hours *in vacuo* at 298K or after 30 mins in THF or acetone solutions under N_2 above 273K; this prevented its further characterisation.

No reaction was observed between $[Rh([9]aneS_3)(C_2H_4)_2]$-$(PF_6)$ and C_2F_4 in THF at 298K, with the *bis*-ethene complex being recovered unchanged.

Attempts to protonate $[Rh([9]aneS_3)(C_2H_4)_2]^+$ and $[Rh([9]aneS_3)(cod)]^+$ with HBF_4 via dropwise addition of $HBF_4.CH_3OCH_3$ to CH_2Cl_2 solutions of these complexes under N_2 at 298K were unsuccessful, leading only to recovery of unreacted starting material. Similarly, no reaction was observed between $[Rh([9]aneS_3)(C_2H_4)_2]^+$ and CS_2 in THF under N_2 at 298K or 338K.

The results described in this section contrast with the behaviour of $[(cp)Rh(C_2H_4)_2]$ and $[(acac)Rh(C_2H_4)_2]$, which readily form stable adducts with electrophiles $[(L)Rh(C_2H_4)(E)]$ (L = cp^-, $acac^-$; E = SO_2, C_2F_4, tcne)[214,238,239]. The square-planar complex $[Rh([14]aneS_4)]^+$ also gives stable 1:1 complexes with tcne, H^+, SO_2, BF_3 and O_2[202]. The reluctance of $[Rh([9]aneS_3)(C_2H_4)_2]^+$ and $[Rh([9]aneS_3)(C_8H_{12})]^+$ to form adducts with electrophiles such as tcne or C_2F_4 shows that the Rh centres in these complexes have relatively low nucleophilic character in comparison to many other Rh^I compounds. This is consistent with the low barrier to ethene rotation observed for $[Rh([9]aneS_3)(C_2H_4)_2]^+$ (Sections 5.2.1, 6.2.2), and with the overall positive charge for these cations.

5.2.12 Other Reactions of $[Rh([9]aneS_3)(L)(L')]^+$ (L = C_2H_4, CO; L' = C_2H_4, PR_3)

Reaction of $[Rh([9]aneS_3)(C_2H_4)_2]^+$ or $[Rh([9]aneS_3)(C_2H_4)(Pcyc_3)]^+$ with stoichiometric amounts of CH_3COCl, Me_3SiCl, I_2 or CH_3I in acetone or THF or by stirring in $CHCl_3$ or CH_2Cl_2, under N_2 at temperatures above 273K resulted in the rapid formation of insoluble yellow (for Cl-containing substrates) or orange (for I_2 or CH_3I) products. On the basis of I.R. spectroscopy and micro-analytical data, these products were formated as $[Rh([9]aneS_3)X_3]$ (X = Cl, I). The I.R. spectrum of $[Rh([9]aneS_3)Cl_3]$ showed, in addition to peaks from the $[9]aneS_3$ ligand, absorbances at 340 and 290 cm^{-1} which could correspond to Rh-Cl stretching vibrations. This implies that this compound has a mononuclear structure, with terminally bound Cl^- ligands; the insolubility of both $[Rh([9]aneS_3)X_3]$ complexes in solvents other than dmso prevented their further characterisation, however.

Most attempts to isolate soluble intermediates from the above reactions were unsuccessful: below *ca.* 273K no reaction occurred, whilst above 273K the formation of the $[Rh([9]aneS_3)X_3]$ products was complete within 3 minutes of the initial mixing of the reactants. However, the reaction of $[Rh([9]aneS_3)(C_2H_4)(Pcyc_3)](PF_6)$ with neat CH_2Cl_2 at 298K occurred less rapidly, and a small amount (<5 mg) of orange solid could sometimes be isolated from this reaction mixture, after reduction of the solution and

filtration, by crystallisation with ^{n}hexane at 253K. I.R. spectroscopy of this product confirmed the presence of [9]aneS_3, Pcyc$_3$ and PF_6^-, and its f.a.b. mass spectrum exhibited peaks at M^+ = 647, 611, 598, 563 and 332, which were assigned to $[^{103}Rh([9]aneS_3\text{-}H)(Pcyc_3)(CH_2{}^{35}Cl)^{35}Cl]^+$, $[^{103}Rh([9]aneS_3\text{-}H)(Pcyc_3)(CH_2{}^{35}Cl)]^+$, $[^{103}Rh([9]aneS_3)(Pcyc_3)^{35}Cl]^+$, $[^{103}Rh([9]aneS_3)(Pcyc_3)]^+$ and $[^{103}Rh([9]aneS_3)(CH_2{}^{35}Cl)]^+$ respectively. This led to the tentative formulation of this species as the initial oxidative addition product $[Rh([9]aneS_3)(Pcyc_3)\text{-}(CH_2Cl)Cl](PF_6)$, although full characterisation was not attempted because of the low yields obtained.

No reaction was observed between $[Rh([9]aneS_3)\text{-}(C_8H_{12})]^+$ and CH_3I, CH_3COCl or CH_2Cl_2 at 298K or under reflux using the methodology described above. $[Rh([9]aneS_3)(CO)(PPh_3)](PF_6)$ did not react with CH_2Cl_2 under reflux, but rapidly formed $[Rh([9]aneS_3)I_3]$ on reaction with CH_3I in refluxing acetone under N_2.

The reactivity of $[Rh([9]aneS_3)(C_2H_4)_2]^+$ towards benzene (in C_6H_6) and $HSiEt_3$ (two-fold excess in THF) was examined. At 298K under N_2 no reaction was observed between $[Rh([9]aneS_3)(C_2H_4)_2](PF_6)$ and C_6H_6 or $HSiEt_3$ after 1 hr, the *bis*-ethene complex being recovered intact from the reaction mixtures. When reacted under refluxing conditions under N_2 for 30 mins, both C_6H_6 and $HSiEt_3$ reactions afforded red solutions from which rust-red solids could be isolated by reduction to 1 cm^3 and

addition of diethyl ether. The products from both reactions exhibited I.R. and f.a.b. mass spectra similar to those given by the thermal decomposition products of $[Rh([9]aneS_3)(C_2H_4)_2]^+$ (*vide infra*), and gave complex ^1H n.m.r. spectra in d^6-acetone at 298K indicative of a mixture of $[9]aneS_3$-containing complexes. No evidence for incorporation of C_6H_6 or $HSiEt_3$ into the metal-based products of these reactions was observed in any of these spectra. These results imply that intra-molecular decomposition of $[Rh([9]aneS_3)(C_2H_4)_2]^+$ occurs preferentially over activation of external aryl C-H or silane Si-H bonds under thermal conditions.

The decomposition reaction of $[Rh([9]aneS_3)(C_2H_4)_2]^+$ in refluxing acetone or THF under N_2 for 30 mins gave a red solution, from which red-brown solids could be isolated after filtration and reduction of the solutions by addition of diethyl ether. The same product could be obtained by the thermal decomposition of solid $[Rh([9]aneS_3)(C_2H_4)_2](PF_6)$ at 298K *in vacuo* for 2 weeks. These red compounds exhibited I.R. spectra that showed peaks due to coordinated $[9]aneS_3$ and PF_6^- only. F.a.b. mass spectroscopy showed major peaks at M^+ = 477, 449, 421, 393, 365 and 337, which correspond to the molecular ions $[^{103}Rh([9]aneS_3)(C_2H_4)_n\text{-}2H]^+$ (n = 2-7, Figure 5.16). This reaction was followed by ^1H n.m.r. spectroscopy in d^6-acetone in a sealed tube at 298K. After 30 mins at 298K, the reaction mixture exhibited new resonances at δ =

5.64, 5.38 and 1.62 ppm in addition to peaks due to coordinated [9]aneS$_3$ ($\delta \simeq 3.1$ ppm) and π-bound C_2H_4 (δ = 2.76 ppm, Figure 5.17a). After a further 30 mins, the peaks at δ = 5.64, 5.38, 3.10 and 2.76 ppm were still present, whilst several new resonances between δ = 4.5 and 1.5 ppm were also observed (Figure 5.17b). Neither spectrum exhibited resonances at negative chemical shift that could be assigned to hydride ligands. A ^{13}C d.e.p.t. n.m.r. spectrum obtained after *ca.* 2 hours reaction at 298K showed an intense peak at δ = 34.62 ppm due to the [9]aneS$_3$ ligand, together with weaker resonances at δ = 52.3, 46.4, 41.4, 37.1 and 32.0 ppm. These results suggest that [Rh([9]aneS$_3$)$(C_2H_4)_2$]$^+$ decomposes via the coupling of ethene ligands. Further experiments are required to determine the mechanism of this reaction and to characterise the products formed. However, the absence of hydride resonances in the ^1H n.m.r. spectra described above shows that if ethene activation proceeds via oxidative addition across the ethene C-H bonds, then the resultant Rh-H product must be very short-lived. Given the known electrophilic characters of the [Rh([9]aneS$_3$)]$^+$ fragment (Sections 5.2.1 and 5.2.11), more likely mechanisms for ethene activation in this system are nucleophilic attack at a coordinated ethene ligand (61), or the formation of a Rh^{III} metallacyclopentane species (62). In both cases, insertion of coordinated ethene into the resultant Rh-C bond would cause coupling of the ethene

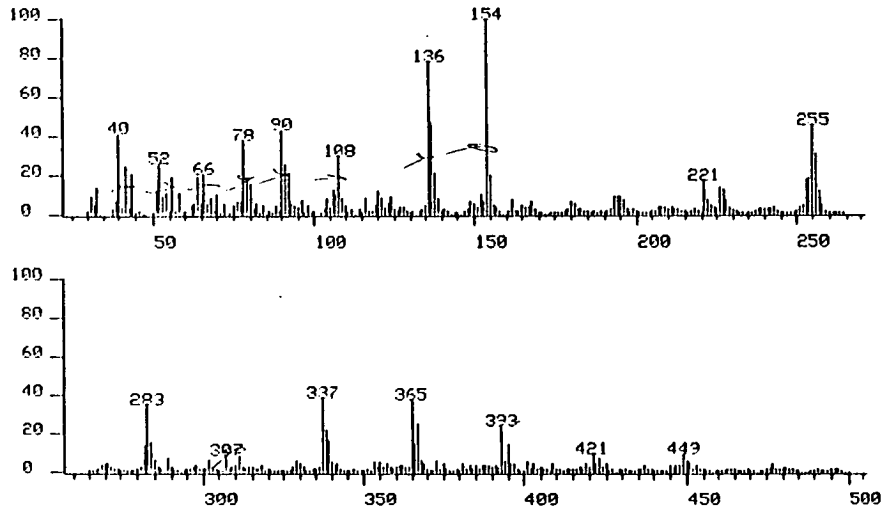

Figure 5.16: F.a.b. Mass Spectrum of the Thermal Decomposition Product of [Rh([9]aneS_3)-(C_2H_4)$_2$](PF_6) (3-NOBA matrix).

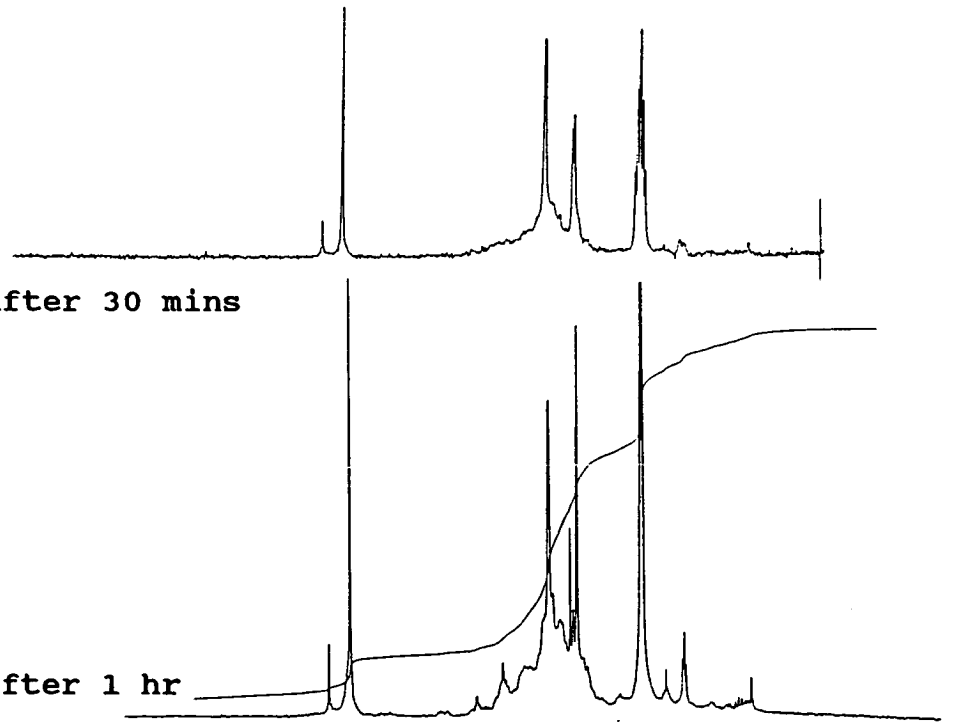

a) After 30 mins

b) After 1 hr

Figure 5.17: ^{1}H n.m.r. Spectra Following the Thermal Decomposition of [Rh([9]aneS_3)(C_2H_4)$_2$]-(PF_6) (200.13 MHz, d^6-acetone, 298K).

ligands (c.f. Ziegler-Natta polymerisation of alkenes[240]).

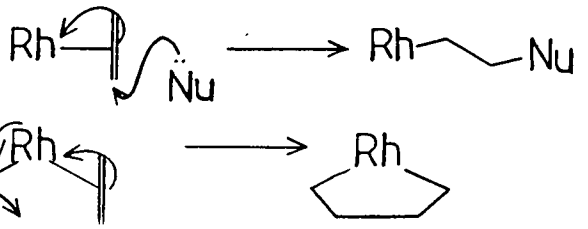

(61)

(62)

5.2.13 Electrochemical Study of $[Rh([9]aneS_3)(L)_2](PF_6)$

Cyclic voltammetry of $[Rh([9]aneS_3)(L)_2](PF_6)$ (L = C_2H_4, $\frac{1}{2}C_7H_8$, $\frac{1}{2}C_8H_{12}$, $\frac{1}{2}C_4H_6$) and of $[Rh([9]aneS_3)(CO)(PPh_3)](PF_6)$ in CH_3CN/0.1M $^nBu_4NPF_6$ at 298K showed in each case a single broad irreversible oxidation wave, with no well defined return waves from daughter products (Table 5.9, Figure 5.18). These processes remained irreversible at scan rates between 100 and 1000 mV/s at 298K and 253K. Coulometric determinations of these processes in CH_3CN/0.1M $^nBu_4NPF_6$ at 298K at a Pt basket electrode gave variable results between n = 1.5 and 2.0 electrons (Table 5.9), and controlled potential electrolysis of bulk samples of these compounds in CH_3CN/0.1M $^nBu_4NPF_6$ at 298K afforded pale yellow e.p.r. silent solutions. These results show that any Rh^{II} species formed from these Rh^I complexes decompose rapidly, probably via spontaneous oxidation to Rh^{III} products, or by disproportionation to form Rh^{III} and Rh^I species which are then re-oxidised. For those complexes that gave n<2, it is possible that a dimerisation process may also occur, to form diamagnetic metal-metal bonded

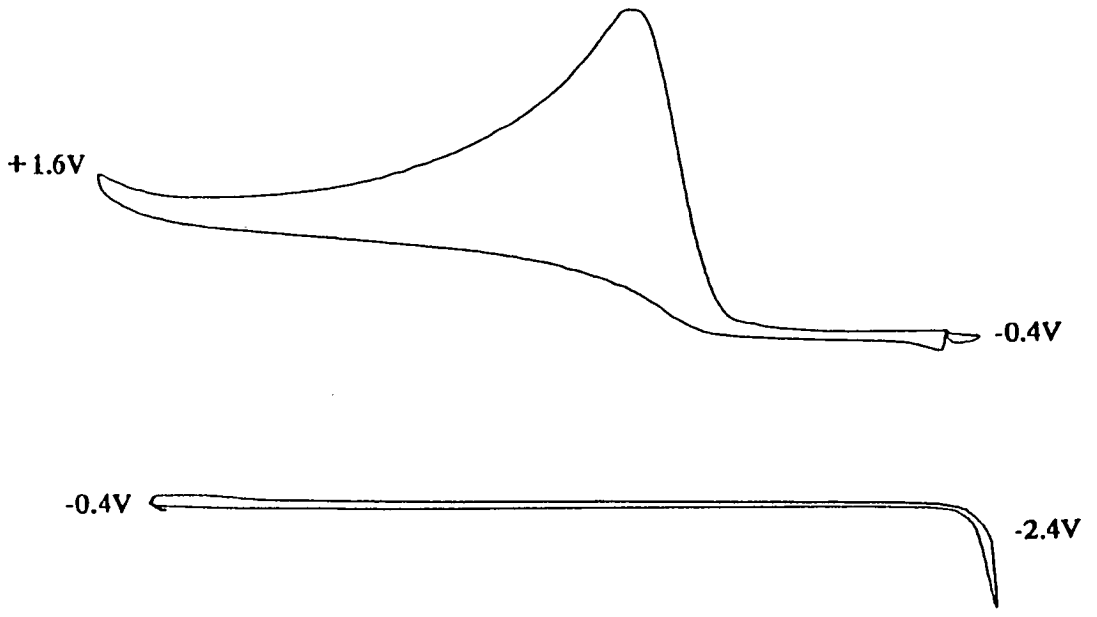

Figure 5.18: Cyclic Voltammogram of $[Rh([9]aneS_3)(C_8H_{12})](PF_6)$ (CH_3CN/0.1M $^nBu_4NPF_6$, 298K, scan rate 400 mV/s).

Complex	Ep_a(V)	n
$[Rh([9]aneS_3)(C_2H_4)_2](PF_6)$	+0.48	1.63
$[Rh([9]aneS_3)(C_8H_{12})](PF_6)$	+0.29	2.07
$[Rh([9]aneS_3)(C_7H_8)](PF_6)$	+0.30	1.78
$[Rh([9]aneS_3)(C_4H_6))](PF_6)$	+1.10	1.94
$[Rh([9]aneS_3)(CO)(PPh_3)](PF_6)$	+0.30	1.91

Table 5.9: Electrochemical Data for $[Rh([9]aneS_3)(L)_2](PF_6)$ (Potentials quoted *vs.* Fc/Fc^+ in CH_3CN/0.1M $^nBu_4NPF_6$, 298K, scan rate 400 mV/s).

Rh^{II}-Rh^{II} complexes (c.f. the complexes $[Ir([9]aneS_3)(L)_2]^+$, Section 6.2.10). Further experiments would be needed to characterise the processes occurring and products formed during oxidation of the complexes $[Rh([9]aneS_3)(L)_2]^+$.

5.3 CONCLUSIONS

The complexes $[Rh([9]aneS_3)(L)(L')]^+$ (L = C_2H_4, L' = C_2H_4, P^iPr_3, $Pcyc_3$; L,L' = $\frac{1}{2}C_7H_8$, $\frac{1}{2}C_8H_{12}$, $\frac{1}{2}C_4H_6$; L = CO, L' = PPh_3) have been synthesised and characterised. The compounds $[Rh([9]aneS_3)(C_2H_4)_2](BF_4)$, $[Rh([9]aneS_3(C_8H_{12})](BF_4)$ and $[Rh([9]aneS_3)(CO)(PPh_3)](PF_6)$ have been shown to adopt a variety of five-coordinate geometries in the solid state, which are related by rotation of the $[9]aneS_3$ macrocycle about the central Rh-$[9]aneS_3$ axis. This is consistent with the observed low barrier for this rotation process in solution, which suggests that slippage of the $[9]aneS_3$ ring from a tridentate to a bidentate mode of coordination in solution is not a favourable process and hence that the complexes maintain an 18-electron structure in solution. This is confirmed by the observed inactivity of $[Rh([9]aneS_3)(C_2H_4)_2]^+$ towards thermal nucleophilic substitution.

The low barrier to rotation of the ethene ligands in $[Rh([9]aneS_3(C_2H_4)_2]^+$ shows that Rh→ethene π-back donation is weak in this complex, and hence that the $[Rh([9]aneS_3)]^+$ fragment has greater electrophilic

character than analogous $[(C_5R_5)Rh]$ species (R = H, CH_3). This is confirmed by the low affinity of the $[Rh([9]aneS_3)]^+$ fragment for the electrophilic ligands C_2F_4, tcne and H^+. The electrophilicity of the complexes $[Rh([9]aneS_3)(L)_2]^+$ probably arises from their cationic charge, as well as from the properties of the $[9]aneS_3$ protecting group. The electronic structures of the complexes $[Rh([9]aneS_3)(C_2H_4)_2]^+$ and $[Rh([9]aneS_3)-(C_4H_6)]^+$ are discussed further in Chapter 6.

Reaction of $[Rh([9]aneS_3)(C_2H_4)(L)]^+$ (L = C_2H_4, $Pcyc_3$) with halide-containing substrates or chlorinated solvents rapidly affords the insoluble complexes $[Rh([9]aneS_3)X_3]$. There is some evidence that these reactions may proceed via the oxidative addition products $[Rh([9]aneS_3)(L)(R)X]^+$ (for reaction with the substrate R-X), although no such intermediates were fully characterised. No reactions were observed between $[Rh([9]aneS_3)(C_2H_4)_2]^+$ and C_6H_6 or $HSiEt_3$ under thermal conditions. This is consistent with the electrophilic character of the Rh centre in this complex, since oxidative addition by a Rh^I complex across a C-H or Si-H bond involves formal nucleophilic attack by the metal ion at the C-H or Si-H σ^*-orbital and is therefore disfavoured for an electrophilic metal centre[241]. The thermal decomposition of $[Rh([9]aneS_3)(C_2H_4)_2]^+$ was studied by n.m.r. spectroscopy and f.a.b. mass spectrometry, which showed that this reaction probably involves coupling of the ethene ligands, although no

products or intermediates from the reaction mixture could be identified.

The complex $[Rh([9]aneS_3)(CO)_2]^+$ was unstable with respect to dimerisation to $[Rh_2([9]aneS_3)_2(\mu\text{-}CO)_2]^{2+}$. Heating this latter complex caused decomposition to a blue product(s) exhibiting several C≡O stretching frequencies. The attempted synthesis of $[Rh([9]aneS_3)(CO)Cl]$ caused the rapid formation of a different product which also showed several I.R. absorbances due to C≡O ligands. These unknown products may be mixtures of complexes, or they could be cluster compounds analogous to those derived from $[(cp)Rh(CO)_2]$[242]. The tendency of thioether ligands to form polynuclear or polymeric species with $[Rh_2(CO)_4Cl_2]$ has been noted previously[199].

These results show that the chemistry of the complexes $[Rh([9]aneS_3)(L)_2]^+$ merits further study, both to fully characterise the reactions described in this work and to investigate other forms of reactivity. In particular, the photochemistry of these Rh complexes in the presence of nucleophiles or oxidative addition substrates might yield interesting results, since they exhibit several absorptions in the visible and near U.V. regions of the spectrum. The analogous species $[(C_5R_5)M(L)_2]$ (R = H, CH_3; M = Rh, Ir; L = C_2H_4, CO) readily undergo nucleophilic substitution and oxidative addition of C-H and Si-H bonds under photolytic conditions, although these reactions are slow under thermal conditions.

5.4 EXPERIMENTAL

5.4.1 Synthesis of $[Rh_2(C_2H_4)_4Cl_2]$[243]

$RhCl_3.3H_2O$ (1.00 g, 3.8 x 10^{-3} mol) was dissolved in methanol (30 cm^3) and water (2 cm^3). The solution was purged with ethene at room temperature for 2 hrs, then left to stand under an ethene atmosphere for 24 hrs. The resulting red crystals were filtered and washed with cold methanol. Yield 0.37 g, 60%. Mol. wt. 388.94. Elemental analysis: found C = 24.5, H = 4.08%; calculated for $[C_8H_{16}Rh_2Cl_2]$ C = 24.7, H = 4.15%. I.R. spectrum (KBr disc): 3050 w, 2980 w, 2890 w, 1505 m, 1425 s, 1210 s, 990 s, 950 m, 925 m, 810 w, 710 m, 670 m, 495 w, 390 s, 300 w cm^{-1}.

5.4.2 Synthesis of $[Rh_2(C_8H_{14})_4Cl_2]$[244]

$RhCl_3.3H_2O$ (1.00 g, 3.8 x 10^{-3} mol) and cyclooctene (3 cm^3) were dissolved in 4:1 2-propanol/water (25 cm^3). The mixture was degassed, and then left to stand under N_2 at room temperature for 5 days. The product was an orange precipitate, which was filtered and washed with 2-propanol (Yield 0.89 g, 65%). Mol. wt. 717.53. Elemental analysis: found C = 53.4, H = 7.93%; calculated for $[C_{32}H_{56}Rh_2Cl_2]$ C = 53.6, H = 7.87%. I.R. spectrum (KBr disc): 2970 m, 2910 s, 2840 s, 2660 w, 1460 s, 1440 m, 1380 w, 1350 m, 1320 w, 1270 w, 1255 w, 1230 w, 1165 w, 1140 w, 1120 w, 1085 w, 1015 w, 980 w, 970 w, 950 m, 895 m, 875 w, 840 w, 825 w, 810 w, 765 w, 730 w, 700 w,

615 m, 550 m, 520 s, 410 m, 315 w cm^{-1}.

5.4.3 Synthesis of $[Rh_2(C_8H_{12})_2Cl_2]$[245]

$RhCl_3.3H_2O$ (0.60 g, 2.3 x 10^{-3} mol) and 1,5-cycloocta-diene (1 cm^3) were dissolved in 5:1 ethanol/water (6 cm^3), and the resulting solution refluxed for 18 hrs during which time an orange precipitate formed. The mixture was allowed to cool, and the product was filtered and washed with pentane. Yield 0.46 g, 82%. Mol. wt. 493.09. Elemental analysis: found C = 39.1, H = 4.83%; calculated for $[C_{16}H_{24}Rh_2Cl_2]$ C = 39.0, H = 4.90%. I.R. spectrum (KBr disc): 2980 w, 2920 m, 2860 m, 2820 m, 1465 m, 1420 m, 1365, w, 1320 m, 1300 m, 1225 w, 1210 w, 1170 m, 1150 w, 1075 w, 990 m, 960 s, 870 m, 830 w, 815 s, 790 w, 770 m, 690 w, 510 w, 475 m, 430 w, 380 m cm^{-1}.

5.4.4 Synthesis of $[Rh_2(CO)_4Cl_2]$[246]

$RhCl_3.3H_2O$ (1.00 g, 3.8 x 10^{-3} mol) was placed on a medium porosity glass frit in a reaction vessel[246], and heated in an oil bath to 95°C. CO gas was blown over the $RhCl_3.3H_2O$ for 20 hrs, whereupon a red solid sublimed up the reaction tube. The product was extracted from the vessel with diethyl ether (200 cm^3). The resulting solution was filtered, reduced to ~30 cm^3, and the red crystalline product left to crystallise at -30°C. Yield 0.54 g, 73%. Mol. wt. 388.75. Elemental analysis: found C = 12.3%; calculated for $[C_4O_4Cl_2Rh_2]$ C = 12.4%. I.R.

spectrum ($MeNO_2$ solution) 2095 s, 2030 s cm^{-1}.

5.4.5 Synthesis of $[Rh(CO)Cl(PPh_3)_2]$[247]

$RhCl_3.3H_2O$ (0.50 g, 1.9 x 10^{-3} mol) and PPh_3 (2.49 g, 9.5 x 10^{-3} mol) were refluxed in dmf (30 cm^3) for 2 hrs. Hot MeOH (60 cm^3) was then added to the yellow solution, and the mixture left to crystallise at -30°C. The golden yellow microcrystalline product was filtered, washed with methanol and dried *in vacuo* (Yield 1.12 g, 86%). Mol. Wt. 690.95. Elemental analysis: found C = 63.7, H = 4.30%; calculated for $[C_{37}H_{30}P_2ClORh]$ C = 64.3, H = 4.37%. I.R. spectrum ($CHCl_3$ solution) 1980 cm^{-1}. I.R. spectrum (KBr disc) 3060 w, 3040 w, 1965 s, 1920 2, 1585 w, 1570 w, 1480 s, 1435 s, 1385 w, 1330 w, 1305 w, 1285 w, 1180 m, 1160 w, 1120 w, 1090 s, 1070 w, 1025 m, 1000 m, 970 w, 925 w, 845 w, 745 s, 705 m, 690 s, 620 w, 575 s, 550 m, 520 s, 510 s, 455 m, 440 m, 420 m, 380 w, 340 w, 310 m cm^{-1}.

5.4.6 Synthesis of $[Rh([9]aneS_3)(C_2H_4)_2](BF_4)$

Reaction of $[Rh_2(C_2H_4)_4Cl_2]$ (0.032 g, 0.8 x 10^{-4} mol) with $[9]aneS_3$ (0.030 g, 1.6 x 10^{-4} mol) and $NaBF_4$ (0.018 g, 1.6 x $1_0{}^{-4}$ mol) in acetone (6 cm^3) under N_2 at room temperature for 15 mins yielded an intense yellow solution. this solution was filtered, reduced to 1 cm^3 volume, and the crude product crystallised with diethyl ether. The yellow complex was recrystallised from

CH_2Cl_2/hexane at 243K (yield 0.025 g, 35%). Mol. wt. 426.12. Elemental analysis: found C = 27.3, H = 4.55%; calculated for $[C_{10}H_{20}S_3Rh](BF_4).\frac{1}{2}CH_2Cl_2$ C = 26.9, H = 4.52%. F.a.b. mass spectrum: found M^+ = 339, 311, 283; calculated for

$[^{103}Rh([9]aneS_3)(C_2H_4)_2]^+$ $M^+ = 339$

$[^{103}Rh([9]aneS_3)(C_2H_4)]^+$ $M^+ = 311$

$[^{103}Rh([9]aneS_3)]^+$ $M^+ = 283$

^1H n.m.r. spectrum (360.13 MHz, 233K, d^6-acetone) δ = 3.22-3.02 ppm (m, 12H, [9]aneS$_3$), 2.76 (d, $^2J_{Rh-H}$ = 1.6 Hz, 4H, C_2H_4). ^{13}C D.E.P.T. n.m.r. spectrum (50.32 MHz, 233K, d^6-acetone) δ = 51.41 ppm (d, $^1J_{Rh-C}$ = 9.6 Hz, C_2H_4), 33.78 (s, [9]aneS$_3$). U.V./vis spectrum (CH_3CN) λ_{max} = 380 nm (ε_{max} = 590 $dm^3.mol^{-1}.cm^{-1}$), 298 (2,360), 234 (9,295). I.R. spectrum (KBr disc) 3040 w, 2940 m, 2900 w, 1515 w, 1440 s, 1410 s, 1380 w, 1300 m, 1255 w, 1165 m, 1060 vs, 1030 m, 990 w, 970 w, 940 w, 905 m, 815 s, 770 w, 660 w, 620 w, 570 w, 525 s, 480 m, 450 w, 410 w cm^{-1}.

5.4.7 Single Crystal Structure of [Rh([9]aneS$_3$)(C_2H_4)$_2$](BF$_4$)

Solvent diffusion of hexane into a CH_2Cl_2 solution of the complex under N_2 at -35°C yielded yellow plates of x-ray quality. A suitable crystal was selected, mounted on a glass fibre, and cooled to 173K with an Oxford Cryosystems low temperature device.

Crystal data:

$[C_{10}H_{10}S_3Rh](BF_4)$, Mr = 426.12. Monoclinic, space group $P2_1/c$, a = 10.720(12), b = 8.547(17), c = 32.890(49) Å, β = 92.622(105)°, V = 3010.6 Å^3 (by least-squares refinement on diffraction angles for 12 centred reflections measured at $\pm\omega$ [$15<2\theta<26°$, λ = 0.71073 Å]), Z = 8, D_C = 1.880 g.cm^{-3}. Crystal dimensions 0.46 x 0.27 x 0.019 mm, μ(Mo-K_α) = 1.541 mm^{-1}, $F(000)$ = 1712.

Data Collection and Processing:

Stoë STADI-4 four-circle diffractometer, $\omega/2\theta$ scan mode with ω scan width (1.40 + 0.347 tanθ)°. Graphite-monochromated Mo-K_α radiation: 5030 data measured ($2\theta_{max}$ = 45°, h -11→11, k 0→9, l 0→35), 3237 unique (R_{int} = 0.0912) giving 1612 with $F>4\sigma(F)$. No crystal decay, no absorption correction.

Structure Analysis and Refinement:

A Patterson synthesis located the Rh atoms, and the structure was developed using least-squares refinement and difference Fourier synthesis to reveal all other non-H atom positions. An empirical absorption correction was made using DIFABS (maximum correction 1.689, minimum 1.127). Anisotropic thermal parameters were refined for Rh, S and F atoms. The H atoms were included in fixed,

calculated positions, with the ethene H atoms fixed so that C-H = 1.08 Å, C-C-H = 120°, Rh-C-C-H = ±103° [248]. At convergence R = 0.0825, R_W = 0.0910, S = 1.179 for 233 parameters. The weighting scheme $w^{-1} = \sigma^2(F)+0.000185F^2$ gave satisfactory agreement analyses. The final difference Fourier synthesis contained no peak above + 1.11 or below -1.17 eÅ^{-3}.

5.4.8 Synthesis of [Rh([9]aneS$_3$)(C$_8$H$_{12}$)](PF$_6$)

Reaction of [Rh$_2$(cod)$_2$Cl$_2$] (0.041 g, 0.8 x 10^{-4} mol) with [9]aneS$_3$ (0.030 g, 1.6 x 10^{-4} mol) and NH$_4$PF$_6$ (0.027 g, 1.6 x 10^{-4} mol) in acetone (6 cm^3) under N$_2$ at 298K for 30 mins yielded a yellow solution. This solution was filtered, reduced to ~1 cm^3, and the crude compound crystallised with diethyl ether. The yellow solid product was recrystallised from dichloromethane/hexane, and dried *in vacuo* (yield 0.062 g, 70%). Mol. wt. 536.34. Elemental analysis: found C = 31.4, H = 4.47%; calculated for [C$_{14}$H$_{24}$S$_3$Rh](PF$_6$) C = 31.4, H = 4.51%. F.a.b. mass spectrum: found M$^+$ = 391, 282; calculated for

[^{103}Rh([9]aneS$_3$)(cod)]$^+$ M$^+$ = 391

[^{103}Rh([9]aneS$_3$-H)]$^+$ M$^+$ = 282

^{1}H n.m.r. spectrum (360.13 MHz, CD$_3$NO$_2$, 298K) δ = 4.10 ppm (br, 4H, cod C*H*), 3.01-2.79 (m, 12H, [9]aneS$_3$), 2.52 (M, 4H, cod C*H*$_2$), 2.20 (M, 4H, cod CH$_2$). ^{13}C D.E.P.T. n.m.r. spectrum (50.32 MHz, CD$_3$NO$_2$, 298K) δ = 78.33 ppm (d, $^1J_{Rh-C}$ = 11 Hz, cod *C*H), 33.84 (s, [9]aneS$_3$), 30.80 (s,

cod CH_2). U.V./vis spectrum (MeCN): λ_{max} = 390 nm (sh), 304 (ε_{max} = 2,460 $dm^3.mol^{-1}.cm^{-1}$), 245 (14,780), 220 (25,870). I.R. spectrum (KBr disc) 2980 w, 2920 m, 2860 m, 2810 m, 1470 w, 1440 s, 1410 s, 1380 w, 1325 m, 1300 m, 1285 m, 1260 w, 1245 m, 1215 m, 1170 s, 1120 w, 1090 w, 1010 w, 980 w, 935 m, 900 m, 890 w, 875 m, 840 vs, 780 w, 685 w, 660 w, 620 w, 560 s, 505 w, 480 m, 445 w, 385 w cm^{-1}.

5.4.9 Single Crystal Structure of [Rh([9]aneS$_3$)-(C_8H_{12})](BF$_4$)

A sample of [Rh([9]aneS$_3$)(cod)](BF$_4$) was prepared in an analogous method to the PF_6^- salt, using $NaBF_4$ (0.018 g, 1.6 x 10^{-4} mol) as the counterion metathesis agent. Recrystallisation of this complex from acetonitrile/diethyl ether yielded orange plates of x-ray quality.

Crystal Data:

$[C_{14}H_{24}S_3Rh](BF_4)$, Mr = 478.20. Triclinic, space group $P\bar{1}$, a = 11.4911(134), b = 12.8026(64), c = 13.3770(145) Å, α = 88.121(66), β = 70.300(80), γ = 74.683(70)°, V = 1783.5 $Å^3$ (by least-squares refinement at angles for 14 centred reflections measured at $\pm\omega$ [41<2θ<44°, λ = 1.54184 Å]), Z = 4, D_C = 1.781 $g.cm^{-3}$. Crystal dimensions 0.61 x 0.61 x 0.39 mm, μ(Cu-K_α) = 11.48 mm^{-1} F(000) = 968.

Data Collection and Processing:

Stoë STADI-4 four-circle diffractometer, $\omega/2\theta$ scan mode with ω scan-width $(0.70 + 0.347 \tan\theta)°$. Graphite-monochromated Cu-K_α radiation; 2838 reflections measured to $2\theta = 90°$ (h-9→10, k-11→11, ℓ0→12), 2787 unique, giving 2608 with $F>6\sigma(F)$. An initial absorption correction was applied using ψ-scans (max. and min. transmission factors 0.0889 and 0.0182 respectively). No crystal decay.

Structure Analysis and Refinement:

A Patterson synthesis located the Rh atom positions, and successive cycles of least-squares refinement and difference Fourier synthesis located all other non-H atoms. During refinement, the C atoms of one [9]aneS_3 ring were found to be disordered over two orientations; this was modelled using the fixed distances S-C = 1.83 Å, C-C = 1.52 Å, S-C-C = 2.74 Å. At isotopic convergence, an empirical absorption correction was applied using DIFABS (maximum correction 1.060, minimum 0.794). Anisotropic thermal parameters were refined for Rh, S, F and wholly occupied C atoms. H atoms were included in fixed, calculated positions. A secondary extinction coefficient was refined to 0.01607(79). The weighting scheme $w^{-1} = \sigma^2(F) + 0.007496\ F^2$ gave satisfactory agreement analyses. At final convergence $R = 0.0577$, $R_W = 0.0843$, $S = 1.038$ for 452 independent parameters, and the final ΔF map

exhibited maximum and minimum residuals +1.05 and -0.55 eÅ^{-3} respectively.

5.4.10 Synthesis of [Rh([9]aneS$_3$)(C$_7$H$_8$)](PF$_6$)

A solution of [Rh$_2$(nbd)$_2$Cl$_2$] was generated by stirring [Rh$_2$(C$_2$H$_4$)$_4$Cl$_2$] (0.032 g, 0.8 x 10^{-4} mol) with an excess of norbornadiene (2 drops) in CH_2Cl_2 (6 cm^3) under N_2 at 298K for 1 hr. [9]aneS$_3$ (0.030 g, 1.6 x 10^{-4} mol) and NH_4PF_6 (0.027 g, 1.6 x 10^{-4} mol) were added to the resulting yellow solution, and the mixture was stirred for a further 30 mins. The solution was filtered, reduced to ~ 1 cm^3, and the yellow product crystallised with hexane. Yield 0.045 g, 52%. Mol. wt. 520.29. Elemental analysis: found C = 30.1, H = 3.91%; calculated for [C$_{13}$H$_{20}$S$_3$Rh](PF$_6$) C = 30.0, H = 3.88%. F.a.b. mass spectrum: found M$^+$ = 375, 282; calculated for

[^{103}Rh([9]aneS$_3$)(nbd)]$^+$ M$^+$ = 375

[^{103}Rh9[9]aneS$_3$-H)]$^+$ M$^+$ = 282

^{1}H n.m.r. spectrum (200.13 MHz, d^6-acetone, 298K) δ = 3.58 ppm (dd, $^2J_{Rh-H}$ = 2.1 Hz, $^3J_{H-H}$ = 4.7 Hz, 4H, nbd sp^2-C*H*), 3.49 (tt, $^3J_{H-H}$ = 1.6, 4.7 Hz, 2H, nbd sp^3-C*H*), 2.87-2.66 (m, 12H, [9]aneS$_3$), 1.17 (t, $^3J_{H-H}$ = 1.6 Hz, 2H, nbd C*H*$_2$). ^{13}C D.E.P.T n.m.r. spectrum (50.32 MHz, d^6-acetone, 298K) δ = 59.32 ppm (d, $^3J_{Rh-C}$ = 4.8 Hz, nbd *C*H$_2$), 46.10 (s, nbd, sp^3-*C*H), 41.45 (d, $^1J_{Rh-C}$ = 8.4 Hz, nbd sp^2-*C*H), 33.71 (s, [9]aneS$_3$). U.V./vis spectrum (CH_3CN): λ_{max} = 388 nm (sh), 309 (ε_{max} = 2,360 dm^3.mol^{-1}. cm^{-1}), 222

(20,600). I.R. spectrum (KBr disc) 3060 w, 2990 w, 2960 m, 2910 m, 2840 w, 1450 m, 1435 w, 1410 s, 1385 w, 1340 w, 1305 s, 1285 w, 1260 w, 1245 w, 1225 w, 1170 m, 1140 w, 1110 w, 1035 m, 995 w, 940 w, 920 w, 905 m, 890 w, 840 vs, 790 m, 770 w, 740 w, 685 w, 660 w 560 w, 550 s, 490 w, 440 w, 360 m cm^{-1}.

5.4.11 Synthesis of [Rh([9]aneS$_3$)(C$_4$H$_6$)](PF$_6$)

Butadiene was bubbled through a solution of [$Rh_2(C_2H_4)_2Cl_2$)] (0.032 g, 0.8 x 10^{-4} mol) in CH_2Cl_2 (6 cm^3) at room temperature for 10 mins. The solution was then transferred to a Schlenk tube containing [9]aneS$_3$ (0.030 g, 1.6 x 10^{-4} mol) and NH_4PF_6 (0.027 g, 1.6 x 10^{-4} mol), and the mixture stirred under N_2 for 10 mins. The yellow solution was filtered, reduced in volume to ~1 cm^3, and the product crystallised with hexane. The complex was a pale yellow microcrystalline solid (yield 0.038 g, 4 7%). Mol. wt. 482.25. Elemental analysis: found C = 25.2, H = 3.78%; calculated for [$C_{10}H_{18}S_3Rh$](PF$_6$) C = 24.9, H = 3.76%. F.a.b. mass spectrum: found M^+ = 337, 282; calculated for

[^{103}Rh([9]aneS$_3$)(C$_4$H$_6$)]$^+$ M^+ = 337

[^{103}Rh([9]aneS$_3$-H)]$^+$ M^+ = 282

^{1}H n.m.r. spectrum (360.13 MHz, d^6-acetone, 298K) δ = 5.60 ppm (m, 2H, C_4H_6CH), 3.22-2.85 (br, 12H, [9]aneS$_3$), 2.32 (m, 2H, C_4H_6 CH_2), 1.08 (m, 2H, C_4H_6 CH_2). ^{13}C D.E.P.T. n.m.r. spectrum (90.56 MHz, d^6-acetone, 298K) δ = 89.98

ppm (d, $^1J_{Rh-C}$ = 5.0 Hz, C_4H_6 *CH*), 36.24 (s, [9]aneS_3), 35.37 (d, $^1J_{Rh-C}$ = 12.1 Hz, C_4H_6 *CH_2*), 34.69 (s, [9]aneS_3). U.V./vis spectrum (CH_3CN): λ_{max} = 352 nm (sh), 283 (ε_{max} = 3,360 $dm^3.mol^{-1}.cm^{-1}$), 229 (18,900). I.R. spectrum (KBr disc) 3040 w, 3000 m, 2960 m, 2920 w, 2840 w, 1470 s, 1445 s, 1430 m, 1410 s, 1385 w, 1370 m, 1290 m, 1280 m, 1265 w, 1240 m, 1195 m, 1180 w, 1170 w, 1130 w, 1115 w, 1050 m, 1005 m, 990 w, 960 m, 935 s, 910 s, 870 m, 840 vs, 790 w, 740 w, 715 w, 680 m, 655 m, 620 w, 555 s, 495 m, 480 m, 450 w, 415 w, 400 m, 365 w cm^{-1}.

5.4.12 Single Crystal Structure of [Rh([9]aneS_3)-(C_4H_6)](PF_6).½($C_2H_5OC_2H_5$)

Yellow laths of x-ray quality were grown by vapour diffusion of diethyl ether into an acetone solution of the complex. A suitable crystal was mounted on a glass fibre, and cooled to 277K on an Oxford Cryosystems low temperature device.

Crystal Data:

[$C_{10}H_{18}S_3Rh$](PF_6).½($C_4H_{10}O$), *Mr* = 500.56. Monoclinic, space group *C2/c*, *a* = 18.612(6), *b* = 8.679(5), *c* = 23.756(5) Å, β = 96.844(18)°, *V* = 3810 $Å^3$ (by least-squares refinement on diffractometer angles for 22 centred reflections measured at $\pm\omega$[30<2θ<32°, λ = 0.71073 Å]), *Z* = 8, D_C = 1.746 $g.cm^{-3}$. Crystal dimensions 0.82 x 0.43 x 0.23 mm, μ(Mo-K_α) = 1.326 mm^{-1}, *F*(000) =

2004.

Data Collection and Processing:

Stoë STADI-4 four-circle diffractometer, $\omega/2\theta$ scan mode using the learnt-profile method. Graphite-monochromated Mo-K_α radiation: 2684 reflections measured ($2\theta_{max}$ = 45°, h-20→19, k0→9, l0→25), 2446 unique, giving 2329 with $F>4\sigma(F)$. No crystal decay, no absorption correction.

Structure Analysis and Refinement:

A Patterson synthesis located the Rh position, and the structure was developed by least-squares refinement and difference Fourier synthesis to reveal all other non-H atoms. During refinement the PF_6^- counterion was found to be disordered; this was modelled using twelve half-occupied F atoms. A half-occupied diethyl ether solvent molecule was also located lying across a crystallographic two-fold axis; this was itself disordered over two equally occupied orientations. Anisotropic thermal parameters were refined for Rh, S, P, F, O and non-solvent C atoms. Macrocyclic and solvent H atoms were included in fixed, calculated positions; butadiene H atom positions were refined with a fixed C-H bond length of 1.08 Å, and constraints such that all C-C-H, and both H-C-H, angles were equal. The fixed weighting scheme $w^{-1} = \sigma^2(F) + 0.000500\ F^2$ gave satisfactory agreement

analyses. At convergence R = 0.0467, R_W = 0.0671, S = 2.676 for 281 independent parameters. The final difference Fourier synthesis exhibited the maximum and minimum residuals +0.82 and -1.08 eÅ^{-3} respectively.

5.4.13 Synthesis of [Rh([9]aneS$_3$)(C$_2$H$_4$)(P^{i}Pr$_3$)](PF$_6$)

[Rh$_2$(C$_2$H$_4$)$_4$Cl$_2$] (0.032 g, 0.8 x 10^{-4} mol) and P^{i}pr$_3$ (1.6 cm^3 of a 0.1M solution in THF) were stirred in acetone under N$_2$ at 298K for 30 mins. The resultant yellow solution was then treated with [9]aneS$_3$ (0.030 g, 1.6 x 10^{-4} mol) and NH$_4$PF$_6$ (0.027 g, 1.6 x 10^{-4} mol), and stirred for a further 15 mins, giving a pale yellow solution and yellow precipitate. The solution was filtered, reduced to 1 cm^3 volume, and addition of diethyl ether afforded a pale yellow solid which was recrystallised from CH$_2$Cl$_2$/hexane at 253K (Yield 0.030 g, 29%). Mol. wt. 616.45. Elemental analysis: found C = 33.4, H = 6.13%; calculated for [C$_{17}$H$_{33}$S$_3$PRh](PF$_6$) C = 33.1, H = 6.05%. F.a.b. mass spectrum: found M$^+$ = 471, 443; calculated for

[^{103}Rh([9]aneS$_3$)(C$_2$H$_4$)(P^{i}pr$_3$)]$^+$ M$^+$ = 471

[^{103}Rh([9]aneS$_3$)(C$_2$H$_4$)(P^{i}pr$_3$)]$^+$ M$^+$ = 443

U.V./visible spectrum (CH$_3$CN): λ_{max} = 360 nm (sh), 260 (sh), 236 (ε_{max} = 16,740 dm^3.mol^{-1}.cm^{-1}). I.R. spectrum (KBr disc) 2970 s, 2930 m, 2880 w, 2720 w, 1450 s, 1410 s, 1390 m, 1370 w, 1290 w, 1250 m, 1175 w, 1145 m, 1090 s, 1055 w, 1035 m, 950 s, 840 vs, 740 m, 720 w, 655 m, 640 w,

605 w, 555 s, 530 m, 490 w, 470 w, 405 w cm^{-1}.

5.4.14 Synthesis of $[Rh([9]aneS_3)(C_2H_4)(PCyc_3)](PF_6)$

$[Rh_2(C_2H_4)_4Cl_2]$ (0.032 g, 0.8 x 10^{-4} mol) and $PCyc_3$ (0.046 g, 1.6 x 10^{-4} mol) were stirred in CH_2Cl_2 (6 cm^3) under N_2 at 298K until all the solid had dissolved, giving an orange/yellow solution. $[9]aneS_3$ (0.030 g, 1.6 x 10^{-4} mol) and NH_4PF_6 (0.027 g, 1.6 x 10^{-4} mol) were then added, and the mixture stirred for a further 10 mins. The resulting pale yellow solution was filtered, reduced to 1 cm^3 volume, and the yellow product crystallised with hexane (Yield 0.073 g, 59%). Mol. wt. 736.64. Elemental analysis: found C = 42.2, H = 6.78%; calculated for $[C_{28}H_{49}S_3PRh](PF_6)$ C = 42.4, H = 6.71%. F.a.b. mass spectrum: found M^+ = 591, 562; calculated for

$[^{103}Rh([9]aneS_3)(C_2H_4)(PCyc_3)]^+$ $M^+ = 591$

$[^{103}Rh([9]aneS_3\text{-}H)(PCyc_3)]^+$ $M^+ = 562$

^1H n.m.r. spectrum (200.13 MHz, d^6-acetone, 298K) δ = 3.08-2.95 ppm (m, 12H, $[9]aneS_3$), 2.52 (m, 2H, C_2H_4), 2.18 (m, 2H, C_2H_4), 2.04-1.28 (m, 33H, $PCyc_3$). ^{13}C D.E.P.T. n.m.r. spectrum (50.32 MHz, d^6-acetone, 298K) δ = 35.02 (d, $^1J_{P-C}$ = 19.2 Hz, b-$PCyc_3$), 34.43 (s, $[9]aneS_3$), 29.15 (d, $^1J_{Rh-C}$ ~ 12Hz, C_2H_4), 28.85 (s, α-$PCyc_3$), 26.66 (d, $^3J_{P-C}$ = 9.5 Hz, β-$PCyc_3$), 25.28 (s, γ-$PCyc_3$). ^{31}P n.m.r. spectrum (81.02 MHz, d^6-acetone, 298K) δ = 36.75 ppm (d, $^1J_{Rh-P}$ = 130.4 Hz, $PCyc_3$). U.V./vis spectrum (CH_3CN): λ_{max} = 365 nm (sh), 260 (sh), 239 (ε_{max} = 14,860

$dm^3.mol^{-1}.cm^{-1}$). I.R. spectrum (KBr disc) 3070 w, 3020 w, 2920 s, 2840 s, 2650 w, 1490 w, 1445 s, 1410 s, 1380 w, 1345 w, 1330 w, 1295 m, 1270 m, 1225 w, 1200 m, 1170 m, 1150 m, 1115 m, 1070 w, 1045 w, 1020 w, 1000 m, 940 m, 915 w, 895 w, 875 w, 840 vs, 780 w, 730 m, 700 w, 665 w, 555 s, 515 m, 495 w, 450 w, 435 w, 420 w, 400 w cm^{-1}.

5.4.15 Synthesis of $[Rh_2([9]aneS_3)_2(\mu\text{-}CO)_2](PF_6)_2$

$[Rh_2(CO)_4Cl_2]$ (0.032 g, 0.8 x 10^{-4} mol) was reacted with [9]$aneS_3$ (0.030 g, 1.6 x 10^{-4} mol) and NH_4PF_6 (0.027 g, 1.6 x 10^{-4} mol) in acetone (6 cm^3) under N_2 at 298K. After stirring for 30 mins, the resultant dark green solution was filtered and reduced to 1 cm^3 volume, and the green product crystallised with diethyl ether. The product was recrystallised from CH_3NO_2/diethyl ether (Yield 0.060 g, 79%). Mol. wt. 912.32. Elemental analysis: found C = 17.3, H = 3.09%; calculated for $[C_{14}H_{24}S_6O_2Rh_2](PF_6)_2.3H_2O$ C = 17.4, H = 3.13%. F.a.b. mass spectrum: found M^+ = 622, 593, 339, 283; calculated for

$[^{103}Rh_2([9]aneS_3)_2(CO)_2]^+$	$M^+ = 622$
$[^{103}Rh_2([9]aneS_3)([9]aneS_3\text{-}H)(CO)]^+$	$M^+ = 593$
$[^{103}Rh_2([9]aneS_3)(CO)_2]^+$	$M^+ = 339$
$[^{103}Rh_2([9]aneS_3)]^+$	$M^+ = 283$

^1H n.m.r. spectrum (80.13 MHz, CD_3NO_2, 298K) δ = 3.22 ppm (m, [9]$aneS_3$). ^{13}C {^1H} n.m.r. spectrum (50.32 mHz, CD_3NO_2, 298K) δ = 202.51 ppm (t, $^1J_{Rh-C}$ = 26.9 Hz, *CO*),

32.71 (s, [9]aneS$_3$). U.V./visible spectrum (CH_3CN): λ_{max} = 894 nm (ε_{max} = 75.1 $dm^3.mol^{-1}.cm^{-1}$), 532 (sh), 388 (sh), 346 (sh), 310 (14,390). I.R. spectrum (CH_3NO_2 solution) 1855 cm^{-1}. I.R. spectrum (KBr disc) 2990 m, 2960 m, 2920 m, 1915 w, 1850 vs, 1775 w, 1445 s, 1410 s, 1360 w, 1295 m, 1270 w, 1250 w, 1180 m, 1135 w, 1070 w, 1040 w, 1015 w, 990 w, 935 m, 840 vs, 740 m, 680 s, 625 m, 555 s, 540 m, 480 w, 440 w cm^{-1}.

5.4.16 Synthesis of [Rh([9]aneS$_3$)(CO)(PPh$_3$)](PF$_6$)

Reaction of [Rh(CO)Cl(PPh$_3$)$_2$] (0.115 g, 1.6 x 10^{-4} mol with [9]aneS$_3$ (0.030 g, 1.6 x 10^{-4} mol) and NH_4PF_6 (0.027 g 1.6 x 10^{-4} mol) in dichloromethane (6 cm^3) under N_2 at room temperature yielded an intense yellow solution. This was filtered, reduced to ~ 1 cm^3, and the yellow product crystallised with hexane (Yield 0.065 g, 55%). Mol. wt. 718.45. Elemental analysis: found C = 41.4, H = 3.71%; calculated for [$C_{25}H_{27}S_3PORh$](PF$_6$) C = 41.8, H = 3.76%. F.a.b. mass spectrum: found M^+ = 573, 545, 468; calculated for:

[^{103}Rh([9]aneS$_3$)CO)(PPh$_3$)]$^+$ M^+ = 573

[^{103}Rh([9]aneS$_3$)(PPh$_3$)]$^+$ M^+ = 545

[^{103}Rh([9]aneS$_3$)(PPh$_2$)]$^+$ M^+ = 468

^{1}H n.m.r. spectrum (200.13 MHz, CD_3CN, 298K) δ = 7.80-7.45 ppm (m, 15H, PPh$_3$), 2.57-2.40 (m, 12H, [9]aneS$_3$). ^{13}C{^{1}H} n.m.r. spectrum (50.32 MHz, CD_3CN, 298K) δ = 133.51 ppm (d, $^2J_{P-C}$ = 11.4 Hz, o-PPh$_3$), 131.75 (d, $^1J_{P-C}$

= 51 Hz, b-PPh_3), 131.06 (d, J_{P-C} = 2.5 Hz, m-PPh_3), 128.43 (d, J_{P-C} = 10.7 Hz, p-PPh_3), 33.44 (s, [9]aneS_3). ^{31}P n.m.r. spectrum (81.02 MHz, CD_3CN, 298K) δ = 43.80 ppm (d, $^1J_{Rh-P}$ = 129 Hz, PPh_3). U.V./vis spectrum (CH_3CN): λ_{max} = 370 nm (sh), 278 (sh), 251 (ε_{max} = 21,980 $dm^3.mol^{-1}.cm^{-1}$). I.R. spectrum (CH_3NO_2 solution) 1960 cm^{-1}. I.R. spectrum (KBr disc) 3070 w, 3040 m, 3000 w, 2950 w, 2920 w, 2840 w, 1955 s, 1905 w, 1580 w, 1570 w, 1480 m, 1450 m, 1435 s, 1410 s, 1335 w, 1315 w, 1300 m, 1270 w, 1175 m, 1150 w, 1115 w, 1090 s, 1075 w, 1025 w, 1000 m, 985 w, 970 w, 940 w, 905 w, 870 w, 840 vs, 765 s, 755 m, 745 m, 710 s, 695 s, 660 w, 620 w, 560 s, 545 s, 535 s, 510 s, 485 w, 470 w, 445 w, 430 m cm^{-1}.

5.4.17 Single Crystal Structure of [Rh([9]aneS_3)(CO)-(PPh_3)](${PF_6}$)

Solvent diffusion of hexane into a solution of the complex in dichloromethane gave yellow columnar crystals.

Crystal Data:

[$C_{25}H_{27}S_3PORh$](${PF_6}$), *Mr* = 718.45. Orthorhombic, space group *Pnma*, *a* = 12.4367(8), *b* = 12.7190(6), *c* = 18.0229(8) Å, *V* = 2850.9 Å^3 (by least-squares refinement on diffraction angles for 39 reflections measured at $\pm\omega$ [28<2θ<30°, λ = 0.71073 Å]), *Z* = 4, D_C = 1.674 g.cm^{-3}. Crystal dimensions 0.65 x 0.15 x 0.12 mm, μ(Mo-K_α) = 0.968 mm^{-1}, F(000) = 1448.

Data Collection and Processing:

Stoë STADI-4 four-circle diffractometer, $\omega/2\theta$ scan mode with ω scan-width $(0.99 + 0.347 \tan\theta)^\circ$. Graphite-monochromated Mo-K_α radiation: 2028 reflections measured ($2\theta_{max}$ = 45°, h0→11, κ0→13, l0→19) giving 1401 with $F>6\sigma(F)$. No significant crystal decay, no absorption correction.

Structure Analysis and Refinement:

A Patterson synthesis located the Rh atom lying on a crystallographic mirror plane, and the structure was developed by iterative cycles of least-squares refinement and difference Fourier synthesis. The [9]aneS_3 C atoms were found to be disordered over two orientations; this was modelled using the constraints S-C = 1.83 Å, C-C = 1.52 Å, S-C-C = 2.74 Å. The PF_6^- counterion was also disordered, and was modelled using partial F atoms such that the total number of F atoms equalled six. Anisotropic thermal parameters were refined for all non-H atoms with site occupancy factor above 0.5, and H atoms were included in fixed, calculated positions. The weighting scheme $w^{-1} = \sigma^2(F) + 0.000373F^2$ gave satisfactory agreement analyses. At final convergence R, R_w were 0.0498, 0.0691 respectively, S = 1.252 for 202 parameters, and the final ΔF synthesis showed maximum and minimum residuals of +1.53 and -0.80 $Å^{-3}$.

5.4.18 Synthesis of [Rh([9]aneS$_3$)(tcne)(CH$_3$CN)](BF$_4$)

[Rh([9]aneS$_3$)(cod)](BF$_4$) (0.040 g, 8.4 x 10^{-4} mol) and tcne (0.011 g, 8.4 x 10^{-5} mol) were refluxed in acetonitrile (6 cm^3) under N$_2$ for 2 hrs. The resulting yellow solution was filtered, reduced to 1 cm^3, and the pale yellow product crystallised with diethyl ether. Yield 0.035 g, 78%. Mol. wt. 539.16. Elemental analysis: found C = 31.7, H = 2.88, N = 12.4%; calculated for [C$_{14}$H$_{15}$S$_3$N$_5$Rh)](BF$_4$) C = 31.2, H = 2.80, N = 13.0%. F.a.b. mass spectrum: found M$^+$ = 452, 411, 385, 323, 283; calculated for

[^{103}Rh([9]aneS$_3$)(tcne)(CH$_3$CN)]$^+$	M$^+$ = 452
[^{103}Rh([9]aneS$_3$)(tcne)]$^+$	M$^+$ = 411
[^{103}Rh([9]aneS$_3$)tcne-CN)]$^+$	M$^+$ = 385
[^{103}Rh([9]aneS$_3$-H)(CH$_3$CN)]$^+$	M$^+$ = 323
[^{103}Rh([9]aneS$_3$)]$^+$	M$^+$ = 283

^{1}H n.m.r. spectrum (200.13 MHz, CD$_3$CN, 298K0 δ = 3.64 ppm (m, 6H, [9]aneS$_3$), 1.96 (s, 3H, C*H*$_3$CN), 1.79 (m, 6H, [9]aneS$_3$). ^{13}C {^{1}H} n.m.r. spectrum (50.32 MHz, CD$_3$CN, 298K) δ = 37.27 (s, [9]aneS$_3$), 34.06 (s, [9]aneS$_3$), 33.53 (s, [9]aneS$_3$), 24.77 (s, *C*H$_3$CN). U.V./vis spectrum (CH$_3$CN) λ_{max} = 330 nm (sh), 299 (ε_{max} = 14,345 dm^3.mol^{-1}.cm^{-1}), 255 (26,900). I.R. spectrum (KBr disc): 2980 m, 2930 m, 2860 w, 2320 m, 2295 m, 2245 w, 2220 s, 2150 w, 1440 s, 1410 s, 1380 w, 1300 m, 1285 m, 1260 w, 1245 w, 1210 s, 1190 w, 1170 w, 1140 m, 1125 m, 1060 vs,

945 m, 910 s, 850 w, 830 s, 770 w, 660 w, 625 w, 560 w, 525 s, 490 m, 330 m cm^{-1}.

5.4.19 Synthesis of $[Rh([9]aneS_3)Cl_3]$

The reaction of $RhCl_3.3H_2O$ (0.044 g, 1.6 x 10^{-4} mol) with [9]$aneS_3$ (0.030 g, 1.6 x 10^{-4} mol) in refluxing ethanol (15 cm^3) under N_2 for 3 hrs yielded a pale yellow precipitate. The product was filtered, washed with ethanol, and dried *in vacuo* (Yield 0.042 g, 64%). Mol. wt. 389.6. Elemental analysis: found C = 18.6, H = 3.16%; calculated for $[C_6H_{12}S_3Cl_3Rh]$ C = 18.5, H = 3.10%. I.R. spectrum (KBr disc): 2980 m, 2920 m, 2880 w, 1440 s, 1400 s, 1365 w, 1295 w, 1280 m, 1260 m, 1170 w, 1120 m, 1010 w, 940 m, 905 s, 830 s, 675 w, 660 w, 560 w, 430 w, 340 s, 295 s cm^{-1}.

5.4.20 Synthesis of $[Rh([9]aneS_3)I_3]$

$[Rh([9]aneS_3)(C_2H_4)_2](PF_6)$ (0.060 g, 1.2 x 10^{-4} mol) was reacted with excess CH_3I (4 drops) in acetone under N_2 at 298K for 15 mins. The resultant orange precipitate was filtered, and washed with acetone and diethyl ether (Yield 0.041 g, 51%). Mol. wt. 663.95. Elemental analysis: found C = 10.9, H = 1.85%; calculated for $[C_6H_{12}S_3I_3Rh]$ C = 10.9, H = 1.82%. I.R. spectrum (KBr disc) 2940 m, 2880 m, 2840 w, 1435 s, 1400 s, 1360 w, 1290 w, 1260 m, 1235 w, 1160 m, 1120 m, 1090 w, 1020 w, 930 m, 900 s,

820 s, 675 w, 590 w, 480 w cm^{-1}.

CHAPTER 6

HALF-SANDWICH IRIDIUM (I) COMPLEXES OF [9]aneS$_3$

6.1 INTRODUCTION

This chapter describes the synthesis and characterisation of the half-sandwich complexes $[Ir([9]aneS_3)(L)_2]^+$ (L = C_2H_4, C_8H_{14}, $\frac{1}{2}C_8H_{12}$, $\frac{1}{2}C_4H_6$, CO, PPh_3). The metal-alkene bonding in the complexes $[M([9]aneS_3)(C_2H_4)_2]^+$ and $[M([9]aneS_3)(C_4H_6)]^+$ (M = Rh, Ir) is also discussed. See Section 5.1 for an introduction to this work, and to the chemistry of analogous cyclopentadienyl complexes.

Very few Ir complexes of thioether ligands have been reported. The reaction of $[Ir_2(cod)_2Cl_2]$ with dth and $S(CH_2CH_2SPh)_2$ was found to lead to the complexes [Ir(dth)(cod)Cl] and $(Ir\{S(CH_2CH_2SPh)_2\}(cod)]Cl$ (dth = 2,5-dithiahexane), which were assigned five-coordinate geometries[199]. Two isomers of stoichiometry $[Ir(SR_2)_3Cl_3]$ (R = alkyl, aryl) have been observed: the yellow *mer*-octahedral neutral species, and the red ionic *trans*-$[Ir(SR_2)_4Cl_2]^+$ *trans*-$[Ir(SR_2)_2Cl_4]^-$ [249].

The Edinburgh group has investigated the formation and chemistry of $[Ir([9]aneS_3)_2]^{3+}$ [250]. Reaction of $[Ir_2(coe)_4Cl_2]$ with four equivalents of $[9]aneS_3$ in the presence of 40% HBF_4 afforded the unusual octahedral species $[Ir([9]aneS_3)_2H]^{2+}$, containing a bidentate $[9]aneS_3$ ligand (Figure 6.1a). Abstraction of the H^- ligand from this complex with aqueous HNO_3 gave $[Ir([9]aneS_3)_2]^{3+}$ (Figure 6.1b). In contrast to its Rh analogue, $[Ir([9]aneS_3)_2]^{3+}$ exhibits one irreversible

one-electron reduction at Ep_C = -1.38V *vs.* Fc/Fc^+ in $CH_3CN/^nBu_4NPF_6$. Bulk electrogenerated samples of the reduction product were e.p.r. inactive, implying the formation of a metal-metal bonded Ir^{II}-Ir^{II} dimeric species.

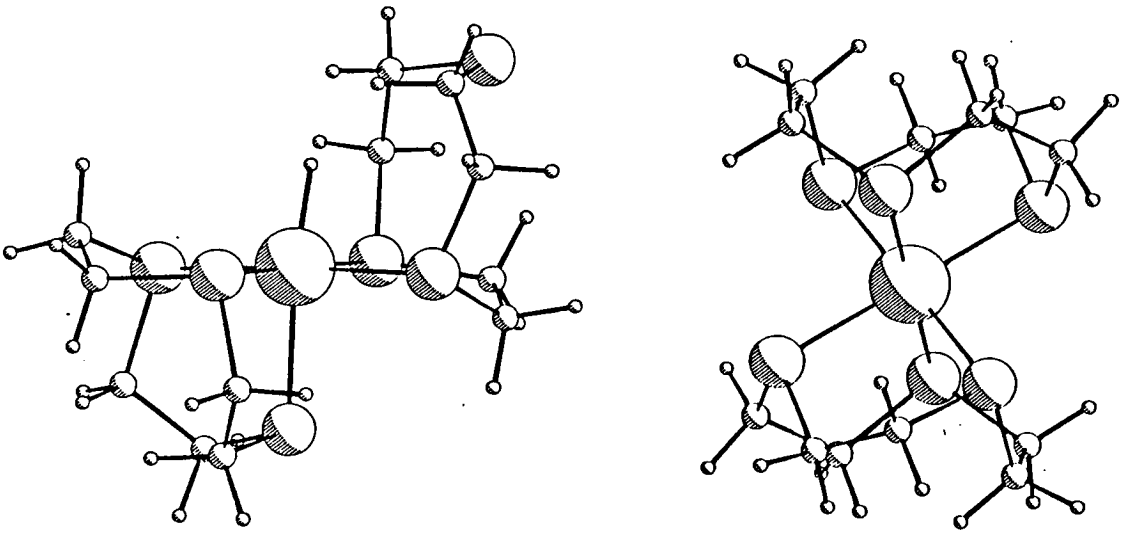

Figure 6.1: Views of the Single Crystal Structures of
a) $[Ir([9]aneS_3)_2H]^{2+}$ and
b) $[Ir([9]aneS_3)_2]^{3+}$.

The octahedral complex *cis*-$[Ir([14]aneS_4)Cl_2]^+$ has been structurally characterised[105].

6.2 RESULTS AND DISCUSSION

6.2.1 $[Ir([9]aneS_3)(C_2H_4)_2](PF_6)$

A solution of $[Ir(C_2H_4)_4Cl]$ was generated *in situ* by bubbling C_2H_4 through a THF solution of $[Ir_2(coe)_4Cl_2]$ at 298K[251,270]. Addition of two molar equivalents of [9]aneS$_3$ and NH_4PF_6 to this mixture afforded a pale yellow solution, which was reduced to dryness to remove residual cyclooctene. Recrystallisation of the resulting crude product from CH_2Cl_2/hexane gave a pale yellow crystalline solid in 50% yield.

The f.a.b. mass spectrum of this compound showed peaks at M^+ = 429, 401 and 373, which are consistent with the assignments $[^{193}Ir([9]aneS_3)(C_2H_4)_2]^+$, $[^{193}Ir([9]aneS_3)(C_2H_4)]^+$ and $[^{193}Ir([9]aneS_3)]^+$ respectively. The product was, therefore, formulated as $[Ir([9]aneS_3)(C_2H_4)_2](PF_6)$; this was supported by I.R. spectral and microanalytical data.

The U.V./visible spectrum of $[Ir([9]aneS_3)(C_2H_4)_2]^+$ in CH_3CN exhibited similar bands to its Rh analogue [λ_{max} = 356 nm (ε_{max} = 750 $dm^3.mol^{-1}.cm^{-1}$), 290 (2,350), 229 (8,230); cf for $[Rh([9]aneS_3)(C_2H_4)_2]^+$ λ_{max} = 380 nm (ε_{max} = 590 $dm^3.mol^{-1}.cm^{-1}$), 298 (2,360), 234 (9,295)]. This suggests that the structures of $[M([9]aneS_3)(C_2H_4)_2]^+$ (M = Rh, Ir) in solution are similar, and hence that $[Ir([9]aneS_3)(C_2H_4)_2]^+$ adopts an 18-electron, five-coordinate geometry. This was supported by the observation that no reaction occurred between

$[Ir([9]aneS_3)(C_2H_4)_2]^+$ and an excess of cod or CO in refluxing THF, which is also consistent with an 18-electron formulation (Section 5.2.1).

6.2.2 Low Temperature N.m.r. Studies on $[Ir([9]aneS_3)(C_2H_4)_2](PF_6)$

The ^1H n.m.r. spectrum of $[Ir([9]aneS_3)(C_2H_4)_2]^+$ in d^6-acetone at 298K showed a multiplet at δ = 3.11-2.98 ppm, corresponding to the SCH_2 protons of coordinated $[9]aneS_3$, and a singlet resonance at δ = 2.19 ppm from the ethene H atoms (Figure 6.2). Cooling the sample to 178K (the limit of the solvent) caused partial decoalescence of the C_2H_4 resonance, implying a coalescence temperature T_C of 165-180K: no change was observed in the $[9]aneS_3$ resonance on cooling. An accurate value of T_C was obtained using a 2:1 CD_2Cl_2:d^8-THF solvent mixture, which allows access to temperatures approaching 140K. In this solvent mixture, the decoalescence temperature for $[Ir([9]aneS_3)(C_2H_4)_2]^+$ was measured as 177±1K, and further cooling to 158K caused the resolution of two new signals at δ = 2.57 and $\delta \simeq$ 1.89 ppm (obscured by a solvent peak, Figure 6.3), corresponding to the "inner" and "outer" C_2H_4 H environments (52). Using these data, the activation energy for ethene rotation can be calculated from the Eyring equation[252]:

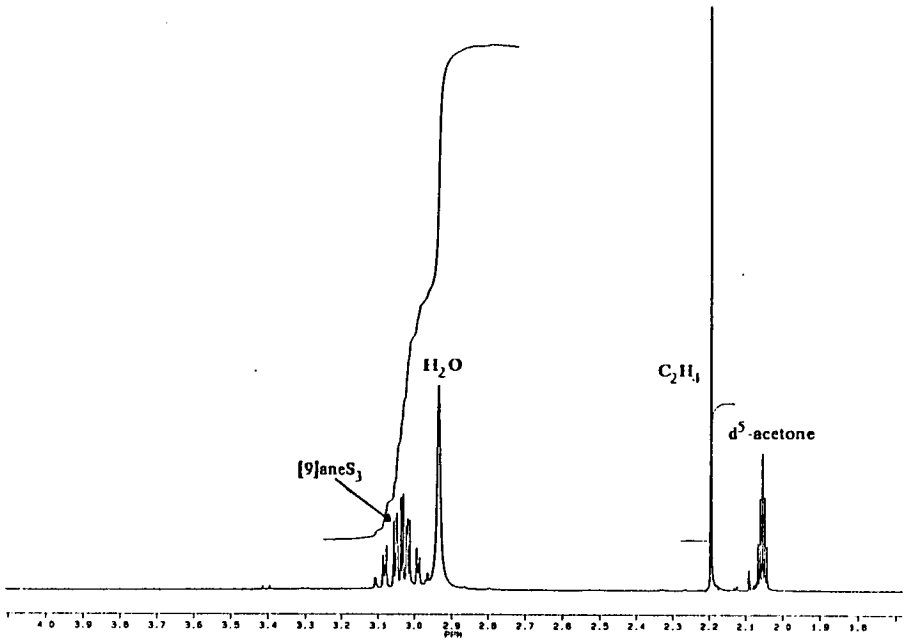

a) ^{1}H (360.13 MHz).

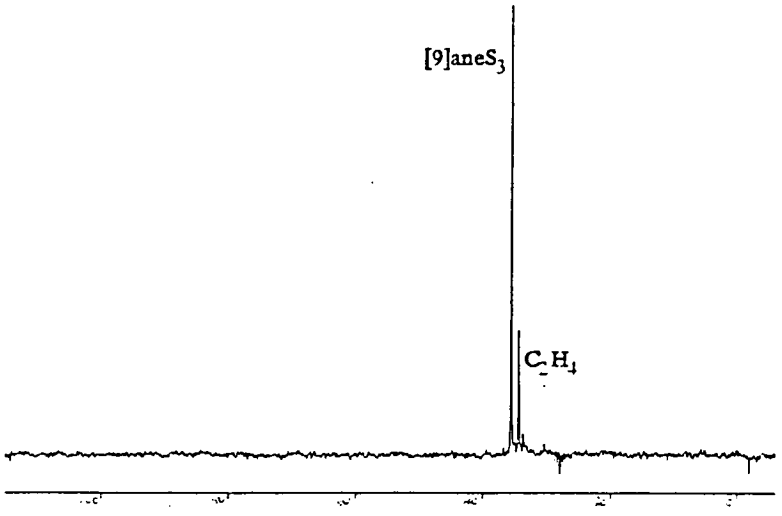

b) ^{13}C DEPT (50.32 MHz)

Figure 6.2: N.m.r. Spectra of $[Ir([9]aneS_3)(C_2H_4)_2](PF_6)$ (d^6-acetone, 298K).

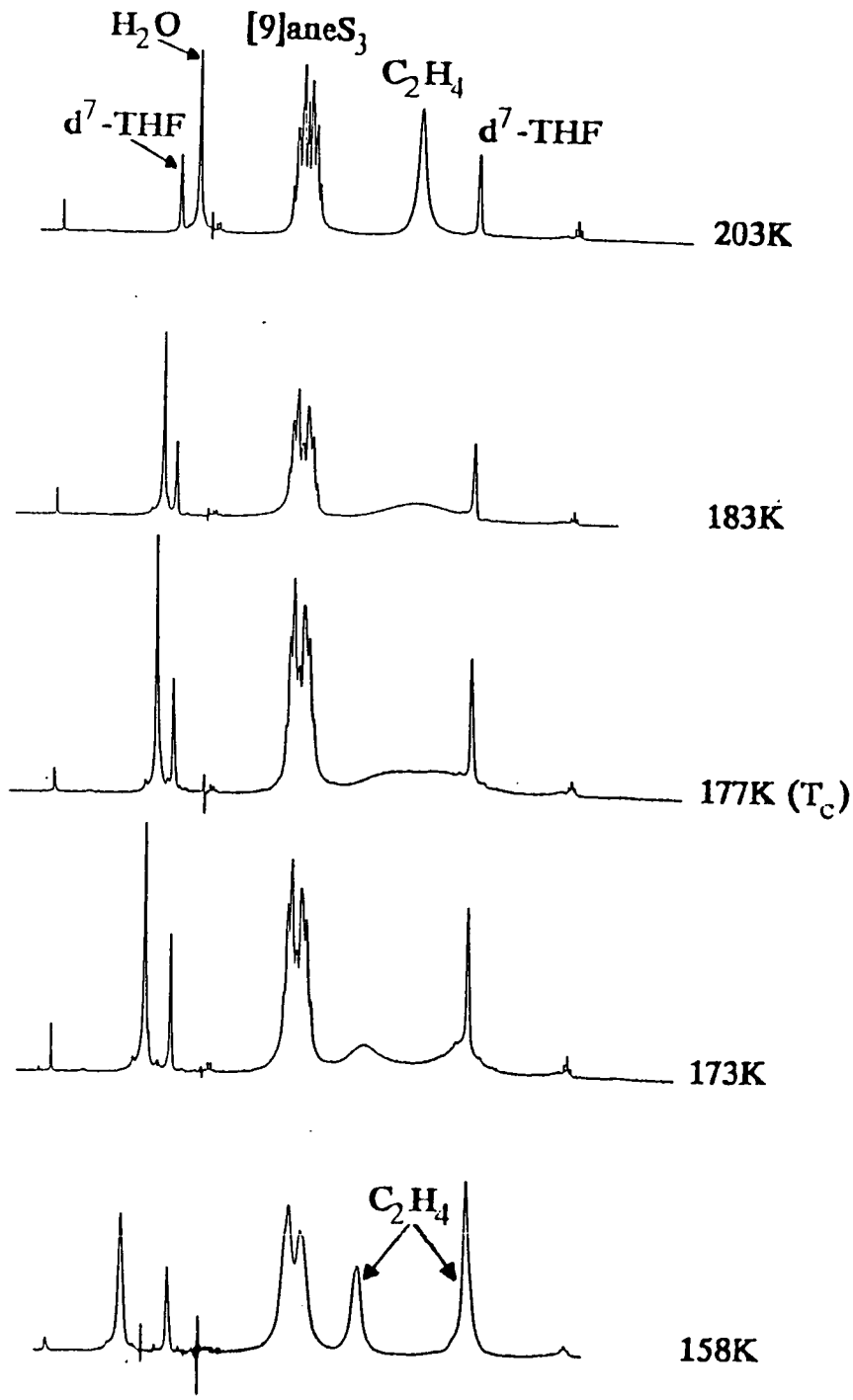

Figure 6.3: Low Temperature ^1H N.m.r. Study of $[Ir([9]aneS_3)(C_2H_4)_2](PF_6)$ (2:1 CD_2Cl_2:d^8-THF, 360 MHz).

$$k_r = \kappa . \frac{k_b T}{h} . \exp\left[\frac{\Delta G^{\dagger}}{RT}\right] \qquad (63)$$

where k_r = rate constant at temperature T, κ = transmission coefficient (usually set equal to 1), k_b = Boltzmann's constant, h = Planck's constant and $\Delta G^{\dagger}$ = free energy of activation at temperature T. Using an approximation for the rate constant at the n.m.r. coalescence temperature (T_C) for exchange between two equally occupied environments[253]

$$k_r(T_C) = \frac{\pi(\delta\nu)}{\sqrt{2}} \qquad (64)$$

where $\delta\nu$ = the n.m.r. frequency difference between the decoalesced resonances in Hz, the following expression for $\Delta G^{\dagger}$ at T_C is obtained:

$$\Delta G^{\dagger}(T_C) = -RT_C \ln\left[\frac{\pi(\delta\nu)h}{\sqrt{2}k_b T_C}\right] \qquad (\text{J.mol}^{-1},\ 65).$$

For $[Ir([9]aneS_3)(C_2H_4)_2]^+$, T_C = 177±1K and $\delta\nu$ was estimated as 240±10 Hz. This gives $\Delta G^{\dagger}(T_C)$ = 33.3±0.2 kJ.mol^{-1}.

Coalescence temperatures for alkene ^{1}H resonances and the associated free energies of activation for selected transition metal ethene complexes are listed in Table 6.1. It should be noted that the mechanism of such

equilibration in some of these complexes may be inter-molecular ethene exchange, rather than intra-molecular ethene rotation[209]. For iso-electronic complexes of similar coordination geometry (e.g. five-coordinate d^8 complexes), however, the $\Delta G^{\dagger}$ parameter is a useful indicator to the properties of a metal centre, since rotation about a metal-alkene bond will be hindered by increased metal→alkene π-back donation[260] (Figure 6.4). The $\Delta G^{\dagger}(T_C)$ values derived for $[M([9]aneS_3)(C_2H_4)_2]^+$ (M = Rh, Ir) are substantially lower than those reported for analogous complexes such as $[(C_5R_5)M(C_2H_4)_2]$ (M = Rh, Ir; R = H, CH_3). This implies that metal→alkene π-donation is unusually weak for $[M([9]aneS_3)(C_2H_4)_2]^+$, and hence that the $[M([9]aneS_3)]^+$ fragments are highly electrophilic in

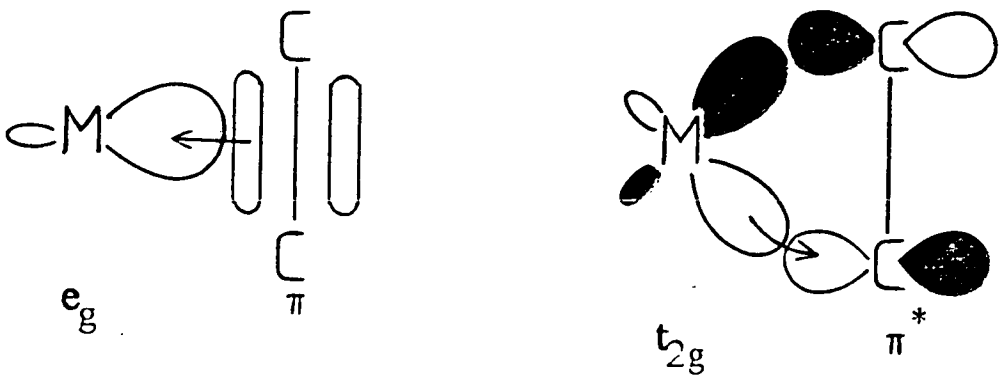

Figure 6.4: Chatt-Dewar-Duncanson Model for Metal-alkene Bonding[261].

Table 6.1: Free Energies of Activation for Alkene H-exchange for Some Ethene Complexes

Compound	T_c (K)	$\Delta G^{\dagger}(T_c)$ (kJ.mol^{-1})	Reference
$[Rh([9]aneS_3)(C_2H_4)_2]^+$	<175	<33	This work
$[Ir([9]aneS_3)(C_2H_4)_2]^+$	177	33.3	This work
$[Rh(C_5H_5)(C_2H_4)_2]^+$	328	64	209
$[Rh(C_5Me_5)(C_2H_4)_2]$	>333	>70	209b
$[Rh(C_9H_7)(C_2H_4)_2]$	240	43	254
$[Ir(C_5Me_5)(C_2H_4)_2]$	>383	>80	255
$[Ir(HBPz_3)(C_2H_4)_2]$	263	54	269
[Ir(triso)$(C_2H_4)_2$]	<298	<58	85
$[Ru(C_6Me_6)(C_2H_4)_2]$	>389	>84	256
[Os(CO)(NO)$(PPh_3)(C_2H_4)$]	208	40	257
[Pt(acac)(C_2H_4)Cl]	253	51.1	258
$[Pt(PPh_3)(C_2H_4)_2]$	225	42.7	259

$HBPz_3$ = hydridotris(pyrazolyl)borate

triso = tris(diphenyloxophosphoranyl)methanide

acac = 2,4-pentanedionate

character. It is unclear how much this reflects the binding properties of the [9]aneS$_3$ macrocycle, since the cationic +1 charge on these complexes should also reduce metal→ligand back-bonding.

In order to further quantify the Ir-ethene bonding in this complex, and to ascertain the coordination geometry adopted, an x-ray structural analysis of [Ir([9]aneS$_3$)(C$_2$H$_4$)$_2$](PF$_6$) was undertaken.

6.2.3 Single Crystal Structure of [Ir([9]aneS$_3$)(C$_2$H$_4$)$_2$](PF$_6$)

Details of the structure solution and refinement are given in Section 6.4.5. Selected bond lengths, angles and torsions are listed in Table 6.2, and an ORTEP plot displaying the complex's molecular geometry is given in Figure 6.5.

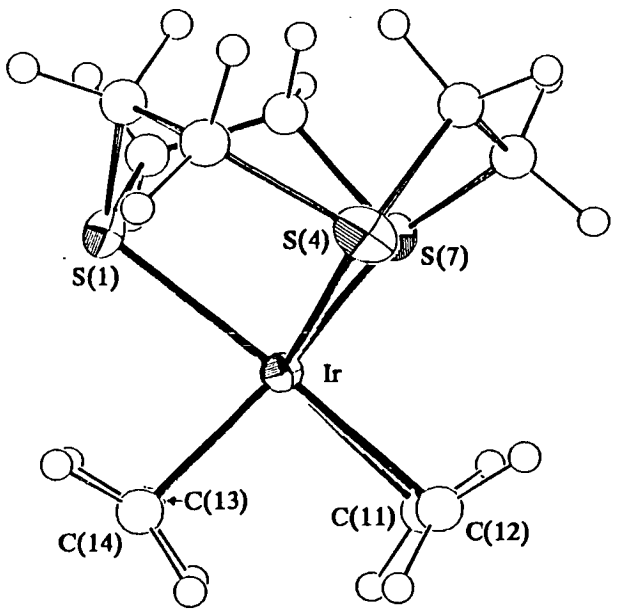

Figure 6.5: View of the Single Crystal Structure of [Ir([9]aneS$_3$)(C$_2$H$_4$)$_2$]$^+$.

Single Crystal Structure of $[Ir([9]aneS_3)(C_2H_4)_2](PF_6)$

Table 6.2. Bond Lengths(A), angles(degrees) and torsion angles(degrees) with standard deviations

Ir	- S(1)	2.3165(18)	C(2)	- C(3)	1.505(10)
Ir	- S(4)	2.4024(18)	C(3)	- S(4)	1.822(8)
Ir	- S(7)	2.3835(16)	S(4)	- C(5)	1.842(7)
Ir	-C(11)	2.173(9)	C(5)	- C(6)	1.529(10)
Ir	-C(12)	2.194(10)	C(6)	- S(7)	1.812(7)
Ir	-C(13)	2.146(8)	S(7)	- C(8)	1.818(7)
Ir	-C(14)	2.118(7)	C(8)	- C(9)	1.524(10)
S(1)	- C(2)	1.818(8)	C(11)	-C(12)	1.366(13)
S(1)	- C(9)	1.820(8)	C(13)	-C(14)	1.443(11)

S(1)	- Ir	- S(4)	87.32(6)	C(13)	- Ir	-C(14)	39.5(3)
S(1)	- Ir	- S(7)	87.52(6)	Ir	- S(1)	- C(2)	106.68(24)
S(1)	- Ir	-C(11)	156.81(23)	Ir	- S(1)	- C(9)	102.22(25)
S(1)	- Ir	-C(12)	165.8(3)	C(2)	- S(1)	- C(9)	101.4(3)
S(1)	- Ir	-C(13)	83.56(21)	S(1)	- C(2)	- C(3)	112.6(5)
S(1)	- Ir	-C(14)	86.30(20)	C(2)	- C(3)	- S(4)	114.6(5)
S(4)	- Ir	- S(7)	86.30(6)	Ir	- S(4)	- C(3)	100.74(24)
S(4)	- Ir	-C(11)	113.46(23)	Ir	- S(4)	- C(5)	105.54(23)
S(4)	- Ir	-C(12)	83.9(3)	C(3)	- S(4)	- C(5)	101.2(3)
S(4)	- Ir	-C(13)	148.94(21)	S(4)	- C(5)	- C(6)	111.9(5)
S(4)	- Ir	-C(14)	110.39(20)	C(5)	- C(6)	- S(7)	114.2(5)
S(7)	- Ir	-C(11)	83.86(23)	Ir	- S(7)	- C(6)	103.11(22)
S(7)	- Ir	-C(12)	102.9(3)	Ir	- S(7)	- C(8)	104.81(22)
S(7)	- Ir	-C(13)	122.73(21)	C(6)	- S(7)	- C(8)	100.9(3)
S(7)	- Ir	-C(14)	161.87(20)	S(7)	- C(8)	- C(9)	111.3(5)
C(11)	- Ir	-C(12)	36.4(3)	S(1)	- C(9)	- C(8)	113.7(5)
C(11)	- Ir	-C(13)	83.1(3)	Ir	-C(11)	-C(12)	72.6(5)
C(11)	- Ir	-C(14)	95.3(3)	Ir	-C(12)	-C(11)	70.9(5)
C(12)	- Ir	-C(13)	98.4(3)	Ir	-C(13)	-C(14)	69.2(4)
C(12)	- Ir	-C(14)	86.4(3)	Ir	-C(14)	-C(13)	71.3(4)

C(9)	- S(1)	- C(2)	- C(3)	-133.3(5)	S(4)	- C(5)	- C(6)	- S(7)	49.3(6)
C(2)	- S(1)	- C(9)	- C(8)	64.4(6)	C(5)	- C(6)	- S(7)	- C(8)	64.3(5)
S(1)	- C(2)	- C(3)	- S(4)	48.0(7)	C(6)	- S(7)	- C(8)	- C(9)	-135.3(5)
C(2)	- C(3)	- S(4)	- C(5)	65.5(6)	S(7)	- C(8)	- C(9)	- S(1)	50.6(6)
C(3)	- S(4)	- C(5)	- C(6)	-132.9(5)					

Examination of the internal angles about the Ir centre in the five-coordinate cation (Table 6.8) shows that $[Ir([9]aneS_3)(C_2H_4)_2]^+$ adopts a distorted trigonal bipyramidal geometry, similar to that of molecule 1 of the single crystal structure of $[Rh([9]aneS_3)(C_2H_4)_2](BF_4)$ (Section 5.2.2). The Ir-S distances in $[Ir([9]aneS_3)(C_2H_4)_2]^+$ are slightly shorter than for the Rh complex [Ir-S(1) = 2.3165(18), Ir-S(4) = 2.4024(18), Ir-S(7) = 2.3855(16) Å; c.f. Rh-S(1) = 2.322(9), Rh-S(4) = 2.437(9), Rh-S(7) = 2.432(9) Å]. The metal-C and ethene C=C bond lengths in the two cations are not significantly different [Ir-C(11) = 2.173(9), Ir-C(12) = 2.194(10), Ir-C(13) = 2.146(8), Ir-C(14) = 2.118(7), C(11)-C(12) = 1.366(13), C(13)-C(14) = 1.443(11) Å; c.f. Rh-C(11) = 2.21(4), Rh-C(12) = 2.21(5), Rh-C(13) = 2.12(5), Rh-C(14) = 2.05(4), C(11)-C(12) = 1.33(6), C(13)-C(14) = 1.43(6) Å].

The axial Ir-S bond is significantly shorter than the equatorial Ir-S bonds, as expected for a d^8 trigonal bipyramidal complex[145]. However, the axial ethene ligand is less closely bound than the equatorial ethene, which suggests a strong *trans*-effect for a π-bound alkene *trans* to a thioether S-donor. The equatorial S atoms are not directly *trans* to the equatorial C_2H_4 ligand, so no *trans*-effect lengthening is observed for these donors. It is unclear whether this *trans*-effect arises from a greater capacity for σ-donation, or for π-back bonding, of the

[9]aneS$_3$ S-donors compared to the ethene ligands.

The pattern of metal-alkene bond distances described above has been observed previously in trigonal bipyramidal Rh^I and Ir^I complexes of chelating dialkenes (e.g. [Rh{$(CF_3CO)_2CH$}{2,3-dicarbomethoxy-nbd}(py)] and [Ir(dppe)(cod)(CH_3)])[262,263]. It is possible that the shortened metal-C, and lengthened C=C bonds observed for equatorial alkene ligands in those complexes may reflect tautomerism between a five-coordinate M^I-alkene complex, and an octahedral M^{III} metallacyclopropane species[264].

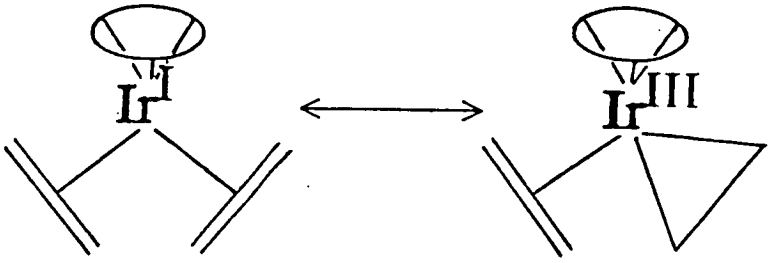

Rh and Ir complexes of alkenes containing strongly electronegative substituents, such as tetracyanoethene (tcne), have been shown to have substantial metallacyclopropane character, and are often described as formally M^{III} species[265-267]. The low barrier to ethene rotation observed for [M([9]aneS$_3$)(C_2H_4)$_2$]$^+$ (*vide supra*), and the oxidations observed in their cyclic voltammograms (Sections 5.2.13, 6.2.10), imply that these complexes are

best regarded as five-coordinate M^{I} species.

6.2.4 $[Ir([9]aneS_3)(C_8H_{14})_2](PF_6)$

Reaction of $[Ir_2(coe)_4Cl_2]$ with two molar equivalents of $[9]aneS_3$ and NH_4PF_6 in acetone under N_2 at 298K for 15 mins gave a pale yellow solution, which was filtered, reduced to ~1 cm^3 volume, and the pale yellow product crystallised with diethyl ether. Recrystallisation from CH_3CN/diethyl ether yielded a yellow microcrystalline solid. The I.R. spectrum of this compound contained peaks attributable to $[9]aneS_3$ and coe ligands, and the PF_6^- counterion. F.a.b. mass spectrometry revealed peaks at M^+ = 593, 483 and 372, which were assigned to the molecular ions $[^{193}Ir([9]aneS_3)(C_8H_{14})_2]^+$, $[^{193}Ir([9]aneS_3)(C_8H_{14})]^+$ and $[^{193}Ir([9]aneS_3\text{-}H)]^+$. The product was therefore assigned the formulation $[Ir([9]aneS_3)(C_8H_{14})_2](PF_6)$, which was borne out by elemental analytical data.

The ^1H n.m.r. spectrum of $[Ir([9]aneS_3)(C_8H_{14})_2](PF_6)$ in CD_3NO_2 at 298K exhibited a multiplet peak at δ = 5.62 ppm (4H), assigned to the coe vinyl H atoms, and a complex series of multiplets at δ = 2.97-2.10 ppm (36H), arising from the $[9]aneS_3$ and coe alkyl H's. The ^{13}C n.m.r. spectrum of this compound measured under identical conditions showed peaks at δ = 61.44 ppm (coe vinyl *C*H), 35.19 ($[9]aneS_3$), 31.00, 28.41 and 25.02 (coe alkyl *C*H_2, Figure 6.6). Hence, the complex was formulated as an Ir^{I} π-complex (66). No evidence for σ- or η^3-bound coe

ligands (67, 68) was observed; these types of structure have been observed for $[Ir(HBPz_3)(\eta^2\text{-}C_8H_{14})(\sigma\text{-}C_8H_{13})(H)]$ and $[Ir(HBPz_3)(\eta^3\text{-}C_8H_{13})(H)]$[$HBPz_3$ = hydridotris-(pyrazolyl)borate][268,269].

$[Ir([9]aneS_3)(coe)_2]^+$ is stable indefinitely at 298K in air in the solid state, and for *ca.* 2 days at 298K under N_2 in CH_3NO_2 or CH_3CN solution. This contrasts with $[Rh([9]aneS_3)(coe)_2]^+$, which decomposes rapidly above 250K (Section 5.2.1).

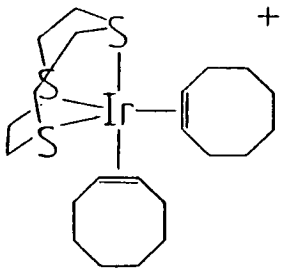

(66)

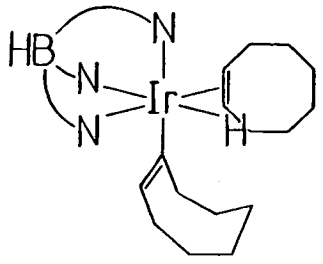

(67)

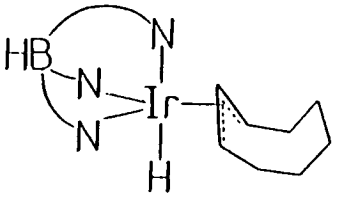

(68)

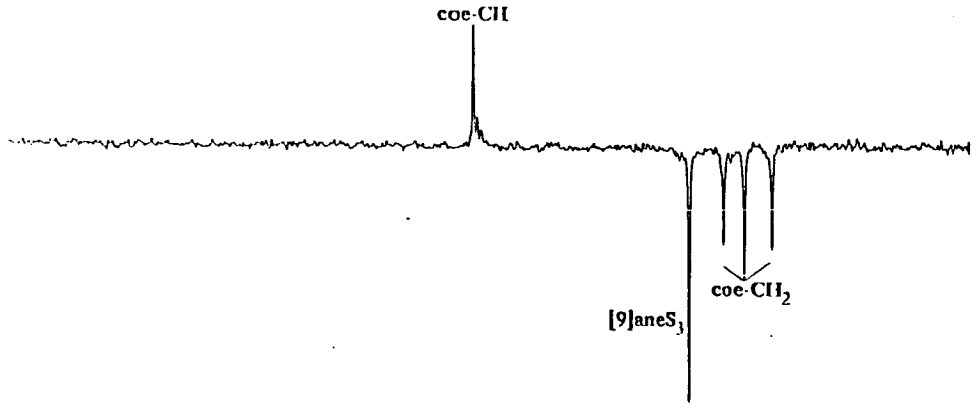

Figure 6.6: ^{13}C d.e.p.t. n.m.r. Spectrum of $[Ir([9]aneS_3)(coe)_2](PF_6)$ (CD_3NO_2, 298K, 50.32 MHz).

6.2.5 $[Ir([9]aneS_3)(C_8H_{12})](PF_6)$

Reaction of $[Ir_2(cod)_2Cl_2]$ with two molar equivalents of $[9]aneS_3$ and NH_4PF_6 in CH_2Cl_2 at room temperature afforded a pale orange solution. After filtration and reduction, addition of *n*-hexane to this solution yielded a tan solid, which could be analysed without further purification.

The f.a.b. mass spectrum of this product showed peaks at M^+ = 625 and 480, which correspond to the species $[^{193}Ir([9]aneS_3\text{-}H)(C_8H_{12})(PF_6)]^+$ and $[^{193}Ir([9]aneS_3)\text{-}(C_8H_{12})]^+$ respectively. The ^1H n.m.r. spectrum of the complex in CD_3CN at 298K exhibited multiplets at δ = 3.64 ppm (cod vinyl C*H*), 2.84-2.54 ([9]aneS$_3$ SC*H*$_2$), 2.32 and 2.12 (cod alkyl C*H*$_2$); the ^{13}C d.e.p.t. n.m.r. spectrum showed singlet peaks at δ = 63.03 ppm (cod vinyl *C*H), 35.57 ([9]aneS$_3$ S*C*H$_2$) and 32.27 (cod alkyl *C*H$_2$). This information, together with microanalytical and I.R. spectral data, led to the formulation of the product as $[Ir([9]aneS_3)(\eta^2,\eta^2\text{-cod})]\ (PF_6)$.

In order to confirm this structural assignment, the single crystal structure of $[Ir([9]aneS_3)(cod)](PF_6)$ was determined.

6.2.6 Single Crystal Structure of $[Ir([9]aneS_3)(C_8H_{12})](PF_6)$

The structure solution and refinement are described in Section 6.4.8. Relevant bond lengths, angles and torsions

are listed in Tables 6.3-6.5, and the geometry of the complex cation is displayed in Figure 6.7.

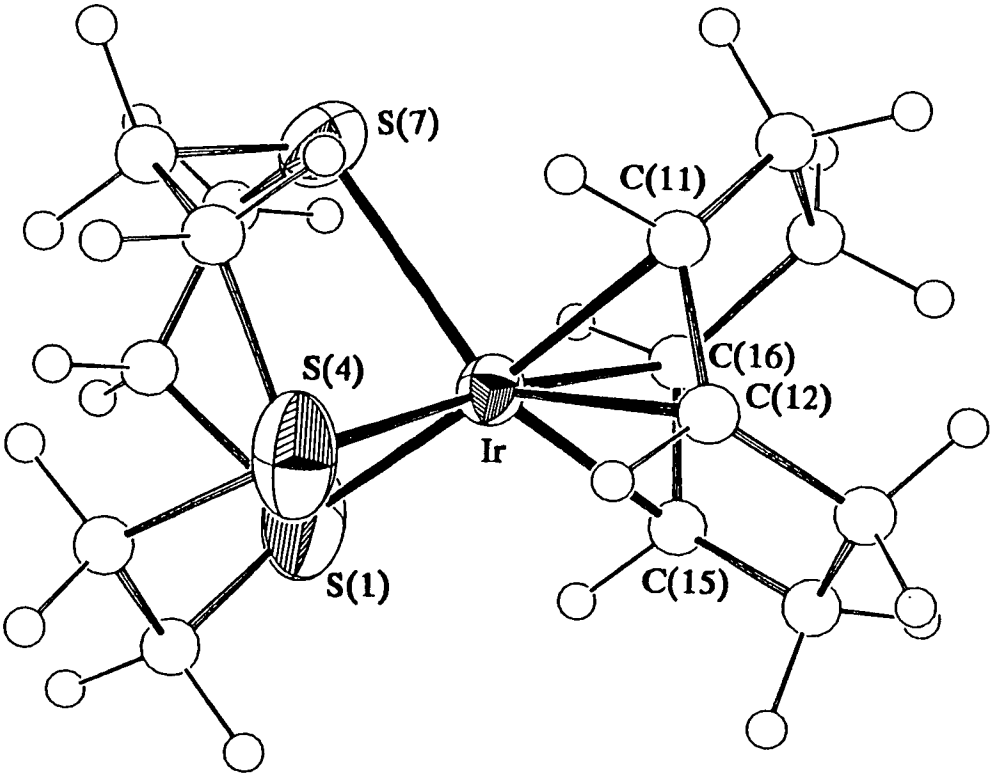

Figure 6.7: View of the Single Crystal Structure of $[Ir([9]aneS_3)(C_8H_{12})]^+$

Like molecule 1 of the single crystal structure of $[Rh([9]aneS_3)(C_8H_{12})]^+$ (Section 5.2.4), $[Ir([9]aneS_3)(C_8H_{12})]^+$ exhibits a highly distorted five-coordinate geometry. All three Ir-S distances are different from each other [Ir-S(1) = 2.319(5), Ir-S(4) = 2.343(4), Ir-S(7) = 2.419(4) Å]; in contrast to the Rh complex, however, all four Ir-C bond lengths are similar [Ir-C(11) = 2.166(14), Ir-C(12) = 2.199(14), Ir-C(15) = 2.188(15), Ir-C(16) = 2.141(15) Å]. Examination of the

Single Crystal Structure of [Ir([9]aneS$_3$)(C$_8$H$_{12}$)](PF$_6$)

Table 6.3. Bond Lengths(A) with standard deviations

Ir - S(1)	2.319(5)	C(11) -C(18)	1.499(21)
Ir - S(4)	2.343(4)	C(12) -C(13)	1.528(21)
Ir - S(7)	2.419(4)	C(13) -C(14)	1.474(23)
Ir -C(11)	2.166(14)	C(14) -C(15)	1.482(23)
Ir -C(12)	2.199(14)	C(15) -C(16)	1.418(21)
Ir -C(15)	2.188(15)	C(16) -C(17)	1.566(21)
Ir -C(16)	2.141(15)	C(17) -C(18)	1.528(21)
C(11) -C(12)	1.411(19)		

Table 6.4. Angles(degrees) with standard deviations

S(1) - Ir - S(4)	86.35(15)	Ir - S(4) -C(3')	102.3(5)
S(1) - Ir - S(7)	86.79(15)	Ir - S(4) - C(5)	100.6(4)
S(1) - Ir -C(11)	174.2(4)	Ir - S(4) -C(5')	105.2(6)
S(1) - Ir -C(12)	147.5(4)	C(3) - S(4) - C(5)	102.0(7)
S(1) - Ir -C(15)	84.3(4)	C(3') - S(4) -C(5')	97.8(7)
S(1) - Ir -C(16)	95.3(4)	Ir - S(7) - C(6)	103.5(5)
S(4) - Ir - S(7)	85.99(14)	Ir - S(7) -C(6')	100.6(5)
S(4) - Ir -C(11)	97.2(4)	Ir - S(7) - C(8)	98.8(5)
S(4) - Ir -C(12)	86.8(4)	Ir - S(7) -C(8')	102.6(5)
S(4) - Ir -C(15)	134.5(4)	C(6) - S(7) - C(8)	105.8(7)
S(4) - Ir -C(16)	171.9(4)	C(6') - S(7) -C(8')	101.0(7)
S(7) - Ir -C(11)	88.9(4)	Ir -C(11) -C(12)	72.4(8)
S(7) - Ir -C(12)	124.3(4)	Ir -C(11) -C(18)	110.3(9)
S(7) - Ir -C(15)	137.6(4)	C(12) -C(11) -C(18)	124.8(13)
S(7) - Ir -C(16)	102.0(4)	Ir -C(12) -C(11)	69.9(8)
C(11) - Ir -C(12)	37.7(5)	Ir -C(12) -C(13)	114.3(9)
C(11) - Ir -C(15)	96.3(5)	C(11) -C(12) -C(13)	123.3(12)
C(11) - Ir -C(16)	81.8(5)	C(12) -C(13) -C(14)	111.4(13)
C(12) - Ir -C(15)	78.1(5)	C(13) -C(14) -C(15)	115.1(14)
C(12) - Ir -C(16)	87.6(5)	Ir -C(15) -C(14)	112.1(10)
C(15) - Ir -C(16)	38.2(6)	Ir -C(15) -C(16)	69.1(8)
Ir - S(1) - C(2)	103.6(5)	C(14) -C(15) -C(16)	123.9(14)
Ir - S(1) -C(2')	106.0(6)	Ir -C(16) -C(15)	72.7(8)
Ir - S(1) - C(9)	105.1(5)	Ir -C(16) -C(17)	111.5(10)
Ir - S(1) -C(9')	100.9(5)	C(15) -C(16) -C(17)	125.0(13)
C(2) - S(1) - C(9)	97.2(7)	C(16) -C(17) -C(18)	113.8(12)
C(2') - S(1) -C(9')	101.9(7)	C(11) -C(18) -C(17)	112.9(12)
Ir - S(4) - C(3)	105.2(5)		

Table 6.5. Torsion angles(degrees) with standard deviations

C(9) - S(1) - C(2) - C(3)	-59.8(11)	C(3') - S(4) -C(5') -C(6')	-144.1(11)
C(2) - S(1) - C(9) - C(8)	142.8(10)	S(4) -C(5') -C(6') - S(7)	60.8(12)
S(1) - C(2) - C(3) - S(4)	-56.6(11)	C(5') -C(6') - S(7) -C(8')	55.0(12)
C(2) - C(3) - S(4) - C(5)	142.1(10)	C(6') - S(7) -C(8') -C(9')	-139.3(10)
C(3) - S(4) - C(5) - C(6)	-52.7(11)	S(7) -C(8') -C(9') - S(1)	61.4(12)
S(4) - C(5) - C(6) - S(7)	-60.8(11)	C(18) -C(11) -C(12) -C(13)	3.6(22)
C(5) - C(6) - S(7) - C(8)	137.3(10)	C(12) -C(11) -C(18) -C(17)	47.7(19)
C(6) - S(7) - C(8) - C(9)	-54.1(11)	C(11) -C(12) -C(13) -C(14)	-96.3(17)
S(7) - C(8) - C(9) - S(1)	-61.4(12)	C(12) -C(13) -C(14) -C(15)	31.6(19)
C(9') - S(1) -C(2') -C(3')	-140.4(11)	C(13) -C(14) -C(15) -C(16)	45.9(21)
C(2') - S(1) -C(9') -C(8')	54.7(12)	C(14) -C(15) -C(16) -C(17)	1.4(23)
S(1) -C(2') -C(3') - S(4)	56.7(12)	C(15) -C(16) -C(17) -C(18)	-88.9(18)
C(2') -C(3') - S(4) -C(5')	57.9(12)	C(16) -C(17) -C(18) -C(11)	26.6(17)

angles about the Ir centre (Table 6.8) shows that the cation is best described as a distorted square-pyramidal complex [*trans*-angles within the basal plane <S(1)-Ir-X(1) = 166.1(4), <S(4)-Ir-X(2) = 153.2(4)^0; apical-basal angles <S(7)-Ir-X(1) = 106.9(4), <S(7)-Ir-X(2) = 120.2(4)^0, where X(1), X(2) are the midpoints of the C(11)=C(12) and C(15)=C(16) double bonds respectively]. This distortion from a more symmetrical structure is probably caused by crystal packing forces: it is unlikely that steric repulsions between the [9]aneS$_3$ and cod ligands would be sufficient to impose a particular geometry onto the complex (c.f. the complexes [Ni([9]aneS$_3$)(PP)]$^{2+}$, Chapter 3).

6.2.7 [Ir([9]aneS$_3$)(C$_4$H$_6$)](PF$_6$)

Bubbling butadiene through a CH_2Cl_2 solution of [Ir$_2$(coe)$_4$Cl$_2$] at 298K for 5 mins afforded a colourless solution of [Ir(C$_4$H$_6$)$_2$Cl]^{270}, to which one molar equivalents of [9]aneS$_3$ and NH_4PF_6 were added. After stirring under N_2 at 298K for 15 mins, the resultant solution was filtered, reduced to *ca.* 1 cm^3 in volume, and the crude product crystallised with *n*-hexane. Recrystallisation from CH_3NO_2/diethyl ether afforded an off-white microcrystalline solid.

The f.a.b. mass spectrum of the complex showed peaks at M^+ = 427, 399 and 372, which were assigned to the fragments [^{193}Ir([9]aneS$_3$)(C$_4$H$_6$)]$^+$, [^{193}Ir([9]aneS$_3$)

$(C_2H_2)]^+$ and $[^{193}Ir([9]aneS_3\text{-}H)]^+$ respectively. This data, together with I.R. and n.m.r. spectroscopy and elemental analysis, were consistent with the desired formulation of $[Ir([9]aneS_3)(C_4H_6)](PF_6)$.

The ^1H n.m.r. spectrum of $[Ir([9]aneS_3)(C_4H_6)](PF_6)$ in d^6-acetone at 298K exhibited complex multiplet resonances at δ = 5.29 ppm (corresponding to the C_4H_6 CH protons), 3.08-2.92 ([9]$aneS_3$ SCH_2), 2.25 and 0.69 (C_4H_6 CH_2, Figure 6.8). The ^{13}C d.e.p.t. n.m.r. spectrum of the complex under similar conditions showed peaks at δ = 80.94 and 22.34 ppm, arising from the butadiene CH and CH_2 atoms respectively. Interestingly, this spectrum also exhibited three resonances in the region expected for the [9]$aneS_3$ SCH_2 groups, at δ = 37.63, 36.46 and 35.04 ppm (Figure 6.9a), implying that this complex has a static structure

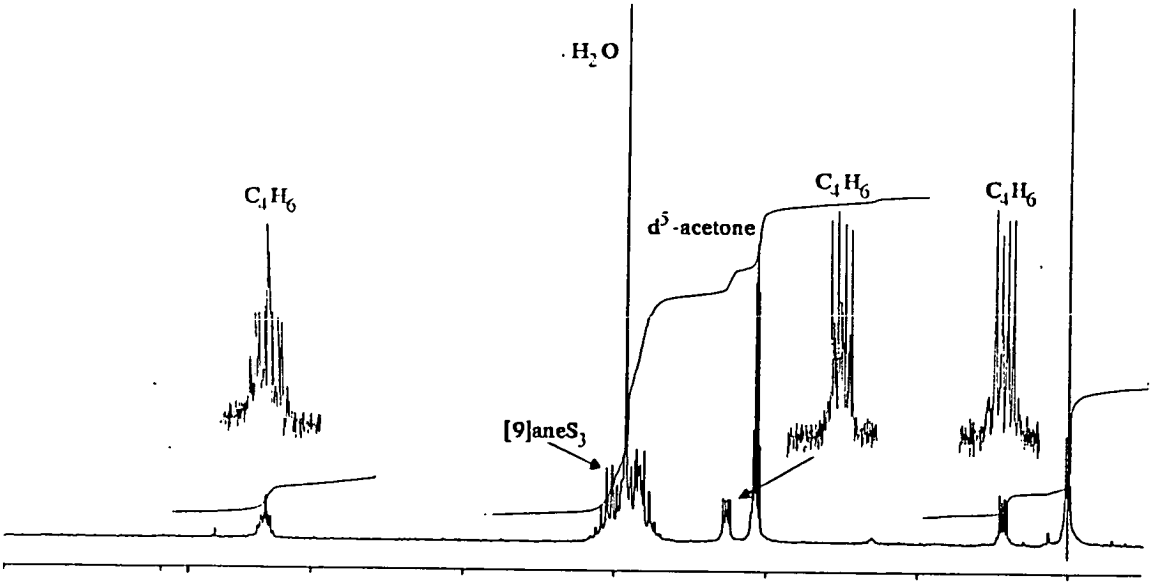

Figure 6.8: ^1H n.m.r. Spectrum of $[Ir([9]aneS_3)(C_4H_6)](PF_6)$ (200.13 MHz, d^8-acetone, 298K).

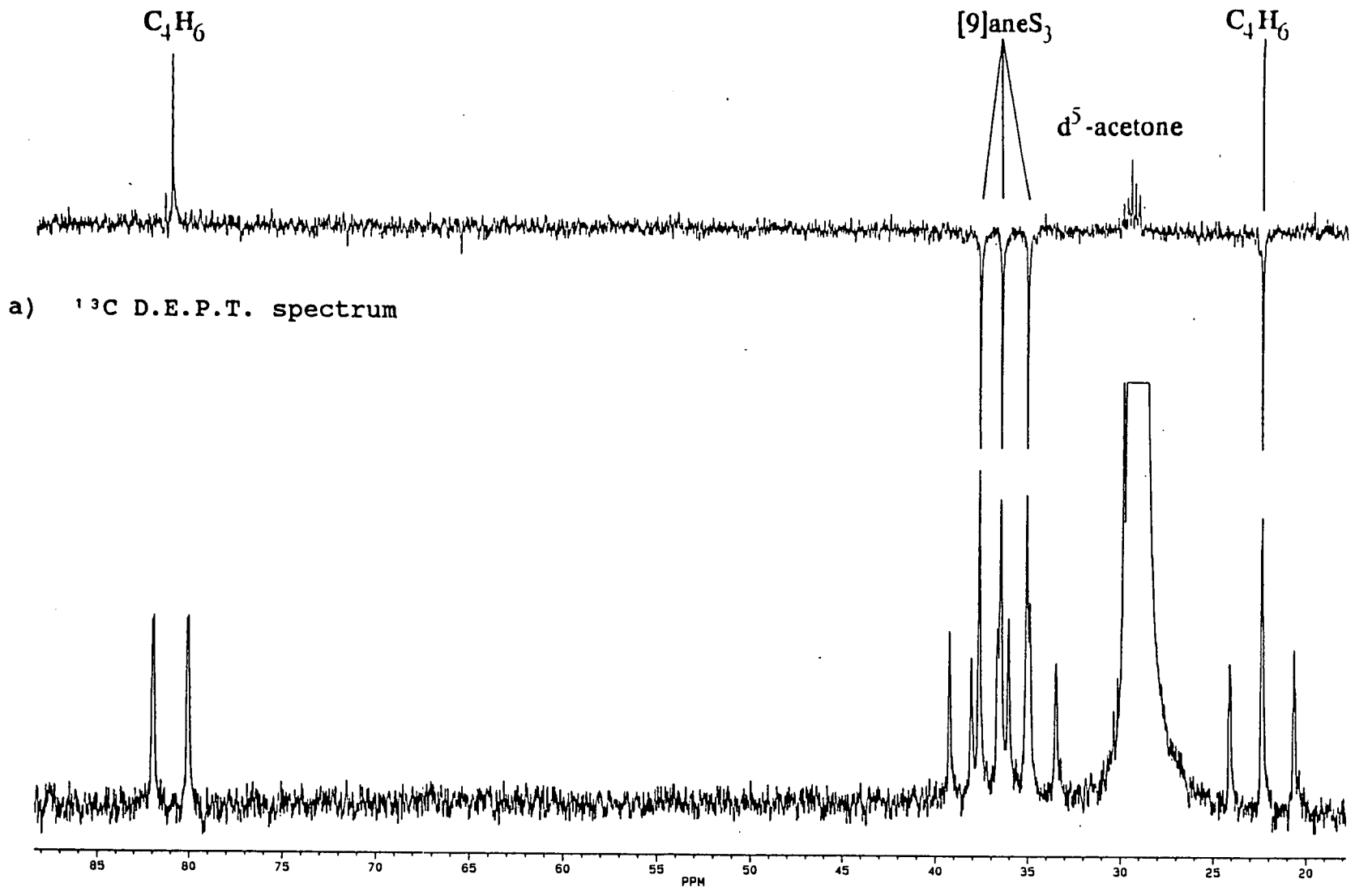

Figure 6.9: ^{13}C n.m.r. Spectra of [Ir([9]aneS$_3$)(C_4H_6)](PF$_6$) (90.56 MHz, d^6-acetone, 298K).

in solution with three distinct C-environments for the coordinated [9]aneS$_3$ (a, b and c, 58). This contrasts with [Ir([9]aneS$_3$)(C$_2$H$_4$)$_2$]$^+$, where no decoalescence is observed for the coordinated [9]aneS$_3$ down to 173K (Section 6.2.2). The ^{1}H and ^{13}C resonances for [9]aneS$_3$ in [Rh([9]aneS$_3$)(C$_4$H$_6$)]$^+$ do exhibit coalescence at *ca*. 319K, however (Section 5.2.5).

The non-fluxional behaviour of [Ir([9]aneS$_3$)(C$_4$H$_6$)]$^+$ can be explained if the complex cation is assumed to maintain its solid state geometry (Section 6.2.8) in solution. It has been observed that the activation barrier for CO scrambling in complexes [Fe(CO)$_3$(1,3-diene)], which are iso-electronic with [Ir([9]aneS$_3$)(C$_4$H$_6$)]$^+$, is significantly higher than for Fe(CO)$_3$ complexes of non-conjugated dienes[271]. For [Fe(CO)$_3$(C$_4$H$_6$)], this process is thought to occur by rotation of the [Fe(CO)$_3$] fragment about the central Fe-diene axis rather than via a Berry pseudo-rotation pathway, the barrier to rotation being measured as 40 kJ.mol^{-1} ($T_C \approx 230$K)[271a]. This behaviour has been rationalised by molecular orbital analysis (Figure 6.10)[272,273]. The rotation of the [Fe(CO)$_3$] fragment towards the transition state D (69) reduces the overlap of the butadiene $2\pi_S$ orbital with the Fe-based $2\pi_S$ orbital, leading to a significant destablilisation of the HOMO *4a'*. For an analogous non-conjugated diene complex, $2\pi_S$ lies >1 eV higher in energy than for butadiene. Hence, the *4a'*

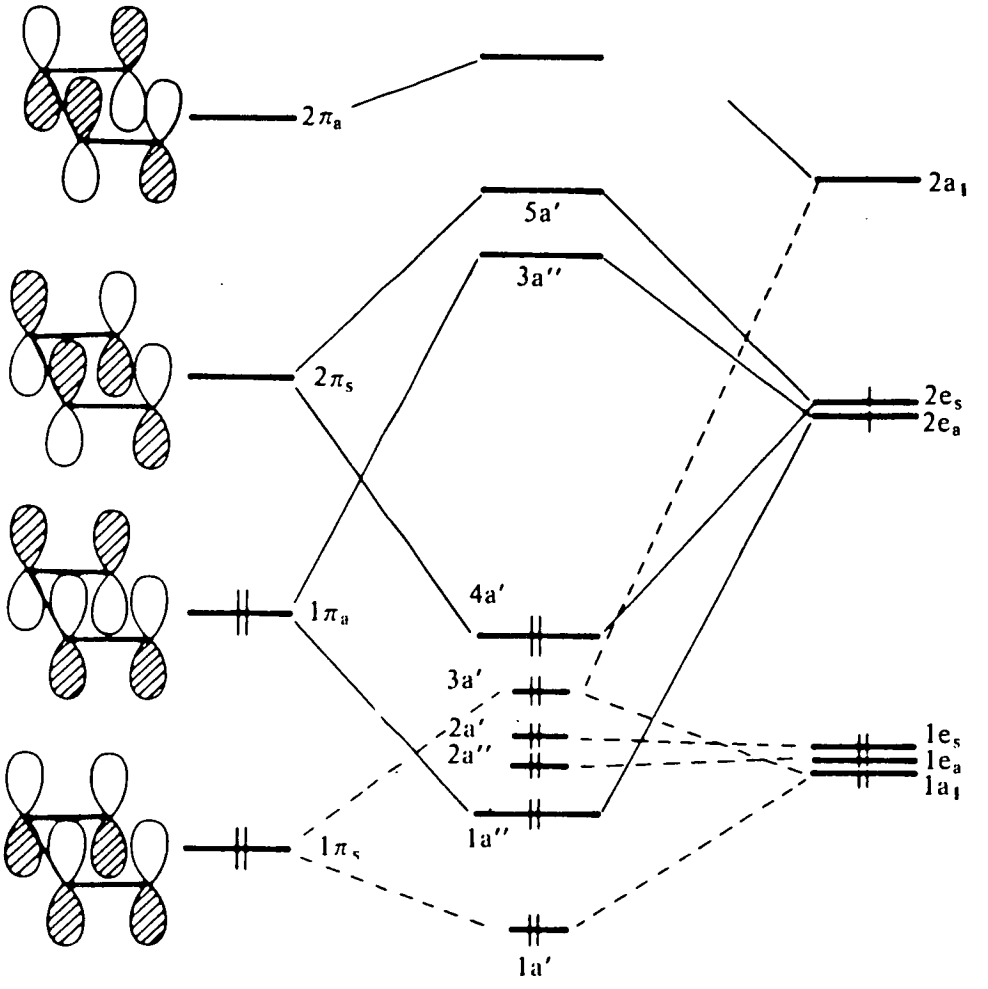

Figure 6.10: Molecular Orbital Diagram for $[Fe(CO)_3(C_4H_6)]$.

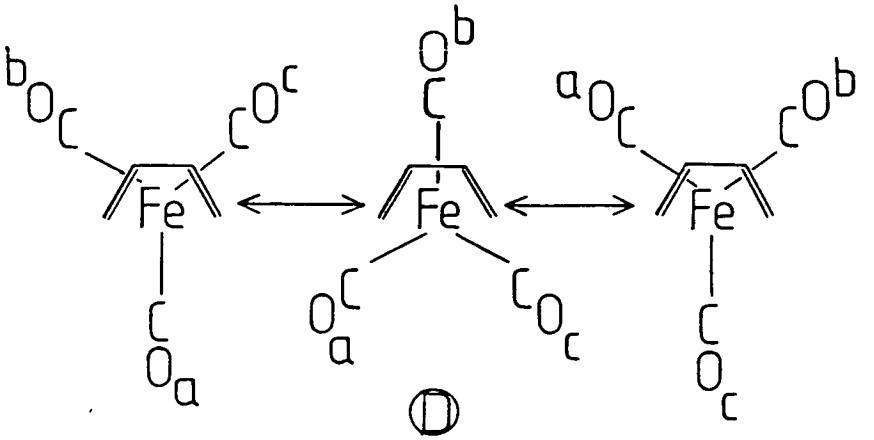

(69)

HOMO is now mainly Fe-based, and is relatively unaffected by rotation of the $[Fe(CO)_3]$ moiety, so the barrier to rotation is much reduced. For the third row transition metal complex $[Ir([9]aneS_3)(C_4H_6)]^+$, the barrier to rotation of the $[ML_3]^+$ fragment would be expected to be greater than for the first row Fe species, because the increased energy of the metal-based frontier orbitals of the $[Ir([9]aneS_3)]^+$ moiety allows greater interaction with the diene π-orbitals; this is indeed observed.

Other explanations for the static solution structure of $[Ir([9]aneS_3)(C_4H_6)]^+$ might be that the cation adopts a square planar geometry in solution, which would inhibit rotation of the $[9]aneS_3$ ring. Alternatively, significant $Ir^{I} \leftrightarrow Ir^{III}$ tautomerism of the type discussed previously (Section 6.3) would also restrict fluxionality about the Ir centre, which would posess significant d^6 Ir^{III} character. In order to determine the molecular geometry adopted by the complex, a single crystal x-ray analysis of $[Ir([9]aneS_3)(C_4H_6)](PF_6)$ was undertaken. A ^1H-coupled ^{13}C n.m.r. spectrum of the compound was also obtained (Figure 6.9b); the ^{13}C-^1H coupling constant thus derived are discussed below.

6.2.8 Single Crystal Structure of $[Ir([9]aneS_3)(C_4H_6)](PF_6) \cdot \frac{1}{2}[(C_2H_5)_2O]$

Details of the structure solution and refinement are given in Section 6.4.10, and selected bond lengths, angles and torsions are listed in Table 6.6. An ORTEP plot of the complex cation is shown in Figure 6.11.

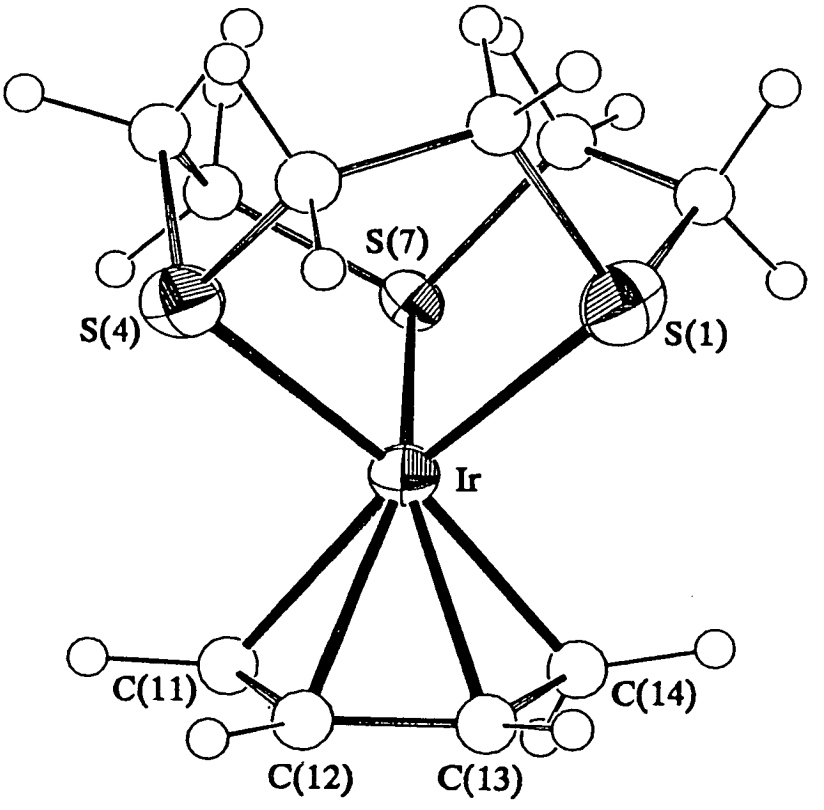

Figure 6.11: View of the Single Crystal Structure of $[Ir([9]aneS_3)(C_4H_6)]^+$.

Single Crystal Structure of $[Ir([9]aneS_3)(C_4H_6)](PF_6)\cdot \frac{1}{2}[(C_2H_5)_2O]$

Table 6.6. Bond Lengths(A), angles(degrees) and torsion angles(degrees) with standard deviations

Ir - S(1)	2.3310(25)	C(3) - S(4)	1.838(10)
Ir - S(4)	2.3249(23)	S(4) - C(5)	1.837(9)
Ir - S(7)	2.3206(20)	C(5) - C(6)	1.522(12)
Ir -C(11)	2.149(9)	C(6) - S(7)	1.830(8)
Ir -C(12)	2.141(9)	S(7) - C(8)	1.843(9)
Ir -C(13)	2.146(9)	C(8) - C(9)	1.508(13)
Ir -C(14)	2.115(10)	C(11) -C(12)	1.433(13)
S(1) - C(2)	1.824(10)	C(12) -C(13)	1.381(12)
S(1) - C(9)	1.828(10)	C(13) -C(14)	1.461(14)
C(2) - C(3)	1.517(13)		

S(1) - Ir - S(4)	89.07(8)	Ir - S(1) - C(9)	102.2(3)
S(1) - Ir - S(7)	88.06(8)	C(2) - S(1) - C(9)	100.7(4)
S(1) - Ir -C(11)	167.95(25)	S(1) - C(2) - C(3)	112.2(7)
S(1) - Ir -C(12)	129.11(24)	C(2) - C(3) - S(4)	113.4(7)
S(1) - Ir -C(13)	99.68(25)	Ir - S(4) - C(3)	101.5(3)
S(1) - Ir -C(14)	94.7(3)	Ir - S(4) - C(5)	105.4(3)
S(4) - Ir - S(7)	88.87(8)	C(3) - S(4) - C(5)	100.0(4)
S(4) - Ir -C(11)	94.86(25)	S(4) - C(5) - C(6)	111.9(6)
S(4) - Ir -C(12)	98.29(24)	S(7) - C(6) - C(5)	114.4(6)
S(4) - Ir -C(13)	125.73(25)	Ir - S(7) - C(6)	102.2(3)
S(4) - Ir -C(14)	165.8(3)	Ir - S(7) - C(8)	106.1(3)
S(7) - Ir -C(11)	103.38(25)	C(8) - S(7) - C(6)	102.0(4)
S(7) - Ir -C(12)	141.97(24)	S(7) - C(8) - C(9)	111.5(6)
S(7) - Ir -C(13)	144.33(25)	S(1) - C(9) - C(8)	114.4(7)
S(7) - Ir -C(14)	105.0(3)	Ir -C(11) -C(12)	70.2(5)
C(11) - Ir -C(12)	39.0(3)	Ir -C(12) -C(11)	70.8(5)
C(11) - Ir -C(13)	68.8(3)	Ir -C(12) -C(13)	71.4(5)
C(11) - Ir -C(14)	78.9(4)	C(11) -C(12) -C(13)	119.1(8)
C(12) - Ir -C(13)	37.6(3)	Ir -C(13) -C(12)	71.0(5)
C(12) - Ir -C(14)	68.8(4)	Ir -C(13) -C(14)	68.8(5)
C(13) - Ir -C(14)	40.1(4)	C(12) -C(13) -C(14)	115.5(8)
Ir - S(1) - C(2)	104.5(3)	Ir -C(14) -C(13)	71.1(5)

C(9) - S(1) - C(2) - C(3)	136.1(7)	S(4) - C(5) - C(6) - S(7)	-46.9(7)
C(2) - S(1) - C(9) - C(8)	-64.7(8)	C(6) - S(7) - C(8) - C(9)	132.9(6)
S(1) - C(2) - C(3) - S(4)	-50.2(8)	C(8) - S(7) - C(6) - C(5)	-68.1(7)
C(2) - C(3) - S(4) - C(5)	-65.4(7)	S(7) - C(8) - C(9) - S(1)	-46.9(8)
C(3) - S(4) - C(5) - C(6)	132.2(6)	C(11) -C(12) -C(13) -C(14)	0.2(13)

$[Ir([9]aneS_3)(C_4H_6)](PF_6)$ is isostructural with its Rh analogue (Section 5.2.6). The $[9]aneS_3$ ligand is bound symmetrically to the Ir atom, with all three Ir-S distances being identical [Ir-S(1) = 2.3310(25), Ir-S(4) = 2.3249(23), Ir-S(7) = 2.3206(20) Å], and the butadiene ligand is bound in *cis* η^4-fashion [Ir-C(11) = 2.149(9), Ir-C(12) = 2.141(9), Ir-C(13) = 2.146(9), Ir-C(14) = 2.115(10) Å]. The angles about the Ir centre are consistent with a *quasi*-square pyramidal geometry (Table 6.8). However, the cation is probably best described as a mixed sandwich complex, with the $[Ir([9]aneS_3)]^+$ fragment binding to the butadiene ligand in a manner analogous to other d^8 $[ML_3]$ fragments such as $[M(CO)_3]$ (M = Fe, Ru). The stereochemistry observed for the complex cation, with one Ir-S bond pointing towards the open edge of the C_4H_6 ligand, is the same as that observed for other iso-electronic complexes such as $[Fe(CO)_3(C_4H_6)]$ and $[Co(PMe_3)_3(C_4H_6)]^+$ [274]: this orientation of the $[ML_3]^{n+}$ fragment relative to the C_4H_6 ligand has been found to be electronically favoured[272].

The C-C bond lengths within the coordinated butadiene ligand in $[Ir([9]aneS_3)(C_4H_6)]^+$ are very different from those of free C_4H_6 [C(11)-C(12) = 1.433(13), C(12)-C(13) = 1.381(12), C(13)-C(14) = 1.461(13) Å; c.f. for free C_4H_6 C=C = 1.343(1), C-C = 1.467(1) Å from electron diffraction data[275]]. Whilst equalisation of the butadiene C-C bond lengths would be expected on coordination to a metal

centre[273,276], the degree of distortion observed for $[M([9]aneS_3)(C_4H_6)]^+$ (M = Rh, Ir) is unusual for butadiene complexes of group 8-10 metals. This may reflect $M^{I} \leftrightarrow M^{III}$ tautomerism similar to that discussed for $[Ir([9]aneS_3)(C_2H_4)_2]^+$ (Section 6.2.3):

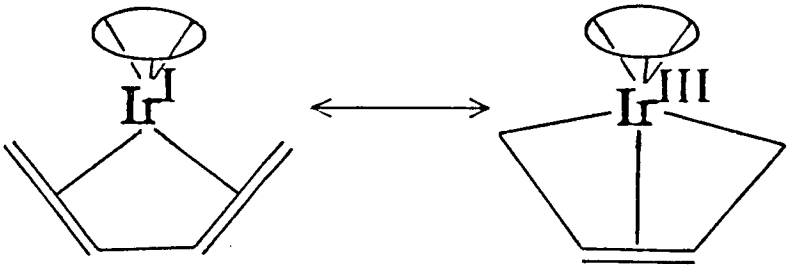

Metallacyclopent-3-ene structures have been proposed for some 1,3-diene complexes of Nb, Ta and Zr[277,278]. For these species, the central C-C bond of the butadiene fragment is shorter than the outer two, and the metal-C bonds to the two outer C atoms are shorter than those to the inner C atoms; e.g. for $[(C_5H_5)TaCl_2(C_4H_6)]$ Ta-C(1) = 2.258(12), Ta-C(2) = 2.424(11), Ta-C(3) = 2.410(12), Ta-C(4) = 2.257(11), C(1)-C(2) = 1.458(16), C(2)-C(3) = 1.375(16), C(3)-C(4) = 1.453(16) Å (70)[278].

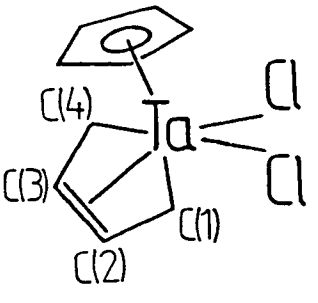

Table 6.7: ^{13}C n.m.r. Data for Some Butadiene Complexes

	^{13}C δ,ppm($^{1}J_{C-H}$,Hz) for: C(1)/C(4)	C(2)/C(3)	Reference
$[Rh([9]aneS_3)(C_4H_6)]^+$	35.4(158,158)	90.0(170)	This work
$[Ir([9]aneS_3)(C_4H_6)]^+$	20.9(156,160)	79.5(171)	This work
$[Fe(CO)_3(C_4H_6)]$	41.1(158,161)	85.8(169)	279
$[Ru(CO)_3(C_4H_6)]$	32.7(156,160)	86.3(168)	279
$[Ta(C_5H_5)Cl_2(C_4H_6)]$	62.4(146,146)	126.1(169)	278
$[Zr(C_5H_5)_2(C_4H_6)]$	48.4(145,145)	110.9(154)	280
Free C_4H_6	116.6(158,158)	137.2(158)	281

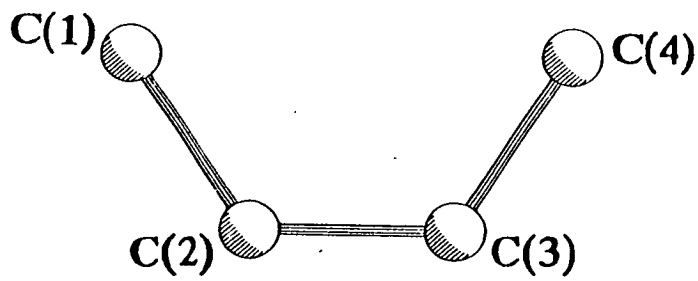

The metallacyclopentene form of these complexes is also reflected in their ^1H and ^{13}C n.m.r. spectra. In particular, the $^1J_{C-H}$ coupling constants for the butadiene CH_2 groups of metallacyclopentene species are 10-25 Hz lower than those in η^4-π-complexes[278], reflecting the increased sp^3 hybridisation at these C atoms for the former compounds.

In order to quantify the metal-butadiene bonding in the complexes $[M([9]aneS_3)(C_4H_6)]^+$ (M = Rh, Ir), their ^1H-coupled ^{13}C n.m.r. spectra were obtained (Figures 5.11b, 6.9b). The $^1J_{C-H}$ coupling constants derived from these spectra are listed in Table 6.7. The $^1J_{C-H}$ coupling constants for both the Rh and Ir complexes are very similar to those observed previously for $[M(CO)_3(C_4H_6)]$[279], but are significantly greater than those of Ta and Zr species such as $[Ta(C_5H_5)Cl_2(C_4H_6)]$ and $[Zr(C_5H_5)_2(C_4H_6)]$[278,280]. Using the semi-empirical expression relating $^1J_{C-H}$ coupling constants to the degree of hybridisation at the C atom[282]:

$$^1J_{C-H}(Hz) = 5.70(\%s) - 18.4 \qquad (71)$$

we obtain a figure of 30.9% s-character at the butadiene outer C atoms for $[M([9]aneS_3)(C_4H_6)]^+$ (M = Rh, Ir). This corresponds to n=2.2 for sp^n hybridisation at the C_4H_6 CH_2 groups; metallacyclopentene species generally give n=2.6-2.7 for these atoms[278]. For the butadiene CH C

atoms of $[M([9]aneS_3)(C_4H_6)]^+$ the s-character is calculated as 33.1%, giving n=2.0.

The above results show that the complexes $[M([9]aneS_3)(C_4H_6)]^+$ (M = Rh, Ir) are best considered as 18-electron M^I species containing an η^4 butadiene ligand, in common with other late transition metal C_4H_6 complexes. The highly distorted C-C bond lengths within the butadiene ligands in these species could arise from either abnormally efficient $C_4H_6 \rightarrow M$ σ-donation or from significant $M \rightarrow C_4H_6$ π-back bonding. Given the +1 charge on the complexes, and the low barriers to ethene rotation observed for the analogous compounds $[M([9]aneS_3)(C_2H_4)_2]^+$, the former explanation is more likely.

	$[Rh([9]aneS_3)(L)_2]^+$					$[Ir([9]aneS_3)(L)_2]^+$		
	$L=C_2H_4$		$L=\frac{1}{2}(cod)$					
	Molecule 1	Molecule 2	Molecule 1	Molecule 2	$L=\frac{1}{2}(C_4H_6)$	$L=C_2H_4$	$L=\frac{1}{2}(cod)$	$L=\frac{1}{2}(C_4H_6)$
M-S(1) (Å)	2.322(9)	2.337(9)	2.3213(25)	2.3059(24)	2.3417(15)	2.3165(18)	2.319(5)	2.3310(25)
M-S(4) (Å)	2.438(9)	2.327(10)	2.3966(25)	2.4443(24)	2.3374(14)	2.4024(18)	2.343(4)	2.3249(23)
M-s(7) (Å)	2.433(9)	2.469(10)	2.4457(24)	2.4358(23)	2.3580(12)	2.3835(16)	2.419(4)	2.3206(20)
M-X(1) (Å)	2.11(4)	2.02(4)	2.098(9)	2.101(10)	2.011(5)	2.074(9)	2.066(15)	2.022(9)
M-X(2) (Å)	1.96(4)	2.07(4)	1.977(9)	1.979(9)	1.989(5)	2.006(9)	2.045(15)	2.002(9)
<S(1)-M-X(1)°	178.2(12)	161.7(11)	172.40(24)	174.07(28)	149.68(14)	173.90(26)	166.1(4)	148.62(26)
<S(1)-M-X(2)°	85.9(13)	88.7(10)	88.37(26)	88.97(26)	98.12(15)	84.61(22)	89.7(4)	97.65(28)
<S(4)-M-X(1)°	92.5(12)	88.1(11)	96.33(24)	97.64(27)	97.73(14)	98.74(26)	92.1(4)	96.97(26)
<S(4)-M-X(2)°	140.3(10)	160.1(10)	144.16(26)	135.80(26)	147.21(15)	129.94(22)	153.2(4)	145.61(28)
<S(7)-M-X(1)°	95.5(12)	110.6(11)	100.72(24)	97.19(27)	121.70(14)	93.57(25)	106.9(4)	122.69(26)
<S(7)-M-X(2)°	132.8(13)	112.8(10)	128.74(26)	137.48(26)	123.42(15)	142.26(22)	120.2(4)	124.88(28)
<X(1)-M-X(2)°	93.0(17)	90.7(14)	84.9(3)	85.1(4)	61.52(20)	90.9(3)	85.5(6)	61.1(4)

X = midpoint of alkene C=C bond.

All <S-M-S angles lie between 86 and 90°.

Table 6.8: Selected Structural Parameters for $[M([9]aneS_3)(L)_2]^+$ (M = Rh, Ir; L = C_2H_4, ½cod, ½C_4H_6).

6.2.9 $Ir([9]aneS_3)(CO)PPh_3)](PF_6)$

Treatment of $[Ir(CO)Cl(PPh_3)_2]$ with one molar equivalent of $[9]aneS_3$ and $TlPF_6$ in refluxing CH_2Cl_2 under N_2 afforded a pale yellow solution and white precipitate. The solution was filtered, reduced to *ca.* 1 cm^3 volume, and the addition of *n*-hexane yielded a pale yellow solid which was recrystallised from CH_3CN/diethyl ether.

The I.R. spectrum of this compound indicated the presence of $[9]aneS_3$, PPh_3 and CO ligands (ν_{CO} = 1,945 cm^{-1} in CH_3NO_2) and PF_6^- counterion. F.a.b. mass spectrometry showed peaks at M^+ = 663, 634, 483 and 455, which were assigned to the molecular ions $[^{193}Ir([9]aneS_3)(CO)(PPh_3)]^+$, $[^{193}Ir([9]aneS_3\text{-}H)(PPh_3)]^+$, $[^{193}Ir(CO)PPh_3)]^+$ and $[^{193}Ir(PPh_3)]^+$. The ^1H n.m.r. spectrum of the complex in d^6-acetone at 298K exhibited two multiplets at δ = 7.86-7.54 ppm (15H) and 2.75-2.55 (12H), corresponding to the H atoms of the PPh_3 and $[9]aneS_3$ ligands respectively. The $^{13}C\{^1H\}$ n.m.r. spectrum exhibited resonances at δ = 133.49, 131.09, 130.75 and 127.95 ppm assigned to the PPh_3 ligand, and 34.04 ppm from the $[9]aneS_3$ macrocycle; no ^{13}C n.m.r. resonance was observed in the region expected for the CO ligand, due to the low solubility of the complex. These spectra are all consistent with the formulation $[Ir([9]aneS_3)(CO)(PPh_3)(PF_6)$; this assignment was supported by elemental analytical data.

The C≡O stretching frequency of $[Ir([9]aneS_3)(CO)$

$(PPh_3)](PF_6)$ in solution and the solid state is very similar to that for $[Rh([9]aneS_3)(CO)(PPh_3)]^+$ (ν_{CO} = 1,945 cm^{-1} for M = Ir, c.f. 1,960 cm^{-1} for M = Rh, in CH_3NO_2 solution]. This implies that $[Ir([9]aneS_3)(CO)(PPh_3)]^+$ is probably isostructural with its Rh analogue, which adopts a trigonal bipyramidal stereochemistry in the solid state (Section 5.2.10).

6.2.10 Electrochemical Study of $[Ir([9]aneS_3)(L)_2]^+$

The cyclic voltammograms of all the complexes described in this chapter were measured in CH_3CN/0.1M $^nBu_4NPF_6$ at 298K. Each compound exhibited a single irreversible oxidation (Table 6.9, Figure 6.12); there is no obvious correlation between the oxidation potentials of the Ir complexes and their Rh analogues (Table 5.9). No reductive behaviour was observed for any of the compounds.

Coulometric measurements on the oxidation processes for the complexes $[Ir([9]aneS_3)(L)_2](PF_6)$ gave n = 0.90-1.07 (Table 6.9), consistent with overall one-electron processes. Bulk solutions of the oxidation products generated by controlled potential electrolysis were pale yellow in colour, and e.p.r. silent; no current flow was observed on attempting re-reduction of the samples at OV *vs.* Ag/AgCl. This is consistent with the formation of diamagnetic metal-metal bonded Ir^{II}-Ir^{II} dimeric species, possibly with bridging S-donors, although in the absence of supporting data this assignment must

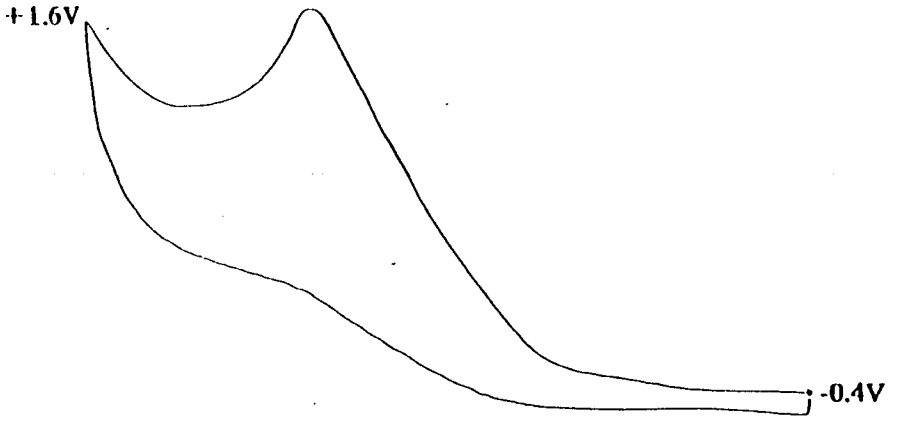

Figure 6.12: Cyclic Voltammogram of [Ir([9]aneS$_3$)(C_2H_4)$_2$](PF$_6$) ($CH_3CN/^nBu_4NPF_6$, 298K, scan rate 400 mV/s).

Complex	Ep_a(V) *vs.* Fc/Fc^+	n
[Ir([9]aneS$_3$)(C_2H_4)$_2$](PF$_6$)	+0.97	1.03
[Ir([9]aneS$_3$)(C_8H_{14})$_2$](PF$_6$)	+0.48	0.90
[Ir([9]aneS$_3$)(C_8H_{12})](PF$_6$)	+0.39	0.92
[Ir(9]aneS$_3$)(C_4H_6)](PF$_6$)	+1.05	1.07
[Ir(9]aneS$_3$)(CO)(PPh_3](PF$_6$)	+0.19	0.95

Table 6.9: Electrochemical Data for [Ir([9]aneS$_3$)(L)$_2$](PF$_6$). (Potentials measured in CH_3CN/0.1M $^nBu_4NPF_6$, 298K, scan rate 400 mV/s: n = Coulometric determination).

remain highly tentative. The chemistry of Ir^{II} is dominated by the formation of binuclear complexes; with the exception of Ir^{II} porphyrin species, most known Ir^{II}-Ir^{II} dimers are supported by bridging ligands such as RS^- or H^- [43,283,284].

Further experiments would be necessary to confirm the dimeric nature of the oxidation products. In particular, *in situ* experiments to follow the oxidations by U.V./visible or e.p.r. spectroscopy might allow the detection of transient mononuclear intermediates.

6.3 CONCLUSIONS

A series of half-sandwich compounds of formula $[Ir([9]aneS_3)(L)_2]^+$ (L = C_2H_4, C_8H_{14}, $\frac{1}{2}C_8H_{12}$, $\frac{1}{2}C_4H_6$, CO, PPh_3) has been synthesised and characterised. Like their Rh analogues (Chapter 5), the Ir *bis*-C_2H_4 and C_8H_{12} complexes adopt five-coordinate structures in the solid state, although the geometries observed are not identical to those of the Rh species (Table 6.8). It has been shown that rotation of the [9]aneS$_3$ ring about the central Ir-[9]aneS$_3$ axis in solution is a facile process: hence, the stereochemistry adopted by $[M([9]aneS_3)(L)_2]^+$ (M = Rh, Ir; L = C_2H_4, $\frac{1}{2}C_8H_{12}$) in the solid state is probably strongly influenced by crystal packing forces. The unreactivity of $[Ir([9]aneS_3)(L)_2]^+$ (L = C_2H_4, C_8H_{14}) towards CO or cod under thermal conditions implies that these complexes maintain five-coordinate, 18-electron

structures in solution. Unlike the other Ir compounds, the ^{13}C n.m.r. spectrum of $[Ir([9]aneS_3)(C_4H_6)]^+$ at 298K indicates a static structure for this complex in solution. This is also consistent with it also adopting a five-coordinate geometry in solution, however.

The single crystal structures of $[M([9]aneS_3)(C_2H_4)_2]^+$ and $[M([9]aneS_3)(C_4H_6)]^+$ (M = Rh, Ir) show that the C-C bond lengths within the coordinated alkenes are distorted from those of the free alkenes to an unusual degree. It has been shown that this is not due to oxidative addition across the alkene C=C bonds to give formally M^{III} metallacyclic species. Rather, it is probably evidence of high electrophilic character at the Rh^I and Ir^I centres. This is supported by the low barriers to ethene rotation observed for $[M([9]aneS_3)(C_2H_4)_2]^+$ (M = Rh, Ir). No electrochemically or chemically reversible processes were observed in the cyclic voltammograms of the complexes $[Ir([9]aneS_3)(L)_2]^+$. Each complex exhibited a single irreversible one-electron oxidation, giving e.p.r. inactive products which were tentatively assigned to dimeric structures (c.f. the reduction product of $[Ir([9]aneS_3)_2]^{3+}$ [250].

Due to time constraints, the reactivity of the Ir^I complexes towards oxidative addition substrates was not examined. It should be noted that these Ir^I-compounds are considerably more thermally and air-stable than the analogues Rh^I species, suggesting that the Ir^I compounds

may be more inert to electrophilic attack than their Rh analogues.

6.4 EXPERIMENTAL

6.4.1 Synthesis of $[Ir_2(C_8H_{14})_4Cl_2]$[285]

$IrCl_3.3H_2O$ (1.00 g, 2.8 x 10^{-3} mol) and cyclooctene (2 cm^3) were refluxed in 2-propanol (11 cm^3) and H_2O (4 cm^3) under N_2 for 3 hrs. The resulting orange precipitate was filtered, washed with cold methanol and dried *in vacuo*. Yield = 0.60 g, 47%. Mol. wt. 896.15. Elemental analysis: found C = 42.7, H = 6.21%; calculated for $[C_{32}H_{56}Ir_2Cl_2]$ C = 42.9, H = 6.29%. I.R. spectrum (KBr disc): 2970 m, 2900 s, 2840 s, 2660 w, 1460 s, 1450 s, 1380 w, 1365 s, 1355 m, 1345 w, 1320 w, 1300 w, 1275 m, 1255 w, 1245 w, 1230 m, 1210 w, 1170 m, 1150 m, 1120 w, 1090 w, 1065 w, 1040 w, 1020 w, 985 w, 970 w, 955 m, 930 w, 915 s, 890 w, 880 w, 865 w, 850 m, 840 m, 810 m, 765 m, 750 w, 735 m, 635 m, 580 s, 550 s, 460 w, 435 m, 315 m cm^{-1}.

6.4.2 Synthesis of $[Ir_2(C_8H_{12})_2Cl_2]$[285]

$IrCl_3.3H_2O$ (1.00 g, 2.8 x 10^{-3} mol) was refluxed with cod (3 cm^3) in 2:1 ethanol/water (25 cm^3) under N_2 for 24 hrs. The yellow-orange precipitate product was filtered, and washed with cold methanol (Yield 0.47 g, 50%). Mol. wt. 671.71. Elemental analysis: found C = 28.4, H = 3.65%; calculated for $[C_{16}H_{24}Ir_2Cl_2]$ C = 28.6, H = 3.60%.

I.R. spectrum (KBr disc): 2960 w, 2930 m, 2900 w, 2870 m, 2820 m, 1465 m, 1445 s, 1420 m, 1355 w, 1320 s, 1290 m, 1260 w, 1230 m, 1205 m, 1165 m, 1150 m, 1070 m, 1000 s, 980 s, 905 s, 870 m, 830 s, 805 m, 780 m, 700 w, 670 w, 600 w, 560 w, 530 m, 510 w, 500 m, 450 w, 415 m, 340 w cm^{-1}.

6.4.3 Synthsis of $[Ir(CO)Cl(PPh_3)_2]$[247]

$IrCl_3.3H_2O$ (0.58 g, 1.6 x 10^{-3} mol) and PPh_3 (2.16 g, 8.2 x 10^{-3} mol) were refluxed in DMF (24 cm^3) under N_2 for 15 hrs. The resulting yellow solution was filtered hot, then hot methanol (50 cm^3) was added to the warm filtrate and the mixture left to cool. The product crystallised as fluorescent yellow microcrystals (Yield 1.03 g, 80%). Mol. wt. 780.26. Elemental analysis: found C = 57.3, H = 3.93%; calculated for $[C_{37}H_{30}P_3OClIr]$ C = 57.0; H = 3.88%. I.R. spectrum ($CHCl_3$ solution): 1968 cm^{-1}. I.R. spectrum (KBr disc): 3060 w, 3050 w, 3000 w, 2000 w, 1950 s, 1900 w, 1585 w, 1570 w, 1475 s, 1430 s, 1380 s, 1330 w, 1310 w, 1180 m, 1160 w, 1120 w, 1095 s, 1070 w, 1025 m, 1000 m, 970 w, 920 w, 840 w, 745 s, 705 s, 690 s, 620 w, 600 m, 570 w, 545 w, 520 s, 510 s, 500 s, 460 w, 440 w, 420 m, 315 m cm^{-1}

6.4.4 Synthesis of $[Ir([9]aneS_3)(C_2H_4)_2](PF_6)$

Ethene was bubbled through a solution of $[Ir_2(coe)_4Cl_2]$ (0.075 g, 0.8 x 10^{-4} mol) in THF (6 cm^3)

for 10 minutes, until the solution became colourless. To the resulting solution was added [9]aneS$_3$ (0.030 g, 1.6 x 10^{-4} mol) and NH_4PF_6 (0.027 g, 1.6 x 10^{-4} mol), and the mixture was stirred at room temperature under N_2 for 15 mins. The solution was filtered, and the solvent removed under vacuum. The crude product was recrystallised from CH_2Cl_2/hexane, and isolated as a pale yellow solid (Yield 0.048 g, 50%). Mol. wt. 573.57. Elemental analysis: found C = 20.7, H = 3.42%; calculated for $[C_{10}H_{20}S_3Ir](PF_6)$, C = 20.9, H = 3.49%. F.a.b. mass spectrum: found M^+ = 429, 401, 373; calculated for

$[^{193}Ir([9]aneS_3)(C_2H_4)_2]^+$ $M^+ = 429$

$[^{193}Ir([9]aneS_3)(C_2H_4)]^+$ $M^+ = 401$

$[^{193}Ir([9]aneS_3)]^+$ $M^+ = 373$

^1H nmr spectrum (360.13 MHz, d^6-acetone, 298 K) δ 3.11-2.98 ppm (m, 12H, [9]aneS$_3$), 2.19 (s, 8H, C_2H_4). ^{13}C d.e.p.t. nmr spectrum (50.32 MHz, d^6-acetone, 298 K) δ = 35.51 ppm (s, [9]aneS$_3$), 34.35 (s, C_2H_4). U.V./vis spectrum (CH_3CN) λ_{max} = 356 nm (ε_{max} = 750 dm^3 mol^{-1} cm^{-1}), 290 (2,350), 229 (8,230). I.R. spectrum (KBr disc): 3040 w, 2990 m, 2920 w, 1470 w, 1450 s, 1435 w, 1410 s, 1300 w, 1285 w, 1265 w, 1225 m, 1190 w, 1170 w, 1130 m, 1015 m, 995 w, 970 w, 860 vs, 740 m, 680 w, 660 w, 555 s, 490 w, 445 w, 390 w cm^{-1}.

6.4.5 Single Crystal Structure of [Ir([9]aneS$_3$)-(C$_2$H$_4$)$_2$](PF$_6$)

Pale yellow crystals of the title compound were grown by vapour diffusion of diethyl ether into an acetone solution of the complex. A suitable crystal was mounted on a glass fibre, and placed in a cold stream of CO_2 at 150 K.

Crystal Data:

$[C_{10}H_{20}S_3Ir](PF_6)$, M_r = 573.57. Monoclinic, space group $P2_1/n$, a = 11.461(3), b = 9.521(5), c = 15.653(8) Å, β = 105.44(4)°, V = 1646 Å^3 (by least-squares refinement on diffractometer angles for 26 centred reflections [30<2θ<32°, λ = 0.71073 Å]), Z = 4, D_c = 2.314 g cm^{-3}. Crystal dimensions 0.70 x 0.39 x 0.12 mm, μ (Mo-K$_\alpha$) = 8.588 mm^{-1} $F(000)$ = 1096.

Data Collection and Processing:

Stoë STADI-4 four circle diffractometer, $\omega/2\theta$ scan mode using the learnt profile method. Graphite-monochromated Mo-K$_\alpha$ radiation: 3574 data measured ($2\theta_{max}$ = 45°, h = -12→11, k = Ø→10, l = Ø→16), 2094 unique (R_{int} = 0.0349), giving 1897 with $F>4\sigma(F)$. No crystal decay, no absorption correction.

Structure Analysis and Refinement:

The Ir atom was located using a Patterson synthesis,

and the structure was then developed using iterative rounds of least-squares refinement and difference Fourier synthesis. At isotropic convergence, a final empirical absorption correction was made using DIFABS (maximum correction 1.509, minimum correction 0.799). During refinement, the PF_6^- counterion was found to be disordered by rotation about one F-P-F axis; this was modelled using three distinct, equally occupied orientations. Anisotropic thermal parameters were refined for Ir, C, S, P and ordered F atoms. The H atoms were included in fixed, calculated positions, the ethene H atoms fixed so that C-H = 1.08 Å, C-C-H = 120°, Ir-C-C-H = $\pm 103^{\circ 248}$. At final convergence R = 0.0278, R_W = 0.0360, S = 1.099 for 202 parameters, and in the final difference Fourier synthesis the maximum and minimum residuals were +0.88 and -0.87 eÅ^{-3} respectively. The weighting scheme $w^{-1} = F^2 + 0.000105\sigma^2(F)$ gave satisfactory agreement analyses.

6.4.6 Synthesis of $[Ir([9]aneS_3)(C_8H_{14})_2](PF_6)$

$[Ir_2(coe)_4Cl_2]$ (0.075 g, 0.8 x 10^{-4} mol), $[9]aneS_3$ (0.030 g, 1.6 x 10^{-4} mol) and NH_4PF_6 (0.027 g, 1.6x10^{-4} mol) were stirred in acetone (6 cm^3) under N_2 at 298 K. After 15 mins the solution was filtered and reduced to ~2 cm^3, and the product crystallised with diethyl ether. Recrystallisation from acetonitrile/diethyl ether under N_2 yielded pale yellow microcrystals (Yield 0.081 g, 65%). Mol. wt. 737.86. Elemental analysis: found C = 35.5, H =

5.55%; calculated for $[C_{22}H_{40}S_3Ir](PF_6)$ C = 35.8, H = 5.46%. F.a.b. mass spectrum: found M^+ = 593, 483, 372; calculated for:

$[^{193}Ir([9]aneS_3)(C_8H_{14})_2]^+$ $M^+ = 593$

$[^{193}Ir([9]aneS_3)(C_8H_{14})]^+$ $M^+ = 483$

$[^{193}Ir([9]aneS_3\text{-}H)]^+$ $M^+ = 372$

^1H nmr spectrum (200.13 MHz, CD_3NO_2, 298 K) δ = 5.62 ppm (m, 4H, coe C*H*), 2.97-2.10 (m, 36H, [9]aneS_3 + coe CH_2). ^{13}C D.E.P.T. nmr spectrum (50.32 MHz, CD_3NO_2, 298 K) δ = 61.44 ppm (s, coe *C*H), 35.19 (s, [9]aneS_3), 31.00 (s, coe α-CH_2), 28.41 (s, coe β-CH_2), 25.02 (s, coe γ-CH_2). U.V./vis spectrum (CH_3CN): λ_{max} = 335 nm (sh), 285 (ε_{max} = 2,300 dm^3 mol^{-1} cm^{-1}), 245 (8,370). I.R. spectrum (KBr disc): 3000 w, 2970 m, 2910 s, 2860 s, 2670 w, 1465 s, 1450 s, 1435 s, 1410 s, 1355 m, 1340 w, 1320 w, 1290 w, 1280 m, 1260 w, 1240 m, 1225 m, 1205 w, 1190 w, 1175 m, 1145 m, 1120 w, 1090 m, 1070 w, 1040 w, 1020 w, 985 w, 970 w, 960 w, 930 w, 905 m, 840 vs, 740 s, 680 w, 660 w, 635 w, 605 w, 560 s, 540 m, 520 w, 485 w, 435 w, 420 w cm^{-1}.

6.4.7 Synthesis of $[Ir([9]aneS_3)(C_8H_{12})](PF_6)$

[9]aneS_3 (0.030 g, 1.6 x 10^{-4} mol) and NH_4PF_2 (0.027 g, 1.6 x 10^{-4} mol) were added to $[Ir_2(cod)_2Cl_2]$ (0.056 g, 0.8 x 10^{-4} mol) in dichloromethane (6 cm^3), and the resulting mixture stirred at room temperature under N_2 for 15 minutes. After filtration and reduction in volume,

the pale tan product was crystallised with hexane (Yield 0.035 g, 30%). Mol. wt. 625.65. Elemental analysis: found C = 26.7, H = 3.90%; calculated for $[C_{14}H_{24}S_3Ir](PF_6)$ C = 26.9, H = 3.87%. F.a.b. mass spectrum: found M^+ = 625, 480; calculated for

$[^{193}Ir([19]aneS_3\text{-}H)(cod)(PF_6)]^+$ $M^+ = 625$

$[^{193}Ir([9]aneS_3\text{-}H)(cod)]^+$ $M^+ = 480$

^1H nmr (200.13 MHz, CD_3CN, 298 K) δ = 3.64 (m, 4H, cod *CH*), 2.84-2.54 (m, 12H, [9]aneS$_3$), 2.32 (m, 4H, cod H_2), 2.12 (m, 4H, cod CH_2). ^{13}C d.e.p.t. nmr spectrum (50.32 MHz, CD_3CN, 298 K) δ = 63.03 ppm (s, cod *C*H), 35.57 (s, [9]aneS$_3$), 32.27 (s, cod CH_2). U.V./visible spectrum (CH_3CN): λ_{max} = 335 nm (sh), 285 (ε_{max} = 2,300 $dm^3\ mol^{-1}\ cm^{-1}$), 249 (15,300). I.R. spectrum (KBr disc): 2980 w, 2940 s, 2910 m, 2870 m, 2820 m, 1470 w, 1445 s, 1410 s, 1370 w, 1330 m, 1300 m, 1260 w, 1245 m, 1210 w, 1170 w, 1155 m, 1140 w, 1120 w, 1075 w, 1025 m, 1010 w, 995 w, 965 w, 940 w, 920 m, 905 m, 875 m, 840 vs, 780 w, 740 w, 705 w, 680 w, 660 w, 560 s, 525 w, 480 w, 450 w, 400 w, 380 w cm^{-1}.

6.4.8 Single Crystal Structure of [Ir([9]aneS$_3$)-(C_8H_{12})](PF$_6$)

Vapour diffusion of diethyl ether into a solution of the complex in acetonitrile yielded pale yellow plates of X-ray quality.

Crystal Data:

$[C_{14}H_{24}S_3Ir](PF_6)$, M_r = 625.65. Monoclinic, space group $P2_1/c$, a = 9.6404(8), b = 11.9222(14), c = 17.2174(18) Å, β = 103.957(8)°, V = 1920.5 Å^3 (by least-squares refinement on diffractometer angles for 42 reflections [24<2θ<26°, λ = 0.71073 Å]), Z = 4, D_c = 2.164 g cm^{-3}. Crystal dimensions 0.290 x 0.084 x 0.031 mm, μ (Mo-k$_\alpha$) = 7.372 mm^{-1}, F(000) = 1208.

Data Collection and Processing:

Stoë STADI-4 diffractometer, $\omega/2\theta$ scan mode using the learnt profile method. Graphite-monochromated Mo-k$_\alpha$ radiation; 3709 data collected ($2\theta_{max}$ = 45°, h -10→10, k Ø→12, l Ø→18), 2372 unique (R_{int} = 0.0345) giving 1919 data with $F>6\sigma(F)$. An initial absorption correction was applied using ψ-scan data (maximum transmission factor 0.4855, minimum 0.3312). No crystal decay.

Structure Analysis and Refinement

The Ir position was located from a Patterson synthesis, and iterative cycles of least squares refinement and difference Fourier synthesis located all other non-H atoms. During refinement, the [9]aneS$_3$ C atoms were found to be disordered over two equally occupied orientations. This was modelled using the constraints S-C = 1.83 Å, C-C = 1.52 Å, S-C-C = 2.74 Å. At isotropic convergence, a final empirical absorption

correction was made using DIFABS (maximum correction 1.144, minimum correction 0.801). Anisotropic thermal parameters were refined for Ir, S, P, F and cod-C atoms and H atoms were included in fixed calculated positions. The weighting scheme $w^{-1} = \sigma^2(F) + 0.000354\ F^2$ gave satisfactory agreement analyses. At final convergence R = 0.0407, R_W = 0.0521, S = 1.162 for 220 parameters, and the final Fourier difference map exhibited no peaks above +1.40 or below -0.78 eÅ^{-3}.

6.4.9 Synthesis of [Ir([9]aneS$_3$)(C$_4$H$_6$)](PF$_6$)

Butadiene was bubbled through a solution of [Ir$_2$(coe)$_4$Cl$_2$] (0.075 g, 0.8 x 10^{-4} mol) in dichloromethane (6 cm^3) for 5 mins. The resulting colourless solution was then stirred with [9]aneS$_3$ (0.030 g, 1.6 x 10^{-4} mol) and NH$_4$PF$_6$ (0.027 g, 1.6 x 10^{-4} mol) under N$_2$ at 298 K for 30 mins. The colourless solution was filtered, and the solvent removed under vacuum. The crude product was recrystallised from nitromethane/diethyl ether, giving a colourless microcrystalline solid (Yield 0.030 g, 25%). Mol. wt. 571.56. Elemental analysis: found C = 21.1, H = 3.14%; calculated for [C$_{10}$H$_{18}$S$_3$Ir](PF$_6$) C = 21.0, H = 3.17%. F.a.b. mass spectrum: found M$^+$ = 427, 399, 372; calculated for:

[^{193}Ir([9]aneS$_3$)(C$_4$H$_6$)]$^+$	M$^+$ = 427
[^{193}Ir([9]aneS$_3$)(C$_2$H$_2$)]$^+$	M$^+$ = 399
[^{193}Ir([9]aneS$_3$-H)]$^+$	M$^+$ = 372

^{1}H nmr spectrum (360.13 MHz, d^6-acetone, 298 K) δ = 5.29 ppm (m, 2H, C_4H_6 CH), 3.08-2.72 (m, 12H, [9]aneS_3), 2.25 (m, 2H, C_4H_6 CH_2), 0.43 (m, 2H, C_4H_6 CH_2). ^{13}C D.E.P.T. nmr spectrum (90.56 MHz, d^6-acetone, 298 K) δ = 80.94 ppm (s, C_4H_6 CH), 37.63 (s, [9]aneS_3), 36.46 (s, [9]aneS_3), 35.04 (s, [9]aneS_3), 22.34 (s, C_4H_6 CH_2). U.V./vis spectrum (CH_3CN): λ_{max} = 278 nm (ε_{max} = 2,270 dm^3 mol^{-1} cm^{-1}), 246 (3,900). I.R. spectrum (KBr disc): 3030 w, 2970 m, 2920 w, 1450 m, 1420 m, 1405 s, 1385 w, 1360 w, 1295 m, 1260 w, 1240 w, 1170 m, 1120 w, 1050 w, 1030 m, 1010 w, 980 w, 965 w, 940 m, 910 m, 875 w, 550 vs, 740 w, 680 m, 660 w, 560 s, 500 m, 485 w, 460 w, 405 m cm^{-1}.

6.4.10 Single Crystal Structure of [Ir([9]aneS_3)-(C_4H_6)](PF_6). ½[$(C_2H_5)_2O$]

Vapour diffusion of diethyl ether into an acetone solution of the complex yielded colourless tablets. A suitable crystal was mounted on a glass fibre, and cooled to 150 K in the cold stream of an Oxford Cryostems low temperature device.

Crystal Data:

[$C_{10}H_{18}S_3Ir$](PF_6).½($C_4H_{10}O$), M_r = 608.62. Monoclinic, space group $C2/c$, a = 18.397(6), b = 8.593(4), c = 23.571(13) Å, β = 97.79(3)°, V = 3692 Å^3 (by least-squares refinement on diffractometer angles for 23 reflections [31<2θ<32°, λ = 0.71073 Å]), Z = 8, D_c = 2.190 g cm^{-3}.

Crystal dimensions 0.47 x 0.35 x 0.23 mm, μ (Mo-K_α) = 7.669 mm^{-1}, $F(000)$ = 2344.

Data Collection and Processing:

Stoë STADI-4 four-circle diffractometer, $\omega/2\theta$ scan mode with ω scan-width (1.05 + 0.347 tan θ)°. Graphite-monochromated Mo-K_α radiation, 2614 reflections measured to 2θ = 45° (h -19→19, k Ø→9, l Ø→25), 2283 unique (R_{int} = 0.0215) giving 2064 with $F>4\sigma(F)$. An initial absorption correction was applied using ψ-scan data (maximum and minimum transmission factors 0.1585 and 0.0954 respectively). No crystal decay.

Structure Analysis and Refinement:

A Patterson synthesis identified the Ir atom position, and repeated least-squares refinement and difference Fourier syntheses located all other non-H atoms. A diethyl ether solvent molecule was located lying across a crystallographic two-fold axis, and was disordered over two equally occupied orientations. At isotropic convergence a final absorption correction was applied using DIFABS (maximum correction 1.618, minimum correction 0.760). Anisotropic thermal parameters were refined for Ir, S, P, F, O and all fully occupied C atoms. Macrocyclic and solvent H atoms were included in fixed, calculated positions; the butadiene H atoms positions were refined with a fixed C-H bond length of 1.08 Å, and all

C-C-H, and both H-C-H, angles constrained to be equal. The weighting scheme $w^{-1} = \sigma^2(F) + 0.000154\ F^2$ gave satisfactory agreement analyses. At final convergence R = 0.0315, R_W = 0.0405, S = 1.059 for 237 independent parameters, and the final ΔF map exhibited maximum and minimum residuals of +0.95 and -1.14 eÅ^{-3} respectively.

6.4.11 Synthesis of [Ir([9]aneS$_3$)(CO)(PPh$_3$)](PF$_6$)

[Ir(CO)Cl(PPh$_3$)$_2$] (0.130 g, 1.6 x 10^{-4} mol) and [9]aneS$_3$ (0.030 g, 1.6 x 10^{-4} mol) were refluxed with TlPF$_6$ (0.058 g, 1.6 x 10^{-4} mol) in CH_2Cl_2 (6 cm^3) under N_2 for 1 hr. The resulting pale yellow solution was filtered, reduced to ~ 1 cm^3 volume, and the pale yellow product crystallised with hexane. The pale yellow solid was recrystallised from acetonitrile/ether, and dried *in vacuo* (Yield 0.075 g, 56%). Mol. wt. 807.76. Elemental analysis: found C = 37.2, H = 3.30%; calculated for [$C_{25}H_{27}S_3POIr$](PF$_6$) C = 37.1, H = 3.35%. F.a.b. mass spectrum: found M^+ = 663, 634, 483, 455; calculated for:

[^{193}Ir([9]aneS$_3$)(CO)(PPh$_3$)]$^+$	M^+ = 663
[^{193}Ir([9]aneS$_3$-H)(PPh$_3$)]$^+$	M^+ = 634
[^{193}Ir(CO)(PPh$_3$)]$^+$	M^+ = 483
[^{193}Ir(PPh$_3$)]$^+$	M^+ = 455

^{1}H nmr spectrum (200.13 MHz, d^6-acetone, 298 K) δ = 7.86-7.54 ppm (m, 15H, PPh$_3$), 2.75-2.55 (m, 12H, [9]aneS$_3$). ^{13}C {^{1}H} nmr spectrum (50.32 MHz, d^6-acetone, 298 K), δ = 133.49 ppm (d, $^4J_{P-C}$ = 11 Hz, p-PPh$_3$), 131.09

(d, $^{1}J_{P-C}$ = 59 Hz, b-PPh_3), 130.75 (s, m-PPh_3), 127.95 (d, $^{2}J_{P-C}$ = 11 Hz, o-PPh_3), 34.04 (s, [9]aneS_3). U.V./vis spectrum (MeCN): λ_{max} = 360 nm (ε_{max} = 315 dm^3 mol^{-1} cm^{-1}), 262 (sh). I.R. spectrum ($MeNO_2$ solution) 1945 cm^{-1}. I.R. spectrum (KBr disc): 3040 w, 3000 w, 2940 w, 2920 w, 1940 vs, 1885 w, 1585 w, 1570 w, 1480 s, 1445 m, 1430 s, 1405 s, 1335 w, 1315 w, 1295 m, 1265 w, 1245 w, 1205 w, 1180 w, 1165 w, 1125 m, 1100 m, 1090 s, 1070 w, 1025 w, 1010 w, 995 m, 985 w, 970 w, 940 w, 910 w, 840 vs, 765 s, 755 s, 745 s, 710 s, 705 m, 690 s, 675 w, 620 m, 560 s, 530 s, 520 s, 495 m, 450 w, 430 m cm^{-1}.

CHAPTER 7

CONFORMATIONAL STUDIES ON [16]aneS$_4$

7.1 INTRODUCTION

The conformations and modes of coordination adopted by the tetrathia macrocycles [12]aneS_4, [14]aneS_4 and [16]aneS_4 have been discussed previously (Chapter 2). Whilst the coordinative flexibility of [12]- and [14]aneS_4 can be explained by the conformation preferences of the unbound ligands, no equivalent study of [16]aneS_4 had been made. Indeed, the lack of well characterised exocyclic complexes of this ligand implied that the free macrocycle may adopt a different type of conformation from those above. A crystallographic study of free [16]aneS_4 was therefore initiated.

The structures of the unbound 12- and 14-membered tetraoxa and tetrathia crown ethers are related to the conformations preferred by their parent hydrocarbons. Both [12]aneO_4[286] and [12]aneS_4[20] adopt square ([3333] in Dale's notation[287]) conformations in the solid state, which is also the form observed in the crystal structure of $C_{12}H_{24}$[288]. The structures of [12]aneS_4 and [12]aneO_4 differ, however, in the positioning of the heteroatoms within the square ring. This reflects the different 1,4-interactions in gauche X-C-C-X and C-C-X-C fragments (X = O, S)[20]. A gauche placement at an O-CH_2-CH_2-O bond results in a weakly attractive dispersive (i.e. electron-nuclear) attraction, whereas a gauche S-CH_2-CH_2-S unit gives rise to a repulsive inter-electron repulsion, because of the greater size of the S heteroatoms (Figure

7.1). In contrast, a gauche torsion about a CH_2-CH_2-O-CH_2 fragment is strongly disfavoured because of Van der Waals repulsions between H atoms; this interaction is less significant for a gauche CH_2-CH_2-S-CH_2 unit, because of the increased length of the C-S bond (Figure 7.2). These effects reinforce each other, to create a generally observed preference for *anti* placements about C-O bonds, and *gauche* placements about C-S bonds, in oxo- and thia-macrocycles. Hence, in [12]aneO_4 the O atoms lie along the sides of the square ring (72), giving the maximum possible number of four *anti* and four *gauche* C-O torsions, whilst in [12]aneS_4 the S atoms lie at the corners of the ring (73, Figure 2.1a) with all eight C-S bonds adopting *gauche* placements.

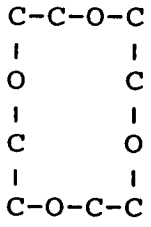

(72)

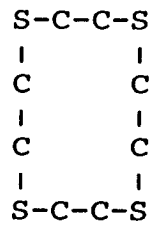

(73)

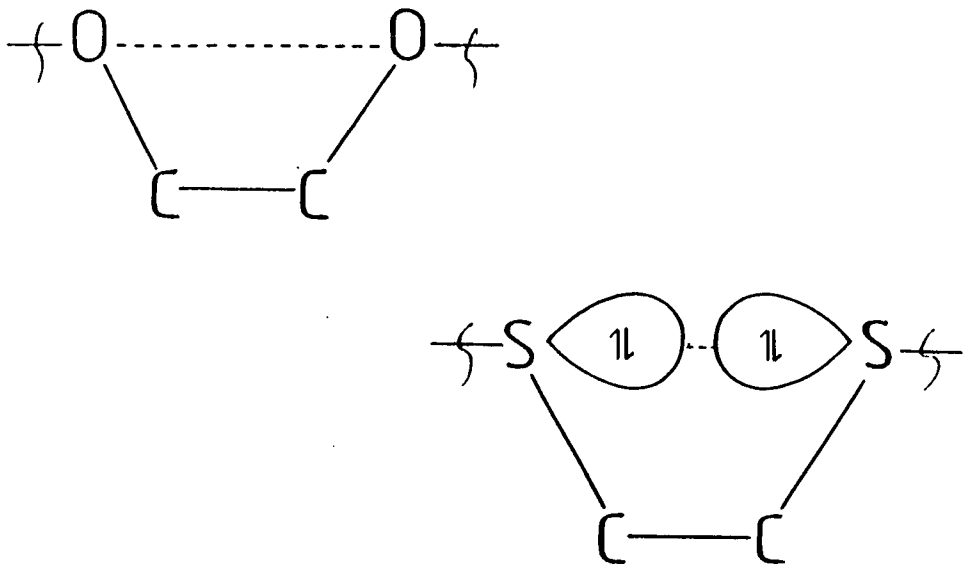

Figure 7.1: Representation of Interactions in Gauche $X-CH_2-CH_2-X$ Fragments (X = O, S).

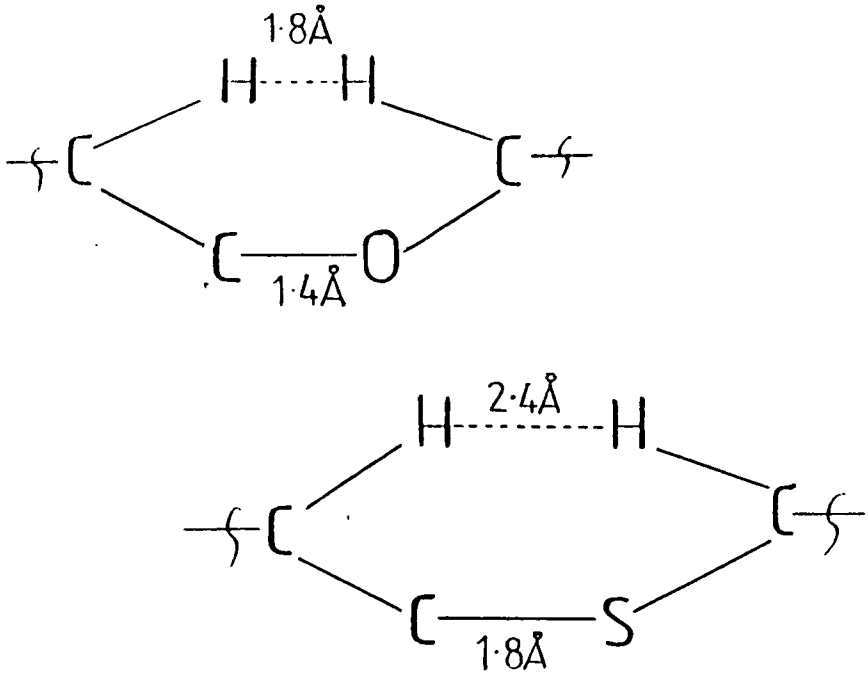

Figure 7.2: Representation of Interactions in Gauche $CH_2-CH_2-X-CH_2$ Fragments (X = O, S).

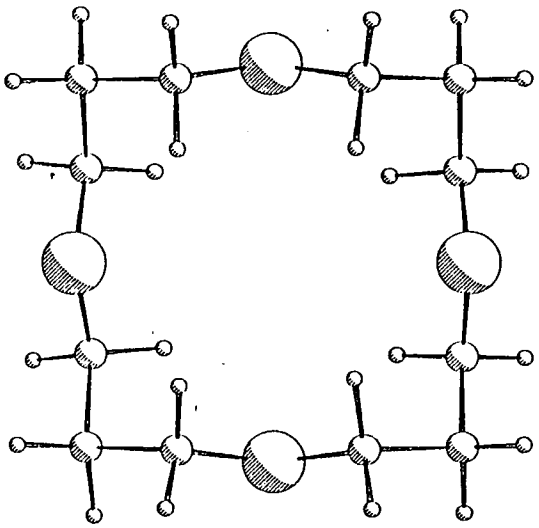

a) [16]aneO_4

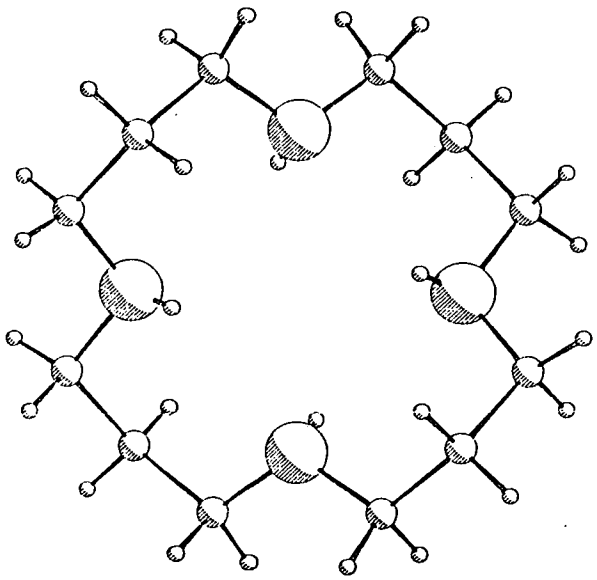

b) [16]aneN_4

Figure 7.3: Views of the Single Crystal Structures of Sixteen-Membered Macrocycles.

The structures of [14]aneO$_4$[289], [14]aneS$_4$ (Figure 2.1b)[19] and [16]aneO$_4$ (Figure 7.3a)[290] exhibit similar features to those above. The tetraprotonated {[14]aneN$_4$H$_4$}$^{4+}$ macrocycle also adopts a rectangular conformation in the solid state[291]. However, the saturated tetraza rings [14]aneN$_4$[17] and [16]aneN$_4$ (Figure 7.3b)[292] show endodentate conformations, similar to those observed in tetragonal metal complexes of these ligands.

The conformational structure of cyclohexadecane, $C_{16}H_{32}$, is still the subject of some controversy. Early I.R.[293], n.m.r.[294] and molecular mechanics studies[295] implied that this molecule adopts a square [4444] conformation at low temperatures, with a rectangular [3535] isomer lying 1.2-3.5 kcal mol^{-1} higher in energy being populated at higher temperatures. A pseudo-rotation mechanism for the interconversion of these forms was proposed by Dale (Figure 7.4)[296], and the barrier to pseudorotation was measured as 6.7±0.2 kcal mol^{-1} [294]. However, a more recent analysis of the I.R. and Raman spectra of crystalline and liquid $C_{16}H_{32}$ has thrown considerable doubt on these results, with the C_{16} ring being rather more flexible than expected from the earlier studies[297]. Molecular mechanics calculations did not successfully interpret these new measurements. Hence, there was considerable doubt as to the conformation(s) free [16]aneS$_4$ might exhibit. 1,1,9,9,-Tetramethylcyclohexadecane exhibits a [4444]

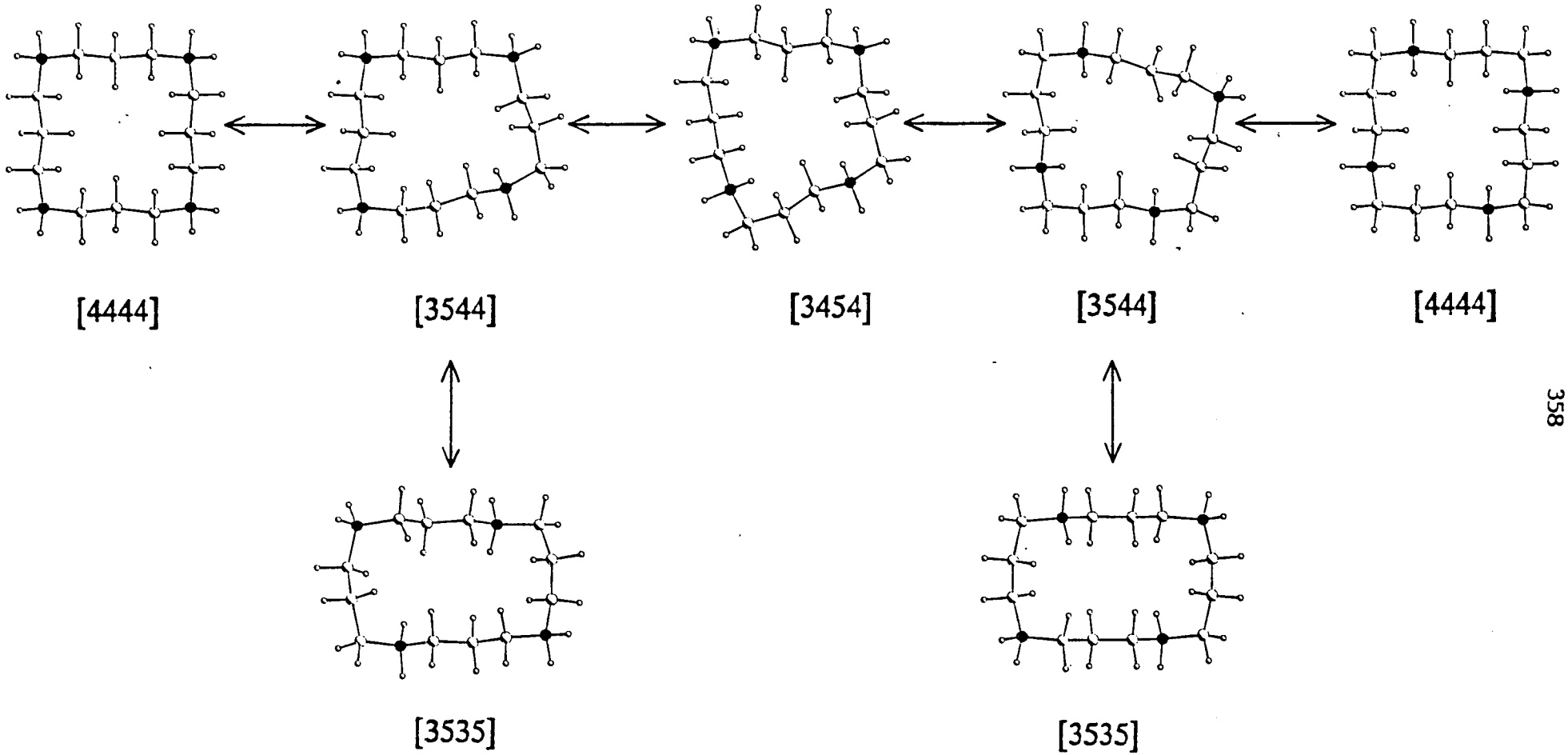

Figure 7.4: Dale's Pseudo-rotation Mechanism for Cyclohexadecane.

conformation in the solid state[298]. However, a preliminary refinement of a badly disordered single crystal structure implied that [16]aneSe$_4$, the tetra-selena analogue of [16]aneS$_4$, adopts a rectangular [3535] conformation in the solid state[299].

Some of the results described in this chapter have been published[316].

7.2 RESULTS AND DISCUSSION

7.2.1 Single Crystal Structures of [16]aneS$_4$

The recrystallisation of a commercial sample of [16]aneS$_4$ by solvent diffusion of hexane into a CH_2Cl_2 solution of the free ligand yielded colourless crystals. Detailed examination of these revealed three distinct crystal morphologies: acicular (needles), lamellar (plates) and columnar, which were labelled α, β and γ-[16]aneS$_4$ respectively.

In order to confirm that three different crystalline forms of [16]aneS$_4$ were present, melting points and mixed melting points were determined for the three types of crystal (Table 7.1). The melting point of each mixture was lower than those of its pure components, confirming that each morphology corresponded to a distinct crystalline phase. However, the changes observed were small, implying that the intermolecular forces, and therefore the crystal packing, were similar in all three polymorphs.

Crystal Form	T_M (°C)
α	59.5-60.2
β	57.8-59.0
γ	60.0-60.9
$\alpha+\beta$	56.5-57.5
$\alpha+\gamma$	55.5-57.0
$\beta+\gamma$	56.6-57.2

Table 7.1: Melting Point and Mixed Melting Point Data for [16]aneS_4.

The single crystal structures of the α- and β-forms of [16]aneS_4 were successfully collected and refined. Details of the structural solutions are described in Section 7.4.1 and 7.4.2, and bond lengths, angles and torsions are listed in Tables 7.2 and 7.3. ORTEP plots of the structures are shown in Figures 7.5 and 7.6.

The conformation of the macrocycle is the same in both structures. The molecule adopts a rectangular [3535] conformation, with local two-fold symmetry. Two sulphur donors lie at opposite corners of the ring, in exo positions; the other two occupy positions along the longer sides of the rectangle, and can be regarded as either exo or endo. The trans-annular S...S distances are 5.626(2) (α-form) and 5.550(9) Å (β-form), ruling out any charge-transfer interactions of the type observed in several 1,5-dithiocane derivatives (74)[300].

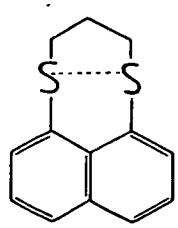

(74)

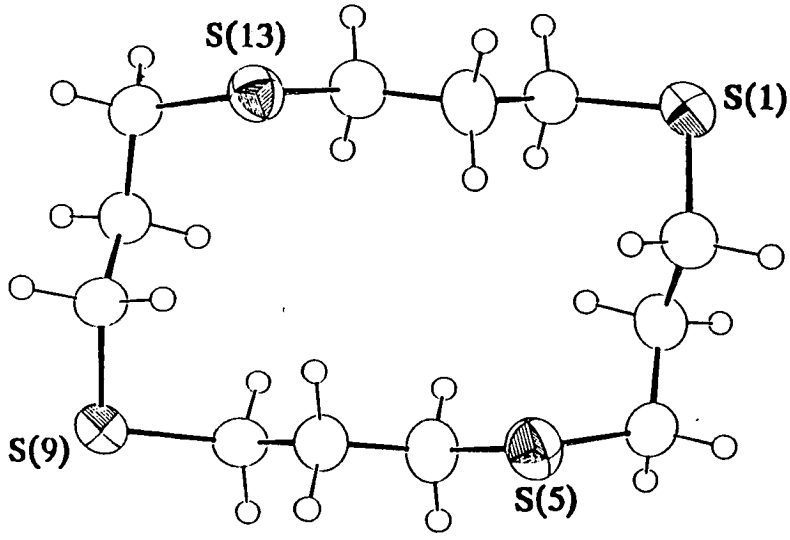

a) α-[16]aneS$_4$

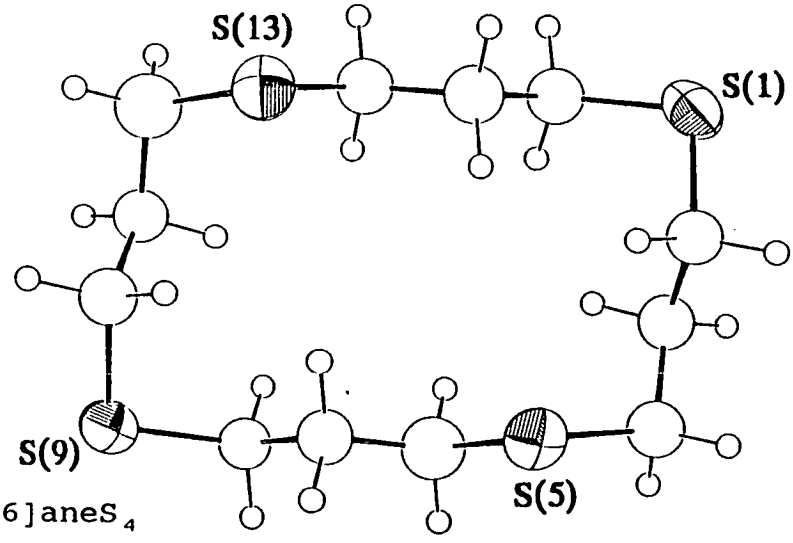

b) β-[16]aneS$_4$

Figure 7.5: Views of the Single Crystal Structures of α- and β-[16]aneS$_4$.

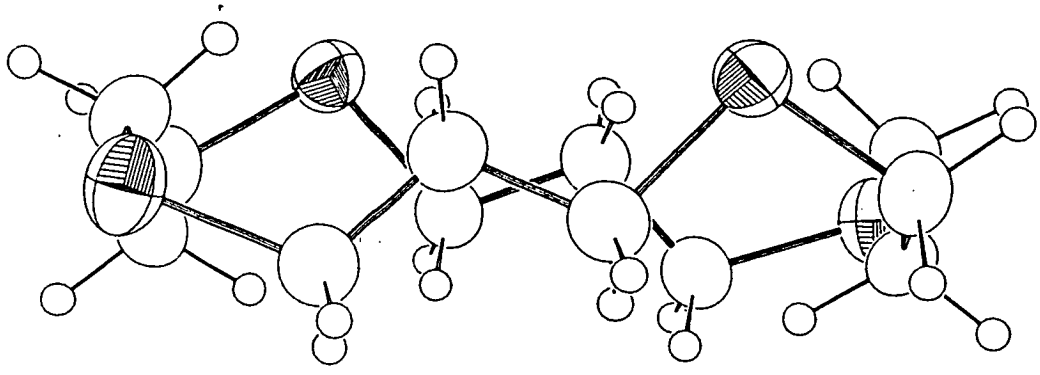

a) α-[16]aneS_4

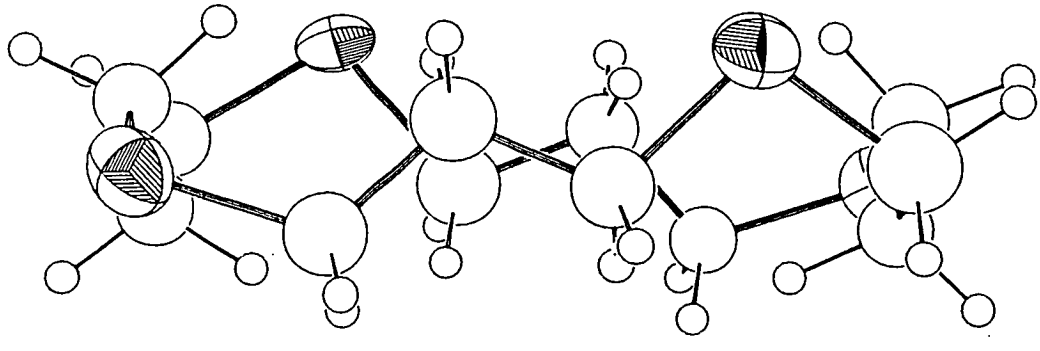

b) β-[16]aneS_4

Figure 7.6: Alternative Views of the Single Crystal Structures of α- and β-[16]aneS_4.

Single Crystal Structure of α-[16]aneS_4.

Table 7.2. Bond Lengths(A), angles(degrees) and torsion angles(degrees) with standard deviations

S(1) - C(2)	1.808(4)	C(8) - S(9)	1.815(4)
S(1) -C(16)	1.816(4)	S(9) -C(10)	1.805(3)
C(2) - C(3)	1.525(5)	C(10) -C(11)	1.523(5)
C(3) - C(4)	1.530(5)	C(11) -C(12)	1.520(5)
C(4) - S(5)	1.807(4)	C(12) -S(13)	1.815(4)
S(5) - C(6)	1.803(4)	S(13) -C(14)	1.810(4)
C(6) - C(7)	1.511(5)	C(14) -C(15)	1.518(5)
C(7) - C(8)	1.516(5)	C(15) -C(16)	1.509(5)

C(2) - S(1) -C(16)	101.62(17)	C(8) - S(9) -C(10)	101.24(15)
S(1) - C(2) - C(3)	114.19(25)	S(9) -C(10) -C(11)	115.08(23)
C(2) - C(3) - C(4)	112.4(3)	C(10) -C(11) -C(12)	112.7(3)
C(3) - C(4) - S(5)	113.8(3)	C(11) -C(12) -S(13)	114.17(23)
C(4) - S(5) - C(6)	101.05(17)	C(12) -S(13) -C(14)	101.03(16)
S(5) - C(6) - C(7)	110.29(25)	S(13) -C(14) -C(15)	110.0(3)
C(6) - C(7) - C(8)	111.3(3)	C(14) -C(15) -C(16)	112.6(3)
C(7) - C(8) - S(9)	114.78(24)	S(1) -C(16) -C(15)	114.0(3)

C(16) - S(1) - C(2) - C(3)	62.1(3)	C(7) - C(8) - S(9) -C(10)	62.9(3)
C(2) - S(1) -C(16) -C(15)	61.5(3)	C(8) - S(9) -C(10) -C(11)	66.6(3)
S(1) - C(2) - C(3) - C(4)	-174.47(24)	S(9) -C(10) -C(11) -C(12)	-173.81(22)
C(2) - C(3) - C(4) - S(5)	69.2(3)	C(10) -C(11) -C(12) -S(13)	66.8(3)
C(3) - C(4) - S(5) - C(6)	74.6(3)	C(11) -C(12) -S(13) -C(14)	75.0(3)
C(4) - S(5) - C(6) - C(7)	-167.59(25)	C(12) -S(13) -C(14) -C(15)	-165.59(25)
S(5) - C(6) - C(7) - C(8)	179.00(24)	S(13) -C(14) -C(15) -C(16)	-178.8(3)
C(6) - C(7) - C(8) - S(9)	-177.99(24)	C(14) -C(15) -C(16) - S(1)	178.40(25)

Single Crystal Structure of β-[16]aneS_4.

Table 7.3. Bond Lengths(A), angles(degrees) and torsion angles(degrees) with standard deviations

S(1) - C(2)	1.790(18)	C(8) - S(9)	1.817(18)
S(1) -C(16)	1.789(19)	S(9) -C(10)	1.806(19)
C(2) - C(3)	1.517(25)	C(10) -C(11)	1.52(3)
C(3) - C(4)	1.53(3)	C(11) -C(12)	1.53(3)
C(4) - S(5)	1.848(19)	C(12) -S(13)	1.807(21)
S(5) - C(6)	1.866(21)	S(13) -C(14)	1.774(19)
C(6) - C(7)	1.50(3)	C(14) -C(15)	1.50(3)
C(7) - C(8)	1.524(25)	C(15) -C(16)	1.50(3)

C(2) - S(1) -C(16)	101.0(8)	C(8) - S(9) -C(10)	102.7(9)
S(1) - C(2) - C(3)	116.1(12)	S(9) -C(10) -C(11)	114.5(13)
C(2) - C(3) - C(4)	112.2(15)	C(10) -C(11) -C(12)	113.1(15)
C(3) - C(4) - S(5)	112.0(12)	C(11) -C(12) -S(13)	112.3(14)
C(4) - S(5) - C(6)	99.9(9)	C(12) -S(13) -C(14)	100.9(9)
S(5) - C(6) - C(7)	107.6(13)	S(13) -C(14) -C(15)	112.0(13)
C(6) - C(7) - C(8)	109.6(15)	C(14) -C(15) -C(16)	113.1(16)
C(7) - C(8) - S(9)	113.6(12)	S(1) -C(16) -C(15)	118.6(13)

C(16) - S(1) - C(2) - C(3)	65.8(14)	C(7) - C(8) - S(9) -C(10)	60.1(14)
C(2) - S(1) -C(16) -C(15)	64.0(16)	C(8) - S(9) -C(10) -C(11)	61.6(15)
S(1) - C(2) - C(3) - C(4)	-172.6(12)	S(9) -C(10) -C(11) -C(12)	-175.6(13)
C(2) - C(3) - C(4) - S(5)	68.2(17)	C(10) -C(11) -C(12) -S(13)	70.3(18)
C(3) - C(4) - S(5) - C(6)	76.7(14)	C(11) -C(12) -S(13) -C(14)	75.1(15)
C(4) - S(5) - C(6) - C(7)	-169.7(13)	C(12) -S(13) -C(14) -C(15)	-168.0(14)
S(5) - C(6) - C(7) - C(8)	179.7(12)	S(13) -C(14) -C(15) -C(16)	178.2(13)
C(6) - C(7) - C(8) - S(9)	-178.0(13)	C(14) -C(15) -C(16) - S(1)	-178.2(13)

Six of the eight C-S bonds, and two of the eight C-C bonds, have *gauche* placements. This is surprising, given the known tendency of thioether macrocycles to maximise the number of gauche C-S torsions (*vide supra*). However, [16]aneS_4 contains only propyl S-CH_2-CH_2-CH_2-S linkages, and destabilising S...S interactions should be much reduced in comparison with [12]aneS_4 and [14]aneS_4, which contain ethyl linkages. Clearly, S...S repulsions are now no longer sufficiently large to impose an all exodentate conformation onto the [16]aneS_4 macrocycle. This effect has been observed previously for the all-propyl linked [12]aneS_3 macrocycle, which adopts a square conformation with only four gauche C-S bonds[21]. This [3535] conformation is the same as that proposed for the crystal structure of [16]aneSe_4[299].

The crystal packing in the two polymorphs is quite similar. The [16]aneS_4 molecules are approximately planar, with a central cleft corresponding to the two non-exo S atoms. Both structures contain stacks of molecules; in α-[16]aneS_4 these stacks are related by *b* and *c* glides perpendicular to the *a* and *b* axes to give a sheet structure (Figure 7.7), whilst in the β-form the stacks are related by a 2_1 screw axis parallel to *b*, such that adjacent stacks lie perpendicular to each other (Figure 7.8).

Crystals of the γ-phase of [16]aneS_4 suffered from twinning, and whilst a dataset was collected from this

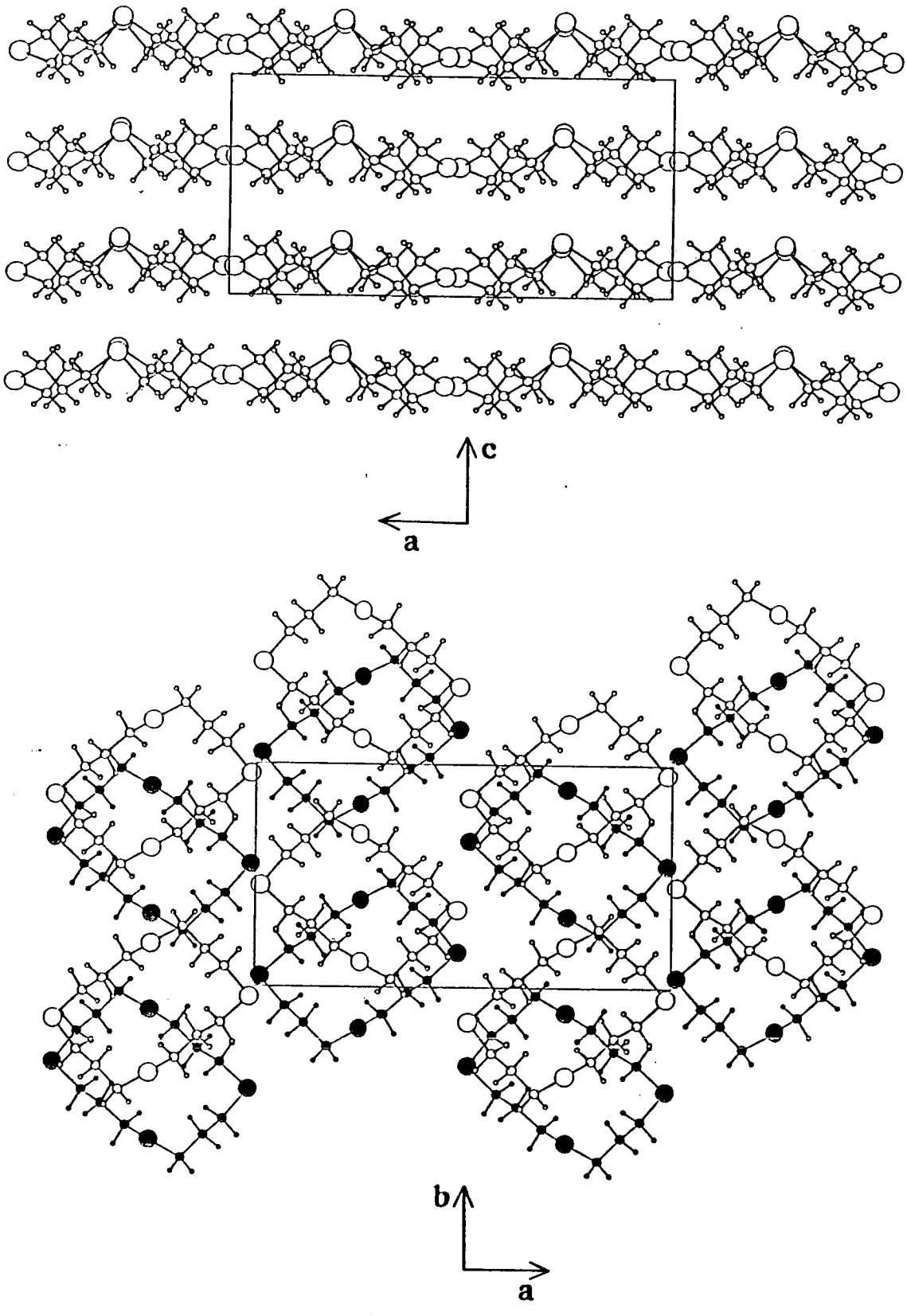

Figure 7.7: Packing Diagrams for α-[16]aneS$_4$.

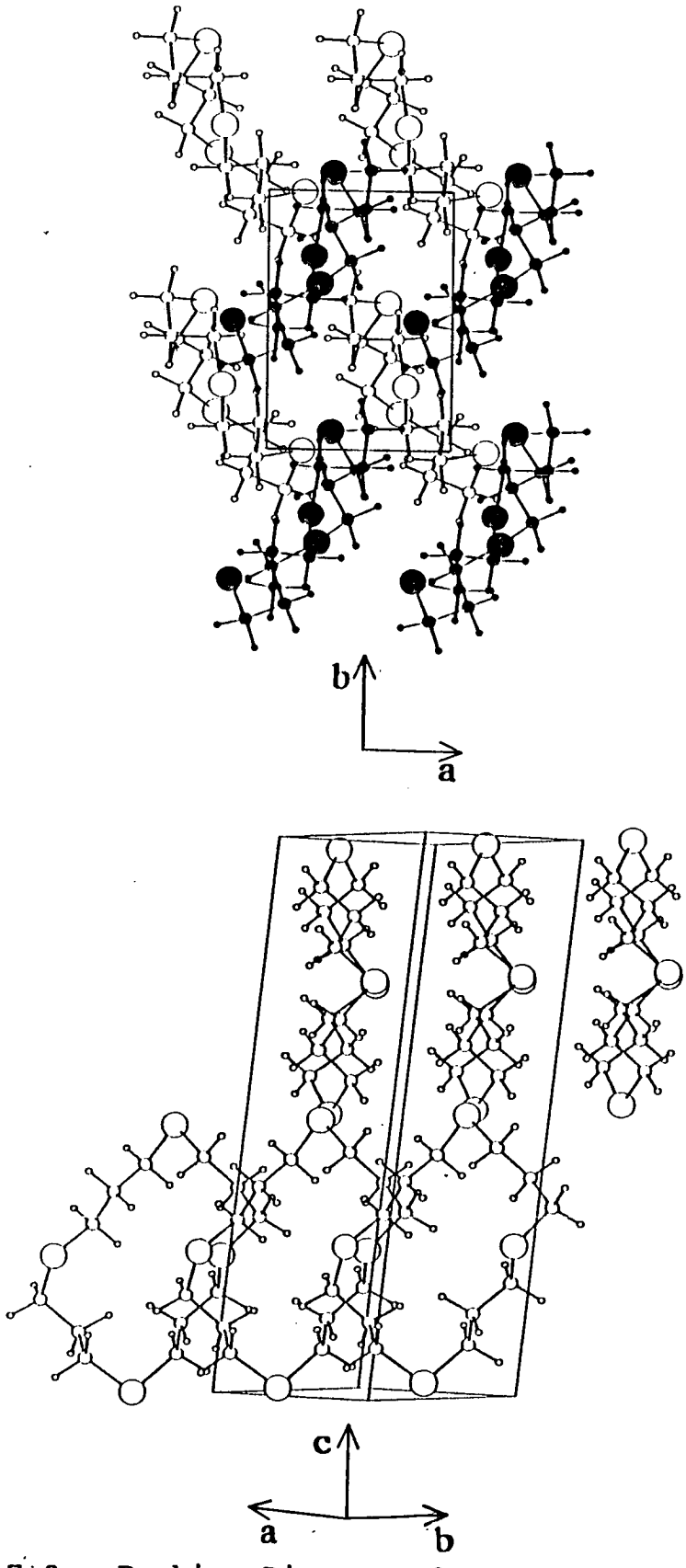

Figure 7.8: Packing Diagrams for β-[16]aneS$_4$.

polymorph no structural information could be derived.

7.2.2 Molecular Mechanics Calculations on [16]aneS$_4$ and Cyclohexadecane

In order to quantify the conformational flexibility of [16]aneS$_4$, and to explain its adoption of a [3535] conformation in the solid state, molecular mechanics calculations were performed on selected conformers of this molecule and of $C_{16}H_{32}$. The conformations chosen for study were those proposed in Dale's pseudo-rotation mechanism for 16-membered rings (Figure 7.4)[296], and those observed in complexes of [16]aneS$_4$ (Figure 7.9). The calculations were performed using the MM2(87) force field[301], and initial model structures were taken from crystal structure coordinates, or generated using the MINP input generation program[302]. The results of the calculations are listed in Table 7.4. The strain energies calculated for $C_{16}H_{32}$ are the same as those previously reported[295].

The calculations imply that for both the molecules examined, the conformation with the lowest strain energy is a square [4444] conformation. For [16]aneS$_4$, the [4444] ring with S atoms occupying corner positions is preferred over other [4444] conformers by 0.7-0.8 kcal mol^{-1}: this is the form with the maximum number of gauche C-S torsions. However, the [3535] conformation is significantly stabilised for [16]aneS$_4$, so that it lies

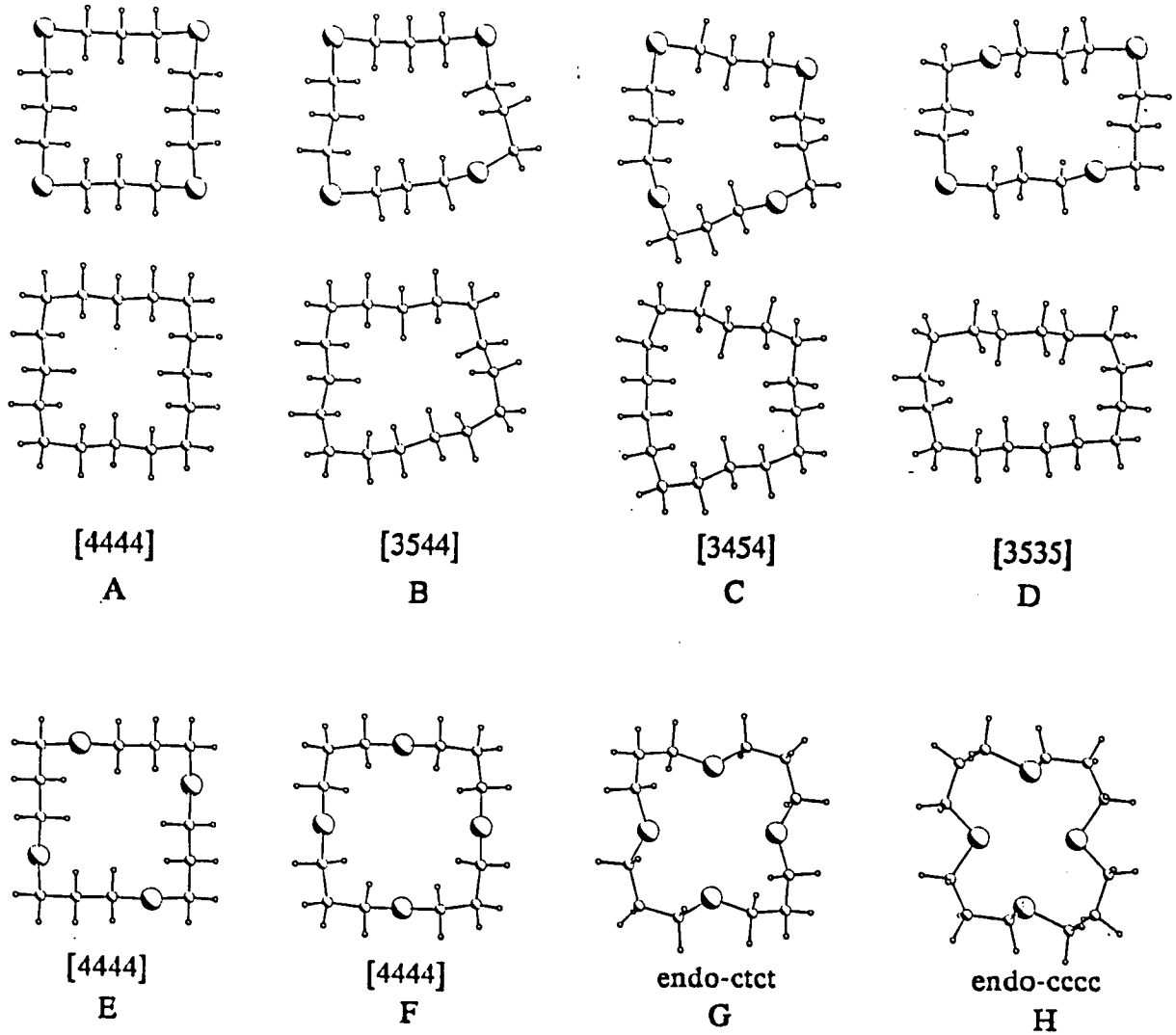

Figure 7.9: Conformers of [16]aneS$_4$ and Cyclohexadecane used in the Molecular Mechanics Calculations.

Table 7.4: Minimised Strain Energies from Molecular Mechanics Calculations.

Conformation[a]	[16]aneS$_4$		$C_{16}H_{32}$[b]	
	E (kcal mol^{-1})	ΔE (kcal mol^{-1})	E (kcal mol^{-1})	ΔE (kcal mol^{-1})
A	12.83	0	16.58	0
B	14.16	+1.3	18.99	+2.4
C	14.74	+1.9	18.69	+2.1
D	13.56	+0.7	19.99	+3.4
E	13.57	+0.7		
F	13.68	+0.8		
G	20.03	+7.2		
H	19.37	+6.5		

a) See Figure 7.9. b) See refs.

reduction in the number of unfavourable Van der Waals interactions between H atoms on adjacent sides of the ring due to the substitution of four CH_2 groups by S atoms (Figure 7.10). Other conformers of [16]aneS_4 are also stabilised over their $C_{16}H_{32}$ analogues, for the same reason. The two endo conformations of [16]aneS_4 examined lay *ca.* 6 kcal mol^{-1} above the other forms, and it is unlikely that these would be significantly populated in the absence of a metal ion[303].

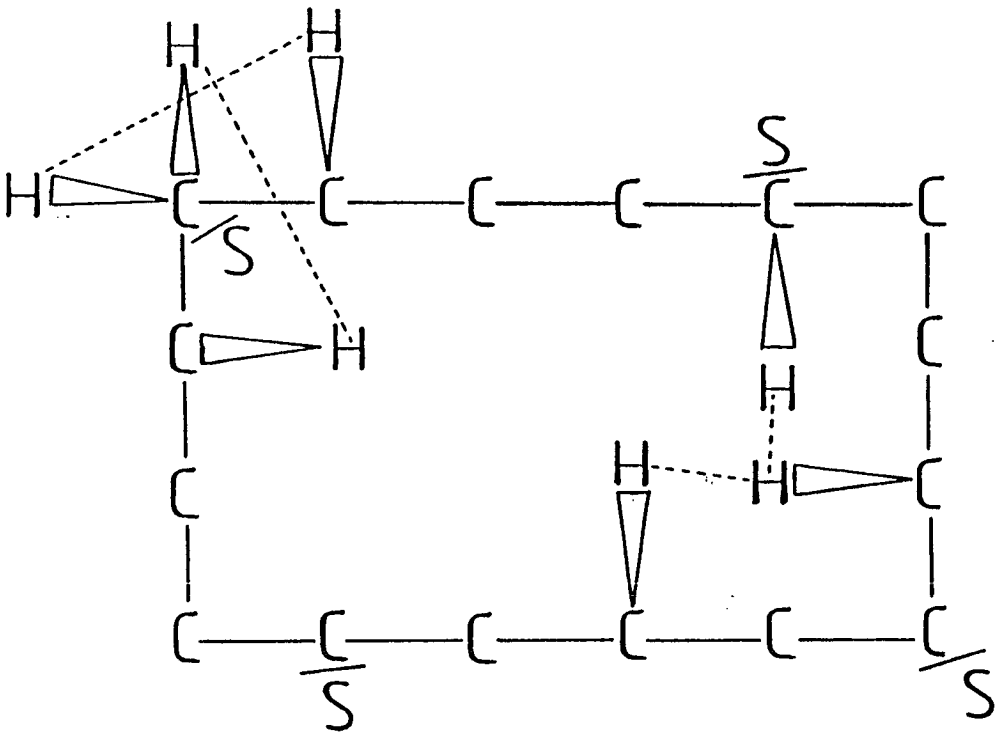

Figure 7.10: Unfavourable 1,2 and 1,4 H...H Repulsions in the [3535] Ring Conformer.

The structural models derived from the calculations were as expected, with bond lengths C-S ≙ 1.82, C-C ≙ 1.54 and C-H ≙ 1.12 Å, and angles <C-S-C = 98-103, <C-C-S and <C-C-C = 108-116°.

7.3 CONCLUSIONS

It has been shown that [16]aneS$_4$ adopts a rectangular [3535] conformation in the solid state. Molecular mechanics calculations have shown that this is probably not the minimum energy conformer, the ground state being a [4444] conformation with S atoms occupying the corners of the square ring. However, the energy differences involved are very small (< 1.5 kcal mol^{-1}), so that other forms are likely to be significantly populated at room temperature. Hence, the observation of a [3535] in the crystal structures of [16]aneS$_4$ can probably be attributed to crystal packing forces. It should be noted that molecular mechanics calculations have been shown to be unreliable for describing the conformational preferences of medium ring cycloalkanes[297,304]. Therefore, whilst it seems likely from these results that [16]aneS$_4$ should be more conformationally flexible than cyclohexadecane, no further firm conclusions about the conformational behaviour of either molecule can be drawn.

7.4 EXPERIMENTAL

Recrystallisation of a commercial sample of [16]aneS_4 by solvent diffusion of hexane into dichloromethane solution yielded colourless crystals of all three forms.

7.4.1 Single Crystal Structure of α-[16]aneS_4.

Crystal Data:

$C_{12}H_{24}S_4$, M_r = 296.56. Orthorhombic, space group $Pbc2_1$, a = 17.7366(17), b = 9.8219(7), c = 9.0558(11) Å, V = 1577.6 Å^3 (by least-squares refinement on diffraction angles for 40 reflections at ±ω [28<2θ<32°, λ = 0.71073 Å]). Z = 4, D_C = 1.248 g cm^{-3}. Crystal dimensions 0.96 x 0.15 x 0.10 mm, μ (Mo-K_α) = 0.556 mm^{-1}, F(000) = 640.

Data Collection and Processing:

Stöe STADI-4 four-circle diffractometer, $\omega/2\theta$ scan mode using the learnt profile method. Graphite-monochromated Mo-K_α radiation, 3256 reflections measured ($2\theta_{max}$ = 50°, h = 0→21, k 0→11, l -10→10), 2576 unique (R_{int} 0.018) giving 1985 with $F>6\sigma(F)$. No significant crystal decay, no absorption correction.

Structure Solution and Refinement:

The structure was solved using automatic direct methods, and refined with successive least-squares cycles on F. Anisotropic thermal parameters were refined for all

non-H atoms. H atoms were included in fixed, calculated positions, with a common U_{iso} = 0.0716(24) Å^2. The absolute polarity was determined by using a published procedure[105] to determine those reflections which were most sensitive to it: these 21 reflections and their Friédel opposites were recollected using Cu-K_α radiation, and a structure factor calculation was performed using the converged model for each polarity. One model gave R = 0.0649, R_w = 0.0852, the other R = 0.0540, R_w = 0.0548; the latter model was accordingly adopted. Using the full dataset, final convergence gave R = 0.0316, R_w = 0.0429, S = 1.153 for 145 independent parameters, and the final Fourier synthesis showed no feature above 0.29 or below -0.23 eÅ^{-3}. The weighting scheme $w^{-1} = \sigma^2(F) + 0.000816 F^2$ gave satisfactory agreement analyses.

7.4.2 Single Crystal Structure of β-[16]aneS$_4$

Crystal Data:

$C_{12}H_{24}S_4$, Mr = 296.56. Monoclinic, space group $P2_1$, a = 5.5608(19), b = 8.1240(22), c = 17.662(10) Å, β = 96.108(17)°, V = 793.4 Å^3 (by least-squares refinement on diffraction angles for 20 reflections at $\pm\omega[36<2\theta<44$, λ = 1.54814 Å]). Crystal dimensions 0.44 x 0.24 x 0.008 mm, μ (Cu-K_α) = 5.227 mm^{-1}, F(000) = 320.

Data Collection and Processing:

Stöe STADI-4 four-circle diffractometer, $\omega/2\theta$ scan mode with ω scan-width $(1.20 + 0.347 \tan \theta)°$. Graphite-monochromated Cu-K_α radiation: 1617 reflections measured ($2\theta_{max}$ = 50°, h-5→5, k0→8, l0→17), 817 unique (R_{int} 0.027) giving 622 with $F>4\sigma(F)$. No crystal decay. Absorption correction was applied using ψ scans (min. and max. transmission factors 0.2905, 0.4137 respectively).

Structure Solution and Refinement:

The structure was solved by automatic direct methods, and refined with successive least-squares cycles on F. At isotropic convergence, a final absorption correction was applied empirically using DIFABS (min. correction 0.735, max. 1.226). Anisotropic thermal parameters were refined for S atoms. H atoms were included in fixed, calculated positions, and a secondary extinction parameter refined to 5.95×10^{-7}. The hand of the structure was determined as described above for the polarity of the α-form. Using 37 reflections and their Friedel opposites, one hand gave R = 0.0873, R_w = 0.1150, the other R = 0.0787, R_w = 0.0942; the latter model was accordingly adopted. Final convergence using the full dataset gave R = 0.0711, R_w = 0.0844, S = 1.153 for 85 parameters, and the final Fourier synthesis contained max. and min. residues 0.65, -0.32 eÅ^{-3} respectively. The weighting scheme $w^{-1} = \sigma^2(F) + 0.0013 F^2$ gave satisfactory agreement analyses.

7.4.3 Single Crystal Structure of γ-[16]aneS$_4$

This form appears to crystallise in the orthohombic space group *Fdd*2, *a* = 18.0183(15), *b* = 21.338(3), *c* = 24.145(3) Å, *V* = 9283 Å^3. However, it suffers from twinning, and no structural information can be obtained.

7.4.4 Molecular Mechanics Calculations on [16]aneS$_4$ and $C_{16}H_{32}$

The calculations were performed using the MM2(87) force field[301], using model structures obtained from crystal structure coordinates, or generated using the MINP input generation program[302].

APPENDIX

EXPERIMENTAL TECHNIQUES

Reagents:

All solvents were purified using standard techniques[305]. Commercial $RhCl_3.3H_2O$ and $IrCl_3.3H_2O$ (Johnson Matthey) were used as supplied. Anhydrous $NiCl_2$ was prepared by dehydrating commercial $NiCl_2.6H_2O$ (Fisons) at 120°C for 2 weeks.

The following ligands were used as supplied: 1,4,7-trithiacyclononane ([9]aneS_3), 1,4,7,10-tetrathiacyclododecane ([12]aneS_4), 1,4,8,11-tetrathiacyclotetradecane ([14]aneS_4), 1,5,9,13-tetrathiacyclohexadecane ([16]aneS_4), 1,4,7,10,13-pentathiacyclopentadecane([15]-aneS_5), bis-diphenylphosphinomethane (dppm), 1,2-bisdiphenylphosphinoethane (dppe), cis-1,2-bis-diphenylphosphinoethene (dppv), 1,3-bisdiphenylphosphino-propane (dppp), triphenylphosphine, cyclooctene, tetracyanoethene (tcne) (Aldrich).

1,2-dicyclohexylphosphinoethane (dcpe), 1,2-dimethyl-phosphinoethane (dmpe), 1,1,1-trisdiphenylphosphinomethyl-ethane (tdpme), tricyclohexylphosphine, triisopropyl-phosphine, tritertiarybutylphosphine (Strem).

Cis,cis-cycloocta-1,5-diene (cod), bicyclo[2.2.1]-hepta-2,5-diene (2,5-norbornadiene, nbd) (B.D.H.).

Tetrafluoroethene (Fluorochem).

Ethene, butadiene (S.I.P. Analytical, Air Products).

Carbon monoxide (B.O.C.)

$^nBu_4NPF_6$ was prepared by the neutralisation of 40% $^nBu_4NOH$ (Aldrich) with 65% HPF_6 (Strem), and

recrystallised from methanol. Electrochemical measurements were performed in "HPLC-grade" CH_3CN (Fisons, Aldrich) without further purification.

Physical Measurements:

Infra-red spectra (4000-200 cm^{-1}) were recorded with a Perkin-Elmer 548 spectrometer using KBr disks, or in 0.2 mm CaF_2 solution cells. Fast atom bombardment mass spectra were run on a Kratos MS 50TC spectrometer using a 3-nitrobenzyl alcohol (3-NOBA) matrix. Elemental analyses were performed by the Edinburgh University Chemistry Department microanalytical service. ^1H nmr spectra were recorded using Bruker WP80, WP200 and WH360 spectrometers operating at 80.13, 200.13 and 360.13 MHz respectively. ^{13}C nmr spectra were measured with the Bruker WP200 or WH360 instruments operating at 50.32 and 90.56 MHz. ^{31}P nmr spectra were run on Jeol FX90Q and Brucker WP200 spectrometers, at 36.23 and 81.02 MHz. U.V./visible spectra were recorded with Pye-Unicam SP8-400 or Perkin-Elmer Lambda-9 spectrophotometers using 1 cm quartz cells.

Electrochemical measurements were performed using a Brucker 310 Universal Modular Polarograph, or Brucker EI30M Modular Potentiostat. Cyclic voltammetric measurements were carried out using a three electrode potentiostat configuration in CH_3CN containing 0.1 M $^nBu_4NPF_6$ as supporting electrolyte, under a dry argon

atmosphere. Platinum button microelectrodes were employed as working and auxiliary electrodes, with an Ag/AgCl reference electrode. All potentials are quoted relative to ferrocene/ferrocenium at +0.40 V vs. Ag/AgCl, unless otherwise stated. Controlled potential electrolysis and coulometry were performed with a three compartment cell, using a three electrode system with Pt basket working and Pt gauze auxiliary electrodes.

X-band electron paramagnetic resonance spectra were measured on a Brucker ER-2000 spectrometer employing 100 kHz field modulation. E.P.R. spectra were measured as frozen glasses at 77 K, or as mobile solutions at 298 K. In both cases, the sample tubes or solution cell were purged with N_2 or Ar gas, and the samples transferred to these by syringe, with rigorous exclusion of air.

The Optically Transparent Electrode (O.T.E.) system was designed and built in the University of Edinburgh, Department of Chemistry, following the original principles of Murray *et al.*[306]. A fine Pt/Rh gauze working electrode (transparency *ca.* 40%) was fitted into an infrasil 0.05 cm quartz cell. A quartz reservoir fitted to the top of the cell contained Pt wire auxiliary and Ag/Ag^+ reference electrodes, both separated from the bulk solution by a porous glass fit to give a three compartment system. This cell was mounted inside the Perkin-Elmer Lambda-9 UV/vis/nir spectrophotometer with a P.T.F.E. cell block (Figure A1). Temperature control was maintained by the

passage of dry, pre-cooled N_2 gas around the cell, and monitored with a thermocouple/digital thermometer.

Solutions of the test compound in 0.1 M $CH_3CN/^nBu_4NPF_6$ were purged with N_2 gas, then placed in the spectrophotometer and cooled to the required temperature. The solution was then electrolysed at the Pt/Rh gauze: the progress of the electrolysis was monitored both spectroscopically and by decay of the current to a residual value. The potential was then reversed, to monitor the chemical reversibility of the process by following the regeneration of the precursor species.

Single crystal X-ray data was collected on a Stöe STADI-4 four-circle diffractometer fitted with an Oxford Cryosystems low temperature device[307].

The following computer programs were used in the solution and refinement of crystal structures: SHELX76[308], SHELX86[309], DIRDIF[310], DIFABS[311], CALC[312], ORTEP[313], PLUTO[314]. Structure factor curves not inlaid in SHELX76 were taken from reference[315].

Key to Fig. A1:

A. Auxiliary electrode.

B. Reference electrode.

C. Working electrode connection protected from bulk solution by P.T.F.E. sleeve.

D. P.T.F.E. cell cap.

E. Test solution, purged with N_2.

F. 0.05 cm Infrasil quartz cell.

G. Pt/Rh grid working electrode.

H. P.T.F.E. cell block.

I. Variable temperature N_2 inlet ports.

J. Dry N_2 inlet ports.

K. Infrasil quartz cell block windows.

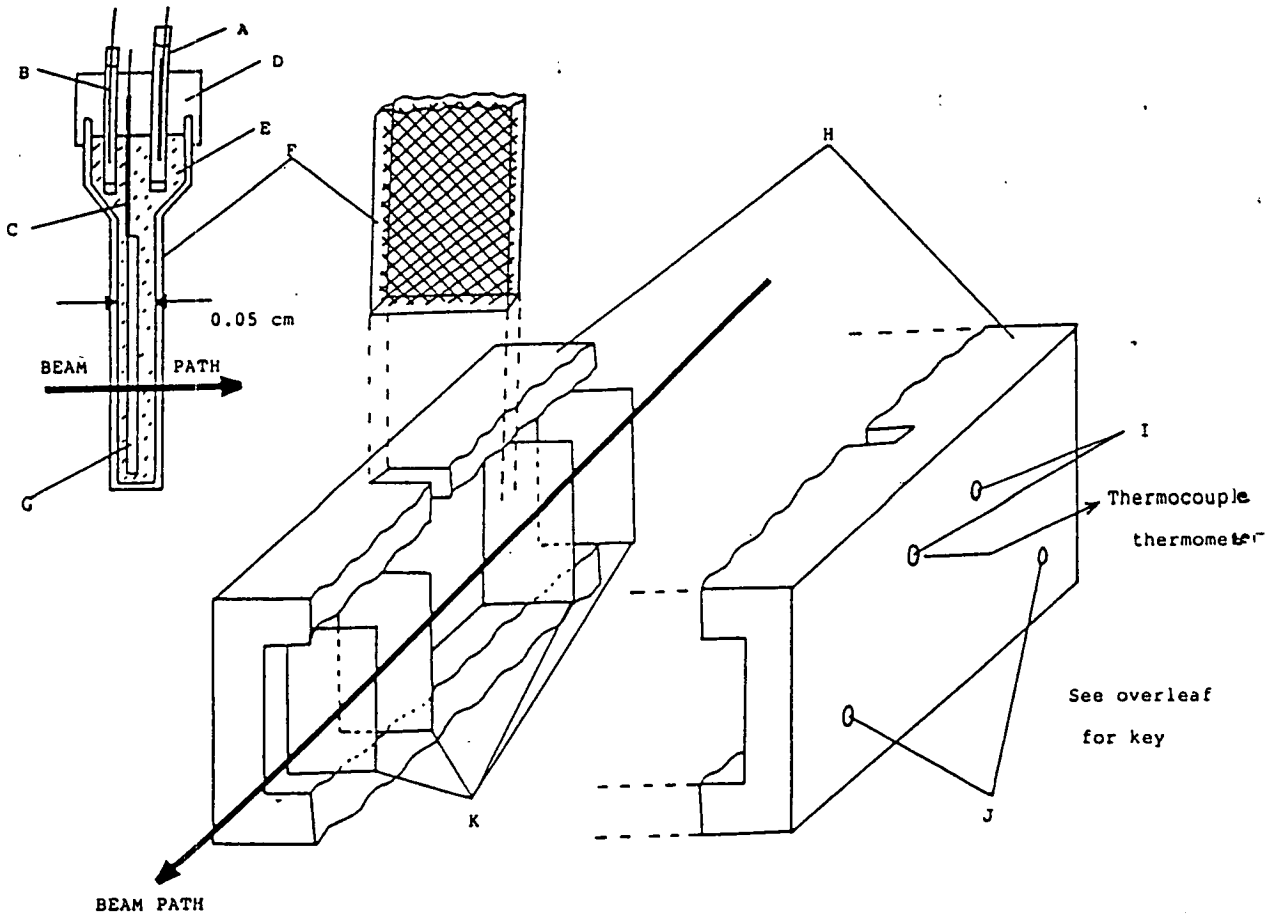

Figure A1: Design of the Optically Transparent Electrode System.

REFERENCES

REFERENCES

1. D.K. Cabbiness and D.W. Margerum, *J.Am.Chem.Soc.*, 91, 6540 (1969).
2. D.K. Cabbiness and D.W. Margerum, *J.Am.Chem.Soc.*, 92, 2151 (1970).
3. "Coordination Chemistry of Macrocyclic Ligands", Ed. G.A. Melson, Plenum, New York, 1979.
4. "The Chemistry of Macrocyclic Ligand Compounds", L.F. Lindoy, Cambridge University Press, Cambridge, 1989.
5. F.P. Kinz and D.W. Margerum, *Inorg.Chem.*, 13, 2491 (1974).
6. D.H. Busch, K. Farmery, V. Goedken, V. Katovic, A.C. Melynk, C.R. Sperati and N. Tokel, *Adv. Chem.Ser.*, 100, 44 (1971).
7. J.D. Lamb, R.M. Izatt, J.J. Christensen and D.J. Etough in "Coordination Chemistry of Macrocyclic Compounds", pp. 166-169 and refs. therein.
8. M. Kodama and E. Kimura, *J.Chem.Soc. Dalton Trans.*, 2341 (1976).
9. L.L. Diaddario, L.L. Zimmer, T.E. Jones, L.S.W.L. Sokol, R.B. Cruz, E.L. Yee, L.A. Ochrymowycz and D.B. Rorabacher, *J.Am.Chem.Soc.*, 101, 3511 (1979).
10. D.H. Busch, *Acc.Chem.Res.*, 11, 392 (1978).

11. K.M. Kadish and R. Guilard, *Chem. Rev.*, 88, 1121 (1988).

12. (a) J-M. Lehn, *Angew.Chem.Int.Ed.Eng.*, 27, 89 (1988).

(b) D.J. Cram, *Angew.Chem.Int.Ed.Eng.*, 27, 1009 (1988).

(c) C.J. Pederson, *Angew.Chem.Int.Ed.Eng.*, 27, 1021 (1988).

13. P. Chaudhuri and K. Wieghardt, *Prog.Inorg.Chem.*, 35, 329 (1987).

14. A.J. Blake and M. Schröder, *Adv.Inorg.Chem.*, 35, 1 (1990).

15. A. Bianchi, L. Bologni, P. Dapporto, M. Micheloni and P. Paoletti, *Inorg.Chem.*, 23, 1201 (1984).

16. G.F. Smith and D.W. Margerum, *J.Chem.Soc.Chem. Commun.*, 807 (1975).

17. N.F. Curtis in "Coordination Chemistry of Macrocyclic Compounds", pp. 219-301 and refs. therein.

18. K. Henrick, P.A. Tasker and L.F. Lindoy, *Prog. Inorg.Chem.*, 33, 1 (1985).

19. R.E. DeSimone and M.D. Glick, *J.Am.Chem.Soc.*, 98, 762 (1976).

20. R.E. Wolf, J-A.R. Hartman, J.M.E. Storey, B.M. Foxman and S.R. Cooper, *J.Am.Chem.Soc.*, 109, 4328 (1987).

21. S.C. Rawle, G.A. Admans and S.R. Cooper, *J.Chem. Soc.Dalton Trans.*, 93 (1988).

22. R.S. Glass, G.S. Wilson and W.N. Setzer, *J.Am. Chem.Soc.*, 102, 5068 (1980).

23. (a) "Inorganic Biochemistry", Ed. G.L. Eichhorn, Elsevier, Amsterdam.

(b) "Bio-Inorganic Chemistry", R.W. Hay, Horwood, Wiley, Chichester, 1984.

24. E. Frieden, *J.Chem.Educ.*, 62, 917 (1985).

25. K.S. Suslick and T.J. Reinert, *J.Chem.Educ.*, 62, 974 (1985).

26. R. Cammack, *Adv.Inorg.Chem.*, 32, 297 (1988).

27. F.P. Guengerich and T.L. Macdonald, *Acc.Chem. Res.*, 17, 9 (1984).

28. S. Lindskog, *Adv.Inorg.Biochem.*, 4, 116 (1982).

29. "Iron-Sulfur Proteins", Ed. T.G. Spiro, Wiley, New York, 1982.

30. A.G. Sykes, *Adv.Inorg.Chem.*, 36, 377 (1990).

31. J.M. Pratt, *Chem.Soc.Rev.*, 14, 161 (1985).

32. J.M. Rifkind in "Inorganic Biochemistry", pp. 832-902.

33. J.J. Katz in "Inorganic Biochemistry", pp. 1022-1066.

34. V.L. Goedken in "Coordination Chemistry of Macrocyclic Compounds", pp. 603-654.

35. R.J.P. Williams, *J.Mol.Catal.*, 1986, 1, (review issue).

36. C-W. Lee, D.J. Ecker and K.N. Raymond, *J.Am.Chem. Soc.*, 107, 6920 (1985).

37. B. Fischer and R. Eisenberg, *J.Am.Chem.Soc.*, **102**, 7361 (1980).

38. M. Beley, J.P. Collin, R. Ruppert and J-P. Sauvage, *J.Chem.Soc.Chem.Commun.*, 1315 (1984); *J.Am.Chem.Soc.*, **108**, 7461 (1986).

39. D.A. Gangi and R.R. Durand, *J.Chem.Soc.Chem. Commun.*, 697 (1986).

40. J.Y. Becker, B. Vainas, R. Eger and L. Kaufman, *J.Chem.Soc.Chem.Commun.*, 1471 (1985).

41. B.B. Wayland and H.W. Bosch, *J.Chem.Soc.Chem. Commun.*, 900 (1986).

42. Y. le Mest, M. L'Her, J. Courtot-Coupez, J.P. Collman, E.R. Evitt and C.S. Bencosme, *J.Chem. Soc.Chem.Commun.*, 1286 (1983).

43. J.P. Collman and K. Kim, *J.Am.Chem.Soc.*, **108**, 7847 (1986).

44. D. Sazou, C. Araullo-McAdams, B.C. Han, M.M. Franzen and K.M. Kadish, *J.Am.Chem.Soc.*, **112**, 7879 (1990).

45. J.P. Collman, J.E. Hutchison, P.S. Wagenknecht, N.S. Lewis, M.A. Lopez and R. Guilard, *J.Am. Chem.Soc.*, 112, 8206 (1990).

46. J.P. Collman, J.E. Hutchison, M.A. Lopez, R. Guilard and R.A. Reed, *J.Am.Chem.Soc.*, 113, 2794 (1991).

47. M.J. Camezind, D. Dolphin and B.R. James, *J.Chem. Soc.Chem.Commun.*, 1137 (1986).

48. T. Yoshida, T. Adachi, M. Kaminaka, T. Ueda and T. Higuchi, *J.Am.Chem.Soc.*, **110**, 4872 (1988).

49. I. Taniguchi, N. Nakashima and K. Yasukouchi, *J.Chem.Soc.Chem.Commun.*, 1814 (1986).

50. J.T. Croves and T.E. Nemo, *J.Am.Chem.Soc.*, **105**, 5786 (1983).

51. J.P. Collman, M. Marrocco, P. Denisevich, C. Koval and F.C. Anson, *J.Electroanal.Chem.*, **101**, 117 (1979).

52. P.J. Brothers and J.P. Collman, *Acc.Chem.Res.*, 19, 209 (1986).

53. R.S. Paonessa, N.C. Thomas and J. Halpern, *J.Am.Chem.Soc.*, **107**, 4333 (1985).

54. T. Yoshida, T. Ueda, T. Adachi, K. Yamamoto and T. Higuchi, *J.Chem.Soc.Chem.Commun.*, 1137 (1985).

55. S.G. Murray and F.R. Hartley, *Chem.Rev.*, **81**, 365 (1981).

56. (a) S.R. Cooper, *Acc.Chem.Res.*, **21**, 141 (1986).

(b) M. Schröder, *Pure Appl.Chem.*, **60**, 517 (1988).

57. G. Reid and M. Schröder, *Chem.Soc.Rev.*, **19**, 239 (1990).

58. A.J. Blake, A.J. Holder, T.I. Hyde and M. Schröder, *J.Chem.Soc.Chem.Commun.*, 1433 (1989).

59. R.M. Christie, PhD Thesis, University of Edinburgh, 1989.

60. (a) S.C. Rawle, R. Yagbasan, K. Prout and S.R. Cooper, *J.Am.Chem.Soc.*, **109**, 6181 (1987).

(b) A.J. Blake, R.O. Gould, A.J. Holder, T.I. Hyde and M. Schröder, *J.Chem.Soc.Dalton Trans.*, 1861 (1988).

61. S.R. Cooper, S.C. Rawle, R. Yagbasan and D.J. Watkin, *J.Am.Chem.Soc.*, **113**, 1600 (1991).

62. A.J. Blake, A.J. Holder, T.I. Hyde and M. Schröder, *J.Chem.Soc.Chem.Commun.*, 987 (1987).

63. A.J. Blake, R.O. Gould, A.J. Holder, T.I. Hyde, A.J. Lavery, M.O. Odulate and M. Schröder, *J.Chem.Soc.Chem.Commun.*, 118 (1987).

64. A.J. Blake, J.A. Greig, A.J. Holder, T.I. Hyde, A. Taylor and M. Schröder, *Angew.Chem.Int.Ed. Eng.*, **29**, 197 (1990).

65. (a) D.B. Rorabacher, M.M. Bernardo, A.M.Q. Vande Linde, G.H. Leggett, B.C. Westerby, M.J. Martin and L.A. Ochrymowycz, *Pure Appl.Chem.*, **60**, 501 (1988).

(b) J-A.R. Hartman and S.R. Cooper, *J.Am.Chem.Soc.*, 108, 1202 (1986).

(c) J.A. Clarkson, R. Yagbasan, P.J. Blower and S.R. Cooper, *J.Chem.Soc.Chem.Commun.*, 1244 (1989).

66. (a) H-J. Küppers, K. Wieghardt, Y-H. Tsay, C. Krüger, B. Nuber and J. Weiss, *Angew.Chem.Int. Ed.Eng.*, 26, 575 (1987).

(b) P.J. Blower, J.A. Clarkson, S.C. Rawle, J-A.R. Hartman, R.E. Wolf, R. Yagbasan, S.G. Bott and S.R. Cooper, *Inorg.Chem.*, 28, 4040 (1989).

(c) G. Reid, University of Edinburgh, unpublished results.

67. (a) A.J. Blake, R.O. Gould, J.A. Greig, A.J. Holder, T.I. Hyde and M. Schröder, *J.Chem.Soc.Chem. Commun.*, 876 (1989).

(b) A. Taylor, PhD Thesis, University of Edinburgh, 1991.

68. W. Rosen and D.H. Busch, *J.Chem.Soc.Chem.Commun.*, 148 (1969); *J.Am.Chem.Soc.*, 91, 4694 (1969).

69. W. Rosen and D.H. Busch, *Inorg.Chem.*, 9, 262 (1970).

70. W.N. Setzer, C.A. Ogle, G.S. Wilson and R.S. Glass, *Inorg.Chem.*, 22, 266 (1983).

71. S.R. Cooper, S.C. Rawle, J-A.R. Hartman, E.J. Hintsa and G.A. Admans, *Inorg.Chem.*, 27, 1209 (1988).

72. W.N. Setzer, E.L. Cacioppo, Q. Guo, G.J. Grant, D.D. Kim, J.L. Hubbard and D.G. VanDerveer, *Inorg.Chem.*, 29, 2672 (1990).

73. K. Wieghardt, H-J. Küppers, E. Raabe and C. Krüger, *Angew.Chem.Int.Ed.Eng*, 25, 1101 (1986).

74. A.J. Holder, PhD Thesis, University of Edinburgh, 1987.

75. G. Reid, PhD Thesis, University of Edinburgh, 1989.

76. A.J. Blake, R.O. Gould, T.I. Hyde and M. Schröder, *J.Chem.Soc.Chem.Commun.*, 431 (1987).

77. K. Nag and A. Chakravorty, *Coord.Chem.Rev.*, 33, 87 (1980).

78. A.G. Lappin and A. McAuley, *Adv.Inorg.Chem.*, 32, 241 (1988).

79. A.J. Blake, A.J. Holder, Y.V. Roberts and M. Schröder, *Acta Cryst.*, C44, 360 (1988).

80. Y.V. Roberts, PhD Thesis, University of Edinburgh, 1991.

81. P.M. Maitlis, *Acc.Chem.Res.*, 11, 301 (1978); *Adv.Chem.Ser.*, 173, 31 (1979).

82. W.A.G. Graham, *J.Organomet.Chem.*, 300, 81 (1986).

83. R.G. Bergman, *J.Organomet.Chem.*, 400, 273 (1990).

84. C.K. Ghosh and W.A.G. Graham, *J.Am.Chem.Soc.*, 109, 4726 (1987); *J.Am.Chem.Soc.*, 111, 375 (1989).

85. R.S. Tanke and R.H. Crabtree, *J.Am.Chem.Soc.*, 112, 7984 (1990).

86. C. Bianchini, E. Farnetti, M. Graziani, G. Nardin, A. Vacca and F. Zanobini, *J.Am.Chem.Soc.*, 112, 9190 (1990).

87. D.C. Olson and J. Vasilevskis, *Inorg.Chem.*, 8, 1611 (1969).

88. F.V. Lovecchio, E.S. Gore and D.H. Busch, *J.Am. Chem.Soc.*, **96**, 3109 (1974).

89. N. Jubran, G. Ginzburg, H. Cohen and D. Meyerstein, *J.Chem.Soc.Chem.Commun.*, 517 (1982); N. Jubran, G. Ginzburg, H. Cohen, Y. Koresh and D. Meyerstein, *Inorg.Chem.*, **24**, 251 (1985).

90. a) K.M. Kadish, M.M. Franzen, B.C. Han, C. Araullo-McAdams and D. Sazou, *J.Am.Chem.Soc.*, 113, 512 (1991) and refs. therein.

b) M.W. Renner, L.R. Furenlid, K.M. Barkigia, A. Forman, H-K. Shim, D.J. Simpson, K.M. Smith and J. Fajer, *J.Am.Chem.Soc.*, **113**, 6891 (1991).

91. R.R. Gagné and D.M. Ingle, *J.Am.Chem.Soc.*, **102**, 1444 (1980).

92. J. Lewis and M. Schröder, *J.Chem.Soc.Dalton Trans.*, 1085 (1982).

93. A.W. Addison, B. Watts and M. Wicholas, *Inorg.Chem.*, **23**, 813 (1984).

94. N.B. Tucker and E.E. Reid, *J.Am.Chem.Soc.*, **55**, 775 (1933).

95. L.A. Ochrymowycz, C.-P. Mak and J.D. Michna, *J.Org.Chem.*, **39**, 2079 (1974).

96. J. Buter and R.M. Kellog, *J.Org.Chem.*, **46**, 4481 (1981).

97. R.E. Wolf, J-A.R. Hartman, L.A. Ochrymowycz and S.R. Cooper, *Inorg.Synth.*, **25**, 122 (1989).

98. R.E. De Simone and M.D. Glick, *J.Am.Chem.Soc.*, 97, 942 (1975).

99. G.H. Robinson, H. Zhang and J.L. Atwood, *Organometallics*, 6, 887 (1987).

100. G.H. Robinson and S.A. Sangokoya, *J.Am.Chem.Soc.*, 110, 1494 (1988).

101. D. Sevdić and L. Fekete, *Inorg.Chim.Acta*, 57, 111 (1982).

102. N.W. Alcock, N. Herron and P. Moore, *J.Chem.Soc. Dalton Trans.*, 394 (1978).

103. M.N. Bell, A.J. Blake, R.O. Gould, A.J. Holder, T.I. Hyde, A.J. Lavery, G. Reid and M. Schröder, *J.Incl.Phenomena*, 5, 169 (1987).

104. P.H. Davis, L.K. White and R.L. Belford, *Inorg.Chem.*, 14, 1753 (1975).

105. A.J. Blake, R.O. Gould, G. Reid and M. Schröder, *J. Organomet.Chem.*, 356, 389 (1988).

106. M.D. Glick, D.P. Gavel, L.L. Diaddario and D.B. Rorabacher, *Inorg.Chem.*, 15, 1190 (1976).

107. V.B. Pett, L.L. Diaddario, E.R. Dockal, P.W. Corfield, C. Ceccarelli, M.D. Glick, L.A. Ochrymowycz and D.B. Rorabacher, *Inorg.Chem.*, 22, 3661 (1983).

108. N. Herron, O.W. Howarth and P. Moore, *Inorg.Chim. Acta*, 20, L43 (1976).

109. J.A. Greig, PhD Thesis, University of Edinburgh, 1990.

110. E.R. Dockal, L.L. Diaddario, M.D. Glick and D.B. Rorabacher, *J.Am.Chem.Soc., 99,* 4530 (1977).

111. R.E. de Simone and M.D. Glick, *Inorg.Chem.*, **17**, 3574 (1978).

112. A.J. Blake, G. Reid and M. Schröder, *J.Chem.Soc. Dalton Trans.*, 1675 (1989).

113. T. Yoshida, T. Adachi, T. Ueda, M. Watanabe, M. Kaminaka and T. Higuchi, *Angew.Chem.Int.Ed.Eng.*, 26, 1171 (1987).

114. L. Sacconi, F. Mani and A. Bencini, in "Comprehensive Coordination Chemistry", ed. G. Wilkinson, R.D. Gillard and J.A. McCleverty, Pergamon, Oxford, 1987, vol. 5, chapter 50, pp. 45-68 and 276-284 and refs. therein.

115. a) "Multiple Bonds Between Metal Atoms", F.A. Cotton and R.A. Walton, Wiley-Interscience, New York, 1982, pp. 235-243 and 282-287 and refs. therein.

b) F.A. Cotton, S.A. Duraj and W.J. Roth, *Inorg.Chem.*, **24**, 913 (1985).

116. See e.g.

a) R.L. Lintvedt, L.L. Born, D.P. Murtha, J.M. Kuszaj and M.D. Glick, *Inorg.Chem.*, **13**, 18 (1974).

b) K.O. Joung, C.J. O'Connor, E. Sinn and R.L. Carlin, *Inorg.Chem.*, **18**, 804 (1979).

c) R.J. Butcher, C.J. O'Connor and E. Sinn, *Inorg.Chem.*, **20**, 3486 (1981).

117. a) G.J. Long and E.O. Schlemper, *Inorg.Chem.*, 13, 279 (1974).

b) R.J. Butcher and E. Sinn, *Inorg.Chem.*, 16, 2334 (1977).

118. a) D.M. Duggan, E.K. Barefield and D.N. Hendrickson, *Inorg.Chem.*, 12, 985 (1973).

b) C.G. Pierpoint, D.N. Hendrickson, D.M. Duggan, F. Wagner and E.K. Barefield, *Inorg.Chem.*, 14, 604 (1975).

119. P. Chaudhuri, H-J. Küppers, K. Wieghardt, S. Gehring, W. Haase, B. Nuber and J. Weiss, *J.Chem. Soc.Dalton Trans.*, 1367 (1988).

120. P.H. Davis, L.K. White and R.L. Belford, *Inorg.Chem.*, 14, 1753 (1975).

121. N.L. Hill and H. Hope, *Inorg.Chem.*, 13, 2079 (1974).

122. M.N. Bell, A.J. Blake, A.J. Holder, T.I. Hyde and M. Schröder, *J.Chem.Soc.Dalton Trans.*, 3841 (1990).

123. J.H. Binks, G.J. Dorward, R.A. Howie and G.P. McQuillan, *Inorg.Chim.Acta*, 49, 251 (1981).

124. A. McAuley and S. Subramanian, *Inorg.Chem.*, 29, 2830 (1990).

125. "Inorganic Electronic Spectroscopy", A.B.P. Lever, Elsevier, Amsterdam, 2nd Edition, 1984, pp. 77-97.

126. L.Y. Martin, L.J. De Hayes, L.J. Zompa and D.H. Busch, *J.Am.Chem.Soc.*, 96, 4046 (1974).

127. R. Yang and L. Zompa, *Inorg.Chem.*, 15, 1499 (1976).

128. a) B.H. O'Connor and D.H. Dale, *Acta Cryst.*, 21, 705 (1966).

b) F. Bigoli, A. Braibanti, A. Tiripicchio and M. Tiripicchio-Cammellini, *Acta Cryst.*, 27, 1427 (1971).

c) A. Zalkin, H. Ruben and D.H. Templeton, *Acta Cryst.*, B38, 610 (1982).

129. A. Bencine, L. Fabbrizzi and A. Poggi, *Inorg.Chem.*, 20, 2544 (1981).

130. K. Wieghardt, H-J. Küppers and J. Weiss, *Inorg. Chem.*, 24, 3067 (1985).

131. L.A. Ochrymowycz, D. Ger, P. Chonsawangvirod and A.K. Leung, *J.Org.Chem.*, 42, 2644 (1977).

132. D. Sellman and L. Zapf, *Angew.Chem.Int.Ed.Eng.*, 23, 807 (1984).

133. P.J. Blower and S.R. Cooper, *Inorg.Chem.*, 26, 2009 (1987).

134. R. Blom, D.W.H. Rankin, H.E. Robertson, M. Schröder and A. Taylor, *J.Chem.Soc.Perkin Trans.2*, 773 (1991).

135. M.N. Bell, PhD Thesis, University of Edinburgh, 1987.

136. A.J. Blake, R.D. Crofts, G. Reid and M. Schröder, *J.Organomet.Chem.*, 359, 371 (1989).

137. S.C. Rawle, T.J. Sewell and S.R. Cooper, *Inorg. Chem.*, 26, 3769 (1987).

138. W.N. Setzer, E.L. Cacioppo, Q. Guo, G.J. Grant, D.D. Kim, J.L. Hubbard and D.G. VanDerveer, *Inorg.Chem.*, 29, 2672 (1990).

139. E. Ercolani, J.V. Quagliano and L.M. Vallarino, *Inorg.Chim.Acta*, 7, 413 (1973).

140. a) G. Booth & J. Chatt, *J.Chem.Soc.*, 3238 (1965).

b) G.R. Van Hecke and W. DeW. Horrocks, *Inorg.Chem.*, 5, 1968 (1966).

141. C.A. McAuliffe and D.W. Meek, *Inorg.Chem.*, 8, 904 (1969).

142. L.M. Venanzi, *J.Chem.Soc.*, 719 (1958).

143. G. Giaccometti, V. Scatturin and A. Turco, *Gazz. Chim.Ital.*, 88, 434 (1958).

144. L. Sacconi, I. Bertini and F. Mani, *Inorg.Chem.*, 7, 1417 (1967).

145. C.M. Harris and E.D. McKenzie, *J.Inorg.Nucl. Chem.*, 29, 1047 (1967).

146. P. Pfeiffer and F. Tappermann, *Z.Anorg.Allg.Chem.*, 215, 273 (1933).

147. A.R. Rossi and R. Hoffmann, *Inorg.Chem.*, 14, 365 (1975).

148. A. Miedaner, R.C. Haltiwanger and D.L. Dubois, *Inorg.Chem.*, 30, 417 (1991).

149. P.W.R. Corfield, C. Ceccarelli, M.D. Glick, I. W-Y. Moy, L.A. Ochrymowycz and D.B. Rorabacher, *J.Am.Chem.Soc.*, **107**, 2399 (1985).

150. T.I. Hyde and M. Schröder, unpublished results.

151. a) A.J. Blake, R.O. Gould, G. Reid and M. Schröder, *J.Chem.Soc.Chem.Commun.*, 974 (1990).

b) G. Reid and M. Schröder, unpublished results.

152. E. Kimura, R. Machida and M. Kodama, *J.Am.Chem. Soc.*, 106, 5497 (1984).

153. P.W. Jolly in "Comprehensive Organometallic Chemistry", ed. G. Wilkinson, F.G.A. Stone & E.W. Abel, Pergamon, Oxford, 1982, vol. 8, chapters 56.1-56.8, pp. 613-797 and refs. therein.

154. a) C. Gosden, K.P. Healy and D. Pletcher, *J.Chem. Soc.Dalton Trans.*, 972 (1978).

b) C. Gosden and D. Pletcher, *J.Organomet.Chem.*, 186, 401 (1980).

c) A. Bakac and J.H. Espenson, *J.Am.Chem.Soc.*, **108**, 713 (1986).

d) M.S. Ram, A. Bakac and J.H. Espenson, *Inorg. Chem.*, 25, 3267 (1986).

155. A.J. Blake, A.J. Holder, A. Taylor and M. Schröder, *New.J.Chem.*, **15**, 511 (1991).

156. A.J. Blake, A.J. Holder, T.I. Hyde and M. Schröder, *J.Chem.Soc.Chem.Commun.*, 1433 (1989).

157. H-J. Küppers, K. Wieghardt, B. Nuber, J. Weiss, E. Bill and A.X. Trautwein, *Inorg.Chem.*, 26, 3762 (1987).

158. L. Alagna, S.S. Hasnain, B. Piggott and D.J. Williams, *Biochem.J.*, 220, 591 (1984).

159. S.P.J. Albracht, D. Ankel-Fuchs, J.W. Van der Zwaan, R.D. Fontijn and R.K. Thauer, *Biochim. Biophys.Acta*, 870, 50 (1986).

160. S.W. Ragsdale, L.G. Ljungdahl and D.V. DerVartanian, *Biochem.Biophys.Res.Commun.*, 115, 658 (1983).

161. S.W. Ragsdale, H.G. Wood and W.E. Antholine, *Proc.Natl.Acad.Sci.USA*, 82, 6811 (1985).

162. V.M. Fernandez, E.C. Hatchikian, D.S. Patil and R. Cammack, *Biochim.Biophys.Acta*, 883, 145 (1986).

163. R. Cammack, D.S. Patil, E.C. Hatchikian and V.M. Fernandez, *Biochim.Biophys.Acta*, 912, 98 (1987).

164. R.H. Crabtree, *Inorg.Chim.Acta*, 125, L7 (1986).

165. M. Zimmer, G. Schulte, X-L. Luo and R.H. Crabtree, *Angew.Chem.Int.Ed.Eng.*, 30, 193 (1991).

166. C.O. Dietrich-Buchecker, J-M. Kern and J-P. Sauvage, *J.Chem.Soc.Chem.Commun.*, 760 (1985).

167. a) P. Chmielewski, M. Grzeszczuk, L. Latos-Grazynski and J. Lisowski, *Inorg.Chem.*, 28, 3546 (1989).

b) L. Latos-Grazynski, M.M. Olmstead and A.L. Balch, *Inorg.Chem.*, 28, 4066 (1989).

168. L.R. Furenlid, M.W. Renner, D.J. Szalda and E. Fujita, *J.Am.Chem.Soc.*, 113, 883 (1991).

169. L. Porri, M.C. Gallazzi and G. Vitulli, *J.Chem. Soc.Chem.Commun.*, 228 (1967).

170. C. Mealli, P. Dapporto, V. Sriyunyongwat and T.A. Albright, *Acta Cryst..*, C39, 995 (1983).

171. a) L. Sacconi and S. Midollini, *J.Chem.Soc.Dalton Trans.*, 1213 (1972).

b) L. Sacconi, C.A. Ghilardi, C. Mealli and F. Zanobini, *Inorg.Chem.*, 14, 1380 (1975).

c) L. Sacconi, P. Dapporto and P. Stoppioni, *Inorg.Chem.*, 15, 325 (1976).

172. a) P. Dapporto, G. Fallani and L. Sacconi, *Inorg.Chem.*, 13, 2847 (1974).

b) A. Gleizes, M. Dartiguenave, Y. Dartiguenave, J. Galy and H.F. Klein, *J.Am.Chem.Soc.*, 99, 5187 (1977).

c) C. Bianchini, D. Masi, C. Mealli and A. Meli, *Cryst.Struct.Commun.*, 11, 1475 (1982).

d) F. Cecconi, S. Midollini and A. Orlandini, *J.Chem.Soc.Dalton Trans.*, 2263 (1983).

173. a) W.E. Geiger, T.E. Mines and F.C. Senftleber, *Inorg.Chem.*, 14, 2141 (1975).

b) W.E. Geiger, C.S. Allen, T.E. Mines and F.C. Senftleber, *Inorg.Chem.*, 16, 2003 (1977).

174. G.A. Bowmaker, P.D.W. Boyd, G.K. Campbell, J.M. Hope and R.L. Martin, *Inorg.Chem.*, 21, 1152 (1982).

175. a) G.A. Bowmaker, P.D.W. Boyd and G.K. Campbell, *Inorg.Chem.*, 21, 2403 (1982).

b) G.A. Bowmaker, P.D.W. Boyd, M. Zvagulis, K.J. Cavell and A.F. Masters, *Inorg.Chem.*, 24, 401 (1985).

176. D.C. Bradley, M.B. Hursthouse, R.J. Smallwood and A.J. Welch, *J.Chem.Soc.Chem.Commun.*, 872 (1972).

177. A.H. Maki, N. Edelstein, A. Davison and R.H. Holm, *J.Am.Chem.Soc.*, 86, 4580 (1964).

178. B.A. Goodman and J.B. Raynor, *Adv.Inorg.Chem. Radiochem.*, 13, 135 (1970).

179. T.I. Hyde, PhD Thesis, University of Edinburgh, 1987.

180. M.C.R. Symons and D.X. West, *J.Chem.Soc.Dalton Trans.*, 379 (1985).

181. K. Wieghardt, W. Walz, J. Bordner, B. Nuber, J. Weiss, A. Ozarowski, H. Stratemeier and D. Reinen, *Inorg.Chem.*, 25, 1650 (1986).

182. J.C. Brodovitch, R.I. Haynes and A. McAuley, *Can.J.Chem.*, 59, 1610 (1981).

183. A.N. Singh and A. Chakravorty, *Inorg.Chem.*, 19, 969 (1980).

184. C.N. Sethulakshmi, S. Subramainan, M.A. Bennett and P.T. Monoharan, *Inorg.Chem.*, 18, 2520 (1979).

185. a) R. Kirmse, J. Stach, W. Dietzsch, G. Steimecke and E. Hoyer, *Inorg.Chem.*, 19, 2679 (1980).

b) C.T. Vance, R.D. Bereman, J. Bordner, W.E. Hatfield and J.H. Helms, *Inorg.Chem.*, 24, 2905 (1985).

186. A. McAuley, P.R. Norman and O. Olubuyide, *Inorg.Chem.*, 23, 1938 (1984).

187. E. Balasivasubramanian, C.N. Sethulekshmi and P.T. Manoharan, *Inorg.Chem.*, 21, 1684 (1982).

188. A.J. Holder, T.I. Hyde and M. Schröder, unpublished results.

189. H-J. Küppers, K. Wieghardt, B. Nuber and J. Weiss, *Z.Anorg.Allg.Chem.*, 577, 155 (1989).

190. A.J. Blake, R.O. Gould, A.J. Holder, A.J. Lavery and M. Schröder, *Polyhedron*, 9, 2919 (1990).

191. M. Botrill, P.D. Gavens, J.W. Kelland & J. McMeeking in "Comprehensive Organometallic Chemistry", vol. 3, chapters 22.1-22.3.

192. D.J. Cardin, M.F. Lappert, C.L. Ralston, and P.I. Riley in "Comprehensive Organometallic Chemistry", vol. 3, chapters 23.1 and 23.2.

193. S.G. Davies, J.P. McNally and A.J. Smallridge, *Adv.Organomet.Chem.*, 30, 1 (1990).

194. G. Erker, *J.Organomet.Chem.*, 400, 185 (1990).

195. P. Jutzi, *Adv.Organomet.Chem.*, 26, 217 (1986).

196. a) C.J. Besecker, V.W. Day and W.G. Klemperer, *Organometallics*, 4, 564 (1985).

b) V.W. Day, W.G. Klemperer, S.P. Lockledge and D.J. Main, *J.Am.Chem.Soc.*, 112, 2031 (1990).

197. D.J. Rauscher, E.G. Thaler, J.C. Huffman and K.G. Caulton, *Organometallics*, 10, 2209 (1991).

198. P. Barbaro, C. Bianchini, A. Meli, M. Peruzzini, A. Vacca and F. Vizza, *Organometallics*, 10, 2227 (1991).

199. J. Chatt, G.J. Leigh, A.P. Storace, D.A. Squire and B.J. Starkey, *J.Chem.Soc.(A)*, 899 (1971).

200. B.R. James and F.T.T. Ng, *J.Chem.Soc.Dalton Trans.*, 355 (1972); *J.Chem.Soc.Dalton Trans.*, 1321 (1972).

201. F. Faraone, R. Pietropaolo and S. Sergi, *J. Organomet.Chem.*, 24, 797 (1970).

202. W.D. Lemke, K.E. Travis, N.E. Takvoryan and D.H. Busch, *Adv.Chem.Ser.*, 150, 358 (1976).

203. T. Yoshida, T. Ueda, T. Adachi, K. Yamamoto and T. Higuchi, *J.Chem.Soc.Chem.Commun.*, 1137 (1985).

204. K. Wieghardt, H-J. Küppers, E. Raabe and C. Krüger, *Angew.Chem.Int.Ed.Eng.*, 25, 1101 (1986).

205. A.J. Blake, A.J. Holder, T.I. Hyde, H-J. Küppers, M. Schröder, S. Stötzel and K. Wieghardt, *J.Chem. Soc.Chem.Commun.*, 1600 (1989).

206. A.J. Blake, G. Reid and M. Schröder, *Polyhedron*, 9, 2925 (1990).

207. D.P. Riley and J.D. Oliver, *Inorg.Chem.*, 22, 3361 (1983).

208. a) E.O. Fischer and K. Bittler, *Z.Naturforsch.Teil B*, 16, 225 (1961).

b) R.B. King, *Inorg.Chem.*, 2, 528 (1963).

209. a) R. Cramer, *J.Am.Chem.Soc.*, 86, 217 (1964).

b) R. Cramer and J.J. Mrowca, *Inorg.Chim.Acta*, 5, 528 (1971).

210. R. Cramer and L.P. Seiwell, *J.Organomet.Chem.*, 92, 245 (1975).

211. J.M. O'Connor and C.P. Casey, *Chem.Rev.*, 87, 307 (1987).

212. P. Caddy, M. Green, E. O'Brien, L.E. Smart and P. Woodward, *Angew.Chem.Int.Ed.Eng.*, 16, 648 (1977); *J.Chem.Soc.Dalton Trans.*, 962 (1980).

213. See e.g.

a) J.W. Kang and P.M. Maitlis, *J.Organomet.Chem.*, 26, 393 (1971).

b) V.W. Day, B.R. Stults, K.J. Reimer and A. Shaver, *J.Am.Chem.Soc.*, 96, 1227 (1974).

c) M. Arthurs, S.M. Nelson and M.G.B. Drew, *J.Chem. Soc.Dalton Trans.*, 779 (1977).

214. R. Cramer, *J.Am.Chem.Soc.*, 89, 5377 (1967).

215. A.J. Oliver and W.A.G. Graham, *Inorg.Chem.*, 9, 243 (1970); *Inorg.Chem.*, 10, 1 (1971).

216. a) J.K. Hoyano and W.A.G. Graham, *J.Am.Chem.Soc.*, 104, 3723 (1982).

b) J.K. Hoyano, A.D. McMaster and W.A.G. Graham, *J.Am.Chem.Soc.*, 105, 7190 (1983).

217. a) S.T. Belt, S.B. Duckett, D.M. Haddleton and R.N. Perutz, *Organometallics*, 7, 1526 (1988); *Organometallics*, 8, 748 (1989).

b) D.M. Haddleton, A. McCamley and R.N. Perutz, *J.Am.Chem.Soc.*, 110, 1810 (1988).

c) T.W. Bell, D.M. Haddleton, A. McCamley, M.G. Partridge, R.N. Perutz and H. Willner, *J.Am.Chem. Soc.*, 112, 9212 (1990).

218. A.J. Rest, I. Whitwell, W.A.G. Graham, J.K. Hoyano and A.D. McMaster, *J.Chem.Soc.Dalton Trans*, 1181 (1987).

219. D.E. Marx and A.J. Lees, *Inorg.Chem.*, 27, 1121 (1988).

220. A.H. Janowicz and R.G. Bergman, *J.Am.Chem.Soc*, 104, 352 (1982); *J.Am.Chem.Soc.*, 105, 3929 (1983).

221. W.D. Jones and F.J. Feher, *Organometallics*, 2, 562 (1983).

222. a) M.J. Wax, J.M. Stryker, J.M. Buchanan, C.A. Kovac and R.G. Bergman, *J.Am.Chem.Soc.*, 106, 1121 (1984).

b) P.O. Stoutland and R.G. Bergman, *J.Am.Chem.Soc*, 107, 4581 (1985); *J.Am.Chem.Soc.*, 110, 5732 (1988).

c) J.M. Buchanan, J.M. Stryker and R.G. Bergman, *J.Am.Chem.Soc.*, **108**, 1537 (1986).

d) B.H. Weiller, E.P. Wasserman, R.G. Bergman, C.B. Moore and G.C. Pimentel, *J.Am.Chem.Soc.*, **111**, 8288 (1989).

223. W.D. Jones and F.J. Feher, *Acc.Chem.Res.*, **22**, 91 (1989) and refs. therein.

224. P. Espinet, P.M. Bailey, P. Piraino and P.M. Maitlis, *Inorg.Chem.*, **18**, 2706 (1979).

225. D.S. Gill, C. White and P.M. Maitlis, *J.Chem.Soc. Dalton Trans.*, 617 (1978).

226. B.R. James, *Adv.Organomet.Chem.*, **17**, 319 (1979).

227. C. Bianchini, A. Meli, M. Perruzzini, F. Vizza, P. Frediani and J. Ramirez, *Organometallics*, **9**, 226 (1990).

228. F. Bachechi, J. Ott and L.M. Venanzi, *Acta Cryst.*, **C45**, 724 (1989); *Acta Cryst.*, **C45**, 876 (1989).

229. S.M. Nelson, M. Sloan and M.G.B. Drew, *J.Chem. Soc.Dalton Trans.*, 2195 (1973).

230. A. Immirzi and G. Allegra, *Acta Cryst.*, **B25**, 120 (1969).

231. C.A. Tolman, *Chem.Rev.*, **77**, 313 (1977).

232. A.J. Blake and M. Schröder, unpublished results.

233. a) A. Nutton and P.M. Maitlis, *J.Organomet.Chem.*, **166**, C21 (1979).

b) M. Green, D.R. Hankey, J.A.K. Howard, P. Louca and F.G.A. Stone, *J.Chem.Soc.Chem.Commun.*, 757 (1983).

234. R.G. Ball, W.A.G. Graham, D.M. Heinekey, J.K. Hoyano, A.D. McMaster, B.M. Mattson and S.T. Michel, *Inorg.Chem.*, **29**, 2023 (1990).

235. J. Powell and B.L. Shaw, *J.Chem.Soc.(A)*, 211 (1968).

236. E. Adman, M. Rosenblum, S. Sullivan and T.N. Margulis, *J.Am.Chem.Soc.*, **89**, 4540 (1967).

237. J.S. Miller, J.C. Calabrese, H. Rommelmann, S.R. Chittipeddi, J.H. Zhang, W. Reiff and A.J. Epstein, *J.Am.Chem.Soc.*, **109**, 769 (1987).

238. R. Cramer and G.W. Parshall, *J.Am.Chem.Soc.*, **87**, 1392 (1965).

239. R. Cramer, J.B. Kline and J.D. Roberts, *J.Am. Chem.Soc.*, **91**, 2519 (1969).

240. H. Sinn and W. Kaminsky, *Adv.Organomet.Chem.*, **18**, 99 (1980).

241. R.H. Crabtree, *Chem.Rev.*, **85**, 245 (1985).

242. a) O.S. Mills and E.F. Paulus, *J.Organomet.Chem.*, 10, 331 (1967).

b) W.D. Jones, M.A. White and R.G. Bergman, *J.Am. Chem.Soc.*, **100**, 6770 (1978).

243. R. Cramer, *Inorg.Synth.*, **15**, 14 (1975).

244. A. Van der Ent and A.L. Onderlinden, *Inorg.Synth.*, **14**, 92 (1974).

245. G. Giordano and R.H. Crabtree, *Inorg.Synth.*, 19, 218 (1979).

246. J.A. McCleverty and G. Wilkinson, *Inorg.Synth.*, 8, 211 (1966).

247. K. Vrieze, J.P. Collman, C.T. Sears and H. Kubota, *Inorg.Synth.*, 11, 101 (1968).

248. R. Cramer and L.J. Guggenberger, *J.Am.Chem.Soc.*, 94, 3779 (1972).

249. a) E.A. Allen and W. Wilkinson, *J.Chem.Soc.A*, 613 (1972).

b) E.W. Abel, G.W. Farrow and K.G. Orrel, *J.Chem. Soc.Dalton Trans.*, 1160 (1976).

250. A.J. Blake, R.O. Gould, A.J. Holder, T.I. Hyde, G. Reid and M. Schröder, *J.Chem.Soc.Dalton Trans.*, 1759 (1990).

251. A. Van der Ent and T.C. Van Soest, *J.Chem.Soc. Chem.Commun.*, 225 (1970).

252. H. Günther, "N.m.r. Spectroscopy", Wiley, New York, 1980, pp. 240-244.

253. D. Kost, E.H. Carlson and M. Raban, *J.Chem.Soc. Chem.Commun*, 656 (1971).

254. a) H. Eshtiagh-Hosseini and J.F. Nixon, *J.Less-Common Met.*, 61, 107 (1978).

b) M. Mlekuz, P. Bougeard, B.G. Sayer, M.J. McGlinchey, C.A. Rodger, M.J. Churchill, J.W. Ziller, S-K. Kang and T.A. Albright, *Organometallics*, 5, 1656 (1986).

255. K. Moseley, J.W. Kang and P.M. Maitlis, *J.Chem. Soc.A*, 2875 (1970).

256. M.A. Bennett and T.W. Matheson, *J.Organomet. Chem.*, 153, 2875 (1978).

257. J.A. Segal and B.F.G. Johnson, *J.Chem.Soc. Dalton Trans.*, 677 (1975).

258. C.E. Holloway, G. Hulley, B.F.G. Johnson and J. Lewis, *J.Chem.Soc.A*, 1653 (1970).

259. N.C. Harrison, M. Murray, J.L. Spencer and F.G.A. Stone, *J.Chem.Soc.Dalton Trans.*, 1337 (1978).

260. T.A. Albright, R. Hoffmann, J.C. Thibeault and D.L. Thorn, *J.Am.Chem.Soc.*, 101, 3801 (1979).

261. a) M.J.S. Dewar, *Bull.Soc.Chim.France*, 18, C79 (1951).

b) J. Chatt and L.A. Duncanson, *J.Chem.Soc.*, 2939 (1953).

262. R.P. Hughes, N. Krishnamachari, C.J.L. Lock, J. Powell and G. Turner, *Inorg.Chem.*, 16, 314 (1977).

263. M.R. Churchill and S.A. Bezman, *Inorg.Chem.*, 11, 2243 (1972); *Inorg.Chem.*, 12, 260, 531 (1973).

264. D.M.P. Mingos in "Comprehensive Organometallic Chemistry", vol. 3, Chapter 19, pp. 47-58 and refs. therein.

265. J.A. McGinnety and J.A. Ibers, *J.Chem.Soc.Chem. Commun.*, 235 (1968).

266. K. Goswami and M.M. Singh, *Transition Met.Chem.*, 5, 83 (1980).

267. M. Haga, K. Kawakami and T. Tanaka, *Inorg.Chem.*, 15, 1946 (1976).

268. M.J. Fernandez, M.J. Rodriguez, L.A. Oro and F.J. Lahoz, *J.Chem.Soc.Dalton Trans.*, 2073 (1989).

269. R.S. Tanke and R.H. Crabtree, *Inorg.Chem.*, **28**, 3444 (1989).

270. A.L. Onderlinden and A. Van der Ent, *Inorg.Chim. Acta*, 6, 420 (1972).

271. a) L. Kruczynski and J. Takats, *J.Am.Chem.Soc.*, **96**, 932 (1974); *Inorg.Chem.*, **15**, 3140 (1976).

b) A.D. English, J.P. Jesson and C.A. Tolman, *Inorg.Chem.*, **15**, 1730 (1976).

c) M.A. Busch and R.J. Clark, *Inorg.Chem.*, **14**, 226 (1975).

272. T.A. Albright, P. Hofmann and R. Hoffmann, *J.Am.Chem.Soc.*, **99**, 7546 (1977).

273. D.M.P. Mingos in "Comprehensive Organometallic Chemistry", vol. 3, chapter 11, pp. 60-67 and refs. therein.

274. a) O.S. Mills and G. Robinson, *Acta Cryst.*, **16**, 758 (1963).

b) L.C.A. de Carvahlo, Y. Peres, M. Dartiguenave, Y. Dartiguenave and A.L. Beauchamp, *Organometallics*, 4, 2021 (1985).

275. W. Haugen and M. Traettenberg, *Acta Chem.Scand.*, 20, 1726 (1966).

276. F.A. Cotton, V.W. Day, B.A. Frenz, K.I. Hardcastle and J.M. Troup, *J.Am.Chem.Soc.*, 95, 4522 (1973).

277. G. Erker, K. Engel, C. Krüger and G. Müller, *Organometallics*, 3, 128 (1984).

278. H. Yasuda, K. Tatsumi, T. Okamoto, K. Mashima, K. Lee, A. Nakamura, Y. Kai, N. Kaneshi and N. Kasai, *J.Am.Chem.Soc.*, 107, 2410 (1985).

279. S. Ruh and W. von Philipsborn, *J.Organomet.Chem.*, 127, C59 (1977).

280. Y. Kai, N. Kaneshi, K. Miki, N. Kasai, M. Akita, H. Yasuda and A. Nakamura, *Bull.Chem.Soc.Jpn.*, 56, 3735 (1983).

281. H.L. Retcofsky, E.N. Frankel and H.S. Gutowsky, *J.Am.Chem.Soc.*, 88, 2710 (1963).

282. M.D. Newton, J.M. Schulman and M.M. Manus, *J.Am.Chem.Soc.*, 96, 17 (1974).

283. H.D. Farnos, B.A. Woods and B.B. Wayland, *J.Am.Chem.Soc.*, 108, 3659 (1986).

284. N. Serpone and M.A. Jamieson, in "Comprehensive Coordination Chemistry", vol. 4, chapter 49, pp. 1120-1124.

285. J.L. Herde, J.C. Lambert and C.V. Senoff, *Inorg.Synth.*, 15, 18 (1974).

286. P. Groth, *Acta Chem.Scand.*, A32, 279 (1978).

287. J. Dale, *J.Chem.Soc.*, 93 (1963).

288. J.D. Dunitz and H.M.M. Shearer, *Helv.Chim.Acta*, 43, 18 (1960).

289. P. Groth, *Acta Chem.Scand.*, **A32**, 91 (1978).

290. P. Groth, *Acta Chem.Scand.*, **25**, 725 (1971).

291. A.J. Blake, J.A. Greig and M. Schröder, *Acta Cryst.*, **C46**, 322 (1990).

292. W.L. Smith, J.D. Ekstrand and K.N. Raymond, *J.Am.Chem. Soc.*, **100**, 3539 (1978).

293. J. Dale and G. Borgen, *J.Chem.Soc.Chem.Commun.*, 1340 (1970).

294. F.A.L. Anet and A.K. Cheung, *J.Am.Chem.Soc.*, **97**, 2420 (1975).

295. N.L. Allinger, B. Gorden and S. Profeta, *Tetrahedron*, **36**, 859 (1980).

296. J. Dale, *Top.Stereochem.*, **9**, 199 (1976).

297. V.L. Shannon, H.L. Strauss, R.G. Snyder, C.A. Elliger and W.L. Mattice, *J.Am.Chem.Soc.*, **111**, 1947 (1989).

298. P. Groth, *Acta Chem.Scand.*, **A28**, 808 (1974).

299. R.J. Batchelor, F.W.B. Einstein, I.D. Gay, J-H. Gu, B.D. Johnston and B.M. Pinto, *J.Am.Chem.Soc.*, **111**, 6582 (1989).

300. R.S. Glass, L. Adamowicz and J.L. Broeker, *J.Am.Chem. Soc.*, **113**, 1065 (1991).

301. N.L. Allinger and Y.H. Yuh, Q.C.P.E. Program No. 423, Quantum Chemical Program Exchange, Indiana University Chemistry Department, Bloomington, Indiana, U.S.A.

302. J-H. Lii and N.L. Allinger, Q.C.P.E. Program No. 543, Quantum Chemical Program Exchange, Indiana University Chemistry Department, Bloomington, Indiana, U.S.A.

303. R.D. Hancock, *Prog.Inorg.Chem.*, 37, 187 (1989).

304. D.M. Ferguson, W.A. Glauser and D.J. Raber, *J.Comput. Chem.*, 10, 903 (1989).

305. "Purification of Laboratory Chemicals", D.D. Perrin, D.R. Perrin and W.L.F Arma, 2nd Edition, Pergamon, Oxford.

306. W.R. Heinemann, R.W. Murray and G.W. O'Dom, *Anal. Chem.*, 39, 1666 (1967).

307. J. Cosier and A.M. Glazer, *J.Appl.Cryst.*, 19, 105 (1986).

308. G.M. Sheldrick, SHELX76, Program for crystal structure refinement, University of Cambridge, 1976.

309. G.M. Sheldrick, SHELX86, Program for crystal structure solution, University of Göttingen, 1986.

310. P.T. Beruskens, W.P. Bosman, H.M. Doesbury, Th. E.M. van den Hark, P.A.J. Prick, J.H. Noordik, G. Beurskeus, R.O. Gould and V. Pathasarathia, DIRDIF, Applications of Direct Methods to Difference Structure Factors, University of Nijmegen, Netherlands, 1983.

311. N. Walker and D. Stuart, DIFABS, *Acta Cryst.*, A39, 158 (1983).

312. R.O. Gould and P. Taylor, CALC, Interactive molecular geometry program, University of Edinburgh, 1985.

313. P.D. Mallinson and K.W. Muir, ORTEPII, *J.App. Cryst.*, 18, 51 (1985).

314. W.D.S. Motherwell and W. Clegg, PLUTO, Program for plotting molecular and crystal structures, University of Cambridge, 1978.

315. D.T. Cromer and J.L. Mann, *Acta Cryst., A24, 321 (1968).*

316. A.J. Blake, R.O. Gould, M. Halcrow and M. Schröder, *Acta Cryst.*, A46, C182 (1990).

317. A.J. Blake, M.A. Halcrow and M. Schröder, *J.Chem.Soc.Chem.Commun.*, 253 (1991).

ABBREVIATIONS

[9]aneN$_3$	1,4,7-triazacyclononane
Me$_3$[9]aneN$_3$	N,N′,N′′-trimethyl-1,4,7-triazacyclononane
[9]aneNS$_2$	1-aza-4,7-dithiacyclononane
[9]aneS$_3$	1,4,7-trithiacyclononane
[10]aneS$_3$	1,4,7-trithiacyclodecane
keto-[10]aneS$_3$	1,4,7-trithiacyclodeca-9-one
[12]aneS$_3$	1,5,9-trithiacyclododecane
[12]aneS$_4$	1,4,7,10-tetrathiacyclododododecane
[14]aneN$_4$	1,4,8,11-tetraazacyclotetradecane
[14]aneS$_4$	1,4,8,11-tetrathiacyclotetradecane
[16]aneS$_4$	1,5,9,13-tetrathiacyclohexadecane
[15]aneS$_5$	1,4,7,10,13-pentathiacyclopentadecane
[18]aneN$_2$S$_4$	1,10-diaza-4,7,13,16-tetrathiacyclooctadecane
Me$_2$[18]aneN$_2$S$_4$	N,N′-dimethyl-1,10-diaza-4,7,13,16-tetrathiacyclooctadecane
[18]aneS$_6$	1,4,7,10,13,16-hexathiacyclooctadecane
ap	apical
ax	axial
bas	basal
bipy	2,2′-bipyridyl
bu	butyl
cod	1,5-cyclooctadiene
cp$^-$	cyclopentadienyl
(cp*)$^-$	pentamethylcyclopentadienyl

cyc	cyclohexyl
cyclam	1,4,8,11-tetraazacyclotetradecane
d	doublet
d.e.p.t.	distortionless enhancement by polarisation transfer
dcpe	1,2-*bis*(dicyclohexylphosphino)-ethane
dmpe	1,2-*bis*(dimethylphosphino)ethane
dppe	1,2-*bis*(diphenylphosphino)ethane
dppm	*bis*(diphenylphosphino)methane
dppp	1,3-*bis*(diphenylphosphino)propane
dppv	*cis*-1,2-*bis*(diphenylphosphino)-ethene
dtco	1,5-dithiacyclooctane
en	1,2-diaminoethane
e.p.r.	electron paramagnetic resonance
eq	equatorial
et	ethyl
EtOH	ethanol
Et_2O	diethyl ether
f.a.b.	fast atom bombardment
fc	ferrocene
hmc	5,7,7,12,14,14-hexamethylcyclam
hr	hour
i.r.	infra-red
M	multiplet
max.	maximum

Me	methyl
MeCN	acetonitrile
$MeNO_2$	nitromethane
MHz	megahertz
min.	minute, minimum
mnt	maleonitriledithiolate
mol.wt.	molecular weight
nbd	2,5-norbornadiene
n.m.r.	nuclear magnetic resonance
3-NOBA	3-nitrobenzyl alcohol
OEP	octaethylprophyrin
o.t.e.	optically transparent electrode
ph	phenyl
phen	1,10-phenanthroline
ppm	parts per million
pr	propyl
s	singlet
sh	shoulder
t	triplet
tcne	tetracyanoethene
tdpme	1,1,1-*tris*(diphenylphosphinomethyl)-ethane
thf	tetrahydrofuran
tht	tetrahydrothiophene
TMC	N,N',N'',N'''-tetramethylcyclam
TPP	tetraphenylporphyrin
U.V./vis	ultra-violet/visible

LECTURE COURSES AND MEETINGS ATTENDED

Lecture Courses:

1. The Lanthanides.
   Dr. S. Cradock, University of Edinburgh.
2. Electronic Structures of Transition Metal Complexes.
   Dr. L.J. Yellowlees, University of Edinburgh.
3. Heavy Metals in the Environment.
   Dr. M. Schröder, University of Edinburgh.
4. Inorganic Medicinal Chemistry.
   Dr. S.K. Chapman, University of Edinburgh.
5. E.P.R. Spectroscopy.
   Dr. R.E.P. Winpenny, University of Edinburgh.
6. Solving and Refining Crystal Structures.
   Drs. A.J. Blake and R.O. Gould, University of Edinburgh.
7. Topics in Inorganic Chemistry.
   Drs. A.J. Welch, S.K. Chapman, M. Schröder and R.E.P. Winpenny, University of Edinburgh.
8. Chemical Uses of Synchrotron Radiation.
   Drs. G.N. Greaves, A. Hopkirk, M. Surman, S.M. Clark and A.J. Dent, S.E.R.C., Daresbury Laboratory.

Meetings:

1. Departmental Inorganic Colloquia and Friday Discussion Meetings (3 years).
2. University of Strathclyde Inorganic Club Conference (1989, 1990, 1991).
3. R.S.C. Scottish Dalton Group Meeting, Glasgow (1990).
4. Butler Postgraduate Electrochemistry Meeting, Edinburgh (1989, 1990).
5. U.K. Macrocyclic Symposium, Durham (1989), Warwick (1989), Manchester (1991).
6. R.S.C. Annual Chemical Congress, Belfast (1990).
7. Platinum Group Metals Conference, Cambridge (1990).
8. A.C.S. National Meeting, Washington D.C. (1990).

Synthesis, Structure and Reactivity of Cationic Rhodium(I) and Iridium(I) Thioether Crowns: Structures of $[M([9]aneS_3)(cod)]^+$ (M = Rh, Ir; cod = cycloocta-1,5-diene) and $[Rh([9]aneS_3)(C_2H_4)_2]^+$ ([9]aneS$_3$ = 1,4,7-trithiacyclononane)

Alexander J. Blake, Malcolm A. Halcrow and Martin Schröder*

Department of Chemistry, University of Edinburgh, West Mains Road, Edinburgh EH9 3JJ, Scotland

Reaction of M^I species with [9]aneS$_3$ affords half-sandwich complexes including $[M([9]aneS_3)(cod)]^+$, $[M([9]aneS_3)(coe)_2]^+$ (M = Rh, Ir; coe = cyclooctene), $[(Rh([9]aneS_3)(C_2H_4)_2]^+$, $[Rh([9]aneS_3)(C_2H_4)(PR_3)]^+$ (R = Ph, cyclohexyl), $[Rh([9]aneS_3)(CO)(PPh_3)]^+$ and $[Rh([9]aneS_3)(tcne)(NCMe)]^+$; crystal structure determinations of $[M([9]aneS_3)(cod)]^+$ (M = Rh, Ir) and $[Rh([9]aneS_3)(C_2H_4)_2]^+$ confirm these complexes to be five-coordinate, and the latter species reacts with C–X (X = halide) bonds.

The insertion of $[M(C_5Me_5)]$ and [M(HBPz)] (Pz - pyrazolyl) fragments into C–H bonds of alkane and aromatic substrates has been reported for M = Rh^I and Ir^I.[1,2] We have been interested in developing alternative methodologies for the stabilisation of facially protected mononuclear Rh^I and Ir^I centres using 6-electron donor ligands. [9]aneS$_3$ is particularly attractive in this respect: its ability to act as an efficient facial blocking group for a range of transition metal centres is now well established,[3] and would afford thioether coordination at the metal centre rather than the more usual N- (pyrazolylborate), P- (triphos) or carbocyclic (arene, cyclopentadienyl) C-donation. In addition, few examples of genuinely low-valent metal complexes of thioether crowns have been reported.[4,5] Most of these are Mo^0 complexes incorporating S_4-donor ligands;[5] no structural or synthetic data on thioether crown complexes incorporating ethylene have been described previously.

Reaction of $[MCl(cod)]_2$ (cod = cycloocta-1,5-diene) with

two molar equivalents of [9]aneS$_3$ in MeOH (for Rh) or in CH_2Cl_2 (for Ir) containing $NaBF_4$ affords [M([9]aneS$_3$)(cod)]$^+$ in 70% (Rh) and 30% (Ir) yields.† The single crystal X-ray structure‡§ of [Rh([9]aneS$_3$)(cod)]$^+$ shows (Fig. 1) five-coordination about Rh^I with [9]aneS$_3$ bound facially *via* all three S-donors. Two crystallographically independent complex cations are observed in the asymmetric unit each having the cod ligand bound in an η^4 manner. A similar five-coordinate structure is observed for [Ir([9]aneS$_3$)(cod)]$^+$.§¶ These complexes are therefore 18-electron species and this is reflected in their relative stability and inertness. Loss of the chelated cod ligand occurs slowly in solution under ambient conditions; thus, reaction of [Rh([9]aneS$_3$)(cod)]$^+$ with tcne (tcne = tetracyanoethylene) in MeCN affords [Rh[9]aneS$_3$(tcne)(NCMe)]$^+$ involving bound tcne.†

Reaction of $[MCl(C_2H_4)_2]_2$ with two molar equivalents of [9]aneS$_3$ in MeOH (for Rh) and in tetrahydrofuran (thf) (for Ir) containing $NaBF_4$ affords the reactive species [M([9]aneS$_3$)$(C_2H_4)_2$]$^+$ in 50% yield for both Rh and Ir. A crystal of the Rh^I complex was picked from the cold mother liquor and protected by an atmosphere of cold CO_2 gas during transfer to a Stoë STADI-4 four-circle diffractometer equipped with an Oxford Cryosystems low-temperature device.[6] The single crystal X-ray structure§ ‖ of

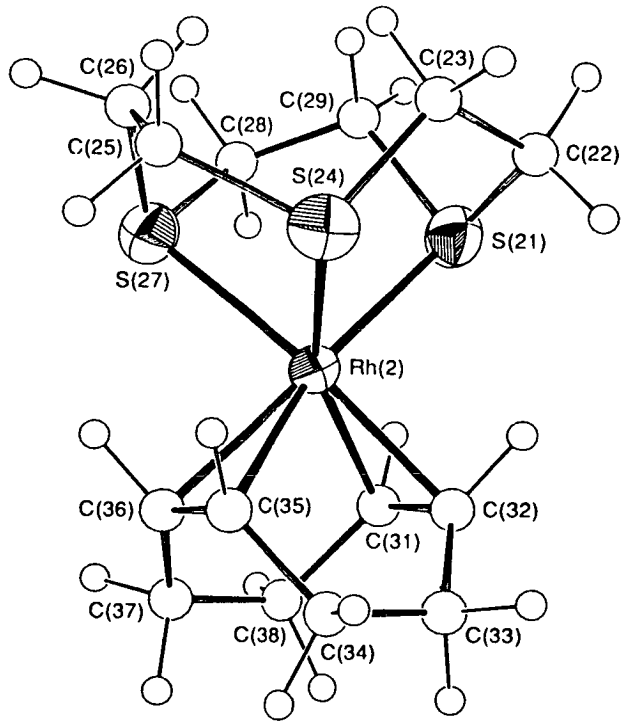

Fig. 1 Single crystal X-ray structure of [Rh([9]aneS$_3$)(cod)]$^+$. Bond lengths (Å) are given for independent cations (*a*) and (*b*). Cation (*b*) is shown. (*a*) Rh(1)–S(1) 2.322(3), Rh(1)–S(4) 2.400(3), Rh(1)–S(7) 2.451(3), Rh(1)–C(11) 2.069(12), Rh(1)–C(12) 2.133(12), Rh(1)–C(15) 2.223(12), Rh(1)–C(16) 2.199(12), C(11)–C(12) 1.424(17), C(15)–C(16) 1.377(17) Å. (*b*) Rh(2)–S(21) 2.305(3), Rh(2)–S(24) 2.441(3), Rh(2)–S(27) 2.436(3), Rh(2)–C(31) 2.108(13), Rh(2)–C(32) 2.080(11), Rh(2)–C(35) 2.193(15), Rh(2)–C(36) 2.214(18), C(31)–C(32) 1.408(17), C(35)–C(36) 1.279(23) Å. Bond lengths (Å) for [Ir([9]aneS$_3$)cod)]$^+$; Ir–S(1) 2.319(5), Ir–S(4) 2.343(4), Ir–S(7) 2.419(4), Ir–C(11) 2.188(15), Ir–C(12) 2.141(15), Ir–C(15) 2.166(14), Ir–C(16) 2.199(14), C(11)–C(12) 1.418(21), C(15)–C(16) 1.411(19) Å.

† These complexes have been characterised by IR and UV spectroscopy, ^{1}H, ^{13}C and, where appropriate, ^{31}P NMR and fast-atom bombardment mass spectroscopy, and by elemental analysis.

‡ *Crystal data* for $C_{14}H_{24}S_3Rh^+BF_4^-$, M = 478.20, triclinic, space group $P\bar{1}$, a = 11.491(13), b = 12.803(6), c = 13.377(15) Å, α = 88.12(7), β = 70.30(8), γ = 74.68(7)°, V = 1784 Å^3 (from setting angles for 14 reflections with 2θ = 42–44°, $\bar{\lambda}$ = 1.54184 Å, T = 298 K), Z = 4, D_c = 1.781 g cm^{-3}, μ = 11.482 mm^{-1}, $F(000)$ = 968. STADI-4 diffractometer, graphite-monochromated Cu-Kα X-radiation, T = 298 K, ω–2θ scans, 2838 unique data collected (2θ_{max} 90°, h −9 → 10, k −11 → 11, l 0 → 12), initial correction for absorption by means of Ψ scans (min. and max. transmission factors 0.0182, 0.0889 respectively), giving 2585 reflections with $F \geq 6\sigma(F)$ for use in all calculations. No significant crystal decay or movement was observed. A Patterson synthesis located both Rh atoms and iterative cycles of least-squares refinement and difference Fourier synthesis located the remaining non-H atoms. At isotropic convergence, final corrections (min. 0.794, max. 1.631) were applied empirically using DIFABS.[11] The structure was then refined (by least-squares on F[12]) with anisotropic thermal parameters for Rh, S, F and C and with H atoms included at fixed, calculated positions.[12] At final convergence R, R_w = 0.0590, 0.0866 respectively, S = 1.069 for 407 refined parameters and the final ΔF synthesis showed no feature above 1.01 e Å^{-3}. An isotropic extinction correction refined to 1.0 × 10^{-6}. The weighting scheme $w^{-1} = \sigma^2(F) + 0.007284F^2$ gave satisfactory agreement analyses and in the final cycle $(\Delta/\sigma)_{max}$ was 0.008.

§ Atomic scattering factors were inlaid[12] or taken from ref. 15, molecular geometry calculations utilised CALC[16] and the Figures were produced by ORTEPII.[17] Atomic coordinates, bond lengths and angles, and thermal parameters have been deposited with the Cambridge Crystallographic Data Centre. See Notice to Authors, Issue No. 1.

¶ *Crystal data* for $C_{14}H_{24}S_3Ir^+PF_6^-$: M = 625.7, monoclinic, space group $P2_1/c$, a = 9.6404(8), b = 11.9222(14), c = 17.2174(18) Å, β = 103.957(8)°, V = 1920.5 Å^3 [from 2θ values of 42 reflections measured at ±ω (2θ = 24–26°, $\bar{\lambda}$ = 0.71073 Å), T = 298 K], Z = 4, D_c = 2.164 g cm^{-3}, μ = 7.372 mm^{-1}. A pale yellow plate, 0.031 × 0.084 × 0.290 mm, grown from MeCN–Et_2O, was mounted on a Stoë STADI-4 four-circle diffractometer. Data collection employing graphite-monochromated Mo-Kα X-radiation, ω–2θ scans and the learnt-profile method[13] yielded 3709 amplitudes to 2θ_{max} = 45°. Initial corrections for absorption were applied by means of Ψ scans. Merging of equivalent reflections gave 2372 unique data (R_{int} = 0.035), of which 1919 with $F \geq 6\sigma(F)$ were used in all calculations. No significant crystal decay or movement was observed. A Patterson synthesis located the Ir and iterative cycles of least-squares refinement and difference Fourier synthesis located the remaining non-H atoms. At isotropic convergence, final corrections for absorption were applied empirically using DIFABS.[11] The structure was then refined (by least-squares on F[12]) with anisotropic thermal parameters for Ir, S, P, F and the C atoms of the cod ligand. The C atoms in the [9]aneS$_3$ ligand were found to be disordered but the application of constraints (S–C = 1.83, C–C = 1.52 Å; ∠SCC = 109.5°) allowed the refinement of two equally occupied conformations. H atoms were included at fixed, calculated positions.[12] At final convergence R, R_w = 0.0407, 0.0521 respectively, S = 1.162 for 220 refined parameters and the final ΔF synthesis showed no $\Delta\rho$ above 1.40 e Å^{-3}.

‖ *Crystal data* for $C_{10}H_{20}S_3Rh^+ \cdot BF_4^-$, M = 426.12, monoclinic, space group $P2_1/c$, a = 10.720(12), b = 8.547(17), c = 32.89(5) Å, β = 92.62(11)°, V = 3011 Å^3 (from setting angles for 12 reflections with 2θ = 15–26°, $\bar{\lambda}$ = 0.71073 Å, T = 173 ± 0.1 K), Z = 8, D_c = 1.880 g cm^{-3}, μ = 1.541 mm^{-1}, $F(000)$ = 1712. STADI-4 diffractometer, graphite-monochromated Mo-Kα X-radiation, T = 173 K, ω–2θ scans, 5030 data collected (2θ_{max} 45°, h −11 → 11, k 0 → 9, l 0 → 35), 3237 unique (R_{int} = 0.091), giving 1612 reflections with $F \geq 4\sigma(F)$. A drift curve based on the variation in the intensity of three standard reflections was applied to the data during processing. A Patterson synthesis located both Rh atoms and iterative cycles of least-squares refinement and difference Fourier synthesis located the remaining non-H atoms. At isotropic convergence, final corrections (min. 1.127, max. 1.689) were applied empirically using DIFABS.[11] The structure was then refined (by least-squares on F[12]) with anisotropic thermal parameters for Rh, S and F. Macrocyclic H atoms were included at fixed, calculated positions,[12] while those of the ethylene molecules were placed by analogy with a related complex.[14] At final convergence R, R_w = 0.0825, 0.0910 respectively, S = 1.179 for 233 refined parameters and the final ΔF synthesis showed no feature above 1.17 e Å^{-3}. The weighting scheme $w^{-1} = \sigma^2(F) + 0.00185F^2$ gave satisfactory agreement analyses and in the final cycle $(\Delta/\sigma)_{max}$ was 0.017.

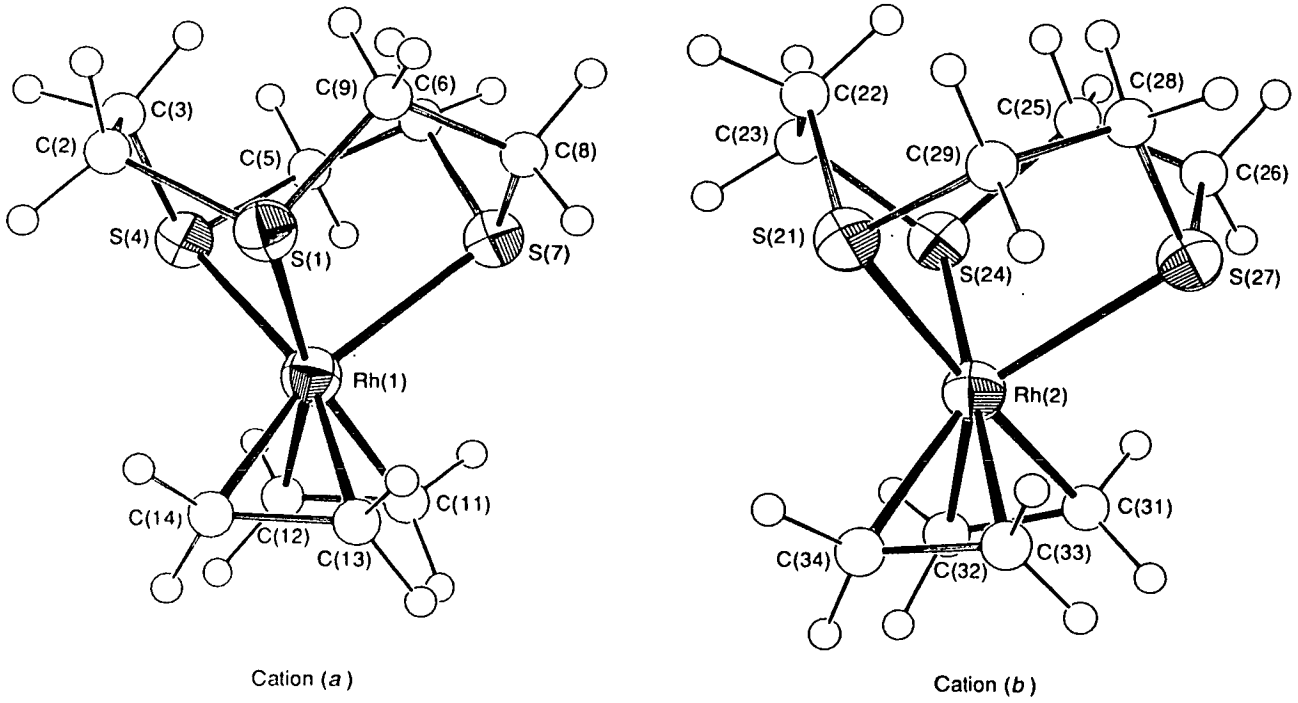

Fig. 2 Single crystal X-ray structure of $[Rh([9]aneS_3)(C_2H_4)_2]^+$. Bond lengths (Å) are given for independent cations (*a*) and (*b*). Both cations are shown. (*a*) Rh(1)–S(1) 2.322(9), Rh(1)–S(4) 2.437(9), Rh(1)–S(7) 2.432(9), Rh(1)–C(11) 2.21(4), Rh(1)–C(12) 2.21(5), Rh(1)–C(13) 2.12(5), Rh(1)–C(14) 2.05(4), C(11)–C(12) 1.33(6), C(13)–C(14) 1.43(6) Å. (*b*) Rh(2)–S(21) 2.337(9), Rh(2)–S(24) 2.327(10), Rh(2)–S(27) 2.469(10), Rh(2)–C(31) 2.11(3), Rh(2)–C(32) 2.18(4), Rh(2)–C(33) 2.15(4), Rh(2)–C(34) 2.22(3), C(31)–C(32) 1.43(5), C(33)–C(34) 1.41(5) Å.

$[Rh([9]aneS_3)(C_2H_4)_2]^+$ confirms (Fig. 2) five-coordination at the Rh^I centre. As with $[Rh([9]aneS_3)(cod)]^+$, two crystallographically independent cations are observed in the asymmetric unit; cation (*a*) shows one short and two long Rh–S distances while the other, cation (*b*), shows two short and one long distances. Cations (*a*) and (*b*) also differ in the relative orientation of the $[9]aneS_3$ ring to the coordinated ethylene. The Rh–S bond lengths in these Rh^I structures are longer than in related Rh^{III} complexes.[7] The related species $[M([9]aneS_3)(coe)_2]^+$ (coe = cyclooctene) can be prepared by reaction of $[MCl(coe)_2]_2$ with two molar equivalents of $[9]aneS_3$, while reaction of $[9]aneS_3$ with $[RhCl(CO)(PPh_3)_2]$ affords $[Rh([9]aneS_3)(CO)(PPh_3)]^+$.†

The C_2H_4 ligands in $[Rh([9]aneS_3)(C_2H_4)_2]^+$ are not particularly labile and substitution of C_2H_4 by PR_3 or CO does not readily occur up to the decomposition temperature of the compound in solution. Thus, no carbonyl complex could be isolated on reaction of $[Rh([9]aneS_3)(C_2H_4)_2]^+$ with CO in refluxing thf. This may reflect the inertness of the 18-electron metal centre. The related complex $[Rh(C_5Me_5)(C_2H_4)_2]$ likewise adds nucleophiles only under vigorous conditions, with alkene exchange occurring very slowly at room temperature.[8] Reaction of $[Rh_2Cl_2(C_2H_4)_2]$ with PR_3 followed by addition of $[9]aneS_3$ and $NaBF_4$ or NH_4PF_6 affords $[Rh([9]aneS_3)(PR_3)(C_2H_4)]^+$ [R = Ph, cyclohexyl (Cy)] and $[Rh([9]aneS_3)(PPh_3)_2]^+$.

Weak metal → alkene π back-bonding would be expected in $[Rh([9]aneS_3)(C_2H_4)_2]^+$ owing to the cationic charge on the complex. The ^1H NMR spectrum (233 K, CD_3COCD_3, 360 MHz) of $[Rh([9]aneS_3)(C_2H_4)_2]^+$ shows alkene resonances at δ 2.76 (d, $^2J_{H-Rh}$ 1.56 Hz) and the ^{13}C NMR spectrum (233 K, CD_3COCD_3, 50.32 MHz) shows δ 51.41 (d, $^1J_{C-Rh}$ 9.63 Hz) for the alkene C-centres. Alkene rotation is not frozen out for this complex down to 183 K. $[Ir([9]aneS_3)(C_2H_4)_2)]^+$ shows alkene resonances at δ 2.19 and 34.35 by ^1H (298 K, CD_3COCD_3, 360 MHz) and ^{13}C (50.32 MHz) NMR spectroscopy respectively. Lowering the temperature to 178 K leads to near collapse of the ^1H NMR signals for the coordinated ethylene suggesting a coalescence temperature of near 170 K, beyond the range of the solvent. The Raman spectrum of $[Rh([9]aneS_3)(PCy_3)(C_2H_4)]^+$ shows the C=C stretching vibration, $\nu_{C=C}$, at 1550 cm^{-1}.

The results described herein confirm that five-coordinate half-sandwich species incorporating the $[Rh([9]aneS_3)]^+$ fragment, the thioether analogues of $[Rh(C_5Me_5)]$ and [Rh(HBPz)], can be synthesised, and suggest that the Rh^I complex[7] $[Rh([9]aneS_3)_2]^+$ is most likely five-coordinate in the solid state. Loss of ethylene from $[Rh([9]aneS_3)(C_2H_4)_2]^+$ would, in principle, afford the 16-electron fragment $[Rh([9]aneS_3)(C_2H_4)]$ which should insert into substrate molecules.[10] Indeed, dissolution of $[Rh([9]aneS_3)(C_2H_4)_2]^+$ or $[Rh([9]aneS_3)(C_2H_4)PR_3]^+$ in CH_2Cl_2 affords $[Rh([9]aneS_3)(CH_2Cl)Cl(C_2H_4)]^+$ and $[Rh([9]aneS_3)(CH_2Cl)Cl(PR_3)]^+$ in low yield; the final product in both reactions is the highly insoluble $[Rh([9]aneS_3)Cl_3]$. It is not clear whether slippage of the tridentate $[9]aneS_3$ to a bidentate coordination to afford a 16-electron intermediate is of relevance here, although examples of bidentate $[9]aneS_3$ have been reported for d^8 complexes.[3,9]

Current work is aimed at studying the reactions of these half-sandwich $[M([9]aneS_3)]^+$ complexes with electrophiles, nucleophiles, aromatics and alkanes.

We are very grateful to ICI Colours and Fine Chemicals Plc and the SERC for a CASE Award to M. A. H., Dr R. Peacock

(University of Glasgow) for Raman spectra, Dr Robin Perutz (University of York) for helpful discussions, the SERC for support, and Johnson Matthey Plc for generous loans of platinum metals.

Received, 6th September 1990; Com. 0/04076B

References

1 A. H. Janowicz and R. G. Bergman, *J. Am. Chem. Soc.*, 1983, **105**, 3926; J. K. Hoyano, A. D. McMaster and W. A. G. Graham, *J. Am. Chem. Soc.*, 1983, **105**, 7190; W. D. Jones and F. J. Feher, *J. Am. Chem. Soc.*, 1986, **108**, 4814; T. T. Wenzel and R. G. Bergman, *J. Am. Chem. Soc.*, 1986, **108**, 4856; M. E. Thompson, S. M. Baxter, A. R. Bulls, B. J. Burger, M. C. Nolan, B. D. Santarsiero, W. P. Schaefer and J. E. Bercaw, *J. Am. Chem. Soc.*, 1987, **109**, 203; W. D. Jones and F. J. Feher, *Acc. Chem. Res.*, 1989, **22**, 91 and references therein.

2 C. K. Ghosh and W. A. G. Graham, *J. Am. Chem. Soc.*, 1987, **109**, 4726; C. K. Ghosh and W. A. G. Graham, *J. Am. Chem. Soc.*, 1989, **111**, 375.

3 A. J. Blake and M. Schröder, *Adv. Inorg. Chem.*, 1990, **35**, 1.

4 T. Yoshida, T. Ueda, T. Adachi, K. Yamamoto and T. Higuchi, *J. Chem. Soc., Chem. Commun.*, 1985, 1137.

5 For example see: D. P. Riley and J. D. Oliver, *Inorg. Chem.*, 1983, **22**, 3361; G. Reid, A. J. Blake, T. I. Hyde and M. Schröder, *J. Chem. Soc., Chem. Commun.*, 1988, 1397. For examples of low valent Mo thioether crown complexes see: D. Sellmann and L. Zapf, *Angew. Chem.*, 1984, **96**, 799: *Angew. Chem., Int. Ed. Engl.*, 1984, **23**, 807; D. Sellmann and L. Zapf, *J. Organomet. Chem.*, 1985, **289**, 57; M. T. Ashby and D. L. Lichtenberger, *Inorg. Chem.*, 1985, **24**, 636; T. Yoshida, T. Adachi, T. Ueda, M. Watanabe, M. Kaminaka and T. Higuchi, *Angew. Chem.*, 1987, **99**, 1182; *Angew. Chem., Int. Ed. Engl*, 1987, **26**, 1171; T. Yoshida, T. Adachi, M. Kaminaka, T. Ueda and T. Higuchi, *J. Am. Chem. Soc.*, 1988, **110**, 4872; T. Yoshida, T. Adachi, T. Ueda, M. Kaminaka, N. Sasaki, T. Higuchi, T. Aoshima, I. Mega, Y. Mizobe and Y. Hidai, *Angew. Chem.*, 1989, **101**, 1053; *Angew. Chem., Int. Ed. Engl.*, 1989, **28**, 1040; T. Adachi, N. Sasaki, T. Ueda, M. Kaminaka and T. Yoshida, *J. Chem. Soc., Chem. Commun.*, 1989, 1320.

6 J. Cosier and A. M. Glazer, *J. Appl. Crystallogr.*, 1986, **19**, 105.

7 A. J. Blake, A. J. Holder, T. I. Hyde and M. Schröder, *J. Chem. Soc., Chem. Commun.*, 1987, 987; S. C. Rawle, R. Yagbasan, K. Prout and S. R. Cooper, *J. Am. Chem. Soc.*, 1987, **109**, 6181; A. J. Blake, R. O. Gould, A. J. Holder, T. I. Hyde and M. Schröder, *J. Chem. Soc., Dalton Trans.*, 1988, 1861.

8 R. Cramer, *J. Am. Chem. Soc.*, 1964, **86**, 217; 1972, **94**, 5681; M. A. Arthurs and S. M. Nelson, *J. Coord. Chem.*, 1983, **13**, 29.

9 A. J. Blake, R. O. Gould, A. J. Holder, T. I. Hyde, M. O. Odulate, A. J. Lavery and M. Schröder, *J. Chem. Soc., Chem. Commun.*, 1987, 118.

10 W. D. Jones and L. Dong, *J. Am. Chem. Soc.*, 1989, **111**, 8722 and references therein.

11 DIFABS, program for empirical absorption correction, N. Walker and D. Stuart, *Acta Crystallogr., Sect. A*, 1983, **39**, 158.

12 SHELX76, program for crystal structure refinement, G. M. Sheldrick, University of Cambridge. 1976.

13 W. Clegg, *Acta Crystallogr., Sect. A*, 1981, **37**, 22.

14 R. Cramer and L. J. Guggenberger, *J. Am. Chem. Soc.*, 1972, **94**, 3779.

15 D. T. Cromer and J. L. Mann, *Acta Crystallogr., Sect. A*, 1968, **24**, 321.

16 CALC, program for molecular geometry calculations, R. O. Gould and P. Taylor, University of Edinburgh, 1985.

17 ORTEPII, interactive version, P. D. Mallinson and K. W. Muir, *J. Appl. Crystallogr.*, 1985, **18**, 51.